

Proceedings of the
TensiNet Symposium 2019

SOFTENING
THE HABITATS

3-5 June 2019 | Politecnico di Milano


MAGGIOLI
EDITORE

ISBN 978-88-916-3245-6

Copyright © 2019 by the authors

Published by Maggioli SpA with License Creative Commons CC BY-NC-ND 4.0 with permission.
Peer-review under responsibility of the TensiNet Association

Proceedings of the TensiNet Symposium 2019

SOFTENING THE HABITATS

Sustainable innovation in minimal mass structures and
lightweight architectures

3-5 June 2019

Politecnico di Milano | Milan | Italy

Edited by:

*Alessandra Zanelli, Carol Monticelli,
Marijke Mollaert, Bernd Stimpfle*

Scientific Committee:

*Adriana Angelotti, Paolo Beccarelli, Katja Bernert, Heidrun Bögner-Balz,
Andrea Campioli, Roberto Canobbio, Valter Carvelli, John Chilton, Jan Cremers,
Lars De Laet, Günther H. Filz, Christoph Gengnagel, Peter Gosling, Sebastian Koch,
Nikolai Kugel, Julian Lienhard, Josep Llorens, Claudia Marano,
Marijke Mollaert (Coordinator), Carol Monticelli (Coordinator), Giorgio Novati,
Arno Pronk, Andrea Ratti, Monika Rychtáriková, Franck Schoefs,
Bernd Stimpfle (Coordinator), Natalie Stranghöner, Martin Tamke, Patrick Teuffel,
Jean-Christophe Thomas, Jörg Uhlemann, Alessandra Zanelli (Coordinator)*

SUPPORTERS



Comune di
Milano



ORDINE DEGLI ARCHITETTI,
PIANIFICATORI, PAESAGGISTI E CONSERVATORI
DELLA PROVINCIA DI MILANO



ORDINE DEGLI INGEGNERI
DELLA PROVINCIA DI MILANO

SPONSORS



Proceedings of the TensiNet Symposium 2019

SOFTENING THE HABITATS

Sustainable innovation in minimal mass structures and
lightweight architectures

3-5 June 2019

Politecnico di Milano | Milan | Italy

Edited by:

*Alessandra Zanelli, Carol Monticelli,
Marijke Mollaert, Bernd Stimpfle*



TABLE OF CONTENTS

Proceedings of the TensiNet Symposium 2019

• Introduction

<i>Sustainable innovation in minimal mass structures and lightweight architectures. Introducing the main themes of the TensiNet Symposium 2019.....</i>	11
---	-----------

SOFT STRUCTURES

• Highlighted lectures

<i>Moveable membranes - smart solutions in the field of architecture.....</i>	17
Christoph Peach	
<i>New Hybrids.....</i>	25
Julian Lienhard	
<i>Lightweight and durable materials for thermal, acoustical and illuminance performance of building envelopes.....</i>	26
Philippe Lussou	
<i>Cable Erection of Adana Stadium Suspended Roof – Turkey.....</i>	34
Daniela Lombardini, Alessandro Stefanucci, Emanuela Di Muro	
<i>Teaching Membrane Architecture.....</i>	46
Robert Roithmayr, Rainer Blum, Horst Dürr, Simon K. Chiu	

• Design & simulation of soft structures

<i>An algorithm to draw simulations of dynamic lightweight structural systems withschemas.....</i>	51
Mesrop Andriasyan	
<i>Pre-stressed cable truss with stiffening girder and design clearance: development and analysis.....</i>	58
Vitalii V. Mikhailov, Andrei V. Chesnokov, Ivan V. Dolmatov	
<i>Numerical technique for estimation of cable roof structural parameters.....</i>	71
Andrei V. Chesnokov, Vitalii V. Mikhailov	
<i>Pressure coefficient distributions for the design of hypar membrane roof and canopy structures.....</i>	84
Jimmy Colliers, Marijke Mollaert, Joris Degroote, Lars De Laet	
<i>Systems for transformative textile structures in CNC knitted fabrics – Isoropia.....</i>	95
Mette Ramsgaard Thomsen, Yuliya Sinke Baranovskaya, Filipa Monteiro, Julian Lienhard, Riccardo La Magna, Martin Tamke	
<i>Bending-active frame: analysis and estimation of structural parameters.....</i>	111
Andrei V. Chesnokov, Ivan V. Dolmatov, Vitalii V. Mikhailov	

<i>Integration of form-finding, analysis process and production of a bending-active textile hybrid into one model.....</i>	123
Rens Vorstermans, Jasper Van Wijk, Patrick Teuffel, Arjan Habraken, Rogier Houtman	
<i>Lightweight structures, heavy foundations?.....</i>	135
Ramon Sastre, Xavier Gimferrer	

- **Air-supported & Pneumatic structures**

<i>Powerful Tools for Formfinding, Statics and Patterning of Pneumatic Structures.....</i>	144
Dieter Ströbel, Jürgen Holl	
<i>Inflatable beams subjected to axial forces.....</i>	160
Jean-Christophe Thomas, Anh Le Van	
<i>Atrium Roof in the New Lilienthalhaus in Brunswick, Job Report.....</i>	172
Bernd Stimpfle, Michael Schäffer	
<i>“Auditorium 1919 Sacmi” - Evaluation of the technological performances in the design phase of the walls and roof subsystem realized with ETFE cushions.....</i>	184
Beniamino Di Fusco, Andrea Angeleri	

- **Demountable structures**

<i>Anchoring emergency lightweight shelters.....</i>	196
Josep Llorens, Daniel Ledesma	
<i>Finite element analysis and design optioneering of an emergency tent structure.....</i>	208
Salvatore Viscuso, Milan Dragoljevic, Carol Monticelli, Alessandra Zanelli	
<i>Innovative Refugee Shelter Design with Pneumatic Sandwich Structure.....</i>	220
Nuerxiati Atawula, Alessandra Zanelli, Carol Monticelli, Carlotta Mazzola	
<i>Manta Bay, the pool in textile architecture.....</i>	231
Alessandro Rizzo, Roberto Canobbio, Francesco Benzi	

SOFTENING THE ENVIRONMENT

- **Highlighted lectures**

<i>Biomimicry for regenerative built environments: mapping design strategies for producing ecosystem services.....</i>	241
Maibritt Pedersen Zari, Katharina Hecht	
<i>Structure and Space of Serendipity Brought by Materials for Art.....</i>	260
Norihide Imagawa	
<i>Softening the environments: Is there anything like an environmentally compatible membrane?.....</i>	268
Katja Bernert	

<i>Eco-design principles for a preliminary eco-efficiency assessment in the design phase: application on membrane envelopes.....</i>	280
Carol Monticelli, Alessandra Zanelli	
<i>Development and testing of a new glass fibre reinforced fluoropolymer membrane.....</i>	292
Maxime Durka	
• Performance and reliability of soft materials	
<i>Increasing the safety of tensile structures.....</i>	304
Heidrun Bögner-Balz, Jochen Köhnlein, Rainer Blum	
<i>Reliability-based analysis of a cable-net structure designed using partial factors.....</i>	316
Elien De Smedt, Marijke Mollaert, Maarten Van Craenenbroeck, Robby Caspeepe, Lincy Pyl	
<i>Strain-rate dependent tensile strengths of PTFE-fabrics by using the Strip Method.....</i>	327
Kübra Talak	
<i>Architectural woven fabrics: Is it possible to classify stiffness values in correlation with strength values?.....</i>	339
Jörg Uhlemann, Natalie Stranghöner	
<i>Uniaxial Strip and Grab Test Methods for Tensile Testing of Architectural Fabrics.....</i>	351
Hastia Asadi, Jörg Uhlemann, Natalie Stranghöner	
<i>Experimental assessment and interpretation of biaxial material parameter variation of a polyester-PVC fabric.....</i>	366
Maarten Van Craenenbroeck, Lars De Laet, Elien De Smedt, Marijke Mollaert	
• Towards new materialities and soft spaces	
<i>Soft Spaces: Hybrid systems from structural membranes and conventional building technologies.....</i>	378
Günther H. Filz, Gerry D`Anza	
<i>TemporActive Pavillion: first loop of design and prototyping of an ultra-lightweight temporary architecture.....</i>	390
Carlotta Mazzola, Bernd Stimpfle, Alessandra Zanelli, Roberto Canobbio	
<i>Achieving complex bending-active structures from flexible planar sheets. Hybrid structure introducing the use of spacer fabrics in architectural field.....</i>	402
Elena Kriklenko	
<i>Computational knitting in architecture: an experimental design process for a performative textile system.....</i>	414
Ingrid Paoletti, Elena Clarke, Andrea Giglio	
<i>FlexHab.....</i>	426
Edoardo Marcandelli, Nicola Giulietti, Francesca Perego, Eleonora Teruzzi, Eleonora Valle	

SOFT SKINS

• Highlighted lectures

- A tensile screen for the windows of Castello Sforzesco: integrating anemometric, optical and mechanical tests in the early-stage design of bespoke textile hybrid structures in historical contexts.....* **439**
Alessandra Zanelli, Elpiza Kolo, Carol Monticelli, Elisabetta Rosina, Tiziana Poli, Alberto Speroni, Andrea Giovanni Mainini
- Textil Akademie Mönchengladbach, Job Report.....* **453**
Bernd Stimpfle, Jürgen Trenkle
- Tension-actuated textiles for architectural applications.....* **465**
Timothy Liddell, Isabella Flore, Massimo Fontana, Nina Romanova, Mahsa B. Zamani, Nataliia Antonenko, Haykaz Poghosyan
- Coating of ETFE – Solar Shading for Architectural Applications.....* **476**
Carl Maywald

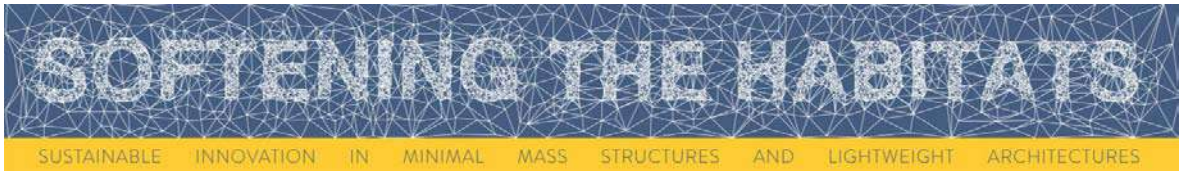
• Soft skins for the built environment

- Optimization of a membrane structure design for existing project of children's playground in the city of Krupina.....* **488**
Vojtech Chmelík, Jozef Kuran, Monika Rychtáriková
- Static assessment of selected transparent and translucent designs of roof over railway exposition.....* **497**
Eva Vojtekova, Matus Turis, Michal Vanek, Olga Ivankova
- Casa Corriere – RCS Media Group pavilion for Expo 2015.....* **505**
Paolo Beccarelli, Monica Armani, Roberto Maffei
- Textile architecture: “dressing the Aurelian walls”.....* **514**
Federica Ottone, Alessandra Zanelli, Dajla Riera
- Application of Atrium Tensile Structure in Historic Building. Case study: Daylight Modeling of Atrium within Historic Building.....* **526**
Beata Polomová, Peter Hanuliak, Andrea Vargová
- Exploring fog harvesting nature-based solution tensile membrane structures towards sustainable development in the Italian urban context.....* **535**
Gabriela Fernandez, Gloria Morichi, Lucas B. Calixto
- A lightweight textile device for urban microclimate control and thermal comfort improvement: concept project and design parameters.....* **547**
Anna Cantini, Adriana Angelotti, Alessandra Zanelli

• Thermal, Optical and Acoustic comfort

- Building Integrated Photovoltaic (BIPV) applications with ETFE-Films.....* **558**
Karsten Moritz
- Extreme Soft Skins: Multilayered ETFE for Challenging Environments.....* **570**
Nebojsa Jakica, Alessandra Zanelli

<i>Thermal performance of pneumatic cushions: an experimental evaluation</i>	580
Andrea Alongi, Adriana Angelotti, Alessandro Rizzo, Alessandra Zanelli	
<i>Assessment of building Physical Aspects of a New Angular Selective 3D – Prototype Foil (ETFE)</i>	592
Jan Cremers, Hannes Marx	
<i>Impact of Technical Textile Envelopes on the Perception of Indoor Comfort in Minor Sports Facilities</i>	602
Aldina Silvestri, Teresa Villani	
<i>Audiovisual comfort in shopping streets covered by structural skins</i>	614
Monika Rychtáriková, Richard Šimek, Paulína Šujanová, Jarmila Húsenicová, Vojtech Chmelík	
<i>Energy performance of film membranes in the retrofitting of Architectural Heritage: An Italian case study</i>	624
Mariangela De Vita, Raffaella D'Antonio, Paolo Beccarelli, Pierluigi De Berardinis	



Proceedings of the TensiNet Symposium 2019

Softening the habitats / 3-5 June 2019, Politecnico di Milano, Milan, Italy
Alessandra Zanelli, Carol Monticelli, Marijke Mollaert, Bernd Stimpfle (Eds.)

Sustainable innovation in minimal mass structures and lightweight architectures. Introducing the main themes of the TensiNet Symposium 2019

Alessandra Zanelli ^a, Carol Monticelli ^a, Marijke Mollaert ^b and Bernd Stimpfle ^c

^a Politecnico di Milano - TextilesHUB Research Laboratory
alessandra.zanelli@polimi.it - carol.monticelli@polimi.it

^b Vrije Universiteit Brussel (VUB), Dept. of Architectural Engineering, Brussel, marijke.mollaert@vub.be

^c form TL Ingenieure für Tragwerk und Leichtbau GmbH, Radolfzell, Germany, bernd.stimpfle@form-tl.de

Introduction

The 6th International TensiNet Symposium “*Softening the Habitats: Sustainable Innovations in Minimal Mass Structures and Lightweight Architectures*” is held from the 3th to the 5th of June 2019 at Politecnico di Milano, in Milan, Italy.

The 2019 TensiNet Symposium (TS19) is organized and hosted by the TensiNet Association and in particular by Politecnico di Milano (PoliMi) and Textile Hub, which is an interdepartmental research laboratory on textiles and polymers at PoliMi.

The 2019 TensiNet edition open a twofold reflection - by means of both the conference and the exhibition - on current innovations, trends and strategies in the field of lightweight membrane structures and mainly on the future of those technologies, which the TensiNet Association is interested in: tensile and pneumatic structures, textile architecture, membranes and foils, ultra-lightweight constructions and structural skins.

Copyright © 2019 by Alessandra Zanelli, Carol Monticelli, Marijke Mollaert and Bernd Stimpfle. Published by Maggioli SpA with License Creative Commons CC BY-NC-ND 4.0 with permission.

Peer-review under responsibility of the TensiNet Association

Innovation in lightweight construction and membrane materials

Lightweight structures have been regularly applied in the field of human construction, and have been so for more than ten thousand years. They have recently seen a considerable expansion due to the promising prospects that they offer, accounting for a larger proportion of the overall volume of buildings. The last few decades have brought numerous significant innovations in terms of materials, design and computation tools, as well as construction detailing and installation methodology. As a consequence of such innovative applications, membrane construction now has an established place in the field of Architecture. However, some imperative questions arise. At what stage of development are the best built examples today? How will textile architecture evolve in the near future? Can we expect any major innovations in this area? What part of our imagination still remains to be explored today? Will current technical advancements in materials production lead to lighter and more efficient structures and to greater environmentally sustainable enclosures? What is the biggest challenge of the next few decades in the field of tensile structures? Can we envision a future where unknown durable and recyclable materials will contribute to decrease the current conflicts between society and nature?

Three mornings of inspiring keynote lectures plus a number of plenary sessions, followed by just as many afternoons of open panel discussions and parallel sessions create a very special event where experts in the areas of membrane architecture and engineering, as well as researchers and industry representatives are contributing to constructive debates on soft structures, softening the environment and soft skins.

The “Softening” admonition

The current regulatory and operative frameworks require designers, researchers and industry executives to systematically consider the theme of societal, economical and environmental sustainability as a pivotal point of their work. Thus, the conference focuses on how building technologies on membranes are being more and more directed towards achieving a smaller environmental footprint and obtaining more resilient cities and landscapes. Worldwide, the lifestyle is increasingly characterized by requirements of flexibility, speed and dematerialization. Further applications of lightness and findings could be foreseen and experimented in the field of extreme living structures, meaning on one side the structures of post-emergency recovery, that have to perform requirements of speed, low-budget and modularity. On the other side, the design of structures for outer space, that need to perform high-tech requirements, in an opposite way, for the extreme living. In this regard, the TensiNet 2019 symposium host a number of panel discussions in order to develop synergies

among all experts of the sector, who are united to redefine the aesthetic and functional principles of today's and tomorrow's textile architecture. Nevertheless, the conference proposes also to deeply reflect on the theme of lightness in architecture, as well as how lighter constructions can potentially generate novel ideas on habitats.

Through the conference and the exhibition, the TS19 shows an exhaustive picture of responsibilities at various levels – academia, industries, practitioners, construction sector and standards – acting on tensile, membrane and foil constructions in Europe and worldwide. This objective is coherent with the main role of the TensiNet Association, disseminating more and more updated information at the regional level and amplifying it to the global scale, and vice-versa.

With the aim to unite academics, industry representatives and leaders in the topic of lightweight material innovations, tools and field advancements, the TS19 works on generating new synergies among professionals and envisioning new perspectives and outlooks within academia and industries. Eventually, again both through conference and the exhibition, a deeper understanding of the latest, most emblematic tensile constructions and of the different team collaborations on specific projects provides an unprecedented mapping of information and material flows. The final topic, in this way, is the promotion of knowledge on recent innovations related to the environmental mitigation and adaptation towards more sustainable materials in textile architecture, and the spreading of a more conscious circular economy-based design approach between TensiNet members, new visitors and new scientists.

Three main discussion focuses envisage new ways for lightening or softening our current spaces, both outdoors and indoors. Novel ideas and concepts of softer habitats, as well as advanced and innovative techniques for optimizing the structures and/or for reducing the environmental impacts of the production of composites materials are inspiring us, thanks the keynote lecturers' contributions, which are dealing with disruptive mind-sets, design methodologies, innovative technologies and advanced manufacturing in the fields of social and environmental sciences and in the field of engineering and construction.

Soft Structures

In the first conference session, the future frontiers of tensile membrane structures are explored thanks the involvement of a variety of disciplines and perspectives. The concept of lightness shifts its essence from vision to necessity, from shape to matter, while lightweight structures have to become fully energy-saving, efficiently load-bearing and, last but not least, carrying on novel concepts of beauty, flexible functions and adaptive structures.

With regard to the session dedicated to the lightening of structures, a comparison between design approaches to the design of membrane structures, through keynote lectures held by professional experts in ultra-lightweight structures and movable and retractable systems, are proposed.

On one hand, the themes of optimizing large-span structures are addressed, and, on other hand, the future approaches on how to reduce the redundancy of the structural parts in favour of their flexibility and adaptability are envisioned.

Further work sessions on soft structures concern then the themes of Design and simulation, as well as the technologies of pneumatic and air-supported structures and demountable structures.

Softening the Environment

This session focuses on the pivotal role of designing, manufacturing and building architectures, structures and landscapes and their impacts on global sustainability challenges. The main goal is to draw the attention to measuring the quality of current and future lightweight constructions in terms of environmental efficiency, user's comfort, materials and building products' durability and end-life scenarios.

At the centre of the debate at this conference session are the themes of: the weight-reduction's opportunities both in designing and manufacturing; the material selection strategies in the field of lightweight construction; updates, constrains and limits of standard regulations; the sustainability targets for the next textile architecture; the environmental impact of membrane structures and composite materials. In parallel, the topics of performances and reliability are also dealt with both on the materials and the building components scale, while a further session of papers is envisioning soft materiality and disruptive concept of spaces, able to expand and change, in relation to the gestures and needs of the users.

Soft Skins

The third conference session is devoted to the crucial and challenging topic of living structures. We have been long wishing for unwoven, seamless, elastic and durable materials, such as a kind of natural fleeces or thin shells. Further fundamental research contains and outstanding practices are leading the development of novel resilient structures and adaptive skins, which will be able to perform a next generation of human construction.

The key topics of this last *Soft skins* session are ranging from novel aesthetics of soft materials to solar design and thermal, optical and acoustic optimization of the building envelope. In particular, the contributions of eminent experts and scientists, which propose new design approaches to the design of adaptive spaces inspired by the essentiality and multiplicity and efficiency of natural organisms, are highlighted. In parallel, more specific issues are addressed, such as the integration of textile and lightweight systems in the built environment and the thermal, optical and acoustic comfort related to the application of ultra-thin and flexible materials, knitted fabrics, woven textiles, coated-textiles and Fluor-polymeric films.

This book contains 55 papers of a multi-form and multi-disciplinary kaleidoscopic set about theoretical and experimental research studies, professional jobs and industrial developments. They were selected through a complex and accurate blind review process, that was led by the TS19 scientific committee and then assigned three expert reviewers for each paper.

A special appreciation goes to all the supporters and the sponsors of this 6th edition of the International TensiNet Symposium; to those of the scientific committee who have actively collaborated in the reading and the revision of different version of the papers; not least, to all to those who, together with us, have patiently taken care of the entire process of organizing this scientific event. In particular, Evi Corne of the TensiNet Association, Carlotta Mazzola, Elpiza Kolo, Anna Cantini, Gabriela Fernandez and Dragana Micavika of Politecnico di Milano. To all them goes our immense gratitude for this result.



SOFT STRUCTURES

HIGHLIGHTED LECTURES

DESIGN & SIMULATION OF SOFT STRUCTURES

AIR-SUPPORTED & PNEUMATIC STRUCTURES

DEMOUNTABLE STRUCTURES

Proceedings of the TensiNet Symposium 2019

Softening the habitats / 3-5 June 2019, Politecnico di Milano, Milan, Italy
Alessandra Zanelli, Carol Monticelli, Marijke Mollaert, Bernd Stimpfle (Eds.)

Moveable membranes - smart solutions in the field of architecture

Christoph PAECH*

*schlaich bergemann partner
Schwabstrasse 43, 70197 Stuttgart, Germany
c.paech@sbp.de

Abstract

In a world of growing and changing demands on buildings and building envelopes, moveable elements help to increase the possible usage of the buildings and to enhance the corresponding characteristics. Over the last decades, an increasing number of projects that include moveable components have been carried out successfully and even more will follow. Projects, which have been completed so far, range in size from small to large scale and reach up to over 10.000 m² in retractable surface. Adaptive façades, retractable courtyard covers and deployable roofs for sport stadia are just a few examples for different kinds of system, which react actively to environmental demands or respond to a specific user requests. The paper describes the basic principles for the conceptual layout of retractable membrane structures. Besides detailed knowledge on material behavior and structural systems, also a comprehensive design approach spanning from architecture, structure to mechanical and electrical engineering is mandatory. To showcase the concepts, some of the recent works by schlaich bergemann partner are presented.

Keywords: membrane, deployable, retractable, movable, driving technology, adaptivity, folding, pneumatic, lightweight

DOI: 10.30448/ts2019.3245.53

Copyright © 2019 by Christoph Paech. Published by Maggioli SpA with License Creative Commons CC BY-NC-ND 4.0 with permission.

Peer-review under responsibility of the TensiNet Association

1. Introduction

schlaich bergemann partner has been working on innovative movable structures for more than 30 years. This includes several fields of engineering and construction like retractable bridges, CSP-technology and movable roofs and facades for concert halls, court yards and sport facilities.



Figure 1 Courtyard City Hall Vienna 2: Black Sea Arena Batumi (© schlaich bergemann partner, Zooey Braun)

The demand for smart buildings with adaptive components is growing from year to year, since they increase the possible usage options and functionality of a building significantly. Retractable roof or façade elements are often implemented in projects of all sizes, to, for example, flexibly protect a space from environmental conditions, enhance a certain user comfort or react on different utilizations. A deployable roof, for example, can transform an outdoor stadium into a mega multipurpose indoor arena within minutes. From an operational point of view, this creates valuable possibilities and helps to successfully run the venue. However, there are of course numerous technical and coordinative challenges that come with designing these structures. Its integration within a building or a fixed structure requires detailed planning and coordination between the involved collaborators, starting from the conceptual layouts, planning, fabrication, construction, developing prototypes until final commissioning. From an aesthetical point of view, it is important that the structural design and mechanical engineering for the retractable elements are developed in close consideration of the overall architecture and appearance of the respective building or space. Therefore, innovative engineering solutions are required using appropriate materials.

2. Adaptive lightweight structures

Lightweight structures are very efficient structural system. The use of low mass materials, such as textile membranes or cables, reduce the overall loads and forces in the global structural system significantly. Since most of the elements are in pure tension and not in bending, the cross sections can be fully utilized leading to a very economic design.

The combination of the lightweight principles and adaptive approaches provides a great opportunity for modern architecture with unique demands to their functionality. A smart structural system in combination with the use of lightweight materials simplifies the driving technology significantly and reduces the overall energy consumption during operation. Various structural concepts are possible using moveable elements. However, the geometry of the supporting structural system must be carefully developed and designed for different configurations, so that beside the structural integrity, the movability of the retractable elements is given under all relevant loading conditions.

The relevant demands on the lightweight membrane materials have to be evaluated on a project specific case. Beside the mechanical properties that are required for the structural design, also further characteristics need to be considered, such as fire resistance, optical parameters, durability in the specific environment, foldability and distinctive folding patterns and the amount of moving cycles during the expected life time – just to mention few of them. A proper material selection in combination with proper design and detailing is important to ensure a durable adaptive membrane structure. Specific material tests are usually required to verify in advance the material before it can be implemented in the project.

3. Moving principles

In most cases retractable membrane structures can accommodate two main configurations: In deployed condition the membrane is either mechanically or pneumatically prestressed and covers a certain space. In this condition the membrane is subject to full environmental loads such as wind, snow, etc. In the second configuration the membrane is retracted and parked. Between these two configurations a defined driving process happens while the membrane is being folded and moved. Using flexible textile membranes or cables allows for the application of folding patterns that reduce the size of the overall system from fully deployed to the storage position. Typical reduction factors are seen in a range from 1/20 to 1/100. The differentiation of driving technology and stressing technology is a key point for large retractable membrane structures in keeping the mechanical driving system simple, reliable and economical. Long distances for travelling require small forces and can be performed in a fast way using winches, whereas short stressing lengths require significant higher forces that can be realized by hydraulic systems.

A movable building component with its associated loads results in a significant variation of boundary conditions for the structural design of the component itself but also for the supporting structure. Various possible configurations and scenarios during the movement process must be considered and well analyzed, assuring that the system is stable and safe not just in the final configuration but also in all intermediate steps. In case just limited loads are allowed during the movement process, it is required to implement a smart monitoring system that is linked directly to the controlling system of the driving technology.

In general, for mechanically prestressed membrane structures a continuous membrane is only able to fold if, during the retraction process, the distance between two supporting points will never be bigger than in the final deployed geometry. Furthermore, the effect of compensation and prestress of the membrane has to be taken into account. Therefore, different moving principles are possible for deployable structures: They are either based on linear movement, radial movement or swinging movements.

Below, some examples of projects that have been designed by schlaich bergemann partner in the past and that apply different moving principles are presented:

3.1 Linear movements

The shade canopy structure for the Barahat Al-Nouq Square in Doha is approx. 35 m wide and 90 m long. In each of the 30 axes two cables are spanning between two building structures on either side of the square. From the fully locked cables 36 membrane covered panels per axis are suspended creating 18 V-shaped folds. At the upper end of the V-shaped fold the panel is fixed to the cable with sliding trolleys that move during operation. In retracted configuration the panels are stored at the perimeter while the folds are nearly vertical.



Figure 1 and 2: Barahat Al-Nouq Square in Doha (© schlaich bergemann partner, transsolar)

In hot weather conditions, when the square needs to be shaded, the system is pulled to the other side of the square, opening the V-shaped folds and creating a zig-zag arrangement of the panels. The panels themselves are 2,70 m x 1,40 m in size and consist of an aluminum frame with a PVC coated polyester membrane cover. Various arrangements of folding – also different in adjacent bays – are possible and provide both adequate shading of the square and a unique visual appearance, too. The result is an elegant movable structure, which on demand can move within a few minutes.



Figure 3 and 4: Barahat Al-Nouq Square in Doha, folded panels in parked configuration © schlaich bergemann partner)

3.2 Radial movements

In the last years, several large-scale convertible roofs have been completed, such as for the National Stadium in Warsaw and the BC Place Stadium in Vancouver. The moving procedure of the membrane roof of the National Stadium in Warsaw shows poetic engineering. Approximately 11,000 m² of PVC coated polyester membrane are supported by 60 single radial cables. The roof can be automatically deployed from the central parking garage along these cables. Electric winches move the driving carriage actively into the reach of the hydraulic stressing cylinders. The membrane itself is connected to the driving carriages and certain sliding carriages, which are all running on the primary steel cables.



Figure 4 and 5: Retracted and deployed roof at the National Stadium in Warsaw (© Marcus Bredt)



Figure 6 and 7: Driving carriage during movement, stressing units at perimeter (© schlaich bergemann partner)

The specific weather conditions in Vancouver can potentially lead to very high snow drifts and loads. To assure the all-year use of the 8,500m² retractable roof, which transforms the stadium within 10 minutes into a fully closed multipurpose arena, inflated and pressure-controlled cushions were integrated instead of a single layer membrane. 36 cushions with a max volume of 105 m³ are attached by sliding carriages to the lower cable of the cable girder. Radial Polyester belts between the cushions transfer the forces into the surrounding structure. They are mechanically stressed before the inflation of the cushion commences. Fluoropolymer coated PTFE fabric with extremely high translucency and excellent performance characteristics, especially in relation to the folding requirements, was chosen. The air pressure in the cushions is variable and responds to the respective environmental conditions. The standard pressure of 500 pa can be adjusted to max 2000 pa, based on load measurements of magnetic sensors at the primary steel cables and local climatic data input.

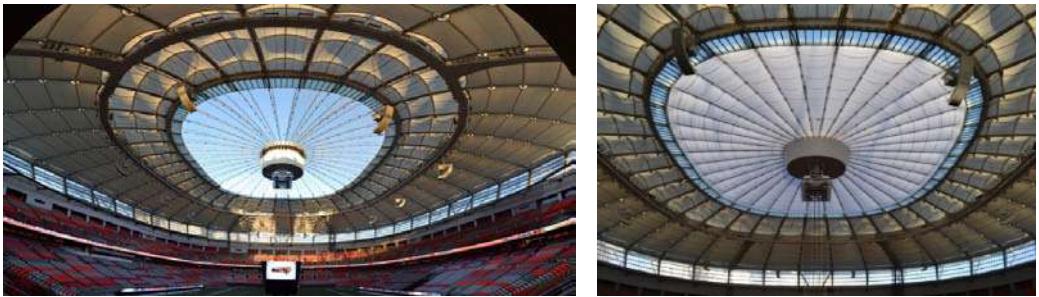


Figure 8 and 9: Deployable roof and pneumatic cushion at the BC Place Stadium, Vancouver (© schlaich bergemann partner)



Figure 10 and 11: Retractable roof at the BC Place Stadium during deployment and interior view of inflated cushion (© schlaich bergemann partner)

4. Future prospects

Various further movable roof structures that use textile membranes are currently under development and construction – often as a result of the continuing development of already implemented and well proven systems. For these retractable roofs, the very different and oftentimes extreme conditions like wind, snow, sun and earthquakes need to be taken in account. Every roof concept and every planning process is unique and needs to be designed and addressed differently to respond to the local situation. In this regard, different movement concepts and geometrical principles are applied, creating outstanding systems with unique appearances. As stated above, the demand for individual roof structures is yet to increase in the future.

Acknowledgements

Barahat Al-Nouq Square: Architecture by Mossessian & Partners

National Stadium Warsaw: Architecture by gmp Architekten von Gerkan, Marg und Partner

References

Paech C., (2016) *Structural membranes used in modern building facades*: In: *Procedia Engineering*, vol. 155 (pp. 61-70).

Goldack A., Gugeler J., Keck T., Paech C., Plieninger S., Sander C., Schlaich M., Stockhusen K., Weinrebe G.: *moveables*, Stuttgart: schlaich bergemann und partner, [online], available at: <http://www.moveables.sbp.de/>, 2014.

Göppert K., Paech C., Balz M., *Faltung von textilen Membranen bei wandelbaren Leichtbaukonstruktionen*: Bautechnik 90 (2013) Heft 4, Ernst&Sohn, Berlin.

Göppert, K., Moschner, T., Paech, C., Stein, M., Werner, M.: *Die Krone von Vancouver – Erneuerung des BC Place Stadions*. Stahlbau 81 (2012), H. 6, page 457-462.

Paech C., Balz M., *Use of textile membranes for adaptive structures*, Proceedings of the Tensinet Symposium 2013, Istanbul, Turkey.

Göppert K., Haspel L., Paech C., *New retractable roof solutions for sports stadia*, Proceedings of the 2011 IASS Symposium, London, Great Britain.

Proceedings of the TensiNet Symposium 2019

Softening the habitats / 3-5 June 2019, Politecnico di Milano, Milan, Italy
Alessandra Zanelli, Carol Monticelli, Marijke Mollaert, Bernd Stimpfle (Eds.)

New Hybrids

Julian LIENHARD*

* str.ucture GmbH, 70176 Stuttgart, Germany

Abstract

Today's challenges in Architecture and Engineering arise from an ever more complex network of boundary conditions, which often address apparently contradicting environmental, social and economic aspects. Within this context, we may not find a single best solution for a construction type or planning method to solve these challenges. In pursuit of efficient solutions for both the digital modelling and the actual construction, we are discovering new hybrids as forerunners of our creative profession. In this context we are also discovering new fields of application for textile architecture for both products and planning techniques beyond their classic application for membrane structures. The talk on 'new hybrids' will address this potential and highlight some challenges of our industry.



DOI: 10.30448/ts2019.3245.50

Copyright © 2019 by Julian Lienhard. Published by Maggioli SpA with License Creative Commons CC BY-NC-ND 4.0 with permission.

Peer-review under responsibility of the TensiNet Association

Proceedings of the TensiNet Symposium 2019

Softening the habitats / 3-5 June 2019, Politecnico di Milano, Milan, Italy
Alessandra Zanelli, Carol Monticelli, Marijke Mollaert, Bernd Stimpfle (Eds.)

Lightweight and durable materials for thermal, acoustical and illuminance performance of building envelopes

Philippe LUSSOU*

*Serge Ferrari, BP 54, 38352 La Tour-du-Pin Cedex, France.
philippe.lussou@sergeferrari.com

Abstract

The envelop is a key component in achieving the comfort in buildings, comfort being considered as the result of the thermal, acoustical and illuminance performances. Fortunately, architectural membranes offer a wide range of solutions and many projects have already achieved good performance by combining several materials in a multilayer composite and/or by using different materials or composites for separate parts of the envelope. The aim of the present study is to showcase few projects that illustrate how flexible materials can contribute to very performing building envelopes. For all the projects presented, the actual performance of the building is achieved thanks to a comprehensive analysis of the building and a strong attention paid to detailing.

Keywords: lightweight structures, structural membrane, durability, performance, thermal, illuminance, translucency, transparency

DOI: 10.30448/ts2019.3245.46

Copyright © 2019 by P. Lussou. Published by Maggioli SpA with License Creative Commons CC BY-NC-ND 4.0 with permission.

Peer-review under responsibility of the TensiNet Association

1. Introduction

Translucency has always been a strong advantage of architectural fabrics compared to other construction materials. Membranes even offer the possibility to play with light and colors by creating variations along the day. A very large variety of building facades, designed by architects, strongly highlight the freedom that is offered by membranes. Among these building facades, we can distinguish two different type depending the function of the membrane: being part of the envelope or not. If no, the membrane mainly provides solar gain control in addition to architectural identity; if yes, then airtightness, water tightness and thermal insulation must also be considered. Each building is then a specific case, each building envelop function need to be studied in detail and proven to the shareholders of the building construction project.

The first part of the present communication focuses on natural daylight then, in the second part, few examples of buildings for which the envelop brings benefits in term of natural daylight, thermal performance and/or acoustical comfort are shown.

2. Natural Daylight

As mentioned earlier, translucency / transparency is a strong advantage of lightweight construction with fabrics compared to other construction types. In most technical documents, this property is given as “Tv” (in percentage) and measured according to EN 410 standard. The aim of this paragraph is to focus on the benefits that daylight provides to people in the building and to the building itself. The physical measures are then different than translucency.

2.1. The benefits of natural daylight

When speaking about the benefits of natural daylight, there're two mains categories to consider: the benefits to people living in buildings and the benefits to the environment (by reducing the footprint of the buildings):

- Well being and performance of people inside the buildings

From Robbins (1986) who has established that daylight improves mood, enhance morale and reduce fatigue and eyestrain, until the latest findings from Hescong (2019) there's a countless number of academic studies about the benefits that natural daylight provide to people. It's now well established that the eye and brain functions respond better to natural light, so concentration capacity is increased. In many different environments: factories, offices classrooms, scientific studies have proven that people perform better with natural light: productivity, attendance rate, even exam results are improved. Some studies even show improved patient recovery rates in hospitals.

- Energy savings from electric lighting

The energy savings for electric lighting from using daylight depends on many factors: the building type (residential, school, office, warehouse, etc), the location of the building, the lighting control system, the occupancy of the building and the behavior of occupants. According to Galasiu (2007) the energy savings for electric lighting from using daylight can range from 20 to 60%. Of course the environmental footprint of a building requires a multiple criteria analysis, it's a matter of optimization.

2.2 Daylight metrics

Over the past decades, the architecture industry has experimented with many metrics for measuring daylighting:

Illuminance

In photometry, illuminance is the total luminous flux incident on a surface, per unit area. It is a measure of how much the incident light illuminates the surface, wavelength-weighted by the luminosity function to correlate with human brightness perception. Similarly, luminous emittance is the luminous flux per unit area emitted from a surface. Luminous emittance is also known as luminous exitance. In SI derived units these are measured in lux (lx), or equivalently in lumens per square metre (lm/m²).

Table 1: Typical illuminance values and minimum levels required for some tasks and activities

Typical illuminance values		Minimum levels tasks and activities	
Direct sunlight	100,000 lux	Residential room	200-500 lux
Diffuse skylight	3,000 – 18,000 lux	Classrooms (general)	300-500 lux
		Workspace lighting	200-500 lux

Daylight Factor

Daylight factor (DF) is a daylight availability metric that expresses as a percentage the amount of daylight available inside a room (on a work plane) compared to the amount of unobstructed daylight available outside under overcast sky conditions (Hopkins,1963).

As Daylight Factor is entirely independent of location, climate, and building orientation, it does not give any information about the actual performance of the building. Point-in-time measures (e.g. illuminance on September 21st at 3:00pm) can still be useful for understanding best- or worst-case scenarios, but don't give a good picture of whether a space or building is performing well overall.

In order to quantify the amount of daylight in a building's interior considering the availability of natural light outside at that location, as well as the properties of the building spaces and its surroundings, a dynamic calculation is needed. The daylight autonomy metric has been developed in that way.

Daylight autonomy

The daylight autonomy "DA_x", given as a percentage, represents the ratio of hours during a period (i.e., year or the occupation time over one year) when the natural indoor illuminance value in an area overcomes a predefined threshold x . As an example, a room achieving 50 of DA₃₀₀ means that for 50% of the occupation time of the room, the target illuminance level of 300 lux is obtained without artificial lighting.

Useful daylight illuminance

Useful daylight illuminance (UDI) is a daylight availability metric that corresponds to the percentage of the occupied time when a target range of illuminances at a point in a space is met by daylight. Daylight illuminances in the range 100 to 300 lux are considered effective either as the sole source of illumination or in conjunction with artificial lighting.

2.3. Codes standards, labels, recommendations

It exists a lot a recommendation guides and specification documents that define minimum lighting levels for wide range of activities. Examples of recommendations for indoor activities are given in Table 1. For sport facilities, depending on the sport league and the competition level the requirement goes from 180 lux to more than 2000 lux (for televised events).

Despite the multiple recommendations for illuminance, there is no building code that enforces a minimum level of daylighting. The design for daylight autonomy is promoted by health authorities (for healthy indoor environments) and sustainable construction institutes like LEED and BREEAM (to reduce environmental footprint of buildings). Applying these recommendations for daylight autonomy require a good understanding of how the entire building is affected by the dynamic nature of daylight. Therefore, they require dynamic simulation programs to be used by both architects and engineers.

3. Combination of daylight, thermal performance and acoustical comfort

In this section, three examples of buildings for which the envelop brings benefits in term of natural daylight, thermal performance and/or acoustical comfort are shown.

3.1 Miramas athletics arena

Stadium Athletics Stadium Miramas Metropole is the largest indoor athletic hall in France. It allows the welcome in track and field configuration of 5,500 spectators. Its gauge can be worn 7,500 spectators for handball and basketball events. The equipment benefits from an incomparable luminous atmosphere thanks to the canvas that covers it, diffusing a homogeneous light at the heart of the project. This performance is achieved thanks to a wooden truss spanning over 80 meters and the use of a double membrane to cover the arena. This specific design provides diffused light, thus blocking sun glare and preventing shadows,



Figure 1: Miramas athletics arena

3.2 The community gym “Julius-Hirsch-Sportzentrum”

The community gym “Julius-Hirsch-Sportzentrum” is located in the German municipality of Fürth. The sport arena is intended to host one indoor soccer/hand ball/basketball match or three small spaces for school sports. The building has a glass façade on the northeast, changing rooms are arranged throughout the basement and ground floor while the sport field is located at the subterranean level of the basement. The membrane roof spans the field and partly the secondary rooms. The scheme of the layer construction of the roof consists of an outer membrane as weather protection, an air space varying from a 0.5 to 2.5 meter thick, a thin cover foil as humidity barrier, a thermal insulation, a small 4 cm air gap and the inner membrane.



Figure 2: The community gym “Julius-Hirsch-Sportzentrum”

Gürlich et al. (2019) carried out a comprehensive study about the daylight performance of the textile roof. The results show that, in comparison to only one glass façade, the additional translucent and thermally insulated membrane roof construction increases the annual daylight autonomy (DA700) from 0% to 1.5% and the continuous DA700 from 15% to 38%. In the roof-covered areas of the sport field, it results in a 30% reduction of the electricity demand for artificial lighting from 19.7 kWhel/m²/a to 13.8 kWhel/m²/a, when a dimming control is used.

3.4 CIRCA

CIRCA is French acronym for Circus Research and Innovation Center, the CIRCA project is an auditorium. The envelop of this building is a double skin system with insulation in between designed by Pauli N. (2015). The distance between the two membranes is 250 mm and insulation panels made of rock wool (160 mm thick, $U = 0.2 \text{ W/m}^2\cdot\text{K}$) are supported by the lower membrane. The advantage of this system is to preserve the aesthetics of the project while providing thermal and acoustic comfort comparable to what is obtained in a theater in conventional construction.



Figure 3: The CIRCA auditorium

In order to achieve the performances required for this project, a special attention has been paid to detailing: the inner membrane is made of one single piece of 2,000 m² that ensures the watertight barrier between the outside and the inside, then several connection systems has been specially designed for the project. As the outer membrane is tensioned by lacing, the connecting devices must allow for adjustment of lacing bars while keeping dismantling possible to allow for future maintenance. In addition, in order to preserve the aesthetics of the project, the connection devices have been designed to remain invisible.

4. Conclusion

The main learnings of this study: 1) the three projects illustrate how flexible materials can contribute to very performing building envelopes 2) the actual performance of the building is achieved thanks to a comprehensive analysis and strong attention paid to detailing 3) even though the flexible materials generally provide excellent daylight benefits, these benefits are rarely quantified. This last point opens an avenue for future works: in past decades, the tensile membrane professionals, especially material suppliers, had to demonstrate the durability of lightweight architecture, Sahnoune (2016). There're now many projects that have been standing for decades that prove the durability of lightweight architecture. Even if there's still few consultants who need to be convinced, one can consider that durability is now established. In order to further develop our industry, we have now to convince about the benefits that can be obtained with highly performing envelopes in terms of thermal, acoustical and illuminance properties. This study modestly wishes to contribute to this objective.

Table 2: a synthetic presentation of the three projects

Project	Roof system	Translucency acc. EN 410	Thermal properties
Miramas arena athletics	TX30-II and 402 HT	Roof: Tv=4,8% Façade Tv=9%	U = 2,9 W/m ² .K
CIRCA project	1002 S2 and 702 S2 opaque with rock wool insulation panels	Opaque	U = 0,2 W/m ² .K
Julius-Hirsch-Sportzentrum	1202 T2 Highly translucent and 1002 S2 Highly translucent with glass wool	Tv=0.74%	U = 0,25 W/m ² .K

Acknowledgements

The author thanks the stakeholders of the projects mentioned in the study. For CIRCA auditorium: the architect Nicolas Novello, the membrane engineer Nicolas Pauli, Abaca, the membrane contractor: VSO – Goupe BHD, the wood frame contractor: Anglade Structures Bois. For Julius-Hirsch-Sportzentrum: the architect: FAB Architekten, Mannheim, the membrane contractor Graboplan. For Miramas athletic arena: the architects: Chabanne + Partenaires, the membrane contractor SMC2.

References

- Robbins, C. (1986). *Daylighting Design and Analysis*. New York: Van Nostrand Reinhold Company
- Heschong, Lisa & Mahone Group, Heschong & L Wright, Roger & Analytics, Rlw. (2019). *Daylighting and Human Performance: Latest Findings*.
- Galasiu, A.D., Newsham G.R., Suvagau, C., Sander, D.M. (2007) Energy saving lighting control systems for open-plan offices: A field study, *Leukos*, 4(1): 7-29.
- R. G. Hopkins, (1963), *Architectural Physics Lighting*, Her Majesty's Stationery Office, London
- Pauli N. (2015), Enveloppe double peau isolée ventilée pour un auditorium, In. *Structural Membranes*, E. Oñate, K.-U. Bletzinger and Kröplin B. (Eds)
- Gürlich, D., Reber, A., Biesinger, A., & Eicker, U. (2018). Daylight Performance of a Translucent Textile Membrane Roof with Thermal Insulation. *Buildings*, 8(9), 118. doi:10.3390/buildings8090118
- Sahnoune F, (2016) Innovative material for long lasting construction Project, *Proceedings of the TensiNet Symposium 2016*

Proceedings of the TensiNet Symposium 2019

Softening the habitats / 3-5 June 2019, Politecnico di Milano, Milan, Italy

Alessandra Zanelli, Carol Monticelli, Marijke Mollaert, Bernd Stimpfle (Eds.)

Cable Erection of Adana Stadium Suspended Roof – Turkey

Daniela LOMBARDINI*, Alessandro STEFANUCCI*, Emanuela DI MURO*

* BU Manager Tensostructures

Via A. Volta 16 20093 Cologno Monzese, Italy,

daniela.lombardini@redaelli.com

Abstract

This paper describes Redaelli contribution to the construction of the New Adana Stadium roof in Turkey.

It will host soccer matches for the two Adana teams. The 33,000 seat capacity stadium roof has a surface area of 24,000m². The roof is covered by a lightweight PVC membrane, supported by the compression ring, secondary arches and the upper cable tension ring in the radial direction, and the radial cables in the transversal direction.

The original stadium design considered a heavier steel structure roof which was subsequently replaced with this lighter cable net roof meaning the compression ring perimeter is more asymmetric than the usual structurally efficient circular shape. This has caused a more accurate design of the roof to assure its stability for all the considered load conditions which was even more sensitive during the lifting phase, particularly the lower ring cable lifting where the forces involved were very high.

Site activities planning and logistics were challenging but ultimately proved to be accurate and efficient, with all Redaelli site activities being performed successfully and to schedule. Despite the complexity of such a large building site and the challenge of several concurring site activities, the greatest control of each stage of cable installation and tensioning system was managed.

DOI: 10.30448/ts2019.3245.49

Copyright © 2019 by D. Lombardini, A. Stefanucci, E. Di Muro. Published by Maggioli SpA with License Creative Commons CC BY-NC-ND 4.0 with permission.

Peer-review under responsibility of the TensiNet Association

Keywords: Stadium, Cable Net Roof, Tension Ring, Radial Cables, Steel Cables, Suspended Roof

1. Introduction

Adana Stadium cable net roof design is based on the bicycle wheel principle using cable “spokes” or radial cables connected to two cable tension rings (one upper & one lower) and one outer steel compression ring. Due to the convex shape of the radial cables, the interconnecting elements between the upper and lower radials are steel strut elements, also known as flying masts.

The radial cables run along 40 axes from the compression ring to the cable tension rings. All the cables which make up the upper and lower cable tension rings are connected by couplers, thus creating a circular ring of cables. Redaelli’s scope for the project was providing the cable net roof design, the cable supply, the cable installation and the big lift synchronized tensioning of the 184 steel cables. The total cable length was 8080m resulting in a total cable net mass of approx. 250 tonnes, including the cable sockets.

The final shape of the radial cables has been designed to reduce the horizontal force on the compression ring, to protect spectator sightlines and to achieve an efficient structural behaviour under live loads, avoiding significant deformations. The stiffness of the roof is provided by prestressing the cables after lifting completion.

The compression ring is placed on top of the existing steel columns, which support the outer façade, and it is duly reinforced to withstand the new roof and supported by spherical bearings. The radial cable spans are between 44m in the long side and 52m in the shorter side and are connected by vertical flying masts and diagonal steel struts, thus forming radial cable trusses.

2. Redaelli design

The roof was designed by Maffei Engineering, who were responsible for the as engineering services, both for roof design (compression ring, cable net and fabric) and for cable net erection. The Adana Stadium Roof consists in a typical spoked-wheel structure, having an outer compression ring and two inner tension rings. In this type of structure, the shape of the compression ring is one of the key parameters and the Designer often investigates different curvature profiles, in order to reduce the bending stresses and optimize the design. Unfortunately, for the Adana Stadium, the compression ring oval shape was already fixed by the concrete bowl geometry and by the presence of a façade structure, standing on the perimeter of the stadium. Hence, the “flat” shape of the compression ring on the long sides of the stands represented the most critical item to be taken into consideration and all the design choices were made in order to avoid overstressing of these weak parts.

The shape of the tension rings was designed in order to achieve an affine geometry with the compression ring ones. “Affine geometry” means that the angle variation of the compression ring and of the tension rings was set to be equal. Studies were carried out in order to perform the best geometry and at the end it was obtained a geometry where the angle changes are exactly the same as it can be seen from the plot below:

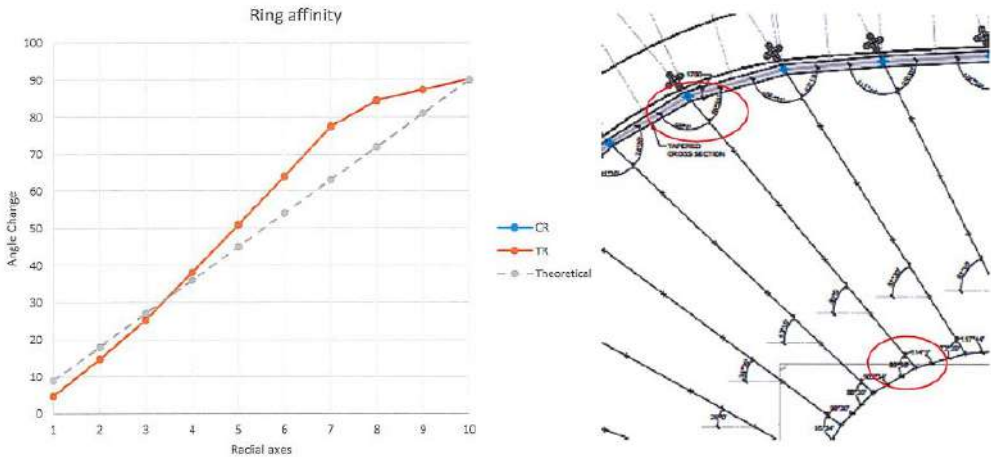


Figure 1. Affine geometry of the roof.

Once the geometry of the rings was achieved, the second step was to determine an appropriate curvature for the radial cables connecting the compression ring to the tension rings. It was found that the more curvature the radial cables have, the less load is introduced in the compression ring, because the force is inversely proportional to the sag [Catenary formula, $H=p l^2/(8f)$]. For the Adana stadium, it was set a low curvature for the radial cables located in the corners (where the compression ring has a strong curvature and therefore it is stiff) and a big curvature on the long sides (where the compression ring is “flat” and it is weak):

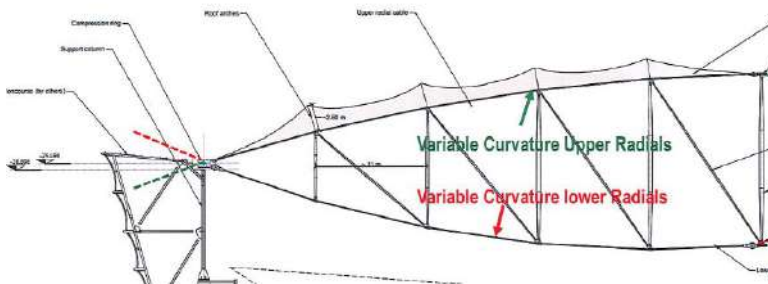


Figure 2. Typical section of the roof.

The third design parameter was the orientation of the radial cables. In order to drag the load on the corners of the compression ring, the radial cables were inclined as much as possible (avoiding excessive deviation forces on the tension ring, which would have led to big ring connectors, and always ensuring to have a regular spacing for the membrane design):

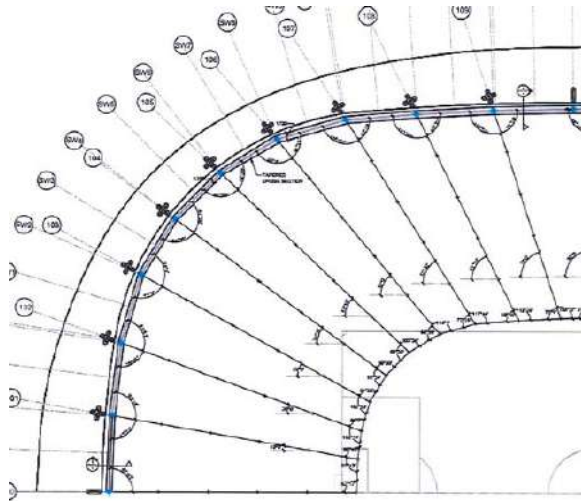


Figure 3. Quarter plan view of the roof.

Horizontal bracings are included in the design in order to reduce the bending moment of the compression ring (mainly on the long sides) and to reduce its displacements.

Diagonal bracings are contemplated between the lower and upper radial cables to reduce the deformations in the central part of the roof under snow and wind loads.

Frontal vertical bracings are contemplated between lower and upper tension ring to increase the stiffness under unbalanced load cases, without the need of increasing the prestress level of the system.

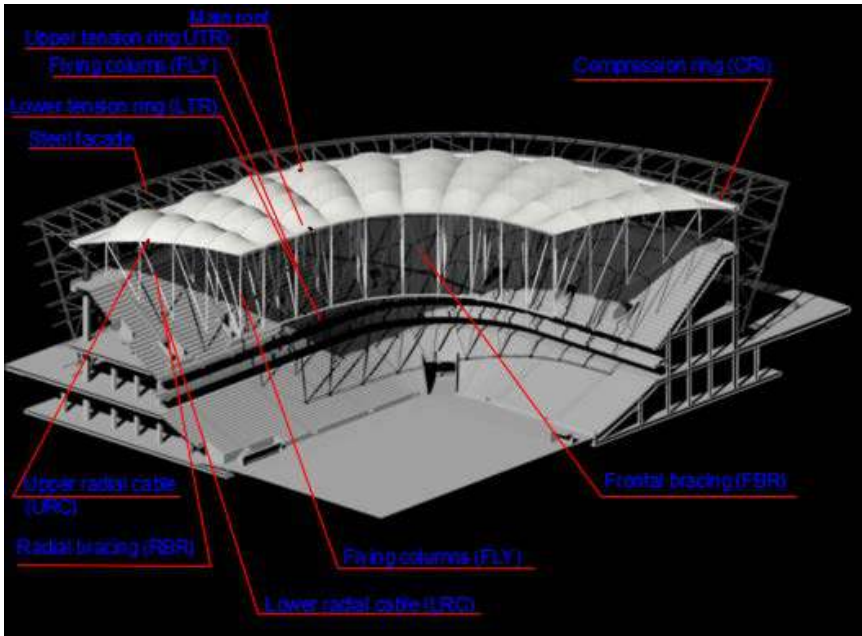


Figure 4. Quarter isometric view of the roof.

Regarding the cladding, a double curvature membrane in PVC was designed which is supported by steel arches. The prestress of the membrane was set to a precise unit value in warp ($\approx 4\text{kN/m}$) and in weft ($\approx 2\text{kN/m}$) direction as a compromise between the installation and the required stiffness against downwards and upwards loads.

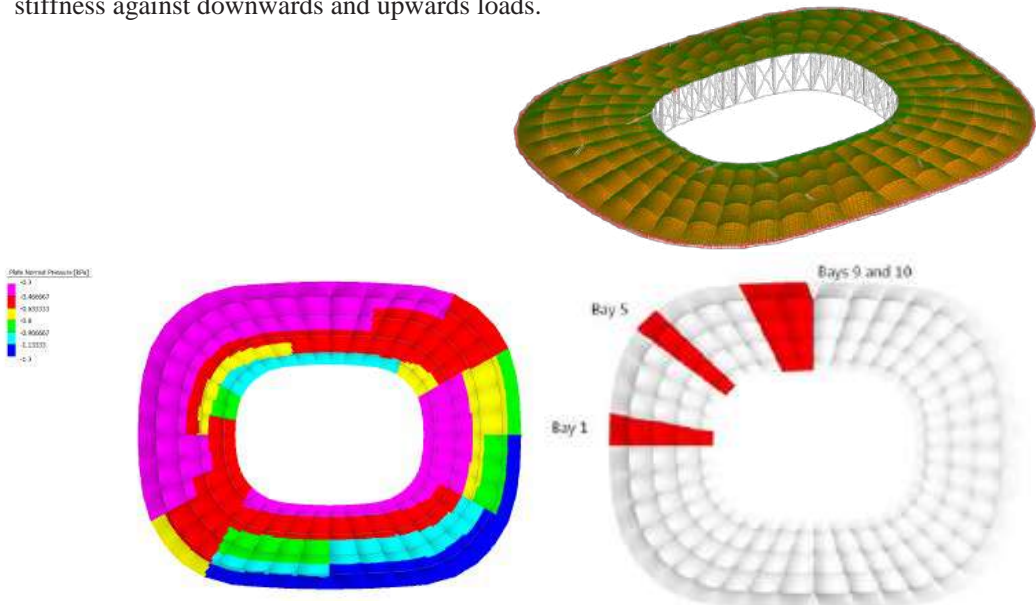


Figure 5. FEM for fabric design.

3. Redaelli supply

Redaelli supplied the cable system for the Adana Stadium Roof. The following table summarizes the scope of supply, in terms of cable type, diameter, number of elements and socket types.

Table 1. Summary of Redaelli Supply.

ITEM	CABLE TYPE & DIAMETER	SOCKET A TYPE	SOCKET B TYPE	M.B.L. (kN)	Q.ty (no.)
Upper Tension Ring	FLC 56	CYC 56	CYC 56	3190	8
Lower Tension Ring	FLC 100	CYC 96	CYC 96	10050	8
Lower Radial 01	FLC 96	TTF 88	TTF 88	9165	24
Lower Radial 02	FLC 60	TTF 56	TTF 56	3660	6
Lower Radial 03	FLC 56	TTF 52	TTF 52	3190	10
Lower Radial split	FLC 40	TTF 40	TTF 40	1605	4
Upper Radial 01	FLC 60	TTF 56	TTF 56	3660	24
Upper Radial 02	FLC 40	TTF 40	TTF 40	1605	6
Upper Radial 03	FLC 40	TTF 40	TTF 40	1605	10
Upper Radial split	FLC 32	TTF 32	TTF 32	1015	4
X cross TR	FLC 32	TTF 32	TBF 32	1015	56
X cross RC	FLC 40	TTF 40	TBF 40	1605	24

All Redaelli cables are made by hot-dip galvanized high strength steel round wires, spun largely in opposite directions around a central core. Full lock coil cables (FLC) have external layers of interlocking Z-shaped wires which provide self-locking of the cable section.

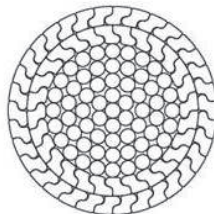


Figure 6. Full Lock Coil Cables.

In order to eliminate initial anelastic strains, the master length of cables were pre-stretched with minimum five cycles. The individual cable lengths and intermediate clamp positions were

precisely marked under specific loads and controlled temperature, a total of 40 marking positions on each ring cable and 4 marking positions on each radial cable was executed.

Fork sockets and connectors were made of high strength cast steel, whereas the cylindrical sockets, turnbuckles, pins and clamps were produced using machined high strength alloy steel. Adana Roof cables were connected to the sockets with Polyester resin.

Hereafter some pictures illustrate the main items of Redaelli's supply.

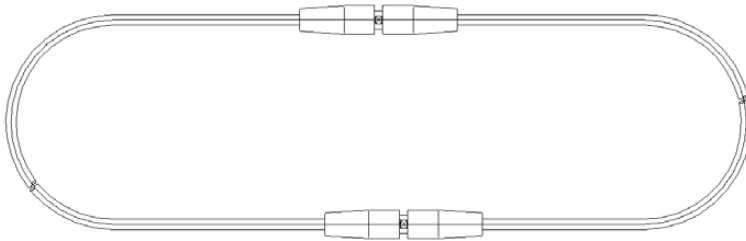


Figure 7. Full Lock Coil Cable (FLC) with CYC Coupler Cylindrical Sockets (Tension Ring Cables).

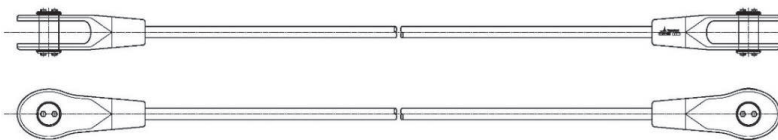


Figure 8. Full Lock Coil Cable (FLC) with TTF/TTF Sockets (Radial Cables).

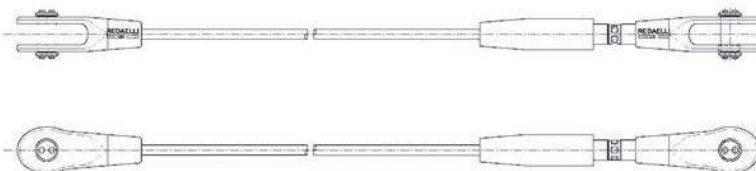


Figure 9. Full Lock Coil Cable (FLC) with TTF/TBF Sockets (Bracings).

The overall quality of the supply was assured by a wide campaign of tests on every component. In addition to destructive and not destructive controls on forged sockets, full scale tensile tests were executed on one cable sample for each size, the samples were fitted with sockets equal to permanent ones. Furthermore, 200-hour long term tests helped to verify the creep on the cables, as well as slipping force tests were used to establish the sliding force of radial clamps and ring cable connectors. Control activities were carefully inspected and examined, also by means of external supervisors, and each step of the production process was accurately tracked and overseen.

4. Site activities

All activities related to cables installation and tensioning were agreed with the Main Contractor so that Redaelli presence on site was organized and synchronized with other site works. Cable installation and tensioning followed the procedure defined by the Designer. Site activities performed by Redaelli are grouped and described in the following paragraphs.

4.1. Site preparation and lay down of the cables

Site preparation was carefully planned considering the necessary storage areas for such a large supply and required assembly areas at proper location according to the site activities schedule.

All cables were supplied in coils and were unwound using uncoilers with the required capacity.



Figure 10. Redaelli cable on the uncoiler.

Figure 11. Site Preparation with reinforced wooden strips.

The first step of cable installation was to uncoil every cable and to lay it down. Cables were uncoiled lifting the top socket with a crane and placing each cable lying at the corresponding position, so that cable system layout was generated on the ground level. For each axis of radial cables, reinforced wooden strips were previously placed on stadium stands and wooden saddles were provided to let the cable sliding over the parapet.

Similarly, timber platforms were built at the location of ring connector castings to protect their surface and the concrete below. The exact position of each timber platform was theoretically calculated according to the cable system layout. These platforms had an internal opening to allow for the sliding of ring connectors during tensioning operations.

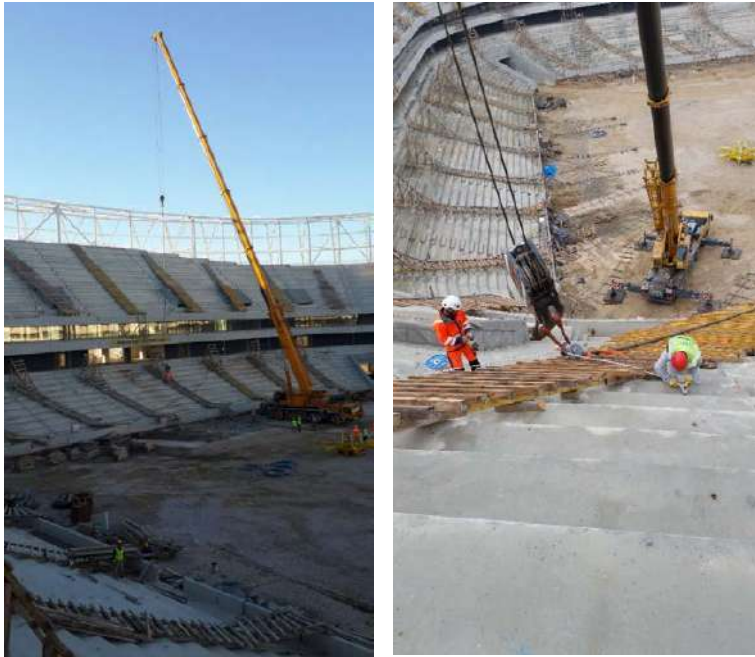


Figure 12 Cables Lay Down

5. Clamps installation and spreader beams

Once radial cables were laid down, radial cable clamps were located at the corresponding marking positions and they were installed and tightened to connect the struts to radial cables, thus forming cable trusses along radial axis. The upper ring cable connectors have been laid down before the lay down of upper ring cables upon the corresponding platforms, while the lower ring cable connectors afterwards.



Figure 13. Ring Cables Connector.

The spreader beams are temporary steel structures used to connect the radial cables to the pulling strands. The beams are two piece components which clamp around the radial cables and transfer the tensioning force of the strands to the cables. A stabilization nose is necessary to prevent the spreader beam from rotating; it is also important that the alignments of the fork sockets are correct to facilitate the insertion of the pins in the final configuration. The spreader beams were assembled on wooden platforms at the top end of radial cables.



Figure 14. Spreader beam.

6. Big Lift

The cable net of the Adana Stadium consists of 8 tension ring cables, 80 radial cables and 80 X-cross bracing cables. Once the tension rings were laid down on the ground, the relevant radial cables were attached to the tension ring connectors and disposed along corresponding axis for final pin connection. A single strand jack for each axis, was installed on the compression ring and upper radial cables were pulled by temporary strands connected to the temporary clamps, lifting the entire cable net. The upper tension ring was lifted pulling each upper radial cable with one strand jack. On the other hand, a double climbing strand jack system was installed on the top of the tribune and lower radial cables were lifted off by spreader beams, connected to the compression ring. The lower tension ring was lifted off pulling each lower radial cable with two strand jacks. It is plain to understand that such a challenging operation requires the greatest care and accuracy at each stage.

6.1. Preliminary activities

It was essential that all equipment was carefully overhauled and inspected prior to transportation on site, equipment testing being documented in detail. Likewise, it was crucial to verify the strands resistance and their safety coefficient with respect to the expected loads.

6.2. Installation of Big Lift equipment

Working on such a large-scale structure, accessibility had to be taken into proper and careful consideration. Particularly, it was necessary to be able to operate promptly and smoothly on socket pins during the final connection, the so called “cable pinning”, so two steel platforms have been installed for each axis, at both side of the radial cable anchorages. For the first lifting of the upper radial cables, a single jack each axis has been located on the top of the compression ring, supported by a steel frame bolted in correspondence with two compression ring segments. A sliding steel saddle positioned at the exit of the strand bundle has been fixed to follow the strand geometry during the entire lifting, especially for the first stage, where the angle is higher.



Figure 15. Single jack on compression ring and steel platforms.

For the second lifting of the lower radial cables, a double climbing jacks each axis have been located on the top of the tribune, connected to the spreader beam. As a consequence, a strand bundle connects the spreader beam to the anchor point positioned on the compression ring, close to the final point.



Figure 16. Pinning of the lower radial cable.

Every jacking system was connected with a control cable to the Lifting Control Centre, which was located in a control room, from where a full and good overview of site operations was guaranteed.

6.3. Cables lifting

Cables were lifted at 40 points strictly following the designer procedure. Some strand jacks had a nominal pulling capacity of 40-70 tonnes, while others had a nominal pulling capacity of 120 tonnes. Hydraulic pumps were used, to achieve an equal pulling speed on radial cables. The main target during lifting operation was to succeed in lifting the entire cable net from its supports minimizing the sliding. At each step of cables lifting, topographic survey of the structure was executed to compare actual positions and theoretical values supplied by the Designer, as geometrical and tensional status of the roof had to be continuously monitored.

6.4. Pinning of cables

The cable net was lifted until external sockets of upper or lower radial cables could be pinned on their final anchor plates. At that point, lifting operation was interrupted and the pinning of upper or lower radial cables was carried out. The cables were adjusted manually towards the anchoring plate. As fork socket was in position, the pin was put in and the tensioning operation was completed. After pinning of upper radial cables, the flying struts were connected to the relevant clamps. While the bottom connection of the struts has been performed during the second lifting, once the cable net geometry and the level were right. Both the upper and the lower pinning have been carried out following the design sequence, to minimize the possible overstress in the cables.

7. Conclusions and remarks.

The overall production process succeeded in delivering the supply within the required time schedule and quality target. Throughout the supply, the characteristics of each component were monitored and evaluated in order to guarantee the final output to be satisfactory. Site activities planning and logistics proved to be accurate and efficient, all site activities were performed successfully. Despite the complexity of such a large building site and the challenge of several concurring site activities, the greatest control of each step related to the installation and tensioning of cable system was upheld. It was also guaranteed the necessary accessibility and broad outlook on working areas, so that any possible difficulty could be promptly detected and solved. The following pictures show the roof after completion.



Teaching Membrane Architecture

Robert Roithmayr^{*}, Rainer Blum^a, Horst Dürr^b, Simon K. Chiu^c

^{*} Formfinder Software GmbH, Josef Gasser Strasse 5, A-9900 Lienz Austria, mail@formfinder.at

^a Danube University Krems, Department for Building and Environment, A-3500 Krems an der Donau

Abstract

In the year 2010 the postgraduate Master's Program for "Tensile Membrane Structures" was initiated in Vienna Austria. Since then positive improvements have been made to provide a pleasant and efficient learning environment.

In 2018 it was possible to enrich the existing curriculum with a collaborative researching and learning method. The basis of this method is a massive amount of content which was provided by experts in the field like Dr. Rainer Blum, Architect Horst Dürr or Prof. Vinzenz Sedlak. The content of these authors is pending for publication but already integrated in a semantic database. Although the amount of information is growing constantly it was possible to keep the access simple and effective. The process to structure and classify relevant information is to make "clever" annotations to each bit of information. So the annotation helps the researcher gain a better view on the available data. It should be possible to share learning's and valuable findings with colleagues and the scientific community. One major goal of this system is to connect experts and researchers with a constantly improved research environment which is pleasant to use an inspiring. As the method is about the visualization and communication of expertise we structured the work in several fields of interest. To mention one pivot point we focus on case studies of existing building projects. The collection of several hundred case studies was used to create a semantic database. Case studies are individually presented including a full digital 3D model that can be addressed online. Each 3D model was described throughout automated object recognition in respect to the geometric properties. Therefore a kind of 3D fingerprint is generated to compare eg. performance parameters. Throughout annotations by researchers the 3D models get more and more information. This process helps to recognize several aspects of a building project. The system is also open to bind other useful information to performance parameters. As we developed with the Danube University Krems a full climate membrane building envelope it is possible

DOI: 10.30448/ts2019.3245.55

Copyright © 2019 by Robert Roithmayr, Rainer Blum, Horst Dürr, Simon K. Chiu. Published by Maggioli SpA with License Creative Commons CC BY-NC-ND 4.0 with permission.

Peer-review under responsibility of the TensiNet Association

to share this information with other researchers when the performance power of one specific project is higher than others. It is a kind of alert system which keeps researchers updated when new knowledge or findings are made.

Based on the semantic database we intend to establish a future "ontology" of membrane architecture. The term ontology describes that it needs a common sense in the scientific world to define and describe parameters. The goal of this system is to provide access to relevant knowledge and to bind together a team of experts and researchers to make membrane architecture better.

Keywords: softening, lightweight structures, structural membrane, sustainability, performance, conceptual design, form finding, formfinder, optimization, manufacturing, climate building envelope, textile facade

Drawing Tools



Image: Drawing interface with integrated "object" recognition to access the online database.

Membrane.Online

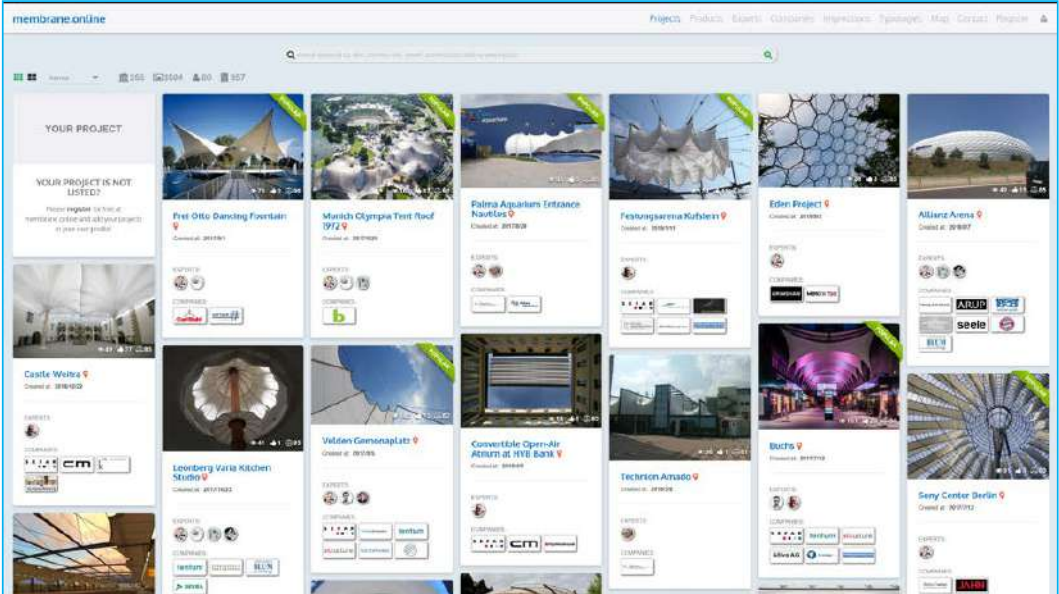


Image: Membrane.Online Platform

membrane.online/project/21

SENFTENBERG STAGE COVER

Project Description

A ventricular stage cover designed by F. Grotz with Bernd Birk, completed in 2011. A transparent membrane covers the outdoor area of Senftenberg stage in Germany from rain and sun mainly throughout the summer season. The main supporting structure is supported by six edge cables departing from the 23 meter high central A frame mast, ending in six forged columns, which are forming the outer edge of the stage stand. The structure is illuminated with colorful lighting. The structure is located in Germany by Senftenberg See in Schwanau and is designed to withstand sun, rain, snow and wind.

Architecture Requirement

Goal of design was to create a significant light-weight membrane large scale structure of around size 200x200m with main use for cultural purpose with 600 places sit. The intention is wanting to have a fast and cost effective permanent cover. The design of the project was a super fast idea reproduction process by architect Bernd Birk who is an expert since 40 years in the field of lightweight membrane structures. The engineering office of Grotz & Grotz has also designed many structures and could a lot of details that they already used over years.

Functional Aspect of the project is a multi-purpose stage cover, used mainly for cultural events (in its dimensions, columns, theater, school).

Materials used for the membrane: PVDF-coated Polyester Structure Steel, Membrane Edges Steel Cable, Membrane Connect, Steel plates.

Engineering Requirement

Structural Geometry of symmetrical structure is designed as a central A-frame mast, membrane support is supported by six edge cables, each leading from the A-frame to one of the six steel high perimeter columns. The entry area is covered by a thin point sail, which is in three points connected to the main membrane surface.

Membrane Connection to Primary Structure is solved using steel cables and steel plates. Steel cables are used as tensioned elements for the main anchoring, for the purpose of attaching the membrane to the main structure and as edge cables at the high points.

Movement in anchors is generally possible to stop that about every membrane structure are subjected to movement depending on the effect of the external load. Reaction force depends on design criteria, Position and Orientation. Position of corner plates depends on making members from the lifting cables according to EN 1993-1-3(23).

Installation/Production

Installation requirement is to build the structure in the easiest way, all though lightweight it has to be an easier structure which could install in diverse situations. The Senftenberg stage cover has large scale structure with big span, the whole building procedure took a business month.

Future Requirement

Since the structure was built, the cover frame has been replaced once due to its age related damage. Client intention in the future (weather protection), fully for sustainability and eye catching lighting.

	Good	Bad	Perfect
Strength	+		Very Good
Unbalanced		+	Harmonious
non-Repeatable		+	Repeatable
Unclear		+	Clear
Confusing		+	Coherent
Unintuitive		+	Intuitive
Temporary		+	Leaving
Provisional		+	Major
Foreign		+	Local
Imprecise		+	Functional
Asymmetrical		+	Symmetrical
Unstable		+	Stable
Crude		+	Elegant
Innovative		+	Imaginative

Total Score: 4900

Architecture	800
Engineering	1000
Installation	300
Future	100
Box	1.300

Image: ForFlexx Research Project with Forsstrom

Membrane.Online

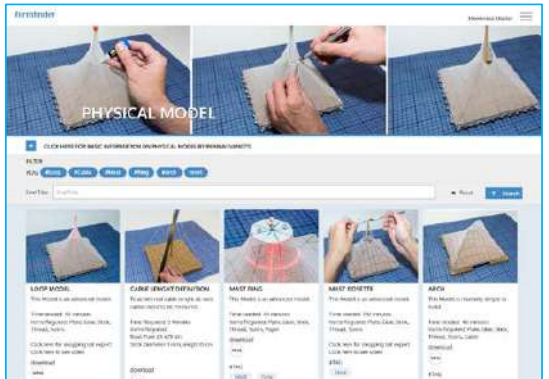
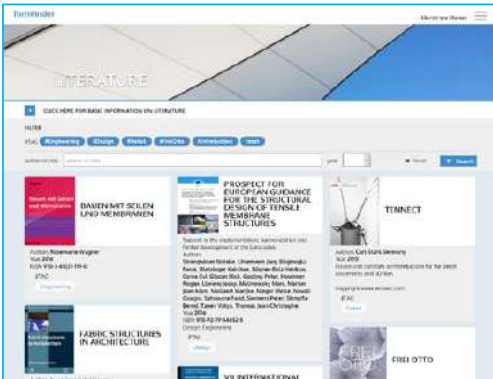
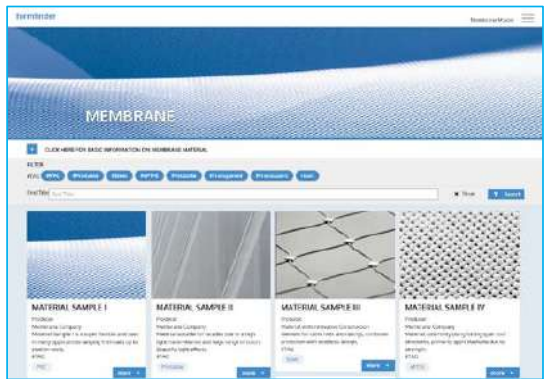
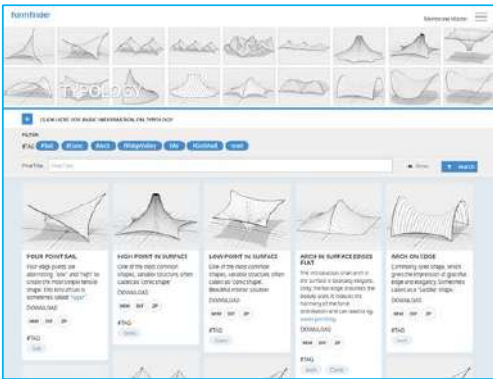
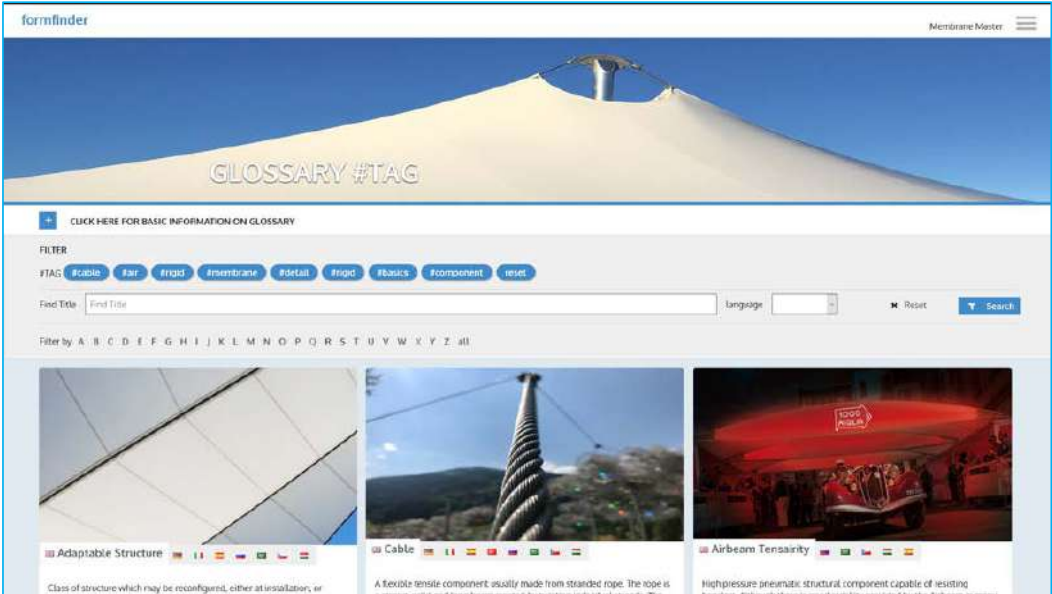


Image: Formfinder Database

Augmented Tools

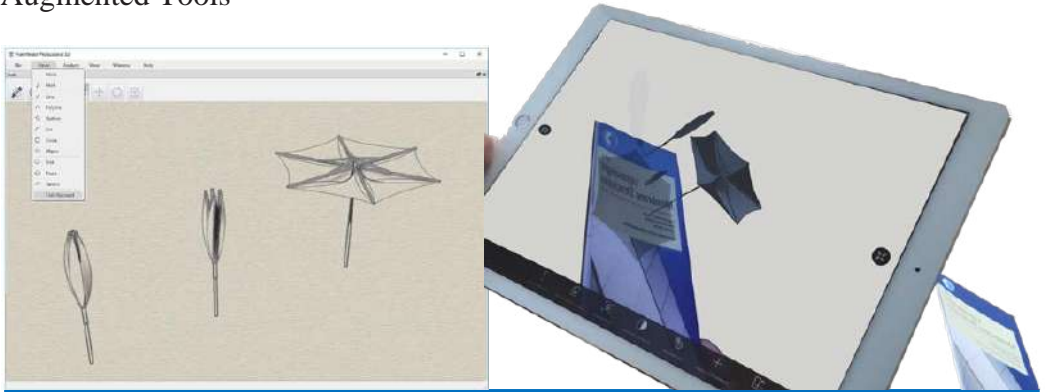


Image: Augmented Reality Tools

References

Blum, R., and Membrane Book to be published

Rosemarie Wagner, R. Bauen mit Membranen 2016

Mollaert, M., European Guidance for the Structural Design of Tensile Membrane Structures

IL Publications, Sedlak, V SDA Database UNSW

Deinhammer, A.V. Ganzheitliche Qualitätsermittlung von Arch. Entwürfen TU Wien,

Supported by Forschungs Förderungs Gesellschaft (FFG), EUREKA, EUROSTARS, Forststrom ForFlexx Research Project, Carl Stahl, SEFAR, Wiener Wirtschaft, Land Tirol Innovationsassistent, aws Austria Wirtschaftsservice, Augmented Art and Architecture Platform Wirtschaftsagentur Wien.

Proceedings of the TensiNet Symposium 2019

Softening the habitats / 3-5 June 2019, Politecnico di Milano, Milan, Italy

Alessandra Zanelli, Carol Monticelli, Marijke Mollaert, Bernd Stimpfle (Eds.)

An algorithm to draw simulations of dynamic lightweight structural systems with schemas

Mesrop ANDRIASYAN*

*Textiles Hub, ABC department, Politecnico di Milano
Via Francesco Cucchi 7, Milan 20133, Italy,
mesrop.andriasyan@polimi.it

Abstract

Architects, designers and structural engineers throughout their education and practice work mostly with visually controlled 3D modelling applications that require manually controlled actions to get the final desired model. On the contrary, we can see the development of visual programming that is now intertwined with traditional software applications and uses data flow to generate geometry. Professionals in the AEC industry witness the capabilities of visual programming mainly by means of its output and the live demonstration of scripts that automate the big amount of manual work. Notwithstanding the fact that visual programming is very appealing as an asset, acquiring the necessary skillset is often a matter of struggle. An example of this is the dynamic simulations of structural systems (tensile, bending active etc.). There are means to perform them but they usually require knowledge of visual programming and several frameworks. This paper attempts to introduce an open-source algorithm cutting short the intricate process of learning new non-conventional software and directly giving the opportunity to design dynamic structural systems as a schema and getting the instant simulations therein.

Keywords: simulation, conceptual design, lightweight structures, form finding

DOI: 10.30448/ts2019.3245.52

Copyright © 2019 by Mesrop Andriasyan. Published by Maggioli SpA with License Creative Commons CC BY-NC-ND 4.0 with permission.

Peer-review under responsibility of the TensiNet Association

1. Introduction

Form finding is a procedure to determine the shape of equilibrium of the desired prestress state and the boundary conditions (Stranghöne & Uhlemann, 2016). It is found that the behaviour of the investigated bending-active structures do not fall into clearly predictable categories, their load bearing is largely dependent on the variety of topologies and geometrical expressions that may be generated. Similarly to membrane structures, the geometry must be form-found, in this case simulating the elastic bending deformation (Lienhard, 2014). Ultra-lightweight structures often include form-active components that have large deformations and complex forms that are difficult to model with conventional 3D modelling processes. In recent years more and more attention is given to visual programming platforms such as Grasshopper for Rhino 3D to develop more complex geometrical solutions. A major step forward was the advent of Kangaroo solver that helps to create dynamic simulations of different structural behaviour. Notwithstanding the fact that kangaroo uses arbitrary values and does not provide accurate structural data it greatly helps in understanding how a certain type of structures might behave. Figure 1 Figure 1 represents the flow chart of the described Grasshopper-Kangaroo workflow.

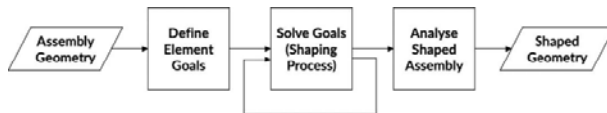


Figure 1 A design modelling pipeline using the Kangaroo2 library
(Deleuran, Pauly, Tamke, Tinning, & Thomsen, 2016)

2. Previous studies

The research presented in this paper is highly inspired by the results published in this paper (Deleuran, Pauly, Tamke, Tinning, & Thomsen, 2016). Several workflows are similar to what has been done. Some of the key differences are that the presented algorithm does not enforce the designer to operate on a given set of subdivision points to input geometry and is extended to incorporate other structural types including rigid elements (with fixed or hinged connections) and membranes. The purpose is the generalisation of the workflow to let the designer's work also on other structural types.

3. Methodology

The algorithm separates the processes of design and visual programming leaving the first part to the designer and automating the second one. What designers draw is considered a static schema of the structural system which is translated into the simulation model and drawn in a real-time manner in the same 3D environment. There are a few sets of rules that the designer has to follow. It is only required to draw the schema of the structural system with few indications of object types and some numerical values and these inputs will, later on, be carried by the algorithm. The algorithm classifies the input in to separate data streams, performs validation procedures and sequential steps of geometrical editing, creates the goal objects which represent the structural behaviour of the given objects, injects the designer's parameters and passes to the Kangaroo solver. The output is also classified into data streams for appropriate real-time visualisations and shape analysis value outputs.

The algorithm is thought to minimize the necessary input, so the designer can focus on the creation process.

3.1. Used tools

Rhino 3D CAD software is the environment where the designer creates the model(schema) of the structural system. The visual programming plug-in Grasshopper is the place where the algorithm is assembled. The fundamental basis of most computational systems used for the design of surface structures is some form of equilibrium modelling (Forster & Mollaert, 2004). This equilibrium is achieved by Kangaroo package which is an interactive physics/constraint solver. Elefront is a plug-in package for both Rhino and Grasshopper together that allows the automated transfer of properties between one another and enables auto-referencing of geometry (Wortmann & Tunçer, 2017). For representation, a package called Human is used, since it creates a pipe-like thick representation of linear elements without affecting heavily the performance. Some parts of the algorithm are developed by Python and C#.

4. The algorithm workflow

When the designer runs the algorithm, it generates a set of layers that will be used by the designer to identify component types. No input from other layers is taken into account and even the elements present in working layers are filtered to match their proper use. For example, the linear elements in the membrane layer will not be taken into account.

The indication of the element type triggers the creation of appropriate properties for that element that the designer can use to input values. These include strengths (non-structural arbitrary quantity for Kangaroo solver), length goal factors, snapping planes for rigid objects etc.). The updated elements with imported values are referenced again.

Later the referenced elements pass through chains of geometrical modelling. This includes:

4.1. Interdivision of linear elements

Kangaroo 2 engine works leveraging the position of the points that comprise elements in regards to the active collection of goals. If we want an element to interact with another one, they must have at least one common vertex. In this regard, all the points that lie within the given distance (a number close to 0) from a linear element will act as a division point. This includes the intersection events between all linear elements, anchors, loads and boundary defining points of membranes Figure 2.

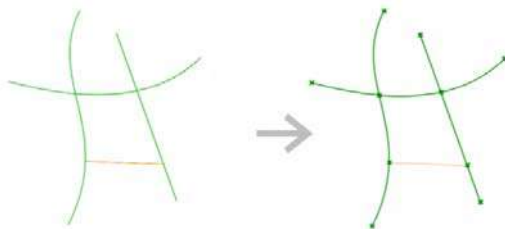


Figure 2 Intersection event of different elements

4.2. Graph connected components

In order to let the designer draw connected rigid components, it was necessary after solving the intersection events of curves to group them by connectivity. Here a sub-algorithm is used to perform flat hard clustering based on curve-curve intersection events (Manning, Raghavan, & Schutze, n.d.). It creates clusters of connected components in the graph. In Figure 3 the nodes represent curves. If the curves are intersecting (including end-to-end connections) then there's a connection line between those nodes. The algorithm clusters together all the connected curves and gives indexes of the curves from the initial unordered list as a data tree.

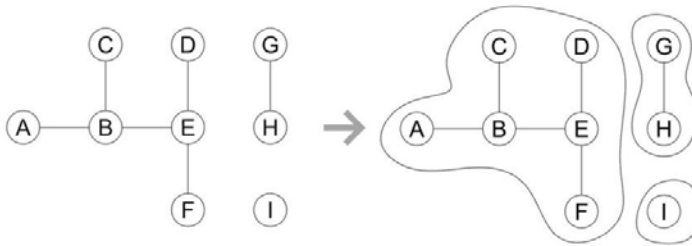


Figure 3 Graph connected components clustering

4.3. Segmentation

Since Kangaroo 2 works with points, in order to simulate the behaviour of curved elements (rods, cables etc.) it is required to divide the designed curve elements into several linear segments Figure 4. The precision is one of the designer's inputs. It is usually based on the scale, the complexity of the project and the computing power of the used processors.

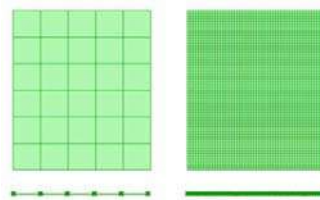


Figure 4 Low and high segmentation controlled by segment size

4.4. Membrane adjacencies

One of the challenges in simulating the membranes with Kangaroo is the solution of adjacencies of different membrane meshes with non-matching edge vertices. In these cases, since there is no vertex wise superposition, the meshes act as separate units. As an inherent part of this algorithm, a special part is written to address this issue. It finds the connected edges between membranes and creates local goals of collinearity for each point with the nearest two points on the other membrane. This ensures that the seams are correctly simulated. The designer has the choice to weld or not different membranes Figure 5.

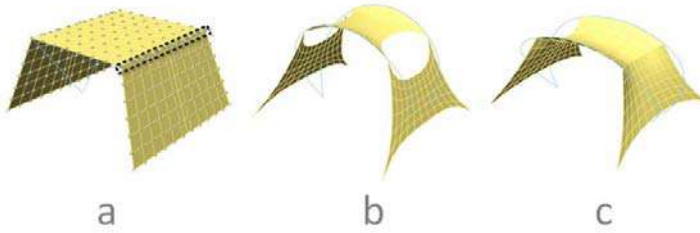


Figure 5 a) drawn model b) separate membranes c) joint membranes

After the presented geometrical operations, each group of geometry is composing a goal of Kangaroo 2 engine. The necessary parameters are passed through the designer's input. The structural and representation goals are combined into an ordered data tree and are inserted into Kangaroo 2 solver. Each time the designers changes the schema, the whole script is recomputed and the simulation model is updated to include the altered schema elements.

4.5. Geometry analysis

The algorithm post-processes and analyses the simulated geometry. Curve-like components that were segmented for simulation are re-interpolated into curves. These curves are used to generate curvature values and provide dynamic output as a curvature graph on top of the model with corresponding numerical values of curvature Figure 6. It also tracks the mean curvature values of the membranes. Although in this case there's a back and forth translation to a surface object which may reduce the accuracy Figure 7.

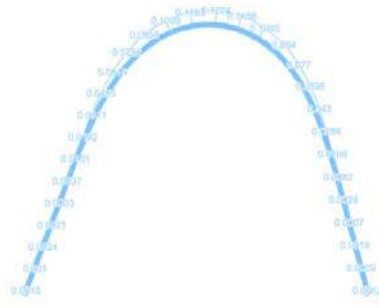


Figure 6 Rod curvature graph

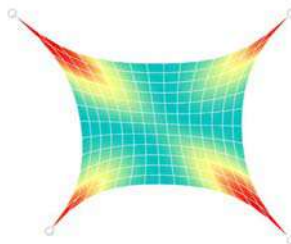


Figure 7 Colored representation of mesh curvatures

Figure 8 Depicts the flow chart of the entire algorithm.

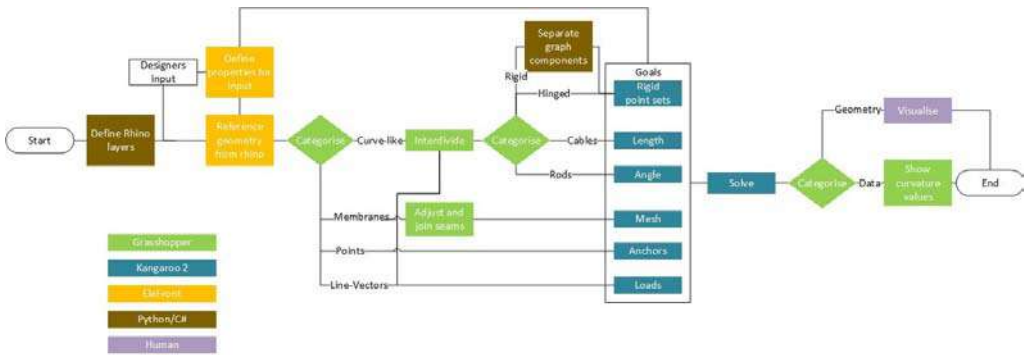


Figure 8 Macro process flow chart of the algorithm

5. Use cases

In order to validate the algorithm, many different design solutions were tested to see if it correctly carries out the simulations. The tool was distributed to the students of the lightweight structure design class and their feedbacks were taken into account to continuously expand the capabilities of the algorithm. This includes the possibility to snap rigid objects to planes, join membrane seams, insert individual strength values and many more. Some of the use cases are described below.

5.1. Gridshell

Conventionally it is possible to simulate a gridshell with the Kangaroo 2 engine. However, it takes some effort and knowledge of both Grasshopper and Kangaroo. With the help of the algorithm, the designer only has to draw a flat network of rods, lines that represent the initial and moved positions of the anchors and a load vector line to lift the structure. This workflow is more intuitive. Figure 9 shows the interaction between rods, moveable anchors and a load.

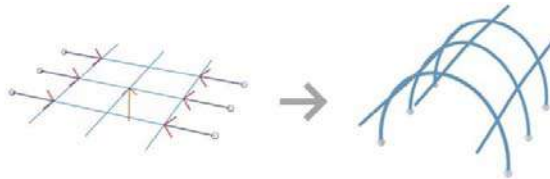


Figure 9 Gridshell schema and the ready model

5.2. Hybrid structure

Hybrid structures are very tedious to model since the joint elements of various structural types close require precise modelling and in case of simulation with Kangaroo, they also require a matching segmentation and anchor positioning. The algorithm streamlines all these processes and the schema that was drawn by the designer is effectively transformed into a correctly interconnected hybrid structure. Figure 10 shows the joint simulation of anchors, membranes and a rod.

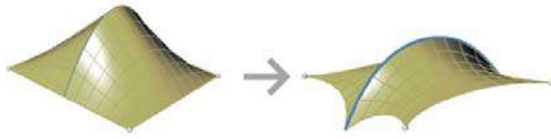


Figure 10 Hybrid structure

6. Conclusion

The aim of the research was to investigate the possibilities of streamlining the workflows of manual creation of Grasshopper+Kangaroo algorithms that are required to perform simulations of various structural systems. As a result, a robust algorithm was developed that works intuitively for the designer to translate the drawn schema into a simulation model and get instant geometry analysis data. However, the algorithm has not been tested yet on large scale projects and predictably will be heavily slowed due to a large number of operations for each component.

7. Further work

The given algorithm helps to easily simulate dynamic structural systems and to understand at a conceptual level how do things work. However, it does not provide accurate structural data. Later on, a FEM package may be incorporated to carry on with the structural calculations and validation. User feedback will be continuously collected to improve the performance and add requested functionality.

References

- Deleuran, A. H., Pauly, M., Tamke, M., Tinning, I. F., & Thomsen, M. R. (2016). Exploratory Topology Modelling of Form-active Hybrid Structures. *Procedia Engineering*, 155, 71–80.
- Forster, B., & Mollaert, M. (2004). *European design guide for tensile surface structures. Tensinet*.
- Lienhard, J. (2014). *Bending-Active Structures* (PhD thesis). Universität Stuttgart.
- Manning, C. D., Raghavan, P., & Schutze, H. Flat clustering. In *Introduction to Information Retrieval* (pp. 321–345). Cambridge University Press.
- Stranghöne, N., & Uhlemann, J. (2016). *Prospect for European Guidance for the Structural Design of Tensile Membrane Structures*. JRC.
- Wortmann, T., & Tunçer, B. (2017). Differentiating parametric design: Digital workflows in contemporary architecture and construction. *Design Studies*, 52, 173–197.

Proceedings of the TensiNet Symposium 2019

Softening the habitats / 3-5 June 2019, Politecnico di Milano, Milan, Italy

Alessandra Zanelli, Carol Monticelli, Marijke Mollaert, Bernd Stimpfle (Eds.)

Pre-stressed cable truss with stiffening girder and design clearance: development and analysis

Vitalii V. MIKHAILOV*, Andrei V. CHESNOKOV*, Ivan V. DOLMATOV*

*Lipetsk State Technical University

Moskovskaya street 30, Lipetsk 398600, Russian Federation

mmvv46@rambler.ru

Abstract

Cable truss systems possess a lot of advantages in comparison to ordinary concrete or steel structures. They are lightweight and able to span large free areas without intermediate supports. At the same time, they are very deformable due to, so-called, kinematic displacements. Horizontal thrust, brought about by cables, should be supported by bearer constructions of the building. It results in increase of material consumption and project expenditures in the whole. In order to equilibrate the thrust and to diminish the deflections of the structure stiffening girders with, so-called, design clearances are proposed to be used. The design clearance allows fine-tuning the cable truss in order to bear external loads in the most efficient way according to material properties of its principal elements. Computational technique for development and analysis of pre-stressed cable truss with stiffening girder and design clearance is given. The results, obtained by the proposed formulas are in a good agreement with data, provided by the specialized software of non-linear structural analysis Easy. The technique may be used either to perform preliminary design or to prepare initial data for software packages of non-linear analysis in order to simulate structural behavior under complex loading conditions. The present work contributes to further development of hybrid roofs.

Keywords: cable truss, stiffening girder, design clearance, hybrid roof, pre-stress

DOI: 10.30448/ts2019.3245.14

Copyright © 2019 by V.V. Mikhailov, A.V. Chesnoko, I.V. Dolmatov. Published by Maggioli SpA with License Creative Commons CC BY-NC-ND 4.0 with permission.

Peer-review under responsibility of the TensiNet Association

1. Introduction

Cable truss systems consist of flexible chords, linked together by struts. They are lightweight and able to span large free areas without intermediate supports. Cable trusses exhibit high load bearing capacity and can be mounted in a short period of time. On the other hand, they are very deformable, especially in the event of non-uniform external loading due to, so-called, kinematic displacements (Wagner, 2016). It significantly reduces the efficiency of high-strength cables. In addition, horizontal thrust, brought about by a cable truss, should be supported by bearer constructions of the building, resulting in substantial increase of project expenditures.

In order to equilibrate the thrust, stiffening girders are used. When connected with the struts, they also reduce deflections of the truss (figure 1). On the other hand, the girder, made of ordinary structural steel, takes the major portion of the load, because its stiffness is substantially higher, in comparison to high-strength cables, which remain underused.

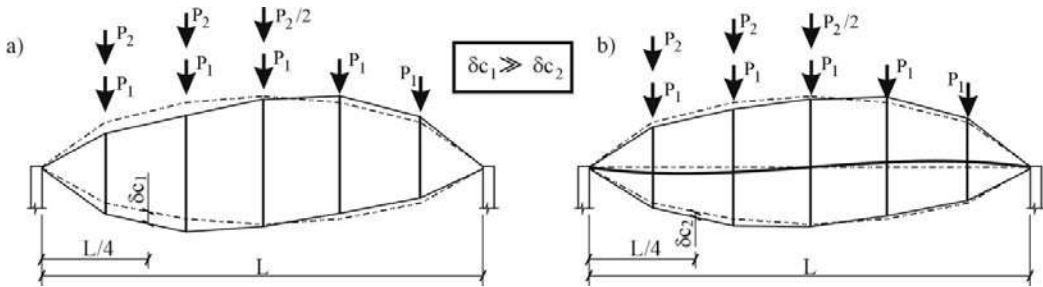


Figure 1: Ordinary cable truss (a) and cable truss with the stiffening girder (b).
(Chesnokov, Mikhailov and Sabitov, 2010)

In order to ensure maximum efficiency of high-strength cables, so-called, design clearances are proposed to be used (Chesnokov and Mikhailov, 2010). The clearance is a gap, which allows the struts of the truss to move freely a certain distance in the vertical direction. While deformations of the cable roof are smaller, than the designed value of the clearance, the stiffening girder does not support the struts. It is loaded only by longitudinal thrust until excessive deformations occur. The girder begins taking transverse load preventing the truss from kinematic displacements. Thus, the design clearance allows fine-tuning the truss in order to bear external loads in the most efficient way, according to material properties of its principal elements.

Computational technique for obtaining stiffness properties of cables and the girder, required pre-stress values and the size of the design clearance is given in the present paper. It is derived from the analytical model of a single cable. Numerical example is considered in order to exhibit and analyze structural behavior of the truss.

The technique may be used either to perform preliminary design of the truss, or to provide initial data for non-linear structural analysis software in order to simulate the influence of all possible load-cases.

The present work contributes to further development of hybrid roof structures, made of flexible and rigid members. It extends the scope of high-strength structural steel for roofs of buildings.

2. Description of the structure

The truss (Chesnokov and Mikhailov, 2010) consists of bearer 1 and restraining 2 chords, made of high-strength cables, spreaders 3, stiffening girder 4 and supports 5 (figure 2). The bearer chord is equipped with tensioning devices, e.g. hydraulic jacks, grip hoists or turnbuckles, which allow to implement preliminary stresses in the truss (Seidel, 2009). The

spreaders 3 and the girder 4 are linked together by means of the design clearance. Retainers (figure 3), rigidly fastened to the spreaders 3, are inserted into the gaps. The length of the gap depends on the required size of the design clearance.

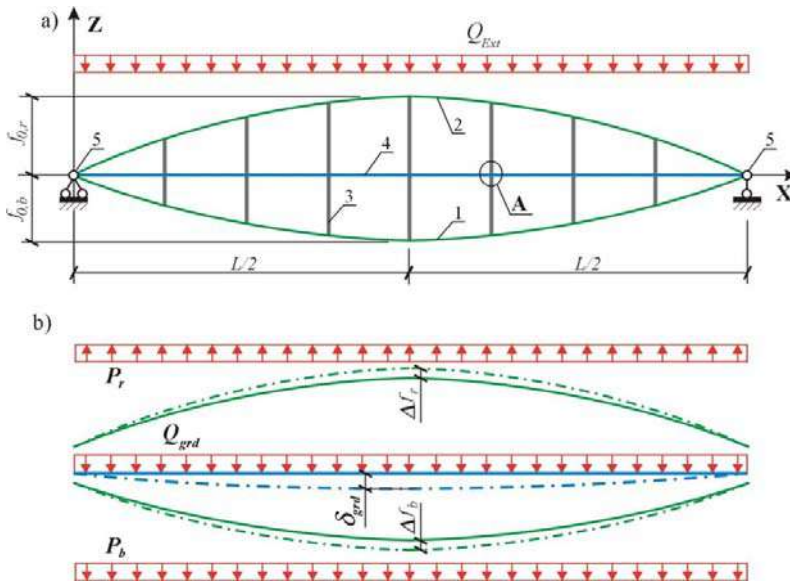


Figure 2: Cable truss with stiffening girder.

a – general view; b – loads on the cables and the girder.

1 – bearer chord; 2 – restraining chord; 3 – spreader; 4 – the stiffening girder; 5 – support; solid line shows initial configuration, while dash-dotted line is used for deformed configuration of the cables and the girder; joint A is illustrated in figure 3

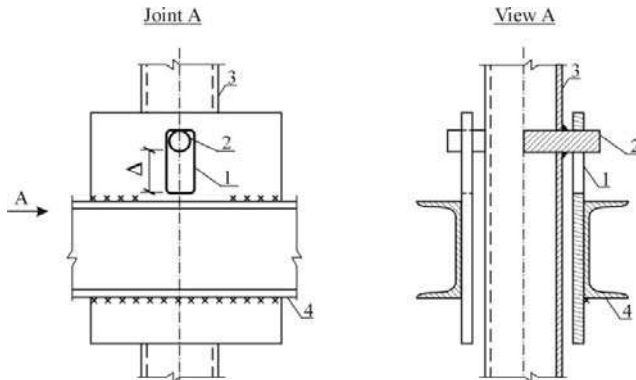


Figure 3: Joint A in figure 2.

1 – the design clearance; 2 – retainer; 3 – spreader of the cable truss; 4 – stiffening girder

3. Analysis of the structure

3.1. General considerations

The behavior of the structure is analyzed in two stages. On the first stage the girder is not connected to the spreaders, and the cable truss is deformed by means of the bearer chord tensioning. Comparatively negligible bending moments arise in the girder, subjected by its own weight in the transverse direction. When the required level of pre-stressing of the truss is achieved the girder is united with the spreaders as shown in figure 3.

On the second stage of structural behavior of the truss operational load Q_{Ld} is applied on the top chord. It results in deflection of the cable truss until the design clearance is exhausted. Then, the girder takes transverse load Q_{grd} . It confines the total deflection of the truss by a limiting value ω_{lim} , which should be provided from the serviceability and operability considerations.

General conditions (1) - (3) for the cable truss may be written:

$$\Delta f_r = -\Delta f_b \quad (1)$$

where Δf_v is the deflection of the corresponding chord of the cable truss, Δf_v -value is measured relative to the initial configuration of the cable (figure 2); hereinafter index “v” is either “r” or “b”, where the index “b” refers to the bearer chord, and the index “r” – to the restraining chord;

$$Q_{Ext} + P_r = P_b + Q_{grd} \quad (2)$$

$$0.01 \leq \Theta_v \leq 1.0 \quad (3)$$

where P_v is the load acting on the chord; Q_{Ext} is an external load, acting on the truss; $\Theta_v = \frac{N_v}{A_v \cdot R_{cab}}$ is a chord ratio; R_{cab} is the load-carrying capacity of steel cables, forming the chords; A_v is the cross section area of the chord; N_v is the force in the chord v:

$$N_v = EA_v \cdot \varepsilon_v \quad (4)$$

where EA_v is the stiffness of the chord; ε_v is the relative deformation of the chord, calculated according to (Chesnokov and Mikhaylov, 2017):

$$\varepsilon = \frac{\Psi_4 \cdot f^4 + \Psi_2 \cdot f^2 + L}{L_{c0}} - 1 \quad (5)$$

where f is the sag of the chord; L is the span of the truss; L_{c0} is the initial length of the chord; Ψ_2 and Ψ_4 are the coefficients, calculated according to (Chesnokov and Mikhaylov, 2017) for uniformly distributed load as follows: $\Psi_2 \approx 2.67/L$ and $\Psi_4 \approx -6.4/L^3$.

Initial length of the restraining chord coincides with its geometric (index “g”) length $L_{c0,r} = L_{g,r}$. Pre-stress of the cable truss is implemented by means of tensioning of the bearer chord ΔL_p . So, initial length of the bearer chord is the following: $L_{c0,b} = L_{g,b} - \Delta L_p$. Geometric lengths of the chords ($L_{g,b}$ and $L_{g,r}$) are calculated according to (Chesnokov and Mikhaylov, 2017) using their initial ordinates in the middle of the span ($f_{0,b}$ and $f_{0,r}$, figure 2) and the coefficients Ψ_2 and Ψ_4 .

Equilibrium equation for a chord v , subjected to uniformly distributed load, is derived from (Mikhaylov and Chesnokov, 2017):

$$EA_v = P_v / \lambda_v \quad (6)$$

where

$$\lambda_v = 8 \cdot \frac{f_v}{L^2} \cdot \varepsilon_v \quad (7)$$

where ε_v is calculated by means of substituting the corresponding value $f = f_v$ into (5).

3.2. The first stage of structural behavior: pre-stress of the cable truss

On the stage of the pre-stress of the cable truss the external load and the girder’s transverse load are omitted: $Q_{Ext,pr} = 0$ and $Q_{grd,pr} = 0$. In accordance to (2):

$$P_{b,pr} = P_{r,pr} \quad (8)$$

Hereinafter index “ pr ” refers to the stage of the pre-stress of the cable truss. The restraining chord ratio reaches its maximum value (3):

$$\Theta_{r,pr} = 1.0 \quad (9)$$

According to (9), the deflection of the restraining chord, brought about by pre-stress of the truss, may be calculated as follows:

$$\Delta f_{r,pr} = \sqrt{\frac{\sqrt{\Psi_2^2 + 4 \cdot \Psi_4 \cdot [(R_{cab} / E_{cab} + 1) \cdot L_{c0,r} - L]} - \Psi_2}{2 \cdot \Psi_4}} - f_{0,r} \quad (10)$$

where E_{cab} is the modulus of elasticity of steel cables.

Equilibrium equation (6) may be written for the stage of the pre-stress of the truss as follows:

$$EA_r = P_{r,pr} / \lambda_{r,pr} \quad (11)$$

$$EA_b = P_{r,pr} / \lambda_{b,pr} \quad (12)$$

Parameters $\lambda_{v,pr}$ are obtained from (7) by substituting the following ordinates for the corresponding chord:

$$f_r = f_{r,pr} = f_{0,r} + \Delta f_{r,pr} \quad (13)$$

$$f_b = f_{b,pr} = f_{0,b} - \Delta f_{r,pr} \quad (14)$$

3.3. The second stage of structural behavior: external load

The external load $Q_{Ext,Ld}$ is equal to, so-called, operational load or payload Q_{Ld} . Hereinafter index “ Ld ” refers to uniformly distributed load on the cable truss. The girder’s transverse load is expressed from (2):

$$Q_{grd} = Q_{Ld} + P_{r,Ld} - P_{b,Ld} \quad (15)$$

The bearer chord ratio reaches the maximum value (3) when the external load acts on the truss:

$$\Theta_{b,Ld} = 1 \quad (16)$$

The pre-tension ΔL_p of the bearer chord is derived from the condition (16):

$$\Delta L_p = L_{g,b} - L_{Ld,b} \cdot \frac{E_{cab}}{E_{cab} + R_{cab}} \quad (17)$$

where $L_{Ld,b}$ is the length of the bearer chord of the loaded truss, calculated according to (Chesnokov and Mikhaylov, 2017), using the ordinate in the middle of the span:

$$f_b = f_{b,Ld} = f_{0,b} - \Delta f_{r,Ld} \quad (18)$$

where the deflection $\Delta f_{r,Ld}$ of the truss under load is confined by the given limiting value ω_{lim} :

$$\Delta f_{r,Ld} = \Delta f_{r,pr} - \omega_{lim} \quad (19)$$

In order to fulfill the left-hand side condition of (3) the limiting value for the deflection of the truss ω_{lim} should be confined as follows:

$$\omega_{lim} \leq \Delta f_{r,pr} + \sqrt{\frac{\Psi_2^2 + 4 \cdot \Psi_4 \cdot \left(\frac{E_{cab} + R_{cab}}{E_{cab} \cdot (1 + \varepsilon_{lim})} \cdot L_{pr,b} - L \right) - \Psi_2}{2 \cdot \Psi_4}} - f_{0,b} \quad (20)$$

and

$$\omega_{lim} \leq \Delta f_{r,pr} - \sqrt{\frac{\Psi_2^2 + 4 \cdot \Psi_4 \cdot \left((1 + \varepsilon_{lim}) \cdot L_{c0,r} - L \right) - \Psi_2}{2 \cdot \Psi_4}} + f_{0,r} \quad (21)$$

where $\varepsilon_{lim} = 0.01 \cdot R_{cab} / E_{cab}$ is the minimum allowable relative tension of a cable chord; $L_{pr,b}$ is the length of the bearer chord of the pre-stressed truss, calculated according to (Chesnokov and Mikhaylov, 2017), using the ordinate in the middle of the span (14).

Equilibrium equation (6) is written for bearer and restraining chords of the loaded truss as follows:

$$EA_r = P_{r,Ld} / \lambda_{r,Ld} \quad (22)$$

$$EA_b = P_{b,Ld} / \lambda_{b,Ld} \quad (23)$$

The parameters $\lambda_{v,Ld}$ are obtained from (7) by substituting the ordinate for the bearer chord (18) and the corresponding ordinate for the restraining chord:

$$f_r = f_{r,Ld} = f_{0,r} + \Delta f_{r,Ld} \quad (24)$$

By means of equating (11) and (22), and also (12) and (23) the expressions for loads, acting on the chords of the truss in the operational stage, are derived as follows:

$$P_{r,Ld} = \frac{\lambda_{r,Ld}}{\lambda_{r,pr}} \cdot P_{r,pr} \quad (25)$$

$$P_{b,Ld} = \frac{\lambda_{b,Ld}}{\lambda_{b,pr}} \cdot P_{r,pr} \quad (26)$$

The load Q_{grd} , obtained from (15), should be positive, otherwise the girder doesn't take transverse load from the cable truss ($Q_{grd} = 0$), and the construction splits into two sub-structures (the truss and the girder), linked together by longitudinal thrust only. From the condition $Q_{grd} > 0$ and expressions (15), (25), (26) the upper bound for the load $P_{r,pr}$ is obtained:

$$P_{r,pr} < P_{r,lim} = \frac{Q_{Ld}}{\frac{\lambda_{b,Ld}}{\lambda_{b,pr}} - \frac{\lambda_{r,Ld}}{\lambda_{r,pr}}} \quad (27)$$

The deflection of the girder, influenced by transverse and longitudinal loads is calculated according to (Galambos and Surovek, 2008):

$$\delta_{grd} = \frac{\delta_Q}{1 - N_{grd} / N_{el}} \quad (28)$$

under the condition:

$$N_{grd} < N_{el} \quad (29)$$

where δ_Q is the deflection, brought about by the transverse load only, obtained from the differential equation of a beam (Fertis, 2006); N_{el} is the Euler load and N_{grd} is the axial force in the girder, equal to the thrust of steel cables:

$$\delta_Q = \frac{5}{384} \cdot Q_{grd} \cdot \frac{L^4}{E_{grd} \cdot I_{grd}} \quad (30)$$

$$N_{el} = \pi^2 \cdot E_{grd} \cdot I_{grd} / L^2 \quad (31)$$

$$N_{grd} \approx N_{r,Ld} + N_{b,Ld} \quad (32)$$

where $N_{v,Ld}$ is the force in the chord v of the truss, calculated from (4), using the corresponding ordinate $f_{v,Ld}$ (18), (24); E_{grd} is the modulus of elasticity of girder's material; I_{grd} is the moment of inertia of the girder's cross section.

Required value of the design clearance in the middle of the span is calculated from (33) (Chesnokov, Mikhailov and Sabitov, 2010). The clearance Δ should be positive.

$$\Delta = \omega_{lim} - \delta_{grd} \quad (33)$$

The strength properties of the girder should be verified by the following criterion:

$$\sigma_{grd} < R_{grd} \quad (34)$$

where R_{grd} is the strength of the material of the girder and σ_{grd} is the stress in the girder:

$$\sigma_{grd} = \frac{N_{grd}}{A_{grd}} + \frac{M_{grd}}{W_{grd}} \quad (35)$$

where A_{grd} and W_{grd} are the cross section area and the elastic section modulus of the girder; M_{grd} is bending moment in the girder:

$$M_{grd} = \frac{Q_{grd} \cdot L^2}{8} + N_{grd} \cdot \delta_{grd} \quad (36)$$

4. Case study

Cable truss, which consists of two flexible chords, linked together by vertical spreaders and horizontal girder, is considered (figure 2). The span of the truss is $L=12$ m. Initial ordinates of the chords are the following: $f_{0,b}=1.5$ m and $f_{0,r}=1.0$ m. The chords consist of steel cables. The strength of the cables is $R_{cab}=700$ MPa and the modulus of elasticity is $E_{cab}=1.3 \cdot 10^5$ MPa (PFEIFER, 2017). The spreaders and the girder are made of structural steel with the following properties: $R_{grd}=210$ MPa and $E_{grd}=2.1 \cdot 10^5$ MPa.

The deflection of the truss under load should be confined by the following values (20), (21): $\omega_{lim} \leq \min(0.112, 0.141)$ m. It is adopted $\omega_{lim} = L/120 = 0.1$ m, while the external load is taken equal to $Q_{Ld} = 25.0$ kN/m.

The bearer chord pre-tension is $\Delta L_p = 0.0932$ m (17), while cambering of the truss on the stage of pre-stress (10) is $\Delta f_{r,pr} = 0.143$ m. The load between the chords of the truss on the stage of the pre-stress is taken $P_{r,pr} = 1.1$ kN/m. It obeys the condition (27), where $P_{r,lim} = 2.96$ kN/m.

Cable cross section areas, calculated from (11) and (12), are the following: the bearer chord $A_b = 1.69 \text{ cm}^2$ and the restraining chord $A_r = 0.25 \text{ cm}^2$.

The forces in the chords are calculated for the stage of the pre-stress $N_{b,pr} = 14.6 \text{ kN}$, $N_{r,pr} = 17.3 \text{ kN}$, and for the stage of the external load $N_{b,Ld} = 118.1 \text{ kN}$, $N_{r,Ld} = 5.0 \text{ kN}$. Corresponding Θ -ratios obey the condition (3): 0.12, 0.99, 0.99 and 0.29.

Transverse (15) and longitudinal (32) loads on the girder are the following: $Q_{grd} = 15.7 \text{ kN/m}$ and $N_{grd} = 123.1 \text{ kN}$. The girder is made of two channel bars (figure 3). It has the following parameters: $A_{grd} = 123.0 \text{ cm}^2$, $I_{grd} = 30440 \text{ cm}^4$ and $W_{grd} = 1493 \text{ cm}^3$. The deflection of the girder (28) is $\delta_{grd} = 0.068 \text{ m}$ and the design clearance (33) is $\Delta = 0.032 \text{ m}$.

Bending moment in the girder (36) is the following $M_{grd} = 291 \text{ kN} \cdot \text{m}$, while the stress in the girder is $\sigma_{grd} = 205 \text{ MPa}$. It obeys the condition (34).

The cable truss was analyzed by the module of non-linear structural simulation BEAM of the specialized software package Easy. Results, provided by Easy, are very close to the ones, calculated by the proposed formulas: $\Delta f_{r,pr} = 0.144 \text{ m}$, $N_{b,pr} = 14.3 \text{ kN}$, $N_{r,pr} = 16.9 \text{ kN}$, $N_{b,Ld} = 120.9 \text{ kN}$, $N_{r,Ld} = 4.02 \text{ kN}$, $\delta_{grd} = 0.066 \text{ m}$, $N_{grd} = 121.0 \text{ kN}$, $M_{grd} = 291 \text{ kN} \cdot \text{m}$ and the total deflection of the truss under load is $\omega = 0.098 \text{ m}$.

The effect of the stiffening girder is illustrated in figure 4, where $\Delta f_{1/2}$ and $\Delta f_{1/4}$ are the deflections of the structure in the middle and in the quarter of the span, respectively, K_{Ld} is the factor of load nonuniformity and $\zeta_{1/2}$, $\zeta_{1/4}$ are relative deflections $\zeta^i = \Delta f^i / \Delta f^0$, where Δf^0 is the deflection under uniform load ($K_{Ld} = 0$).

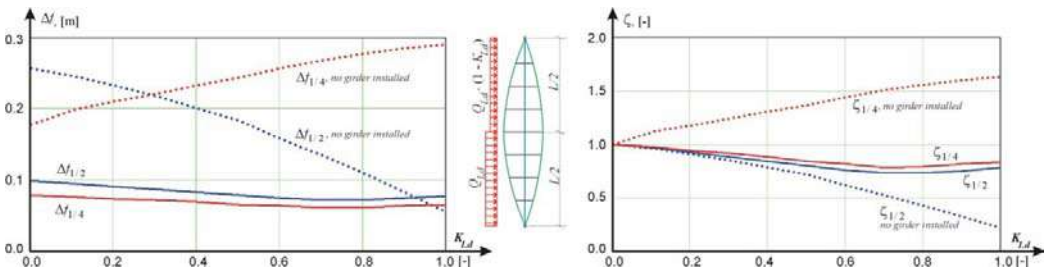


Figure 4: Deflections of the cable truss, obtained by the specialized software Easy (remark: both supports of the truss are fixed when the girder is not installed)

The figure 4 shows, that if the girder is installed, the deflections of the truss are substantially smaller, than that of an ordinary cable truss without the girder. On the other hand, non-linearity of curves, illustrated in figure 4, points to the necessity of asymmetrical load inclusion into the computational technique proposed.

5. Conclusion

Pre-stressed cable truss with stiffening girder and design clearance is considered. Its primary advantages in comparison to ordinary cable structures are smaller deformations under load, self-equilibration of the thrust and efficiency of material consumption.

Computational technique for structural analysis of the truss is given. It ensures to achieve preset deflection of the truss using material properties to the full extent. The technique includes simulation of the stage of the pre-stress and operational stage of the truss. It allows fine-tuning of the main parameters in order to increase the truss competitiveness and to highlight its advantages.

The technique contributes to structural optimization of the truss with stiffening girder. It may be used to perform preliminary design of the truss and to provide initial data for software packages of non-linear analysis in order to simulate complex behavior under different loading conditions.

References

Chesnokov A.V. and Mikhailov V.V. (2010), *Two-chord pre-stressed cable system*. Patent for invention RU2439256, (in Russian). Retrieved January 8, 2019, from <http://new.fips.ru/en/>.

Chesnokov A.V., Mikhailov V.V. and Sabitov L.S. (2010), Two-chord pre-stressed cable system with design clearance, (in Russian). In: *Proceedings of Kazan state University of architecture and construction*, vol. 14 (pp. 137-141).

Chesnokov A.V. and Mikhaylov V.V. (2017), Analysis of cable structures by means of trigonometric series. In: *Proceedings of the VIII international conference on textile composites and inflatable structures*. Munich, 9-11 October 2017, (pp. 455 – 466).

Fertis D.G. (2006). *Nonlinear structural engineering with unique theories and methods to solve effectively complex nonlinear problems*. Berlin Heidelberg: Springer.

Galambos T.V. and Surovek A.E. (2008), *Structural stability of steel: concepts and applications for structural engineers*. New Jersey: John Wiley and Sons.

Mikhaylov V.V. and Chesnokov A.V. (2017), Cable roof structure with flexible fabric covering. In: *Proceedings of the VIII international conference on textile composites and inflatable structures*. Munich, 9-11 October 2017, (pp. 436 – 447).

PFEIFER Tension Members (2017): PFEIFER seil- und hebetchnik GMBH. Retrieved January 8, 2019, from <https://www.pfeifer.info/en/pfeifer-group/business-units/cable-structures/>.

Seidel M. (2009). *Tensile Surface Structures: A Practical Guide to Cable and Membrane Construction*: Ernst and Sohn.

Wagner R. (2016), *Bauen mit seilen und membranen*: Beuth Verlag GmbH.

Numerical technique for estimation of cable roof structural parameters

Andrei V. CHESNOKOV*, Vitalii V. MIKHAILOV*

*Lipetsk State Technical University

Moskovskaya street 30, Lipetsk 398600, Russian Federation

andreychess742@gmail.com

Abstract

Cable roof with reduced overall height is proposed for long-span buildings. It is more attractive from an economic point of view due to diminishing of unused internal space. Bearer cables of the roof are subdivided into primary and ordinary. Primary cables are arranged far from each other. They are directly connected to columns of the building. Ordinary cables are supported by primary ones. The distance between them is comparatively small. Specialized software systems for nonlinear analysis require the basic parameters of the construction to be determined before structural simulation. Numerical technique for estimation of pre-stress values and stiffness properties of elements of the construction is proposed in the present paper. The coordinate descent method is used to perform structural optimization. This approach allows to gain precise analytical results proved by the comparison with data, provided by the non-linear software package EASY. The present study contributes to the improvement and further development of cable and membrane roofs of long-span buildings, particularly in the field of industrial construction. It facilitates structural simulation by means of providing appropriate initial data for computer systems of non-linear static analysis.

Keywords: cable roof, reduced overall height, coordinate descent method, numerical technique

DOI: 10.30448/ts2019.3245.12

Copyright © 2019 by A.V. Chesnokov, V.V. Mikhailov. Published by Maggioli SpA with License Creative Commons CC BY-NC-ND 4.0 with permission.

Peer-review under responsibility of the TensiNet Association

1. Introduction

Cable roofs are widely used for large-span building and constructions. They allow to maximize the distance between internal supports, resulting in huge unobstructed space inside the building.

On the other hand, cable structures are very deformable, especially in the event of non-uniformly distributed external loads. Rigid roof elements, supported by cables, may get damages due to excessive deformations. Thus, flexible polymer membrane, made of polyester or glass fibers, covered with PVC, teflon or silicon (Houtman, 2003), is more attractive to be applied with cable structures. In addition, polymer membrane is lightweight and translucent. It allows to diminish installation and operational costs of the building.

Cable and flexible membrane structures are primarily confined by the field of civil engineering. They are successfully used in stadiums (Grunwald and Seethaler, 2011; Goppert, 2013), railway stations, fair sites, etc. Industrial buildings also need to be covered by such unsurpassed structures. They, however, require to reduce unused internal spaces and to diminish operational expenditures. So, approximately flat roof is much more appropriate for industrial construction in contrast to public buildings, which primarily need impressive architectural appearance.

Cable roof structure, considered in the present paper, consists of bearer and backstay cables, spreaders and ties (Chesnokov and Mikhaylov, 2016; Mikhaylov and Chesnokov, 2017) (figures 1 and 2).

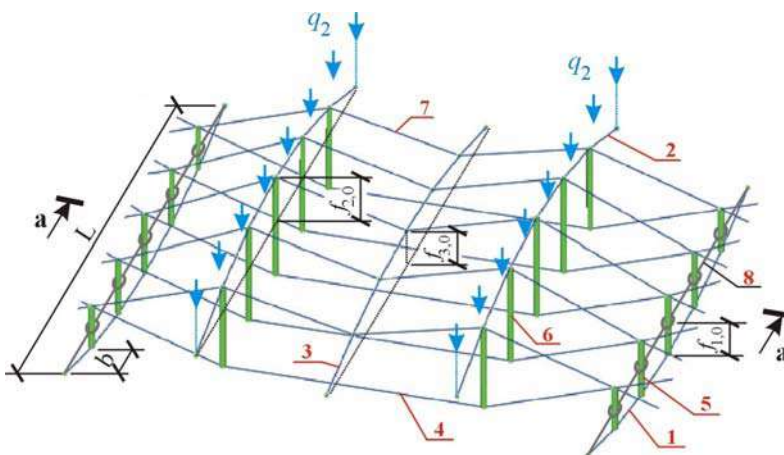


Figure 1: Axonometric view of a section of the roof (Mikhaylov and Chesnokov, 2017).

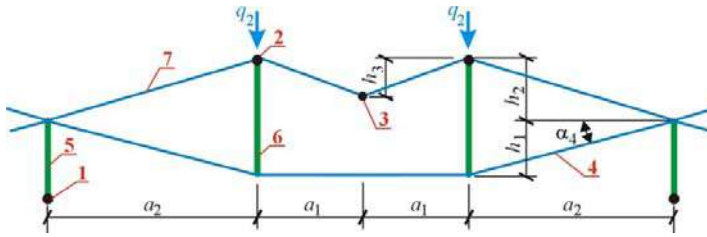


Figure 2: View of the roof along the line a-a in figure 1 (Mikhaylov and Chesnokov, 2017).

Bearer cables are arranged in mutually perpendicular directions. Longitudinal bearer cables 1 are attached fixedly to columns. They are situated far from each other, allowing large free areas to be ensured inside the building. Transverse bearer cables 4 are connected to struts 5, which are, in turn, supported by the cables 1 and fixed by means of ties 8 in the longitudinal direction. Backstay cables 2, supported by struts 6, are convex upwards. Together with ties 3 and 7, they form the top chord of the roof.

The overall height of the roof is smaller in comparison to ordinary cable-membrane structures of the same free span. Membrane curvature, however, is ensured to be in the appropriate range. It allows the membrane to sustain external loads without wrinkles and slackened areas (Forster, 2003).

2. Analysis of the structure

2.1. General considerations

The following parameters of the cable roof structure are taken into account:

- the modulus of elasticity and the strength of the cables and the struts E_{cab} , R_{cab} and E_{str} , R_{str} respectively;
- cross section areas of the cables A_j ($j=1, 2, 3, 4$), diameters of the struts D_5 , D_6 and their thickness-to-diameter ratios $k_{t,5}$, $k_{t,6}$;
- cable tensioning $\Delta L_{p,1}$, $\Delta L_{p,2}$ and $\Delta L_{p,3}$;
- the span of the primary bearer cables L , the distances between the cables a_1 , a_2 and b , initial sags of the cables $f_{i,0}$ and height dimensions h_i ($i=1, 2, 3$).

Cable tensioning $\Delta L_{p,i}$ is implemented by means of an appropriate pre-stressing equipment (Seidel, 2009). It is equal to the difference between, so called, geometrical length of the cable $L_{C_{i,g}}$ and the length of the cable $L_{C_{i,0}}$ in the unstressed state: $\Delta L_{p,i} = L_{C_{i,g}} - L_{C_{i,0}}$. The geometrical length of the cable $L_{C_{i,g}}$ is determined by its shape in the initial state, excluding any deflection of the structure: $\Delta f = 0$.

Numbering of the structural elements is in the figures 1 and 2. Although the pre-stress may be performed by means of the bottom cables 1 only (Mikhaylov and Chesnokov, 2017), tensioning $\Delta L_{p,3}$ of the tie 3 results in more lightweight structure, due to the possibility of force adjustment, which prevents the top chord from slackening. On the other hand, embedding tensioning equipment into the cables 2 is not justified, so the value $\Delta L_{p,2}$ is assumed equal to zero.

Cable cross section areas $\vec{X} = (A_1, A_2, A_3, A_4)^T$ and cable tensioning $\vec{\Delta L}_p = (\Delta L_{p,1}, \Delta L_{p,3})^T$ are taken as independent parameters, which are to be determined by means of a structural optimization technique. Struts diameters D_5 and D_6 are also not preliminary known, but they can be derived from the buckling prevention condition of compressed structural members.

2.2. Flexible steel cable elements

Operability condition of the steel cables, constituting the roof structure, is taken into account as follows:

$$\Theta_{\lim,1} \leq \Theta_j \leq \Theta_{\lim,2} \quad (1)$$

where Θ_j is the ratio (2), while $\Theta_{\lim,1}$ and $\Theta_{\lim,2}$ are the limits of allowable range for the ratio:

$$\Theta_j = \frac{N_j}{A_j \cdot R_{cab}} \quad (2)$$

where N_j is the force in the cable j .

The left-hand side of the condition (1) ensures, that the cable j is in tension and does not slack under load, while the right-hand side prevents the cable from overstress.

The forces N_j are calculated according to (Mikhaylov and Chesnokov, 2017), considering $A_7 = A_8 = A_3$ and $q_1 = q_3 = 0$. They are obtained for the stage of pre-stress of the structure $N_{j,pr}$ and for, so-called, operational stage $N_{j,Ld}$, separately.

It is assumed, that the external load q_2 acts along the cable 2 from top to bottom, as shown in the figures 1 and 2. For the operational stage the load is brought about by the structural own weight, snow and suspended equipment: $q_2 = q$. On the stage of the pre-stress the external load is omitted due to its insignificance: $q_2 = 0$.

The force N_4 in the ordinary bearer cable 4 is obtained from the expression, given in (Mikhaylov and Chesnokov, 2017), using uniformly distributed loads p_i , acting on the cables ($i = 1, 2, 3$). The forces in the primary bearer cable N_1 , the backstay cable N_2 and the longitudinal tie N_3 are obtained from the Hook's law:

$$N_i = E_{cab} \cdot A_i \cdot \varepsilon_i \quad (3)$$

where ε_i is the relative deformation of the cable, derived from (Chesnokov and Mikhaylov, 2017):

$$\varepsilon_i = \varepsilon_i(\Delta f_i, \Delta L_{p,i}) = \frac{\Psi_4 \cdot f_i^4 + \Psi_2 \cdot f_i^2 + L}{Lc_{i,0}} - 1 \quad (4)$$

where Ψ_2 and Ψ_4 are the coefficients, calculated for the middle of the span of the cable: $\Psi_2 \approx 2.67/L$ and $\Psi_4 \approx -6.4/L^3$; $f_i = f_{i,0} + \Delta f_i$ is the cable sag; Δf_i is the deflection of the cable in the middle of the span, obtained from (Mikhaylov and Chesnokov, 2017); $Lc_{i,0}$ is the length of the cable in the unstressed state: $Lc_{i,0} = Lc_{i,g} - \Delta L_{p,i}$.

It is proposed to confine deformations of the roof under load by the following condition:

$$\Delta f_{2,pr} - \Delta f_{2,Ld} \leq \omega_{lim} \quad (5)$$

where ω_{lim} is the limit value of the structural deflection; $\Delta f_{2,pr}$ and $\Delta f_{2,Ld}$ are the deflections of the cable 2 brought about by pre-stressing of the roof and by the external load, respectively.

2.3. Compressed structural members

Diameters of the struts D_5 and D_6 are obtained from the conditions of compressive buckling (6) and flexibility limitation (7):

$$N_v \leq N_E \tag{6}$$

$$\lambda_v \leq \lambda_{lim} \tag{7}$$

where the index v is either 5 or 6, depending on the strut considered, N_E is the Euler load (Galambos and Surovek, 2008), λ_v is the slenderness of the strut, $\lambda_{lim} = 120$ is the limit slenderness, N_v is the force in the corresponding strut:

$$N_5 = p_1 \cdot b \tag{8}$$

$$N_6 = N_4 \cdot \sin(\alpha_4) \tag{9}$$

Conditions (6) and (7) allow to derive the strut diameter:

$$D_v \geq \sqrt{L_v} \cdot \sqrt[4]{\frac{8 \cdot N_v}{\pi^3 \cdot E_{str} \cdot k_{t,v} \cdot (1 - 3 \cdot k_{t,v} + 4 \cdot k_{t,v}^2 - 2 \cdot k_{t,v}^3)}} \tag{10}$$

$$D_v \geq \frac{2 \cdot L_v}{\lambda_{lim} \cdot \sqrt{k_{t,v}^2 - k_{t,v} + 0.5}} \tag{11}$$

where L_v is the length of the strut.

3. Structural optimization of the cable roof

Parameters of the cable roof form a multidimensional space, which consists of two sub-spaces. The first one contains permissible parameter combinations Ξ_p , while the second, or invalid sub-space Ξ_i describes the roof structure, which is either not operable or doesn't comply with the conditions imposed.

Permissible parameter groups Ξ_p are not equivalent. Additional requirements, such as material consumption, expenditures, labor input etc., distinguish them from each other, resulting in the best combination, which should be determined. So, the problem of structural optimization arises.

Complex behavior of the cable roof, reflected in slackening of compressed members and instability of the structure in the whole, substantially complicates gradient optimization techniques and diminishes their effectiveness. Among derivative-free, or zero-order, approaches the coordinate descent method allows to gain reliable and numerically stable

results for the problem considered. It is accepted as a basis for the technique, elaborated in the present work for estimation of cable roof structural parameters (figure 3).

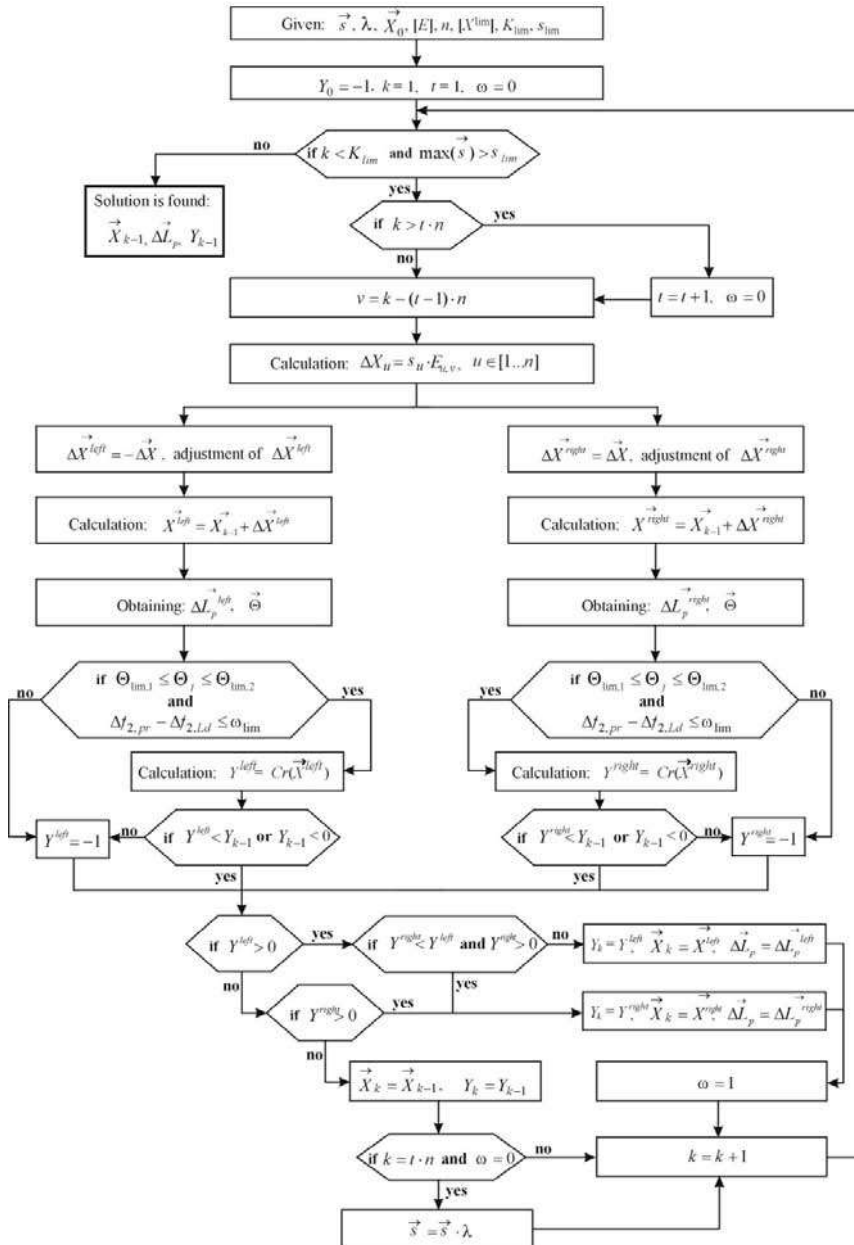


Figure 3: The technique for structural optimization of the cable roof

Parameters of the technique are the following: k is the number of current iteration and K_{lim} is the maximum number of iterations specified; \vec{X}_0 is the vector of initially given values of parameters to be optimized, while \vec{X}_k contains current parameter values; $n=4$ is the number of components of the vector \vec{X} ; $[X^{lim}]$ is the matrix, which consists of n rows and 2 columns, it contains allowable ranges for parameters to be optimized; $[E]$ is the identity matrix of n rows and columns; \vec{s} is a vector of n components, which contains possible variations of the parameters; s_{lim} is a limiting value for a component of \vec{s} ; λ is a reduction factor for \vec{s} .

The criterion function is taken as follows:

$$Cr(\vec{X}) = \Sigma M_{cab} + \Sigma M_{str} \cdot \rho_{str} \tag{12}$$

where ΣM_{cab} and ΣM_{str} are total masses of the cables and the struts belonging to the structure considered, ρ_{str} is the ratio of the average price of struts to the average price of cables.

According to the optimization technique only one component of the vector \vec{X} is modified on each iteration step by means of decrementing X^{left} and incrementing X^{right} the current value. Variations of the vector \vec{X} are adjusted in order that the resultant vector components would be in the appropriate range, specified by the matrix $[X^{lim}]$.

Cable tensioning $\vec{\Delta L}_p = (\Delta L_{p,1}, \Delta L_{p,3})^T$, corresponding to the current vector \vec{X} , is calculated in the step-by-step way (figure 4).

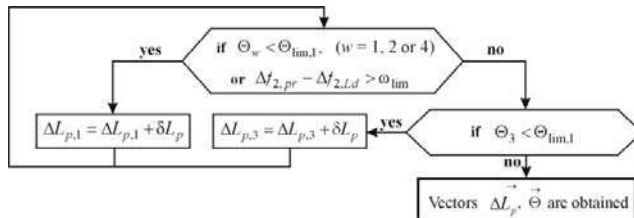


Figure 4: Obtaining cable tensioning $\vec{\Delta L}_p$

The initial components of the vector $\vec{\Delta L}_p$ are assumed equal to the increment $\Delta L_{p,1} = \Delta L_{p,3} = \delta L_p$. If the condition (5) or the left-hand side of the condition (1) are not

satisfied, the increment $\delta \mathcal{L}_p$ is added to the corresponding component. However, if the right-hand side of the condition (1) becomes not valid for any cable j , the step-by-step process is terminated, and current \vec{X} -vector is considered unacceptable.

The criterion function value (12) is saved into variable Y (figure 3). Negative Y -value means either that current parameters are not permissible, or that the criterion function value is worse, than the previously obtained result.

4. Case study

4.1. Initial data

The initial data taken into account are the following: the moduli of elasticity $E_{cab} = 130$ and $E_{str} = 206$ GPa; the strength properties $R_{cab} = 700$ and $R_{str} = 240$ MPa; dimensions of the roof $L = 12.0$ m, $a_1 = 3.0$ m, $a_2 = 3.0$ m, $b = 2$ m, $h_1 = 1.0$ m, $h_2 = 1.5$ m, $h_3 = 0.8$ m; initial sags of the cables $f_{1,0} = 1.0$ m, $f_{2,0} = 1.0$ m and $f_{3,0} = 0.7$ m; thickness-to-diameter ratios of the struts $k_{r,5} = k_{r,6} = 1/20$; the external load $q = 10.8$ kN/m; the limiting value for the structural deflection $\omega_{lim} = L/150 = 0.08$ m; the limiting values for the Θ_j -range (1): $\Theta_{lim,1} = 0.1$ and $\Theta_{lim,2} = 1.0$.

The matrix of admissible ranges for parameters to be optimized is the following:

$$X^{lim} = \begin{bmatrix} A_{lim,1} & A_{lim,2} \\ A_{lim,1} & A_{lim,2} \\ A_{lim,1} & A_{lim,2}/5 \\ A_{lim,1} & A_{lim,2} \end{bmatrix} \quad (13)$$

where $A_{lim,1} = 22$ mm² and $A_{lim,2} = 1560$ mm² are the limiting cross section areas of the cables, corresponding to the interval, which ranges from one cable with the diameter 6.1 mm and up to two cables with the diameter 36.6 mm (PFEIFER, 2017).

Initial vector \vec{s} of variations of parameters is obtained under the following expression: $s_u = (X_{u,2}^{lim} - X_{u,1}^{lim})/20$, where $u = 1..n$, $n = 4$. The limiting value for \vec{s} is adopted the following: $s_{lim} = 0.005$, while the maximum number of iterations is specified $K_{lim} = 500$. The vector \vec{X}_0 of initially given values for parameters is obtained under the following expression:

$X0_u = (X^{\lim}_{u,1} + X^{\lim}_{u,2})/2$. The increment for the cable tensioning is adopted the following: $\delta L_p = 0.01$. The price ratio is taken the following: $\rho_{str} = 1/3$.

4.2. Comparison with results, obtained by the licensed software for non-linear structural analysis

The following \vec{X} -vector (1) is obtained by means of the iteration technique (figure 3):

$$\vec{X} = (4.42 \quad 2.14 \quad 0.22 \quad 1.54)^T \text{ cm}^2 \quad (14)$$

The corresponding $\vec{\Delta L}_p$ -vector is the following:

$$\vec{\Delta L}_p = (0.1248 \quad 0.0347)^T \text{ m} \quad (15)$$

Diameters of the struts, obtained from (10) and (11), are the following: $D_5 = 31$ mm and $D_6 = 62$ mm.

The criterion function value (12) is 254.7. The masses of cables and struts, belonging to the structure considered, are the following: $\Sigma M_{cab} = 213.6$ and $\Sigma M_{str} = 123.3$ kg.

In order to verify the proposed technique, structural analysis of the cable roof was performed by means of the specialized software package EASY. The comparison of results is accomplished by the following expression:

$$\xi = \frac{|\Lambda^e - \Lambda^p|}{0.5 \cdot |\Lambda^e + \Lambda^p|} \cdot 100 \quad (16)$$

where ξ is the relative discrepancy, %; Λ is the structural parameter to be compared; indexes “e” and “p” refer to the results, obtained by the EASY software and by the proposed formulations, respectively.

Comparison of forces in the cables $j=1, 2, 3, 4$ and in the struts 5 and 6 are in the tables 1 and 2. The forces are given in kilonewtons. The deflections of the primary bearer cable 1 and the backstay cables 2, obtained in two ways, are very close to each other: $\Delta f^p_{1,pr} = -0.2024$ m, $\Delta f^p_{1,Ld} = -0.1493$ m, $\Delta f^p_{2,pr} = 0.1436$ m, $\Delta f^p_{2,Ld} = 0.0636$ m, and $\Delta f^e_{1,pr} = 0.2050$ m, $\Delta f^e_{1,Ld} = 0.1518$ m, $\Delta f^e_{2,pr} = 0.1495$ m, $\Delta f^e_{2,Ld} = 0.0690$ m. Corresponding discrepancies (16) are the following: $\xi_{1,pr} = 1.3$ %, $\xi_{1,Ld} = 1.7$ %, $\xi_{2,pr} = 4.0$ % and $\xi_{2,Ld} = 8.1$ %.

Remark: the deflections $\Delta f^{P_{1,pr}}$ and $\Delta f^{P_{1,Ld}}$ are multiplied by -1.0 before substitution into (16), because positive displacements of the cable 1, assumed in the present paper and in the EASY software are opposite to each other.

Table 1: Comparison of forces in the cables

Load-case	N^p_1	N^e_1	Θ^p_1	N^p_2	N^e_2	Θ^p_2	N^p_3	N^e_3	Θ^p_3	N^p_4	N^e_4	Θ^p_4
Pre-stress only	218.8	212.7	0.70	149.6	143.9	1.00	9.65	9.80	0.62	63.5	60.0	0.60
	$\xi_{1,pr} = 2.8\%$			$\xi_{2,pr} = 3.9\%$			$\xi_{3,pr} = 1.6\%$			$\xi_{4,pr} = 5.7\%$		
Pre-stress and vertical load q	309.1	301.8	1.00	64.1	59.5	0.43	1.54	1.68	0.10	92.6	86.0	0.86
	$\xi_{1,Ld} = 2.4\%$			$\xi_{2,Ld} = 7.4\%$			$\xi_{3,Ld} = 8.7\%$			$\xi_{4,Ld} = 7.4\%$		

Table 2: Comparison of forces in the struts

Load-case	N^p_5	N^e_5	$N_{E,5}$	λ_5	N^p_6	N^e_6	$N_{E,6}$	λ_6
Pre-stress only	19.37	19.26	31.7	95.9	20.1	19.9	81.1	120.0
	$\xi_{5,pr} = 0.6\%$				$\xi_{6,pr} = 1.0\%$			
Pre-stress and vertical load q	29.2	28.8	31.7	95.9	29.3	29.2	81.1	120.0
	$\xi_{5,Ld} = 1.4\%$				$\xi_{6,Ld} = 0.3\%$			
Remark:	N_E and λ are designated in the expressions (6) and (7).							

5. Conclusion

Cable roof structure intended for large-span buildings is considered. In spite of comparatively reduced overall height, the roof ensures the membrane covering to be of a required curvature in order to avoid wrinkles and slackened areas.

Numerical technique, based on the coordinate descent method, is used to perform structural optimization. The technique is numerically stable and allows to gain reliable solutions for the problem, multidimensional parameter space of which includes, so-called, invalid sub-spaces Ξ_i . It allows to determine pre-stress values and stiffness properties of structural members, needed for automated computer simulation of the construction. In comparison to graphical approach, used in the previous work, the technique proposed in the present paper is much more effective, providing reliable results in a short period of time.

The future improvement of the optimization technique should be in the field of cost estimation refinement, including expenditures for manufacturing and installation of the cable roof in the whole and also particular joints and details.

References

Chesnokov A.V. and Mikhaylov V.V. (2016), *Cable roof structure*. Utility Model Patent RU169612, (in Russian). Retrieved January 8, 2019, from <http://new.fips.ru/en/>.

Chesnokov A.V. and Mikhaylov V.V. (2017), Analysis of cable structures by means of trigonometric series. In: *Proceedings of the VIII international conference on textile composites and inflatable structures*. Munich, 9-11 October 2017, (pp. 455 – 466).

Forster B. (2003), Engineered fabric architecture – characteristics and behaviour. In: *Proceedings of the TensiNet symposium*. Brussel, 19-20 September, 2003, (pp. 28 – 43).

Galambos T.V. and Surovek A.E. (2008), *Structural stability of steel: concepts and applications for structural engineers*. New Jersey: John Wiley and Sons.

Goppert K. (2013). High tension tensile architecture. New stadium projects. In: *Proceedings of the VI International conference on textile composites and inflatable structures*. Munich, 9-11 October 2013, (pp. 21-26).

Grunwald G. and Seethaler M. (2011). Reconstruction. Olympic stadium. Kiev, Ukraine. In: *Tensinews* N21, (pp. 9 – 10).

Houtman R. (2003), There is no material like membrane material. In: *Proceedings of TensiNet symposium*. Brussel, 19-20 September, 2003, (pp. 178 – 194).

Mikhaylov V.V. and Chesnokov A.V. (2017), Cable roof structure with flexible fabric covering. In: *Proceedings of the VIII international conference on textile composites and inflatable structures*. Munich, 9-11 October 2017, (pp. 436 – 447).

PFEIFER Tension Members (2017): PFEIFER seil- und hebeteknik GMBH. Retrieved January 8, 2019, from <https://www.pfeifer.info/en/pfeifer-group/business-units/cable-structures/>.

Seidel M. (2009). *Tensile Surface Structures: A Practical Guide to Cable and Membrane Construction*: Ernst and Sohn.

Proceedings of the TensiNet Symposium 2019

Softening the habitats / 3-5 June 2019, Politecnico di Milano, Milan, Italy

Alessandra Zanelli, Carol Monticelli, Marijke Mollaert, Bernd Stimpfle (Eds.)

Pressure coefficient distributions for the design of hypar membrane roof and canopy structures

Jimmy COLLIERS^{*}, Marijke MOLLAERT^a, Joris DEGROOTE^b, Lars DE LAET^a

^{*ab}PhD – fellowship, Research Foundation Flanders (FWO), Egmontstraat 5, 1000 Brussel, Belgium
Jimmy.Colliers@vub.be

^aVrije Universiteit Brussel (VUB), Department of Architectural Engineering, Pleinlaan 2, 1050 Brussel, Belgium

^bUniversiteit Gent (UGENT), Department of Flow, Heat & Combustion Mechanics, Sint-Pietersnieuwstraat 41, 9000 Gent, Belgium

Abstract

Membrane structures are used in the built environment as roof or canopy and must therefore be designed to resist the external conditions. Nonetheless, the topologies of membrane structures are not covered by existing wind load standards and relevant wind load distributions for the basic shapes of these structures are almost not available. To have a realistic analysis of the wind loading, wind tunnel tests can be performed for each design. However, due to the lack of resources or time, for many projects the wind analysis will be based on rough approximations by relying on conventional shapes in the Eurocodes, with applying very high safety factors or designing unsafe structures as risk. Therefore, this paper presents a study of the orientation and curvature dependency of the wind load distributions over hypar roof and canopy structures. This study is performed with a numerical wind tunnel, using CFD with Reynolds averaged Navier Stokes equations. The outcomes are summarised in pressure coefficient distribution plots for most important wind orientations for hypar roofs and canopies with different curvature. The presented pressure coefficient distributions can be used in line with the Eurocode to derive more relevant wind load estimations for hypar membrane structures. These wind load estimations will give the engineer information about the average response of these structures under wind loading and will facilitate more reliable wind design of membrane structures.

Keywords: CFD, Cp-distribution, Eurocode, Hypar, Tensile surface structures, Wind loading.

DOI: 10.30448/ts2019.3245.15

Copyright © 2019 by J. Colliers, M. Mollaert, J. Degroote, L. De Laet. Published by Maggioli SpA with License Creative Commons CC BY-NC-ND 4.0 with permission.

Peer-review under responsibility of the TensiNet Association

1. Introduction

Membrane structures are mainly used in the built environment as a canopy structure or as part of a building roof. Therefore, they are subject to the elements and must be designed to resist them. In addition, due to the small self-weight, these lightweight pretensioned structures tend to be vulnerable to wind loading. However, standards for wind design of membrane structures do not exist. The basic anticlastic double curved geometries of membrane structures are not covered by the conventional building standards such as EN 1991-1-4:2005 (CEN, 2005) and even in literature very little studies are available.

1.1. Problem Statement

Membrane structures are used in different applications within the built environment and exist in a wide variety of double curved shapes and dimensions. These double curved shapes are not covered by the existing wind load standards, and the structural engineer has to perform dedicated wind tunnel tests or has to deal with approximations while considering the existing standards. Dedicated wind tunnel testing allows to obtain accurate wind loading, but is very expensive and time consuming. Due to lack of resources or time, wind tunnel testing is only conducted for large projects that have enough time and budget to conduct these tests. Consequently, for most projects the engineer has to make simplifying assumptions and approximations based on the wind load distributions for other shapes that are present in the existing standards. These assumptions will lead to over-dimensioned structures by applying conservative approaches and high safety factors or in some cases under-dimensioned structures that can jeopardise the safety of the users.

The need for general rules in wind design and for accurate wind load determinations over membrane structures has been stipulated in the past (Forster and Mollaert, 2004) (Gorlin, 2009) (Mollaert et al. 2016). The design of membrane structures will benefit from more accurate wind load estimations. Hereby, relevant wind pressure data is essential to conduct the analysis and design process in a reliable manner. Accurate wind load determinations over the 'typical' membrane shapes (hypars, cones, arch forms, and wave types) will allow the structural engineer to perform a more precise wind analysis and to design more efficient and safe membrane structures.

1.2. Outline

The paper starts with a brief introduction of the Eurocode procedure for determining the wind loads over conventional building structures, followed by an overview of the current state in wind design of membrane structures. The main part of the paper discusses the results of the numerical studies towards pressure coefficient (C_p) distributions over hypar roofs and canopies for different wind directions and for different curvatures. This study focusses on hypars with two high and two low corners because this shape can be considered the most basic shape of anticlastic double curved surfaces. The setup of CFD simulations is presented and the obtained wind loads are visualised by C_p -distribution maps. The paper concludes with a comment on the use of the presented C_p -distributions and identifies the additionally required studies in order to draft simplified C_p -distributions over hypar roofs and canopies in line with the Eurocode procedure for wind design of buildings.

2. Wind loading according to EC1 -part 1.4

EN 1991 Eurocode 1: '*Actions on structures*' and more particular, Part 1-4: General actions - Wind actions (CEN, 2005) gives a step by step calculation method to define wind loads over constructions with a height up to 200 m.

2.1. Wind interaction

The wind interacts with any structure that disturbs the free wind flow. During this interaction energy is transferred from the wind flow to the structure. The magnitude of the wind loads depends on amount of energy that is transferred during this interaction and thus the kinetic energy in the wind flow and the aerodynamic parameters of the structure relative to the wind direction. The kinetic energy of the flow is represented by the peak velocity pressure and the aerodynamic parameters are accounted for by pressure coefficients or C_p -values. The Eurocode prescribes a step by step calculation method to calculate the peak velocity pressure at the height of the eave of the roof and gives simplified C_p -distributions for the common building topologies, including flat and pitched roofs and canopies. The wind loads can then be easily computed by multiplying the peak velocity pressure with the C_p -distribution.

2.2. C_p -distributions

The C_p -distributions in EN 1991-1-4 are based on wind tunnel studies in a free flow field. The distributions are given for rectangular ground plans and are subdivided in zones based on geometrical proportions. For each zone, C_p -values are listed in tables, with different C_p -values given for different pitch inclinations in the case of pitched roofs and canopies.

For building roofs, the wind interacts only directly with the external face of the roof and indirectly with the internal face. The loads on these roofs have to be calculated by the summation of the pressure over the external and internal faces. The external pressure is computed by multiplying the external C_p -distribution with the peak velocity pressure at the height of the eave of the roof, while the internal pressure can be defined depending on the building permeability relative to the wind direction. The Eurocode presents external C_p -distributions for the most important wind orientations.

For open canopies, the Eurocode presents only net C_p -distributions, because the upper and lower face of open canopies are directly loaded by the wind. Therefore, these structures can be calculated by multiplying the net C_p -distribution with the peak velocity pressure at the height of the eave of the canopy. Mark that only one net C_p -distribution represents the maximal local values for all wind directions and that six load cases have to be considered. Two cases with the entire roof loaded and four cases with only one pitch of the roof loaded, respectively for net down acting and net uplifting pressure, are defined to cover all possible wind load distributions for canopies.

In addition, in the case of unconventional structures, the Eurocode prescribes that sufficiently safe assumptions have to be made while using pressure coefficients based on the provided data in the norm, or otherwise additional wind investigation is required.

3. Wind loading on membrane structures

The European Design Guide for Tensile Surface Structures (Forster and Mollaert, 2004) could be seen as a first step in the direction of a European Normative document for designing tensile surface structures. This guide emphasizes the need for accurate wind load distributions over the basic shapes of membrane structures as one of the main research priorities.

The current standards point out wind tunnel testing and CFD to study the aerodynamics and to obtain accurate wind load distributions over complex surfaces that are not covered by the current standards. Up to now few studies are performed towards wind load distributions over double curved membrane structures. In (Colliers et al., 2016) the available but fragmented Cp-distributions for these double curved membrane shapes are explored and summarized. This study identified a shortage in available data of wind load distributions over the basic membrane shapes. Due to the high costs of these specialised studies they are almost solely performed for very specific case studies and large-scale projects (Balz and Fildhuth, 2004) (Cook, 2011) (El-ashkar and Novak, 2004) (Irwin and Wardlaw, 1979) (Xuany et al, 2013). For the basic membrane shapes, studies are limited to some conicals (Hincz and Gamboa-Maruffo, 2016) (Nagai et al., 2012), umbrellas (Mall, 2014) (Michalski, 2009) and hypars with high and low points (Colliers, 2014) (Luo and Han, 2009) (Otto, 1954) (Sun et al., 2008) (Takeda et al. 2014) or with arched edges (Rizzo et al., 2012). In addition, recent numerical studies focus on fluid structure interaction frameworks (Kupzok, 2009) (Michalski, 2009) (Wüchner et al., 2006).

Currently, CEN TC 250 WG5 Membrane structures is preparing a technical document about the design and analysis of tensile membrane structures as the next step in the process for developing a Eurocode for membrane structures. In this context, there is need for relevant wind load distributions over the basic shapes of membrane structures in order to draft general recommendations in line with the current standards, which has already been stressed in the science and policy report - Prospect for European Guidance for the structural design of tensile membrane structures (Mollaert et al. 2016).

4. Cp-distributions for hyperbolic paraboloids

In this work, the aerodynamics of hypar roofs and canopies with different orientations and curvatures are studied in a virtual WT using CFD with Ansys Fluent.

The hypars are considered with a square ground plan and with different curvatures in line with the representation of Cp-distributions in the Eurocode. Hypars with a Shape Parameter (SP, sag divided by half the span) (Colliers, 2016) of 0.09, 0.18, 0.27 and 0.35 (Figure 1) are considered, as they directly correspond to pitch inclinations of 5°, 10°, 15° and 20° for the pitched roofs and canopies that are considered in the Eurocode.

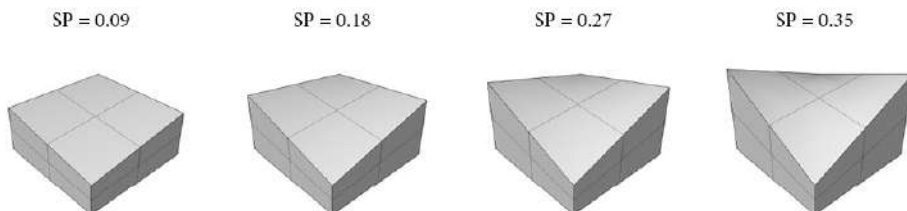


Figure 1: Hypars with an SP of 0.09, 0.18, 0.27 and 0.35 are considered to study the SP dependency of the Cp-distribution over hypar roofs and canopies.

The simulations continue on the numerical validation of previous experimental WT testing at a scale of 1/25. The hypar is considered to have a ground plan of 0,4m by 0,4m and the low corner at 0,13m high, what refers to 10m by 10m and the low corner at 3,25m high in reality.

The Navier Stokes equations are combined with the standard $k\epsilon$ turbulence model. The fluid domain is modelled as a box of 2 m wide by 1 m high by 2 m long, with a velocity inlet, a pressure outlet, a no-slip floor, with symmetry top and symmetry side conditions. A uniform inflow over the height of 15 m/s, with a turbulence intensity of 1% is defined at the inlet. The floor has a 0-sand grain roughness. The grid is fully hexahedral and more refined close to the roof or canopy structure. Grid convergence is achieved with the smallest cells of approximately 5mm (Figure 2). Results are less qualitative by double cell sizes (10 mm) and do almost not improve by half the cell sizes (2.5 mm).

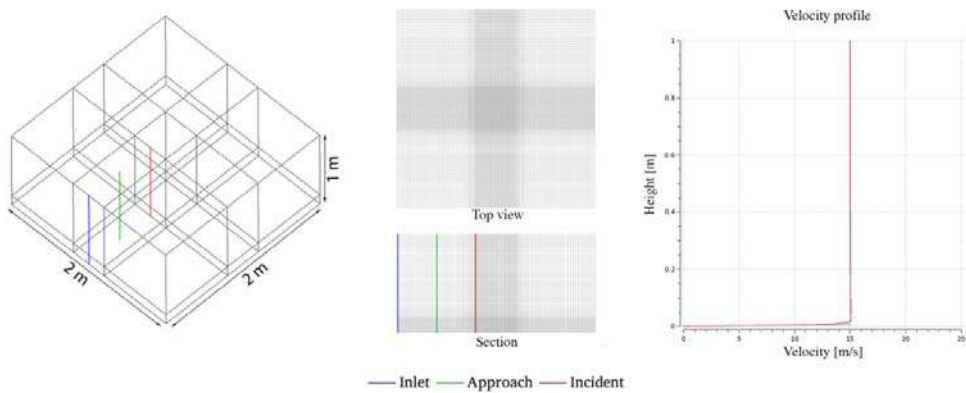


Figure 2: Mesh of the virtual wind tunnel in Ansys Fluent CFD and the velocity profile in the fluid domain.

The size of the fluid domain in these CFD simulations is rather small, because it results from the size of the test section of the WT that has been used in preliminar tests for the validation of the results. To confirm the accuracy of the results, the numerical studies are also performed at scale 1/1 and for a larger fluid domain in line with the best practice guidelines for CFD simulations of flows in the urban environment (Franke et al., 2007), and this for hypars with the lowest and the highest SP. Furthermore, the simulations are also run at lower wind speeds to verify the Reynolds independence. All simulations yield identical results, what indicates that hypars can be considered as bluff bodies and that the smaller fluid domain can be used to reduce computation time without jeopardising the accuracy of the results for the intermediate SP.

4.1. Orientation dependency

The orientation dependency of the C_p -distribution has been identified for a hypar roof and canopy with an SP of 0.09. The external C_p -distributions over the hypar roof are presented for different wind orientations, in steps of 15° ranging between the 45° with the high corner under attack and the 135° orientation with low corner under attack (Figure 3). For all orientations the hypar roof is entirely subject to suction, with highest suction near the upwind edges and corners. Mark that the asymmetric solution is the stable variant when the corner is under attack.

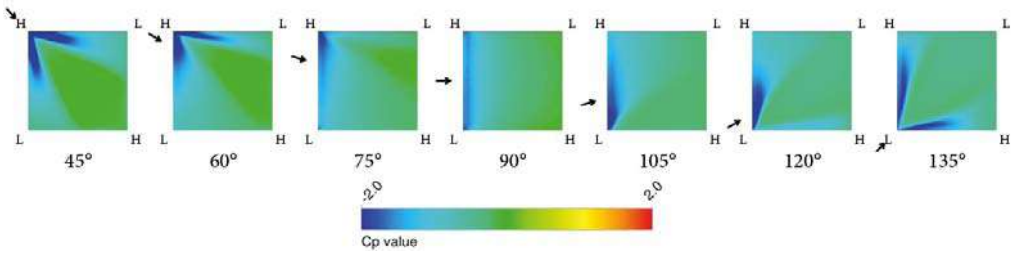


Figure 3: The orientation dependency of the Cp-distributions over a hypar roof with a SP of 0.09 with increments of 15 degrees in wind orientation.

The same sequence is shown for the hypar canopy, with Cp-distributions over the upper and over the lower face of the canopy separately (Figure 4). The Cp-values for hypar canopies have reduced significantly compared to the Cp-values for hypar roofs. Hypar canopies are not only subject to suction such as hypar roofs, but they are loaded by differential pressure and suction, depending on the local inclination of the roof relative to the wind flow.

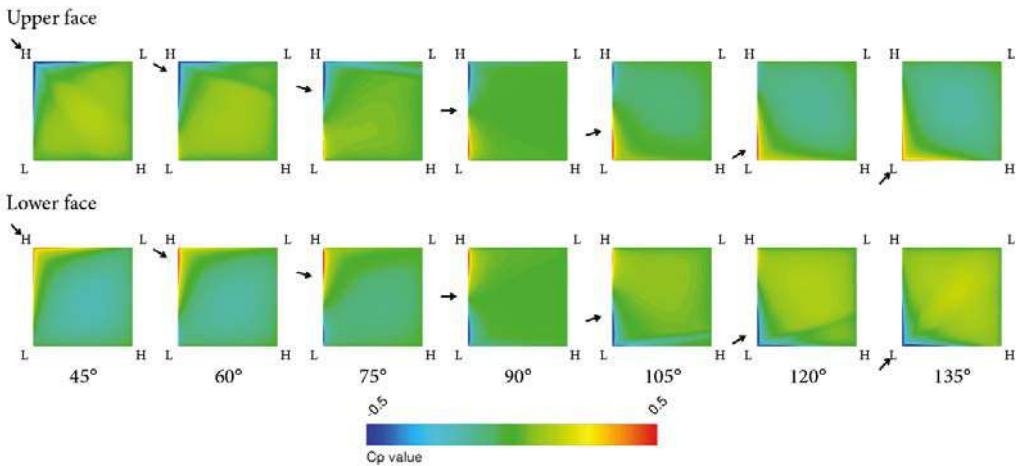


Figure 4: The orientation dependency of the Cp-distributions over the upper and lower face of a hypar canopy with a SP of 0.09 with increments of 15 degrees in wind orientation.

Three important wind orientations are identified for the hypar roof and canopy, respectively with the high corner under attack, the low corner under attack and with the leading edge perpendicular to the flow. Two of these orientations, respectively with the high and the low corner under attack were already proposed in the Design Guide (Forster and Mollaert, 2004) based on wind tunnel tests over a hypar roof with an SP of 0.18, done by Otto Frei in (Otto, 1954). Both orientations yield strongly different Cp-distributions with the highest absolute values near the upwind corners. The third orientation, with the leading edge perpendicular to the flow, should also be considered due to the highest total lift in the case of a roof, and the almost uniform net loading in the case of a canopy.

4.2. Curvature dependency

The SP-dependency of the C_p -distribution has been studied for hypar roofs and canopies for the most important wind orientations. Hypars with a SP of 0.09, 0.18, 0.27 and 0.35 are considered for this study, all with the same height of the low corner to span ratio in order to study only the influence of surface curvature on the C_p -distributions. Simulations are performed for the three important wind orientations that have been identified during the orientation dependency, respectively with the high corner under attack, with the low corner under attack and with the leading edge perpendicular to the flow.

The C_p -distributions for hypar roofs are more different with increasing SP (Figure 5). With the high corner under attack pressure develops near the downwind corner, while the suction zone spreads near the upwind corner. Only for the highest SP of 0.35, a significant reduction of suction near the upwind corner is observed, due to the local separation of the flow. With the low corner under attack, pressure develops at the upwind corner, while the highest suction zones move more downwind over the leading edges and suction increases in the middle of the roof.

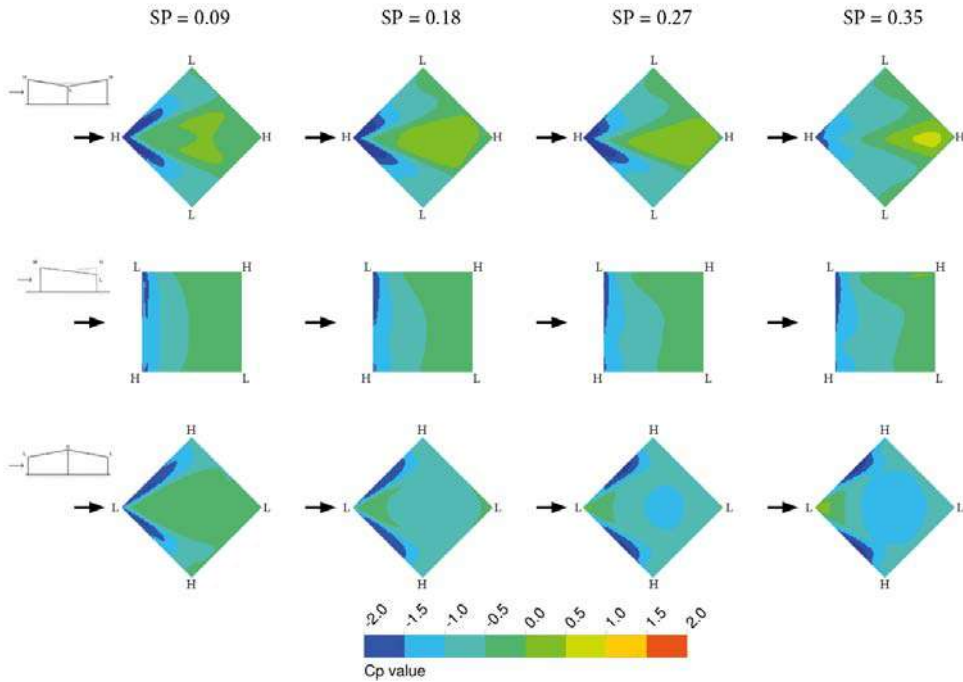


Figure 5: The SP-dependency of the C_p -distributions over hypar roofs with different SP for the three most important wind orientations.

For canopies, the C_p -distributions are also more pronounced with increasing SP (Figure 6). In general, rather similar changes take place as for hypar roofs, but for canopies the flow does not separate for high SP.

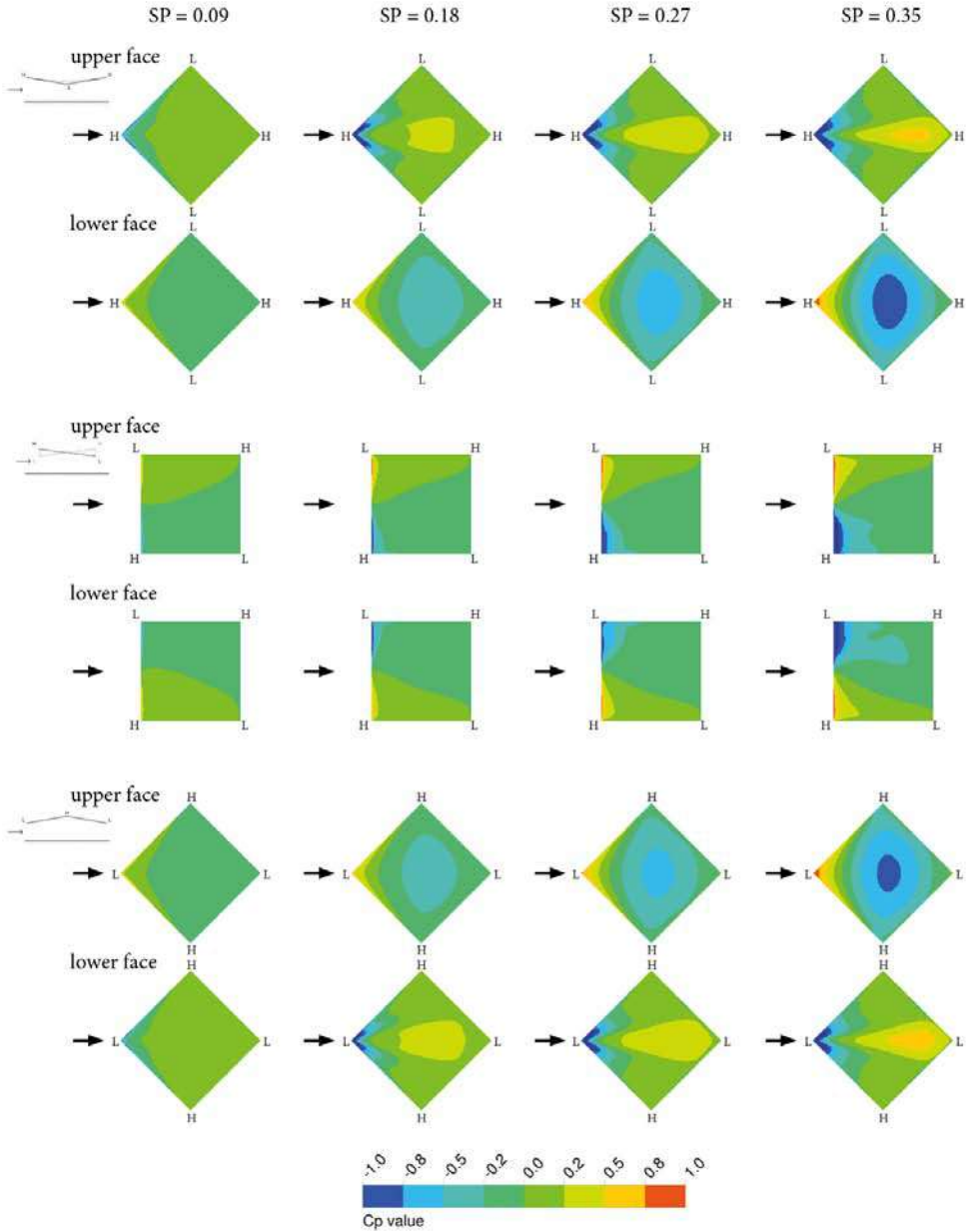


Figure 6: The SP-dependency of the Cp-distributions over the upper and lower face of hypar canopies with different SP for the three most important wind orientations.

5. On the use of Cp-distributions in line with the Eurocode

More studies are required in order to define simplified Cp-distributions that fully cover the wind load distributions over hypar roof and canopies in the same way as done for pitched roofs and canopies in the Eurocode. For example, different height of the low corner to span ratio will cause different displacements of the air flow and thus different Cp, especially when considering the atmospheric boundary layer.

With precautions the average results of these RANS simulations can be used for the design of hypar membrane structures with similar height of the low corner to span ratio. Furthermore, the presented Cp-distributions should be used in combination with the peak velocity pressure to account for the effects of wind gusts as established by the Eurocode for quasi static responses. Nonetheless, the accuracy of these gust loads and the influence of turbulence should be verified for aeroelastic responses of these structures, using extreme value analysis of real scale measurements, specialised WT tests or LES simulations.

6. Conclusion

This paper presents a clear overview of the orientation and curvature dependency of the Cp-distribution for hypar roofs and canopies under wind loading and could form a basis for further research on wind loading over the basic shapes of tensioned membrane structures within the scope of a prospect Eurocode on membrane structures.

The presented Cp-distributions can be used in line with EN 1991-1-4 to have information about the average response under wind loading of hypar membrane structures with similar height of the low corner to span ratio, but the influence of turbulence fluctuations on the Cp-values should be verified with extreme value analysis in further research.

Acknowledgements

This research is conducted under PhD fellowship of the Research Foundation Flanders (FWO-Vlaanderen).

The authors would like to thank the COST Association for facilitating a European framework within the COST Action TU1303 Novel Structural Skins, and in particular the expert discussions of Working Group 5 – From material to structure and limit states: codes and standardization.

References

Balz M., Fildhuth T., Schlaich Bergermann and Partners, "Wind Loading on Stadia Roof Structures, in: M. Mollaert M., Haase J., Chilton J., Moncieff E., Dencher M., Barnes M. (Eds.), TensiNet Symposium 2003 Designing Tensile Architecture, VUB, Brussels, pp. 140-149, 2004.

CEN European Committee for Standardizations, "EN 1991-1-4:2005. Eurocode 1: Actions on structures - Part 1-4: General actions - Wind actions." CEN, 2005.

Colliers J., " Wind Loading on Tensile Surface Structures -Experimental Approach -," Master Thesis, Vrije Universiteit Brussel, Brussels, 2014.

Colliers J., Mollaert M., Vierendeels J. and De Laet L., "Collating Wind Data for Doubly-curved Shapes of Tensioned Surface Structures (Round Robin Exercise 3)," TensiNet – COST TU1303 International Symposium 2016 Novel Structural Skins – Improving sustainability and efficiency through new structural textile materials and designs. In *Procedia Engineering*, vol. 155, pp.152-162, 2016.

Cook M.J., Buro Happold Engineers Ltd., 1981. *Wind Tunnel Tests for Large Surface Stresses Structure In Kuwait*. Irwin P., *Wind Engineering Research Needs*, 2011.

El-ashkar I. and Novak M., "Wind Tunnel Studies of Cable Roofs", *Journal of Wind Engineering and Industrial Aerodynamics*, vol. 13, pp. 407–419, 1983.

Forster B., Mollaert M. and Tensinet, *European Design Guide for Tensile Surface Structures*. Brussels: VUB, 2004.

Franke J., Hellsten A., Schlünzen H. and Carissimo B., "Best practice guidelines for the CFD simulation of flows in the urban environment", *Cost Action 732: Quality assurance and improvement of microscale meteorological models*. P.52, University of Hamburg, Hamburg, 2007.

Gorlin W.B., "Wind Loads for Temporary Structures: Making the Case for Industrywide Standards," *Journal of Architectural Engineering*, vol. 15, no. 2, pp. 35–36, 2009.

Hincz K. and Gamboa-Maruffo M., "Deformed Shape Wind Analysis of Tensile Membrane Structures", *Journal of Structural Engineering*, vol. 142, no. 3, p. 5, 2016.

Irwin H. and Wardlaw R.L., "A Wind Tunnel Investigation of a Retractable Fabric Roof for the Montreal Olympic Stadium", *Proceedings of 5th International Conference on Wind Engineering*, pp. 925–938, 1979.

Kupzok A., "Modeling the Interaction of Wind and Membrane Structures by Numerical Simulation", *Dissertation, Technischen Universität München, Munchen*, 2009.

Luo J. and Han D., "3D wind-induced response analysis of a cable-membrane structure", *Journal of Zhejiang University SCIENCE A*, vol. 10, no. 3, pp. 337–344, 2009.

Mall F., "Ermittlung von Windlasten auf Bauwerke mit Hilfe von CFD-Berechnungen", *Master Thesis, Hochschule für Technik, Wirtschaft und Gestaltung Konstanz, Radolfzell*, 2014.

Michalski A., “Simulation leichter Flächentragwerke in einer numerisch generierten atmosphärischen Grenzschicht”, Dissertation, Technischen Universität München, München, 2009.

Nagai Y., Okada A., Miyasato N., and Saitoh M., “Wind Response of Horn-Shaped Membrane Roof and Proposal of Gust Factor for Membrane Structures”, *Journal of the International Association for Shell and Spatial Structures*, vol. 53, no. 3, pp. 169–176, 2012.

Otto F., “Das hängende Dach”, Dissertation, Technische Universität Berlin, Berlin, 1954.

Rizzo F., D’Asdia P., Ricardelli F., and Bartoli G., “Characterisation of pressure coefficients on hyperbolic paraboloid roofs”, *Journal of Wind Engineering and Industrial Aerodynamics*, vol. 102, pp. 61–71, 2012.

Stranghöner, N., Uhlemann, J., Bilginoglu, F., et al., “Prospect for European Guidance for the Structural Design of Tensile Membrane Structures: Support to the implementation, harmonization and further development of the Eurocodes.” Mollaert M., Dimova S., Pinto A. and Denton S. (Eds), Joint Research Center science and policy report. Luxembourg: Publications Office of the European Union, 2016.

Sun X., Wu Y., Yang Q., and Shen S., “Wind Tunnel Tests on the Aeroelastic Behaviors on Pretensioned Saddle-Shaped Suspended Roofs”, presented at the 6th International Colloquium on Bluff Body Aerodynamics and Applications, Milano, pp. 1–10, 2008.

Takeda F., Yoshino T., and Uematsu Y., “Design Wind Force Coefficients for Hyperbolic Paraboloid Free Roofs”, *Journal of Physical Science and Application*, vol. 4, no. 1, pp. 1–19, 2014.

Wüchner R., Kupzok A. and Bletzinger K.-U., “Simulation of fluid-structure -interaction with free form membrane structures using an implicit coupling scheme with adaptive under relaxation”, *European Conference on Computational Fluid Dynamics*. p. 17, 2006.

Xuanyi Z., Zhihui H., Ming G., An-an Z., Weiyu Z. and Wei F., “Research on wind-induced responses of a large-scale membrane structure”, *Earthquake Engineering and Engineering Vibration*, vol. 12, No. 2, pp. 297-305, 2013.

Systems for transformative textile structures in CNC knitted fabrics – Isoropia

Mette RAMSGAARD THOMSEN*, Yuliya SINKE BARANOVSKAYA*, Filipa MONTEIRO^a, Julian LIENHARD^b, Riccardo LA MAGNA^b, Martin TAMKE*

*CITA, 1435 Copenhagen, Denmark, martin.tamke@kadk.dk

^a A. Ferreira & Filhos SA, 4815-901 Caldas de Vizela, Portugal

^b Str.ucture GmbH, 70176 Stuttgart, Germany

Abstract

Extending recent work on Form Active Hybrid Structures of Active Bend and CNC knitted (Computer Numerical Control) tensile members we present a set of innovations in design and manufacturing, which together allow to build structural systems, that morph across multiple structural states. While state of the art tools and fabrications methods in textile hybrid structures provide architects and engineers with means to adopt the geometry of a chosen textile system to the requirements of a given site, constraints in design thinking, tools and manufacturing however still limit the ability to change the spatial and structural qualities and expressions within a textile object. The potentials of our developments to create new spatial expressions and atmospheres in textiles structures are demonstrated and evaluated through the large-scale installation Isoropia designed and built for the Danish Pavillion in the 2018 Venice Architectural Biennale.

Keywords: Architecture, Digital Design, Bending Active Textile Membrane Hybrids, Digital Chain - Integration of Design, Simulation and Fabrication, CNC Knit

DOI: 10.30448/ts2019.3245.08

Copyright © 2019 by M. Ramsgaard Thomsen, Y. Sinke Baranovskaya, F. Monteiro, J. Lienhard, R. La Magna and M. Tamke. Published by Maggioli SpA with License Creative Commons CC BY-NC-ND 4.0 with permission.

Peer-review under responsibility of the TensiNet Association

1. Introduction

Tensile membrane structures are per se customized, as the shape of the membrane can only be determined through the process of form finding. In here the final membrane shape emerges as equilibrium of forces. As result tensile membrane structures are usually one-offs, designed and engineered specifically to the context, they are situated in, and fabricated to project specific specifications of predominately non-standard elements. Current state of the art membrane projects, are however dominated by a desire to repeat the same or similar elements, restricting the expression and spatial potential, which resides in the bespoke nature of membrane technology. In this paper we propose to use digital workflows for the design and fabrication of bespoke materials and elements to create in an efficient manner membrane architectures, which create radical new spatial atmospheres, exemplified in the 2018 installation *Isoropia* (Fig. 1).



Fig. 1. *Isoropia* - a bespoke textile installation for the Danish Pavilion at the Architectural Biennale 2018.

In architectural fields outside of membrane structures new spatial experiences and expressions have in the last decade been enabled through the use of non-standard design and fabrication methods. The success of these designs is based on the implementation of computational techniques in design and analysis and an integration of digital design and digital fabrication (Tamke & Thomsen, 2009).

These digital design methods and workflows have enabled new spatial and tectonic solutions across all scales (Fig. 2-6) in which elements change and morph in order to change the atmosphere and expression for the humans within. As shown in the 2009 CITA exhibition design for “It’s a small World” a non-standard design approach allows structures to adapt seamlessly to different scales and environments and act as a physical mediator between spatial requirements. Furthermore the underlying computational approaches provide the base for future

highly material efficient structures, which rely on the total integration of design and robotic manufacturing (Nicholas, Zwierzycki, Nørgaard Clausen, Hutchinson, & Thomsen, 2017; Solly, Frueh, Saffarian, Prado, & Menges, 2018)



Fig. 2-6 Interior Panels in Oslo Opera Hall (Olafur Eliasson), It's A small World (CITA), Arch Union Architects), Dongdaemun Design Plaza (Zaha Hadid architects), Aqua Tower (Studio Gang) - all photos CC

In the field of tensile architectures the use of non-standard approaches has been tested early on in small scale academic prototypes, such as the 2007 AA Component Membrane installation and related work (Hensel & Menges, 2008). However similar site and human scale specific installations, that are based on the morph of the size and shape of membranes across the structure, have until now not seen a wide implementation in the field. Instead discrete and varying membrane fabric elements of same size are repeated, as in the case of the King Fahad National Library (2014) (Dupont, 2014), or an intended morphing expression is created through a combination of a customised steel structure and standard membrane elements, as in the Nizhny Novgorod Stadium (2018) (Bernert, 2018).

While the authors of the latter structure do not reveal the reason, why their design shifted from a non-standard approach towards the pattern cut of the membrane elements to standard ones, accounts from small scale structures with non-standard approaches to geometry and detailing (Hensel & Menges, 2008), point at the labor intensity in design, simulation, fabrication and assembly as a challenge. Moreover, the inherent stiffness of traditional laminated membranes limits the scales by which it can be applied, as the need for seams to assemble patches to achieve double curvature and integrate detailing further limits the scales by which the membranes can be used.

New opportunities for spatial expression and tactile experiences emerge through the integration of design, analysis and fabrication combined with the shift of the textile system from weave to CNC-knit (Ahlquist & Menges, 2013; Popescu et al., 2018; Sabin, 2013; Thomsen et al., 2015). The inherent flexibility of knit, the ability to integrate shaping and detailing in the textile fabrication process opens especially opportunities for designing membranes at the smaller scale of state of the art membrane architecture, as in Ron Herrons Imagination Building (Lyll & Herron Associates, 1992). Current application of CNC knitting in the field have focused on

small scale prototypes, but didn't engage in building scale or devised knitted textiles a role as structural member, as needed in Form Active Hybrid Structures of Active Bend and Tensile members (Thomsen et al., 2015).

1. Isoropia - Outset and framework

Isoropia, which in Greek means balance, equilibrium and stability, is a 35m long structure made from 41 custom CNC knitted patches of up to 7m length for the 2018 Venice Biennale Installation. The textile membrane is set in structural equilibrium with bend glass fibre rods of varying thickness and strength.

In this paper we ask how state of the art materials and structural systems, design and fabrication workflows can create avenues for new spatial experiences in textile architecture. Detailed questions of digital design and analysis workflows in isoropia have been discussed in a previous publication (La Magna, Fragkia, Noël, Baranovskaya, & Thomsen, 2018).

The structure creates a spatial and structural continuum through the Danish Pavilion, forming differentiated outdoor canopy structures on the two outer sides and a vaulted space in the interior in a reaction to the specific program and sites (Fig. 7):

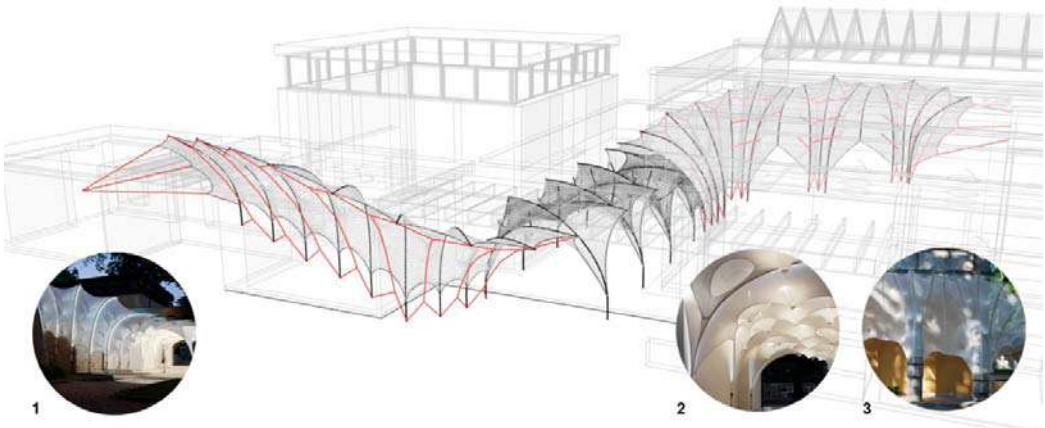


Fig 7. Architectural concept of Isoropia. 1) The southern exterior part (left) welcomes visitors to the Biennale and creates a canopy like structure guiding visitors into the Danish Pavilion. 2) The interior passage (middle) is the only entrance to the Danish Pavilion. The aim was to create a dense textile space, which creates curiosity on side of the visitors, allows them to slow down, study movies and text about the installation and finally redirects them into the further exhibition of the pavilion. 3) The northern exterior part (right) is directed towards the lively cafe zone of the Biennale and creates an shading entrance canopy, which adapts to the rhythm of the colonade of the existing Danish Pavilion.

Further forming requirements have been:

- the status of the Danish Pavilion as quasi listed building, which prohibits irreversible modifications to the construction
- the need to connect the structure to “Danish ground” only, which prohibited any ties to the directly surrounding “Italian” ground and the large amount of ca. 150.000 visitors, which required a sturdy construction and detailing in compliance to structural and historical conservation code, that had to be documented in a building permission to the authorities
- the pavilion had to work at day and night, which required the integration of artificial lighting.

Most important of all the time given from commissioning of the installation to its completion was only 4,5 months.

1. Isoropia solutions

The conceptual answer to the total amount of ideas and demands, was to create a structure, which can morph and adopt on relatively small scale yet high level and quality of textile surfaces and detail. In order to overcome the above listed constraints we had to devise new solutions on several levels. These are highly interconnected in terms of the processes in design, analysis and fabrication as well across scales.

1.1. Structural system - Bending Active Textile Hybrid

The building system employed for the canopy falls into the category of bending-active membrane hybrids (Ahlquist, Lienhard, Knippers, & Menges, 2013). These are defined as systems that achieve equilibrium through the combination of bending-active elements (the GFRP rods) with purely tensile elements (the membrane patches and cables), hence the hybrid nature of the structure. The bending-active elements provide the required mechanical supports to prestress the tensile elements, which in turn lock the bent rods into position. In this way, a subtle equilibrium solution is achieved in which the interdependency between the individual components is necessary for the stability of the structural system. The shape of the canopy is therefore the result of the interplay of internal forces conveyed by the individual structural elements.

In order to morph, the Isoropia structural system shifts from a cablenet system on the exteriors, which pre-stresses and stabilises the structure, to a tensegrity-like structure in the interior in which compression elements pre-stress the knitted membrane (Fig. 7). Each arrangement posed a specific challenge in terms of analysis and assessment of the structural behaviour.

The *outdoor areas* derive their shape from the mutual force interaction between the bent rods, tensile Dyneema® membrane and Dyneema® cables. The only support being the dedicated steel fixtures on the building's wall. The rods with diameter and wall thickness (24.3/20.3mm and 26/19mm), bespoke to local performance requirements, cantilevered outwards and were kept in position solely by the prestressed tensile elements (Fig. 7). In terms of form-finding and structural analysis, this area presented particular challenges due to the high nonlinearities deriving from the minimal amount of supports and mechanical constraints in the system.

The *interior* is made of bending-active elements, which alternate their direction and create a crossing pattern visible in Fig. 7. Here the GFRP rods (22/17mm) were connected to the building's walls and ceiling, creating a continuous support condition of the beams. Less demanding from a computational point of view thanks to the forgiving boundary conditions, this area presented particular challenges in terms of analysis due to the topological arrangement of the membrane patches and the stretched sections where the compression rods were inserted.

Finally the listed building status of the Danish pavilion coupled with the bending-active hybrid nature of the canopy, pushed for solutions that reduced to the bare minimum the interventions on the surroundings and consequently the support areas that could be used to secure the structure.

1.2. Design system

For the purpose of the project these constraints were translated into a dedicated design system (Gengnagel, La Magna, Ramsgaard Thomsen, & Tamke, 2018) that seamlessly connected the digital design pipeline used for geometrical exploration, based on Projection Dynamics (Bouaziz, Martin, Liu, Kavan, & Pauly, 2014), with an intermediate Isogeometric Analysis tool (Längst, Bauer, La Magna, & Lienhard, 2018), which provided frequently feedback on the structural performance of the canopy and finally a robust and detailed analysis using more established tools for simulation (Julian Lienhard, Bergmann, La Magna, & Runberger, 2017). In this way, the behavior of the structure could be constantly monitored during the development of the project, providing valuable information to all the parties involved throughout the conceptual and development phases.

1.2.1. Digital Design Workflow

The developed continuous membrane system is based on a single principle structural unit, consisting of a pair of bend GFRP rods (Beams), which carry a connecting membrane, stressed by cablenets or compression sticks. Through variations, of parameters in this basic units, such as the width between the supporting rods, their lengths and the interposition of the fabrics in relation to the rods, a continuous yet adapting structure is possible.

Around this basic parameters a generative design pipeline using Kangaroo2 (Quinn et al., 2016) was built (Fig 8). This setup allowed rapid design variations, through changes of only a few parameters, such as the beam locations in space (A), the beam length (B) and Z-position.

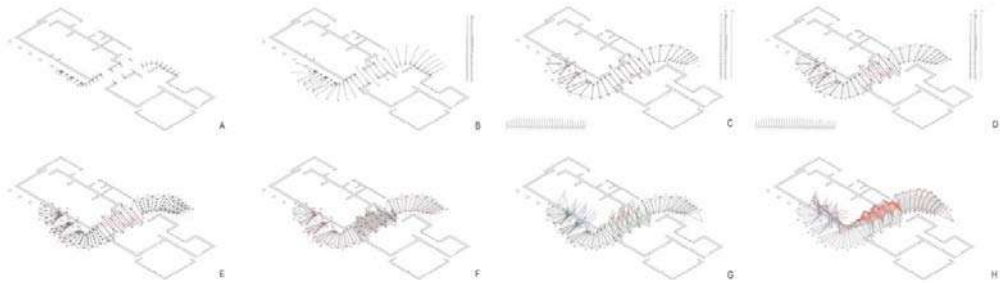


Fig. 8: Steps of the workflow for the Digital Design Tool A) Positions for the beams are indicated on 2D ground level, considering the maximum fabrication width of the membranes. At each position a vector perpendicular to the existing building indicates the direction of the beams. B) Based on the vectors beams are generated in determined length. C) Z-values are given for the target locations of beam start and end, as well as values for start and end of fabric on beams. The discretisation of the beams (30cm) is used to generate a membrane outline as quads. The type of membrane is indicated (double or single-sided with cablenet)
 E) All quads get discretized in custom resolutions, as either single or double layer membranes. The amount of coverage of the second layer is increasing gradually F)The cablenets and the amount of pulling points are introduced. G)The interior membranes are generated and compression sticks are introduced and iteratively optimised in order to find an equilibrium position in the textile. H)External constraints for the relaxation are introduced: anchors, external tension ropes, links to the ceiling in the interior and back tension ropes for the non-cablenet units. I) Kangaroo Force values are applied to the goals of the digital design tool pipeline and the overall shape is found.

1.2.2. Analysis Workflows

The digital design tool provided an agile platform for quick design explorations and geometrical variations of the canopy throughout its conception and development. Though, the high level of documentation requested by the authorities, a detailed analysis of the structure was necessary in order to assess its performance under high wind loading and its effects on the surroundings, especially the reaction forces exerted by the canopy on the support areas fixed to the building. A dedicated workflow between the design and analysis was set up to quickly provide feedback to the design process.

Kiwi3d, a new tool for Isogeometric Analysis, was used for intermediate quick analysis. In particular, Kiwi3d incorporates modules for linear and nonlinear analysis, as well as form-finding based on the URS (Updated Reference Strategy) method (Philipp, Breitenberger, D’Auria, Wüchner, & Bletzinger, 2016). To speed up the transfer between the two platforms, a

geometry processing workflow was set up which took care of the discrepancies between the geometric models. This meant converting discrete lines and surfaces into continuous spline and NURBS patches through interpolation of the nodes. This geometry conversion was robust and reliable and an analysis of the full building process of the canopy could be simulated: the bending of the GFRP rods, the attachment and form-finding of the membrane patches and linking the cables to the membrane and prestressing it. Besides this initial assessment of the structural behaviour under wind loading (930 mm vertical deformation for wind suction, 640 mm vertical deformation for wind pressure) and the corresponding reaction forces took place in Kiwi3D.

The analysis of the canopy was completed by running a Finite Element simulation on the final design (SOFiSTiK coupled with the dedicated Grasshopper plugin STiKbug) (J. Lienhard, La Magna, & Knippers, 2014). This step was necessary to validate the intermediate results using well-established tools which have been extensively tested both in research and in practice. The Finite Element tools allow for a very detailed description and simulation of the structural behaviour, giving the analyst the possibility to incorporate advanced aspects such as long-term behaviour and plasticity. Specific to this case, compressive springs were added in the final simulation model to take into account the contact between the bending-active rods and the building's walls, an aspect that needed to be verified due to the scrupulous requirements of the organization.

1.3. Material Systems

In Isoropia we further develop the inter-scalar approach first suggested in the Hybrid Tower projects (Holden Deleuran et al., 2015; Thomsen et al., 2015). Here, design takes place at multiple scales from the overall structural system, to the single patch, the implemented knit structure and down to fibre selection and fibre surface.

1.3.1. Knitted membrane: an inter-scale approach

In difference to Hybrid Tower, in which a single patch design is repeated to achieve the rotational geometry, Isoropia works with mass customised patches. As the structure morphs from canopy to vault and back again and as it twists through the Danish Pavilion building, each patch is differentiated both in size and shape. This differentiation creates variances in the patch design from a variation of protruding cones and slits (Fig.9).

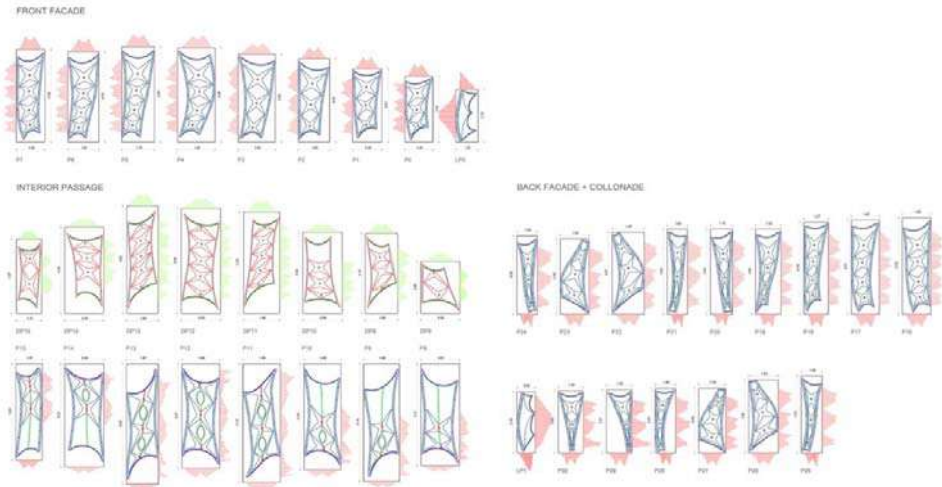


Fig 9: Outline drawings of all patches produced for the three zones of Isoropia. The graph lines surrounding the bounding boxes indicate the amount of elasticity in areas of the patches through combination of different knit structures.

Isoropia also further develops the innovative membrane design from Hybrid Tower, where we detailed the membrane through tubular jersey for double surface channels, interlocking for reinforcement parts and holes for tying and pre-stressing (Tamke et al., 2016). Isoropia further differentiates between various knit patterns within the patch surface (Fig 10). Initial tests using only one base knit pattern (Piquet Lacoste) revealed to be too tight to achieve the strong three dimensionality needed for the cones, which provides together with the cablenet structural depth and capacity. To increase cone depth we defined a fourth stitch pattern, in which the interlocking between needles is less, therefore allowing more flexibility of the yarn and better deformation. This fourth stitch pattern is introduced in star-shaped zones around the cones grading the material locally for performance

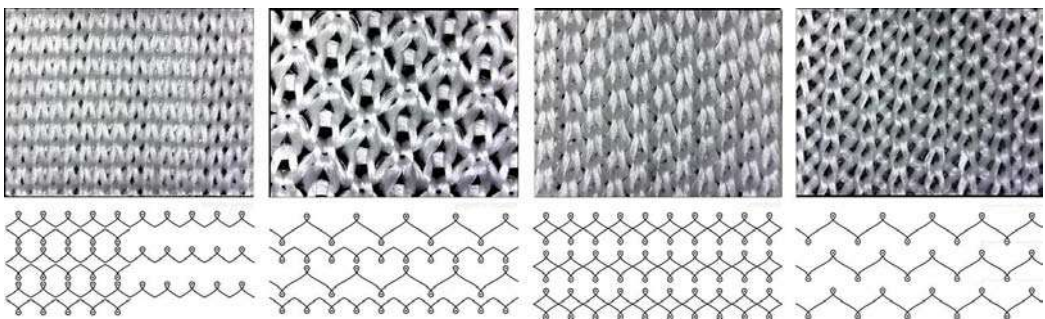


Fig 10: The in Isoropia used knit patterns (from left: tubular, piquet lacoste, interlock, piquet)

The double patches are assembled using a knit logic (Fig. 11&12). By linking the two surfaces together, in the way that garment patches are linked together, we employ a knit stitch and use the same fibres as in the patches. In this we achieve similar performance of the assembly stitch as in the overall patch allowing better pre-stressing of the membrane.

1.3.2. Fibre system - manufacturing bespoke knit

At fibre level the material, machine requirement and final textile structure had to be considered in order to achieve a promising textile system, which could handle the variations in pattern and mechanical stress that characterizes Isoropia. It was further important, to create a welcoming and soft haptic experience for visitors who touch the fabric, unlike the plastic nature of state of the art building membranes. From a limited range of available high performance yarns, ultra high molecular weight polyethylene yarns Dyneema® SK65 was selected due to its enhanced mechanical properties specifically 3,3-3,9 GPa of Tensile Strength; 109-132 GPa of Tensile Modulus and 3-4% Elongation at Break (Fig. 13&14)



Fig 11-14: Linking using Dunkermotoren linker (BG83 14GG),Dyneema® SK75 220DText

1.4. Fabrication Systems

In Isoropia the development of design, knit specification and fabrication system ran in parallel and each step of this rapid process was evaluated in 1:1 prototypes. This required to have early on an automatic link between the digital design tool at CITA, and the CNC knitting machines at the textile producer AFF.

1.4.1. Digital Fabrication Interface

The interface between design and production takes place through bitmap files (Thomsen et al., 2016). These files are automatically generated from planarised meshes of the digital design system (Fig. 15)

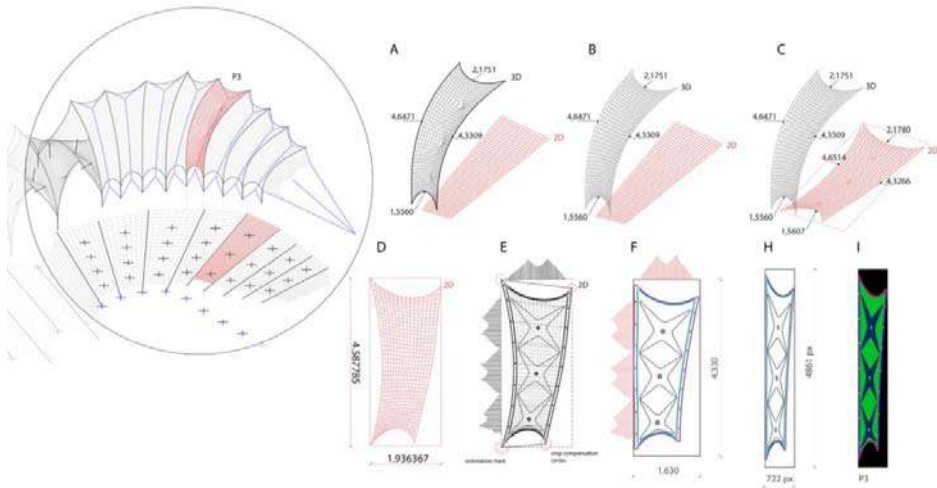


Fig. 15: Workflow for the Digital Fabrication Tool: A) A 2D mesh with identical mesh topology to the formfound 3d mesh is generated. B) The protrusion of each cone is “relaxed” into a simplified 3d mesh, as the cones are formed as the result of textile stretch only. The outer edge lengths are maintained. C) The internal and external edges of the 3d mesh are measured and used as constraints for a K2 relaxation of the 2D mesh with a 0.01m tolerance for the output edge lengths. D) A best fitting bounding box is generated and tested against the max width of the CNC knitting machine. E) The 2D mesh and the transposed cone centres serve as base for the automated specification of the boundaries of areas with different knit structures (rods channels, details for the lighting details, reinforcement edge and the expandable cone stars, large slits). Visual feedback is provided on the relation between zones of different stretch (Piquet and Piquet Lacoste). F) Colours are assigned to the different areas, the lines in linework was set a colour. H) In order to accommodate the non-square nature of knit stitches, a non-uniform scaling is performed. I) Lineworks is processed with Squid (Grasshopper Plug-In, developed at CITA by Mateusz Zwierzycki), filled with predefined colours and exported as bmp.

The development of the digital fabrication workflow did take place through iterative testing and prototyping of samples in increasing size (Fig. 16). 1:1 prototyping of the system was instrumental in order to understand and measure the interplay of all elements and materials across all scales, instead of working on assumptions gained from isolated tests. Each prototype allowed the project to leap to a more reliable level and gain validated correction values for the parameters in the design and fabrication workflow.

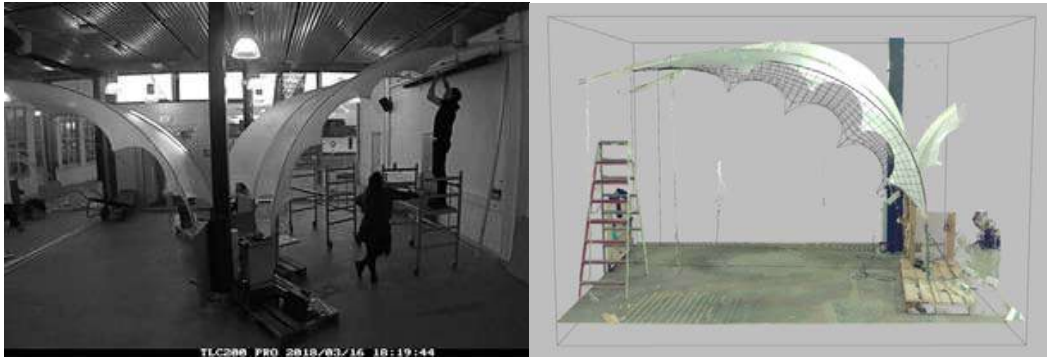


Fig. 16 1:1 Prototyping of the membrane units Fig.17: Evaluation through 3d scanning

1.4.2. Producing CNC Knit - Machines

The complexity of Isoropia on knit level required a high degree of freedom on side of production machinery. For this a Shima Seiki M183514 14GG flat knitting machine and APEX3 software was selected, due to their ability to interface on level of design and programming code (Barfield, 2015). The process of converting the bitmap knit information from the design level to CNC knitting code (Fig. 18 & 19) entailed that the single colour fills of the bmps were assigned a smaller scale pixel pattern, which contains a particular information for every single needle. This required the computationally powerful SHIMA SEIKI computer units and novel processing steps and design planning for knitting procedures. Some challenges were faced regarding the yarn flow, the structural detail of the textile area itself and the pre-defined outer shape. Structural detail meaning the interfaces of the different structures in the knit (Fig. 15). Techniques had to be developed in order to absorb or spread tension between structures where needed and also allow a proper knitting flow whenever the knit code changes between different structures. These three distinct textile architectures had to be precisely programed and tested to resist mechanical solicitations without compromising neighboring structural requirements. Though the project was based on previous collaborations (Tamke et al., 2016) any new development posed challenges. The use of the inelastic and hence demanding Dyneema® yarn required for instance an adjustment of the knitting machine in order to be able to knit on a high speed without mistakes or damages to the machine. But as well interdisciplinary challenges occurred, when new processes, as the linkage of two single layer into a double membrane were introduced. In here the existing work procedures and the lack of integrated markers on the fabric of the positions to link the fabric created a situation where the fabrics were linked wrong, which resulted in a non-matching assembly. Fortunately the issue could be very easily solved by simply delinking the fabrics and linking them once again in the right places.

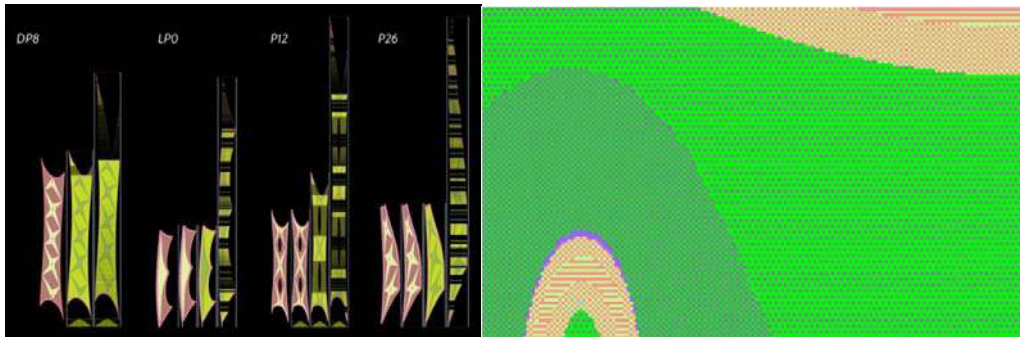


Fig. 18-19: Processing of the CNC-knitting files for the membranes at AFF and final production resolution

2. Conclusion and Potentials

The realisation of the bending-active membrane hybrid Isoropia was only possible, through an integration of the Structural, Design, Material and Fabrication system. This transdisciplinary and interscalar approach allowed us to design and build a morphing structural membrane system in only 4,5 months, which delivers new spatial experiences and a new level of detailing to the field of small scale membrane structures. Isoropia is until today the largest structure made in preprogrammed CNC-knit, with every single membrane being unique (Fig. 20-22).



Fig. 20 - 22: Interior view. Textile membrane ceiling together with integrated light created a special atmosphere and invited guests to interact with the environment.

The approach chosen in Isoropia opens up opportunities for new design expressions in textile architectures and an integrative approach towards other building elements. Isoropia morphs between two very radically structural systems and spatial expressions: from a more normative outer appearance to the radically textile space in the inner area. A unified impression is created through the use of similar design features - the textile cones - in both systems and the ability to specify gradual shifts in families of elements and materials.

The ability to morph provides the structure with modes to adapt and create highly local interfaces to the existing buildings. This was beneficial for the design of structures in historic context. A further factor, which contributed to the minimal invasive character of Isoropia was, that we could avoid tension connections to the existing structures, as the prestressing of the membranes was provided within the hybrid structure itself.

Despite being a first of its kind, the overall installation of Isoropia took only 8 days. Most of the time was used to install the infrastructure, such as electrics and support, while the actual assembly and tensioning of the hybrid structure only hours. This shows, how the integration of functionality and performance in elements and materials, allows to minimise the overall complexity and costs of building, which would else arise through on-site fabrication, assembly and the handling of many parts.

During the exhibition we observed, that most of the more than 100.000 visitors touched the textile surfaces of Isoropia with interest and pleasure. CNC knit is able to create surface qualities on level with apparel, even when it is made from high performance yarns.

Finally Isoropia is giving rise to an environmental friendly architecture and smart production strategy through CNC knit, which is able to address zero waste and low labor intensity production, deliver elements with highly customised shapes, functions and behaviours and new freedom in design of membrane architecture. In this aspect Isoropia is a stepping stone and the exploration of designed movement of similar hybrid structures, the further integration of lighting and the production of non-manifold surfaces are obvious next steps.

3. Acknowledgments

The realisation of Isoropia builds on an interdisciplinary collaboration between CITA, Centre for IT and Architecture (design and computation), structure (engineering), AFF - A. Ferreira & Filhos, SA (knit fabrication), DSM Dyneema B.V (fibre) and alurays lighting technology GmbH (lighting). The project is kindly sponsored by Topglass Italy (GFRP tubes), Sofistik (FE analysis)WK Led Netherlands (flexible LEDs) and SIKA (Glue) and financially supported by Danish Ministry of Higher Education and Science - Complex Modelling - Sapere Aude: DFF-Starting Grant / <https://ufm.dk/>

4. References

- Ahlquist, S., Lienhard, J., Knippers, J., & Menges, A. (2013). Physical and numerical prototyping for integrated bending and form-active textile hybrid structures. In *Rethinking Prototyping: Proceeding of the Design Modelling Symposium, Berlin* (pp. 1–14).
- Ahlquist, S., & Menges, A. (2013). Frameworks for Computational Design of Textile Micro-Architectures and Material Behavior in Forming Complex Force-Active Structures. In *Proceedings of the 33rd Annual Conference of the Association for Computer Aided Design in Architecture (ACADIA)* (pp. 281–292). Cambridge.
- Barfield, W. (2015). *Fundamentals of wearable computers and augmented reality*. CRC Press.
- Bernert, K. (2018, September). Facade made of blue and white membrane Panels, Russia Nizhniy Novgorod Stadium. *TensiNews*, pp. 16–17.
- Bouaziz, S., Martin, S., Liu, T., Kavan, L., & Pauly, M. (2014). Projective Dynamics: Fusing Constraint Projections for Fast Simulation. *ACM Transactions on Graphics*, 33(4), 154:1–154:11.
- Dupont, S. (2014, September). Architectural shrouding: A second skin for façade and ceiling, Riyadh, Saudi Arabia King Fahad National Library. *TensiNews*, pp. 12–13.
- Gengnagel, C., La Magna, R., Ramsgaard Thomsen, M., & Tamke, M. (2018). Shaping hybrids--Form finding of new material systems. *International Journal of Architectural Computing*, 16(2), 91–103.
- Hensel, M. U., & Menges, A. (2008). Membrane spaces (Architectural design), 78(192)), 74–79.
- Holden Deleuran, A., Schmeck, M., Quinn, G., Gengnagel, C., Tamke, M., & Ramsgaard Thomen, M. (2015). The Tower: Modelling, Analysis and Construction of Bending Active Tensile Membrane Hybrid Structures. In *Future Visions - Proceedings of the IASS Annual Symposium 2015*. Amsterdam, The Netherlands.
- La Magna, R., Fragkia, V., Noël, R., Baranovskaya, Y. S., & Thomsen, M. R. (2018). Isoropia: an Encompassing Approach for the Design, Analysis and Form-Finding of Bending-Active Textile Hybrids. In S. A. Caitlin Mueller (Ed.), *Creativity in Structural Design*. Boston, USA: MIT.
- Längst, P., Bauer, A. M., La Magna, R., & Lienhard, J. (2018). Isogeometric Methods at the Interface of Architecture and Engineering. In *Creativity in Structural Design - Proceedings of the IASS Annual Symposium - 2018*. Boston.
- Lienhard, J., Bergmann, C., La Magna, R., & Runberger, J. (2017). A collaborative model for the design and engineering of a textile hybrid structure. In B. A. Manfred (Ed.), *Proceedings of the IASS Annual Symposium 2017 "Interfaces: architecture . engineering . science."* Hamburg, Germany.
- Lienhard, J., La Magna, R., & Knippers, J. (2014). Form-finding bending-active structures with temporary ultra-elastic contraction elements. In *Mobile and Rapidly Assembled Structures IV* (Vol. 1, pp. 107–115). Southampton, UK: WIT Press.

Lyll, S., & Herron Associates. (1992). *Imagination Headquarters: Herron Associates*. Phaidon.

Nicholas, P., Zwierzycki, M., Nørgaard Clausen, E., Hutchinson, C. R., & Thomsen, M. (2017). Adaptive Robotic Fabrication For Conditions Of Material Inconsistency Increasing The Geometric Accuracy Of Incrementally Formed Metal Panels. In A. Menges, B. Sheil, R. Glynn, & M. Skavara (Eds.), *Fabricate: Rethinking Design and Construction - Proceedings of Fabricate 2017* (pp. 114–121). Stuttgart: UCL Press.

Philipp, B., Breitenberger, M., D’Auria, I., Wüchner, R., & Bletzinger, K.-U. (2016). Integrated design and analysis of structural membranes using the Isogeometric B-Rep Analysis. *Computer Methods in Applied Mechanics and Engineering*, 303, 312–340.

Popescu, M., Reiter, L., Liew, A., Van Mele, T., Flatt, R. J., & Block, P. (2018). Building in Concrete with an Ultra-lightweight Knitted Stay-in-place Formwork: Prototype of a Concrete Shell Bridge. *Structures*, 14, 322–332.

Quinn, G., Deleuran, A. H., Piker, D., Tamke, M., Brandt-Olsen, C., Thomsen, M. R., & Gengnagel, C. (2016). Calibrated and Interactive Modelling of Form-Active Hybrid Structures. In *Proceedings of the IASS Annual Symposium 2016 “Spatial Structures in the 21st Century.”* Tokyo, Japan.

Sabin, J. E. (2013). myThread Pavilion: Generative Fabrication in Knitting Processes. In *Proceedings of the 33rd Annual Conference of the Association for Computer Aided Design in Architecture (ACADIA)* (pp. 347–354). Cambridge.

Solly, J., Frueh, N., Saffarian, S., Prado, M., & Menges, A. (2018). ICD/ITKE Research Pavilion 2016/2017: Integrative Design of a Composite Lattice Cantilever. In S. A. Caitlin Mueller (Ed.), *Proceedings of the IASS Symposium 2018*. Massachusetts Institute of Technology.

Tamke, M., Baranovskaya, Y., Deleuran, A. H., Monteiro, F., Stranghöner, N., Uhlemann, J., ... Thomsen, M. R. (2016). Bespoke Materials For Bespoke Textile Architecture. In *Proceedings of the IASS Annual Symposium 2016 “Spatial Structures in the 21st Century.”* Tokyo, Japan.

Tamke, M., & Thomsen, M. R. (2009). Implementing digital crafting: developing: it’s a SMALL world. In *Design Modelling Symposium Berlin*. University of the Arts.

Thomsen, M. R., Tamke, M., Deleuran, A. H., Tinning, I. K. F., Evers, H. L., Gengnagel, C., & Schmeck, M. (2015). Hybrid Tower, Designing Soft Structures. In Thomsen, M.R., Tamke, M., Gengnagel, C., Faircloth, B., Scheurer, F. (Ed.), *Modelling Behaviour* (pp. 87–99). Copenhagen: The Royal Danish Academy of Fine Arts, Schools of Architecture, Design and Conservation.

Thomsen, M. R., Tamke, M., Karmon, A., Underwood, J., Gengnagel, C., Stranghöner, N., & Uhlemann, J. (2016). Knit as bespoke material practice for architecture. In K. V. S. A. M. Del Campo Geoffrey Thün (Ed.), *Proceedings of the 36th Annual Conference of the Association for Computer Aided Design in Architecture (acadia): Posthuman Frontiers: Data, Designers, and Cognitive Machines, 2016* (pp. 280–289). Ann Arbor .

Thomsen, M. R., Tamke, M., Karmon, A., Underwood, J., Gengnagel, C., Stranghöner, N., & Uhlemann, J. (2016). Knit as bespoke material practice for architecture. In K. V. S. A. M. Del Campo Geoffrey Thün (Ed.), *Proceedings of the 36th Annual Conference of the Association for Computer Aided Design in Architecture (acadia): Posthuman Frontiers: Data, Designers, and Cognitive Machines, 2016* (pp. 280–289). Ann Arbor.

Proceedings of the TensiNet Symposium 2019

Softening the habitats / 3-5 June 2019, Politecnico di Milano, Milan, Italy

Alessandra Zanelli, Carol Monticelli, Marijke Mollaert, Bernd Stimpfle (Eds.)

Bending-active frame: analysis and estimation of structural parameters

Andrei V. CHESNOKOV*, Ivan V. DOLMATOV*, Vitalii V. MIKHAILOV*

*Lipetsk State Technical University

Moskovskaya street 30, Lipetsk 398600, Russian Federation

andreychess742@gmail.com

Abstract

Bending-active frame, considered in the research, consists of high-strength low-modulus beams, hinged struts and flexible cables. The beams, forming the top chord of the frame, are initially straight. Cable tensioning results in substantial deformation of the beams, and the frame turns into an arch or dome-shaped structure. Specialized software packages of nonlinear structural design require that parameters of the frame would be known in advance, before the analysis. The present work is aimed at estimation of initial span of the frame and the diameter of the top-chord beam. The parameters are checked for compliance with system requirements. The differential equation of a curved beam (the Euler–Bernoulli law for large deformations) is used. The results are verified by comparison with data, provided by the computer software of nonlinear analysis EASY. The present work contributes to the process of design of bending-active structures. It facilitates preliminary calculations required for approval or rejection of a specific design solution. The results of the work may also be used for structural optimization of the bending-active frame in order to obtain its geometrical dimensions and cable tensioning, which correspond to the minimum consumption of material. The work allows to expand the field of application of non-metallic constructions, which require smaller environmental footprint.

Keywords: pre-stressed, flexible beam, fiber reinforced polymer, bending-active

DOI: 10.30448/ts2019.3245.13

Copyright © 2019 by A.V. Chesnokov, V.V. Mikhailov, I.V. Dolmatov. Published by Maggioli SpA with License Creative Commons CC BY-NC-ND 4.0 with permission.

Peer-review under responsibility of the TensiNet Association

1. Introduction

The frame, considered in the research, belongs to bending-active structures, which “derive their geometry from the elastic deformation of initially straight elements” (Knippers, Cremers, Gabler and Lienhard, 2011). Bending-active structures with flexible pre-stressed membrane are state-of-the-art constructions having significant potential for possible applications (Lienhard, 2012). The frame, considered in the research, is capable to sustain assembly loads without the membrane attached and the loads caused by the membrane during its hanging, tensioning and operation. It simplifies the construction process in comparison to structures, “which only have sufficient stability through the interaction of stiff and flexible elements” (Seidel, 2009).

The top chord of the frame is made of high-strength low-modulus beams 3, supported by hinged struts and steel cables underneath (figure 1, a) (Chesnokov, Mikhaylov and Dolmatov, 2017). The beams are initially straight. They are situated in a common plane and arranged in parallel or radial directions. Tensioning of cable 1 transforms the frame from its original, so-called “flat”, configuration into the operational or dome-shaped one. The joints of the top chord should be implemented according to the specialized design guides, for example (FIBERLINE, 2019). Steel sleeves are to be provided in connections for protection of fiberglass beams.

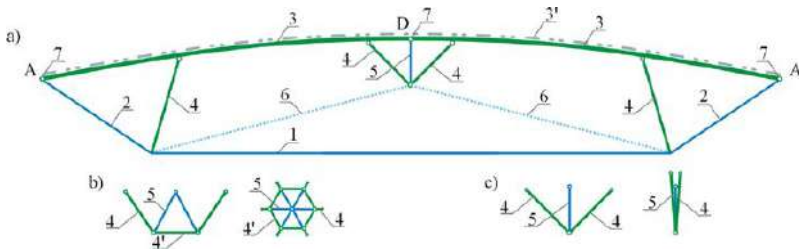


Figure 1: The frame, considered in the research. a – general view; b, c – central lattice structures (different embodiments). 1 – tensioning cable, 2 – diagonal cable, 3, 3’ – top chord beams (different embodiments), 4, 4’ – hinged struts, 5 – central tie, 6 – additional tie, 7 – hinge at the end of the beam

The outer ends of the beams are pivotally connected to the supports of the frame at points A and A’. Due to high slenderness it is proposed to apply half-span (short) beams 3 linked together by hinges 7 (point D, figure 1, a), rather than full-span (long) beam 3’, connecting the opposite supports. It allows to achieve compact size of the frame, prepared for transportation from one site to the other.

In order to rigidly unite the beams, lattice structures of two types are considered (figure 1, b, c). The structures consist of hinged struts 4, 4’ and flexible ties 5.

The first embodiment of the lattice structure (figure 1, b) is derived from (Chesnokov, Mikhaylov and Dolmatov, 2015). It improves stability of the top chord in, so-called, out-of-plane direction. On the other hand, flexible polymer membrane, attached to the top chord, performs a similar function preventing compressed members from buckling in the horizontal direction (Mele, Laet, Veenendaal, Mollaert and Block, 2013). The second embodiment or triangular-like lattice structure consists of fewer members. It can be easily adjusted in-situ. The structure of the second type, even if applied in the spatial frame, can be compactly folded (figure 1, c, right), while the ring-shaped bottom chord of the first embodiment (figure 1, b, right) complicates packaging, increasing transportation expenditures.

Non-uniform load may result in substantial deformations of the frame, but installation of additional ties 6 ensures its serviceability reducing the deflections to an appropriate level (Chesnokov, Mikhaylov and Dolmatov, 2017). Unlike direct connection of additional ties 6 to the beams, the lattice structures allow to adjust stresses and moments in the top chord.

The frame, considered in the research, is proposed to be delivered to the construction site in form of particular members: top chord beams 3 with struts 4, the central lattice structure in folded configuration and the cables with anchors. Having assembled the frame, pre-stressing is implemented by means of tensioning devices, such as turnbuckles or threaded rods. When the desired frame shape is reached, the devices are replaced with connecting links (Seidel, 2009).

The present work is aimed at estimation of initial span of the frame and the diameter of the top-chord beam. It allows to facilitate structural analysis of the frame using specialized software packages of nonlinear design and contributes to the process of optimization in order to achieve minimum consumption of material. The parameters of the frame are checked for compliance with system requirements, such as the strength properties and the conditions of compressive buckling of the top-chord. The differential equation of a curved beam is used.

2. Parameters of the frame

It is assumed in the research, that the beams of the frame are of a tubular cross section, and the pre-stress of the frame is performed by means of cable 1 tensioning. The plain model of the frame is taken into account. Parameters, considered in the research, may be broken down into the following groups:

- geometrical dimensions (given parameters are marked with red color in figures 2 and 3): initial frame span S_0 and the span S_1 of the frame in the operational state, horizontal dimensions a_0 , b_0 , c_0 and angles between the frame members α_0 , β_0 and γ_0 ;

- tensioning of cable 1 ΔL_p ;
- material properties: the modulus of elasticity and the strength of the beam and the cables - E_b , R_b and E_{cab} , R_{cab} , respectively;
- properties of the frame members: cross section area of the cables A_{cab} , diameter of the beam D_b and thickness-to-diameter ratio k_t .

Material properties are assumed to be given in advance. According to (PFEIFER, 2017) the properties of steel cables are the following: $E_{cab} = 130$ GPa and $R_{cab} = 700$ MPa. The beams should be made of materials with the ratio $R_b / E_b \geq 2.5$ (Lienhard, Alpermann, Gengnagel and Knippers, 2013). Pultruded glass-fiber reinforced polymer (FIBERLINE, 2019) is an appropriate material for this purpose due to its superior properties: $E_b = 24$ GPa and $R_b = 185$ MPa. These values are, however, for short-term use only (Kotelnikova-Weiler, Douthe, Hernandez, Baverel, Gengnagel and Caron, 2013).

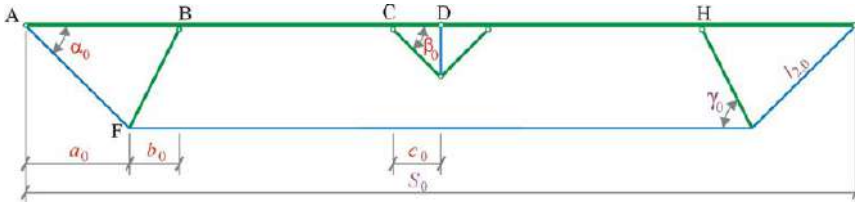


Figure 2. Geometrical parameters of the frame

The following condition, regarding to the linear dimensions of the frame, may be written:

$$a_0 + b_0 + c_0 \leq S_0 / 2 \tag{1}$$

Angle dimensions α_0 and β_0 are assumed to be in the range $[20...70]^\circ$. Low bound for the angle α_0 is also determined by the following condition:

$$\alpha_0 - \Delta\alpha > \alpha_{lim} \tag{2}$$

where $\Delta\alpha$ is the angle alteration by the frame transformation into the operational state (figure 3), α_{lim} is a given limiting value for the angle α .

3. Determination of the initial frame span S_0

The span of the frame in the operational state S_1 is considered to be given. Thus, the span S_0 is to be determined in order to obtain the initial lengths of the frame members.

It is approximately assumed, that the triangle ABF rotates like a rigid body, while the internal part of the frame, situated between points B and H, takes on parabola-like shape with the span S_p and the rise f_p (figure 3).

The length of the parabola is determined by the following simplified expression:

$$L_p = S_p + \frac{8}{3} \cdot \frac{f_p^2}{S_p} \quad (3)$$

It is approximately equal to the unstressed length of the beam parts, situated between points B-D and H-D:

$$L_p \approx S_0 - 2 \cdot (a_0 + b_0) \quad (4)$$

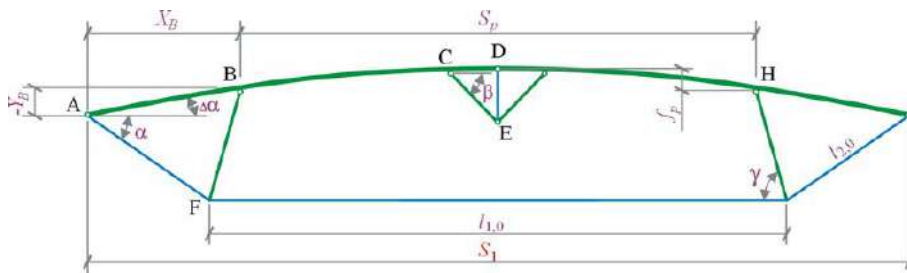


Figure 3. The frame configuration in the operational state

Line AB passes along the tangent to the parabola at the end point:

$$\tan(\Delta\alpha) = 4 \cdot \frac{f_p}{S_p} \quad (5)$$

Substituting the ratio f_p / S_p from (5) into (3) gives:

$$\cos(\Delta\alpha) = \frac{1}{\sqrt{6 \cdot L_p / S_p - 5}} \quad (6)$$

On the other hand:

$$\cos(\Delta\alpha) = \frac{S_1 - S_p}{2 \cdot (a_0 + b_0)} \quad (7)$$

Substituting (4) and (7) into (6), the dependence for the initial span of the frame S_0 is derived:

$$S_0 = \left[2 \cdot \left(\frac{a_0 + b_0}{S_1 - S_p} \right)^2 + 2.5 \right] \cdot \frac{S_p}{3} + 2 \cdot (a_0 + b_0) \quad (8)$$

The expression for the span S_1 is the following:

$$S_1 = l_{1,0} + 2 \cdot l_{2,0} \cdot \cos(\alpha_0 - \Delta\alpha) \quad (9)$$

where $l_{1,0}$ and $l_{2,0}$ are the initial lengths of the cables, forming the bottom chord (figure 3):

$$l_{1,0} = S_0 - 2 \cdot a_0 - \Delta L_p, \quad l_{2,0} = a_0 / \cos(\alpha_0).$$

Substituting (8) into (9), considering (7), the following equation in one unknown is derived:

$$\Theta(\Delta\alpha) = S_1 + \Delta L_p - 2 \cdot b_0 \quad (10)$$

where

$$\Theta(\Delta\alpha) = 2 \cdot a_0 \cdot (\cos(\Delta\alpha) + \tan(\alpha_0) \cdot \sqrt{1 - \cos(\Delta\alpha)^2}) + \left(\frac{1}{\cos(\Delta\alpha)^2} + 5 \right) \cdot \frac{S_1 - 2 \cdot (a_0 + b_0) \cdot \cos(\Delta\alpha)}{6} \quad (11)$$

Having obtained the angle $\Delta\alpha$ from (10) by a diagram or numerically, the initial span of the frame S_0 is calculated from (8), considering (7).

4. Estimation of the diameter of the beam

4.1. Structural behavior of the beam

The shape of the beam may be approximately represented as follows (figures 3, 4):

– segment A-B ($0 \leq x < X_B$, $X_B = (a_0 + b_0) \cdot \cos(\Delta\alpha)$):

$$Y(x) = -x \cdot \tan(\Delta\alpha) \quad (12)$$

– segment B-D ($X_B \leq x \leq X_D$, $X_D = 0.5 \cdot S_1$ and $Y_B = -(a_0 + b_0) \cdot \sin(\Delta\alpha)$):

$$Y(x) = \frac{4 \cdot f_p}{S_p^2} \cdot (x - X_B) \cdot (x - X_B - S_p) + Y_B \quad (13)$$

The differential equation of a beam, subjected to bending, is the following (Fertis, 2006):

$$\frac{Y''(x)}{(1 + Y'(x)^2)^{1.5}} = -\frac{M(x)}{E_b \cdot I_b} \quad (14)$$

where $M(x)$ is a bending moment at point x of the beam; I_b is the second moment of area of the beam.

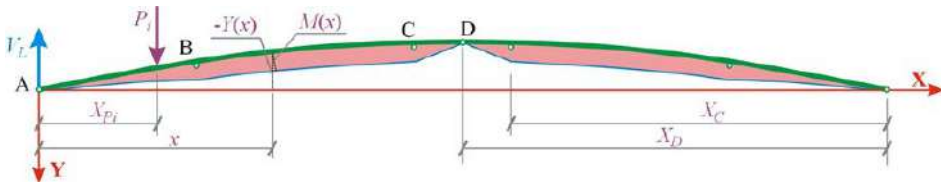


Figure 4. Schematic diagram of bending moments in the beam

Diagram of bending moments in the beam of the frame is shown in the figure 4. In case of symmetric load distribution, the moments are also symmetric relatively to the vertical axis, passing through the point D. Expressions for the moments $M(x)$ are the following:

– segment A-B ($0 \leq x < X_B$):

$$M_{A-B}(x) = m_{ab}(x) \quad (15)$$

where $m_{ab}(\xi) = N_2 \cdot (Y(\xi) \cdot \cos(\alpha) - \xi \cdot \sin(\alpha)) + M_{LD}(\xi)$; N_2 is the force in the cable 2 (figure 1); $M_{LD}(\xi)$ is the bending moment, brought about by external loads P_i situated on the left relatively to the corresponding section ξ of the beam:

$$M_{LD}(\xi) = V_L \cdot \xi - \sum_i P_i \cdot (\xi - X_{Pi}) \quad (16)$$

where V_L is the vertical support reaction, brought about by the external loads; X_{Pi} is the load coordinate, $X_{Pi} < \xi$; $\alpha = \alpha_0 - \Delta\alpha$ is the angle between the cable and the horizontal axis;

– segment B-C ($X_B \leq x < X_C$, $X_C = 0.5 \cdot S_1 - c_0$):

$$M_{B-C}(x) = m_{bc}(x) \quad (17)$$

where $m_{bc}(\xi) = m_{ab}(\xi) + N_2 \cdot \sin(\alpha) \cdot [(Y(\xi) - Y(X_B)) / \tan(\gamma) + \xi - X_B]$; $\gamma = \gamma_0 + \Delta\alpha$;

– segment C-D ($X_C \leq x \leq X_D$):

$$M_{C-D}(x) = m_{bc}(x) + m_{bc}(X_D) \cdot \frac{X_C - x}{X_D - X_C} \quad (18)$$

Maximum stress in the beam σ_b must be less than the strength of the material:

$$\sigma_b < R_b \quad (19)$$

The stress is expressed according to (FIBERLINE, 2019) as follows:

$$\sigma_b = \frac{N_b}{A_b} + \frac{1}{1 - \frac{N_b}{N_{cr}}} \cdot \frac{|M_{b,\max}|}{W_b} \quad (20)$$

under the condition:

$$N_b < N_{cr} = \frac{F_d}{1 + F_d / N_{el}} \quad (21)$$

where $F_d = A_b \cdot R_b$ and N_{el} is the Euler load $N_{el} = \pi^2 \cdot E_b \cdot I_b / (K \cdot L_u)^2$, where K is the effective length factor and L_u is the length of a half of an arch, formed by the curved beam (EN 1993-2:2006).

The maximum moment $M_{b,\max}$ is obtained from (15), (17), (18), while the axial force in the beam N_b , the second moment of area I_b , the cross section area A_b and the elastic section modulus W_b are expressed as follows:

$$N_b = N_2 \cdot k_b \quad (22)$$

where $k_b = \sin(\alpha_0 + \gamma_0) / \sin(\gamma_0 + \Delta\alpha)$ and

$$I_b = \frac{\pi \cdot D_b^4}{8} \cdot k_t \cdot (1 - k_t) \cdot [2 \cdot k_t \cdot (k_t - 1) + 1] \quad (23)$$

$$A_b = I_b \cdot \frac{8}{D_b^2 \cdot [2 \cdot k_t \cdot (k_t - 1) + 1]} \quad (24)$$

$$W_b = \frac{2 \cdot I_b}{D_b} \quad (25)$$

4.2. Estimation of the upper bound for the diameter of the beam

Lets consider the stage of the frame pre-stress. In the assumption, that own weight of the frame is negligible, external loads P_i are omitted and $M_{LD(x)} = 0$. Thus, bending moments in the beam may be expressed as follows:

$$M(x) = M_1(x) \cdot N_{2,pr} \quad (26)$$

where index “pr” refers to the stage of the frame pre-stress; $M_1(x)$ is the moment in x -section of the beam (15), (17), (18), considering the force in the cable $N_2 = 1$.

The differential equation (14) may be written for the point B as follows:

$$\frac{8 \cdot f_p \cdot S_p}{[S_p^2 + 16 \cdot f_p^2]^{3/2}} = \frac{-M_1(X_B)}{E_b} \cdot \mu \quad (27)$$

where μ is the ratio:

$$\mu = N_{2,pr} / I_b \quad (28)$$

Having obtained μ -value from (27), the upper bound for the diameter of the beam $D_b < D_{lim,up}$ is expressed from the conditions (19) and (21) as follows:

$$D_{lim,up} = \min \left\{ \frac{-\lambda_1 \cdot \mu + \sqrt{(\lambda_1 \cdot \mu)^2 + 8 \cdot \lambda_2 \cdot \mu \cdot R_b}}{2 \cdot \lambda_2 \cdot \mu}, \sqrt{\frac{8 \cdot R_b}{2 \cdot k_t \cdot (k_t - 1) + 1} \cdot \left[\frac{1}{\mu \cdot k_b} - \frac{1}{E_b} \cdot \left(\frac{K \cdot L_u}{\pi} \right)^2 \right]} \right\} \quad (29)$$

where

$$\lambda_1 = \frac{|M_{1,max}|}{1 - \left(\frac{K \cdot L_u}{\pi} \right)^2 \cdot \frac{\mu \cdot k_b}{E_b}} \quad \text{and} \quad \lambda_2 = \frac{k_b}{4} \cdot [2 \cdot k_t \cdot (k_t - 1) + 1] \quad (30)$$

where $M_{1,max}$ is the maximum moment in the beam, considering $N_2 = 1$ and $M_{LD(x)} = 0$.

4.3. Estimation of the lower bound for the diameter of the beam

The lower bound for the diameter of the beam $D_b \geq D_{lim,low}$ is proposed to be found in the step-by-step manner. Having started from the minimum permissible value $D_{b,min}$, the diameter of the beam D_b is incremented until the conditions (19) and (21) are fulfilled and the lower bound is reached $D_{lim,low} = D_b$. If, however, $D_{lim,low} > D_{lim,up}$, the set of structural

parameters, such as geometrical dimensions, cable tensioning and material properties, is not permissible for the given value of external load.

The diagonal cable force $N_{2,Ld}$, needed to calculate the force N_b and the moment $M_{b,max}$ in the beam, is obtained from the following expression:

$$N_{2,Ld}(D_b) = N_{2,pr}(D_b) + \Delta N_2 \quad (31)$$

where $N_{2,pr}(D_b)$ is expressed from (28), considering (23); ΔN_2 is the force alteration, brought about by the external load:

$$\Delta N_2 = \frac{- \int_0^{x_p} M_1(x) \cdot M_{LD}(x) \cdot \sqrt{1 + \left(\frac{d}{dx} Y(x)\right)^2} dx}{\int_0^{x_D} [M_1(x)]^2 \cdot \sqrt{1 + \left(\frac{d}{dx} Y(x)\right)^2} dx} \quad (32)$$

where $Y(x)$ is the shape function of the beam, given by (12) and (13).

The expressions (31) and (32) are obtained by the flexibility method, which is valid for small shape alterations of the frame in case of symmetrical external loading.

5. Case study

The frame with the following parameters is considered as an example: the span $S_1 = 12.0$ m, horizontal dimensions $a_0 = 1.5$, $b_0 = 0.0$, $c_0 = 1.0$ m, angles between the frame members $\alpha_0 = 45^\circ$, $\beta_0 = 45^\circ$ and thickness-to-diameter ratio of the tubular beam $k_t = 1/20$. Tensioning of the cable 1 is assumed $\Delta L_p = 1.0$ m. Uniformly distributed external load $q_{LD} = 0.5$ kN/m is taken into account for operational stage of the frame.

From the equation (10), considering (11), the angle alteration is obtained the following $\Delta\alpha = 16.7^\circ$, the span of the parabola is calculated from (7) $S_p = 9.127$ m and the initial span of the frame is obtained from (8) $S_0 = 12.263$ m. Equation (27) allows to determine μ -value, $\mu = 1.307 \cdot 10^6$ kN/m⁴, while the upper bound for the diameter of the beam is obtained from (29) $D_{lim,up} = 0.153$ m, considering the effective length factor $K = 1.04$ (EN 1993-2:2006) (two-hinged arch with rise-to-span ratio 0.1) and the length of a half of the arch $L_u = S_0 / 2 = 6.132$ m.

Having calculated the force alteration $\Delta N_2 = 5.33$ kN, considering (17), (20), (22)-(25) and (31), the appropriate beam diameter $D_b = 0.125$ m is found from the conditions (19) and (21): $\sigma_b / R_b = 0.99$ and $N_b / N_{cr} = 0.35$.

In order to verify results, obtained by the proposed expressions, numerical simulation of the bending-active frame is performed by means of the software package of structural analysis EASY. After the stage of the pre-stress, the span of the frame is $S_{1,EAS} = 12.025$ m (discrepancy is $\varepsilon = 0.2\%$), the angle alteration $\Delta\alpha_{EAS} = 17.3^0$ ($\varepsilon = 3.6\%$) and the distance between points B and H (figure 3) is $S_{p,EAS} = 9.159$ m ($\varepsilon = 0.4\%$), where index “EAS” refers to results, obtained by the EASY software and ε is the relative discrepancy between the proposed results and the results by EASY. The force alteration, caused by the external load, is $\Delta N_{2,EAS} = 5.3$ kN ($\varepsilon = 0.6\%$). The conditions (19) and (21) are fulfilled as well: $\sigma_{b,EAS} / R_b = 0.93$ ($\varepsilon = 6.5\%$) and $N_{b,EAS} / N_{cr} = 0.36$ ($\varepsilon = 2.9\%$).

6. Conclusion

Light-weight bending-active frame is considered in the research. It requires less expenditures for transportation and installation, than ordinary building constructions. The frame is intended for temporary sheltering of areas of social occasions, entertaining events, points of retail, bus stations, etc.

In accordance to (Lienhard, Alpermann, Gengnagel and Knippers, 2013) the proposed work belongs to, so-called, “geometry based approach”, which uses analytical techniques for structural simulation of bending-active systems. On the other hand, it provides essential data for rapidly developing “integral” approach, which is based on specialized software packages of nonlinear structural design.

The present work contributes to the development of bending-active structures. It facilitates the conceptual design stage, allowing to consider a lot of competing design options and to select the best one. The results of the work may also be used for structural optimization of the bending-active frame. The work allows to expand the field of application of non-metallic constructions, which require smaller environmental footprint.

The future work should take into account arbitrary external load distribution, including loads in the horizontal direction. Time-dependent material behavior and temperature variations during the operational period are to be considered.

References

Chesnokov A.V., Mikhaylov V.V. and Dolmatov I.V. (2015), Development of the hybrid dome and research of its behavior under load. In: *Proceedings of the VII international conference on textile composites and inflatable structures*. Barcelona, 19-21 October 2015, (pp. 469-476).

Chesnokov A.V., Mikhaylov V.V. and Dolmatov I.V. (2017), Bending-active dome-shaped structure. In: *Proceedings of the VIII international conference on textile composites and inflatable structures*. Munich, 9-11 October 2017, (pp. 427 – 435).

EN 1993-2:2006. *Eurocode 3. Design of steel structures. Part 2: Steel Bridges* (2006). Brussels: EUROPEAN COMMITTEE FOR STANDARDIZATION.

Fertis D.G. (2006), *Nonlinear structural engineering with unique theories and methods to solve effectively complex nonlinear problems*. Berlin Heidelberg: Springer.

FIBERLINE Composites. Design Manual. Retrieved January 9, 2019, from <https://fiberline.com/design-manual>

Knippers J., Cremers J., Gabler M. and Lienhard J. (2011), *Construction Manual for Polymers + Membranes*. Munchen: Institut fur internationale Architektur-Dokumentation.

Kotelnikova-Weiler N., Douthe C., Hernandez E.L., Baverel O., Gengnagel C. and Caron J.F. (2013), Materials for actively-bent structures. In: *International Journal of Space Structures*. Vol. 28, No. 3-4 (pp. 229-240).

Lienhard J. (2012), Bending-active membrane structure. In: *Tensinews*. No. 22 (p. 9).

Lienhard J., Alpermann H., Gengnagel C. and Knippers J. (2013), Active bending, a review on structures where bending is used as a self-formation process. In: *International Journal of Space Structures*, vol. 28, No. 3 & 4 (pp. 187-196).

PFEIFER Tension Members (2017): PFEIFER seil- und hebetechnik GMBH. Retrieved January 8, 2019, from <https://www.pfeifer.info/en/pfeifer-group/business-units/cable-structures/>.

Seidel M. (2009), *Tensile surface structures: a practical guide to cable and membrane construction*. Berlin: Ernst and Sohn.

Van Mele T., De Laet L., Veenendaal D., Mollaert M. and Block P. (2013), Shaping tension structures with actively bent linear elements. In: *International Journal of Space Structures*. Vol. 28, No. 3-4 (pp. 127-135).

Integration of form-finding, analysis process and production of a bending-active textile hybrid into one model

Rens VORSTERMANS*, Jasper VAN WIJK^a, Patrick TEUFFEL^b, Arjan HABRAKEN^b,
Rogier HOUTMAN^a

*Tentech BV, Rotsoord 9A, NL-13523CL Utrecht, Netherlands, rens@tentech.nl

^a Tentech BV, Rotsoord 9A, NL-13523CL Utrecht, Netherlands

^b Eindhoven University of Technology, P.O. box 513, 5600 MB Eindhoven, Netherlands

Abstract

The goal of this research is integrating the form-finding, analysis process and production of bending-active textile hybrids (BATH) into one model, in these systems bending-active elements are combined with membrane elements. For this project Easy FSCB is used which is a software package for the engineering of membrane structures. The simultaneous form-finding approach is used which is described by Lienhard (Lienhard, 2014). Here first the bending-active element is form-found, followed by the coupled form-finding process of the membrane. Now the membrane is attached to the bending-active element in the form-finding process. To simulate the bending-active behavior in Easy FSCB, the Local Coordinate System of each beam link is manually adjusted. Here the initially straight configuration of the bending-active element is implemented. In fact, the beam links want to reset to its initial straight configuration but are attached to the membrane. In the next step the calculation of the hybrid system is executed. Here the Force-density method is used to form-find the membrane according to the deformation of the bending-active element. For validating purposes, a scale model is constructed. In fact, a prototype of the workflow described in this project. The already determined routines of Easy are used in producing the prototype including cutting patterning, compensating and plotting.

Keywords: Active Bending (softening), form-finding, statical analysis, integration, production process, installation sequence

DOI: [10.30448/ts2019.3245.33](https://doi.org/10.30448/ts2019.3245.33)

Copyright © 2019 by Rens Vorstermans, Jasper Van Wijk Patrick Teuffel, Arjan Habraken, Rogier Houtman. Published by Maggioli SpA with License Creative Commons CC BY-NC-ND 4.0 with permission.

Peer-review under responsibility of the TensiNet Association

1. Introduction

Lightweight structures have never been more contemporary and necessary than today. Especially temporary lightweight structures are more and more used in the current built environment. For example, if we compare the number of music or big sports events to that of 25 years ago, it can be concluded that there is an increasing demand for temporary safe structures in this sector. It's the architect's and structural engineer's task to facilitate these structures in the most efficient, aesthetic and safe way. The principles of lightweight engineering are used in combination with the daily developing simulation and analysis tools to reach this goal.

Even more efficient lightweight systems can be constructed while combining the principles of lightweight membrane engineering with bending-active elements. In fact, bending-active elements store bending energy which can be used in pre-stressing, in this case, membrane elements. The need of the bending-active elements to go back to its initial configuration is pre-stressing the membrane elements. Another advantage of building with bending-active elements is that a curved geometry can be achieved by just bending the elements instead of producing actual curved elements. Initial straight or planar elements are used to produce double curved building envelopes.

The goal of this research is integrating the form-finding, analysis process and production of bending-active textile hybrids (BATH) into one model. This model will also contain the information to realize the final model. For this project Easy is used which is a software package for the engineering of membrane structures.

The research on bending-active structures by Julian Lienhard is used as a starting point to construct a workflow on the form-finding process of these hybrid systems. First, the bending-active element is form-found, followed by the coupled form-finding process of the membrane. Here the membrane is attached to the bending-active element in the form-finding process. This will result in an updated membrane geometry according to the deformation of the hybrid system. In fact, both elements in the model are optimized to the behavior of the hybrid system (see BATH by Ahlquist in Figure 1).



Figure 1: SensoryPLAYSCAPE v1.0 (Ahlquist Sean, 2017)

The Local Coordinate System (LCS) of the beam links which are the bending-active elements in the model is reset to an initial straight configuration. In fact, the beam links want to reset to its initial straight configuration but are restrained to the membrane. In the next step, the calculation of the hybrid system is executed. Here the Force-density method is used to find the membrane according to the deformation of the bending-active element.

For validating purposes, a scale model is constructed. A prototype of the workflow described in this research to design and construct a bending-active textile hybrid. The already determined routines in Easy are used in producing the prototype including patterning, compensating and plotting. Detailing and determining the building sequence of the prototype also contribute to the relevance of the result of the research.

The workflow presented in this paper can be used in further research of integrating bending-active elements into traditional membrane engineering.

2. Methods

2.1 BATH types

In the last decade just a few bending-active tensile textile hybrids have been built. With every new structure a new combination of words has been used to present the work. Slabbinck introduces a terminology to categorize different types of bending-active tensile hybrids (BATH) (Slabbinck, Suzuki, Solly, Mader, & Knippers, 2017). She states three important requirements to categorize these hybrid systems.

- (1) The membrane keeps the bending-active element bent
- (2) The buckling strength of the bending-active element is enhanced by the membrane
- (3) The membrane is pre-stressed and doubly curved by the bending-active element

In this research a local BATH structure is analyzed. In this type of BATH the bending-active element is coupled by itself (straight element coupled into a ring). The membrane is only deforming the coupled bending active elements into a 3D sculpture.

2.2 Local Coordinate System update (LCS update)

In this research the first step in implementing the bending-active behavior in the model is simulating theastica curve within the used software package Easy. Theastica curve describes a beam's elastic deformation. It was found that manipulating the local coordinate system of beam links would make it possible to set the initially straight configuration of beam elements, in fact resetting the LCS of every beam element. The LCS of one beam element can be defined according to 2 vectors namely the local X direction in global coordinates and the

local Y direction in global coordinates. With adjusting the LCS it is possible to implement the initially straight configuration of beam elements in a deformed state.

The Elastica curve simulation can now be explained according to LCS example 1 of Figure 2. A polyline is drawn in external CAD software and imported into Easy. In default the LCS is set along the direction of the beam links. This indicates that nothing will happen when a calculation would have been executed because the beam is already in its initial configuration. It will only deform by its own weight if this is relatively high.

In the second step the LCS is adjusted. The LCS of every beam element is set in the same direction corresponding to an initially straight configuration of the system. The calculation will result in one of the Elastica curves because the beam links will find its shape of maximal bending radius and thus minimal bending moment, within the two pinned supports. If one support would allow sliding over the x-axis the beam will tend to go to its initially straight configuration without any curvature and bending moment.

Next, a new support and 3 cables are added to the model (LCS example 2, Figure 2). The cables are connecting the beam to the new support and thus are restraining the system. When the LCS update is performed and the calculation is executed. It can be seen that the Elastica curve is restrained by the cables and the final result is tending towards the initial design curve. Now the beam again wants to find its way of minimal bending moment but is restrained by cables and 2 pinned supports. A new Elastica curve is found with new boundary conditions. The need of the beam to go back to its initial configuration is now used to tension the cable elements and find a new equilibrium. This simulation will be used in the next steps of the research to implement the bending-active behavior in a hybrid system with membrane elements.

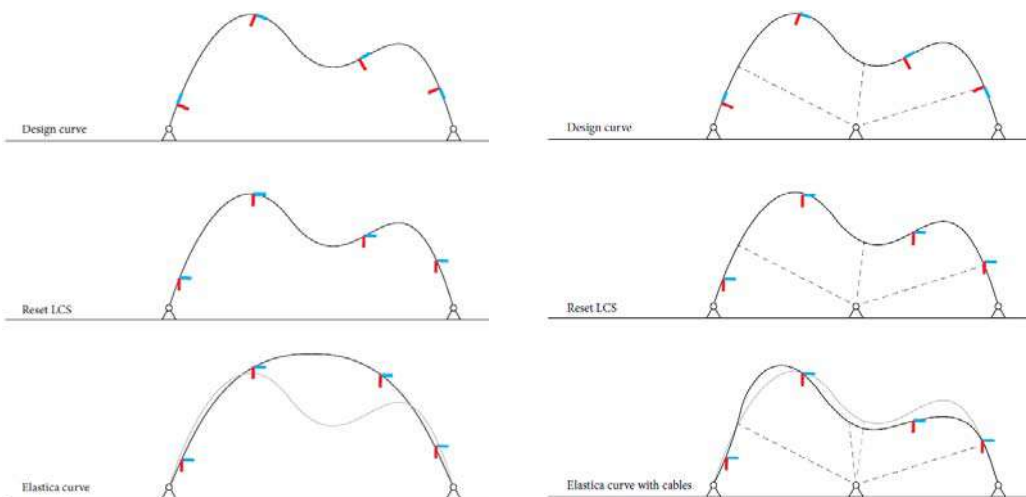


Figure 2: LCS example 1 (left), LCS example 2 (right)

2.3 Successive form-finding approach

“The process is separated into first, the form-finding of an elastically bent beam structure and second, the form-finding of the membrane attached to the beams. Here, the second form-finding step serves to generate an intricate equilibrium system which is based on further deformations in the beam structure.” (Lienhard, 2014)

In the previous section it is elaborated how the initial straight configuration of a beam element can be set to a design curve in Easy. In fact, first the elastically bent beam structure is form-found and the LCS is adjusted to an initial straight configuration. Secondly, the membrane is attached and the form-finding step can be executed using the Force Density Method. Finally, a calculation of the hybrid system is executed. The successive form-finding approach can be explained according to the following steps.

2.3.1 Geometric input

The design curve can be drawn or form-found with external CAD software and imported in Easy as a polyline. Easy translates this DWG file into an Ein-file. This Ein-file consists of point coordinates and defines the link elements. In this case the design curve is form-found with Karamba in Rhino/Grasshopper. Now the initial configuration and the design curve can be used to simulate the bending-active behavior of the beam elements.

2.3.2 Initial configuration

The local coordinate system (LCS) update is used to implement the bending-active behaviour in the calculation of the hybrid system. For the LCS update it is required to determine the initial configuration of the model.

2.3.3 Form-edit model

In the Form-edit module of Easy the mesh settings are set for the first form-finding step of the membrane. In the Form-edit model the mesh boundary and the geometry boundary can be defined separately. In other words, the fixed points of the form-finding procedure can be defined separate from the projected mesh. In the form-finding step the projected mesh will be form-found towards the fixed points of the geometry. In Figure 3 an overview is shown of the Form-edit model.

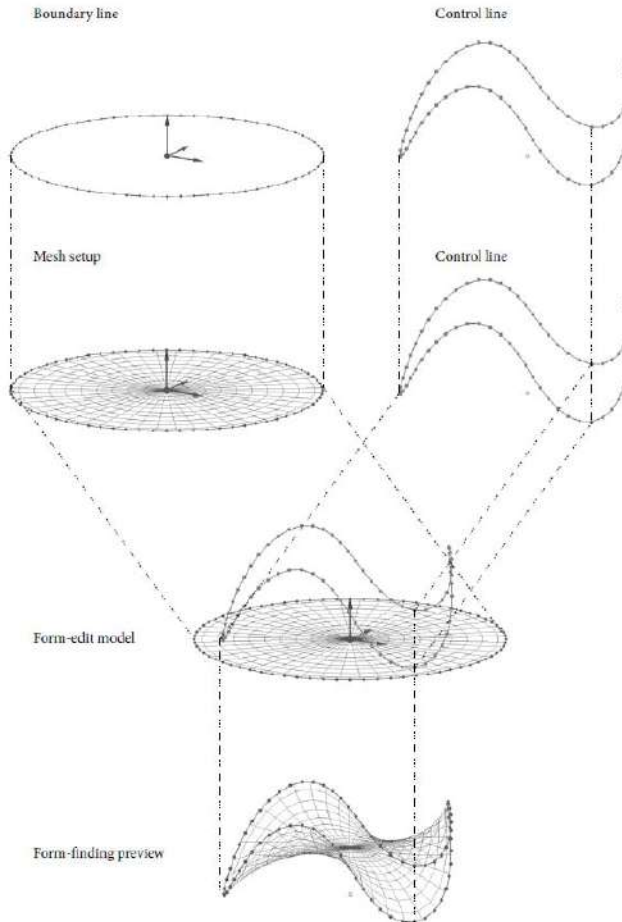


Figure 3: Form-edit model

2.3.4 Form-finding

The form-finding calculation of the membrane is executed in Easy. The Force-Density Method is used in this form-finding calculation.

The result of the form-finding calculation is again an Ein-file which contains the coordinates of the free points after the form-finding step. With these coordinates the link lengths and the new width of every link in the mesh can be calculated. This recalculation of the mesh width is needed to obtain realistic membrane stresses. The width is changed because the mesh is changed from a 2D configuration to a 3D configuration. The width of the membrane elements is calculated with a polygon file which defines polygon elements in between the points of the net.

2.3.5 Easy Beam

The calculation of the hybrid system will be executed in two different Easy Beam models. Here the form-finding result of the membrane is combined with the bending-active simulation of the beam links.

Easy Beam model (1)

In this model the membrane links can still change in length with the use of the Force Density Method. The membrane links are not translated into elastic elements but are still force-density links. Here the membrane geometry can still change according to the deformation of the bending-active element. This results in a membrane geometry which is updated according to the deformation of the beam.

Easy Beam model (2)

From the result of Easy Beam model (1) the unstressed lengths for the membrane elements in Easy Beam model (2) can be calculated.

Now the final calculation is executed with updated membrane geometry and material properties for beam and membrane element.

3. Prototype

3.1 Prototype properties

The global dimensions of the prototype are presented in the Figure 4. The membrane of the prototype is produced at Buitink Technology. The membrane consists of 12 patterns. The stiffness parameters for the used flexible membrane are 11.95 / 15.59 kN/m (warp/weft). These stiffness parameters are used to compensate the cutting patterns.

In the structural model a Young's modulus of 45 GPa is used for the material properties of the GFRP rod. The resulting geometry of the simulation model is checked on bending. The strain by bending is calculated with the height of the profile and its radius (1) where the maximal strain of the material is assumed to be 1.5%.

$$\epsilon = \frac{h}{2 \cdot R} = \frac{10}{2 \cdot 660} = 0.75\% \quad (1)$$

The minimal radius of the geometry results in the highest strain of the outer fiber, here a radius of 660mm in the model results in a strain of 0.75% with a profile with a height of 10mm. It can be concluded that it is safe to bent the 10mm rods into the desired radius.

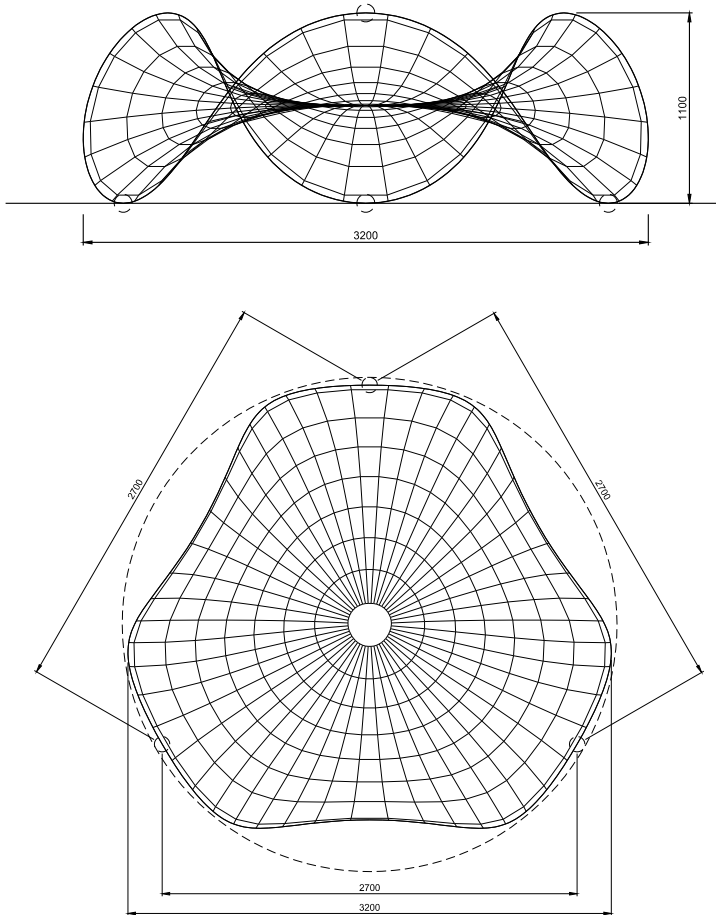


Figure 4: Dimensions of the prototype

3.1 Computational model

The model for the prototype is constructed according to the same procedure as described in the successive form-finding method. The design curve is scaled uniformly towards a total circumference of 12m. This 12m can be divided into 6 equal lengths of 2m. The material properties for the bending-active element are set according to the results of the bending test and consultation with the composite engineer ($E = 45 \text{ GPa}$). The cross section of the bending-active element in the Easy Beam model is constructed out of 3 GFRP (glass-fibre-reinforced-polymers) profiles with a diameter of 10mm.

From the Easy Beam model which is calculated with 3 profiles of diameter 10mm the membrane stresses can be extracted. These membrane stresses will be used in compensating the cutting patterns of the membrane. The cutting patterns must be compensated with the strains (Figure 5)

calculated from the membrane stresses. This is required because the cutting patterns are generated from the geometry of the stretched membrane.

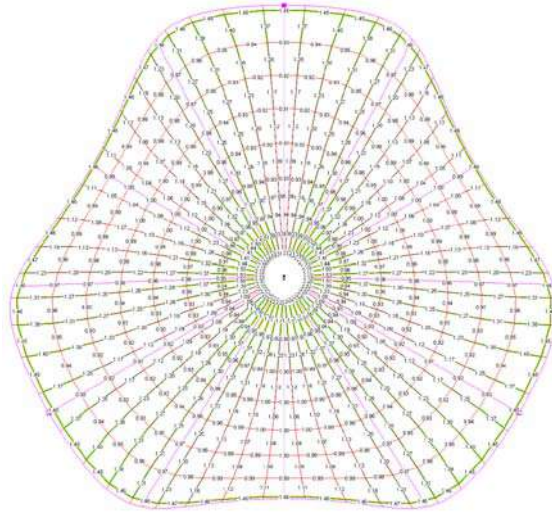


Figure 5: Membrane strains from hybrid calculation

3.2 Building sequence

The setting up of the tent is described by means of several steps. These steps are important to evenly distribute the forces in the membrane and deform the GFRP element into the 3D curve. The prototype is setup within 30 minutes with one person and 3 ground anchors. Wooden slats are used to determine the locations of the ground anchors. In order to setup the tent with one person these anchors are used to connect the GFRP ring to the low points of the tent, this is shown in Figure 6. (The membrane production and test setup is executed at Buitink Technology)



Figure 6: GFRP rings with 3 ground anchors (left), GFRP rings connected to ground anchors (right)



Figure 7: Connect low points to high points in steps

In Figure 7, it is shown that first the high and low points of the membrane are connected to the GFRP element. Thereafter the remaining points of the membrane are connected to the GFRP ring to evenly pre-stress the membrane and deform the GFRP element.



Figure 8: Prototype side view (1)

3.3 Prototype analysis

In the final computational model no horizontal supports are required to stabilize the full system. The low points of the system are free to slide and will find equilibrium with the membrane. In fact, this is required because the bending-active element must find equilibrium with the membrane and concentration of forces at fixed points must be prevented.

In contrast to the Easy Beam model, the prototype model requires the horizontal supports (anchors) to maintain in the current equilibrium state. It is measured that a force of 6kg is required in the direction of the membrane towards the common middle point to keep this shape.

It can be concluded from the test setup that there is significant stress in the membrane. The forces transferred by the S-hooks (connecting membrane to GFRP ring) corresponds to the forces in the Easy Beam model which indicate that the stresses in the membrane will correspond to the stresses in the Easy Beam model. In Table 1, the prototype is compared with the Easy Beam model. Here the high and midpoint of the models are compared. The comparison of geometry can be improved by performing it with a 3D scanner.

Table 1: Comparison of Easy Beam model with the prototype

Comparison	Easy Beam	Prototype
High point [mm]	1058	1050
Midpoint [mm]	543	550
Force in S-hooks [kN]	0.059	0.055

4. Conclusions

It can be concluded that simulating the Elastica curve and thus the bending-active behavior in beam elements with the LCS update can be used in the design and form-finding process of bending-active textile hybrids. In this research it is used within the software package Easy and combined with membrane form-finding using the force-density method.

In the Easy Beam model exact equilibrium is found between the bending-active element and the membrane. Because the prototype shows instability problems without horizontal supports at the low points it can be concluded that realizing this exact equilibrium in the prototype is very sensitive to inaccuracies in the stiffness parameters of the bending-active or membrane elements.

The use of a membrane material with higher stiffness parameters could possibly increase the stability of the model but this leads to a decrease of compensation values which increases the influence of inaccuracies in the production process.

An additional attention point of the required anchors points is that shear forces will concentrate at the connection of the GFRP ring to the anchor. Here the ring is loaded perpendicular to the direction of the glass fibre orientation. The shear capacity of these pultruded profiles is limited in this direction. It is thus very important to limit the peak forces and locate the anchors at the right position if they are required to keep the desired shape.

Throughout this project one design curve is used for constructing the workflow of the form-finding, calculation and realization model. In further research it would be interesting to start a new project with a design analysis on physical models. In this way different types of bending-active textile hybrids can be modelled and the use of the workflow of this research can be extended.



Figure 9: Prototype front view at night (1)



Figure 10: Prototype top view at night (2)

Copyright photos

All photos presented in this paper are taken by the author.

References

Ahlquist Sean. (2017). Sensorial Playscape: Advanced Structural, Material Andresponsive Capacities of Textile Hybrid Architectures as Therapeuticenvironments for Social Play. In S. M. Menges Achim, Sheil Bob, Glynn Ruairi (Ed.), *Fabricate 2017* (pp. 234–241).

Lienhard, J. (2014). *Bending-Active Structures*. University of Stuttgart.

Slabbinck, E., Suzuki, S., Solly, J., Mader, A., & Knippers, J. (2017). Conceptual framework for analyzing and designing bending-active tensile hybrid structures. *Proceedings of the International Association for Shell and Spatial Structures (IASS)*.

Lightweight structures, heavy foundations?

Ramon SASTRE*, Xavier GIMFERRER *

* ETSAV, UPC, Pere Serra, 1-15, St Cugat del Vallès, Spain.

ramon.sastre@upc.edu

Abstract

It is well known that most of tensile structures foundations are made with concrete footings. Not because it is the best form to solve this part of the structure, but because it is the easiest way for many builders-manufacturers. And it is not a surprise either, the comments about the big size of these footings.

It is also curious, at least, the absence of regular bibliography about tensile structure foundations. Although we can find some special texts (PhD Theses, papers...), it's not so easy to find regular books about them.

A serious approach to this subject must consider the different types of typical actions¹ arriving or demanding these foundations (footings). Pushing forces (vertical or inclined), pulling forces (vertical or inclined) and moments without vertical force are the most common situations we must face.

But not only actions are different. Lightweight structures foundations behave quite differently from regular foundations in regular buildings. The importance of the settlements (the importance of the lower soil layers), the horizontal resistance of soil, the situation and size-form of the reinforcement, etc. are concepts that must be revised since they can be completely different.

DOI: 10.30448/ts2019.3245.17

Copyright © 2019 by R. Sastre, X. Gimferrer. Published by Maggioli SpA with License Creative Commons CC BY-NC-ND 4.0 with permission.

Peer-review under responsibility of the TensiNet Association

In this paper, a complete catalog of situations and solutions are studied and proposed for most of all the situations we can find in this type of foundations.

Main discussion is placed about horizontal resistance and overturning resistance. These are probably the maximum difference between this type of foundations and regular ones. But we cannot forget about rain protection, soil-concrete friction, existence of pavement slab, etc., since these aspects can be crucial in the lightweight structures foundations design and absolutely negligible in most of regular building foundations.

If reinforced concrete is used (as it happens most of the time) position and evaluation of the reinforcement are key elements to be taken into account. Exactly the same about pulling elements and their anchorages to the footing.

This paper pretends to fill succinctly a gap in the footing foundation design procedure, so well covered in regular building bibliography.

Keywords: foundations, passive earth pressure, cohesion, soil friction, footing, anchorage

1. Foundations of tensile buildings



Foundations of traditional buildings (structures of stone, brick, wood, steel, etc.) are very different. Depending on the type of soil, its stratification, the type of the structure (frames, continuous...) and the type and magnitude of loads, a typology of diverse foundations is generated: isolated, strip, off-centre footings; foundation beams and slabs; piles, etc.

However, despite this diversity, often a common factor is found. The predominant load on the foundation is compression. A force pushing down the foundation and must be countered by the resistance of the soil beneath the foundation (or next to it, friction, in some types such as certain piles).

It is true that we also can find other cases with other types of loads; especially in structures with columns built in the foundations (at least this is the usual way to calculate the structures). These columns have at its bottom shear forces and bending moments that have to be balanced. Shear forces are usually not very important and, therefore, in most cases the problem is solved with the tensile or compression resistance offered by horizontal braces that are arranged between different footings.

As for the bending moment, it may be important at the border columns of frames and especially in the off-centre footings (for example, under border walls). In these cases solutions are diverse, but often strap beams between this footing and the next one inwards is the most usual solution.

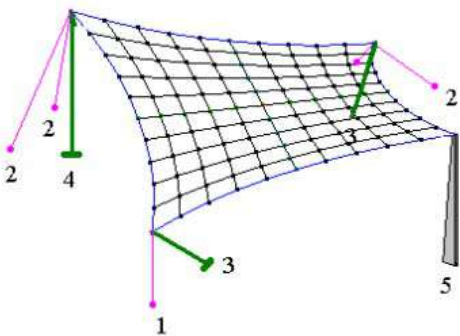
Even so, in all these cases, vertical load of compression is the most important load and the one which determines the type of foundation to use.

In tensile buildings we can also find foundations like those just discussed, for example, in the central vertical mast of a conoid-shaped roof, but these cases are less frequent.

2. Typology of Foundations

In general, foundations of typical tensile buildings can be classified depending on the load to be resisted, in any of these types:

1. Vertical pulling load (vertical cable)
2. Leaning pulling load (any cable or guy-rope fixed to the ground)
3. Leaning pushing load (tilted masts, base of an arch, etc.).
4. Vertical pushing load (vertical mast)
5. Bending moment, with vertical and horizontal loads of lesser importance (especially vertical columns supporting a membrane, without stays or guy-ropes)

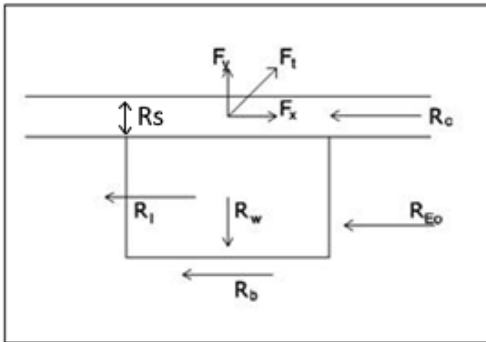


As we can see, only type 4 is what we would call traditional foundation. Type 3 could be considered traditional if the horizontal component was very small or if it was possible to establish a grid of straps between these and other footings. If not, we'll see that the design of the foundation is quite different.

2.1. Balance resources

To balance the loads produced by the structural elements of the tensile constructions, foundations use a different set of resources that, although they could be used in any type of foundation, are more common in this typology.

So, we can consider the following resources:



The compressive strength of the soil at the bottom of the foundation.

The compressive strength of the soil, at the sides of the foundation.

The friction between the sides and the bottom of the foundation with the soil.

The weight of the foundation and all other materials or structural elements located above the foundation: soil, base, slab, pavement ...

The mechanical resistance of a possible continuous reinforced concrete slab, on the foundation.

3. Study of cases

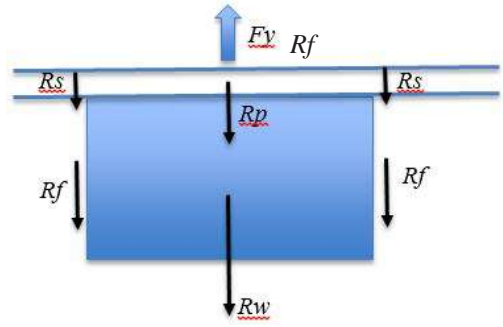
If we accept that tensile structures foundations can be classified in these five categories, now we can consider each one in an independent analysis. This analysis can be very extensive ^[1] but in this paper we will just introduce the main points to be considered.

3.1 Vertical pulling load



This is the simplest case. The foundation is subject to the vertical pulling load F_y . To provide stability, the foundation will resist this force in several ways:

- R_w by its own weight
- R_p by the weight of the pavement that may exist on the foundation
- R_f by the lateral friction against the ground
- R_s by the shear strength by the slab of pavement, if any



3.2 Inclined pulling load

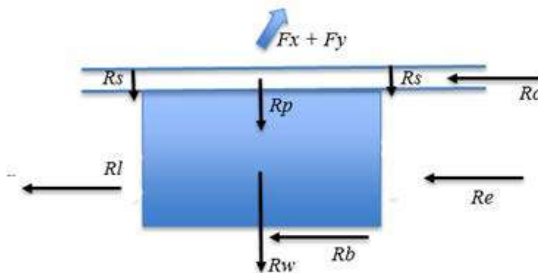
In this case pulling force F_t has two components vertical F_y and horizontal F_x . F_y has already been studied in the previous section (although it will be re-studied later on when considering footing rotation). Now we will pay attention to the behaviour of F_x .



In order to guarantee stability the footing will put up resistance to F_x in some different ways.

- R_e soil lateral resistance. produced by lateral earth pressure E_0 (passive earth pressure E_p could be used, but problems with displacement would appear)
 - R_f friction of the footing base R_b and lateral sides R_l against the soil.
 - $R_f = R_b + R_l$
 - R_c compression resistance of pavement only if it exists.
 - R_s by the shear strength by the slab of pavement, if any.

$$F_x \leq R_x = R_e + R_f + R_c$$



3.3 Vertical pushing force



This type of foundation is the one that most resembles the foundations of traditional constructions. In these cases, the vertical load is much more important than the horizontal one or the moment. The analysis of the foundation is practically reduced to find a contact surface that produces a stress on the ground smaller than the soil bearing capacity.

$$N / A \leq s_a$$

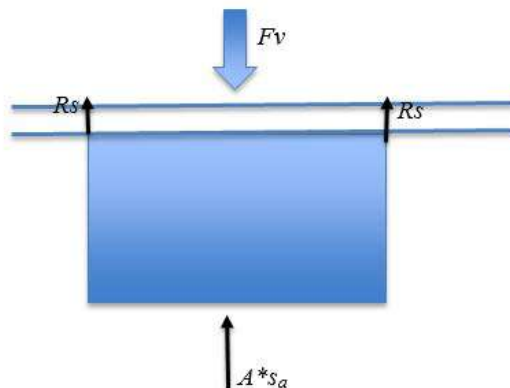
where

N = vertical load

A = footing horizontal surface

s_a = soil bearing capacity

Note that in this case, unlike the case with a pulling force, we do not contemplate at all the friction of lateral sides of the footing. That's because the foundation will not easily move down independently. When we pull up, footing can move up, but when we push down the foundation does not move independently of the adjacent soil (settlement is not considered a movement that causes friction). In any case, if we continued to push the soil, it would break, locally or in a generalized manner, and we would surpass the value of the breaking load or stress. Generally, the value of the soil bearing capacity is obtained by applying a safety factor of 3 or 4 to the breaking stress.



3.4 Inclined pushing force



Inclined compression force is a very common case in tensile constructions. In fact, it is usually more common than vertical compression. Inclined masts are used, above all, to increase the lever arm of the moment that form the vertical reactions at the base of the masts and the stay cables, in most of the perimeter supports (bipods or tripods) .

If we decompose the inclined force F_t in its vertical components F_v and horizontal F_h we can see that the problem is similar to the one we have studied in chapter: Inclined Pulling Load. In any way the vertical compression force has to meet the requirement of

$$F_v / A \leq s_a$$

where

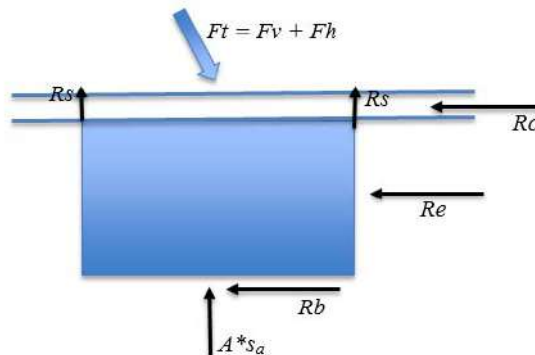
F_v = vertical load

A = footing horizontal surface

s_a = soil bearing capacity

with all the considerations that we have taken into account in the previous section “vertical pushing force”. Moreover we must remember:

- R_e soil lateral resistance. produced by lateral earth pressure E_0 (passive earth pressure E_p could be used, but problems with displacement would appear)
- R_b and R_s could not exist



3.5 Embedded mast



In some cases, especially in the perimeter of tensile constructions we find solutions based on bipods (a mast and a stay cable) or tripods (one or two masts with two or one stay cables respectively) and even more complex sets of masts and stay cables.

Stay cables usually are usually a hindrance, since they are normally very thin, not easily seen and can cause accidents. They also occupy a space that is not usable, so very often you tend to eliminate them.

To do this, it is necessary to have an element embedded in the base, able to work as a cantilever and support the force that is applied at its top, as seen in the attached image.

The typical triangular shape responds to the distribution of forces in a cantilever. However, sometimes for aesthetic or economical reasons it is preferred to have a vertical element of constant section, as a column or a tube, although it means we use more material than necessary.

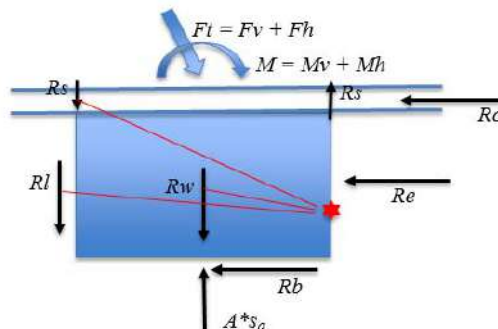
In a first approximation it could seem that this is a more economical solution than using a bipod or tripod, but this can be misleading, since one of the great differences between these solutions is precisely the foundation. This foundation will have to be able to transmit the following forces to the ground:

F_h = horizontal force

F_v = vertical force (pulling or pushing force)

M_h = moment due to the horizontal force

M_v = moment due to the vertical force (if the element is not completely vertical)



4. Conclusions.

Designing foundations for tensile structures is a complex task that involves structural and soil technology knowledge as well as very important economical and construction factors. What can be the best solution for a precise case in one location is completely different from what might be chosen in another location. And it should not be considered an error or a mistake.

Equilibrium or balance must be achieved, of course, but to get to this point displacements and other external variables must be taken into account (rain protection, concrete slab pavement existence...). It can be argued that these factors must be taken into account in any type of foundation, but the relative importance is very different when tensile structures are involved. Balancing forces with friction or passive earth pressure implies that significant displacement might exist, and in this case a relaxation of tensile structure stresses might occur as well. Trying to avoid it by ignoring these balancing forces would imply an over-dimensioning of foundations.

References

- [1] R. Sastre, <http://www.wintess.com/wintess-manual/foundation/introduction/>, WinTess, 2007

Proceedings of the TensiNet Symposium 2019

Softening the habitats / 3-5 June 2019, Politecnico di Milano, Milan, Italy

Alessandra Zanelli, Carol Monticelli, Marijke Mollaert, Bernd Stimpfle (Eds.)

Powerful Tools for Formfinding, Statics and Patterning of Pneumatic Structures

Dieter STRÖBEL*, Jürgen HOLL ^a

*Dieter Ströbel, Pestalozzistraße 8, Stuttgart 70563, Germany.

dieter.stroebel@technet-gmbh.com

^a Jürgen Holl, Pestalozzistraße 8, Stuttgart 70563, Germany.

Abstract

Formfinding is needed to create a pneumatically feasible surface. Therefore, the force density approach is extended with additional constraints. The additional constraints are one or several chambers, which can be loaded by different internal pressure values or even simpler by their volumes. By this method forms can be generated without any limitations concerning the boundary conditions. A harmonically stressed surface is guaranteed. Reinforcements by cables, belts, etc. can be considered already in the form finding procedure.

Statics starts with the definition of the material properties. In general, we define for textile membranes: warp- and weft stiffness, and, if available, crimp- and shear stiffness. We must fix an internal (operating) pressure and now the non-deformed geometry of the finite membrane elements, we can say the patterns, can be calculated. Load case calculations can be performed now by 3 different modes: Constant inner pressure ($p=\text{constant}$), constant volume ($V=\text{constant}$), constant product of inner pressure and volume ($p \cdot V=\text{constant}$, gas law of Boyle-Mariotte) or even the general gas equation ($p \cdot V/T=\text{constant}$). Sometimes belts or cables are used to reinforce the structure. We can define those elements by either fixing them onto the membrane or leave them completely free on the membrane. The pneumatically stressed membrane surface is usually attached to a bending stiff primary structure. The common interaction between the pneumatically stressed membrane and the primary structure is considered by a hybrid model.

DOI: 10.30448/ts2019.3245.45

Copyright © 2019 by D. Ströbel, J. Holl. Published by Maggioli SpA with License Creative Commons CC BY-NC-ND 4.0 with permission.

Peer-review under responsibility of the TensiNet Association

We show that the disregarding of the common interaction leads to 'wrong' results and should be not applied. We try to improve the computer models in many aspects: as an example, we would like to mention the wind-loads; in our calculation the wind changes its direction and size with respect to the deformation, we apply so-called non-conservative loads. Very important in membrane engineering is to avoid ponding problems, so we developed tools to show the flow of the water onto the surface.

After the form is found the patterning can be done. We show how to divide the form in several substructures and how to pattern the different parts individually. Automatic tools for the optimization of the widths can be used. Fast methods for compensation, seam allowances, welding marks, help to produce high quality patterns. We also provide so-called evaluation numbers for the patterning to help the membrane engineers to get perfect patterns without any wrinkles.

Keywords: Pneumatic structures, Biogas plants, Lightweight structures, Formfinding, Statics, Patterning, Gas law, Hybrid structures, Membranes, Foils, Force density, Optimization

1 Formfinding

The Formfinding procedures of mechanically and pneumatically stressed structures is very similar at first view. In both cases prestress values for the membranes are set; for pneumatically structures we need additionally also an internal pressure or a specific volume (which is finally caused by an internal pressure). This procedure has one disadvantage concerning the pneumatic structures: the geometry cannot be controlled as it is the result of the Formfinding method. But in some cases, the geometry should be as simple as possible (as a geometrical function) in order to end up with simple patterns, etc. Here we must make sure that these surfaces are pneumatically feasible. Only a few geometrical functions such as spheres, cylinders, torus shaped forms are useful.

This is the reason why we distinguish between model generation by a Formfinding procedure and model generation by geometrical forms being pneumatically feasible.

1.1 Model generation with Formfinding procedure

In the following we describe the Formfinding procedure of pneumatically stressed structures. It is known that a Formfinding procedure solves the 'inverse' problem. 'Inverse' is related to Statics where the geometry and its elements including size, stiffness, etc. are given and forces, stresses and (small) deflections are searched. The Formfinding procedure in contrast inputs stress values for the elements and ends up with a balanced geometry of a pneumatically prestressed surface. As usual Formfinding procedure of pneumatic structures works as follows: a membrane field (with its material directions) is inputted with 'desired' prestress-values in warp and weft directions and volume or an internal pressure. In Figure 1 we have a typical

example. The red mesh shows the membrane field and the blue line is the polygon where the membrane is finally fixed to.

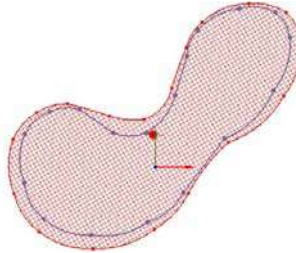


Figure 1: Top view of a meshed boundary as input for a Formfinding

The result of the method (here the force-density approach was used) is the balanced shape in 3D with very uniform stress values. If the same input stresses are used in warp and weft direction we end up with a minimal surface.

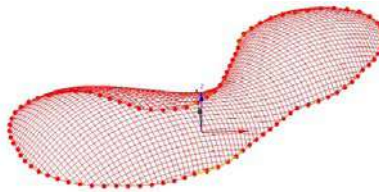


Figure 2: Formfinding result

This example consists of only the membrane surface and the membrane is simply fixed by a closed line onto a plane. This line can be assumed as absolutely fixed.

Theoretical background: The Formfinding of pneumatic chambers has its basics in the well-known Force-Density Method ([1], [2] and [3]). The Force-Density Method creates a linear system of equations for the form-finding procedure by defining the ratio between Force S and stressed length l to be known. Hereby the nonlinear equations of the equilibrium change to a linear system.

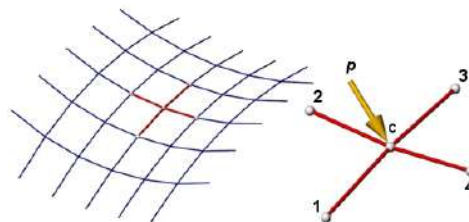


Figure 3: Four cables in point C

In order to clarify these facts Figure 3 shows a point C which is connected by cables to 4 points $(1,2,3,4)$. The nonlinear equations of the equilibrium in the point C are as follows, where the external load vector can be expressed $\mathbf{p}^t = (p_x \ p_y \ p_z)$.

$$\begin{aligned} (x_c - x_1) \frac{S_1}{l_1} + (x_c - x_2) \frac{S_2}{l_2} + (x_c - x_3) \frac{S_3}{l_3} + (x_c - x_4) \frac{S_4}{l_4} &= p_x \\ (y_c - y_1) \frac{S_1}{l_1} + (y_c - y_2) \frac{S_2}{l_2} + (y_c - y_3) \frac{S_3}{l_3} + (y_c - y_4) \frac{S_4}{l_4} &= p_y \\ (z_c - z_1) \frac{S_1}{l_1} + (z_c - z_2) \frac{S_2}{l_2} + (z_c - z_3) \frac{S_3}{l_3} + (z_c - z_4) \frac{S_4}{l_4} &= p_z \end{aligned} \quad (1)$$

These equations become linear by assuming known force-densities, e.g. $q_1 = \frac{S_1}{l_1}$, and analogue for q_2, q_3 and q_4 . The force-density equations are as follows:

$$\begin{aligned} (x_c - x_1)q_1 + (x_c - x_2)q_2 + (x_c - x_3)q_3 + (x_c - x_4)q_4 &= p_x \\ (y_c - y_1)q_1 + (y_c - y_2)q_2 + (y_c - y_3)q_3 + (y_c - y_4)q_4 &= p_y \\ (z_c - z_1)q_1 + (z_c - z_2)q_2 + (z_c - z_3)q_3 + (z_c - z_4)q_4 &= p_z \end{aligned} \quad (2)$$

The coordinates of the point C are the solution of these linear equations. In the following step we want to write the system above by considering m neighbors in the point C :

$$\begin{aligned} \sum_{i=1}^m (x_i - x_c)q_i - p_x &= 0 \\ \sum_{i=1}^m (y_i - y_c)q_i - p_y &= 0 \\ \sum_{i=1}^m (z_i - z_c)q_i - p_z &= 0 \end{aligned} \quad (3)$$

The energy which belongs to the system (1) can be written as (see also [4], [5]).

$$\Pi = \frac{1}{2} \mathbf{v}^t \mathbf{R} \mathbf{v} - p_x(x - x_0) - p_y(y - y_0) - p_z(z - z_0) \Rightarrow stat. \quad (4)$$

The internal energy is the expression $\frac{1}{2} \mathbf{v}^t \mathbf{R} \mathbf{v}$. The vector $\mathbf{v}^t = (v_x \ v_y \ v_z)$ and the matrix $\mathbf{R} = diag(q_i \ q_i \ q_i)$ show this energy with respect to a single line element i . We can write the inner energy as $\frac{1}{2} q_i (v_x^2 + v_y^2 + v_z^2)$, precisely:

$$\begin{aligned}
 v_x &= x_i - x_c \\
 v_y &= y_i - y_c \\
 v_z &= z_i - z_c
 \end{aligned}
 \quad
 \mathbf{R} = \begin{bmatrix} q_i & 0 & 0 \\ & q_i & 0 \\ sym. & & q_i \end{bmatrix}
 \quad (5)$$

The chamber of a pneumatic structure has a volume V , which is made by an internal pressure p_i . The product from internal pressure and volume is a part of the total energy Π : a given volume V_0 leads directly to a specific internal pressure p_i : hence the total energy for the Formfinding of a pneumatic chamber is $\Pi = \frac{1}{2} \mathbf{v}^t \mathbf{R} \mathbf{v} - p_x(x - x_0) - p_y(y - y_0) - p_z(z - z_0) - p_i(V - V_0) \Rightarrow stat$. The derivation of the total energy to the unknown coordinates and to the unknown internal pressure ends up with

$$\begin{aligned}
 \frac{\partial \Pi}{\partial x} &= \sum_{i=1}^m (x_i - x_c) q_i - p_x - p_i \frac{\partial V}{\partial x} = 0 \\
 \frac{\partial \Pi}{\partial y} &= \sum_{i=1}^m (y_i - y_c) q_i - p_y - p_i \frac{\partial V}{\partial y} = 0 \\
 \frac{\partial \Pi}{\partial z} &= \sum_{i=1}^m (z_i - z_c) q_i - p_z - p_i \frac{\partial V}{\partial z} = 0 \\
 \frac{\partial \Pi}{\partial p_i} &= V - V_0 = 0
 \end{aligned}
 \quad (6)$$

In the system (6) the internal pressure p_i can be seen as a so-called Lagrange multiplier. The fourth row in (6) shows, that our boundary condition $V = V_0$ is obtained by the derivation of the energy to this Lagrange multiplier. The vector $(\frac{\partial V}{\partial x} \quad \frac{\partial V}{\partial y} \quad \frac{\partial V}{\partial z})$ describes the normal direction in the point (x, y, z) and the size is the according area. By a set of given force-densities for all elements and a given volume V_0 we end up with a pre-stressed and of course balanced pneumatic system with a volume V_0 and an internal pressure p_i .

Each additional chamber leads to an additional volume and Lagrange multiplier, which allows to calculate multi-chambered structures (see Figure 4).

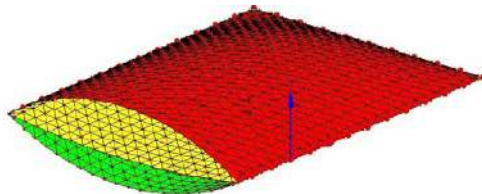


Figure 4: 2 chambers with 3 layers.

If the internal pressure p_i is given or set by user row number 4 of formula (6) is dropped off. The former unknown Lagrange multiplier p_i becomes a known external load.

$$\begin{aligned} \frac{\partial \Pi}{\partial x} &= \sum_{i=1}^m (x_i - x_c) q_i = p_x + p_i \frac{\partial V}{\partial x} \\ \frac{\partial \Pi}{\partial y} &= \sum_{i=1}^m (y_i - y_c) q_i = p_y + p_i \frac{\partial V}{\partial y} \\ \frac{\partial \Pi}{\partial z} &= \sum_{i=1}^m (z_i - z_c) q_i = p_z + p_i \frac{\partial V}{\partial z} \end{aligned} \tag{7}$$

The force-densities q and the internal pressure p_i are not independent from each other. This can be simple noted in equation (7). In case of no external loads p_x, p_y, p_z the force densities q_i and the internal pressure p_i are proportional to each other. If we double the prestress we end up with the doubled internal pressure with an unchanged geometry.

Sometimes the membranes are fixed for example to bending stiff beam elements and now we have a situation that the boundary line is not fixed totally. The flexibility of the boundary line should be considered already in the Formfinding stage (also very important for ETFE-cushions). The procedure works as follows. We perform a so-called ‘mixed’ Formfinding, where the boundary lines are defined with all its mechanical properties and for the membrane, we still use the ‘desired’ stress values as always. Now the boundary line deflects but the membrane stresses are perfect with respect to the ‘desired’ input values.

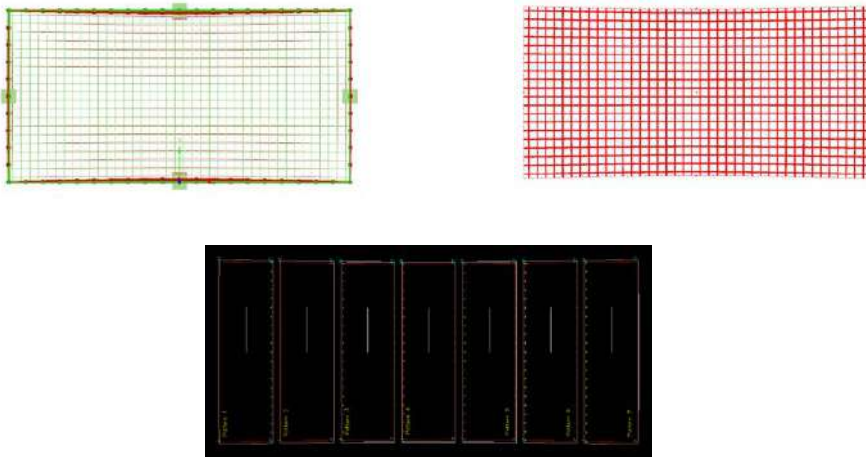


Figure 5: Deflected boundary with uniform stress and cutting patterns

The boundary deflects but the desired prestress in the membrane is maintained. The biggest deflection of the outer beam is as expected in the middle. Therefore, the patterns are smaller in this area.

Very often the membrane system and the primary steel structure are calculated in separated systems by loading the steel elements with the reaction forces of the pneumatic membrane which was fixed at its boundaries in a first calculation step. This procedure is wrong with respect to Formfinding and Statics. Separation is only allowed if the deflections are very small and this is never the case for membrane structures. In case of Statics it is only a first - very imprecise (and expensive) estimation. Users should always calculate with computer models consisting of primary structure and membrane in one holistic model.

1.2 Model generation with geometrically defined surfaces

As already mentioned geometrically defined surfaces must be pneumatically feasible. In this case a Formfinding procedure is not needed. After materialization (=definition of the material properties) a static calculation with a specific internal pressure should not change the geometry significantly (by neglecting elastic deformations). If we find significant geometrical differences the geometry was not perfect with respect to pneumatic feasible forms. The example below seems to be perfect as we have a cylinder and 2 quarter spheres. But the combination of both disturbs the stress-distribution. The lines where the spheres are connected to the cylinder are the problem as the cylinder has the stress $p \cdot R$ and the sphere stress $\frac{1}{2} p \cdot R$. In order to check the differences, we simply perform a static calculation with the internal pressure.

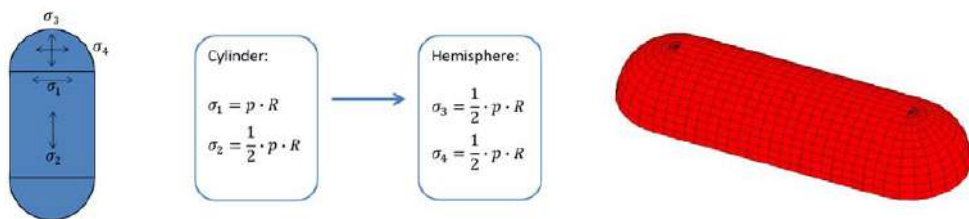


Figure 6: Geometrically defined volume surfaces and stresses

We find the geometrical form under internal pressure more or less unchanged in this example.

1.3 Formfinding with sliding cables

If additional reinforcement cables in case of big wind loads are needed, we perform a Formfinding procedure for those cables in order to find their optimal positions. In Figure 7 we see the cable net in a flat situation.

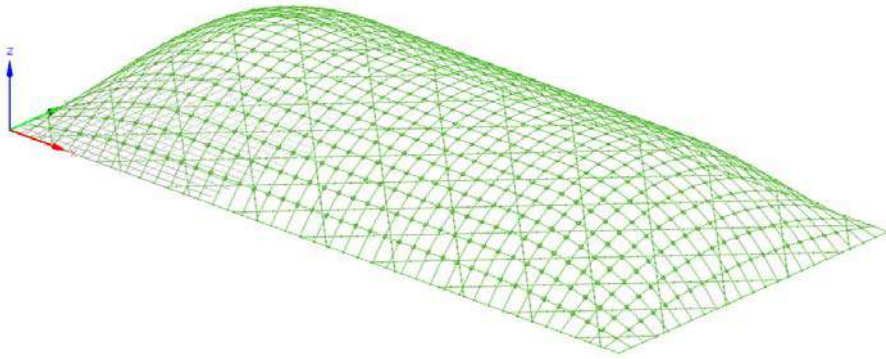


Figure 7: Start situation with a flat cable mesh

The Formfinding procedure calculates the coordinates of the intersection points of the cables onto the surface - which is assumed as fixed – under the constraints that all cable forces are the same. The result is shown in Figure 8.

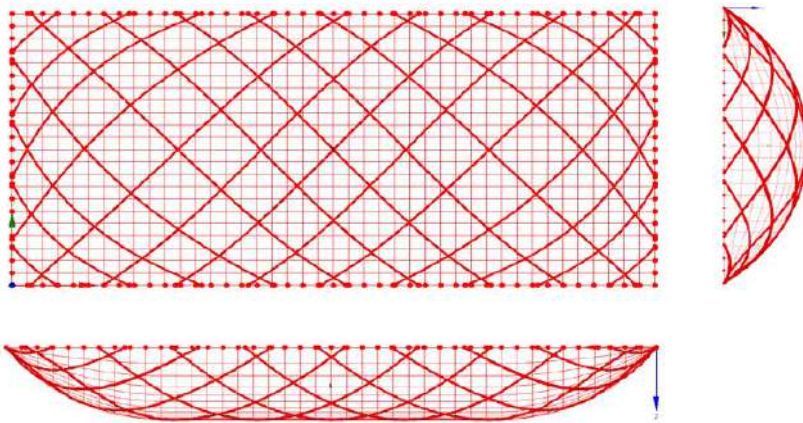


Figure 8: Sliding cables with identical forces after Formfinding (top-, side- and front view)

2 Statics

A static calculation for membranes is geometrically nonlinear. We need material properties for all elements and its nondeformed geometry. The nondeformed geometry of a cable element for instance is the unstressed length of this cable. Next, we need the external loads and the internal pressure or volume information. After the Formfinding-procedure a geometry is available, and Statics can be performed.

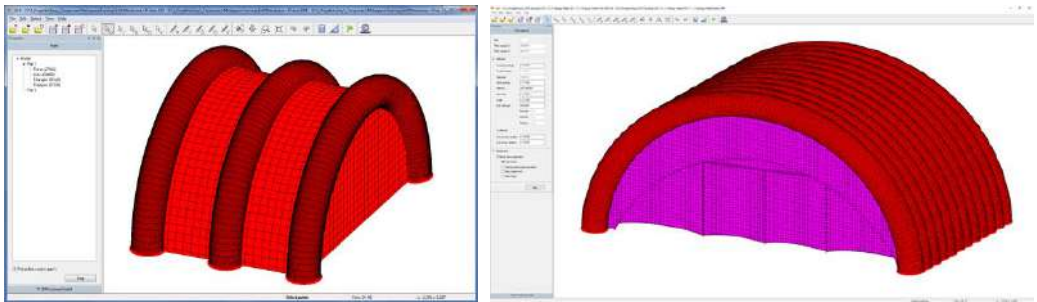


Figure 9: Pneumatic tube systems combined with mechanically stressed membranes

2.1 Statics with Formfinding models

When a usual Formfinding procedure was made also prestress values for all elements exist. We can define material properties for the membranes and then we can calculate the unstressed 'lengths' (= non-deformed geometry) of all elements as we have prestress values from the Formfinding result. Usually the first load-case in statics to be calculated should be 'internal operation pressure'. The result of this calculation must be identical with the Formfinding result as we 'shortened' the membrane elements in this way.

2.2 Statics with geometrically defined models

When a geometrical Formfinding was made, prestress values are usually not available or at least these values do not balance the structure in general. Here we recommend the following procedure:

Define the material properties. The unstressed geometry cannot be calculated by prestress values; therefore, we simply set the stressed lengths to be the unstressed lengths. Now after the load case 'internal operation pressure' we end up with a different geometry. The geometrical differences should be small in this case.

2.3 Theoretical background

2.3.1 Membrane Elements

We extend the form-finding theory by introducing the constitutive equations for the membrane elements to the system (1). Now the force-densities q from the form-finding are unknowns and they belong to the material equations.

$$\begin{bmatrix} \sigma_u \\ \sigma_v \\ \tau \end{bmatrix} = \begin{bmatrix} m_{11} & m_{12} & 0 \\ & m_{22} & 0 \\ sym. & & m_{33} \end{bmatrix} \begin{bmatrix} \varepsilon_u \\ \varepsilon_v \\ \Delta\gamma \end{bmatrix} \quad (8)$$

We must consider, that the membrane axial-stress in u - or v - direction can be expressed as $\sigma_u = \frac{S_u}{b_u}$ and $\sigma_v = \frac{S_v}{b_v}$. b_u and b_v are the widths of the u - and v -lines. The force-densities q can be introduced now as: $S_u = q_u l_u$ and $S_v = q_v l_v$. The strains in u - and v -direction can be written as follows:

$\varepsilon_u = \frac{l_u - l_{u0}}{l_{u0}}$ and $\varepsilon_v = \frac{l_v - l_{v0}}{l_{v0}}$. The angle difference $\Delta\gamma = \gamma - \gamma_0$ is needed for the shear-stress calculation. γ is the angle between u and v -direction; γ_0 refers to the ‘non-deformed start-situation’ without any shear-stress.

The geometrical compatibility has to be considered as follows:

$l_i = \sqrt{(x_i - x_c)^2 + (y_i - y_c)^2 + (z_i - z_c)^2}$ and $\gamma = \arccos\left(\frac{l_u * l_v}{l_u l_v}\right)$, in which $(l_u * l_v)$ means the inner (scalar-) product between u and v -direction.

The shear-stress calculation is guaranteed also for a continuous membrane by the fact that the shear angle is between the non-deformed u - and v -direction of the material [4].

2.3.2 General calculation modes

For static calculations we recommend 4 calculation modes:

1. Given internal pressure p (snow)
2. Given volume V (water)
3. Given product $p \cdot V$ (Boyle-Mariotte, for example wind)
4. Given product $\frac{p \cdot V}{T}$ (General gas equation, consideration of temperature)

$$\begin{aligned}
 \frac{\partial \Pi}{\partial x} &= \frac{1}{2} \frac{\partial(v^t R v)}{\partial x} - p_x - \frac{\partial V}{\partial x} p_i = 0 \\
 \frac{\partial \Pi}{\partial y} &= \frac{1}{2} \frac{\partial(v^t R v)}{\partial y} - p_y - \frac{\partial V}{\partial y} p_i = 0 \\
 \frac{\partial \Pi}{\partial z} &= \frac{1}{2} \frac{\partial(v^t R v)}{\partial z} - p_z - \frac{\partial V}{\partial z} p_i = 0 \\
 \frac{\partial \Pi}{\partial p_i} &= V - \frac{(p_{abs} \cdot V)_0}{(p_{atm} + p_i)} = 0
 \end{aligned}
 \tag{9}$$

Mode 1 is very simple, and we showed the principle in equation (7).

Mode 2 is standard case where row 4 is $V - V_0 = 0$, see equation (6).

Mode 3 (consideration of gas-laws) enables the realistic behavior of the internal pressure. This mode is important in case of e.g. fast wind gusts. Here the pump systems cannot update the inner pressure in the short time. We can see it as a closed system and by considering the temperature as constant we get the gas law of Boyle and Mariotte $p \cdot V = const$ in this case. Only if the gas law is fulfilled the membrane stresses get the correct size. Equation (9) refers to mode 3, here the constant value $(p_{abs} \cdot V)_0$ is the given product and row 4 of (9) has to be fulfilled in iterations where the unknown internal pressure p_i is adapted.

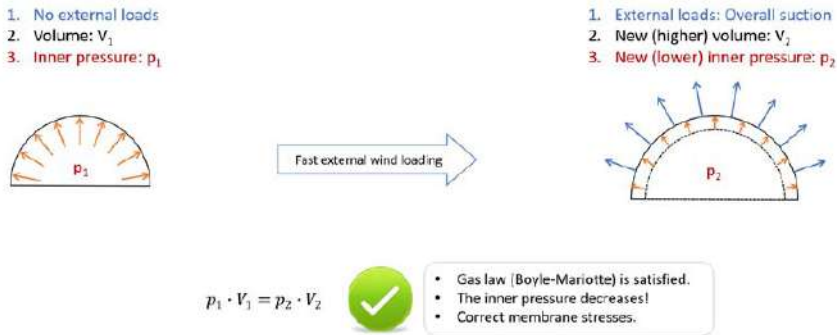


Figure 10: The physical principles of the gas law (mode 3)

On the left-hand side of Figure 10 we see an air hall with an absolute inner pressure p_1 and a volume V_1 . The absolute inner pressure is the sum of the over pressure in the air hall and the atmospheric pressure. On the right-hand side, the structure is loaded by an overall wind suction. By considering the Boyle-Mariotte gas law we end up in this case with a higher volume and a lower inner pressure.

Mode 4 considers also the temperature, the principle itself is the same as mode 3 with minor modifications.

By using these modes most cases are covered. The modes can be used e.g. as follow:

1. An air hall under snow-loading (a specific internal pressure is set to resist the snow-loads)
2. A membrane filled with an incompressible fluid (water-bag) and
3. A pneumatic cushion loaded by a fast wind-gust; here, the gas law ($p \cdot V = const$) is valid.
4. A pneumatic cushion loaded by a fast wind-gust; here, the gas law ($\frac{p \cdot V}{T} = const$) is valid.

2.3.3 Non-conservative loads

It is to mention that the internal pressure effect is always perpendicular to the deformed geometry. These loads are called non-conservative as all wind loads. In order to get correct results software packages should consider these effects.

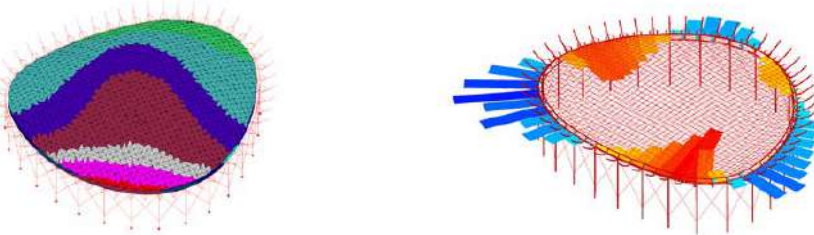


Figure 11: Wind load case with different load zones (left) and bending moments in steel ring in a holistic model (right)

2.3.4 Statics with cables as reinforcements

If the membrane stresses are too big, membranes can be combined with cable nets. We distinguish between cables which are fixed to the membrane and “free” sliding cables. These different cases have to be considered in the statico calculation by different calculation strategies. The interaction of membrane and sliding cables has to be modeled correctly. In the cable net (see Figure 12) it is important to receive constant forces in the cables between the crossing points.

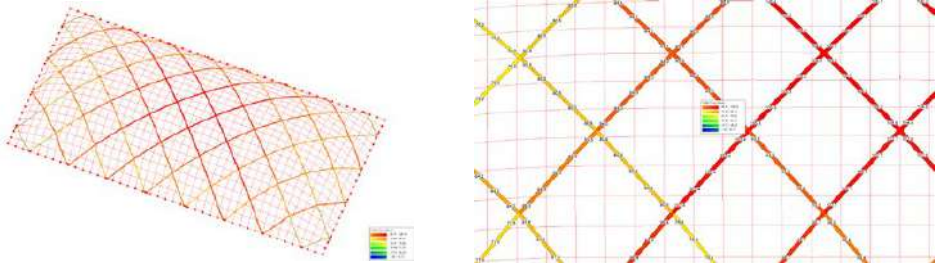


Figure 12: Sliding cable net partially fixed on air hall surface with loops

In Figure 13 the sliding cable is completely free and therefore it is detached from the membrane.

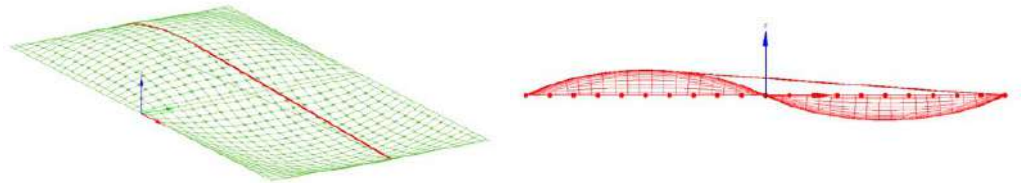


Figure 13: Totally free sliding cable (perspective view and side view)

In Figure 14 we show a situation where an air hall is loaded by wind pressure. The free sliding cables (green lines on right side) are lifted.

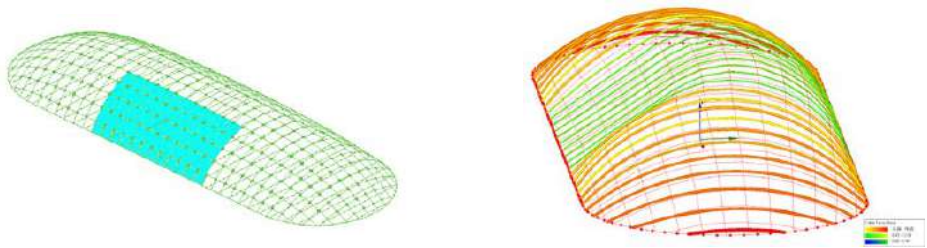


Figure 14: Wind pressure load zone (left), totally free sliding cables detached from the membrane (right)

3. Cutting pattern generation

The cutting patterning is an essential part of the engineering process for pneumatic structures. In the past it was very cost- and time-intensive if the waste of material was to be minimized. Nowadays efficient or even automatic patterning tools are existing where those problems are solved.

2.4 Manual patterning

The first step in the manual patterning procedure is the definition of seam lines. The seam lines can be either geodesic lines or plane cuts defined by starting and ending points. Another possibility is to define so called semi geodesic lines, these are lines with a starting and ending point and a control point in between. If at least 2 lines are defined a flat strip can be generated and its width can be determined.

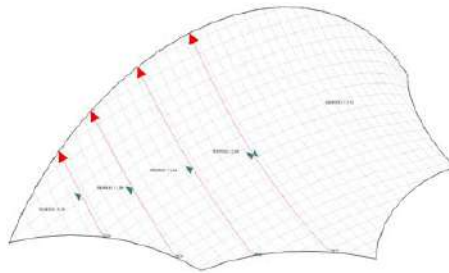


Figure 15: Geodesic seam lines in 3d model

After the determination of the seam lines a flattening method must be executed. The manual patterning is with respect to width optimization and mass production a time-consuming procedure. Therefore, very often automatic methods are used.

2.5 Automatic patterning

In order to optimize the widths of patterns automatically we need optimization variables. The widths of the patterns depend on the position of the seam-lines (mainly geodesic lines). In order to achieve appropriate widths for all patterns the position of those seam lines must be modified until the desired widths of the patterns are reached. Therefore, the position of the geodesic lines must be changed during the iteration process.

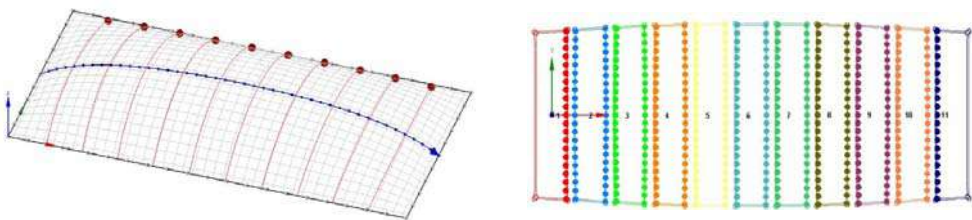


Figure 16: Cushion with automatic created geodesic lines and flattened patterns with identical widths

In case of a non-regular geometry guide lines can be used, if the cutting lines do not intersect themselves, see Figure 17. If not, the seam line definition has to be made manually line by line.



Figure 17: Non-regular geometry with guide lines and patterns

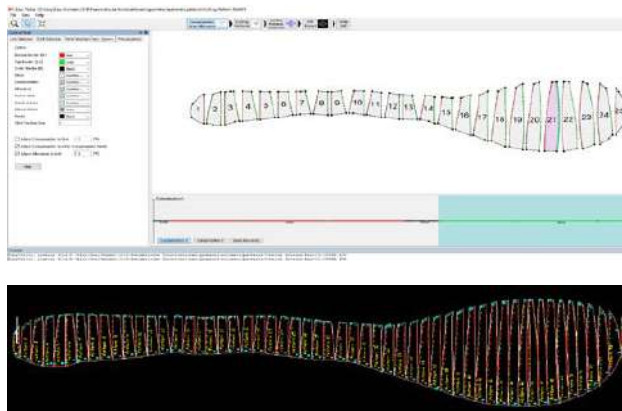


Figure 18: Air hall with automatic created geodesic lines

The cutting pattern layout of air halls should be width optimised but also satisfy the aesthetic sensations. Hierarchical cuts should be possible, this means that the whole surface can be divided in subsurfaces and those parts are patterned independently. In Figure 19 the whole air hall surface is separated in 3 parts and individually patterned (Figure 20). For each individual part automatic pattern procedures were used.

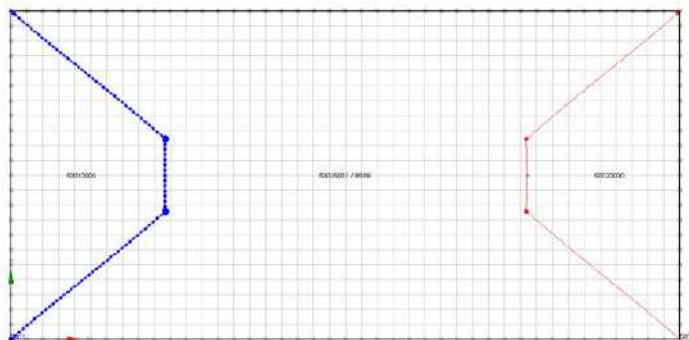


Figure 19: Separation of air hall surface by cutting lines

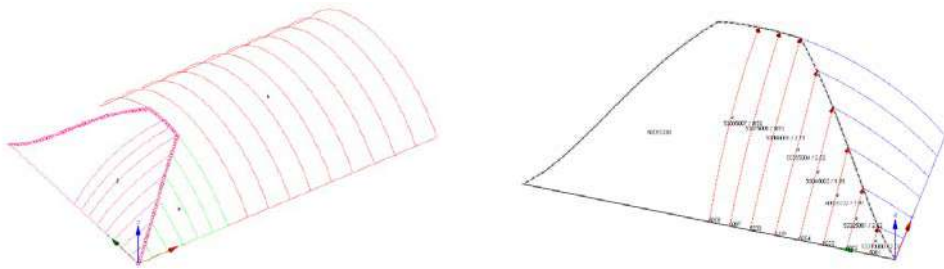


Figure 20: Compliance with geometrical boundary conditions

In Figure 20 we can see that the seam lines of different parts are meeting in one point. Therefore one part can be patterned automatically, the second one has to be done manually.

References

- [1] Ströbel, D., Singer, P., Holl, J. „Analytical Formfinding”, *International Journal of Space Structures*, Volume: 31 issue: 1, page(s): 52-61, March 1, 2016
- [2] Holl, J., Ströbel, D., Singer, P. “Formfinding and Statical Analysis of Cable Nets with flexible covers”, *VI International Conference on Textile Composites and Inflatable Structures STRUCTURAL MEMBRANES 2013*, Munich, Germany.
- [3] Singer, P. (1995), „Die Berechnung von Minimalflächen, Seifenblasen, Membrane und Pneus aus geodätischer Sicht“, *Dissertationsschrift, DGK Reihe C*, Nr. 448, 1995.
- [4] Ströbel, D. (1997), „Die Anwendung der Ausgleichsrechnung auf elastomechanische Systeme“, *Dissertationsschrift, DGK, Reihe C*, Nr. 478.
- [5] Ströbel, D. Singer, P, Holl, J: Holistic Calculation of (Multi)-Chambered ETFE-Cushions, *Tensinet, TensiNet Istanbul*, 2013.

Proceedings of the TensiNet Symposium 2019

Softening the habitats / 3-5 June 2019, Politecnico di Milano, Milan, Italy

Alessandra Zanelli, Carol Monticelli, Marijke Mollaert, Bernd Stimpfle (Eds.)

Inflatable beams subjected to axial forces

Jean-Christophe THOMAS*, Anh LE VAN^a

*GeM (Institute for Research in Civil and Mechanical Engineering),
Université de Nantes-Ecole Centrale Nantes, UMR CNRS 6183
2, rue de la Houssinière, BP 92208, 44322 Nantes Cedex 3, France
jean-christophe.thomas@univ-nantes.fr

^aGeM (Institute for Research in Civil and Mechanical Engineering),
Université de Nantes-Ecole Centrale Nantes, UMR CNRS 6183

Abstract

The inflatable beam is one of the simplest models to understand the mechanics of the inflatable structures in general. In this study, we address the problem of an inflatable beam subjected to compressive and transverse loads. Although the strength of materials for inflatable beams is now well established for inflatable beams subjected to transverse loads, the case of the combined axial and transverse loads has received few studies. Contrary to what one may think, one must not superimpose the two loads in as much as the axial loads modify the stiffness of the beam. For example, a compressive load counteracts the effect of the pressure on the end surface of the beam and reduces its stiffness. The authors present here some new formulations for the bending of inflatable beams subjected to compressive forces.

Also addressed in this work is the buckling of inflatable beams subjected to compressive loads. Analytical formulas are proposed, taking into account the effect of the internal pressure.

Keywords: lightweight structure, structural membrane, pneumatic structure, inflatable beam, buckling

DOI: 10.30448/ts2019.3245.32

Copyright © 2019 by Jean-Christophe Thomas and Anh Le Van. Published by Maggioli SpA with License Creative Commons CC BY-NC-ND 4.0 with permission.

Peer-review under responsibility of the TensiNet Association

1. Introduction

Pneumatic structures are an important part of lightweight structures. They are very various, and some of them can be seen of the website (Tensinet association website). They can be divided into different families: air-supported structures which are mono-membranes, air-inflated structures – also named here inflatables, which are generally composed of air beams or/and air cushions, and hybrid structures, which can be composed of both. Air beams are the simplest model to understand the behavior of inflatable structures: deflection of the beam, apparition of wrinkle, collapse of the beam under bending, buckling. Some previous studies have been conducted on these key-points and allow predicting precisely the behavior of inflatable beams (Fichter 1966, Le Van and Wielgosz 2005, Nguyen and al. 2013, 2015, Thomas and Bloch 2016). Knowing precisely the performance of the models used to design membrane structures is a current and important issue. Working Group 5 of CEN TC 250 is working on rules of design in Europe (Eurocode), which should be obtained from reliability analysis. In this frame, it is of importance to know the performance of the models used to conduct the analysis. The analytical models used to calculate inflatable beams submitted only to transverse loads have been compared with 3D simulation results and with experiments. These models have been used to conduct a reliability analysis of a pedestrian inflatable bridge (Thomas and al. 2018). These studies should now be extended to the case of combined loads.

Some inflatable structures are submitted to combination of loadings, for example bending and compression. This can be the case of an inflatable mast supporting heavy loads due to lighting systems, monitoring systems, etc. It is usual to superimpose the effects of the actions in the case of beams made of conventional materials (steel, aluminum, concrete..). But the stiffness of inflatable beams comes from the pretension due to the internal pressure. The pressure applied on the ends of the beams leads to a normal load, which is transmitted in the membrane along the beam and gives a reserve of axial positive stresses. This study addresses the influence of compressive axial forces that counteract the pretension in the case of a combination compression-bending for an inflatable beam.

To answer this question, we will first present the model of a uncompressed inflatable beam and explain how to adapt logically the results to answer our problem. Then, in a second part, we present a new formulation dedicated to the deflection of inflatable beams under compression. We then give the formulations for the buckling and propose finally a comparison between our analytical results and numerical results obtained with a 3D membrane code.

All the 3D numerical computations of this study are done with a homemade code dedicated to membrane structures. It is based on the total Lagrangian formulation. The non linear equations are solved by an iterative Newton scheme. The material can be isotropic or orthotropic.

2. Behaviour of inflatable beams subjected to transverse loads

For this study, the membrane is supposed orthotropic, and one orthotropy direction is supposed parallel to the axis of the beam. This will represent a coated fabric for which the warp is aligned with the axis of the beam. The local orthotropy basis is $(\vec{e}_\ell, \vec{e}_t, \vec{e}_z)$, where ℓ means axial, and t refers to transverse, Fig. 1.

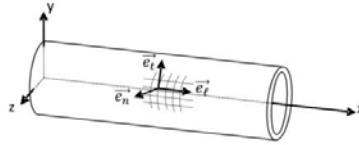


Figure 1: local orthotropy basis

2.1. The different steps

Let us consider an inflatable beam subjected to a transverse load applied in its middle. Figures 2 and 3 present some key-points of its behaviour. Figure 2.a shows the step of inflation. This step is particularly important because it gives the beams its stiffness. The red mesh corresponds to the beam submitted to a very low pressure, which allows balancing the own weight of the fabric and ensuring the section of the beam to be quasi-circular. This corresponds to the natural state of the beam, which is denoted by the sign Φ in the following. For example, R_Φ and L_Φ are the radius and the length of the beam in the natural state. The grey mesh corresponds to the beam at the end of the pressurization. This state is called initial state. R and L are the radius and length in this initial state. Figure 2.b shows the deflected beam. Once loaded transversely, the beam attains the so-called actual state. It has been experimentally verified that the deflection of the beam depends linearly on the load provided that a certain level of loading is not exceeded. Current strength of material theory studies the behaviour between the initial and the actual state. For beams made of more conventional materials (steel, aluminium, concrete, wood...), there is no natural state.



Figure 2: inflation and bending of an inflatable beam

The level of loading mentioned not to be exceeded to remain in the linear domain corresponds to the apparition of plasticity in the cases of conventional materials. The case of inflatable beams is different. The first phase of linear behaviour ends as soon as a wrinkle appears at the upper

surface of the beam in this case. The wrinkling load is reached. Note that the apparition of the wrinkle does not imply the collapse of the beam. There exists a reserve of stiffness. Increasing the load beyond the wrinkling load leads to a propagation of the wrinkle around the section (Fig 3.a) and the collapse occurs when the wrinkle reaches the middle of the beam section (Fig 3.b). This property had been verified theoretically and experimentally verified (Thomas and Bloch 2016).

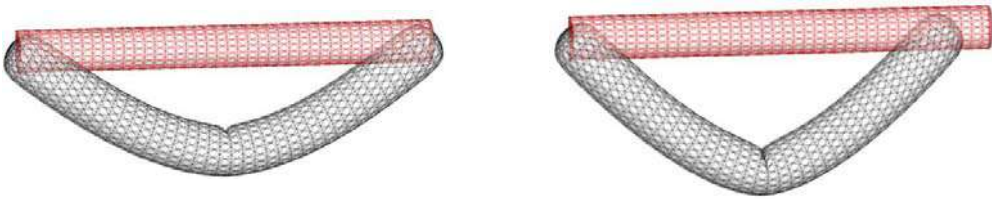


Figure 3: inflatable bended beam- propagation of wrinkle (a) and collapse of the beam (b)

A parallel can be drawn between the plasticity load in the case of conventional materials and the collapse load of inflatable beams.

Not that there exists another specificity of inflatables: when unloaded, they come back to the initial state. It means that, if one neglects the effects of creep, the behaviour is reversible. Reversible collapse is not correct from a semantic standpoint, but it is a physical reality.

2.2. Stresses in the membrane

To understand the behaviour of inflatable beams, it is necessary to detail with precision the distribution of longitudinal stresses in the various cases of loading. Figure 4.a shows the distribution of stresses when no wrinkle appears in the membrane. The longitudinal stresses due to the inflation (in blue) are superimposed with the longitudinal stresses due to the bending (in black), which leads to the final distribution (in blue). Figure 4.b presents the same distribution when a wrinkle appears in the membrane. It happens when a principal stress of the beam vanishes. It allows getting a criterion: the wrinkling load is attained when the longitudinal stress is nil. For example, in the case of a cantilever inflatable beam, one can calculate the wrinkling load function of the pressure p and the geometric parameters:

$$F_W = \frac{p\pi R^3}{2L} \quad (1)$$

Note that the material coefficients (elasticity moduli) do not appear explicitly in the formula. They only impact the length and the radius in the initial state, calculate from the length and the radius in the natural state with the relations:

$$L = L_\phi \left(1 + \frac{pR\phi}{2\phi_{E_\ell}} (2 - \phi_{\nu_{\ell t}}) \right) \quad \text{and} \quad R = R_\phi + \frac{pR_\phi^2}{2\phi_{E_t}} (2 - \phi_{\nu_{\ell t}}) \quad (2)$$

where ϕ_{E_ℓ} and ϕ_{E_t} are the elasticity moduli in the longitudinal and transverse directions, $\phi_{\nu_{\ell t}}$ is a Poisson's coefficient. The shear coefficient is denoted $\phi_{G_{\ell t}}$.



Figure 4: longitudinal stresses in the membrane

2.3. Deflection of the beam

Precise details of the strength of materials theory written at the GeM laboratory can be found in (Le Van and Wielgosz 2005, Nguyen and al. 2013, 2015). We only recall here the key points that will allow to get a linear system of equations useful for the study of an inflatable beam submitted to a combination of axial and transverse loads. The starting point is the total Lagrangian formulation that allows accounting properly the work of the internal pressure. Timoshenko's kinematic must be used for such thin-walled beams to account the effect of shear: the straight section remains in a plane, but doesn't remain orthogonal to the neutral axis of the beam. The constitutive laws of the material are $\Sigma_{xx} = \Sigma_{xx}^0 + E_\ell E_{xx}$ and $\Sigma_{xy} = \Sigma_{xy}^0 + 2G_{\ell t} E_{xy}$, where Σ_{xx}^0 and Σ_{xy}^0 are the stresses in the initial state. It has also been showed that the elasticity moduli used in these constitute laws which refers to the initial state must be calculated from the elasticity moduli of the material in the initial state (Nguyen and al. 2015).

The material coefficients are calculated with two coefficients that characterise the changes of geometry between the natural state and the initial state: $k_x = L/L_\phi$ and $k_\theta = R/R_\phi$.

$$E_\ell = \phi_{E_\ell} \frac{k_x^3}{k_\theta} \quad \text{and} \quad G_{\ell t} = \phi_{G_{\ell t}} k_{\theta x} k_\theta \quad (3)$$

After development of the virtual power principle and a final linearization, the following equations are obtained for a beam subjected to local forces and torques at its extremities .

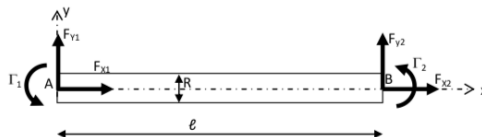


Figure 5: inflatable beam subjected to local forces and torques

$$-\frac{dN}{dx} = 0 \tag{4}$$

$$-(N + kG_{\ell t}S) \frac{d^2v}{dx^2} + (P + kG_{\ell t}S) \frac{d\theta}{dx} = 0 \tag{5}$$

$$\left(E_{\ell}I + \frac{NI}{S}\right) \frac{d^2\theta}{dx^2} + (P + kG_{\ell t}S) \left(\frac{dv}{dx} - \theta\right) = 0 \tag{6}$$

k is a correcting coefficient usually used to account properly the shear in thin membranes. It is equal to 0,5 for circular sections.

The boundary conditions are:

$$N(0) - P = -F_{x1} \quad , \quad N(\ell) - P = F_{x2} \tag{7}$$

$$\begin{aligned} (N + kG_{\ell t}S) \frac{dv}{dx}(0) - (P + kG_{\ell t}S)\theta(0) &= -F_{y1} \\ (N + kG_{\ell t}S) \frac{dv}{dx}(\ell) - (P + kG_{\ell t}S)\theta(\ell) &= F_{y2} \end{aligned} \tag{8}$$

$$\left(E_{\ell}I + \frac{NI}{S}\right) \frac{d\theta}{dx}(0) = -\Gamma_1 \quad \left(E_{\ell}I + \frac{NI}{S}\right) \frac{d\theta}{dx}(\ell) = \Gamma_2 \tag{9}$$

Equations (5) to (8) can be simplified in the case of a beam for which no axial force is superimpose. In this case, equation (4) and (7) show that the normal force N(x) is constant and equal to P. We consider in the following an inflatable cantilever beam only subjected to a load F at its extremity . Equation (5) and (8) lead to

$$(P + kG_{\ell t}S) \left(\frac{dv}{dx} - \theta\right) = F \quad \xrightarrow{\text{yields}} \quad \frac{dv}{dx} = \theta + \frac{F}{P+kG_{\ell t}S} \tag{10}$$

which make evidence of the influence of the shear. Using (6), (9) and $\theta(0) = 0$ gives $\theta(x)$. Equation (10) and the boundary condition $v(0)=0$ lead finally to:

$$v(x) = \frac{F}{E_{\ell}I + \frac{PI}{S}} \left(\ell \frac{x^2}{2} - \frac{x^3}{6}\right) + \frac{Fx}{P+kG_{\ell t}S} \tag{11}$$

Eq. (11) shows the influence of the pressure p on the stiffness. It reinforces the stiffness of the beam, which follow the intuition.

3. Inflatable beams subjected to transverse and compressive loads

The principle of inflatable beams is simple: the effects of the pressure on the two surfaces at each end of the end inducts is equal to P, and is equal to the normal force. An external compression load will then counteract P, and then reduce the stiffness. Let study now the new

problem: a cantilever beam subjected to a transverse load $F_{y2} = F$ and a compression load $F_{x2} = -Q$.

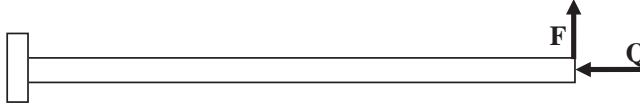


Figure 6: case studied: inflatable beam submitted to a transverse load F and a compressive load Q

3.1. Deflection of the compressed bended beam: adaptation of the uncompressed beam solution

The load Q counteracts the effect off the pressure P on the circular section at the extremity of the beam. It means that the normal force in the beam is no more equal to P, but is equal to $P-Q$. It seems then logical to replace P with $P-Q$ in eq. (11). This leads to the deflection:

$$v(x) = \frac{F}{E_{\rho}I + \frac{(P-Q)I}{S}} \left(\ell \frac{x^2}{2} - \frac{x^3}{6} \right) + \frac{Fx}{(P-Q) + kG_{\ell t}S} \quad (12)$$

This has been done without any demonstration. We propose to solve the problem properly in the following to verify if this solution is valuable or not.

3.2. Deflection of the compressed bended beam: theory

The equations of the theory (4) to (9) are always valuable and allow getting an analytical solution of this new problem. Eqs. (4) and (7) lead to

$$N(x) = P - Q \quad (13)$$

Eqs. (5) and (8) yield to

$$\frac{dv}{dx} - \theta = \frac{Q}{N + kG_{\ell t}S} \theta + \frac{F}{N + kG_{\ell t}S} \quad (14)$$

Including Eq. (13) into (6) allows to eliminate $v(x)$, and gives a second order linear differential equation:

$$\frac{d^2\theta}{dx^2} + \frac{P + kG_{\ell t}S}{N + kG_{\ell t}S} \frac{Q}{E_{\rho}I + \frac{NI}{S}} \theta = - \frac{P + kG_{\ell t}S}{N + kG_{\ell t}S} \frac{F}{E_{\rho}I + \frac{NI}{S}}$$

Introducing the variable $\Omega = \sqrt{\frac{P + kG_{\ell t}S}{N + kG_{\ell t}S} \frac{Q}{E_{\rho}I + \frac{NI}{S}}}$ gives the following equation, for which the solutions are well-known:

$$\frac{d^2\theta}{dx^2} + \Omega^2\theta = - \frac{P + kG_{\ell t}S}{N + kG_{\ell t}S} \frac{F}{E_{\rho}I + \frac{NI}{S}} \quad (15)$$

Finally, the rotation of the section is obtained:

$$\theta(x) = A \cos \Omega x + B \sin \Omega x - \frac{F}{Q}$$

In the case of the cantilever inflatable beam studied here, A and B can be calculated with $\theta(0) = 0$ and eq. (10). This finally gives:

$$\theta(x) = \frac{F}{Q} (\cos \Omega x - 1 + \tan \Omega \ell \sin \Omega x) \quad (16)$$

Knowing that $\frac{dv}{dx} = \frac{P+kG_{\ell t}S}{N+kG_{\ell t}S} \theta + \frac{F}{N+G_{\ell t}S}$ and using the boundary condition $v(0)=0$ gives finally the solution for the deflection:

$$v(x) = \frac{F}{N+kG_{\ell t}S} \left[\frac{P+kG_{\ell t}S}{Q} \left(\frac{\sin \Omega x}{\Omega} - x + \frac{\tan \Omega \ell}{\Omega} (1 - \cos \Omega x) \right) + x \right] \quad (17)$$

This equation could be compared with eq. (11) and eq.(12), but the influence of the compression force Q on the stiffness is not easily understandable in eq. (17) because Ω depends also on Q.

3.3. Deflection of the compressed bended beam for small compressive loads

Let now see what happens if the compression load Q is small. If Q tends to 0, then Ω tends to 0. It is possible to use the Taylor expansion for $\sin \Omega x \approx \Omega x - \frac{\Omega^3 x^3}{6}$, and $\cos \Omega x \approx 1 - \frac{\Omega^2 x^2}{2}$, which finally leads to:

$$v(x) = \frac{F}{N+kG_{\ell t}S} \left[\frac{P+kG_{\ell t}S}{Q} \Omega^2 \left(\ell \frac{x^2}{2} - \frac{x^3}{6} \right) + x \right]$$

Replacing Ω^2 with its value gives:

$$v(x) = F \left[\frac{(P+kG_{\ell t}S)^2}{(N+kG_{\ell t}S)^2} \frac{1}{E_{\ell}I + \frac{NI}{S}} \left(\ell \frac{x^2}{2} - \frac{x^3}{6} \right) + \frac{x}{N+kG_{\ell t}S} \right]$$

The assumption of small compressive loads leads finally to:

$$v(x) = F \left(\frac{1}{E_{\ell}I + \frac{NI}{S}} \left(\ell \frac{x^2}{2} - \frac{x^3}{6} \right) + \frac{x}{N+kG_{\ell t}S} \right) = F \left(\frac{1}{E_{\ell}I + \frac{(P-Q)I}{S}} \left(\ell \frac{x^2}{2} - \frac{x^3}{6} \right) + \frac{x}{(P-Q)+kG_{\ell t}S} \right) \quad (18)$$

One recognizes eq. (12). So, this shows that it is theoretically possible to account the change of the pretension effect due to the compressive loads, by replacing the longitudinal load P do to the pressure inside the beam with $P-Q$, in the case of small compressive loads. This allows then using the “usual” solution for the deflection with a very little modification.

3.4. Buckling of the beam

When a beam is subjected to a pure compressive load, buckling can occur. This leads to a new limit load F_B that has to be added to the wrinkling load F_w and to the collapse load F_c . To calculate the buckling load, results of paragraph 3.1 have to be used. Eq. (15) gives

$$\frac{d^2\theta}{dx^2} + \Omega^2\theta = 0$$

for which the solution is $\theta(x) = A \cos \Omega x + B \sin \Omega x$. The boundary conditions are $\theta(0) = 0$ (the beam is clamped), and $\frac{d\theta}{dx}(\ell) = 0$ from eq. (10). This leads finally to:

$$\cos \Omega \ell = 0 \xrightarrow{\text{yields}} \Omega \ell = \frac{\pi}{2} + n\pi \quad (n = 1.. \infty)$$

There exist an infinity of solution for Ω . It is then possible to calculate the buckling load:

$$\Omega^2 = \frac{P+kG_{\ell t}S}{N+kG_{\ell t}S} \frac{Q}{E_{\ell}I+\frac{NI}{S}} = \frac{P+kG_{\ell t}S}{P-Q+kG_{\ell t}S} \frac{Q}{E_{\ell}I+\frac{(P-Q)I}{S}}$$

Then:

$$\Omega^2 \left[\frac{Q^2 I}{S} - Q \left(E_{\ell} I + \frac{PI}{S} + \frac{I}{S} (P + kG_{\ell t} S) \right) + (P + kG_{\ell t} S) \left(E_{\ell} I + \frac{PI}{S} \right) \right] = (P + kG_{\ell t} S) Q$$

Finally, if one considers the first term (in bold) to be negligible compared to the others in the preceding equation, it is possible to calculate directly Q . The buckling load of the inflatable beam is then obtained by replacing $\Omega \ell$ with its value $\pi/2$.

$$F_B = \frac{E_{\ell} I + \frac{PI}{S}}{\frac{E_{\ell} I + \frac{PI}{S}}{P+kG_{\ell t}S} + \frac{I}{\pi^2} + \frac{I}{S}} \quad (19)$$

3.5. Wrinkling load for the compressed bended beam

The apparition of wrinkle limits the domain of transverse loads for this study. The wrinkling load for the compressed inflatable beam must be calculated. Fig.7 shows the repartition of the longitudinal stresses due to the loadings. Fig 7.a. corresponds to the repartition of the stresses at the end of the inflation, for which the stresses are well known: $\Sigma_{xx}^0 = pR/2$. The black repartition of stresses in fig.7.b corresponds to the longitudinal stresses due to the compression which are superimposed to the stresses due to the inflation. This leads then to the decrease of Σ_{xx}^0 :

$$\Sigma_{xx}^0 = \frac{P-Q}{2\pi R} = \frac{pR}{2} - \frac{Q}{2\pi R} \quad (20)$$

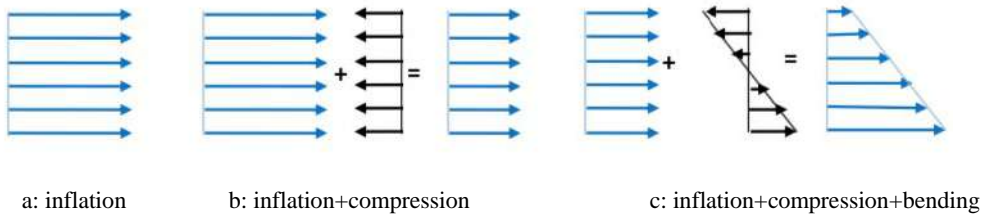


Figure 7: longitudinal stresses in the membrane for an inflatable compressed bended beam

Finally, it is possible to obtain the distribution of stresses for a compressed bended inflatable beam by adding the stresses due to the bending. Considering always the same criterion for the wrinkling load than in paragraph 2.2, this leads finally to:

$$F_W = \frac{p\pi R^3}{2L} - \frac{QR}{2L} \tag{21}$$

4. Analysis of results in a case studied

We present here some results for an inflatable compressed beam. Comparisons are made with the results of the 3D homemade software SAFE dedicated to inflatable structures. For practical reasons, the 3D simulations are conducted on the right configuration of the beam (see fig.8), which is equivalent to the left configuration: clamped compressed inflatable beam.

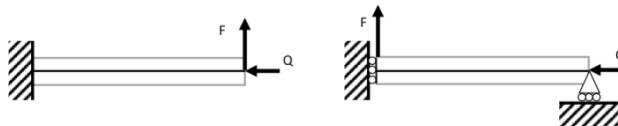


Figure 8: Boundary conditions for a compressed bended beam

The material properties and the geometrical parameters are given table 1.

Table 1: Material coefficients and geometrical parameters for the example

Parameter	Value	
Length in the natural state	L_ϕ	2.5 (m)
Radius in the natural state	R_ϕ	0,125 (m)
Longitudinal elasticity modulus in natural state	${}^\phi E_\ell$	210 (kN/m)
Transverse elasticity modulus in natural state	${}^\phi E_t$	210 (kN/m)
Shear elasticity modulus in natural state	${}^\phi G_{\ell t}$	50 (kN/m)
Poisson's coefficient in the natural state	${}^\phi \nu_{\ell t}$	0,2

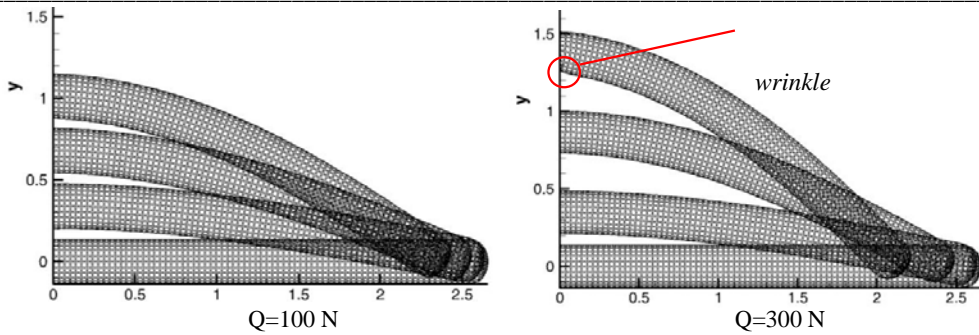


Figure 9: Results of the 3D membrane computations

Figure 9 shows the deflections of the beam for 2 compressive loads. The pressure in both cases is equal to $2 \cdot 10^5$ Pa. Three following increasing transverse loads have been used for each figure: $F=60\text{N}$, 156N and 267N for $Q=100\text{N}$, and $F=61\text{N}$, 169N and 248N for $Q=300\text{N}$. Since the three loads are closed for each series of simulation, the influence of the compressive load is clear. The higher the compressive load, the higher the deflection.

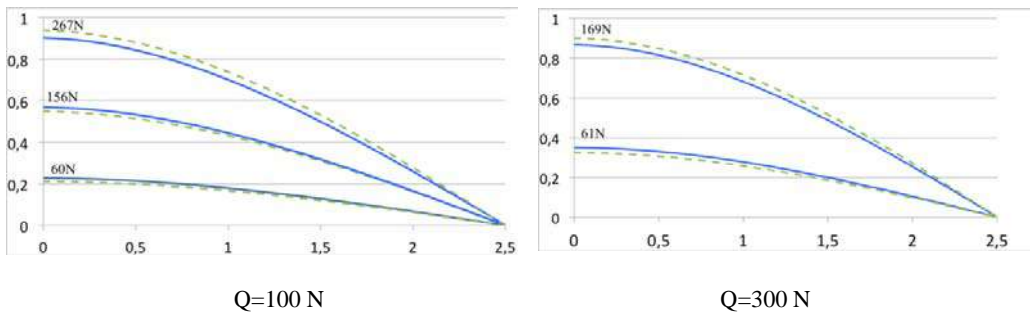


Figure 10: Comparison between the 3D results (blue) and the theoretical results (green)

Figure 10 presents the comparison between the results of the software SAFE and the theoretical results obtained with eq. (17). It shows that the effect of the compressive load is taken into account correctly because the differences between both calculations are less than 7% for the cases studied here. For the case $Q=300\text{N}$, the curves for the highest load are not given because the wrinkle has appeared at the left extremity, as can be seen on figure 9 (right).

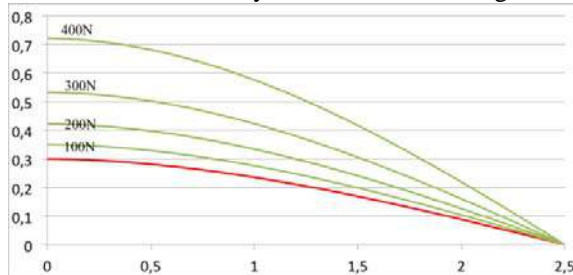


Figure 11: Influence of the compressive load

Fig.11 shows more clearly the effect of the compression. The radius of the beam in its initial state is 0,125m. This means that the force P inside the beam due to the pressure has an order of magnitude of 12kN. The compression loads used here are very small compared to P (less than 4%) here, but has clearly a significant effect. Ignoring the compression lead to an error in the deflection (red curve on fig 11). Moreover, it is also clear that replacing P with $P-Q$ (eq. 12) will not have an effect for the orders of magnitudes that are used in such applications. This formulation is valuable if P and Q are comparable, and for low values of Q .

5. Conclusion

Inflatable beams can be subjected to combination of loads. Although the strength of materials for inflatable beams is now well established for beams subjected only to transverse loads, combinations of loads have not been really investigated. To fill this gap, this study gives analytical solutions for compressed inflatable beams and comparisons with 3D membrane simulations, which have shown the accuracy of the solution. It has also been showed that the beams are very sensitive to the compressive loads.

References

- Tensinet association website. Retrieved from <http://www.tensinet.com>
- Fichter W. (1966), "A theory for inflated thin-wall cylindrical beams", *NASA Technical Note*, NASA TND-3466.
- Le Van A. and Wielgosz C. (2005), "Bending and buckling of inflatable beams: some new theoretical results", *Thin-Walled Structures*, vol 43, pp. 1166-1187.
- Nguyen Q.-T., Thomas J.-C., and Le Van A. (2013), "An analytical solution for an inflated orthotropic membrane tube with an arbitrarily oriented orthotropy basis". *Engineering Structures*, 56 (0), 2013, 1080 - 1091.
- Nguyen Q.-T., Thomas J.-C., and Le Van A. (2015), "Inflation and bending of an orthotropic inflatable beam". *Thin-Walled Structures*, 88 (0), 2015, 129 - 144.
- Thomas J.-C., Bloch A. (2016), "Non linear behaviour of an inflatable beam and limit states", *Procedia Engineering* 155, 2016, 398 – 406
- Thomas J.-C., Schoefs F., Caprani C. & Rocher B. (2018). Reliability of inflatable structures: challenge and first results, *European Journal of Environmental and Civil Engineering*

Proceedings of the TensiNet Symposium 2019

Softening the habitats / 3-5 June 2019, Politecnico di Milano, Milan, Italy
Alessandra Zanelli, Carol Monticelli, Marijke Mollaert, Bernd Stimpfle (Eds.)

Atrium Roof in the New Lilienthalhaus in Brunswick, Job Report

Bernd STIMPFFLE*, Michael SCHÄFFER*

*form TL Ingenieure für Tragwerk und Leichtbau GmbH, Güttinger Straße 37, 78315 Radolfzell, Germany,
bernd.stimpfle@form-tl.de

Abstract

Vis-à-vis to the Brunswick research airport the new Lilienthalhaus, a four storied service and office building has been opened as the first part of the new developed Lilienthalquarter. Not only the location is vis-à-vis to the airport building, also the architecture is in contrast to the 1940th airport design. The architect Hartmut Rüdiger from Architekten Rüdiger Brunswick wants to represent the new break up at this area with new technologies and services. Nearby the German Luftfahrt Bundesamt and several aviation research plants are located. The Volksbank Brunswick as building owner together with the city of Brunswick want to develop a new progressive business park. The triangular plan view with its rounded sides was developed based on the site plot and other boundary conditions. The building is a monolith without extensions exceeding from its primary shape. Also the transparent roof structure and the entrance is placed behind the primary border lines.

Keywords: ETFE, cushion, pneumatic, cable surrounded, inflation system, integrated drainage, structural design, analysis, installation

DOI: 10.30448/ts2019.3245.09

Copyright © 2019 by Bernd Stimpfle, Michael Schäffer. Published by Maggioli SpA with License Creative Commons CC BY-NC-ND 4.0 with permission.

Peer-review under responsibility of the TensiNet Association

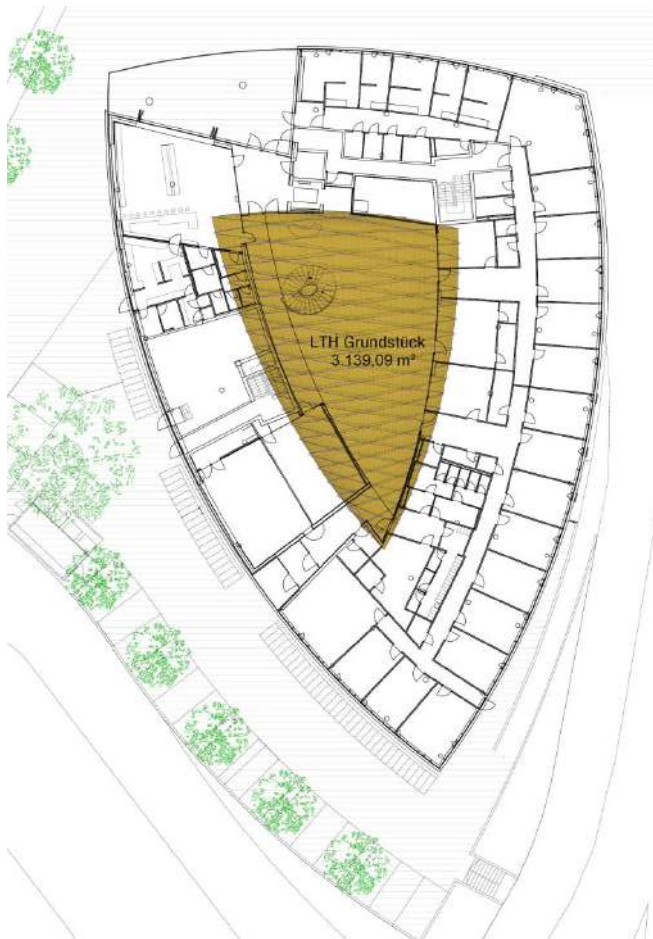


Figure 1: plan view Lilienthalhaus with highlighted ETFE-cushion roof (Rüdiger Architekten/formTL)

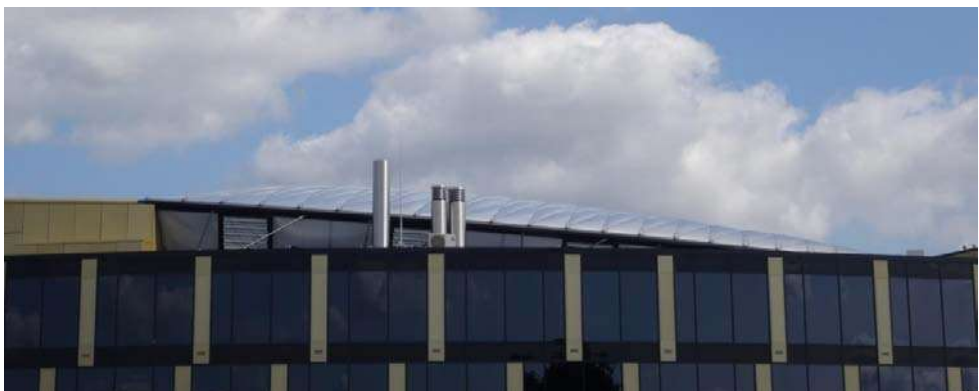


Figure 2: façade with ETFE-cushion-roof (formTL)

The entrance leads into the bright atrium with a sculptural spiral stair. The roofing of this area is almost invisible. The transparent roof is not located directly on the concrete structure. The roof is lifted up, so that the skylounge which is placed on top of the fourth floor is integrated to the atrium area. So the roof surface is inclined from top of fourth floor to the top of third floor at the tip of the triangle. To get a complete open image the border frame of the roof is placed behind the concrete parapet. Hence the roof-facade is inclined and has also transparent cladding.



Figure 3: Atrium (Hanno Keppel)

In the initial design step a glass roof was intended. The heavy primary steel structure for the glass roof required a sprinkler system. To avoid additional cost the client searched for alternative solutions. With the big ETFE-cushion this was solved. The primary steel structure is a perimetral steel frame, placed on the concrete structure. The load carrying cables forming the cushion reinforcement are the only primary steel parts placed upon the atrium.

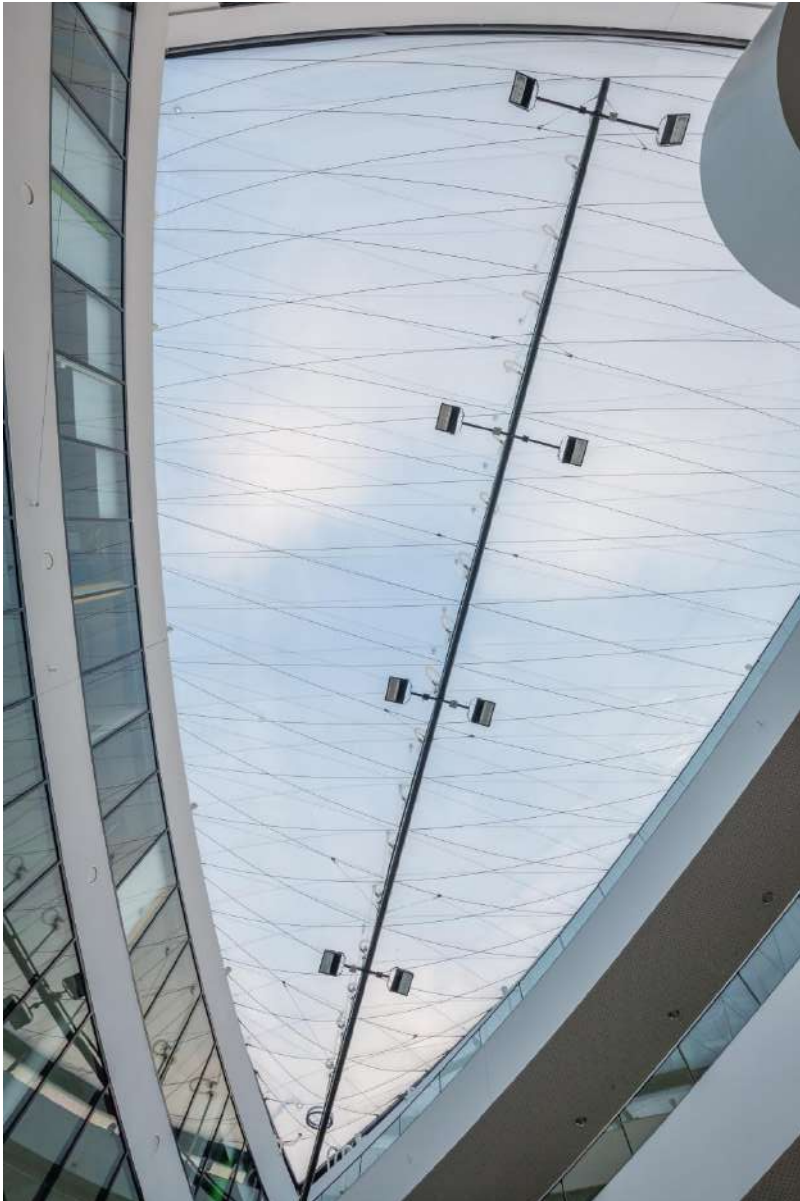


Figure 4: view from below to the atrium roof (Hanno Keppel)

The stainless steel cables with a diameter of 10 mm have an overall weight of 711 kg on a covered ground area of 430 m² which gives a unit weight of just 1.7kg/m². In case of fire the ETFE foil with its melting temperature of approx. 270°C will open the roof before reaching melting point of the stainless steel cables, so that the primary atrium structure cannot fall down due to fire. The ETFE-foil with its B1 certificate according to DIN 4102 and being not dripping burning was approved by the authorities.



Figure 5: ETFE-cushion with stainless steel cable reinforcement (Hanno Keppel)

The structural principle of the large cushion structure is a perimetral steel frame according to the shape of the atrium area raised on the upper concrete slab. With this raise the frame moves back and opens a larger space than the ground floor itself, so the roof gets even more light. The inclined sidewalls are also covered with ETFE-cushions and allow more light coming in.

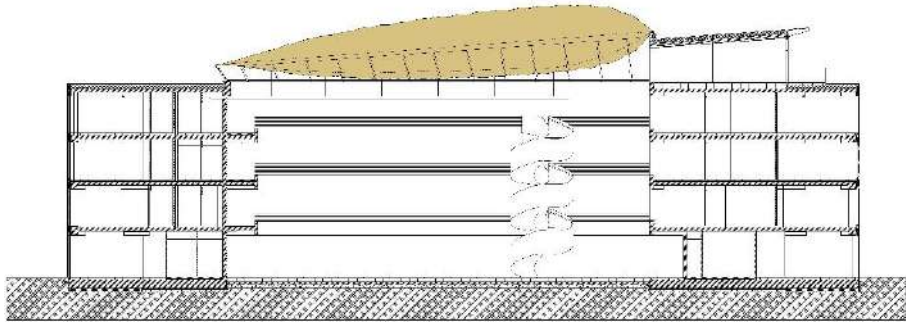


Figure 6: longitudinal section (formTL)

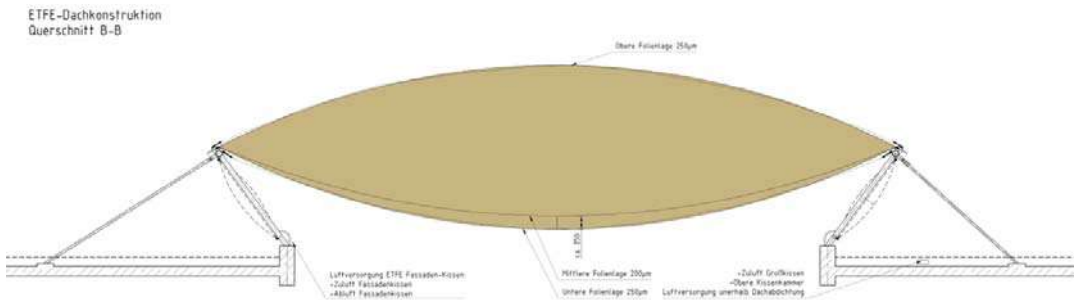


Figure 7: cross section (formTL)

The main space upon the atrium is covered by a single cushion consisting of three layers. The cushion with its covered area of 430m² was fabricated in one piece. The upper and lower layer are supported by steel cables so that the maximum foil stress can be safely carried.

Brunswick is located in the area called North German Plain where high snow loads have to be applied. 1.5 kN/m² as accidental snow load case has to be carried by the increased inner pressure in the cushion. So the maximum pressure is defined with 1600 Pa. To reduce the forces in the cables and also to the steel structure the sag of the ETFE-cushion was increased. The result was the reduction of the forces in the cables. Stainless steel cables 1x19 with a diameter of 10 mm are sufficient. The ETFE-foil is not connected to the cables, so the cables can slide on the foil and local stress peaks between cables and foil are avoided. The horizontal loads of the cables are guided to the border frame and then into the concrete slab. The concrete structure is has no expansion joint so the inner forces of the cushion are coupled in the slab level.

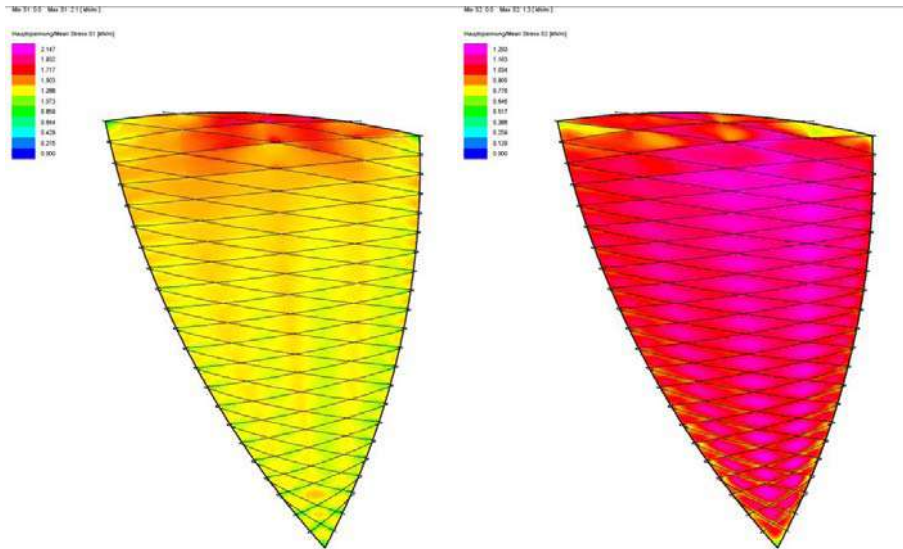


Figure 8: foil tension in longitudinal and cross direction at 800 Pa inner pressure (formTL)

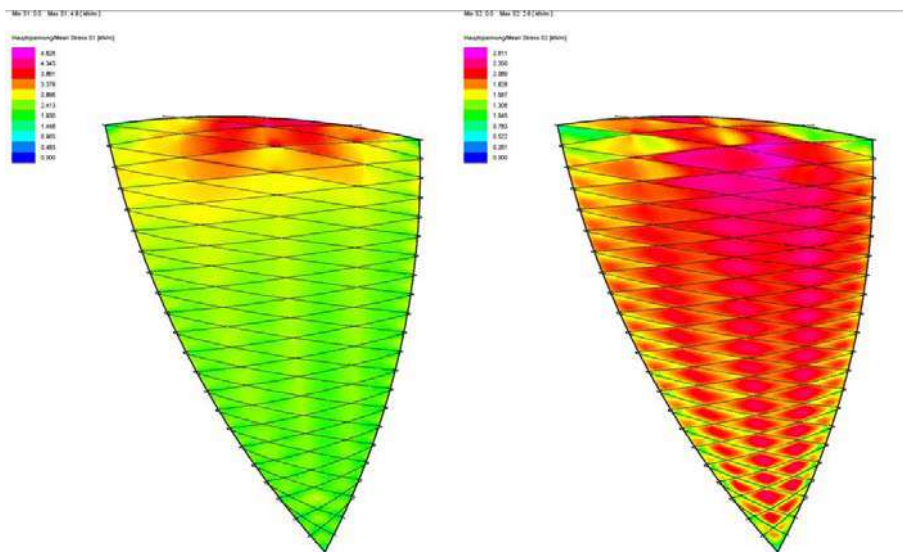


Figure 9: foil tension in longitudinal and cross direction at 1600 Pa inner pressure (formTL)

The cushion volume is about 1100 m³ split in two chambers. The middle foil layer is located near to the lower layer so the chambers have different volumes. The lower volume has also less convection and so a better thermal insulation. The U-value for a three layer cushion is about 2.0 W/(m²K). The inner layer is not reinforced. To avoid wrinkles in the foil the pressure between the upper and the lower chamber is 50 Pa. With this little difference in pressure the foil has a significant prestress. The usual inner pressure is 350/300 Pa. In case of

snow load the pressure is increased according to the snow height up to 1600/1550 Pa controlled by a snow sensor. The differential pressure in the chambers is controlled by the blower system which is executed as circuit. Only air loss, due to leakage and diffusion must be replaced with air from the outside. With this closed system the required energy for drying can be reduced significantly.

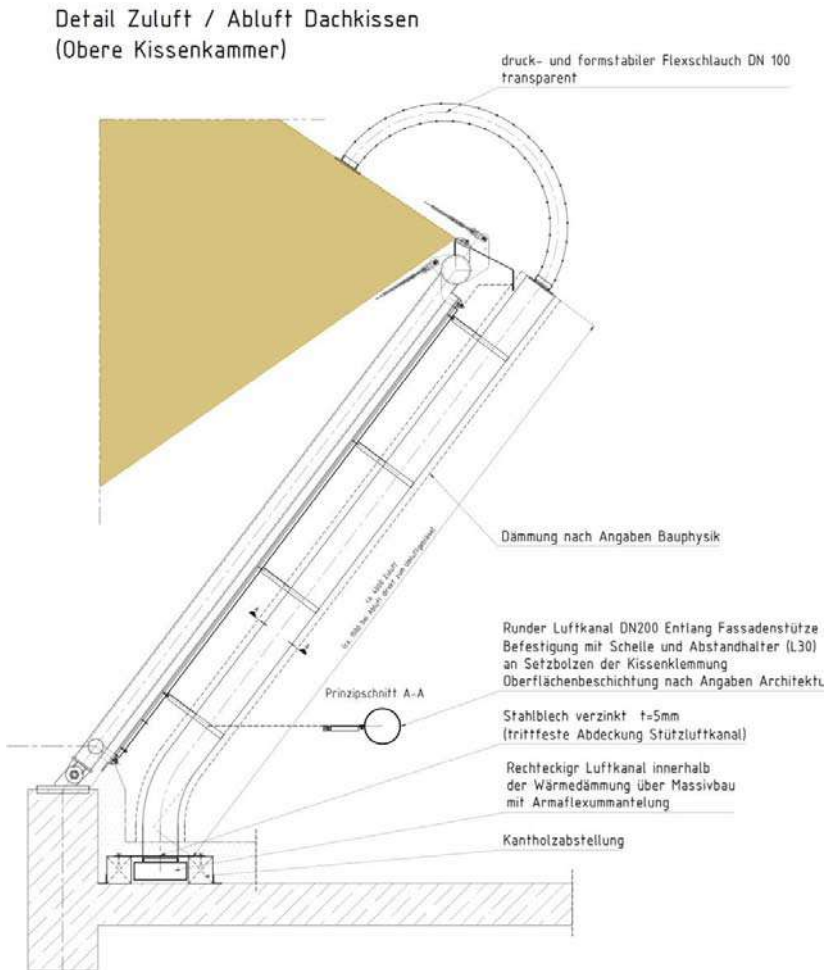


Figure 10: detail air supply for ETFE-cushion (formTL)

In case of pressure loss in the cushion over longer period, the cushion deflates and the three layer of foil lay on each other. The middle foil layer is stretched to the inner layer. This strain is not big because of the close location of the two foils. The strain is in the elastic range of the foil. So once the cushion is up again the inner foil will return to its initial state. When the three foils lay on each other water cannot drain over the border frame. To avoid water accumulation several flexible drainage pipes connect the outer and the inner foil so that water

take a look at a small sample of foil. In the overall appearance of the roof a silver shadow is realized, but it remains transparent and light. Only in direct comparison with the printing is realized.



Figure 13: cable connection detail with printed upper cushion layer (formTL)

In comparison to a glass covered roof structure the installation is easier and also faster on site. The primary steel structure is placed on the upper concrete slab. So the installation of the elevated surrounding steel frame can be done directly from the main building roof without scaffolding.

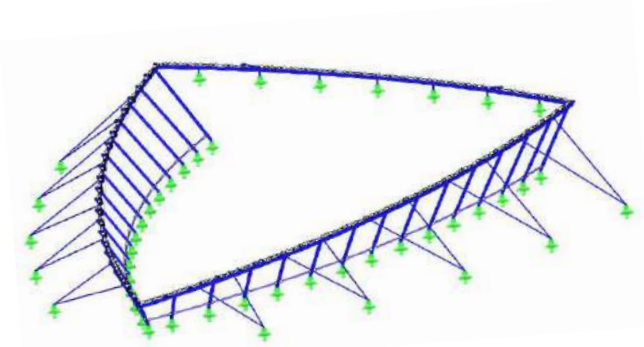


Figure 14: primary steel frame (formTL)

The lower cable layer was installed from the border of the atrium. Afterwards the pipe for the emergency drainage and the atrium lighting was lifted up and installed by using the crane before closing the roof. For the following installation of the cushion an installation net was fixed to the steel-frame. The three layer ETFE-cushion was completely prefabricated. All three layer were welded tight and have only one surrounding keder. This is the only fixation of the cushion to the primary structure. The whole foil-package has an overall weight of 450 kg and was lifted up in a timber box with a mobile crane to the middle of the installation net.



Figure 15: installation web, view from below (formTL)

To avoid elongation in the foil, horizontal belts were spanned in plane of the frame. The foil was spread out on this support and the border was clamped to the pre installed border clamps. On the horizontal installation plane the ETFE-cushion was clamped without any stress. Afterwards the upper cables were installed, the belts removed and the cushion was inflated.

Acknowledgements

Client: Volksbank BraWo Projekt GmbH, Braunschweig

Architect: Hartmut Rüdiger, Braunschweig/DE

Structural design of the atrium roof formTL ingenieure für tragwerk und leichtbau gmbh

Contractor: Temme // Obermeier GmbH, Rosenheim

Picture credits: Hanno Keppel, Braunschweig and formTL, Radolfzell

References

Schäffer, M., Stimpfle, B.: ETFE Großkissendach über dem Lilienthalhaus in Braunschweig, *Stahlbau* 87 (2018), Heft 7

Schäffer, M., Stimpfle, B.: Luftfahrtpionier als Namensgeber, Membranüberdachung für ein Atrium, *DIB*, 7-8-2018

Sauerbrei, C.: Fast so leicht wie Luft, Lilienthalhaus, Braunschweig, *DBZ*, 7-8-2018

Proceedings of the TensiNet Symposium 2019

Softening the habitats / 3-5 June 2019, Politecnico di Milano, Milan, Italy
Alessandra Zanelli, Carol Monticelli, Marijke Mollaert, Bern Stimfle (Eds.)

“Auditorium 1919 Sacmi” - Evaluation of the technological performances in the design phase of the walls and roof subsystem realized with ETFE cushions.

Beniamino DI FUSCO*, Andrea ANGELERI^a

*Eoss Architettura, Napoli, Italy, b.difusco@eoss.it

^aCanobbio Textile Engineering

Abstract

"Auditorium 1919" is a building of high qualitative value both in terms of content and aesthetics, an innovative, eco-friendly auditorium linked to the size of man and his wellbeing signed by the architecture studio A2 studio Gasparri e Ricci Bitti Associated Architects.

EOSS Architettura and Canobbio Textile Engineering dealt with the executive design, construction and installation of the façade and the roof realized with ETFE cushions. During the engineering phase of the aforementioned building components, particular attention has been given to the correct definition of the technological performance requirements like energy optimization, thermal properties, definition of design service life, durability, focus on minimum ordinary maintenance activities.

In this regard, considering the continuous technological progress of technical fabrics for building industry and the methods of application of the same, various operators (fabric producers, research centers, etc...) have been involved. For example, for the definition of the thermal performance of the façade and the roof, necessary to verify the environmental sustainability of the chosen solution, the Politecnico Milano Textile Hub was involved through a computational simulation "*Optical and Thermal characterization of a multi-layered ETFE*"

DOI: 10.30448/ts2019.3245.44

Copyright © 2019 by B. Di Fusco, A. Angeleri. Published by Maggioli SpA with License Creative Commons CC BY-NC-ND 4.0 with permission.

Peer-review under responsibility of the TensiNet Association

1. Introduction

"Auditorium 1919" is a building of high qualitative value both in terms of content and aesthetics, an innovative, eco-friendly auditorium linked to the size of man and his wellbeing signed by the architecture studio A2 studio Gasparri e Ricci Bitti Associated Architects.

According to Sacmi 1919 auditorium designers, developing a project with apparently simple shapes but a channeling of attention, where light and architectural volumes merge, giving the structure dynamism and lightness, it was the main challenge "... *the quality of the result essentially depended on two elements: transparency and ... absence*". "So we thought about *"textile walls"*, inspired by the use of this extraordinary material - bubble-like air cushions defined by ETFE fluoropolymer membranes - used in the most modern and famous sports facilities of the world, such as the Allianz Stadium of Munich or the Sea World of Beijing, but also in projects at the forefront of urban furnishing. *"Appropriately hooked to the iron structure and" inflated with compressed air, these membranes make it possible to create covered spaces while maintaining the same light as open spaces, with extraordinary performance in terms of resistance to climatic conditions. The result, in terms of aesthetic effect, is a building almost suspended within these "bubbles"*.



Figure 1: View of the building (photographer Lorenzo Rinella).



Figure 2: View of the ETFE skin (photographer Lorenzo Rinella).

A structure where transparency dominates, that polite, never brazen transparency that is well suited to a high-level professional, social and cultural environment: permeable inside, from the outside the “bubbles” play a double effect, sometimes veil, some other mirror. On the other hand, the protagonist is the natural light that intervenes, redefining the rooms according to the time of day, the appearance of the sky, even the mood of the individual visitor. Light and transparent, the bubbles envelop the structure, and allow a dialogue between the volumes that seem to float in them.

The notes given by the architects Gasparri and Ricci Bitti, designers of the auditorium, express the intentions at the base of the project, and more specifically define the architectural and performance characteristics that the building envelope should have guaranteed. The architects Di Fusco and De Rosa, of EOSS Architettura Studio associated, with Canobbio Textile Engineering, engineer Angeleri, took care of the executive design and construction of steel structures and ETFE cushions.

2. Design Development.

Referring to the reported standards and to the requests made by A2 Designers, in the executive design phase of the facades and roofs made with ETFE multi-layer cushions, particular attention was paid to defining the performance requirements of the following technological components that would later define the building envelope:

- etfe cushions
- cushions anchoring system
- metal support structure
- connecting elements with the other surfaces of the building
- arrangements for the passage of technical systems

In this respect, the executive design proceeded together with the verification, at Canobbio manufacturing company, of connection details of metal parts, the technical joints, the pillow detailing, etc. and with the verification at some research laboratories of the performance characteristics of the materials used such as the determination of the thermal transmittance of the ETFE cushions, the latter performed by the Politecnico di Milano through the computational simulation "Optical and thermal characterization of a multilayer ETFE"

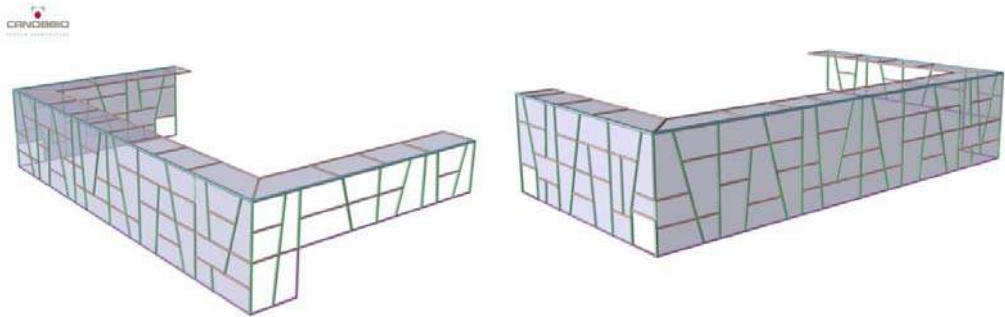


Figure 3: Geometrical model.

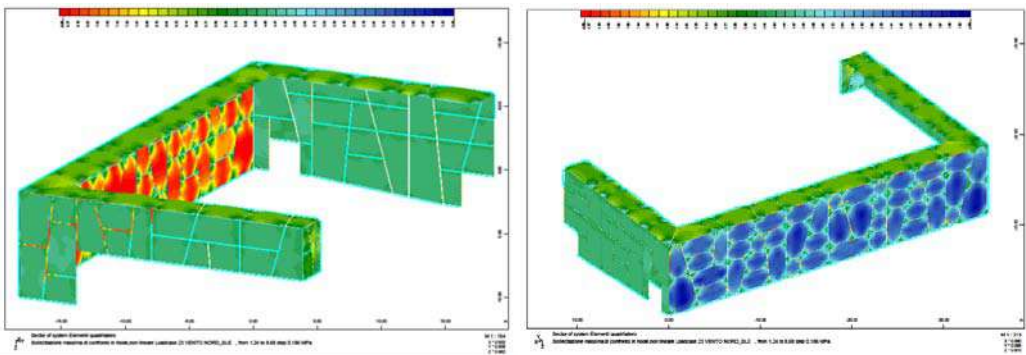


Figure 4: Structural model.

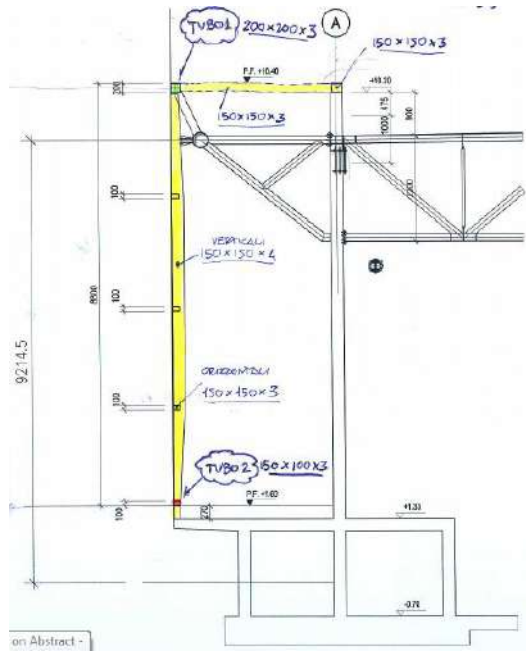


Figure 5: Typical cross section view.

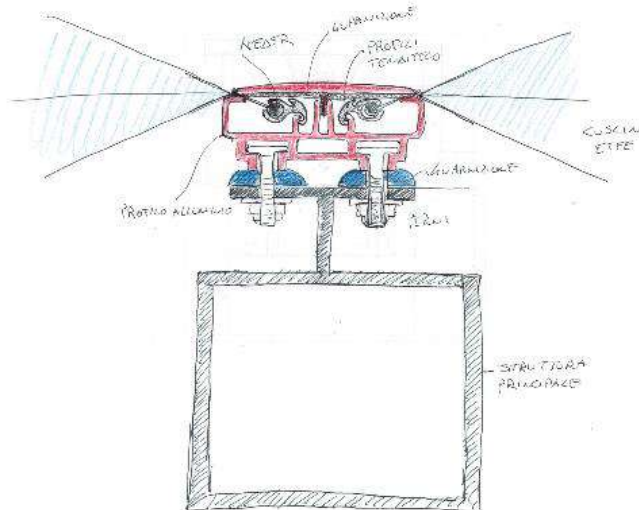


Figure 6: Connection detail between steel structure and ETFE pillows

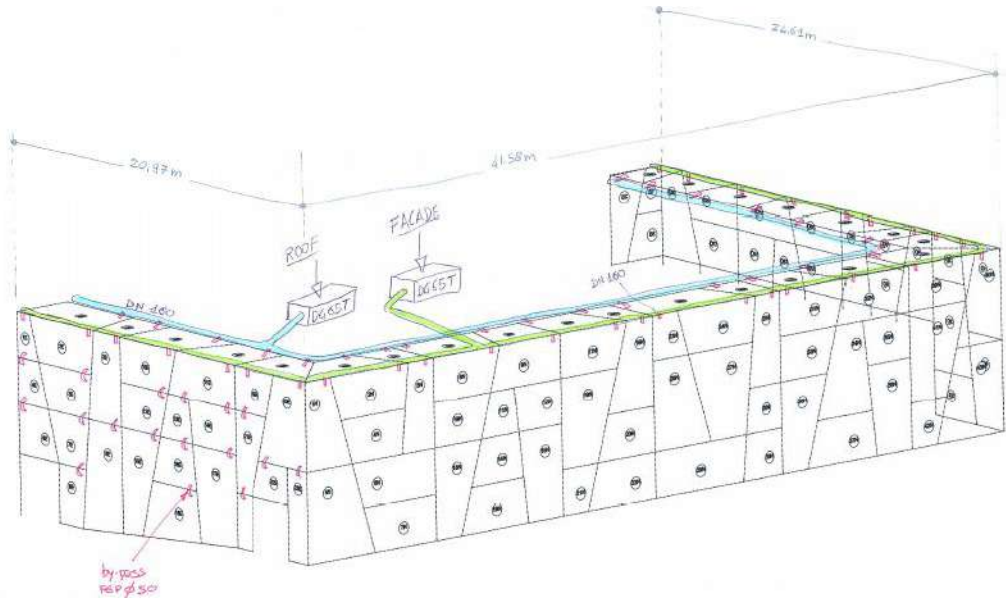


Figure 7: Air inflating concept.

3. Mock-up

The construction of the Mock up of a portion of the façade in a space made available by the client allowed to check definitively with the architects of the A2 Studio, with the client and with the other technicians involved, whether the objective of building an high quality cladding, capable of meeting all the requirements established in the preliminary design phase was achieved.



Figure 8: Mock-up drawing and mock-up at the Client's shop.

The result was the design and construction of a building with a very slender metal structure thanks to the lightness of the ETFE, weighing about one percent of the glass while providing the same standard of insulation. The design and construction of a building organization that, according to the principles of "biomimesis", allows the building to be changeable: the cushions depending on the incidence of sunlight are more or less reflective, more or less transparent; it also allows dynamic response to climate stresses: the air cushions, with the right sensors and controls, inflate / deflate depending on the weather conditions of the climate

4. Some Numbers

Pneumatic Structure is performed with "3 layer pillows" with ETFE films $250\mu\text{m} + 100\mu\text{m} + 250\mu\text{m}$. The pillows are stabilized with an internal pressure of 400Pa for the facade, and 400 Pa for the roof, up to 600Pa in case of snow.

It represents the perfect fusion of aesthetics and technique. The façade and part of the cover made of 3-layer ETFE cushions demonstrates its ability to innovate not only the world of architecture, but in terms of technology and design.

Amount of roof cushions = 17x

Amount of facade cushions = 86x

Total cladded area = 1.000 sqm

The objective of the thermal and solar transmittance was:

U value = 1.9 [W/m²k]

g-value = 0.71

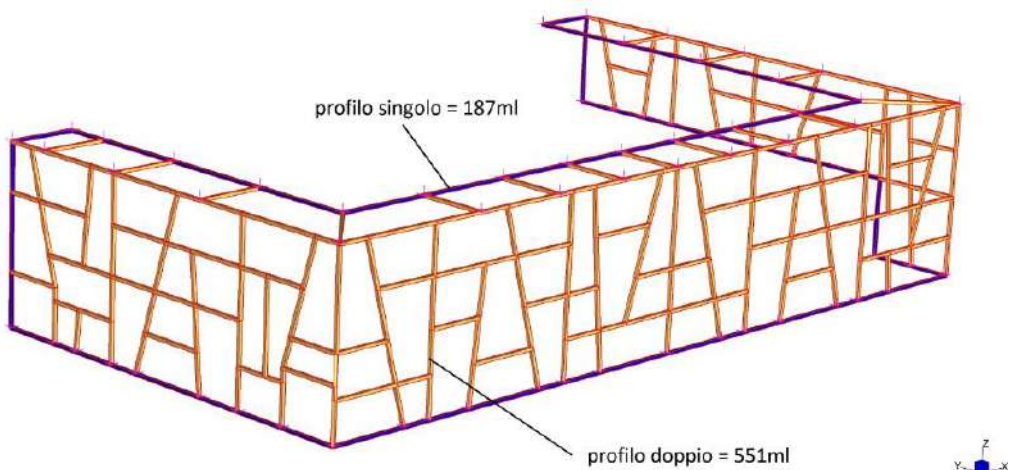


Figure 9: supporting structure layout.



Figure 10: ETFE pillows of the facade

5. Optical and Thermal characterization of a multi-layered ETFE - SACMI

In the project “Auditorium 1919” the thermal performance of the facade was a fundamental issue for the correct evaluation of the environmental sustainability of the solution. Therefore, Politecnico di Milano Textiles hub has been involved to determine the parameters by means of a computational simulation “Optical and Thermal characterization of a multi-layered ETFE – SACMI”. According to the results obtained from the analysis, it has been determined that the 3-layer ETFE cushion solution meets the general given sustainability requirements.

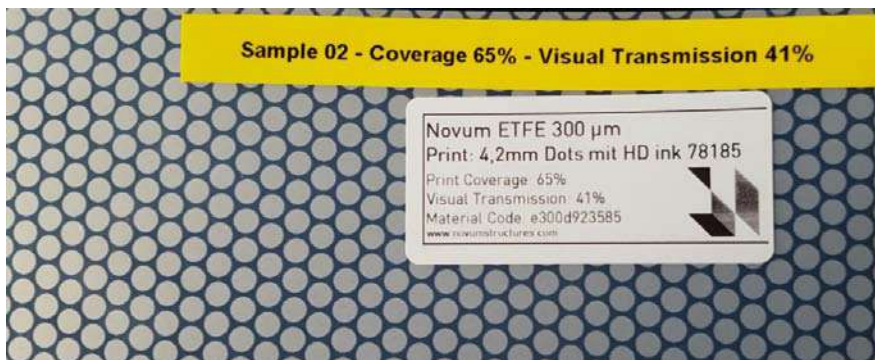


Figure 11: Fritted layed chosen for the top pillows.

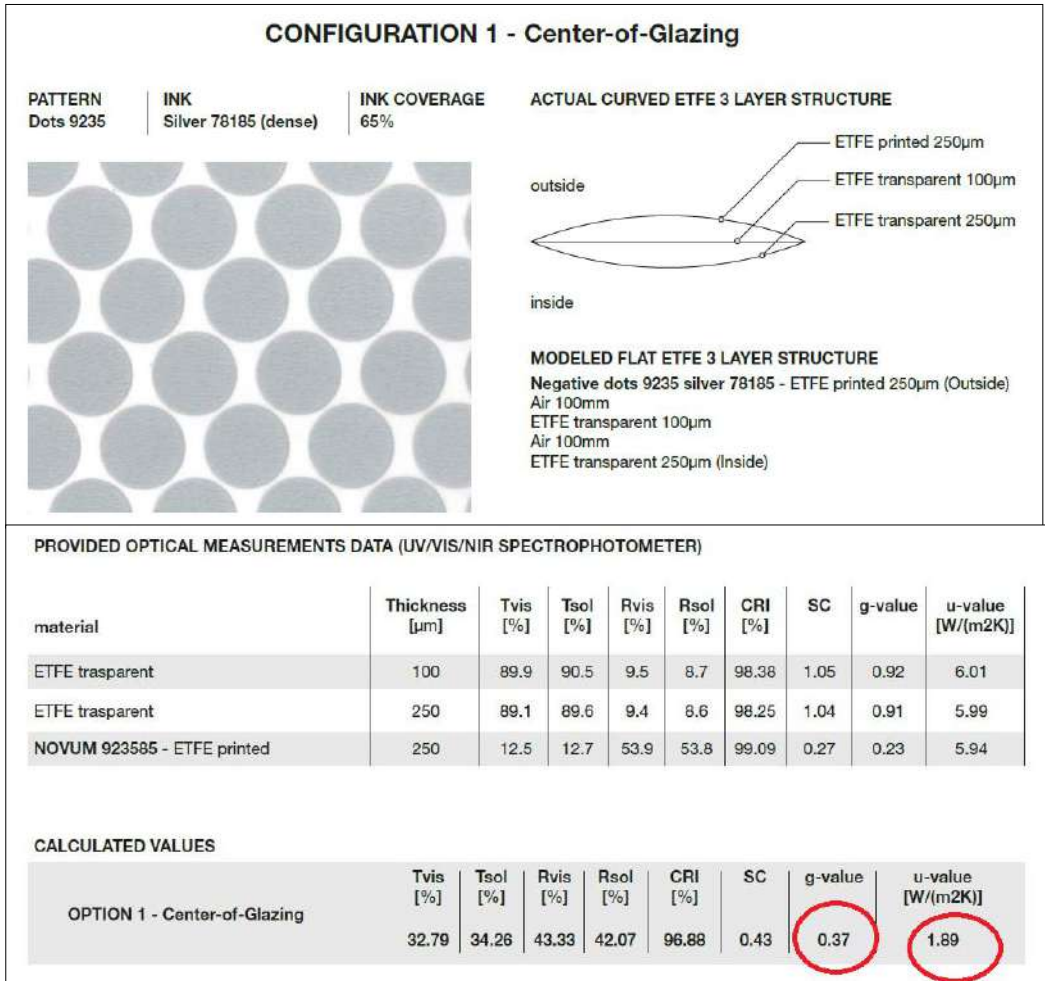


Figure 12: Optical and thermal characterization

6. Site Installation



Figure 13: Main supporting structure.

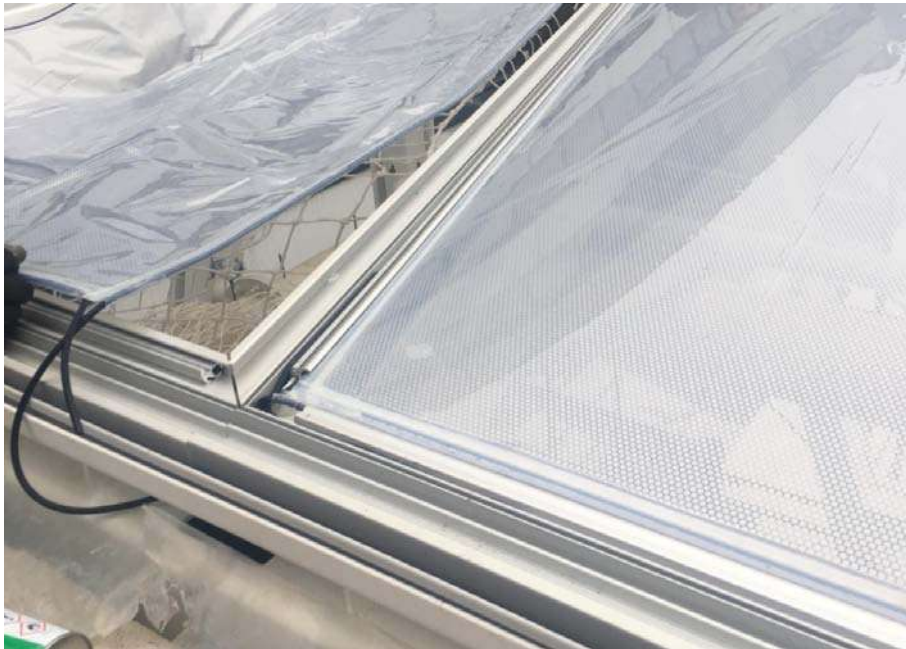


Figure 14: Typical roof corner detail.



Figure 15: Installation of the facade pillows.

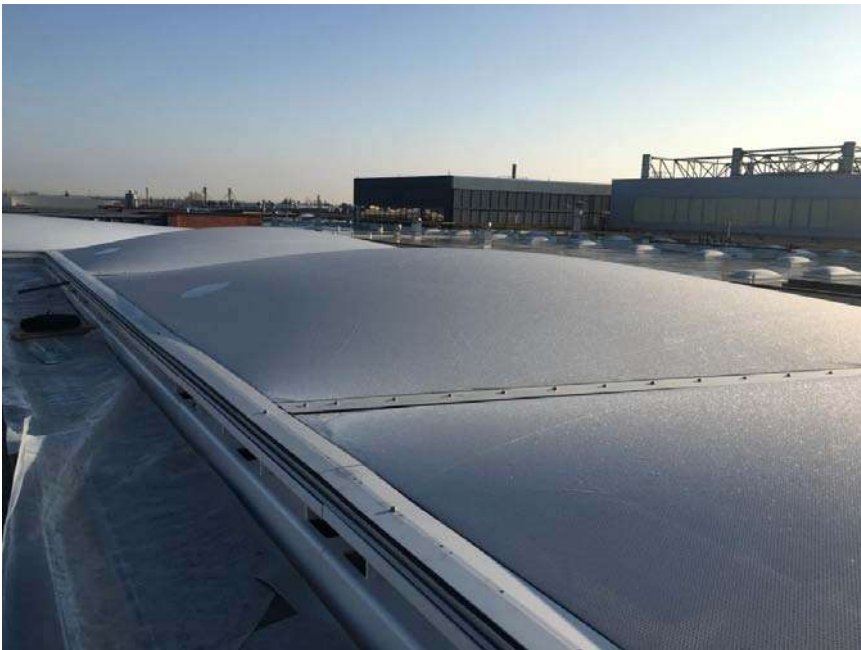


Figure 16: Inflated roof ETFE pillows



Figure 17: Inflated facade ETFE pillows.



Figure 18: View of the complex by night with the effects of the lighting system embedded in the pillows (Photographer: Lorenzo Rinella).

Proceedings of the TensiNet Symposium 2019

Softening the habitats / 3-5 June 2019, Politecnico di Milano, Milan, Italy
Alessandra Zanelli, Carol Monticelli, Marijke Mollaert, Bernd Stimpfle (Eds.)

Anchoring emergency lightweight shelters

Josep LLORENS*, Daniel LEDESMA^a

*School of Architecture of Barcelona (ETSAB), Universitat Politècnica de Catalunya
Diagonal 649, 08028 Barcelona, Spain
ignasi.llorens@upc.edu

^a International Federation of Red Cross and Red Crescent Societies - Shelter Research Unit (IFRC-SRU)
10 Cité Henri Dunant, L-8095, Bertrange

Abstract

Field tests have been conducted to address the question: ‘what are the major aspects to consider using anchors in the humanitarian sector?’. Influence of soil, weather, type and combination of anchors, installation, orientation, inclination, depth, displacement and price have been measured. An extensive study of anchor usage, practice recommendations with step by step checklists and a handout for humanitarian field practitioners is provided to identify the best anchoring option for their context of intervention.

Keywords: soil anchors, emergency shelters, tents

DOI: 10.30448/ts2019.3245.04

Copyright © 2019 by Josep Llorens, Daniel Ledesma. Published by Maggioli SpA with License Creative Commons CC BY-NC-ND 4.0 with permission.

Peer-review under responsibility of the TensiNet Association

1. Introduction

Anchors and foundations play an essential role in the structure of emergency shelters. A failure of the anchors can be the first in a series of dramatic ones. Its undesirable consequences are either the shelter being blown away by the wind as ground resistance is lost or the shelter collapses due to loss of structural stability. Good anchoring is a prerequisite to reach the effective shelter lifetime, and it is relevant to economic and effective material usage, because within the family tent ridge-2015 it accounts for a significant percentage of the total mass.

Soil anchors have been extensively investigated and documented for permanent and heavy applications. They involve frequently the consumption of concrete and, therefore, cannot be considered light, neither recoverable nor sustainable. On the other hand, available data on anchors for emergency shelters and tents is commercial, scarce, dispersed and insufficient.

This anchoring study starts from the specific requirements of emergency lightweight shelters and tents formulated by the International Federation of Red Cross and Red Crescent Societies - Shelter Research Unit (IFRC-SRU), with the overall objective of contributing to the reduction of shelter related vulnerabilities that put the inhabitants' lives at risks.

Field tests on 18 commercial anchors of three types (pegs, screws and buried anchors) have been conducted in five different soils measuring forces and displacements. The anchors were selected according to their appropriateness for emergency shelters and availability. A total of 66 suppliers were contacted, 37 anchors were received, out of which 18 were finally chosen.

2. Antecedents

Antecedents of passive anchors can be found in Nature. Roots feed plants and provide uplift resistance against the wind **involving a volume of soil** (fig.01). Stakes have been used for anchoring tents like the Bedouin tent (fig.02), the Tabernacle, the military tents or the circus tent.

Sea anchors attach the ships to the sea bed. A high efficiency ratio is needed in order to withstand heavy loads with minimum self-weight. Metal flukes bury themselves in the soft bottom or hook on to rocks. They are installed from a long distance through the chain that attaches it to the mooring vessel. They are recoverable breaking them out of the bottom by shortening the rode until the vessel is directly above the anchor.

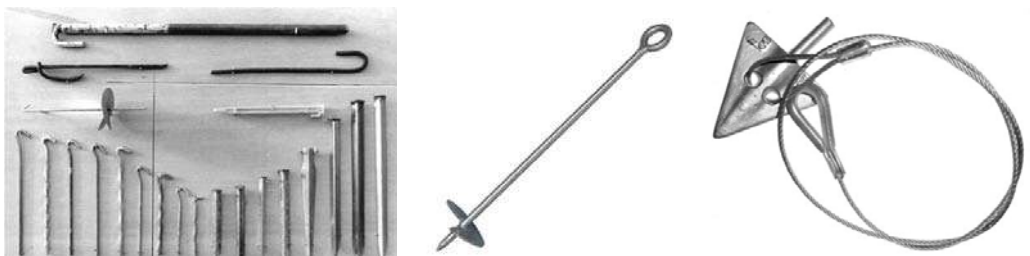


Figures 1,2: Antecedents of anchoring shelters can be found in Nature and vernacular architecture.

More recent examples are the anchors for bridges, mobile homes, antennas, poles, transmission towers, pipelines, buried tanks, equipment, runways, agricultural installations and cattle.

3. Typology

Soil anchors can be active or passive. Active anchors are prestressed by initially tensioning against a steel bearing plate. The level of prestress is a percentage of the design-working load. When the prestressed anchor is externally loaded, it behaves as a much stiffer member than a dead anchor. Passive anchors act only against the soil when loaded. They move more than active anchors, but they are simpler and involve fewer problems of relaxation and durability. They can be subdivided into two main groups according to whether they reach the surface of the ground or are buried.



Figures 3, 4, 5: Pegs, screw anchor and arrowhead anchor (percussion-driven).

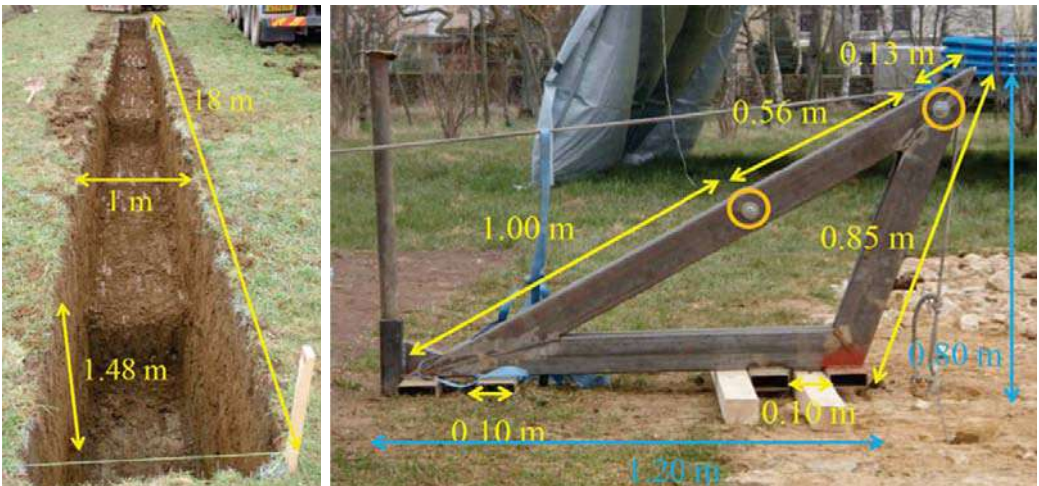
Anchors reaching the surface are mostly pegs (fig.03), also called stakes: various profiles include round, flat, V-shaped or T-shaped. Most common materials are metal, plastic and wood. Force is essentially transferred by compressing the soil. Another type of anchor that can reach the surface or be buried is the ballast anchor. It is generally made of a heavy

material such as concrete, earth or water and uses its own weight. If the ballast anchor is buried, the friction surface is bigger and the anchor is stronger.

Two other types of buried anchors are the screw anchors (fig.04) or helical anchors and the percussion-driven anchor (fig.05). The screw anchor consists of a rod with a helix straddling or in some cases of a body in the form of a helix itself. It is inserted into the soil just as a screw and use the surfaces of the helix in order to create resistance by compression of the soil above. The percussion-driven anchor (or mechanical anchors) is composed of a base attached to a cable called tendon. Similarly to the screw anchor, it uses the surface of the buried and armed base to create resistance by compression.

4. Field tests. Equipment

In order to obtain useful data inputs for the identification of important aspects, a series of test was conducted. The materials used include:



Figures 6: Soil trench. Figure 7: Pulling system

a) Pulling system composed of a steel cable, a motorized winch and a triangular steel construction to control the angle of pull (fig.07).

b) Measuring system: dynamometer.

c) Four soil trenches, dimensions $\ell=18$, $w=0.8$ and $h=0.6$ to 1.5 m were filled with different kinds of soils, compacted in layers of 30cm (fig.06). These soils were chosen in order to

create a representative diversity (sand, silt, rocky sand and clay rocky sand). A fifth sample was provided by the original natural soil (clay + sand).

d) 18 Anchors belonging to three categories: 8 pegs, 3 screws and 7 percussion-driven ones (see annex for more details). A total of 66 suppliers were contacted, 37 anchors were received, out of which 18 were finally selected for the final test sets.

5. Field tests. Procedure

Similarly, to wind loads applying punctually, the test was conducted by activating the winch step by step, hereby pulling each time a bit more on the anchor. Each time, the displacement of the anchor in the direction of the pull and the forces were measured and written down. The obtained data resulted in two outputs: the maximum performance for a displacement lower or equal to 5 cm (+/- 1) and the absolute maximum performance measured independently from the displacement. Preliminary tests were carried out to determine the relevant effects of inclination and position. The reference IFRC-SRU 2018 includes a complete description.

6. Field tests. Results

A detailed exposition can be found at IFRC-SRU, 2018. Most important findings concern to:

- **Weather** exists under the ground too. Different performances have been measured depending on temperature and precipitation.

- **Limit states.** Two outputs were obtained with the tests: the overall peak performance without constraints and the peak performance reached with a constraint, a displacement limit of 5 cm (+/-1). Big differences between the values, were sometimes observed. Pegs and screws show a difference smaller than 3 times while percussion-driven anchors can reach as much as 8. Thus, percussion-driven anchors can need substantially more displacement before reaching their maximum capacity.

- **Maximum resistance.** The highest resistances were observed for percussion-driven anchors. Independently of the soil, the strongest anchors always reach 6 kN and in some cases the output was higher than 12 kN. For the case of screw anchors, forces measured were considerably lower: for all compatible soils, the most performing anchor reaches 3 kN in all of them. For pegs, only one model in one soil reaches the 3 kN threshold.

- **Incompatibilities.** Observed incompatibilities were screw anchors in 'Gravel-Sand' and 'Silt' and the biggest percussion-driven anchors in 'silt' and 'rocky-sand' soil.

- **Ease of use.** Pegs and screw anchors are relatively easy to set up. The only drawback which applies, especially for pegs is the hazard risk once installed (for instance with children playing). Therefore, sharp ends should be removed in pegs design. For percussion-driven anchors, the situation is clearly different: the arming process is a fundamental step which needs special skills. As it takes place invisibly, skilled experience is needed to correctly estimate whether the correct position is reached.

- **Removability, reusability.** For pegs and screw anchors, removal is rather easy. For pegs, pulling on the axis is generally sufficient as resistance is weaker in that setting. For screws, repeating the set-up instructions in the opposite order is sufficient and if the anchor is not damaged, it can be reused for future endeavors. For percussion-driven anchors, removal is only possible using a shovel if the soil allows burying but it is very time-intensive. Therefore, percussion-driven anchors should be perceived as single-use. A wrong placed percussion-driven anchor becomes a spilled anchor. (Percussion-driven anchors with a second rope for disarming and removal are not recommended for use in the humanitarian sector as inverting the ropes can have dramatic consequences).

- **Warning indicators.** In the case of screw and peg anchors, upward movements have a clear and strong visual impact, even if the displacement is only of a few centimeters. Strengthening measures must be taken urgently if anchors slide out. For percussion-driven anchors, the indicator is much subtler as only the distance between the eye-loop and the soil can serve as such. Regular measuring and recording is necessary.

- **Price is not a reliable indicator.** The ratio between price and performance is not stable. Two anchors of the same type and with the same price can show significant differences in terms of performance.

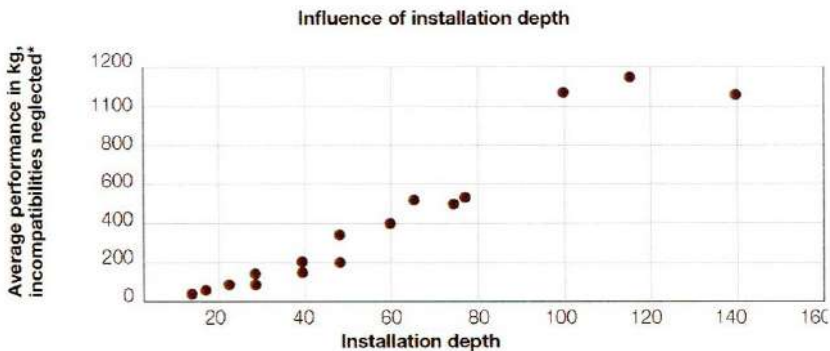


Figure 8: Depth increases performance independently of the type. In opposition to the unit price, a clear link does exist between the average performance and the depth of the 18 tested anchors.

- **X-crossing pegs is a limited improvement.** The resistance of three anchors, one being the peg itself and the other two creating additional resistance, is 10% higher than the one of a single peg.
- **Combination of pegs.** In order to increase forces, pegs can be combined by connecting several of them to the same guy rope. As, the same soil might be compressed twice, the force transferred per peg decreases.
- **Combination of percussion-driven anchors.** The resistance of combined percussion-driven anchors increases but the ratio overall peak performance without constraints / peak performance reached with a displacement limit of 5 cm is unstable.

7. Recommendations, observations and comments

- 1** Don't take any risks if shelters cannot be strengthened. The consequences of dismantling for a few days are much smaller than the ones of unusable or blown away shelters.
- 2** Forces applying to the shelter are highly dependent on the exact situation and shelter.
- 3** Wind speed is different from wind pressure, one of the forces impacting buildings.
- 4** Even after completion, weather conditions need to be monitored. If those ones become higher than the one structures are designed for, measures need to be taken.
- 5** The differences between the types of anchors are fairly big and need to be taken into account.
- 6** Instructions about how to use the anchors should always be distributed with the products.
- 7** If percussion-driven anchors are chosen, special attention should be paid to the arming process.
- 8** If the force is pulling in a different direction than the axis of resistance, the anchor might loosen the guy rope by moving. This is a risk to be considered beforehand.
- 9** Pegs use compression to transfer horizontal forces and friction to transfer vertical ones.
- 10** Screws and percussion driven anchors use both friction and compression in the same axis.
- 11** Always attach the rope as close as possible to the ground as this reduces the force applying to the anchor.
- 12** An anchor which is difficult to insert into the ground indicates a ground which is more difficult to compact and finally, a bigger resistance.
- 13** Anchors which do not reach their intended implementation depth are considerably weaker.
- 14** Check regularly anchors after installation and correct them if necessary. If an anchor cannot be fully inserted, attach the rope at the bottom, close to the soil.
- 15** Two types of soil are never 100% identical: different contexts = different soils = different anchor performances.

- 16** Don't trust previous experiences when using pegs. A peg which worked in the same location a few years ago will not necessarily work in that location again.
- 17** When identifying a location, cross-checking at different depths and at different points is necessary. A few meters are sufficient to change the type of soil.
- 18** Even once identified, the performance of an anchor can change as it is impacted by external influences (i.e. humidity variations).
- 19** Screw anchors are better suited for vertical than for diagonal pull.
- 20** Pegs were observed working best when implemented vertically into the soil. However, a guy rope pulling in the axis of the peg should always be avoided. Therefore, if the angle between the guy rope and the soil is smaller than 45° , the angle should always be installed vertically. Correct installation increases the performance by approximately 20%.
- 21** V and T-sections showed best performances when used with the sharp side pointing in the direction of the tent/guy rope. Correct usage increases the performance by approximately 20%. Together with the correct inclination, approximately 45% more resistance can be obtained.
- 22** The climatic context has a major impact on the anchor performances. Depending on the day, the performances of an anchor in a given soil can be different.
- 23** Depending on the type of anchors and soils, displacements bigger than 5 cm (+/- 1) might be required before reaching the full potential of the anchor (the maximum resistance). This is especially the case for percussion-driven anchors.
- 24** The best test performances are reached by percussion-driven anchors, followed by screw ones and pegs.
- 25** Pegs were found compatible with all tested soils and show best results in 'clay sand' and 'rock sand'.
- 26** All tested screw anchors and some big percussion-driven anchors cannot be installed with human force in 'silt' and 'rocky sand' soils.
- 27** All tested screw anchors loose resistance in sand soils.
- 28** Tested percussion-driven anchors which can be implemented with human force in 'Silt' and 'Rocky sand' show best performances in this type of soil.
- 29** Percussion-driven are the most complicated to install. Especially the arming process which takes place invisibly requires trained people.
- 30** Percussion-driven anchors are generally of single use as removal is very time-intensive if not impossible (need to dig). Therefore, an implemented anchor cannot be corrected (i.e. moved).
- 31** Pegs and screw anchors are easier to set up and to reuse. Also, displacements which should warn people are easier to perceive.
- 32** Hazard risk for beneficiaries (i.e. playing children) should be minimized by avoiding sharp ends.

- 33** The price of an anchor is not a reliable indicator. Performance is clearly influenced by other factors.
- 34** Depth is a reliable indicator: independently of the type of anchor, performance will increase with increasing depth.
- 35** Pegs perform better if combined as active ones rather than as x-crossing.
- 36** Combining percussion-driven anchors is also an option to increase resistance.
- 37** When choosing an anchor, one should not only bear the soil and weather conditions but also the installation procedure in mind. Who is going to install the anchors in the soil? If the answer to this question is unsure, choose an anchor which is easy to install. Otherwise, the risk of wrong installation increases.
- 38** Furthermore, it was noticed that one can increase the performance of anchors by either combining them or using longer models. However, simply buying a more expensive anchor is not recommended.
- 39** Many other alternative approaches exist. The ones discussed in this part are only examples to illustrate possible strategies.
- 40** Sometimes, alternatives require extensive research before becoming applicable. Examples are the durability of buried wood and textiles. The lifetime of anchors should in fact exceed the one of the building itself.
- 41** Inspiration can often be gathered from related fields. For instance, sheet piling within earth engineering can give ideas for combinable anchors.

8. Alternative approaches

1 Appropriate tools of other uses. This first approach was tested during the test sets. It is a screw tool (hand auger) used by gardeners to make holes. This one was inserted into the soil and reached a considerable maximum value of 512 kg for a displacement of 5cm(+/-1) and an absolute maximum resistance of 1500kg. This shows that product being designed for a different purpose can very effectively be used as anchors, sometimes even showing better results than specifically designed anchors themselves.

2 Local practices. Vernacular architecture. Nomad populations exist or existed in many regions of the world. As their buildings are lightweight and temporary, they have been confronted to similar challenges. In fact, some groups use interesting alternatives. Bedouins for instance use local bush vegetation which they dig into the sand before attaching the guy rope. This shows that knowledge of local and nomad populations can be of major interest. Means to identify those practices include not only members of the practicing groups but also local populations, publications, archives, etc.

3 Use local resources. Textile earth bags, rocks, refilled oil barrels, cars, trucks, car tires, wheels, etc. Before using this method, further studies concerning its influence on the soil and the environment are needed (influence on vegetation, humidity and textiles). Also, the durability of several types of textile should be explored to choose the most appropriate one.

9. Conclusion table

Comparison of the different anchor options considering technical and practical aspects.

					
Technical aspects	Resistances observed	Low	Medium	High	
	Difficult soils	None	Hard and compact soils		None
	Combinations	Possible	With a reduction of performance per unit		Possible
Practical aspects	Extra material	Hammer	Bar	Hammer and bar	Bag or container
	Instructions	Instruction manual		Skilled people	Instruction manual
	Time of installation	Very little time	Little time	Some more time	Little time
	Monitoring	Visual inspection		Inspection + measuring + recording	Visual inspection
Balance	Performance	Limited resistance		Highest resistances	
	Complexity	Ease of installation		Complex	Easy

(*) Ballast anchors were not tested. They are included as a reference due to their simplicity, compatibility and performance.

10 Annex. Tested anchors.

Supplier	Model	Family	Weight (N)	Dimension (mm)	Installation depth (cm)	Unit price(*)
Delta Ground Anchors	Plastic stake	Peg	0,48	155	15	1.86
IFRC catalogue	Family tent stake	Peg	1,43	220	18	0.39
	Family tent stake	Peg	2,82	280	24	0.6
	Family tent stake	Peg	4,00	350	30	1.06
	Multipurpose tent stake	Peg	4,85	510	50	1.55
SRU	Prototype	Peg	3,15	350	30	1.3
Toughstake	Sand/Snow stake 3	Peg	1,98	444	40	40
Vortex	Yard anchor	Peg	0,20	150	15	1.75
Anchor System	Auger 40	Screw	13,10	600	50	Not provided
Shelter Logic	Shelter auger 30	Screw	7,00	762	60	5
Vortex	Spiral anchor 16	Screw	7,75	400	40	13.97
Duckbill	68-D8D	Percussion driven	0,92	68	75	5.72
	MR4	Percussion driven	5,00	138	140	20.7
Milspec Anchors	Arrowhead 3	Percussion driven	2,38	75	78	3.1
	Arrowhead 6	Percussion driven	7,07	150	115	18.2
Platipus	Platipus S2	Percussion driven	0,50	70	50	2.96
	Platipus S4	Percussion driven	1,80	121	67.5	4.75
	Platipus S6	Percussion driven	5,30	171	100	9.87

(*) US \$ - Nov.2016

References

- Al-Mosawe, 1979: "The effect of repeated and alternating loads on the behaviour of dead and prestressed anchors in sand". Thesis, University of Sheffield.
- R.H.Basset, 1977: "A model study of the load capacity of under reamed anchors in clay". Special Session n° 4: "Ground Anchors", International Conference on Soil Mechanics and Foundation Engineering, Tokyo.
- Clemence, S.P. 1982: "Uplift and bearing capacity of helix anchors in soil". Research Report, Niagara Mohawk Power Corporation, Syracuse, NY.
- Das, B.M. & Shukla, S.K. 2013: "Earth anchors". J.Ross Publishing, Plantation.
- Hubell/Chance, 2012: "Encyclopaedia of anchoring". A.B.Chance Company, Centralia, Mo.
- IFRC-SRU, 2018: *Anchoring study. Recommendations for the good usage of anchors in the humanitarian shelter sector*. Available at:
http://ifrc-sru.org/wp-content/uploads/2018/02/IFRC-SRU_AnchoryStudy_2018.pdf
- A.Kovacs et al. 1975: "On the theory of ground anchors". Technical Report 258, Cold Regions Research and Engineering Laboratory, U.S.Army Corps of Engineers, Hanover, NH.
- Kovacs, W.D. & Yokel, F.Y. 1979: "Soil and rock anchors for mobile homes. A state of the art report". NBS Building Science Series 107, U.S.Department of Commerce.
- J.Kwasniewski et al. 1975: "Anchors with vertical tie rods". Proceedings of the First Baltic Conference on Soil Mechanics and Foundation Engineering, Gdansk, Poland.
- Llorens, J. 2013: "Tension anchors for structural membranes" in Beltzinger, K.U., Kröplin, B & Oñate, E. (ed.) *"VI International Conference on Textile Composites and Inflatable Structures"*. CIMNE, Barcelona.
- Rowe, R.K. & Davis, E.H. 1982: "The behaviour of anchor plates in sand". University of Ontario Research Report, Géotechnique vol.32, n° 1, pp.25-41.
- Shahin, M.A. & Jaksa, M.B. 2003: "Modelling the pullout capacity of marquee ground anchors". Research Report n° R174, University of Adelaide.
- Tent Rental Division, 2006: "Pullout capacity of tent stakes". Industrial Fabrics Association International, Roseville, MN.
- Yokel, F.Y. et al. 1982 : « Load-displacement characteristics of shallow soil anchors ». National Bureau of Standards, Building Science Services, Washington .

Proceedings of the TensiNet Symposium 2019

Softening the habitats / 3-5 June 2019, Politecnico di Milano, Milan, Italy

Alessandra Zanelli, Carol Monticelli, Marijke Mollaert, Bernd Stimpfle (Eds.)

Finite-element analysis and design optioneering of an emergency tent structure

Salvatore VISCUSO*, Milan DRAGOLJEVIC^a, Carol MONTICELLI^b, Alessandra ZANELLI^c

*^{a,b,c} Politecnico di Milano, Dept. of Architecture, Built Environment and Construction Engineering
Via Ponzio 31, 20133 Milan, Italy

* salvatore.viscuso@polimi.it, ^a milan.dragoljevic@polimi.it, ^b carol.monticelli@polimi.it,
^c alessandra.zanelli@polimi.it

Abstract

The paper focuses on the structural analysis of the “Multipurpose Shelter - Type 2” (T2 MP), designed and prototyped by the authors during the research activities of the European collaborative project S(P)EEDKITS. Research institutes, universities, non-profit organizations and manufacturers designed novel shelters concepts, medical care resources and other facilities provided in case of emergency. Specifically, this contribution proposes an optimized solution of the tent structure, in order to meet the UNICEF criteria for collective tents.

Keywords: lightweight structure, temporary structure, emergency sheltering, finite element analysis, structural optimization, snow load, wind load

1. Introduction

Since 2014 UNICEF has been publishing diverse Target Product Profiles (TPPs) to communicate requirements for products - shelters and others NFIs (*Non-food items*) included in procurement specifications of NGOs, which are currently not available on the market but which fulfil a priority need to be used in the unique context in which UNICEF and its partners operate. TPPs include information on how the new product will be used, by or for whom, and the minimum and ideal performance criteria. The purpose of TPPs is to guide industry to develop products that meet UNICEF’s needs, however they do not act as the final procurement

DOI: 10.30448/ts2019.3245.42

Copyright © 2019 by Salvatore Viscuso, Milan Dragoljevic, Carol Monticelli, Alessandra Zanelli.
Published by Maggioli SpA with License Creative Commons CC BY-NC-ND 4.0 with permission.

Peer-review under responsibility of the TensiNet Association

specifications but rather as a list of desired requirements that combined describes the ideal product considering the context. UNICEF recognizes that innovation is an iterative process, and that suppliers must balance sometimes competing requirements against product development progress. To allow for creativity, and the innovation process to take its course, TPPs are less prescriptive than procurement specifications, and can therefore be challenged by the industry.

TPP shelter list included requirements for multipurpose tents with various ground area (24m², 48m² and 72m²). In emergency settings, multipurpose tents and relative add-ons (winterization kit, shade net, electrical lighting kit, inner partitioning layers etc.) are commonly used whenever timely delivery of services to affected populations can be life-saving. The capacity of UNICEF and its implementing partners to provide such services is dependent on the timely availability of fit-for-purpose spaces. Impacting negatively on the timely availability of multipurpose tents are mostly the mobilisation and transport process and, once tents have reached their final destination, the set-up complexity. Some multipurpose tents are used beyond the emergency phase and are transformed into transitional structures allowing UNICEF to move into the recovery phase. Therefore, the frame of the tent is fitted with more durable wall materials and a hard floor, sourced locally or internationally, and often also a full electrical system.

In agreement with Ferrino SpA, the commercial partner that leaded the fabrication of T2 MP during the exploitation and dissemination plan of S(P)EEKITS, the Textile Architecture Network (TAN) of Politecnico di Milano studied an optimization plan, in order to satisfy the UNICEF requirements (Table 1), and verify which is the sufficient dimension of the aluminium structure in order to optimize the balance safety and cost-effectiveness.

	<i>Minimum performance</i>	<i>Ideal performance</i>
Max weight	400 kg (packaging included)	250 kg (packaging included)
Wind load	80 km/h	120 km/h
Snow load	300 N/m ²	300 N/m ²

Table 1: UNICEF Target Product Profile referred to structural requirements of 48 m² Multipurpose tent

Although the T2 MP tent has a net internal area of 48 m², the proposed structural optimization is compliant with snow and wind load specifications of UNI EN 13782:2015 (Temporary structures. Tents. Safety) that describes safety requirements which need to be observed at design, calculation, manufacture, installation, maintenance, of mobile, temporary installed tents with more than 50 m² ground area. According to the European Standard, the limit states due to the combinations of actions is calculated, thus verifying that the design value of internal forces or moments does not exceed the corresponding design resistance of the respective part and the ultimate or serviceability limit state is not exceeded. All verifications are performed for the most unfavourable loading. For this purpose, the permanent, variable and accidental actions are always assumed to have the position and magnitude, which result in the most unfavourable limit, states for the structural components to be calculated (Bernuzzi, Mazzolani, 2007).

2. Methodology and procedure

The simulation procedure is divided in two main activities. The first phase consists in a deep analysis of the current T2 MP tent for all of the required criteria. T2 MP tent (Figure 1) has a covered area of 48 m², and a primary structure made of aluminium tubes with diameter of 35 mm and thickness of 3mm. The second phase is the changing of certain parameters in order to get an updated tent made of a different combinations of variables, in order to meet the UNICEF requirements. The performed assessment is dealing with the weight of the tent and its general structural stability as well as with the properties of its parts.



Figure 1: Multipurpose tent - Type 2 (T2 MP) developed in S(P)EEDKITS project

In both phases, the main tools for the analyses are Grasshopper and Karamba - a plug-in for parametric design and structural calculations used within 3D modelling software Rhinoceros. By using Grasshopper tools, the geometrical model of current T2 MP tent is realized including poles, fabrics and connections with its diameters and thicknesses. The model is completely parametrized, so it is possible to directly control and change the diameters and thicknesses of poles as well as their lengths, mutual angles and positions. In that way the total weight of the tent, obtained by multiplying the volume of poles and fabrics with corresponding specific weights, can be checked for infinite design combinations (Figure 2). Subsequently, Karamba allows to link material properties, support points and loads to the analytical models extracted from the geometrical one. As any FEA application, Karamba has its limitations, and the model has to be made according to the software specifications (Preisinger, Moritz, 2014). In the case of the T2 MP tent, more than one analytical model need to be used, so it's necessary to manually transfer the load data list obtained in the first analytical model to the second one (structure).

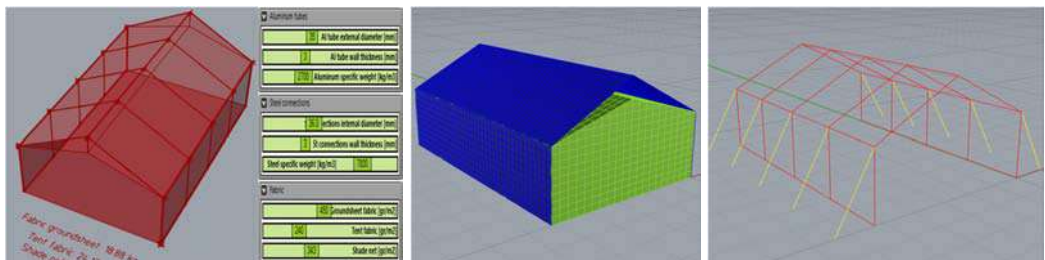


Figure 2 (from the left to the right): geometrical model and parameter sliders (data input); analytical model of a fabrics; analytical model of poles and diagonal ropes

3. Material characterization

3.1 Fabric

The fabric analytical model represents the envelope of the tent, and is done by creating a mesh surface and giving it “shell” element properties in Karamba. It is made of three different parts: groundsheet fabric, tent fabric and shade net. Groundsheet and tent fabric are fixed, while the shade net can change its position. Polyester coated PVC is used as a material of groundsheet, poly-cotton for tent fabric and shade net is made of polyester net (Table 2).

In order to perform realistic simulation, the other elements attached to the fabric sheets are replaced by support elements (Knippers et al., 2011). Those include aluminium poles and strings that connect tent with the ground. Loads are distributed over the whole surface in vertical direction. Karamba performs an approximation of the surface load with a grid of point loads, corresponding to each node of the mesh replicating the surface load.

3.2 Structure

The second analytical model replicates the system of aluminium poles and ropes by means of “beam” elements of Karamba. Poles are made of 6060 aluminium, furnished in the T6 temper (Table 2). This model includes also strings that connect poles to the ground. Supports are set on the bottom horizontal poles (that are attached to the ground) as well as on the points where the strings are anchored to the ground. For the diagonal ropes that stabilize the aluminium frame, belt fasteners made of polyester are proposed. They can withstand loads up until 8351 N; at that tension force, belts can break. In order to add this impact on the model, ropes are replaced with forces applied to the corresponding nodes of the structure.

<i>Component</i>	<i>Material</i>	<i>Traction resistance</i> [N/5cm]	<i>Young's Modulus</i> [kN/cm ²]	<i>Shear Modulus</i> [kN/cm ²]	<i>Specific Weight</i> [kN/m ³]	<i>Coeff. therm. expansion</i> [1/°C]
Groundsheet	PES/PVC 450 g/m ²	2400	252.63	94.74	11.04	0.01
Tent fabric	PES/COT 343 g/m ²	2100	246.32	92.37	7.48	0.01
Shade net	PES/PVC 240 g/m ²	1800	240.00	90.00	3.92	0.01
Poles	ALU 6060 T6 temper	-	6800	2600	26.49	23x10 ⁻⁶

Table 2: Mechanical properties of analytical models

3.3 Preliminary check on the total weight

A preliminary check of the weight requirement is performed on the geometrical model before starting the structural behaviour simulation, in order to verify the compliance of T2 MP tent with UNICEF Standards. Current tent uses aluminium poles with external diameter of 35 mm and thickness of 3 mm. Weights of single parts can be seen in Table 3.

<i>Fabrics</i>	<i>Weight [kg]</i>	<i>Structure</i>	<i>Weight [kg]</i>
Groundsheet fabric	18.88	Aluminium poles	73.06
Tent fabric	21.71	Steel joints	45.31
Shade net	27.51	Pegs and ropes	70.00
Total	68.10		188.37

Table 3: Weight of the T2 MP tent components

4. Simulation of snow and wind loads

4.1 Transfer of load from fabric to poles

Since both of load types (wind and snow) are interacting with the fabric, which transfers them to the poles. First, the whole loaded surface needs to be divided to tributary areas according to position of the poles underneath. Tributary areas are formed by the rule of equal distribution of an area load to the edges of surface. The border of tributary area is formed as a symmetry line of the angle between edges (Figure 3).

In the next step, each of these areas is approximated to a series of rectangles (similarly to integral approximation in mathematics). The precision depends on the number of the rectangles. Since every of these rectangles have its own length and width, their area can be calculated. This area is further used for determining the load that is transferred from each of these rectangles to the pole, that is simply done by multiplying the surface with the area load.

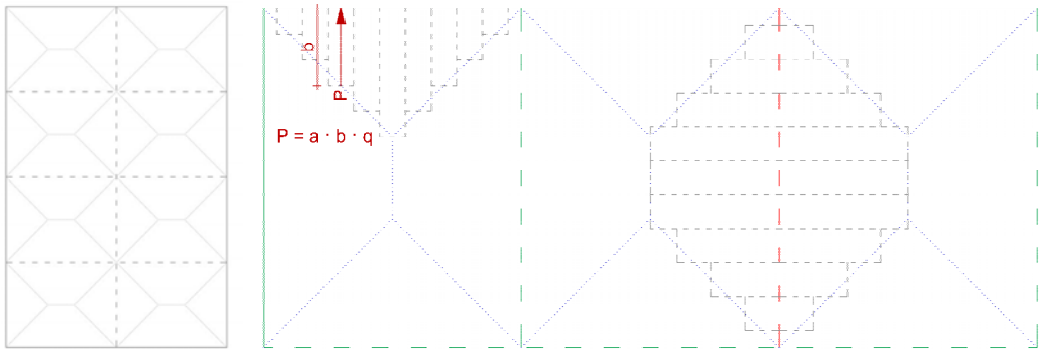


Figure 3: tributary areas subdividing the upper surface of the tent and equation for transferring an area load to a local point load (green lines represents the poles underneath)

4.2 Analysis procedure

Computation of current tent is organized in the following steps (Christensen et al., 2015):

1. Defining properties of material used for both analytical models. Properties inserted are: specific weight, Young's modulus of elasticity, shear modulus, thermal of the structure like hinges.

2. Defining direction and intensity of loads for both analytical models. At this point, for every load case is created different simulation: side wind load (of 120 km/h) and vertical snow/sand load (300 N/m²). Gravity load is added in each case.
3. Assembling all of the above defined values and elements into analytical models.
4. Performing simulation based on appropriate theory of deformations. For the sheet fabric, algorithm based on theory of large deformations is used. As it is known, in this simulation there are multiple iterations, where after every one of them the position of the structure is updated. In this way, more precise simulation is achieved. For examined case, there are used 400 iterations for the fabric computation. For the system of poles, the first order theory for small deflections was more appropriate.
5. Displaying deformed structure and values for various design options and evaluating results in a decision matrix.

5. Results of load simulation and bending moment verification

Moment of inertia determines the torque needed for a desired angular acceleration about a rotational axis. For the round hollow section the used formula is:

$$I = \frac{\pi(D^4 - d^4)}{64} \quad (1)$$

Where D is external diameter of the pole and d is the internal one. For the aluminium poles involved in calculation (diameter 35 mm, thickness 3 mm), the moment of inertia is 38943.18 mm⁴. The minimum needed moment of inertia for the poles depends on the maximum deflection based on the load and allowed deflection based on the length of the beam. If U_f is maximum deflection based on the load and U_{max} maximum allowed deflection, then the minimum moment of inertia equals to:

$$I_{min} = \frac{U_f}{U_{max}} \quad (2)$$

Since the analysed case includes a system of point loads, calculating U_f is quite complex and needs the help of the algorithm. Karamba output includes internal forces, displacement and utilization for both analytical models, the fabric one and structural one (Figures 4, 5, 6). In case of multiple loads applied, the total nodal displacement - calculated through the software at all points where the fabric is connected to the frame - can be obtained through superposition (adding displacements each other). For example, for the point A, it is calculated separately the deflection that is caused by every point load $P_1 \dots P_n$ and then all of these will be added (Bernuzzi, Mazzolani, 2007). To perform this, the following three formulas are used; at the end, for the point A, all the deflections caused by the “left” loads, “right” loads and the load exactly at the point A are added each other (Figure 7).

$$U_x = \frac{Pa(l-x)}{6EI} (2lx - x^2 - a^2), a < x \quad (3)$$

$$U_x = \frac{Pa^2b^2}{3EI}, a = x \tag{4}$$

$$U_x = \frac{Pbx}{6EI} (l^2 - b^2 - x^2), a > x \tag{5}$$

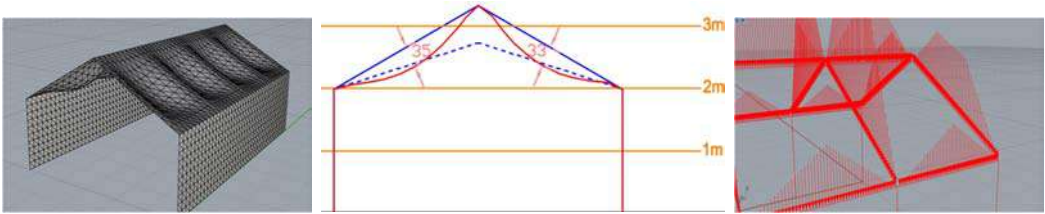


Figure 4: deformation of shade net under snow load, performed on the fabric analytical model, and load transfer to the structural analytical model

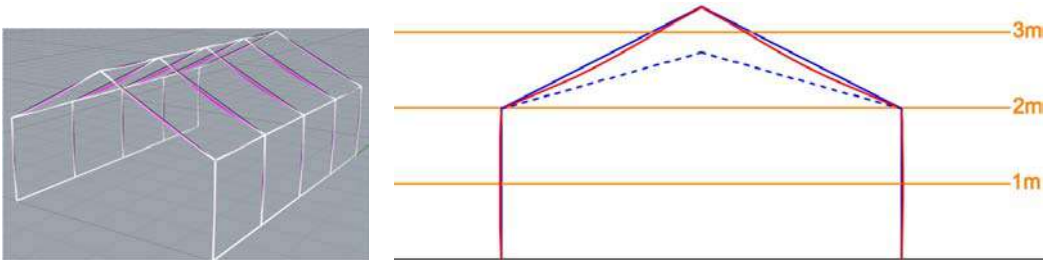


Figure 5: displacement of aluminium poles, performed on the structural analytical model under snow load

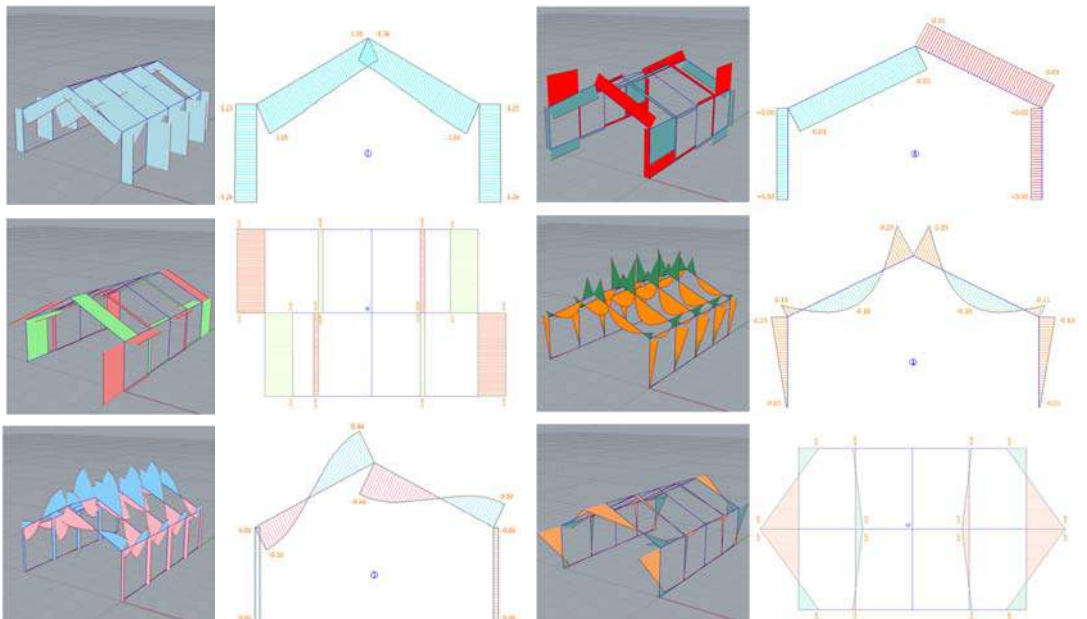


Figure 6: normal force (on the left) and bending moment (on the right) along X-axis (top row), Y-axis (centre row) and Z-axis (bottom row), performed on the structural analytical model under snow load

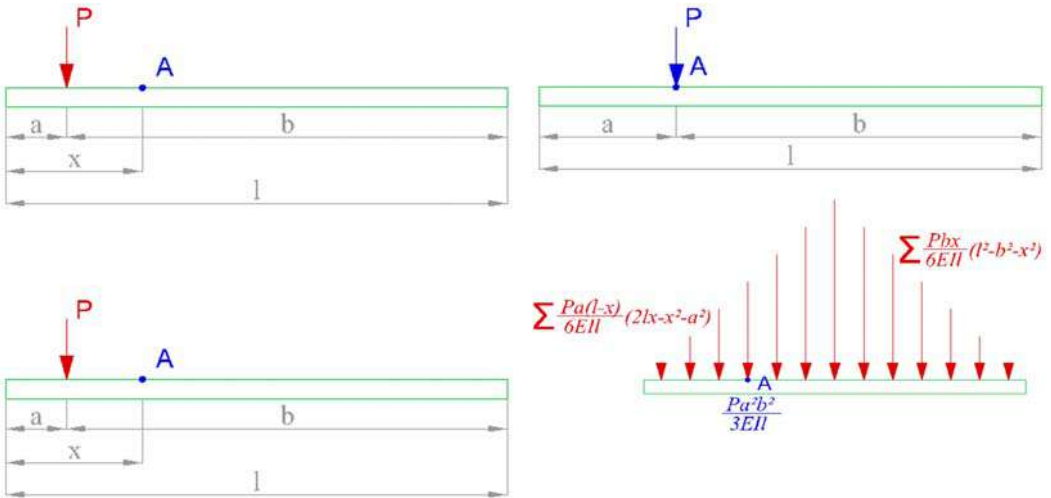


Figure 7: three cases for calculating deflection of the point A in relationship to the position of the load P, and sum of all loads that cause total deflection of the point A

Obtained values of deflection produce a minimum required moment of inertia of 629.54 mm⁴ for the snow load, while for the wind load the minimum moment of inertia is 1297.56 mm⁴. As it is shown above, required moments of inertia are highly below the moments of inertia of cross section used, so the poles are possible to resist the torque created by both snow and wind. Considering the resistance to the bending moment, plastic section modulus needs to be calculated first and then using, the maximum bending moment that poles can resist. Formula are the following ones:

$$W = \frac{D^3-d^3}{6} \tag{6}$$

$$M_{c,Rd} = \frac{W \times f_d}{Y_{MO}} \tag{7}$$

Where D is external diameter of the pole and d is the internal one. For used sections of poles W is 3081.0 mm³, while $Y_{MO}=1.1$ and represents partial factor for resistance of cross sections. Referring to the material characterization, the computation considers an Aluminium 6060-T6, with $f_d = 160$ N/mm² and tensile strength $\sigma_d = 160$ N/mm².

Allowed bending moments for observed poles and material are 0.48 kNm. The performed analysis shows that the maximum bending moment is 0.55 kNm for the snow load and 0.37 kNm for the wind load, so the conclusion comes that the aluminium poles with yield strength of 160 N/mm² cannot resist the bending moments generated in the structure.

6. Design optioneering stage

6.1 Optimization of fabrics - adding diagonal reinforcement

Deformation cause by side wind as this can disable normal use of interior space. This is the reason why some types of the reinforcement need to be added. The most effective is adding linear diagonal reinforcements on the lateral fields. In Karamba it is possible to model and determine the needed strength of the reinforcements. First, on the already deformed model, diagonal section of the deformation is extracted. This part will be observed as a string and theoretical model of the tension in strings will be applied. And by this model, if the string is strained with the force R , every part of the string is applying force R in its own direction.

Each of these forces can be “split” into its components R_x that has direction as the load and R_y in the perpendicular direction to the load. For the calculations, only R_x is taken into the consideration. After several iterations of tests, it is obtained a result that reinforcing the fabric with the string able to resist tension of 165 N, because that is the force needed for resisting the wind of 120 km/h. Additionally, all the analyses are again performed on the reinforced tent. As it can be seen in Figure 8, the deformation is significantly decreases up to 8 ± 10 cm. In this way, the tent can remain useful even under the lateral wind of 120 km/h.

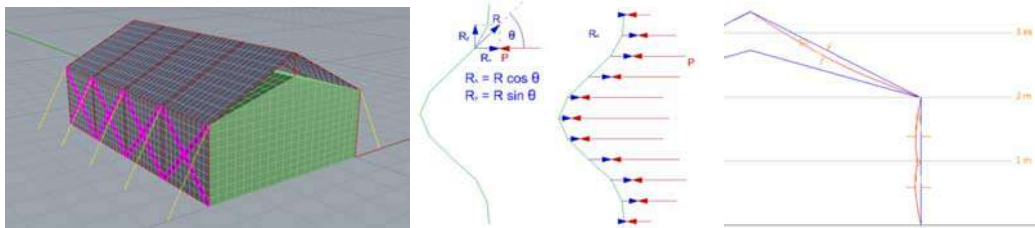


Figure 8: position of reinforcements on the lateral sides; diagram of tensile force at each point of the string and its components R_x and R_y ; diagram of resistance of R_x to the load P ; final shell deformation

6.2 Optimization of the cross section of Aluminium 6060-T6 poles

As it can be seen in par. 5, current steel poles are unable to resist the maximum bending moment that is occurring in the structure. This moment is present in the case of the snow load and equals 0.55 kNm. By combining formula (6) and (7), it is easily noticeable that the maximum allowed moment can be increased either by increasing the external diameter D (in comparison to d) or by increasing the minimum yield strength of the material.

In Table 4 it is possible to see value of maximum allowed moment depending on the external and internal diameter of poles in Aluminium 6060-T6. Change of the material (or more precisely its minimum yield strength) has a proportional impact on the values in the table. In this work, this change is not examined.

In the further step, the tested diameters can be set as parameters for the geometrical model that computes the total weight of the tent. Thus it is possible to verify if the needed profiles fulfil the UNICEF weight requirements. As the final conclusion, it is possible to see that the aluminium 6060-T6 poles that can resist maximum bending moment of the snow (still remaining below the weight of 400 kg) are:

- diameter of 31 mm and thickness of 6 mm; total tent weight of 289.20 kg;
- diameter of 32 mm and thickness of 5.5 mm; total tent weight of 286.50 kg;
- diameter of 33 mm and thickness of 5 mm; total tent weight of 282.70 kg;
- diameter of 34 mm and thickness of 4.5 mm; total tent weight of 277.70 kg;
- diameter of 35 mm and thickness of 4 mm; total tent weight of 271.60 kg.

$M_{c,Rd}$		Internal diameter (d) [mm]																
External diameter (D) [mm]	[kNm]	17	18	19	20	21	22	23	24	25	26	27	28	29	30	31	32	
	27	0.36	0.34	0.31	0.28	0.25	0.22	0.18	0.14	0.10	0.05							
	28	0.41	0.39	0.37	0.34	0.31	0.27	0.24	0.20	0.15	0.11	0.06						
	29	0.47	0.45	0.42	0.40	0.37	0.33	0.30	0.26	0.21	0.17	0.11	0.06					
	30	0.53	0.51	0.49	0.46	0.43	0.40	0.36	0.32	0.28	0.23	0.18	0.12	0.06				
	31	0.60	0.58	0.56	0.53	0.50	0.46	0.43	0.39	0.34	0.30	0.25	0.19	0.13	0.07			
	32	0.68	0.65	0.63	0.60	0.57	0.54	0.50	0.46	0.42	0.37	0.32	0.26	0.20	0.14	0.07		
	33	0.75	0.73	0.70	0.68	0.65	0.61	0.58	0.54	0.49	0.45	0.39	0.34	0.28	0.22	0.15	0.08	
	34	0.83	0.81	0.79	0.76	0.73	0.69	0.66	0.62	0.57	0.53	0.48	0.42	0.36	0.30	0.23	0.16	
	35	0.92	0.90	0.87	0.85	0.81	0.78	0.74	0.70	0.66	0.61	0.56	0.51	0.45	0.38	0.32	0.25	

Table 4: maximum allowed moment of the pole in relation to its external and internal diameter

Weight		Internal diameter (d) [mm]																
External diameter (D) [mm]	[kg]	17	18	19	20	21	22	23	24	25	26	27	28	29	30	31	32	
	27	256.6	249.9	242.9	235.5	227.7	219.5	210.9	202.0	192.6	182.9							
	28	267.6	261	253.9	246.5	238.7	230.5	222.0	213.0	203.7	194.0	183.9						
	29	279.0	272.3	265.3	257.9	250.1	241.9	233.3	224.4	215.1	205.4	195.3	184.8					
	30	290.8	284.1	277.1	269.6	261.8	253.7	245.1	236.2	226.8	217.1	207.0	196.6	185.7				
	31	302.9	296.3	289.2	281.8	274.0	265.8	257.2	248.3	239.0	229.3	219.2	208.7	197.9	186.6			
	32	315.4	308.8	301.7	294.3	286.5	278.3	269.8	260.8	251.5	241.8	231.7	221.2	210.4	199.2	187.6		
	33	328.3	321.7	314.6	307.2	299.4	291.2	282.7	273.7	264.4	254.7	244.6	234.1	223.3	212.1	200.5	188.5	
	34	341.6	334.9	327.9	320.5	312.7	304.5	295.9	287.0	277.7	268.0	257.9	247.4	236.6	225.3	213.7	201.7	
	35	355.3	348.7	341.6	334.2	326.4	318.2	309.6	300.7	291.4	281.7	271.6	261.1	250.3	239.1	227.5	215.5	

Table 5: total weight of the tent in relation to the external and internal diameter of the pole

7. Conclusion

In conclusion, a set of last considerations to take into account while a workflow for structurally designing of temporary tents is established. The difficulty to work inside the emergency field is to arrange a standard solution adaptable to different situations and conditions. Needs are related to the context, to the cultural and economic background of affected population, to the climate zone and to the entity of the disaster. Therefore, the solutions should be extremely flexible, but at the same time ready to be used and highly customizable. Finally, novel shelter designs have to face strong project limits: structural reliability, cost and weight for the transportation.

The methodology elaborated allows the creation of a decision matrix on which is based the selection of the structural optimization strategy for the S(P)EEDKITS “Multipurpose Shelter - Type 2” (Ulrich, Eppinger, 2012). The State of Art analysis allows to create an overview on the current T2 MP tent - already commercialized as multipurpose or collective solution in emergency – and shows its limitations in terms of compliance with both UNICEF targets and European regulation on temporary structures. The decision matrix is not the only factor influencing the design optioneering. At the same time, the still ongoing collaboration with the shelter team of S(P)EEDKITS and Ferrino SpA can produce different score evaluations for each required criterion (e.g., reducing cost may be the most influencing requirement for humanitarian applications). Further studies shall evaluate the use of different kind of structural materials, e.g. composite materials for the framework or for connectors, or simply a more resistant aluminium in substitution of 6060, would allow the decrease of weight without losing the required safety.

Acknowledgements

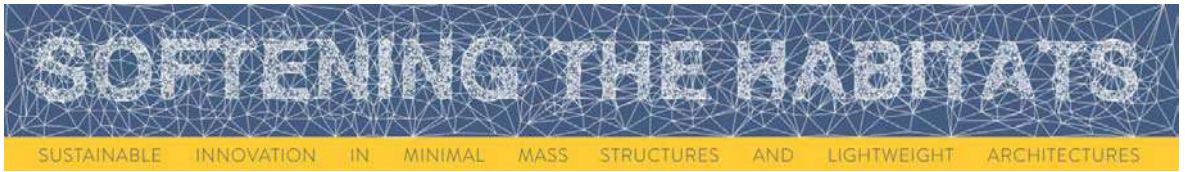
The research work presented in this paper is part of the collaborative project S(P)EEDKITS, co-financed by European Union’s 7th Framework Programme under the Security Theme (SEC-2011.4.2-3). The authors would like to express their deepest gratitude to all the partner of the European project, with special thanks to Centexbel, IFRC-SRU, VUB University, Ferrino SpA and Sioen Industries NV for the profitable collaboration and support in research activities.

This study is also related to the research activity of COST Action TU1303 (Novel structural skins - Improving sustainability and efficiency through new structural textile materials and designs). The authors would like to thank the COST initiative to support all the scientific exchanges between the involved partners.

Mechanical tests on fabrics are performed at the biaxial testing station of TEXTILES HUB, the interdepartmental laboratory of Politecnico di Milano focused on testing and prototyping lightweight material and structures; special thanks to all the researchers, students and collaborators that daily contribute to the grow of this multidisciplinary group.

References

- Bernuzzi C., Mazzolani F.M. (2007), *Edifici in acciaio, materiale calcolo e progetto secondo l'Eurocodice EN 1993-1-1*, Hoepli, Milan.
- Christensen J.T., Parigi D., Kirkegaard P.H. (2015), *Interactive tool that empowers structural understanding and enables FEM analysis in a parametric design environment*. Proceedings of IASS IASS 2014 Brasilia Symposium: Shells, Membranes and Spatial Structures: Footprints - Computational Methods, pp. 1-8(8).
- European Commission (2011), *Regulation (EU) No 305/2011 of the European Parliament and of the Council of 9 March 2011 laying down harmonised conditions for the marketing of construction products and repealing Council Directive 89/106/EEC Text with EEA relevance*. European Product Reg. Off. J. Eur. Union.
- European Committee for Standardization (2015), UNI EN 13782 - *Temporary structures. Tents. Safety*. ICS 91.040.99. Start Validity Date: 8 October 2015.
- Ferrino Spa (2016), *T2 Multipurpose Collective Shelter*. Available at: <https://www.ferrino.it>. Accessed: 13 March 2019.
- Knippers J., Cremers J., Gabler M., Lienhard J. (2011), *Construction manual for Polymers + Membranes. Materials, semi-finished products, form-finding, design*. Edition Detail, Munich.
- Leitão, António, Renata Castelo Branco, and Carmo Cardoso (2017), *Algorithmic-Based Analysis. Protocols, Flows, and Glitches*. Proceedings of the 22nd Annual Conference of the Association for Computer-Aided Architectural Design Research in Asia, Suzhou, pp. 137–147.
- Preisinger C., Moritz H. (2014), *Karamba - A Toolkit for Parametric Structural Design*. Structural Engineering International, n. 24 (2), pp. 217–221.
- Ulrich K.T., Eppinger S.D. (2012), *Product Design Development*, McGraw-Hill, New York.
- UNICEF Supply Division Innovation Unit (2014), *Supplies and Logistics: Target Product Profiles*. Available at: https://www.unicef.org/supply/index_91816.html. Accessed: 21 February 2019.
- UNICEF Supply Division Innovation Unit (2016), *Target Product Profile: Multipurpose tent*. Version: 3.0. Available at: https://www.unicef.org/supply/files/Multipurpose_Tents_TPP_-_V3.pdf. Accessed: 13 March 2019.
- Zanelli A, Buyle G., Giabardo G., Viscuso S. (2014), *S(P)EEDKITS & Smart Packaging. Nuove applicazioni tessili per ridefnire la risposta alle emergenze*. TECHNE n. 8, Firenze University Press, pp. 250-260.



Proceedings of the TensiNet Symposium 2019

Softening the habitats / 3-5 June 2019, Politecnico di Milano, Milan, Italy
Alessandra Zanelli, Carol Monticelli, Marijke Mollaert, Bernd Stimpfle (Eds.)

Innovative Refugee Shelter Design with Pneumatic Sandwich Structure

Nuerxiati ATAWULA*, Alessandra ZANELLI^a, Carol MONTICELLI^a,
Carlotta MAZZOLA^a

* Politecnico di Milano, Campus Leonardo, piazza Leonardo da Vinci, 32, 20133 Milano, Italy,
nuerxiati.atawula@mail.polimi.it

^a Politecnico di Milano, Architecture, Built Environment and Construction Engineering Department (ABC)
Campus Leonardo, via Bonardi 9, 20133 Milano, Italy

Abstract

According to the record of United Nations Refugees Agency UNHCR in July, 2018 there are 68.5 million people around the world have been forced to flee from home. This is a huge number of population and they need a new place to live in.

In the present work, a proposal design of refugee shelter that made by “pneumatic sandwich” structure is demonstrated. The main concept of this design is using the pneumatic material to create a pre-fabricated structure. It is a shaped “airbag” that can be folded into very small size for storing and transporting, when it’s needed it can be set up by pumping air inside. The compression of the air and the tension of the envelope can support the structure itself. Lightweight timber panels were added to both sides to strengthen it. The main goal of this design is easy transporting and quick assembling. This project aiming to provide a shelter that can be assembled in few minutes, without requiring for any technical skills.

Keywords: softening, lightweight structures, pneumatic structure, sustainability, performance, conceptual design, shelter, refugee camp, manufacturing, quick assembling.

DOI: 10.30448/ts2019.3245.35

Copyright © 2019 by N. Atawula, A. Zanelli, C. Monticelli, C. Mazzola. Published by Maggioli SpA with License Creative Commons CC BY-NC-ND 4.0 with permission.

Peer-review under responsibility of the TensiNet Association

1. Introduction

1.1 Background Information

There are more displaced persons today than at any other time of the history in the world. Most of these people have been displaced from their homes by persecution, conflict, environmental disasters, and economic strain. By then they need shelters to live in within a very short time span. A shelter is critical for survival, but it also protects users from the extreme weather conditions and some certain natural threats, provides them with a basic sense of security, and a place for our families to interact. And it is impossible to provide them a real house or refugee camp in very short time in that uncertain situation. Shelter is a vital survival mechanism in times of crisis or displacement. It is also key to restoring personal security, self-sufficiency and dignity.

1.2 Layout of text

This report is divided in four main parts. In the first part the reason of this proposal design is explained by the fact of the world's urgent needs for a new type of quick assembling shelters. Since this design is based on the advantages of lightweight structure, the background knowledge about the lightweight structure is shortly introduced.

In the second part, the prototype of this proposal design is described. Then the detailed structural elements and constructing methods are explained. The following part is an evaluation of this proposal design concept. This part includes the cost analysis report, the advantages of the project and possible further developments.

The last part is the conclusion of this whole research. At last the author's own thoughts on this concept is mentioned.

2. Design Concept

In comparison to issues such as food, water and medical care, shelter design and performance is understudied and rarely evaluated, despite it being known that prolonged exposure to extreme thermal conditions can lead to morbidity and mortality.

2.1 The Current State of Shelters

When a natural disaster or conflict took place, thousands of temporary living spaces are needed within a very short time. At the most of time they are provided with a tent. If the time permits, there will be a short construction of harder shelters according to the local climate and available materials. But usually, considering the essence of the situations the needs for shelters exceeds the logistic capacity; consequently, the heavy and bulky refugee tent is abandoned in favor of simple, but more effective, plastic sheeting.

Even these shelters can provide a basic sense of security and a space at as an intermediate and transitional solution, but it cannot give a real safety condition and protection from the vagaries of climate and other unknown danger. Therefore, a new type of shelter is urgently needed for the refugees which can be transported and built in a short time, at the same time provide the basic living conditions that the current shelters cannot. In this case, the ultra-light weight materials and structures are the most probably competent objects that we can seek an answer from.

2.2 The Ultra-Light Weight Materials

For decades the lightweight structures are widely employed in architecture, engineering and building construction and find application in long span roofs for stadiums and exhibition structures; covered shopping malls; entrance structures; signature structures and sculptures as well as shade and environmental protection canopies. Generally, the self-weight of the structure is a small portion of the applied load or generated forces. Lightweight structures often utilize lightweight and high-strength materials as well as advanced technologies for their design and construction.

2.2.1 The advantages of the ultra-light weight structures

Ultra-light weight materials are coming with very clear advantages. It's widely regarded as the building material of future. From the view of construction, most of the ultra-light materials can be pre-factored in the factory or other spot, then transported to the site. This saves the cost and reduces the construction time. Meanwhile, ultra-light weight materials, such as membrane, timber, coated textiles and plastic materials have very strong flexibility, which allows designers and engineers to express their ideas in a new level that never seen before.

Moreover, as a light weight material, these materials are easy to transport. Beyond that, from the ecological point of view: ultra-lightweight structures are material-efficient due to the materials strengths are optimally used. Thus, no resources are wasted. At last, after use ultra-light weight structures may usually be disassembled, and their elements are recyclable. Therefore, are superior in meeting the requirement for a sustainable development.

In brief, ultra-light weight structures have the advantages such as:

- a. Material saving;
- b. Energy saving;
- c. Construction cost and time saving;
- d. Provide better architectural expressions
- e. Improved durability

All these advantages reduce the restriction in architecture design, especially give more possibilities in emergency shelter design. Then could meet the certain demands we are dealing with, such as: fast, light and low cost.

2.2.2 The Sandwich Structures

The merging of different materials to achieve a new material capability is always the best way to develop and optimize a building material. The reinforced concrete is one of the best and the most successful example of merging well-known materials and get a considerable performance. This allows us to have two or more different material's specific performance at once and take the full advantage of them. Using this method in ultra-light weight materials, we have developed the sandwich structures.

Sandwich structures can be classed as composite materials in that they consist of two or more individual components of differing properties which when combined result in a high-performance material. In contrast to monolithic composites - which consist of an intimate mixture of fibers (glass, Kevlar, carbon, metal, etc.) supported within a continuous matrix (e.g. thermoplastic or thermoset resin) - sandwich structures have a discrete structure in which a core material is bonded to, and faced with, a skin material. The skin material usually has a high stiffness, whereas the core typically has high compressive and shear strength. When these are bonded together, this combination gives the sandwich structure a high flexural modulus. This light weight sandwich structure panels have been used in aircraft and space industry, where a low weight is needed in combination with high stiffness.

As mentioned, the advantages of sandwich structural materials are its stiffness and strength on the one side and its light weight on the other side; without increasing the weight dramatically, higher stiffness and strength can be achieved. Also, sandwich constructions function as a thermal insulation or thermal transfer, depending on the materials used. Moreover, the dampening of vibration and noise is another significant benefit provided by core materials.

2.3 The Design Concept

Generally, Pneumatic Structural Systems are structures or buildings that utilize air pressure to ensure its structural integrity. Due to the flexibility and easy to construction, all the pneumatic structures are pre-fabricated in factories and set up by inflating air in a very short time. Therefore, it is the perfect structure for the emergency shelter. However, the skin material usually made from laminated membranes, consequently the pneumatic structures are not puncture-proof and not suitable for extreme climates.

In this case, the concept of pneumatic sandwich structure design is aimed at using the characteristic advantages of the pneumatic structure and, at the same time, give it an external

protection. Arising from this, the pneumatic sandwich structures for refugee shelter is designed as an inflatable air-bag with thin timber panels on the both sides. The core part is a general pneumatic structure which provides the main structural support, and the timber panels will provide an external protection as a skin. Indeed, the timber panels also provides the extra strength and a considerable thermal insulation.

3. Concept Development

3.1 The Prototype

As it mentioned above, after the design of an innovational pneumatic sandwich structure, a suitable form applied on this structure to shape a shelter. As a result, the prototype of the shelter is a foldable rectangular unit in a transportable size. (Fig 1) The size of the main structure is 1.5m x 2m x 11.2cm. After unfolded there will be 4 sandwich panels connected. It simply needs to be inflated air in the "airbag" and set up to the designed shape. Then insert the base component in the main structure and fill up with soil. At last, use the enhancing pipes and straps to stabilize it. Two of these components creates one whole shelter with 3mx3m inner space. (Fig 2)



Figure 1: The folded shelter



Figure 2: The fully installed shelter

3.2 Structural Detail

3.2.1 The Main Wall

The main wall and roof part are designed as an integrated component. It has four parts connected together and all of these parts designed in same material and in same size (1.5m x 2m x 2cm). The Pneumatic material is around 1cm thick without air. And the plywood panels outside are 9mm thick.

One different design of this proposal from general pneumatic tent is this "airbag" core designed as air mattress which means it only requires air inflating once and seal the air cock, does not require continuous air pumping. And the inflating can be done by a simple hand pump or any other inflator. To strength the structure and reduce the onsite construction, there

are two extra flexible canvas part designed as built-in prefabricated portion of the main structure. They are the triangle canvas including a plastic window and the underlying connection between the two walls. The installation step of the main structure is: first, unfold the structure and expand it to the designed shape. Second, when it is completely unfolded then start to pump air. After it got the required amount of air pressure that can hold the structure. It will become a stabilized structure when it's fully filled with air. (fig 3)

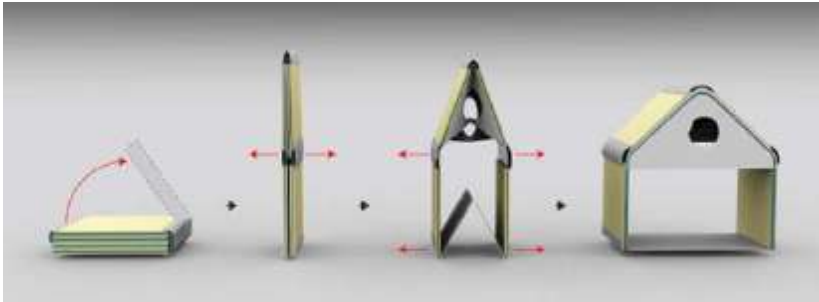


Figure 3: The main structure installation steps.

3.2.2 The Base

The base is designed as a unique component. It's similar to the main part as a sandwich structure. But unlike the main part, this one is a canvas tank and it can be filled with water, soil or sand according to the available source of the site surroundings.

The size of the empty base component is $1.5\text{m} \times 3\text{m} \times 3.4\text{cm}$. It can be folded to $1.5\text{m} \times 1.5\text{m} \times 6\text{cm}$ size for preserving and transporting. When it is filled the full size will be $1.5\text{m} \times 3\text{m} \times 20\text{cm}$. The volume is 0.9m^3 . If it is filled with water, the weight will be 900kg, if it is filled with soil or sand the weight will be around 1.5t. Therefore, it is heavy enough to hold the whole structure fixed on the ground. (Fig 4)



Figure 4: The base installation

3.2.3 The Structural Enhancement Pipe

Even the proposed pneumatic structure can hold the main structures and the self-weight, but due to the unstable shape of the shelter, there is extra structural elements needed to preserve the shelter from horizontal load, such as wind.

The proposal pipes are designed with lightweight aluminum. To make sure it is easy to package and transported with the other components, the pipes are designed as an extendable unit. One end of the pipe can be screwed in to another one's different ending. The original size of the pipe is 1.3 meter. Before the base is filled, extend the pipes by connecting four of them, and put under the base. There will be a notch under the main structure to hold the pipes as well. After the whole structure installed, the pipes will be fixed on the ground by the weight of the shelter. Then use straps to tie the pipes through the designed hole on the end to the strap holder joints (fig 5) on the upper part of the wall. These units can provide an enhanced bearing capacity for horizontal loads. (fig 6).

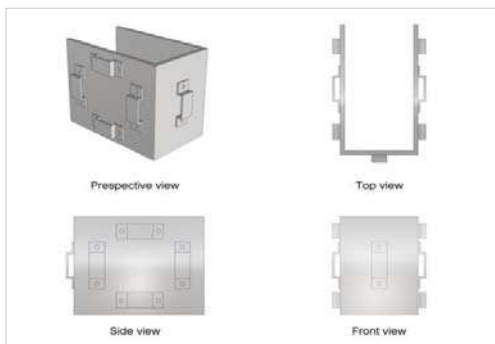


Figure 5: The joint detail

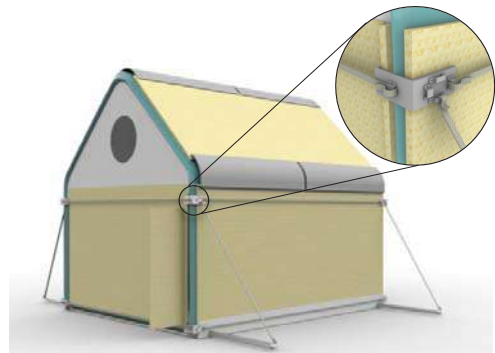


Figure 6: The enhancement structures

3.2.4 The Front and Rear Wall

By using the aforementioned components, a shelter can be completed, yet not enough privacies and protections are provided. To improve the protection, there are two more components designed, using the same material- pneumatic sandwich panels. Both components are in the same size, but the front wall have a simple door that made by a thicker plywood panel.

The installation of these walls also designed as simple as possible. After all the structures installed, the walls can be inflated and tied with straps to the main structure and the base.

4. Concept Evaluation and Further Development

4.1 Cost Analysis

According to the proposal requirements and used materials, a preliminary market (cost) analyzing is made. Due to the most part of this proposal designed as a prefabricated whole unit, the fabrication cost will be the main cost of the project. Considering the main advantage of this proposal is easy installation and it can be set up by only 1~2 users themselves and all the necessary tools will be provided with the kit, then the construction cost is not involved. Because of wide geographical suitability of this proposal shelter, the certain location of the users is not defined. For this reason, the transportation cost is also not considered in this report.

In the view of fact that the lower price is one of the main demands of a refuge shelter, this cost analysis took place in the developing countries such as India and China which having the lower production cost. In extra they can provide inexpensive and convenient mass numbers of product transportation to all over the world by sea. The following cost report (Table1) is based on the lowest price collected from the manufacturers:

Table 1: Cost list of one kit

Item	Dimension	Quantity	Price of one unit	Total price
Inflatable Pneumatic Tent	1.5m×3m *	1	35 €/m ²	157.5 €
Plywood Panel	1.5m×2m×9mm	12	173.5€/ m ³	56.25 €
Strap Holder Joints	20cm×15cm×12cm	8	2.8€/Pieces	22.4 €
Connecting Canvas Unit 1	1.5m×20cm	6	9€/m ²	16.2 €
Connecting Canvas Unit 2	1.5m×3.2m	1	9€/m ²	43.2 €
Foldable Canvas Tank (Base)	1.5m×3m×20cm	1	35€/ m ³	31.5 €
Plywood Panel (Base)	1.5m×1.5m×12mm	4	193.5 €/m ³	20.8 €
Lightweight Aluminum Pipe	1.3m, Ø3cm; 0.894kg	8	4.4 €/kg	31.46 €
Strap	3.2m×3cm	10	0.8 €/m	25.6 €
Total				404.91 €

And we need two of this kit to build one shelter; After a fully cost data collecting and analyzing, the total price of this project is estimated approximately 820€(Transportation not included). There is a list of comparison with other shelters on the market:

Table 2: Cost comparison with the other shelters on the market:

The Project	Type	Size (W×L×H)	Cost
UNHCR framed tent	Non-Pneumatic	4.15m×4m×2.4m	612€
Ikea better shelter	Non-Pneumatic	5.68 m×3.32m	1150€
PNEU-TEX by Ferrino	Pneumatic	5.1m×5.1m	6600€
FSI DAT Series Pneumatic Shelter	Pneumatic	2.13m×2.13m×2.4m	4327€
This Proposal	Pneumatic	3m×3m×2.3	820€

From this comparison we can see that, the pneumatic shelters on the market are extremely expensive that cannot be widely used as a refugee shelter. This market analysis shows that this project has an obvious advantage on cost. Due to the large number of shelters are needed and most of them provided by non-governmental humanitarian foundations and organizations, the low cost certainly is one of the main considerations of refugee sheltering projects.

4.2 The Advantages of The Project

This proposal shelter has several advantages, such as foldable unit, easy to package and transport, easy installation and suitable to various geographic and climatic conditions. At last but not least, this proposal shelter requires relatively low production cost.

Because it is a pneumatic structure, before inflated with air, the whole structure will be in a considerable small size. And the foldable design makes it small and flat panels. This will provide convenience for packaging and transporting. Even a large number of shelters can be piled up to stock or transportation without damaging the shelter and occupying large spaces.

The feature of pneumatic structure makes the shelter very easy to set up. Due to the design of the main structure as a whole unit, it just requires filling air with an inflator or a pump. Even one person can install the shelter without special construction skills.

Because of the moveable base and anchor design, the shelter has a very good compatibility to the various geographic featured areas, such as deserts, forests and grasslands, even some hard ground surfaces. What is more is that, due to the prosperities of pneumatic sandwich structure, this shelter has a good thermal insulation. It can provide relatively comfortable living condition in a hot or cold climate.

4.3 The Further Possibilities

Generally, refugee camps evolve during the time. After settled down and have through sometimes, the users will take some changes according to their daily needs or cultural habits. And what can be expected is the demands of the location that depended on climate and

geographical factors of the place, will drive the further developing or evolution of the shelters. This proposal design allows certain kind of later developing on the shelter. Here are some further development possibilities listed:

However, this proposal project designed as a component unit, it provides more easy way to enlarge or extend the space by merging or connecting more components. As the original shelter is designed to create a 3m x 3m space by connecting two of the components, it allows to create a longer space by connecting more components together. This will provide larger shelter or other service spaces such as temporary classrooms or stock house.

For a long-term use of the shelter as a housing, there is also the possibility to install solar panels on the roof. The original slope roof provides perfect angle and space for the solar panels. And the solar panels can improve the condition of the shelter by providing energy supply.

There is another creative development possibility for a hot climate area. Since the main structure of this shelter is pneumatic structure that needs to inflate air in it, there is also a possibility that fill certain amount of water in the lower part of the wall to get a considerable thermal insulation and a cooling effect. Of course, this concept only suitable in the area that have rich of water resource.

5. Conclusion

Lightweight materials and structures have been used for shelter and refuge housing for decades. The recent developments of new materials and light weight structures are providing more and more possibilities for improving the construction techniques and qualities of the emergency relief and housing.

This work also demonstrates that the innovative development of existing material possibly provides an improved feature for designing and construction processes. The development of this pneumatic sandwich structure started from the demands of the emergency housing, to ensure that the final outcome will satisfy the users and the demands. Among the development of this proposal project, different type of prototypes was considered for providing a better result and more practicability.

From a personal perspective, this proposal concept of a new pneumatic sandwich structure can have a good result in the expected time. The development and use of the pneumatic sandwich structure will provide more effective and efficient solution to the emergency shelter design. It is also possible to expand the use of this structure to other field of housing or temporary building. As a sum up even some most part of this paper is demonstrating the design of proposal shelter however the main purpose of so work is proposing the idea of pneumatic sandwich structure concept and the possible advantages it can provide, especially the

possibilities of providing a new and efficient way shelter design to meet the demands of some mass number of refugees around the world. Therefore, the prototype of this proposal concept may not be the best one but developing it could provide more practical use of pneumatic sandwich structure. The aim of the project is very clear, and its potential outcome in real development is very promising. I was highly motivated to work in this concept.

References

- Albadra, D., Vellei, M., Coley, D., & Hart, J. (2017). Thermal comfort in desert refugee camps: An interdisciplinary approach. *Building and Environment*, vol.124, pp. 460-477. DOI: <https://doi.org/10.1016/j.buildenv.2017.08.016>
- Asefi, M., & Sirus, F. A. (2012). Transformable Shelter: Evaluation and New Architectural Design Proposals. *Procedia - Social and Behavioral Sciences*, vol.51, pp. 961-966. DOI: <https://doi.org/10.1016/j.sbspro.2012.08.270>
- Dahlström, L. (n.d.). Benefits of lightweight construction. Lindabdirect, 2(2006). Retrieved from https://www.lindabgroup.com/English/Documents/News/LindabDirect/LindabDirect_06_2.pdf
- Irit Katz (2017) 'The Common Camp': temporary settlements as a spatio-political instrument in Israel-Palestine, *The Journal of Architecture*, vol. 22:1, pp. 54-103, DOI: <https://doi.org/10.1080/13602365.2016.1276095>
- Nasser, A. V. (2011). Development of a Light Weight Structure for Emergency Housing of Refugees (Unpublished master's thesis). CHALMERS UNIVERSITY OF TECHNOLOGY. Retrieved from <http://publications.lib.chalmers.se/records/fulltext/141887.pdf>
- Schlaich, J., & Schlaich, M. (n.d.). LIGHTWEIGHT STRUCTURES. Retrieved from <https://architecture.mit.edu/sites/architecture.mit.edu/files/attachments/lecture/LightweightStructures.pdf>
- Wouters, N. (2009, November). Pneumatic Structures - A revival of formal experiments. Retrieved from <https://www.yumpu.com/en/document/view/19207499/pneumatic-structures-iam>

Manta Bay, the pool in textile architecture

Alessandro RIZZO*, Roberto CANOBBIO^a, Francesco BENZI^b

*Canobbio Textile Engineering Srl, Strada Sgarbazzo snc, Castelnuovo Scrivia (AL) - 15053, Italy,
alessandro.rizzo@canobbiotextile.com

^a Canobbio Textile Engineering Srl, Strada Sgarbazzo snc, Castelnuovo Scrivia (AL) - 15053, Italy

^b Botany Bay srl, vicolo Scala Santa 1, Verona (VR) – 37129, Italy

Abstract

Everyone knows the above-ground pools like concrete wall or steel frames which have the aim to contain a volume of water. This is the first and ancient meaning of pools and over time it is developed. The pool is a form of architecture and it can follow new ways like contemporary architecture and where people can to enjoy of the wellness. The new challenge is to do an above-ground pools in according to the architectural textile concept, the project had to follow several criteria: 1.maintain the main structure at the minimum size and increase the value of the membrane; 2. maintain the water always light and clean; 3. find a shape typical of the textile structure never see in the pools; 4.to be installed and dismantle easily; 5. modular textile structure, always at the service of simplicity of set-up, use and maintenance. In these ways it was born the project Manta Bay.

The textile pool is composed of tensioned membrane (PVC thermo-sealed) stabilized from selfweight of water and thin steel bracket that it doesn't touch membrane. It is laid on composed matchboard floor (Eco-Friendly composite material, made with rice husk and virgin polymers)

The challenges of this project is the formfinding of the membrane that it should have a deformation against typical behavior of membrane under permanent load (convex shape). It is looking for an concave shape.

DOI: 10.30448/ts2019.3245.39

Copyright © 2019 by A. Rizzo, R. Canobbio, F. Benzi. Published by Maggioli SpA with License Creative Commons CC BY-NC-ND 4.0 with permission.

Peer-review under responsibility of the TensiNet Association

The production of the membrane accessories and steel structure needed of suitable characteristics for working with water plus chlorine, pipes for circulation of water, a little waterfall (solution needed to have an infinity pool).

Keywords: Lightweight structures, design pool, textile architecture, form finding, idrostatic load, softening, temporary structure, membrane stress, above-ground pool, quick installation

1. Design development

Manta Bay become from an architectural approach to pools.

Traditionally the pool has been considered just a commodity that has more to do with structure and systems. As it is a status symbol the only architectural requirement at first is it to be as wide as possible.

During the ages the basic concept has been evolved, as the building technics have. Pools became not mere technical equipmet anymore. The aesthetic approach has introduced for pools specifically designed for wellness, and not only for agonistic sport.

The task is to considering the pool a “volume”, rather than a “hole in the ground”; a “room to live in” rather than a simple “water tank”.

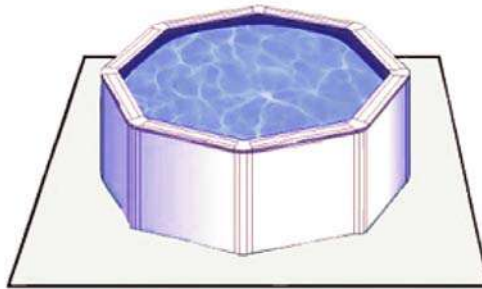


Figure 1: This is a typical outside pool in the trade.

Manta Bay is a step ahead. This concept introduces a brand new point of view: unlikely traditional pools, the volume is designed to be enjoyed from both into and outside the basin. In addition to that, water is not presents as its still surface, but it has an active role in the landscape thanks to the vibrant lamination infinity waterfall.

To keep such concept and to overcomes the traditional limits a modern and versatile building technic is needed.

2. Tensostructure building technology

Tensioned textile architecture is the answer. It allows a way to create basins in many shapes and sizes. Following criteria had been adopted:

- to design the supporting frame at its minimum size, so to emphasize the membrane
- to keep the membrane as much intact as possible, since every flange is a possible leak. This brings to infinity for lamination.
- To set the most organic shape and synclastic form typical for tensostructures, but not common for traditional pools.

Once the technic was defined, we realized that the lightness of tensostructures technology to provide several advantages compared to average pools.

First, such item can be easily set up. This allows to get a pool in sites otherwise not suitable, because of logistic or building permit.

Second, setting up and uninstalling are quick (about 3 hours), so to make Manta Bay a temporary choice. Seasonal use is a topic for reducing pool costs. The possibility to take off the equipment during non bathing season represents a remarkable saving.



Figure 2: 3D Model of textile pool.

Third, as tensostructures does not need heavy supports, Manta Bay does not need further finishin work but the basic kit. Sides and stairs are not needed, that saves a lot of money.

3. Supporting frame and decking

In short time the initial concept gained the traits of an industrial product, according to a specific niche, not yet occupied: high-ended above-ground design pools.

Steel struts as part of a linear frame, mechanical links, make it to be delivered in kit, easy to assemble. More components are adopted for decking and water system, according to a “modular” mind, easy to mantaining and to replace, just in case.

The modular approach allows to design several different models, whose the traits are: longness of struts, membrane surface and number of rthe decking modules.

This fit to the delivery: Manta Bay can be easily exported, where pool is part of local culture or the heat makes it a must to have. Manteniace is easy from far away as well: every components is easy to be sent and install by unskilled persons. Optional systems like whirlpool, heater or spotlights may be added beyond the first season.

Such item needs a brand representing its “organic” design, lighthness and its relationship with water element: therefore Manta Bay.



Figure 3: Picture of textile into design context

4. Design of membrane

The first point to consider for the design of membrane is the behaviour of the hydrostatic force. As usually is known, the hydrostatic thrust is the product between the pressure by the surface where it is applied, as following equation:

$$S = 1/2 * \gamma_{acqua} * h * a * l \tag{1}$$

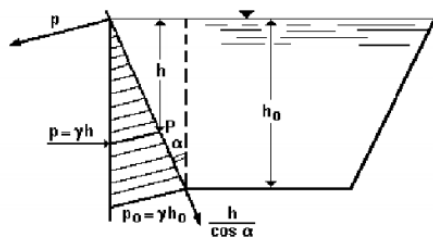


Figure 4: Scheme of hydrostatic force

The situation for textile pool is the following:

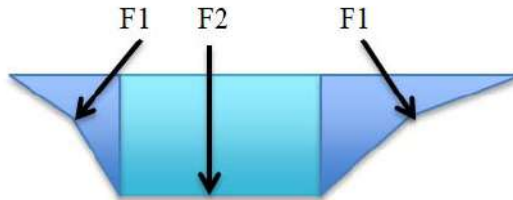


Figure 5: Loads applied in the membrane

Forces involved	Description	Applied	Membrane issue
F1	Vertical forces for the water weight	On membrane in the bottom of pool.	It works in contact with the floor (friction)
F2	Inclinated forces with horizontal and vertical component	On membrane between bottom of pool and steel bracket in the corner	It works with high permanent load and the membrane have to transfer the tension maintaining shape designed

Before formfinding phase it needs to take in account forces named “F1” and its behavior and distribution. The forces named “F2” is important for the stability of entire textile structure where it is involved membrane, steel structure and ropes, but it has less influence in the Formfinding.

4.1. Form-finding

The challenge to win, at least partial, it is the shape of membrane that it doesn't follow the typical deformation of fabric under a permanent load. In fact, when it is in that situation (permanent load as snow, water ponding, etc..) the membrane has following trade:

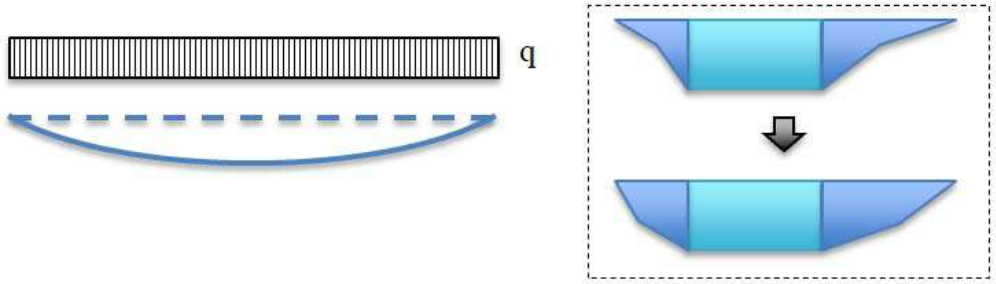


Figure 6: Deformation typical of membrane

In the pool, it means to have a shape with concavity towards the inside of the pool (convex), as shown in the Figure 6.

At the contrary, the formfinding should allow an membrane deformation with concavity towards the outside of the pool (concave) as shown in Figure 6 over black arrow.

4.1.1 Form-finding with software Easy (Technet GmbH)

Without water load, the result of the input geometry into software for formfinding (as Easy, Technet GmbH) has the shape how it seeks for:

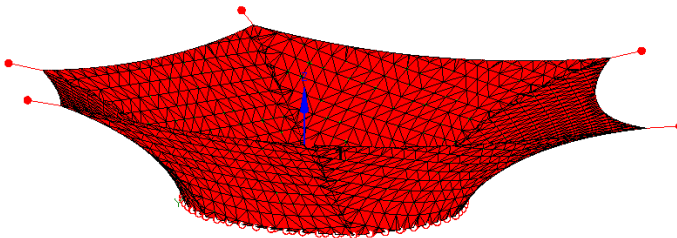


Figure 7: Deformation typical of membrane

Into the software Easy there is a program named Auftr, which creates the external loads caused by water. In order to get correct results it has to define the triangles which are in the hydrostaic force.

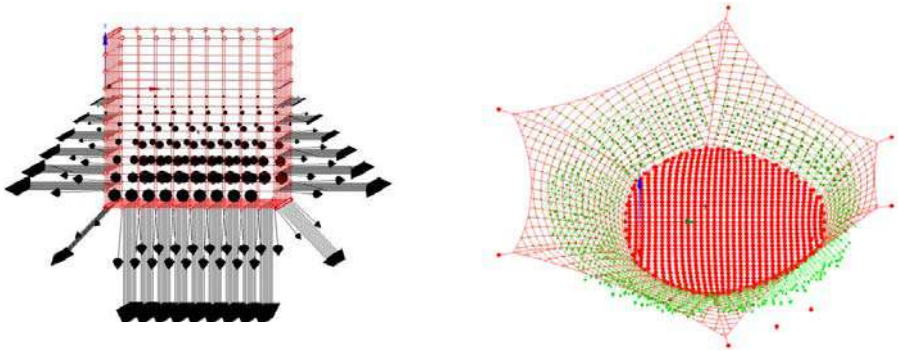


Figure 8: Deformation typical of membrane

4.1.2 Statik analysis with software Easy (Technet GmbH)

Under this water load the software calculate the stress of membrane, but the first observation is that the shape is not like seeked, because the membrane has deformation typical as emntioned before. To reach the final shape, it has to increase the force density along horizontal link and the result is the membrane works with concentric rings and it permits to get convex surface in almost of surface.

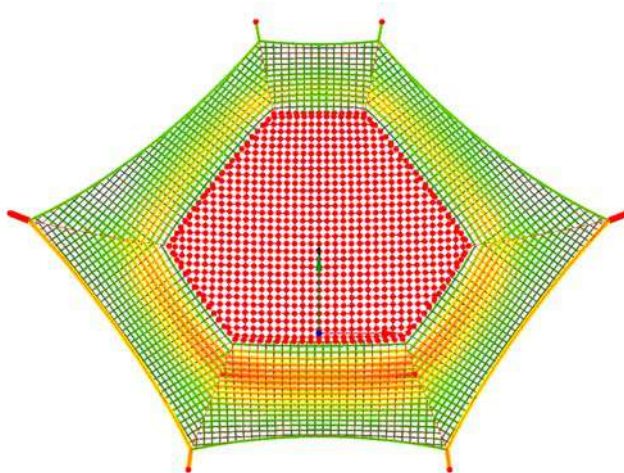


Figure 9: Stress analysis of membrane under water load

At the end, the membrane is made with high compensation along horizontal line and the warp has to be horizontal too. It should to accept the concave shape in the side where there is the water overflow because the membrane is very inclined and the water weight can not be countered by the compensation or the increasing of the force density.

It is due to limit of the membrane, in fact if it increases the stiffness of the horizontal link (concentric rings) the result is high stress of membrane (not existing on the market)

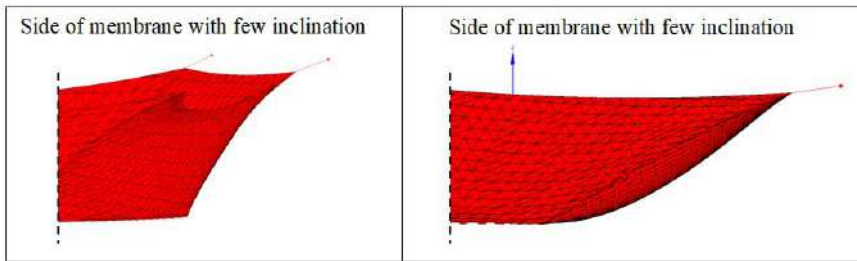


Figure 10: Shape comparison between different sides

4.2. Characteristic of material designed

The static analysis of membrane and its accessories takes to defined a fabric type 2 with low deformation. In the first time the textile pool has been made with standard fabric as “Sioen T2101E” 100% PES and then it has been replaced with pre-stressed fabric as Serge Ferrari Precontraint type 2 because it has a better behavior.

In the edge of membrane there is stainless steel rope with thread swage terminal and turnbuckle. The forces in the rope are transmitted to machined fork-swage turnbuckle (shown in the Figure 11) with round stainless steel plates and bolts for clamping the membrane.



Figure 11: Typical corner of textile pool

4.3. Develop of membrane suitable

The membranes used in the construction of above ground pools are simple PVC fabric. This kind of membrane can be negative affected if subjected to continuous contact with water, but the textile pool designed is temporary and into water there is chlorine.

As an alternative, the market offers membrane solutions used in the field of inflatable boats or in-ground pools, such as the membrane of Renolit (Alkorplan3000) or Mehler (Valmex Boat).

5. Steel structure design

The steel structure to support the membrane has been designed as light as possible, to avoid heavy look. The weight of load is the main contrast to balance the tipping forces and to reduce the arm of the typical force in the cantilever.

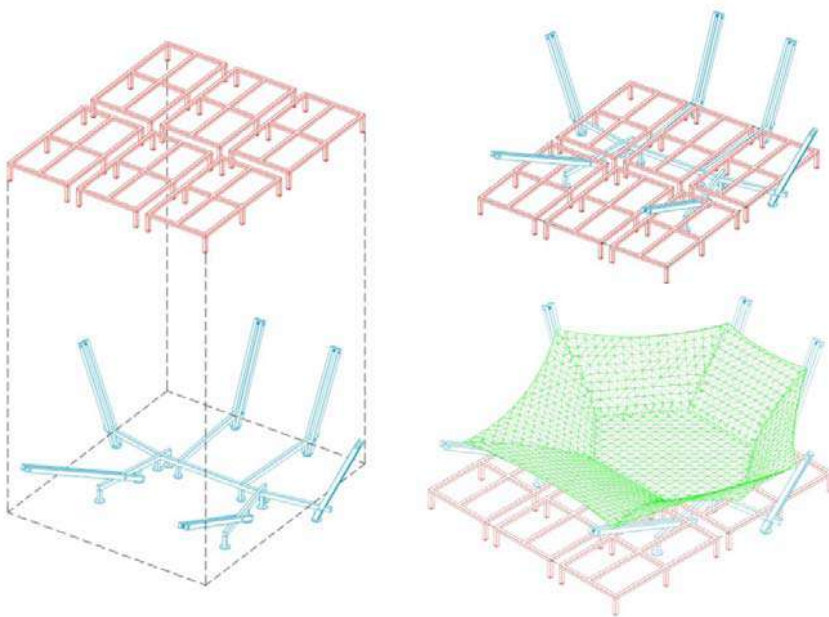


Figure 12: Main steel structure

6. Conclusion

Textile structures can have outlets also in those sectors where at first glance there seems to be no possibility of application. The textile architectural pool shown would open other doors in the pool and wellness sector where the concrete and the steel are the masters.



SOFTENING THE ENVIRONMENT

HIGHLIGHTED LECTURES

PERFORMANCE AND RELIABILITY OF SOFT MATERIALS

TOWARDS NEW MATERIALITIES AND SOFT SPACES

Proceedings of the TensiNet Symposium 2019

Softening the habitats / 3-5 June 2019, Politecnico di Milano, Milan, Italy

Alessandra Zanelli, Carol Monticelli, Marijke Mollaert, Bernd Stimpfle (Eds.)

Biomimicry for regenerative built environments: mapping design strategies for producing ecosystem services

Maibritt PEDERSEN ZARI^{*a}, Katharina HECHT^b

^{*a} School of Architecture, Victoria University of Wellington

PO Box 600, CBD, Wellington 6011, New Zealand

maibritt.pedersen@vuw.ac.nz

^b Department of Biology, Utrecht University

Postbus 80.056, 3508 TB Utrecht, Netherlands

k.hecht@students.uu.nl

Abstract

Redesigning and retrofitting cities so they become complex systems that create ecological and societal health through the provision of ecosystem services is of critical importance. This is due to two key reasons. Firstly, it is well known that cities have a large negative ecological impact, and secondly, the human population is rapidly growing and is now mostly urbanised. As professionals of the built environment are required to solve more urgent and complex problems related to ongoing climate change, and biodiversity loss, it may be useful to examine examples of how the same problems have been solved by other living organisms or ecosystems. This can be termed biomimicry. Biomimicry that emulates whole ecosystems, particularly the function of ecosystems, has been identified as having more potential to positively shift the ecological performance of buildings and urban settings. In this regard the ecosystem services concept is useful. Although a small number of methodologies and frameworks for considering how to design urban environments so that they emulate and provide ecosystem services have been proposed, their use is not wide spread. A key barrier has been identified as a lack of translation of the concept of ecosystem services design into practical examples of design strategies, concepts, and technologies, and case study precedents illustrating the concepts. In response, this

DOI: 10.30448/ts2019.3245.54

Copyright © 2019 by M. Pedersen Zari and K. Hecht. Published by Maggioli SpA with License Creative Commons CC BY-NC-ND 4.0 with permission.

paper presents research seeking to create a qualitative complex map in an online interactive format that relates the ecosystem services concept to design strategies and case studies in a comprehensible format for use by designers and built environment professionals. The paper concludes that buildings, and indeed whole cities should be expected to become active contributors to eco-sociological systems, rather than remaining unresponsive agents of ecosystem degeneration, and that the strategies and technologies to enable this already exist.

Keywords: Ecosystem services; biomimicry; urban design; urban ecology; data visualisation; sustainability; regenerative design.

1. Introduction

The way buildings and cities are designed will need to change rapidly and effectively to address converging drivers of change such as climate change and biodiversity loss. This must occur within the complex context of human population growth, increased per capita consumption, and global urbanisation (Grêt-Regamey et al. 2013). Although cities only occupy approximately 3 to 4% of global land area (van Vliet, Eitelberg, and Verburg 2017, Ruth and Coelho 2007), they are the sites of tremendous concentrations of energy use, water use, materials, greenhouse gas emissions, and other pollutants. Because of the built environment's increasing appropriation of the goods and services of ecosystems, vital ecological services for human society (and other species) such as climate regulation, soil formation, nutrient cycling, pollination, and waste assimilation are negatively affected (Vitousek et al. 1997). Modern cities are primarily sites for cultural expression and the facilitation of trade, rather than for the production of physical resources or the generation of services that produce tangible physical ecosystem or human health (Doughty and Hammond 2004). Despite this, urban environments must be considered in terms of their impact on climate and ecosystems and their potential role in facilitating regeneration of them.

Changes to the climate, and therefore related impacts on the built environment are expected to increase in intensity in the future. This suggests that re-evaluation of the built environment, and rapid expansion of policies and actions to mitigate greenhouse gas (GHG) emissions are urgently required (Masson-Delmotte et al. 2018). The built environment is responsible for approximately a third of global anthropogenic GHG emissions, leading to climate change (de la Rue du Can and Price 2008). The built environment will also have to adapt to climate change impacts, as the main site of human economic, social and cultural life. More than half of all humans now live in urban built environments. It is important therefore that built environment professionals are not only able to work towards mitigating the causes of climate change, but are also able to devise strategies to adapt to the impacts concurrently. In this regard nature inspired; lightweight; membrane; adaptive / intelligent façades; and kinetic technologies and materials with a focus on sustainability have proven to be important (Barozzi et al. 2016, De Vita et al.

2018, Loonen et al. 2013, Romano et al. 2018). Concurrently, biodiversity loss, and with it ecosystem degradation must be addressed. The degradation of ecosystems, along with the fact that there is a positively reinforcing feedback loop between biodiversity loss and climate change (Chapin et al. 2000, Pedersen Zari 2014), is why biodiversity loss is an urgent issue for humans to address (Rastandeh, Brown, and Pedersen Zari 2017), and why this must be considered in built environment design (Pedersen Zari 2018b).

Cities, and the buildings within them must become regenerative (Cole 2012). Regenerative design in this sense means design with an aim to produce quantifiable ecological and social health outcomes rather than design which aims to simply minimise energy or water use, or the emission of pollutants (Reed 2007). The question remains however, how can design professionals practically engage with such an agenda or set of goals? In this regard, there is an obvious and accessible example to investigate and then emulate; that is, the living biological world, and its complex systems. Ecosystems remain the best known example of sustainable organisation of life on this planet (Vincent et al. 2006). It is logical therefore to try to understand, and if possible, to mimic how organisms and ecosystems work and what they do in the creation of a regenerative human habitat.

1.2. Biomimicry for regenerative built environments

By looking to the living world, there may be organisms or systems that can be mimicked to create and maintain a resilient and adaptable built environment, and improve its capacity for regeneration of the health of ecosystems (Pedersen Zari, 2018a). This applies to urban scale interventions, through to the scale of building components and materials, and can be termed ‘biomimicry’ (Benyus 1997). Biomimicry is the emulation of strategies seen in the living world as a basis for design and innovation, and has potential to contribute to the creation of more sustainable architecture and urban environments (Pawlyn 2011). It is the mimicry of an organism, organism behaviour, or an entire ecosystem, in terms of its form, material, construction method, process strategies, or function (Pedersen Zari, 2007). Mimicking living organisms or ecosystems involves a process of translation into suitable solutions for the human context. Several noteworthy contemporary examples of biomimetic architecture or technologies that can assist the built environment in adapting to climate change or becoming an agent of ecological health are examined by (Pedersen Zari, 2018a) and (Pawlyn 2011). Additional historic examples of biomimicry are detailed by Vincent et al. (2006) and Vogel (1998). Biomimetic case studies examined by Pedersen Zari (2015a) suggest that ecosystem biomimicry, that is the emulation of how whole ecosystems function and the ways in which they work, may be the most effective kind of biomimicry to respond to climate change and biodiversity loss. This is because ecosystem biomimicry falls into a paradigm of whole systems thinking and change, rather than design of single components. Ecosystem biomimicry remains the least explored aspect of biomimicry in built form.

1.3 Systemic improvement of the built environment: ecosystem biomimicry

Ecosystems are typically resilient and many are able to move through infrequent abrupt changes while still supporting the survival of organisms (Gunderson and Holling 2002). The ability of ecosystems to adapt to the rapid changes that may come about due to climate change is difficult to predict (Walther et al. 2002). Despite this, mimicking ecosystems can offer insights into how the built environment could function more like a complex living system rather than as a set of unrelated, object-like buildings, and thus become better able to adjust to change.

1.3.1 Mimicking how Ecosystems Work: Process Strategies

Ecosystem processes inspired strategies for addressing climate change and ecological degradation challenge conventional architectural design and procurement thinking, particularly related to the typical boundaries of a building site and design time scales. By mimicking process strategies in ecosystems, designers may have successful models to follow in devising how systems in buildings or urban environments should be put together and how they should work. Typically, such systems mimic the process in ecosystems where waste becomes a resource for another component of the system, or where energy is shared ensuring the system eliminates or reduces duplication of effort. Well known examples of industrial ecology such as Denmark's Kalundborg industrial region illustrate how the process of cycling materials in ecosystems can be mimicked, even between diverse companies. In Kalundborg, this sharing of waste as resource results in a reduction of approximately 30 million m³ of groundwater used, and a reduction in emission of 154 000 tonnes of CO₂ and 389 tonnes of mono-nitrogen oxides (NO_x). Five companies and one local municipality make up the industrial park where twenty different bi-product exchanges occur (Valentine 2016, Jacobsen 2006). The elimination of toxins and pollutants that lead to the degradation of ecosystems is also addressed with such an approach. Examining ecosystem processes other than just the cycling of wastes or sharing of energy, suggests additional strategies for the built environment to mimic.

A comparative analysis of knowledge in the disciplines of ecology, biology, industrial ecology, ecological design, and biomimicry was conducted with an aim of capturing cross disciplinary understandings of how ecosystems work. A group of ecosystem process strategies were formulated that can form the basis of built environment focused biomimetic design (figure 1). For methodology and research sources used to produce figure 1 see: Pedersen Zari (2015b).

1.3.2 Mimicking what ecosystems do: ecosystem services

Mimicking the functions of ecosystems (what they do) has also been investigated in a design context (Birkeland 2009, Pedersen Zari 2017a, Pedersen Zari 2017b). This is different from mimicking the processes of ecosystems (how they work). Mimicking ecosystem processes eventuates in buildings or neighbourhoods that may be biomimetic but not necessarily better than conventional designs in terms of ecological performance. Essentially the emulation of

ecosystem remains at a metaphorical level. Analysing the urban built environment from the perspective of how ecosystems function, and then designing changes to cities, buildings, and building components so that they begin to quantifiably emulate the functions of ecosystems however, could work towards the creation of cities where positive integration with, and restoration of local ecosystem services could be realised (Pedersen Zari, 2018a).

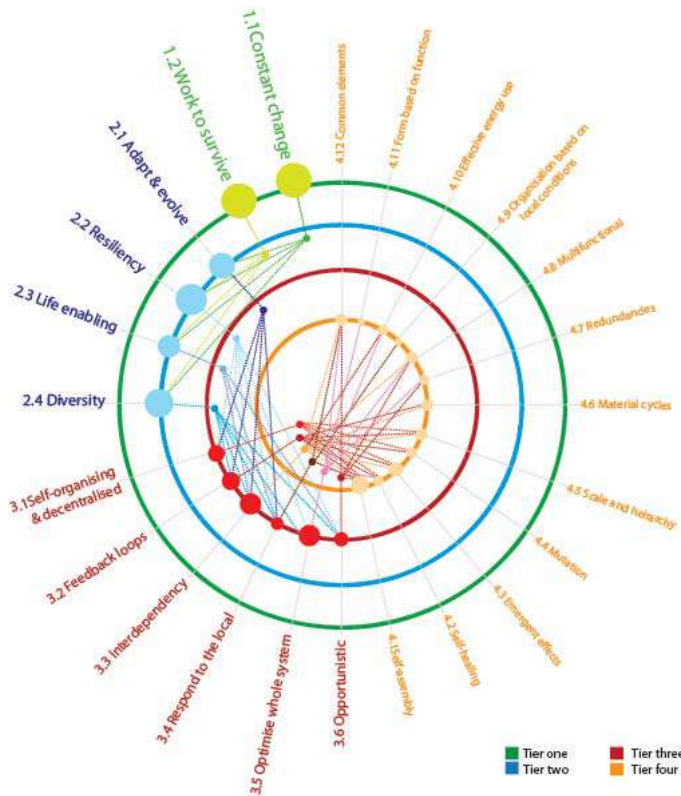


Figure 1: Ecosystem processes. Source: (Pedersen Zari 2015b).

The ecosystem services framework is one way to understand the complexity of ecosystem functions and human interactions with them. Ecosystem services are the benefits that humans (and all living organisms) derive, either directly or indirectly from the functions of ecosystems (Potschin and Haines-Young 2016). Ecosystem services are defined and listed in different ways (Millennium Ecosystem Assessment, 2005, Potschin et al., 2016), but typically are divided into: provisioning services such as food and medicines; regulation services such as pollination and climate regulation; supporting services such as soil formation and fixation of solar energy; and cultural services such as artistic inspiration and recreation. A focus on ecosystem services has been widely adopted among ecology and policy professionals (Martín-López et al. 2014), and

was formalised by the United Nations' Millennium Ecosystem Assessment of Ecosystems and Human Wellbeing (Millennium Ecosystem Assessment, 2005).

One way to reduce the ongoing degradation of ecosystems is to create built environments that mimic or provide ecosystem services and therefore reduce pressure on ecosystems, as the urban environment grows and as the climate continues to change. In urban environments themselves, ecosystem services are less well understood (Gómez-Baggethun and Barton 2013), but are thought to occur at low rates except for cultural ecosystem services (Costanza et al. 2014). Despite this, several important urban ecosystem services have been identified and include: air purification; water flow regulation; micro climate regulation; and carbon sequestration (Gómez-Baggethun and Barton, 2013). Typically, these urban ecosystem services come from urban 'green spaces' such as forests and parks, or 'blue spaces' such as lakes and wetlands and represent important opportunities for novel design interventions, particularly related to increasing resilience to climate change (Elmqvist, Gomez-Baggethun, and Langemeyer 2016) and increasing human wellbeing (Foley and Kistemann 2015). Opportunities also exist for green or grey/green hybrid infrastructure and for buildings themselves to produce ecosystem services however (Escobedo et al. 2019, Birkeland 2009). Mimicking what ecosystems do (provide ecosystem services) can become the overall ecological performance goal generator for a development, while the specific methods or technologies to achieve the goals can be drawn from a wide range of existing design strategies, concepts, and technologies.

By emulating ecosystem services, a building or development could be designed for example to be part of a system that: produces food; produces renewable energy; produces raw materials for the future built environment; collects and purifies water; purifies air and soil; regulates climate through mitigating GHG emissions and the heat island effect; contributes to soil formation and fertility through careful cycling of bio-degradable wastes and recycling of non-biodegradable wastes; and deliberately provides habitat for species suitable for co-habitation with humans in urban built environments (Pedersen Zari, 2018a). New ecologically regenerative developments in turn could act as filters (mechanisms that purify air and water), producers (of food and materials) and generators (of energy) for the rest of the built environment which is still degrading ecosystems and is likely to persist for at least another 50 to 90 years (O'Connell and Hargreaves 2004). If these regenerative nodes became part of the built environment and start to perform even small aspects of ecosystem functions, it is possible that some causes of climate change and biodiversity loss attributed to the built environment would be mitigated, and at the same time the built environment could become more adaptable to climate change, while concurrently creating beneficial biodiversity outcomes.

Ecosystem services analysis (ESA), developed by (Pedersen Zari, 2018a), is a means by which the concept of ecosystem services is applied to built environment contexts, particularly in a context of regenerative design. The purpose of ESA is to measure past, current and future environmental performance of the built environment in terms of ecosystem services provision so that future spatial and temporal ecology derived performance goals can be devised.

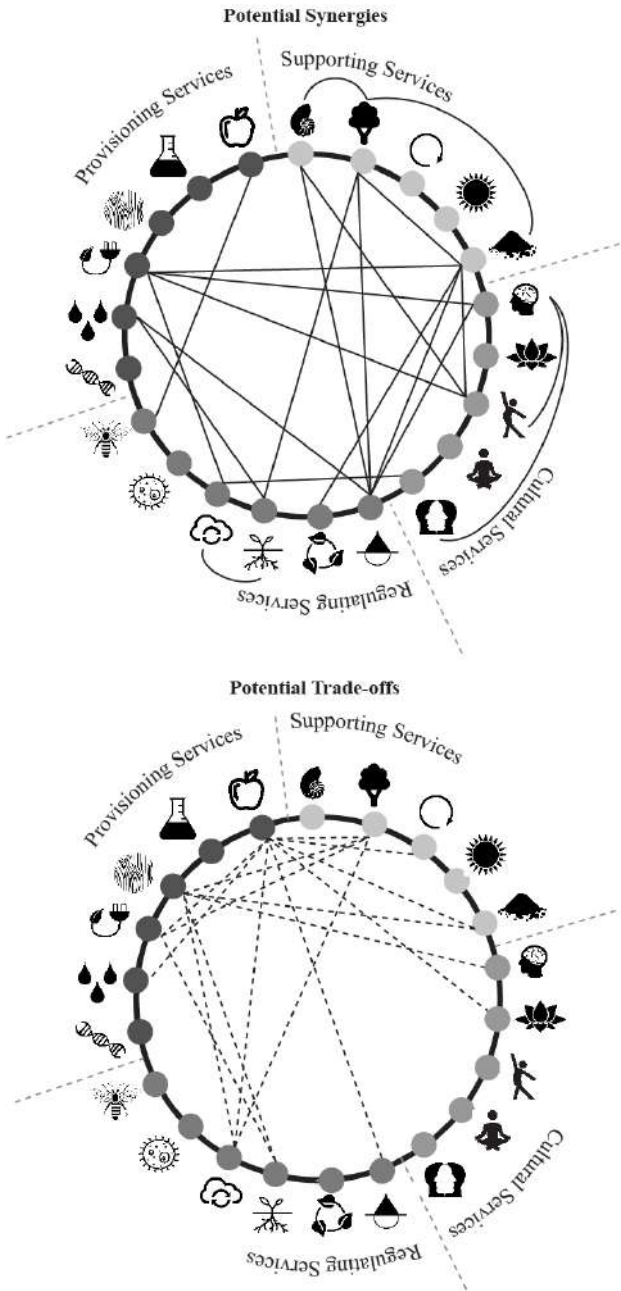


Figure 2: Potential synergies and trade-off relationships between ecosystem services. Source: (Pedersen Zari, 2019). See icon key next page.

If designers and policy makers are to effectively use the ecosystem services model in urban settings they must understand how these ecosystem services are related however (Bennett, Peterson, and Gordon 2009). This is so potential synergies between ecosystem services can be leveraged, but also so that potential trade-off relationships between certain ecosystem services can be avoided or addressed. Recent research by the author (Pedersen Zari 2019) has illustrated relationships between ecosystem services for a design audience based on quantifiable ecological research results devised by Lee and Lautenbach (2016). Further qualifying ecological and socio-economical associations between ecosystem services were provided by (Mouchet et al. 2014), (Howe et al. 2014), Bennett et al. (2009), and (Raudsepp-Hearne, Peterson, and Bennett 2010). See: figure 2.

2.0 The ‘strategies for designing urban ecosystem services’ map

In order to take the concept of emulating the functioning of ecosystem services (a form of ecosystem biomimicry) further, and to make it easier to implement, it is necessary to demonstrate how designers can practically

implement ecosystem services focused design at both the architectural and the urban scale. The aims of this research then are twofold: 1/ Create a database of existing and developing strategies

Key to Figure 2: Ecosystem Services					
Supporting Services		Habitat provision	Cultural services		Aesthetic & artistic inspiration - Aesthetic value - Artistic inspiration
		Nutrient cycling - Retention of nutrients - Regulation of biogeochemical cycles			Recreation and psychological wellbeing - Sport - Outdoor activities - Tourism - Socialisation - Relaxation & psychological benefit
		Species Maintenance			Sense of place and cultural diversity - Celebration of cultural diversity/history - Sense of place
		Fixation of solar energy			Spiritual and religious inspiration
		Soil building - Soil formation - Renewal of soil fertility - Soil quality control - Soil retention			Education and knowledge - Educational - Inspiration & innovation - Cognitive development - Knowledge building
Regulation Services		Disturbance prevention - Noise - Wave - Erosion - Earthquake - Drought - Flood/Storm events - Wind	Provisioning Services		Provision of fuel and energy - Water energy - Wind energy - Active / passive solar energy - Human body heat - Hydrogen energy - Biomass energy - Geothermal energy
		Climate regulation - UV protection - Moderation of temperature - Climate adaptation strategies - GHG mitigation			Provision of fresh water - Drinking water - Sanitation - Irrigation - Industrial processes - Recreational
		Purification - Water purification - Soil purification - Air purification			Provision of food - Small to large scale urban agriculture
		Decomposition - Biodegradation - Material reuse/recycling - Consumption reduction			Biochemicals - Medicine - Natural chemicals
		Biological control - Control of invasive species - Disease/pest regulation			Raw materials
		Pollination			Genetic resources

and technologies that enable the creation of ecosystem services through the medium of buildings, built infrastructure and cities. 2/ map and illustrate this data so it is in an online interactive format comprehensible for designers or built environment researchers. The intention of the ‘strategies for designing urban ecosystem services’ map is that it becomes a tool for designers to use in investigating the practical application of design strategies that have been used to create ecosystem services, or aspects of them.

The online platform and interactive database of ecosystem services focused design methods, strategies, and case studies is the first one that is publicly accessible, interactive and thoroughly researched based. A complete, easily accessible and useful compilation of possible ecosystem services related design strategies will be valuable for people working in the architectural and urban design and planning fields.

3. Methodology

This research was design-led, rather than based on a more traditional science set of quantifiable experiments. Because of this, this methodology section outlines the steps in the research process. The reasoning behind each step and how these relate to the research aims is discussed concurrently, rather than being separated into discrete sections. The methodology used to produce the ‘strategies for designing urban ecosystem services’ map can be understood as follows:

3.1 Step one: literature and design precedent review

The theoretical framework for the map is based on the ecosystem services relationship diagrams and the urban ecosystem services categories described by (Pedersen Zari, 2018a). This work established the initial 22 ecosystem services and 49 subcategories of ecosystem services that were investigated and mapped (see: key to figure 2). A thorough critical literature and design precedent review of existing and developing strategies and technologies that enable the creation of ecosystem services through the medium of building components, buildings, built infrastructure, and cities was conducted. This was combined with and compared to international databases of urban nature-based solutions that focus on climate change adaptation (Keesstra et al. 2018, Pauleit et al. 2017, Raymond et al. 2017, Cohen-Shacham et al. 2016, Pedersen Zari et al. 2017) or climate change mitigation (Hawken 2017). For every strategy, concept or technology, identified, one or more illustrative international built case studies (114 in total) were investigated and summarised. Case studies include: architecture; landscape architecture; urban design; infrastructure design; building technologies / components / materials; and policies.

It should be noted that cultural ecosystem services are benefits that humans obtain from ecosystems related specifically to psychological, cultural, and societal wellbeing. This

ecosystem services type has been well investigated in social sciences literature, and socio-ecological models that link cultural services with ecological functions already exist (Daniel et al. 2012). Due to the existence of such models, the ‘strategies for designing urban ecosystem services’ map currently focuses on design strategies, concepts and technologies for provisioning, regulating and supporting services. Architects and designers are trained to integrate cultural and aesthetic aspects into their design work already and typically are expert at this. This means mapping design strategies that produce cultural ecosystem services is both a large task, and crucially is less urgent in relation to improving the biological ecological performance of urban environments. Future work is planned that integrates and relates cultural services to existing elements in the ‘strategies for designing urban ecosystem services’ map.

3.2 Step two: relational database compilation

The results of step one were compiled as a database that identified relationships between design strategies, concepts, and technologies and specific ecosystem services. Case studies were also added to the database. The database was developed in the Microsoft Excel programme (Microsoft Office Professional Plus 2013). Relationships between 160 distinct design strategies, concepts and technologies that work towards ecosystem services generation were defined.

3.3 Step three: complex system visualisation

The final step was to design an interactive visualisation of the database that captured the ecosystem services and design strategies identified, as well as the relationships between them. In order to create a holistic understanding of complex systems, Suoheimo & Miettinen (2018) suggest employing complexity mapping as a tool. A qualitative visualization of complex systems shows interconnections, patterns, and dynamics of the participating elements (Liebovitch, 2014). In order to understand the relationships between each element in more depth, the complexity map was first drafted manually with sticky notes and hand drawn lines on a board (figure 3). This particular methodology is effective, and common in complex systems mapping (Suoheimo and Miettinen 2018).



Figure 3: Manual complexity mapping.
Photo by K. Hecht

To ensure effective visualisation of the data several online qualitative complexity mapping web-based software and platforms were tested for suitability. The mapping tools investigated for their usability, and functionality included: bubbl.us (Stair 2013); MindMup (Adzic and Chatley 2017); 7Vortex (7Vortex 2018); and Kumu (Liebovitch 2014). Kumu was the platform selected

due to its flexibility in structuring, connecting, and controlling the visualisation of the data. Kumu was created by J. and R. Mohr in 2011 and enables the mapping of relationships and the visualisation of complex systems and large datasets. An additional reason for the selection of Kumu was that the developed database spreadsheet (step two of the research process) could be transferred to the platform for automated updating.

Within the ‘strategies for designing urban ecosystem services’ map each discrete ecosystem service, or design strategy, or case study became a circle on the Kumu map and is termed an ‘element’. In total there are 348 elements in the map, all of which have been manually linked with relationship lines (equating to 1421 individual relationship connections in the map).

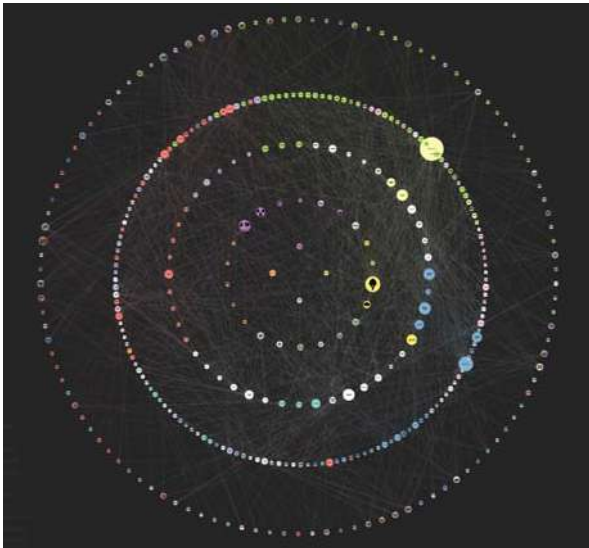


Figure 4: Screenshot of the strategies for designing urban ecosystem services map version 1.0.

The outermost circle are the case studies. The next circle in is the design strategies. The third circle is the ecosystem services subcategories. The second smallest circle is the ecosystem services categories and the innermost circle is the ecosystem services types (provisioning, regulating, supporting, and cultural).

Additional descriptions of each ecosystem service, ecosystem service subcategory, design strategy / technology / concept, and case study were completed and are accessible by clicking on the three grey dots on the left side in the map. References, links to additional material, and video clips where available and relevant, were added to the majority of the descriptions. The element colours were determined by affiliation to one of the seven most applicable ecosystem services to an urban context defined by Pedersen Zari (2018b). These categories are: provision of food; provision of fresh water; provision of fuel / energy; climate regulation; purification; nutrient cycling; and habitat provision. To facilitate the usability of the map, icons were used as background images for the ecosystem services categories and photos were used as element images for the case studies.

Through an iterative design-led research process, it became clear that organising the elements into a series of concentric circles made the complexity map easier to use and meant that users could start from the middle of the map with the intention of designing for a specific ecosystem service, or they could start from the outermost circle from the case studies and work their way inwards to understand how multiple ecosystem services can be generated concurrently (figure 4). A link to version 1.0 of the map is available by contacting the authors.

Additional descriptions of each ecosystem service, ecosystem service subcategory, design strategy / technology / concept, and case study were completed and are accessible by clicking on the three grey dots on the left side in the map. References, links to

4. Results: understanding the ‘strategies for designing urban ecosystem services’ map

The size of each element in the ‘strategies for designing urban ecosystem services’ map was determined through the Kumu programme automatically by the amount of direct connections to it. This means the more relationship links an element has, the larger the element circle appears on the map. By analysing the sizes of the elements it is possible to see which ecosystem services have larger numbers of design strategies attached to them, and which ecosystem services have few existing design strategies associated with their creation in an urban setting. The map displays possible relationships between elements. These relationships can be direct or indirect which means that certain elements are connected via one or more other elements. For instance, the ecosystem service ‘soil building’ is indirectly related to the ecosystem service ‘decomposition’. This can be explained due to the connection via the ‘soil building’ subcategory ‘renewal of soil fertility’ and the ‘decomposition’ subcategory ‘biodegradation’.

Analysing the map based on numbers of connections to each element shows that provisioning services have the highest amount of connections (both direct and indirect), particularly the provision of fuel / energy ecosystem services (connection to 23 different design strategies), and the provision of fresh water ecosystem service (connection to 15 design strategies). This demonstrates that design strategies, concepts, or technologies that generate provisioning ecosystem services are among the most well-known, and developed and are already often integrated into sustainable built environment design. This is not surprising given that these ecosystems services are a familiar and integral part of traditional forms of human economic systems (Daily 1997). They are tangible, and easily understood.

Provisioning ecosystem services tend to be directly reliant on regulating and supporting ecosystem services (Pedersen Zari 2018a). It is important therefore that ecosystem services design does not ignore regulating or supporting services, although these are more difficult to quantify, and indeed to understand for many people (Daily, 1997). The type of ecosystem services with the least amount of connections (both direct and indirect) to known design strategies, concepts, and technologies in the map was supporting services. Supporting services include ecosystem services like ‘soil building’ or ‘nutrient cycling’ and directly support provisioning services. This suggests that future research and effort should be made to devise and test design strategies that produce or contribute to supporting and regulating ecosystem services more readily. The only exception to the low number of known design strategies that relate to supporting ecosystem services was ‘habitat provision’. Habitat provision was actually the ecosystem service with the highest amount of direct connections to known ecosystem services related design strategies (connected to 40 design strategies). This can be explained because of the direct linkage to many design strategies, concepts, and technologies included in the map which are based on vegetation-related concepts such as green roofs, living walls, allotment gardens, and urban wildlife corridors for example.

Ecosystem services and sub categories with the least amount of known design strategies associated with them were: provision of genetic information; fixation of solar energy; and control of invasive species. This can be explained because the nature of these ecosystem services relies heavily on communities of living plants, meaning unless plants themselves are integrated into buildings or urban contexts it is difficult for buildings or grey infrastructure to produce these ecosystem services. Earlier research has shown that if the ecosystem service of habitat provision in urban settings is thought of as a bundle of ecosystem services including: provision of genetic information; biological control; species maintenance; fixation of solar energy; and soil building, these ecosystem services can be more readily integrated into urban contexts (Pedersen Zari, 2015b).

The ecosystem subcategories of greenhouse gas (GHG) mitigation, and climate adaptation, which both relate to the regulating ecosystem service of climate regulation, were among the largest categories in terms of associated design strategies. This may be a result of current effort in the building and urban design communities to devise strategies for design that addresses climate change (both the mitigation of and adaptation to it).

Among the design strategies, concepts, and technologies, ‘revegetation’ had the highest amount of connections to ecosystem services, suggesting that inclusion of green space and living infrastructure into cities will be an important part of achieving ecosystem services based ecological performance goals in urban settings. Applying just this one design strategy in an urban environment can, depending on the exact nature of the design, generate up to nine different ecosystem services including soil building, purification and provisioning of fuel and energy. Other design strategies with large numbers of connections, meaning the potential to contribute to more than one ecosystem service, included urban agriculture and carbon / GHG sequestration technologies.

In summary, the ‘strategies for designing urban ecosystem services’ map shows that there are existing design strategies that relate to the emulation, production, or support of every listed ecosystem service. This suggests that ecosystem biomimicry based on the idea of emulating ecosystem services does not have to rely on new, or un-tested technologies or design ideas. Rather, what is required is a re-imagining of the overall goals for ecological performance and effort to design building or urban spaces that produce multiple interconnected ecosystems.

5. Discussion

That a greater understanding of ecology and systems design is required on the part of design teams is implicit with an ecosystem services approach to architectural and urban design. Increased collaboration between fields that traditionally seldom work together such as architecture or urban design, and biology or ecology would also be required. The built environment varies greatly between different climatic, economic and cultural contexts, and

systems that are appropriate to specific places will therefore also vary greatly. Although each differing geographic region will have to evolve its own unique system over time, knowledge of how to create or evolve such systems can be transferred, particularly through ecosystem services design visualisation tools such as the ‘strategies for designing urban ecosystem services’ map.

A whole-system ecosystem services generation approach to built environment design is a suitable solution for a longer-term response to climate change and biodiversity loss, because it addresses many of the underlying issues with current urban environments that are in need of re-evaluation (Grimm et al. 2008). The difference can be likened to a long-term treatment of the underlying cause of an illness in an individual, rather than a short-term treatment of symptoms which may in fact aggravate the underlying condition. In this case, this is the fact that the majority of human urban settlements are dependent on fossil fuels to heat, feed and transport people in a linear system which creates pollution leading in part to climate change. This system also causes the degradation of water ways, air quality, soil, and human health while at the same time consumes non-renewable resources in such a way that they cannot be re-used. A whole-systems approach to built environment design acknowledges that human developments and therefore humans are not in any way separate from the ecosystems they exist in.

5.1 The evolution of the ‘strategies for designing urban ecosystem services’ map

The ‘strategies for designing urban ecosystem services’ map as illustrated in figure 4 is currently at version 1.0. Version 1.1 will involve verifying the accuracy of existing relationships between map elements, and additional expansion of the text descriptions of each element. In order to better indicate and illustrate the nature of existing relationships, connection lines may need to be modified in terms of their direction / strength / colour etc. Version 1.1 will also require further collaboration with a graphic designer and / or software designer to improve some graphical and usability issues with the existing Kumu map. A revision of how elements are clustered (which currently is determined automatically by the Kumu algorithms) would also be useful. Beyond these minor improvements, it is important to integrate cultural ecosystem services more effectively into the map. The map will require continuous development to include new innovations in the area of design for urban ecosystem services.

The next major phase of the research will involve testing the developed online system practically in a pilot research project with designers, in order to evaluate the usability of the map and to then understand the range of further improvements that should be made. Work on phase 2 in the form of a pilot study using an app based ecosystem services site measurement tool (ESII Tool 2019) has begun with the intention of investigating how existing decision-support tools for ecosystem services measurement (see: Bagstad et al. 2013) can be more effectively translated into practical examples of design strategies using the medium of the ‘strategies for designing urban ecosystem services’ map.

6. Conclusions

Mimicking aspects of living organisms can produce innovations that address sustainability issues in some cases, but without an understanding of the ecological context of these organisms, such innovations can too easily become simple technological add-ons or substitution materials in conventional buildings. Such solutions also miss an opportunity to examine the possibility of systemic change in the built environment and to re-evaluate the nature of the relationship between people, their built environment the ecosystems they exist in.

Positive integration with ecosystems leading to a regenerative rather than damaging effect on them in urban contexts may contribute to maintaining biodiversity and the ecosystem services that humans are dependent upon for survival, particularly as the climate continues to change. Such a concept goes beyond encouraging a basic understanding of ecological processes over time. Instead it is the thorough integration of quantifiable biological ecological knowledge into architecture and urban design for the purpose of altering how buildings fundamentally function in relation to both ecosystems and to each other. Buildings, and indeed whole cities should be expected to become active contributors to ecosystems and social systems, rather than remaining unresponsive agents of ecosystem degeneration.

Acknowledgements

No external funding was received for this research.

References

- 7Vortex. (2018). Everything is Connected. Retrieved from <https://www.sevenvortex.com/>
- Adzic, G., & Chatley, R. (2017). *Serverless computing: economic and architectural impact*. Paper presented at the Proceedings of the 2017 11th Joint Meeting on Foundations of Software Engineering.
- Bagstad, K. J., Semmens, D. J., Waage, S., & Winthrop, R. (2013). A comparative assessment of decision-support tools for ecosystem services quantification and valuation. *Ecosystem services*, 5, 27-39.
- Barozzi, M., Lienhard, J., Zanelli, A., & Monticelli, C. (2016). The Sustainability of Adaptive Envelopes: Developments of Kinetic Architecture. *Procedia Engineering*, 155, 275-284. doi:<https://doi.org/10.1016/j.proeng.2016.08.029>
- Bennett, E. M., Peterson, G. D., & Gordon, L. J. (2009). Understanding relationships among multiple ecosystem services. *Ecology Letters*, 12(12), 1394-1404. doi:10.1111/j.1461-0248.2009.01387.x
- Benyus, J. (1997). *Biomimicry - Innovation Inspired by Nature*. New York: Harper Collins Publishers.
- Birkeland, J. (2009). Design for Eco-Services. In *Environmental Design Guide*. Canberra: The Australian Institute of Architects.
- Chapin, F. S., Zavaleta, E. S., Eviner, V. T., Naylor, R. L., Vitousek, P. M., Reynolds, H. L., . . . Diaz, S. (2000). Consequences of changing biodiversity. *Nature*, 405(6783), 234-242.

- Cohen-Shacham, E., Walters, G., Janzen, C., & Maginnis, S. (2016). Nature-based solutions to address global societal challenges. *IUCN, Gland, Switzerland*, 97.
- Cole, R. J. (2012). Regenerative design and development: current theory and practice. *Building Research & Information*, 40(1), 1-6. doi:10.1080/09613218.2012.617516
- Costanza, R., de Groot, R., Sutton, P., van der Ploeg, S., Anderson, S. J., Kubiszewski, I., . . . Turner, R. K. (2014). Changes in the global value of ecosystem services. *Global Environmental Change*, 26, 152-158.
- Daily, G. C. (1997). *Nature's Services Societal Dependence on Natural Ecosystems*. Washington D.C: Island Press.
- Daniel, T. C., Muhar, A., Arnberger, A., Aznar, O., Boyd, J. W., Chan, K. M. A., . . . von der Dunk, A. (2012). Contributions of cultural services to the ecosystem services agenda. *Proceedings of the National Academy of Sciences*, 109(23), 8812-8819. doi:10.1073/pnas.1114773109
- de la Rue du Can, S., & Price, L. (2008). Sectoral trends in global energy use and greenhouse gas emissions. *Energy Policy*, 36(4), 1386.
- De Vita, M., Beccarelli, P., Laurini, E., & De Berardinis, P. (2018). Performance Analyses of Temporary Membrane Structures: Energy Saving and CO2 Reduction through Dynamic Simulations of Textile Envelopes. *Sustainability*, 10(7), 2548.
- Doughty, M., & Hammond, G. (2004). Sustainability and the Built Environment at and Beyond the City Scale. *Building and Environment*, 39, 1223-1233.
- Elmqvist, T., Gomez-Baggethun, E., & Langemeyer, J. (2016). Ecosystem services provided by urban green infrastructure. In *Routledge Handbook of Ecosystem Services* (pp. 452-464): Routledge.
- Escobedo, F. J., Giannico, V., Jim, C. Y., Sanesi, G., & Laforteza, R. (2019). Urban forests, ecosystem services, green infrastructure and nature-based solutions: Nexus or evolving metaphors? *Urban Forestry & Urban Greening*, 37, 3-12. doi:https://doi.org/10.1016/j.ufug.2018.02.011
- ESII Tool. (2019). ESII Tool. Retrieved from <https://www.esiitool.com/>
- Foley, R., & Kistemann, T. (2015). Blue space geographies: Enabling health in place. *Health & Place*, 35, 157-165. doi:https://doi.org/10.1016/j.healthplace.2015.07.003
- Grimm, N. B., Faeth, S. H., Golubiewski, N. E., Redman, C. L., Wu, J., Bai, X., & Briggs, J. M. (2008). Global Change and the Ecology of Cities. *Science*, 319(5864), 756-760. doi:10.1126/science.1150195
- Grêt-Regamey, A., Celio, E., Klein, T. M., & Wissen Hayek, U. (2013). Understanding ecosystem services trade-offs with interactive procedural modeling for sustainable urban planning. *Landscape and Urban Planning*, 109(1), 107-116. doi:https://doi.org/10.1016/j.landurbplan.2012.10.011
- Gunderson, L. H., & Holling, C. S. (2002). *Panarchy. Understanding Transformations in Human and Natural Systems*. Washington D.C.: Island Press.

- Gómez-Baggethun, E., & Barton, D. N. (2013). Classifying and valuing ecosystem services for urban planning. *Ecological Economics*, 86, 235-245. doi:<http://dx.doi.org/10.1016/j.ecolecon.2012.08.019>
- Hawken, P. (2017). *Drawdown: The most comprehensive plan ever proposed to reverse global warming*: Penguin.
- Howe, C., Suich, H., Vira, B., & Mace, G. M. (2014). Creating win-wins from trade-offs? Ecosystem services for human well-being: A meta-analysis of ecosystem service trade-offs and synergies in the real world. *Global Environmental Change*, 28(Supplement C), 263-275. doi:<https://doi.org/10.1016/j.gloenvcha.2014.07.005>
- Jacobsen, N. B. (2006). Industrial symbiosis in Kalundborg, Denmark: A quantitative assessment of economic and environmental aspects. *Journal of Industrial Ecology*, 10(1-2), 239.
- Keesstra, S., Nunes, J., Novara, A., Finger, D., Avelar, D., Kalantari, Z., & Cerdà, A. (2018). The superior effect of nature based solutions in land management for enhancing ecosystem services. *Science of The Total Environment*, 610, 997-1009.
- Lee, H., & Lautenbach, S. (2016). A quantitative review of relationships between ecosystem services. *Ecological Indicators*, 66(Supplement C), 340-351. doi:<https://doi.org/10.1016/j.ecolind.2016.02.004>
- Liebovitch, L. (2014). *Automated Quantitative Visualization*. Paper presented at the Complexity Mapping in Practice and Research: Methods, Trends, and Future Directions, Honolulu, Hawai'i. https://conflictinnovationlab.files.wordpress.com/2014/06/dst_visualization_23june2014.pdf
- Loonen, R. C. G. M., Trčka, M., Cóstola, D., & Hensen, J. L. M. (2013). Climate adaptive building shells: State-of-the-art and future challenges. *Renewable and Sustainable Energy Reviews*, 25, 483-493. doi:<https://doi.org/10.1016/j.rser.2013.04.016>
- Martín-López, B., Gómez-Baggethun, E., García-Llorente, M., & Montes, C. (2014). Trade-offs across value-domains in ecosystem services assessment. *Ecological Indicators*, 37, 220-228.
- Masson-Delmotte, V., Zhai, P., Pörtner, H.-O., Roberts, D., Skea, J., Shukla, P., & Pirani, A. (2018). *Global warming of 1.5°C*. Retrieved from Switzerland:
- Mouchet, M. A., Lamarque, P., Martín-López, B., Crouzat, E., Gos, P., Byczek, C., & Lavorel, S. (2014). An interdisciplinary methodological guide for quantifying associations between ecosystem services. *Global Environmental Change*, 28(Supplement C), 298-308. doi:<https://doi.org/10.1016/j.gloenvcha.2014.07.012>
- O'Connell, M., & Hargreaves, R. (2004). *Climate Change Adaptation Study Report No. 130: BRANZ*.
- Pauleit, S., Zölch, T., Hansen, R., Randrup, T. B., & Konijnendijk van den Bosch, C. (2017). Nature-Based Solutions and Climate Change – Four Shades of Green. In N. Kabisch, H. Korn, J. Stadler, & A. Bonn (Eds.), *Nature-Based Solutions to Climate Change Adaptation in Urban Areas: Linkages between Science, Policy and Practice* (pp. 29-49). Cham: Springer International Publishing.

- Pawlyn, M. (2011). *Biomimicry in Architecture*. London: RIBA Publishing.
- Pedersen Zari, M. (2007). *Biomimetic Approaches to Architectural Design for Increased Sustainability*. Paper presented at the Sustainable Building Conference (SB07), Auckland, New Zealand.
- Pedersen Zari, M. (2014). Ecosystem Services Analysis in Response to Biodiversity Loss Caused by the Built Environment. *S.A.P.I.E.N.S.*, 7(1). doi:1993-3819
- Pedersen Zari, M. (2015a). Can Biomimicry be a Useful Tool in Design for Climate Change Adaptation and Mitigation? In F. Pacheco-Torgal, J. A. Labrincha, M. V. Diamanti, C. P. Yu., & H. K. Lee (Eds.), *Biotechnologies and Biomimetics for Civil Engineering* (pp. 81-113). Cham: Springer International Publishing.
- Pedersen Zari, M. (2015b). Ecosystem processes for biomimetic architectural and urban design. *Architectural Science Review*, 58(2), 106-119. doi:10.1080/00038628.2014.968086
- Pedersen Zari, M. (2017). Ecosystem services analysis: incorporating an understanding of ecosystem services into built environment design and materials selection. In E. K. Petrović, B. Vale, & M. P. Zari (Eds.), *Materials for a Healthy, Ecological and Sustainable Built Environment: Principles for Evaluation* (pp. 29-64). Duxford, UK: Woodhead
- Pedersen Zari, M. (2017). Utilizing relationships between ecosystem services, built environments, and building materials. In E. K. Petrović, B. Vale, & M. Pedersen Zari (Eds.), *Materials for a Healthy, Ecological and Sustainable Built Environment: Principles for Evaluation* (pp. 1-28). Duxford, UK: Woodhead.
- Pedersen Zari, M. (2018a). *Regenerative Urban Design and Ecosystem Biomimicry*. Oxon: Routledge.
- Pedersen Zari, M. (2018b). The importance of urban biodiversity – an ecosystem services approach. *Biodiversity International Journal*, 2(4), 357-360.
- Pedersen Zari, M. (2019). Ecosystem services impacts as part of building materials selection criteria. *Materials Sustainability Today*, Published online 23 March.
- Pedersen Zari, M., Blaschke, P. M., Livesey, C., Martinez-Almoyna Gual, C., Weaver, S., Archie, K. M., . . . Renwick, J. (2017). *Ecosystem-based Adaptation (EbA) Project Implementation Plans, Port Vila, Vanuatu*. Retrieved from Wellington, New Zealand:
- Potschin, M., & Haines-Young, R. (2016). Defining and measuring ecosystem services. *Potschin, M., Haines-Young, R., Fish, R., Turner, RK (Eds.), Routledge Handbook of Ecosystem Services. Routledge, London and New York*, 25-44.
- Rastandeh, A., Brown, D. K., & Pedersen Zari, M. (2017). *Biodiversity conservation in urban environments: a review on the importance of spatial patterning of landscapes*. Paper presented at the Ecocity World Summit, Melbourne, Australia.
- Raudsepp-Hearne, C., Peterson, G. D., & Bennett, E. M. (2010). Ecosystem service bundles for analyzing tradeoffs in diverse landscapes. *Proceedings of the National Academy of Sciences*, 107(11), 5242.
- Raymond, C. M., Frantzeskaki, N., Kabisch, N., Berry, P., Breil, M., Nita, M. R., . . . Calfapietra, C. (2017). A framework for assessing and implementing the co-benefits of

- nature-based solutions in urban areas. *Environmental Science & Policy*, 77, 15-24. doi:<https://doi.org/10.1016/j.envsci.2017.07.008>
- Reed, B. (2007). Shifting from 'Sustainability' to Regeneration. *Building Research and Information*, 35(6), 674-680.
- Romano, R., Aelenei, L., Aelenei, D., & Mazzuchelli, E. S. (2018). What is an adaptive façade? Analysis of Recent Terms and definitions from an international perspective. *Journal of Facade Design and Engineering*, 6, 65-76.
- Ruth, M., & Coelho, D. (2007). Understanding and managing the complexity of urban systems under climate change. *Climate Policy*, 7(4), 317-336. doi:10.1080/14693062.2007.9685659
- Stair, N. (2013). Bubbl. us–Web 2.0 Mind Mapping. *Compass: Journal of Learning and Teaching*, 4(8).
- Suoheimo, M., & Miettinen, S. (2018). *Complexity MApping and Mess Mapping Tools for Decision-Making in Transportation and Mass Development*. Paper presented at the 21st DMI: Academic Design Management Conference, London, UK.
- Valentine, S. V. (2016). Kalundborg Symbiosis: fostering progressive innovation in environmental networks. *Journal of Cleaner Production*, 118, 65-77.
- van Vliet, J., Eitelberg, D. A., & Verburg, P. H. (2017). A global analysis of land take in cropland areas and production displacement from urbanization. *Global Environmental Change*, 43, 107-115. doi:<https://doi.org/10.1016/j.gloenvcha.2017.02.001>
- Vincent, J. F. V., Bogatyreva, O. A., Bogatyrev, N. R., Bowyer, A., & Pahl, A.-K. (2006). Biomimetics - its practice and theory. *Journal of the Royal Society Interface*, 3(9), 471-482.
- Vitousek, P. M., Mooney, H. A., Lubchenco, J., & Melillo, J. M. (1997). Human Domination of Earth's Ecosystems. *Science*, 277, 494-499.
- Vogel, S. (1998). *Cat's Paws and Catapults*. New York: Norton and Company.
- Walther, G. R., Post, E., Convey, P., Menzel, A., Parmesan, C., Beebee, T. J. C., . . . Bairlein, F. (2002). Ecological responses to recent climate change. *Nature*, 416(6879), 389.

Proceedings of the TensiNet Symposium 2019

Softening the habitats / 3-5 June 2019, Politecnico di Milano, Milan, Italy
Alessandra Zanelli, Carol Monticelli, Marijke Mollaert, Bernd Stimpfle (Eds.)

Structure and Space of Serendipity Brought by Materials for Art

Norihide IMAGAWA*

* Surgical Architect / Director of TIS&PARTNERS. Co., Ltd.

Honorary Professor of Tokyo Denki University

3rd Floor, Eiko Bldg., 1-54 Kanda-Jimbocho, Chiyoda-ku, Tokyo 101-0051 JAPAN

norihide.imagawa@gmail.com

Abstract

Material Speaks: How to effectively utilize materials energy [joules]. Architects, engineers and contractors all know and understand how to review and compare materials and skeletons of the same period. Reviewing and comparing the materials of different architecture and skeletons across time, however, was a different matter. Now, the “Material Speaks Energy Theory” has made it possible for everyone to review and compare not only different materials, architecture and skeletons across time, but the CO2 emissions of special structures, as well. The Material Speaks Energy Theory was formulated by categorizing, analyzing and summarizing the outcomes of more than 2,500 designs, and integrating the value of materials energy based upon the theory of structure design and recognition.

Keywords: tensegrity, serendipity, gravity, earthquake, typhoon, pin joint, art, folly, Nature of Structure, net playground equipment

DOI: 10.30448/ts2019.3245.28

Copyright © 2019 by Norihide Imagawa. Published by Maggioli SpA with License Creative Commons CC BY-NC-ND 4.0 with permission.

Peer-review under responsibility of the TensiNet Association

1. Introduction

Over the last 40 years I have designed 2,500 projects. 50 out of the 2,500, i.e. 1/50, are structural designs for artworks and monuments including follies (foolish structure).

2. Being Aware of Flexibility

As the most representative example of follies, I vividly recall a project by Elia Zenghelis for The International Garden and Greenery Exposition, Osaka, Japan, 1990, FOLLY FOR EXPO'90 #11 composed of a huge column and a huge beam connected to each other. (Figure 1) There, the column and the beam supported each other by utilizing frictional resistance generated on the surfaces touching to each other instead of normal rigid joint delivering bending/shear/axial force.

Folly #8 for the same expo by Morphosis was an asymmetric design. (Figure 2, 3) To balance the asymmetric object under gravity, the outermost end of the lighter side and the ground were connected by pin joint for preload to download. Even though, pin supported structure may become unstable when an earthquake or typhoon hits Osaka. In order to keep the asymmetrically loaded folly from collapsing, tie down belts were attached to each side with proper load for each. The huge 3 flower pots installed on top of the inverted triangle shaped structure were stable under gravity load, though when an earthquake occurs, they quake strongly even do not collapse. The artist brought such a design of art moving three-dimensionally to Japan, land of earthquakes, without knowing how huge earthquakes may occur in Japan. But in this way, the artwork was realized. In the event of



Figure 1: Elia Zenghelis's Folly for EXPO'90 #11



Figure 2: Morphosis' Folly for EXPO'90 #8

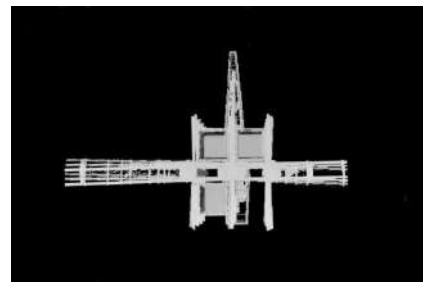


Figure 3: Sway in the Wind Folly #8

earthquakes, thin tie down belts of steel cables on both sides and inverted triangle truss, which was dynamically stable, worked together, as hybrid, to save the folly from collapse. This folly was approx. 10m x 10m.

Mycal Sanda Pororoca, designed with concept of pororoca (huge backward tidal bore), is another example. (Figure 4) Its 2 sloping roofs of 30m x 100m consist of 4,000 glass pieces, but none of the pieces was broken when The Great Hanshin earthquake occurred on January 17, 1995. We designed 3-D structure along with the sloping roofs using basic units of 3-pin structure, which is stable under gravity load but when earthquake occurs the joint solely deforms significantly. (Figure 5) Also, steel pipes of \varnothing -250mm for sloping beams and bottom chords of originally shaped steel rods, which resist tensile stress effectively, were applied. Although these parts are made of steel, they have characteristics to deform flexibly under enormous load due to earthquake or typhoon. In other words, even the example projects above are made of rigid steel, when enormous load by the nature such as earthquake or typhoon is applied, their structure turns around and change their shapes as if soft materials, and once the earthquake or typhoon is over, they return to original position. Concerning materials used for art and its framework, it is material that creates new architectural structure if we find out potential of material and volume of load through listening carefully to invisible voice of material about what form the material wishes to be.



Figure 4: Mycal Sanda Pororoca

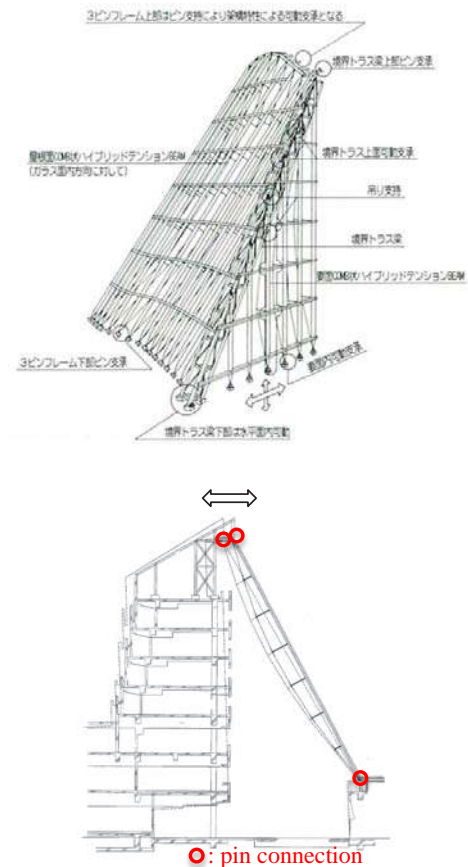


Figure 5: Basic Units of 3-Pin Structure

3. Kenneth Snelson’s “Nature of Structure,” Closest to Animal Skeleton, Art of Wine Bottles, and Prism of Light

A lot of architects and structural engineers have been enchanted by Kenneth Snelson’s Nature of Structure. As its structure has wide variety of potential, diversified designs and technical challenges have been made. Since this Kenneth's invention has been named as “Tensegrity” by Richard Buckminster Fuller, it became known in the field of science and technology. Then it has been analyzed and classified by engineers and scientists over the world. Even though the structural design of Nature of Structure was originally expected to be enjoyed naturally and freely, today degree of freedom to design it seems less than before. This is because Nature of Structure has been classified as Tensegrity - 4 by scientists. I would rather, if I dare to classify it as Tensegrity Structure, Tensegrity – 0. Through structural design for Kenneth’s installation Dragon in Osaka in May 2001, he told me there were 4 aspects to understand materials in its designing concept; muscle, bone, joint, and skin to cover the other invisible factors. Physically, muscle deals with tensile stress, bone with compression stress, joint with stress processed by tensile and compression stress and also it keeps the balance between them. If stress over capacity of the joint is applied, it will be diagnosed with bone fracture. (Figure 6, 7, 8) Thus, for structure of Nature of Structure, Kenneth had animals and plants in the natural world in his mind. As shown on Figure 9, even it is neither an animal or a plant, it floats above a lake. (Figure 9) Nature of Structure draws us in the majestic nature. Needle Tower looks like a tower extended straight to the sky. (Figure 10) Works such as Easy-K are large



Figure 6: Fractured Dragon

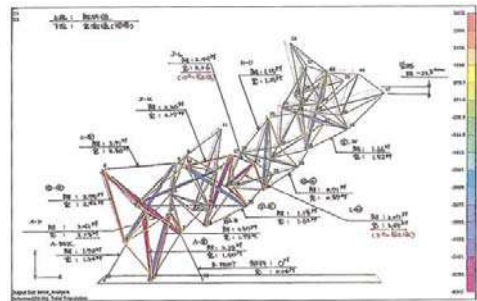


Figure 7: Analytical Result of Dragon



Figure 8: Completed Dragon



Figure 9: Rainbow Arch

cantilever jutting out above lake or pond. (Figure 11) Dragon, which I worked with, is rising up from a lake to heaven. (Figure 12) These examples show the theme of Nature of Structure is nature in a broad sense.

Natural world is greatly affected by gravity, earthquake, typhoon, heavy snowfall and rainfall, etc. Fundamental factors of relationship between such power of nature and Nature of Structure is can be represented by 3 points as below.

1. Despite pin-joint, it is stable under gravity. changes its shape but does not collapse.
3. Detail of joint determines life-span of material and structure.

Nature of Structure has numerous design possibilities and we applied it to realize structural designs for following projects. (Video A)

1. Prism of Light (Figure 13)
2. Recycle Art Pavilion by Jae-eun Choi for The Daejeon International Expo (Figure 14)
3. Foundation for Ambulance Service Development Tokyo Training Facility Gymnasium (Figure 15)

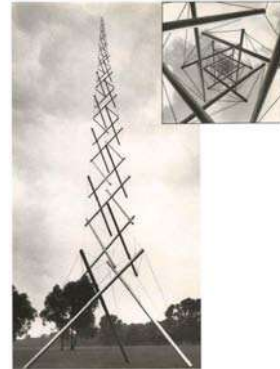


Figure 11: Easy-K

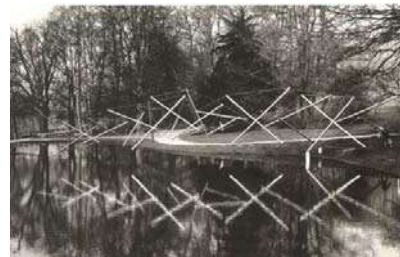


Figure 12: Dragon Rising up from Lake to Heaven



Figure 13: Prism of Light



Figure 14: Recycle Art Pavilion



Figure 15: Emergency Training Center Gymnasium Tokyo

4. Soft But Firmly Hand Crocheted Huge Net for 80 Children

Curved surface of 20m × 25m net made of thin 6mm-in-diameter nylon rope, crocheted into hexagon grids, can support 80 children playing on it. (Figure 16) Just like Nature of Structure, this 3-D structure performances as stable under gravity with deadweight. Once children begin to play with balls hung from top and bottom of the net, the surface starts swinging stronger than earthquake in more complicated ways. The curved surface is controlled by tensile stress and swings unpredictably. Forgetting about time, children enjoy the artwork being synchronized or swung by others. For this art work, 2 types of grid design are used. One is suspension net called “air pocket” formed with hexagon grids where each side is 2.5cm. (Figure 17,23) The other is called as “space net,” HP (hyperbolic paraboloid) net made of square grids of 3.5cm x 3.5cm. (Figure 18,24) This type of playground equipment installation is used in 15 countries today; in Asia, Canada, United States, and Europe. (Figure 19) Children can enjoy hanging, climbing, crawling, sliding, rolling, bouncing, swinging, swaying, balancing, jumping, and combination of them on these nets. (Video B) In structural mechanics, nonlinear analysis is used for structural analysis program and load case includes deadweight and uneven load. (Figure 21, 22)



Figure 16: 80 Children Playing on Net



Figure 17: Air Pocket



Figure 18: Space Net

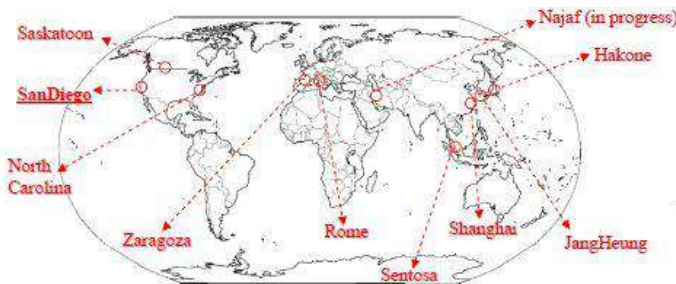


Figure 20: Origin of Horiuchi's Net Art

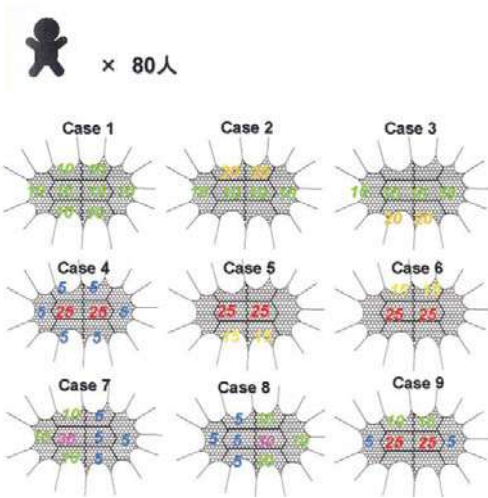
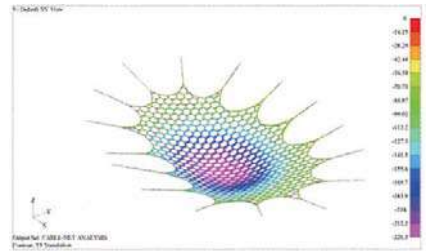
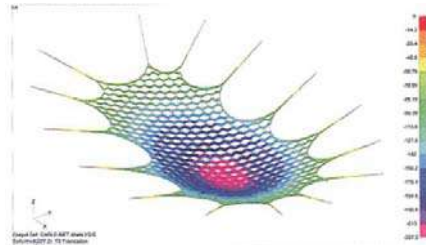


Figure 21: Load Case



Case1



Case8

Figure 22: Nonlinear Analysis



Figure 23: Detail of Air Pocket



Figure 24: Detail of Space Net

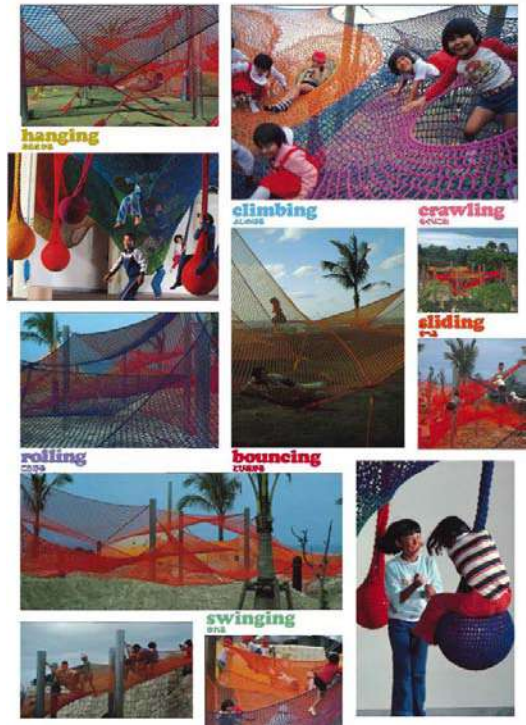


Figure 25: Detail of Space Net

5. CO2 emission efficiency and Materials

Material Speaks Design, below is the function I use.

Structural Energy of Material and Space Function :

$$E_{SS} = \sum_{n=1}^n mEn \text{ [kJ/m}^2\text{]} \times mVn \text{ [m}^3\text{]}$$

E_{SS} : structural energy of material and space [kJ/m²] E : Young' s modulus of material [kJ/m²], m : material,
 V : quantity of used material (volume) [m³], n : number of kinds of used material

(1)

This Structural Energy of Material and Space Function makes possible to compare efficiency of framework in space, and moreover, CO2 emission efficiency until completion of the building beyond material, space, time and place. This means we can compare The Eiffel Tower made of cast-iron and wrought iron, burnt down The Crystal Palace of cast-iron, wrought iron, glass and wood, Villa Savoye of concrete, and "Silver Pavilion" Ginkakuji Temple of wood, located in different parts of the world. Another example, when planing Villa Savoye, originally built in suburban Paris with few earthquakes, in a country with frequent earthquakes, reaction of framework in space and material efficiency can be compared. This new fansion depend on $E=mc^2$. This method is based on the 2,500 projects I realized in 25 countries in 50 years.

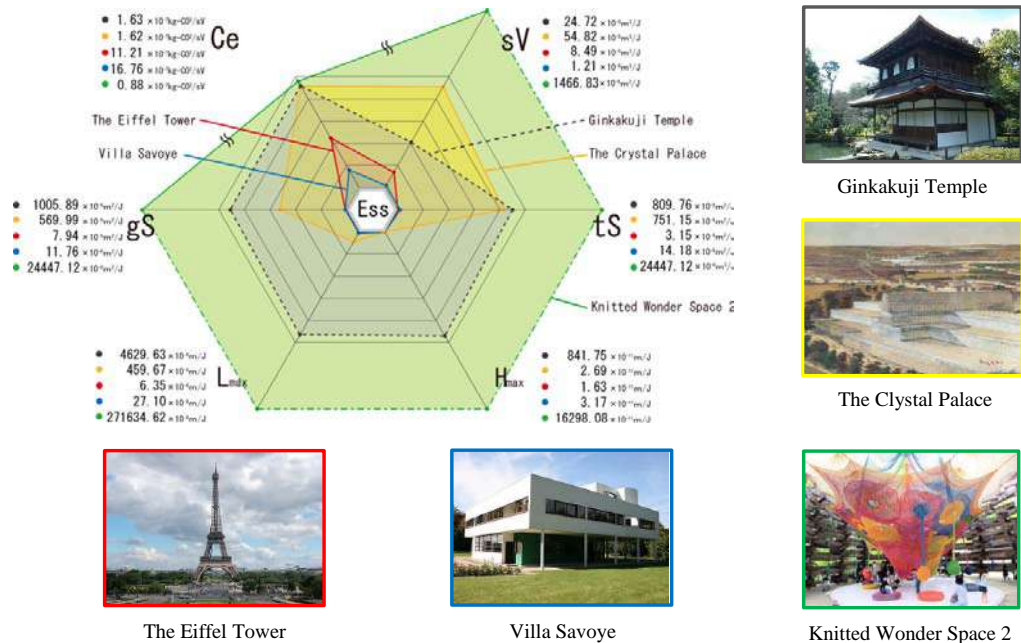


Figure 26: Structural Energy of Material and Space Function Makes Possible to Compare Efficiency of Framework in Space, and CO2 Emission Efficiency

Proceedings of the TensiNet Symposium 2019

Softening the habitats / 3-5 June 2019, Politecnico di Milano, Milan, Italy
Alessandra Zanelli, Carol Monticelli, Marijke Mollaert, Bernd Stimpfle (Eds.)

Softening the environments: Is there anything like an environmentally compatible membrane?

Katja BERNERT*

*Architect, Low & Bonar GmbH
Rheinstr. 11, 41836 Hueckelhoven, Germany
katja.bernert@lowandbonar.com

Abstract

Thoughts about environmentally friendly materials focus on recyclability if not compostability. Opinions about Polyvinylchloride as one of the main components of architectural membranes reflect the opposite of what is commonly described as environmentally friendly. It is the industry's responsibility to explain the compatibility of the composite membrane material and environmental concerns.

Most evident are of course the savings in tons of material - when it comes to a comparison between a fabric and a stone cover for example. Secondly there is the durability of today's membranes that is more and more competitive with other established materials. As these two aspects were previously discussed extensively, this paper will focus on the membranes' other environmentally compatible properties. There are two lines of argument: on the one hand membrane constructions as softening our built environment by their shape and by their soft skills. On the other hand there is the membranes' advantage of adaptivity.

Fabric façades for example are much more than just a textile wrap for a building. The soft forms of a membrane façade are acoustically effective in the cities' micro climate. Additionally they can easily adapt to the user's changing needs. The fabrics' adaptivity is facilitated if the textile has smart properties. Within tensile architecture smartness is only

DOI: 10.30448/ts2019.3245.21

Copyright © 2019 Katja Bernert. Published by Maggioli SpA with License Creative Commons CC BY-NC-ND 4.0 with permission.

Peer-review under responsibility of the TensiNet Association

evolving now: at the end of this development the fabric mesh will be the matrix for all sorts of applications – ranging from leading electricity to supplying lighting as in a vast LED screen. Along with the fabric's inherent soft skills, its growing smartness will facilitate its role in softening our environment.

Keywords: softening, environment, vinyl coating, lightweight structures, sustainability, smartness, textile facades, adaptivity, compatibility

1. Introduction

The technical textiles industry has been repeating two answers when it came to the sustainability question: Yes, the products are environmentally compatible because they are fully recyclable. And: Yes, using an extremely light material makes fabrics sustainable right from the start. The latter is old hat; the former is not true anymore for the European recycling site was closed in summer 2018 due to the lack of recycling orders.

In order to reassure the textile industry's sincerity of still be taking part in the sustainability debate, it has to find new lines of arguments. There is more to technical textiles than their lightness and (now mere theoretical) recyclability. The membrane's soft skills have to take over.

2. Sustainability thoughts up till now

Most likely most architects and planners are fed up with the sustainability debate by now. The longer it has been going on the more its actual content was depraved. Whereas certifications as BREEAM or LEED were initially meant to testify on the buildings green properties they are now more and more degraded to a mere financial issue – mislead by investment companies that focus on the value for money of environmentally compatible materials or ways of building. The same is true for the material suppliers. There are whole industries lobbying on materials like Polyvinylchloride, pushing forward its ecological value.

2.1. Material savings

“The best material is the one that you don't need to use.” Knut Göppert's introductory words in his talk about material savings in membrane structures are of course still valid¹.

2.1.1. Reducing tons – reducing costs

It is obvious that fabrics are apt to wrap buildings at a fraction of the material need for other aesthetical enclosures as stone or aluminium façades. This applies to the sub construction, too,

which is obviously even more important when it comes to roof structures. It is most evident that a spoked wheel construction for a stadium roof is so much lighter than a concrete cover.

The textile industry should not dwell on these evident facts. All players in the market should be striving for new lines of reasoning for the softening of our habitats.

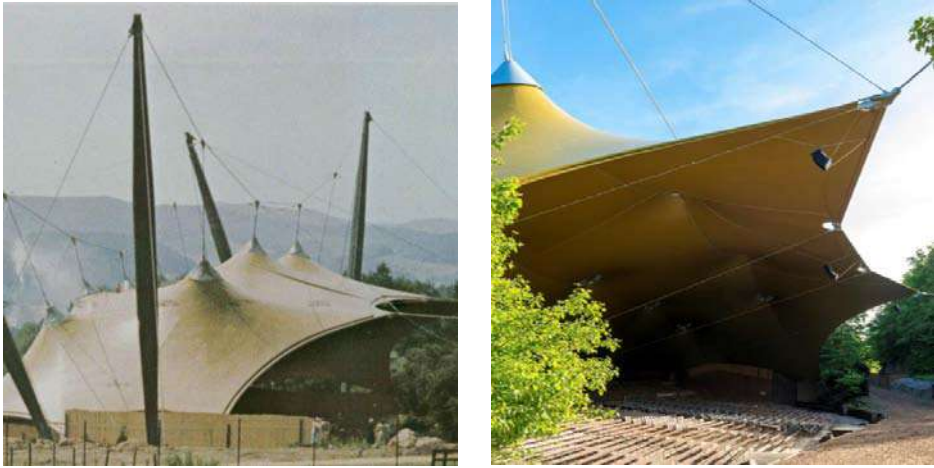
2.1.2. Reusing – recycling

The sustainability debate about fabrics has been mainly dominated by elaborate documentations about the possibility of recycling. It was shown and communicated again and again that principally the PVC-coating can be separated from the Polyester base fabric, that both materials can re-enter a new cycle similar to raw material. About ten years ago even the Glass/PTFE fabric industry showed scientific research programs that enabled the separation from the compound of glass fibres and PTFE coating. The latter never really left the laboratory stage. More frustrating is the outcome of the former: diverse prefixes like vinyl- or texy- were communicated for loop-programs meant to fill a factory in Ferrare, Italy, that was built only for the purpose to separate the two raw materials PES and PVC. Elaborate life cycle assessments made the fabric industry believe that it was worthwhile collecting the used material and bring it all the way to the factory. Unfortunately we now know that these loop-programs failed – at least on the European level².

This is obviously rubbing salt into the sustainability wound of the tensile architecture industry. On the one hand the reason for this failure might have been the business model of the factory itself, not being able to charge adequate prices for all players within the coating industry – no matter which prefix to the loop. On the other hand it very often was a customer decision. When for example fabrics were used as a replacement for older textile wraps, the thermal recycling was most often the customer's choice. The fact that there's a lot of energy in raw oil based material like PVC is only whitewashing the fact that the industry did not succeed in pushing the true recycling program forward.

2.2. Durability

The durability of PVC/Polyester fabrics – for example with Nano topping – now comes close to that of glass/PTFE membranes. Even in the 1970's – in the pre Nano age – the fabric was already extremely durable. This was shown for example in the Elspe paper that was presented at the Tensinet Symposium in Newcastle 2016³.



Figures 1 and 2: Elspe, Grandstand Canopy, Figure 1 shows the original project from 1978 © Mehler Technologies, figure 2 shows the replacement from 2015 © Koch Membranen

The grandstand canopy was originally covered in 1978 with a Type V Mehler membrane. It was thoroughly surveyed – mostly within the last 10 years of its design life. It turned out that the loss of tensile strength was only about 20%. Given these values and the ample safety factors used in tensile architecture, the structure was obviously not in danger of falling down. Nonetheless the client opted for a new roof with Mehler Type V fabric – new lacquer techniques now promise a similarly positive performance of the colour.

Table 1: material residual mechanical values compared with the initial properties

Year 1979	▶	198 kN/m = 9935N/5cm	} Results extract of 30 years periodical tests on yearly base
Year 1989	▶	173 kN/m	
Year 2000	▶	168 kN/m	
Year 2005	▶	197 kN/m	
Year 2007	▶	184 kN/m = 9450 N/5cm	

In the past the PVC/PES players within the tensile architecture range tended to compare themselves with the still more durable glass/PTFE fabric version. Whereas the Vinyl-Industry has been struggling to improve their recipes – not only in terms of REACH compliance – but at the same time in terms of longer durabilities, the glass/PTFE coaters have been relaxing on their quality advantages. The gap within the main two options shrinks: that is to say new benchmarks turn up to be compared to.

2.2.1 Catching up with the big five

The textile industry is now more and more facing the comparison to the big five of building materials: bricks, steel, concrete, glass and timber which have been used for hundreds and

thousands of years. The textile industry's narrative about ancient fabric structures like Bedouin tents or tipis belie the fact that the fabrics which used to be part of the Roman coliseum are no longer in place – as opposed to the stone bricks.

This is yet another reason to look for alternative membrane skills that are apt to show its environmental capability. There is definitely more to environmental compatibility than the hitherto discussed topics of recyclability and durability.

3. Environmental compatibility by soft skills

It is amazing what sorts of positive aspects are mounted when seen through the eyes of the PVC industry. Association like Plastics Europe or the German AGPU frequently publish news on the enormous environmental compatibility of vinyl floors, tubes etc.⁴ Clear enough that political lobbying and re-labelling PVC as Vinyl is still not able to brainwash the architects' minds when it comes to the choice between a Polyvinylchloride coated Polyester Fabric and an organically degradable cotton cloth. Yet there are distinctively soft skills that need to be pushed forward – along with a continuous guidance about the positive properties of PVC et al. in membranes.

3.1. Softening the environment

Which material seems more appropriate to soften our habitats: concrete or fabrics?

Within the trend of parametric architecture buildings tend to be softer than in the technologically dominated style of the 1990s for example. Houses that react sensitively to their environment tend to be softer within their surroundings. Nonetheless we still see lots of glass and steel in these buildings. Whereas their forms pretend tenderness close to fabrics their conventional execution betrays their designer's parametric design approach.

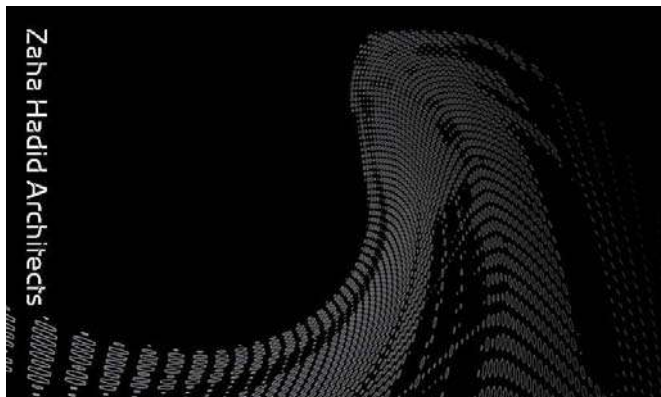


Figure 3: Exhibition poster on Zaha Hadid and Patrick Schumacher's parametric design

The list of the membrane's soft skills can be easily prolonged: a tensile wrap softens the impact of wind for example. With a fabric mesh in front of the glass façade the people in the office spaces are still able to open their windows individually. Another example is the radiation of the sun. Giving shade is a commonly used soft skill of fabrics.



Figure 4: office building in Ecuador with a textile wrap, TF 400

The constant sun shading by the fabric façade is obviously beneficial for the Indoor Environmental Quality (IEQ)⁵. As these softening effects are widely known and often applied the following two examples will put the light on functionalities which are less obvious.

3.1.1. Filtering effects

The membrane's ability to enhance the air's quality is often described as the autocatalytic effect. Indeed special coatings can filter and capture the dirt within the polluted air. With the help of the sun's radiation there is an improvement of the air quality in the textile structure's direct environment. Naturally this effect is biggest near to the fabric. It cannot solve the pollution problems of a whole city. Nonetheless this technique makes sense for example near transportation hubs where pollution caused by vehicles is particularly high. A team of the university in Aachen came forward with proposals in that direction for the local bus station. The situation of that building has been discussed within the city for a long time already. The team of the department of building technology at the architecture faculty developed a scheme to soften the station's environment: covering the run down façade with a fabric mesh that is not only delivering optical improvements but has the ability to improve the air quality with a special coating⁶.



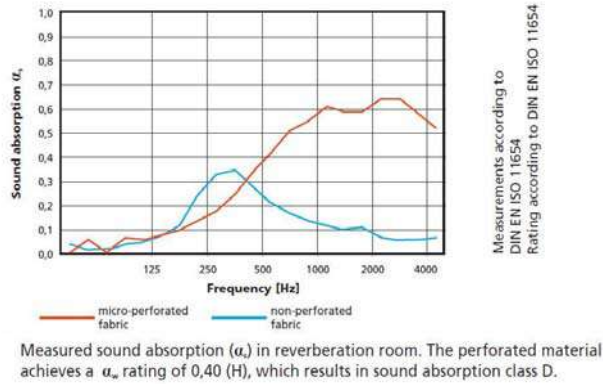
Figures 5 and 6: The main bus terminal in Aachen, as it is (on the left) and as a soft skin could alter it (on the right), computer simulation by Aachen university

There still needs to be more research and development in this direction. Of course it is difficult to measure the actual improvement of air quality. If there were decent numbers and figures that would help enormously to strengthen the fabric's image within the city councils. Just comparing the fabrics' function with the service of a number of trees won't convince decision takers – let alone the investors who need to put these vague numbers into a Green Building certification for example.

3.1.2. Acoustical effects

The transportation hub clad by fabric meshes is exemplary for another of the fabric's soft skills. It is more than obvious that textiles help a lot in the general acoustical comfort. Our comfort zones at home for example are full of textiles. Moreover office spaces can't provide for workable desk zones without implementing perforated textiles for acoustical absorption.

Table 2: exemplary acoustical absorption by a perforated PVC/Polyester membrane



There has been elaborate testing as to the acoustical effects of textiles in inner spaces. Acoustical comfort in the outside environment gets more and more important, too. Here, the absorption effects which have been tested for stadia spaces can be transferred to urban environments. At the moment there is a lot of steel and glass in our city’s central business districts. The future is bright – and much more silent! – if these hard surfaces were more and more covered by acoustically effective fabrics or textile meshes. Replacing Diesel motors by electrical cars will add to this positive effect of silence in our cities

3.2. Smart skins

Up till now fabric façades play a minor role in urban street views. Their functionality is hence limited to providing for a cover of other –probably less presentable- building skins. The building’s climatic wrap is conventionally done with the five main building materials: bricks, concrete, glass, wood or metal. The fabrics’ part in actually shaping the city is still very small.

As smartness and adaptivity are now becoming more and more important for building wraps textiles will eventually play their joker: as opposed to brittle building materials fabric façades have the enormous advantage of being perfectly equipped for adopting this challenge. Developments in this direction are done on a push and pull basis. On the one hand it is the input of architects and designers that strive for innovative solutions for their building skins and hence pull the industry. On the other hand it is the industry itself which pushes the material development forward in order to provide for solutions that are easily applicable by the market.

3.2.1 Smartness by technical features

Smart phones are omnipresent in today’s life. According to the phone analogy smart is everything that facilitates processes. Our smart phones enable actions that used to take a lot of

time – only a couple of years ago. Taken into the material world, smartness hence means that a smart material is able to solve complex specifications at one glance and in one form. That is to say that smartness in material science has a spatial and a temporal notion.

We already live in smart homes that link all our smart devices with the smart materials – enabled by our smart ideas. Following this line, smartness in material science means providing for multifunctionality. Smart wraps are hence building skins that are not mere climatic façades but provide for many other functions at the same time.

One step in the direction of including various technical features within a membrane is the pocket membrane Valmex Systems. On a still analogue level it is meant to give an answer to the users' different needs for including for example lighting or heating elements. The fabric provides for linear pockets in warp or weft direction which can be filled with all sorts of technical features. In this way it is the analogue matrix which is the first step in providing for a digital net that makes the filling process obsolete. The fabric itself would be the matrix, including all technical features in its structure – like the circuit board of a computer.

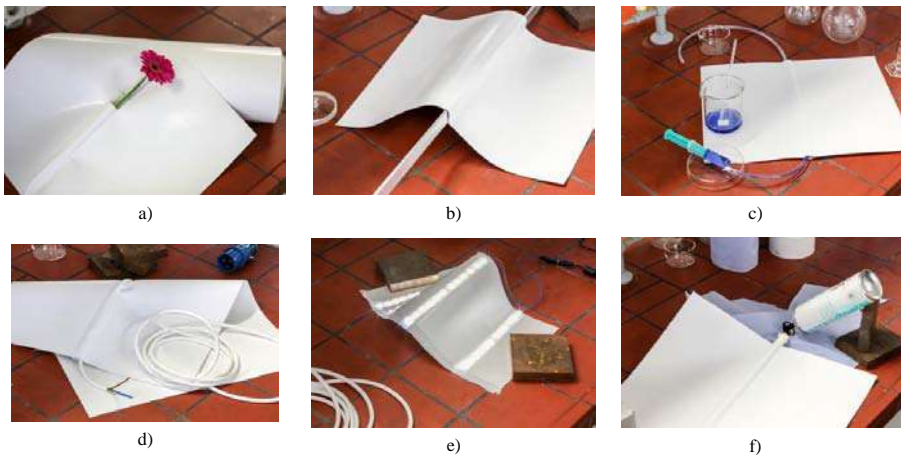


Fig. 7 a), b), c), d), e) and f) pictures of possible technical features within a membrane

3.2.2. *Smartness by adaptivity*

Along with the technical features that today's materials have to provide for there is an additional need for adaptivity. We want to have the above described smartness by technology. Because the users will change along with the building, along with the climatic conditions, along with environmental inputs, these technological features have to be adaptable - making it fit for the contemporary occupant. Almost all building types need to provide for a maximum

of adaptivity when it comes to their ground floor flexibility. Hence they need to be wrapped into a façade with a maximum of adaptivity – reflecting on the inner flexibility.

The easiest way of adapting to a user's new needs is still by replacing one building by the other. This is of course the most extreme adoption – more often it seems to be enough to replace one cover by another. When it comes to replacing building wraps or wrapping-up a building that did not have but the mere thermal skin, textile facades can play their soft card easily. It might be said that on optical change is more an eye catching gimmick than a serious skill. When seen in the context of fast fashion and fast food it is just another fast adopting aspects of a trend which affects the whole society. It is the industry's responsibility to explain that the membrane's skill of quickly adopting to new needs is still compatible with environmental concerns. Smartness in this context is the membrane's skill to adapt easily to new needs.



Figure 8: textile mesh façade for a one family house , printed TF400

About 15 years ago, distinction in textile façades meant for example XXL prints. This was the easiest means to adapt to the user's individual needs and tastes. Obviously that was to do with extravagance rather than adaptivity. Actual smartness by adaptability is only evolving now: at the end of this development the fabric mesh will be the fast adapting matrix for all sorts of applications – ranging from leading electricity through its veins to supplying lighting as in a vast LED screen.

4. Conclusion: environmental compatibility

Whereas the sustainability discourse was dominated by thoughts on material savings and the durability of the material there is now a need to broaden the view on other aspects. There are many more properties in fabrics which are apt to soften the environment. One of them lies in the fabric's flexibility itself. Soft shapes will alter our cities' environment. Up till now technological leadership was primarily expressed by high-tech steel and glass façades. Soft skins will be part of a new corporate identity that focusses on the soft skills of its inner parts.

Another of the membranes' soft skills is its adaptability. A fabric skin is able to adapt to the changing needs of altering users. We see various approaches of adaptable fabrics. The analogous matrix called "Valmex Systems" for example is a first step towards smart adaptivity. Future fabrics must be open for all sorts of applications, not limited in flexibility nor properties.

The necessary invention work will be done by experts in all different fields. It will often be triggered by a project-wise approach. At the same time, there will be scientific research programs. At best these two strands will join-up within the development process.

Cooperation between the above described parties and the ones interested in innovative materials – that is to say architects and designers, respectively their customers - will be vital for bringing the idea of sustainability in fabrics forward.

References

[1] Dipl.-Ing. Knut Göppert, Schlaich Bergermann und Partner, in his presentation at the CIMNE Membranes conference in Barcelona, October 2015

[2] ACTUS-0-53943-sefer-280618-communique-de-presse, press release June 28th 2018

[3] International Symposium on "Novel Structural Skins: Improving sustainability and efficiency through new structural textile materials and designs", Elspe Grand Stand Canopy: Mehler replaces Mehler after 37 years, Dipl.-Ing. Katja Bernert

[4] <https://www.agpu.de/en/all-about-pvc/recycling>, accessed September 2018

[5] according to the US American recommendation of the "Sustainable Facilities Tool", online document, published by the National Institute of Building Science within the "Whole building design guide", <https://www.wbdg.org/>, accessed 6 August 2018

[6] this topic is discussed in detail by Jan Serode, M.Sc. Architect, RWTH Aachen, and his team's research on the environmental skills of fabric façades: <http://www.ita.rwth-aachen.de/cms/ITA/Die-Organisationseinheit/Aktuelle-Meldungen/~reqe/Aachener-Textilfassade-verringert-Sticko/>, accessed September 2018, and on the same topic: <https://www.medlife-ev.de/de/aachener-forscher-stellen-klimafreundliche-textilfassade-green-facade-vor/>, accessed September 2018

Krüger, S. (2009), Textile Architecture: Textile Architektur

Figures and Tables

Figures 1 and 2: Elspe, Grandstand Canopy, Figure 1 shows the original project from 1978 © Mehler Technologies, figure 2 © Koch Membranen

Table 1: Elspe Grand Stand Canopy, Tensinet Symposium 2016, Dipl.-Ing. Katja Bernert

Table 2: taken from Valmex © Silesco flyer, Mehler Technologies

Figure 3: <https://www.flickr.com/photos/eager/6811021943>, accessed September 2018

Figure 4: © Preysi, Quito

Figures 5 and 6: © Institut für Textiltechnik (ITA)

Figure 7: Valmex Systems © Mehler Technologies

Figure 8: © Niggemeyer Bildproduktion

Proceedings of the TensiNet Symposium 2019

Softening the habitats / 3-5 June 2019, Politecnico di Milano, Milan, Italy

Alessandra Zanelli, Carol Monticelli, Marijke Mollaert, Bernd Stimpfle (Eds.)

Eco-design principles for a preliminary eco-efficiency assessment in the design phase: application on membrane envelopes

Carol Monticelli*, Alessandra Zanelli^a

* Politecnico di Milano, Dept. of Architecture, Built Environment and Construction Engineering, Milan 20133, Italy, carol.monticelli@polimi.it

^a Politecnico di Milano, Dept. of Architecture, Built Environment and Construction Engineering, Milan 20133, Italy

Abstract

Stating the necessity of increasing the designers' awareness of both lightweight and flexible materials and their performances, in a life cycle thinking perspective, this contribute is based on the updated identified needs of the membrane sector (Cost Action TU1303, 2017): Life Cycle Assessment, durability aspects, recyclability, social acceptability, thermal, optical, acoustic comforts. Into the frame of the Tensinet association activity, the Textile Architecture Network of Politecnico di Milano is continuing the search of Eco-design strategies and enlarging the mapping of case studies, by the application *ex-post* of two eco-efficiency principles in order to verify their validness and their efficacy for the designer's need, during the design process of a membrane system. The main advancement of this work is here presented adding new membranes case studies to the initial analysis. The aim is to verify the applicability of the principles to a wider and different uses of membranes and the identification of reference rates. The results demonstrate relations between the rate of the eco-efficiency, the year of construction and the evolution of the technology and the importance to take into account in the design phases the environmental impact of membrane structures.

Keywords: Sustainability and comfort, membrane architecture, eco-efficiency principles, ETFE envelope, case studies.

DOI: 10.30448/ts2019.3245.41

Copyright © 2019 by C. Monticelli e A. Zanelli. Published by Maggioli SpA with License Creative Commons CC BY-NC-ND 4.0 with permission.

Peer-review under responsibility of the TensiNet Association

1. Introduction

Currently the construction industry has a considerable impact on the sustainability of the society, and consumes a substantial amount of raw materials (Vivian, Khoa, 2019; EU, 2018). The environmental effects of the construction of a building are dependent on the choice, of materials and construction techniques, made in the design process. It is therefore necessary to opt for solutions suited to the expected performances, with the lowest environmental impact. The material search in architecture is going toward the lightness, with the optimization of the shape and the exploitation of the potentials of new building materials. The search for lightness is research into materials. Research into lightweight materials is all about reducing the thickness, the section and the quantity of materials in a construction. When evaluating the energy performance of a membrane closure, more often employed in permanent buildings, immediate reference is to the requirements of thermal insulation, thermal inertia, solar control, ventilation: the higher the performance, the lower the use of mechanical systems to ensure an optimal microclimate and, consequently, greater energy savings. In addition to these aspects, it is essential to demonstrate also how the design and shape affect the performance of the envelope, in order to improve its eco-efficiency. Light in the shape configuration or lightweight and, therefore, a reduced impact? Some interesting solutions seem to be considered innovative and eco-efficient because of their lightness like the membrane structure: but this alleged correlation does not mean that lighter is more sustainable, even when compared to heavier and more massive solutions. The quality and eco-efficiency of a membrane building are not linearly dependent on the environmental profile of the individual material. Consideration must be given to other factors such as the amount of needed material for one technical solution over another (which is not proportional to the surface of the building, but to the density and thickness of the material involved), the design of the envelope and its parts and structural fixing system.

2. Aim of the study - Eco-design principles for membrane buildings

Due to the current gap between studies and real practice in membrane architectural design, the research takes care of harmonizing the available eco-data for the membranes and proposing a first set of eco-design principles. A strong effort to overcome fragmentation and encourage the sharing of information and experiences between companies is underway thanks to TensiNet, a multidisciplinary association for those interested in building structures of members in tension. Into this activity, the Textile Architecture Network of Politecnico di Milano is continuing the search of Eco-design strategies for the membrane architecture (Monticelli et alii, 2017). The aim of this research is to validate the eco-efficiency principles and to insert them in the design guidelines for membranes to be used during the design process: a. the current stage is focusing on enlarging the mapping of case studies, by the application *ex-post* of two eco-efficiency principles, to verify their validness and their efficacy; b. the expected next step is their introduction in the best practices for membrane

design and their verification on the specific project during the design process of a membrane system.

These eco-efficiency principles aim to be considered as a verification stage in the design process, quite similar as the bioclimatic principles that have to be considered to improve the well-being and energy efficiency of the buildings. They verify the design choices from the point of view of the environmental loads, in relation to the building shape, the correct exploitation of the potentials of the membranes as lightweight materials. They represent a preliminary assessment, for a consequent optimization, of the environmental performance (due to the quantities of involved materials), before and eventual specific Life Cycle Assessment.

Their verification helps to point out the advantages and disadvantages of membrane materials and the correct exploitation of their characteristics. The evaluation criteria mostly concern three relationships: *1st principle* - the comparison between the sum of the Perimeters of the membrane modules with respect to the Surface covered by the envelope solution; *2nd principle* - the comparison between the weight of the membrane and the weight of the fixing systems; *3rd principle* - the comparison between the supporting structure of the membrane and the mechanical load of the structure itself. These principles are applied on membrane structures, roofs and facades.

First principle [P / A] - this principle aims at evaluating the eco-efficiency of a surface, be it a roof or a facade, which has the task of covering or closing a space by highlighting the use of panels and sheets of which a membrane can be formed. When the value resulting from the ratio is very low and approaches zero, it means that the surface taken into consideration is composed of a single cushion or is composed of the fewest possible panels and therefore the frame perimeter that supports the fabric is the minimum essential. This corresponds to a reduction in the structural material used for the fastening system and consequently, a reduction in environmental impacts (the concept of doing more with less).

Second principle [We / Ws] - the second principle aims at analyzing the Life Cycle impact of the membranes and the effectiveness of their choice and to do this it is necessary to verify the quantity and weight of the total elements that make up the casing, or the fastening system, and their real need in terms of structural loads and rigidity, and of the membrane system used as a real dividing element between inside and outside. The higher the value of the ratio is 1 and the closer it is to 1, the more it means that the weight of the fixing systems, which is usually very important with respect to the weight of the fabric, is reduced and optimized.

Third principle - verification of the structure relationship of the membrane / mechanical load of the structure: this principle considers steel and wood as materials mainly involved in membrane structures. Starting from this base, it optimizes the mechanical aspects and the structural behaviors and their form with a relation with respect to the quantity of used material.

3. Application on membrane case studies for the principles' validation

The core advancement of this work is here presented adding new membranes case studies to the collection started in 2017 (Monticelli et alii), in order to enlarge the application of the principles to a wider and different uses of membranes, and to comprehend possible relations between the rate of the eco-efficiency, the year of construction and the evolution of the technology. The previous study (2017) was focused on the application of the two first principles and on the comparison of the built envelope solutions with hypothetical comparisons made by glass or optimized membrane solution. In this study the application was conducted on different case studies, starting with the ex-post application of facades or roofs existing in ETFE. In this case specifically the objective is to evaluate the results obtained for the two principles among the different configurations and to understand which is the objective reference parameter, to compare the project eco-efficiency. This comparison allow to identify which configuration and technological solutions best optimize the use of light technologies and, consequently, reduce environmental impacts. The cases were chosen based on the different aesthetic configurations that were obtained during the design phase, to investigate how the shape can affect technology and then the impact on the environment. The choice was also determined by the level and quality of the information obtained from the project engineering and installation companies.

3.1. Case studies

The first two principles were verified and compared by selecting 13 buildings with ETFE casing, analyzing their formal and material characteristics. Buildings with an ETFE envelope were selected thanks to the necessary information, obtained sometimes more easily or for such cases desumed from the drawings. In some cases the ETFE systems are composed with roof, in others only for the facade and in some others both. Thus a total of 8 cases of coverings and 10 of facades were analyzed (fig. 1).

The Kapuzinerkarree in Aachen, Germany (2002) (an atrium roof on an existing building), the atrium of the Kingsdale School in Dulwich, London, United Kingdom (2004) (part of a new school), the Busbahnhof in Aarau, Swiss (2013) (an enormous cantilever roof, for the bus station with an organic curved shape), the two facades with the ETFE cushions of the Media Tic building in Barcelona, Spain (2009) are part of the calculation developed in the previous studies [4].

Eight additional buildings were added to the previous analysis.

The Sport Hall in Korce, Albania (2018), has a curved roof with three layers ETFE pneumatic cushions and two vertical facades.

The Auditorium 1919 – Sacmi, Imola, Italy (2017), is a tertiary building, of which two sides are built with three layers ETFE pneumatic facades.

The City Life shopping center in Milan, Italy (2015), has a big multicushion roof with three layers ETFE for covering the shopping mall.

The Actor Galaxy Apartments Complex in Sochi, Russia (2014), is a residential multi-storey and multi-owners building with a big multicushion roof with three layers ETFE for covering the internal common courtyard.

The Equipement Polyvalent Lille, France (2013), is a multipurpose cultural center with facades in large regular cushions with two backlit ETFE layers.

The Chemnitz Station, Germany (2012), is the main trains and buses station, renovated by a wrapped double layers ETFE facades.

The Schlosshof in the Dresden Schloss, Dresden, Germany (2008), during the reconstruction of the castle, has the roof of the small courtyard made with two layers rhomboidal ETFE cushions for covering the foyer of the castle museum.

The Unilever Headquarter in Hamburg, Germany (2009), has the second skin of the building built with a single layer ETFE tensioned facade system.

3.2. Methodology and calculation

The necessary details, namely the design drawings and the dimensions of the components, for the calculation of the first and the second principle, were provided by the designers and by the producers and installation companies of the membrane systems.

To calculate the first principle, the dimensions of the components of the considered roof or façade were taken into consideration: the perimeter of the cushions or panels, therefore the sum of the lengths of the profiles (both perimeter and intermediate between a cushion / panel and the other) and the surface area covered by the same layer of the cushions, which usually have slightly higher areas being inflated and curved.

For the second principle, the quantity of materials used is introduced: the weight, expressed in kilograms, of the ETFE membrane and the profiles of the fixing system is taken into consideration. These elements have been calculated for each case study.

The quantification of the dimensions (area and perimeter) is based on precise information provided by the designers and producers of the company taken into consideration. Some companies have provided us with drawings directly and in those cases the data have been calculated based on these drawings, adding the lengths of the profiles and calculating the areas in m². In building systems made up of many panels, the profiles were considered only once in the calculations, being shared between two panels. Also with regard to the data referring to weight, both of the membrane and of the fixing system (not supplied in most cases) an average density of the materials in question was considered, successively multiplied by the total volume. The density considered for ETFE films is 1700 Kg/m³, for aluminum profiles 2700 Kg/m³ and 7800 Kg/m³ for steel profiles. Generally, the results have, understandably, some margins of uncertainty, given some approximate estimate of the dimensions.

To obtain the values referring to the first principle, the perimeter has been divided by the overall area of the roofing material. For the second principle the ratio is obtained by dividing the weight of the roofing material with the weight of the fixing material.



Figure 1: The compared building envelope solutions and their dimensions.

Case study 1: Sport Hall, Xiamen (China) - Architects: OMA	Principle 1 (P1)	Principle 2 (P2)	Case study 8: Chemical Station (Germany) - Architects: Gherkan Ernst Architekten (GEO)	Principle 1 (P1)	Principle 2 (P2)						
E1-E100			E2-E100								
F (kg)	386.08	A (m ²)	304.00	F (kg)	176.06	A (m ²)	787.60	F (kg)	374.17	A (m ²)	1616.91
W (kg)	371.29	W (kg)	376.44	W (kg)	164.17	W (kg)	1616.91	W (kg)	374.17	W (kg)	1616.91
W (kg)	370.48			W (kg)	2148.95			W (kg)	2148.95		
E3-E100			E3-E100								
F (kg)	716.50	A (m ²)	374.00	F (kg)	538.00	A (m ²)	1730.00	F (kg)	594.00	A (m ²)	4116.30
W (kg)	401.40	W (kg)	3836.00	W (kg)	994.00	W (kg)	4116.30	W (kg)	994.00	W (kg)	4116.30
W (kg)	1370.00			W (kg)	2733.30			W (kg)	2733.30		
E2-E100			E9-E100								
F (kg)	88.76	A (m ²)	311.00	F (kg)	486.41	A (m ²)	1307.00	F (kg)	486.41	A (m ²)	13119.00
W (kg)	103.80	W (kg)	8300.00	W (kg)	729.31	W (kg)	13119.00	W (kg)	729.31	W (kg)	13119.00
W (kg)	1750.00			W (kg)	11364.31			W (kg)	11364.31		
E1-E100			E2-E100								
F (kg)	372.08	A (m ²)	389.00	F (kg)	1051.00	A (m ²)	2362.00	F (kg)	2007.00	A (m ²)	2114.50
W (kg)	1045.07	W (kg)	71401.00	W (kg)	2007.00	W (kg)	2114.50	W (kg)	2117.00		
W (kg)	27300.00			W (kg)	2117.00			W (kg)	2117.00		
E1-E100			E2-E100								
F (kg)	100.17	A (m ²)	369.00	F (kg)	316.00	A (m ²)	1360.00	F (kg)	316.00	A (m ²)	1360.00
W (kg)	100.11	W (kg)	1214.00	W (kg)	436.00	W (kg)	4360.00	W (kg)	436.00	W (kg)	4360.00
W (kg)	4110.17			W (kg)	4367.50			W (kg)	4367.50		
E1-E100			E1-E100								
F (kg)	231.07	A (m ²)	1000.00	F (kg)	576.00	A (m ²)	1000.00	F (kg)	576.00	A (m ²)	1000.00
W (kg)	791.17	W (kg)	1040.50	W (kg)	200.50	W (kg)	1170.50	W (kg)	200.50	W (kg)	1170.50
W (kg)	3790.07			W (kg)	1000.00			W (kg)	1000.00		
E1-E100			E1-E100								
F (kg)	177.67	A (m ²)	520.50	F (kg)	177.67	A (m ²)	520.50	F (kg)	177.67	A (m ²)	520.50
W (kg)	401.40	W (kg)	8423.00	W (kg)	401.40	W (kg)	8423.00	W (kg)	401.40	W (kg)	8423.00
W (kg)	7101.00			W (kg)	7101.00			W (kg)	7101.00		

Figure 2: Dimensions of the involved parts of the buildings and results of the 1st and 2nd Principles.

4. Results

A tendency of the evolution of the membrane technology, but at the same time a constraint between the best practice focused to the eco-efficiency and the independent design choices of the designers is gathered. The results obtained allow us to understand how the different configurations of the covers or facades presented start from design will linked to the shape, structural optimization and also to the experimentation of advanced solutions with ETFE pneumatic technology.

The quantification offers indications to understand how the geometry of a façade or have a roof, on which the quantity of material to be used depends, is decisive in influencing the environmental impacts. Moreover it allows understanding if the technology has also evolved over the years or if it is only the result of curious applications without a deep knowledge of the intrinsic possibilities of the membrane systems by the designers.

The graph in figure 3 shows the results divided by type of layer or cushion used and, in each group, listed in chronological order. In order to specify and explain the value derived from the principles, it seemed effective to analyse the case studies by categories:

- a. category 1 Regular facades: Equipment Polyvalent Lille (7) and the Chemnitz Station (8);
- b. category 2 Covers: which includes the coverage of the Korce Sports Center (1A), the Lilientalhaus (3), that of the City Life Shopping Center (4), the Actor Galaxy Complex Sochi (5), the coverage of the Busbahnhof in Aarau (6), the Schlosshof (9), the Kingsdale School (11) and the Kapuzinerkarree (12);
- c. category 3 Irregular facades: including the Sacmi Auditorium (2) and the facades of the Korce sports center (1B - 1C), the Media Tic (10) and Unilever (13).

Additionally the representation of the results follows a chronological order, to understand if research and development in the textile sector have evident improvements, notable during the last years.

As far as the first principle is concerned, it is preferable that the result is very low, closer to zero, or, with respect to the area covered, the perimeter of the cushion profiles is limited: therefore the wrapping solution has been optimized from the point of view maximum surfaces that can be covered with this technology. From an interpolation of data from these case studies and from the parametric analysis of Chilton (2013), it emerges that the value close to 0,7 is a limit above which the first principle is not positively satisfied.

Regarding the second principle, it is preferable that the value is greater, closer to one, since it means that the ratio of the weight between the membrane and fixing profiles is balanced and therefore that the weight of the profiles is not much higher than that one of the membrane. The nature of textile cladding layers suggests their application for a curtain wall, made of big panels instead of many small panels, exploiting all their potentials and especially enhancing the ratio “frame/covered area”, by avoiding the use of lightweight material with a high weight of the structure, which penalizes the environmental performance.

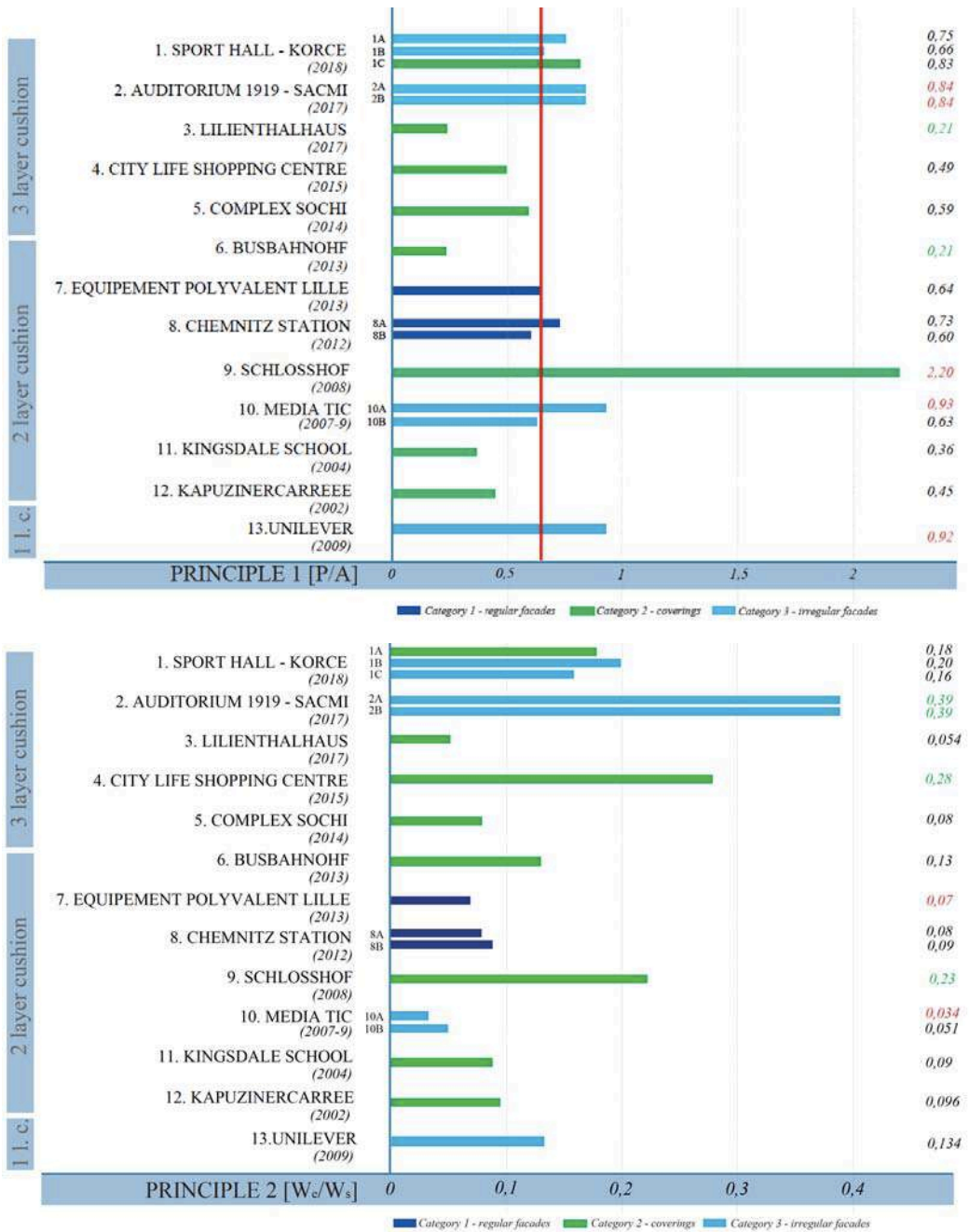


Figure 3: Dimensions of the involved p parts of the buildings and results of the 1st and 2nd Principles

It can be highlighted how, with regard to category 1 of the regular facades, the results are slightly different from each other, both for the first and for the second principle, with a

maximum value of $P/A = 0,73$ of the South facade of Chemnitz Station (8A) for the first principle, which means that, with respect to the West facade with a value of 0,60 and to the facade of the Polyvalent Lille Equipment equal to 0,64, the total profiles' length for the fixing system is greater in relation to the area covered.

For the second principle the obtained results are $W_e/W_s = 0,08, 0,09$ and $0,07$ respectively, values very similar to each other but still far from a balanced relationship between the weights of the materials used.

If the results of category 3 - irregular façades - with those of category 1 are compared, it emerges on average, that the values are higher for the first principle, meaning that the ratio of the surfaces to the area is less optimized. This could be due to the fact that the use of regularized geometries means less use of fixing profiles compared to the use of a more sophisticated design. In fact, a peak is of 0,94 for the facade A of Media Tic and 0,92 for Unilever, then 0,84 and 0,83 for the façades of the Sacmi Auditorium.

For the second principle the results are clearly different than in category 1 with a peak that reaches 0,39 for the Sacmi Auditorium, a higher value than the category 2 - coverings, which reached a maximum of 0,23 with the Schlosshof castle roof in Dresden. Also the facades of the Korce Sports Center show considerable results equal to 0,20 for the main North-West facade and 0,18 for the South-West facade. This means that, for category 3, the material used for the fixing profiles is closer to the weight of the membrane. The reason is due to the choice of the materials: the profiles for the Auditorium and for the Sports Center are made entirely of aluminium while those used for the Chemnitz Station have been used both aluminium and steel, which has a clearly higher density equal to 7800 Kg/m^3 compared to 2700 Kg/m^3 of aluminium. This is demonstrating how the impacts of the design choices has relapses on the eco-profile of the building.

Regarding category 3 - the roofs, the data obtained are quite different from each other. For the first principle the best result is for the case of Lilienthalhaus and the Aarau Busbahnhof, equal to 0,21, a value that is even better compared to categories 1 and 2. This intervention strategy leads to better results having only a huge cushion, the perimeter of the profile is much lower than another technology being present only in the perimeter part. It must be said, however, that this type of structure has disadvantages in terms of maintenance: if a cushion were to break in such a fragmented covering, it would be sufficient to replace only the one in question, whereas in the Lilienthalhaus and Busbahnhof the only solution would be to change the entire membrane. All this to the detriment of the coverage of the Korce Sports Center, which presents a poor result satisfactory equal to 0,83. This means that the area that is covered in Korce is almost the same as the perimeter of the fixing system and this is inconvenient as they could have used less material for the profiles and therefore not only had economic advantages, but also more precautions regarding the environmental impact.

The result for the covering of Schlosshof are higher overall and, for the first principle, they demonstrate, looking the geometry of the panels, the inefficacy thinking to a comparative

solution made by glass: the lightness of the covering material is not exploited to be optimal. But enlarging the evaluation to the second principle the ratio W_e/W_s has a valid result, and that is a good balance between the weight of the double layer envelope and the supporting structure. It has to be noticed here that the last one has the role also of the primary structure, without additional components.

For the second principle, City Life Shopping Center is the most optimized project in category 3 with a value of 0,28. Instead, the Actor Galaxy Complex Sochi has a fairly low result of 0,07. For the sports coverage in Korce the second principle is on average equal to 0,16, this means that it is more optimized in the weight ratio (principle 2) rather than in that of surfaces (principle 1).

As it is notable from the previous work which analysed the cases chosen not only as planned but assuming to replace the ETFE with glass to see the differences, the use of glass would have led to a greater imbalance for the second principle in that the weight of the glass would have been of great length greater than the weight of the fixing structure, bringing the values up to 9, 13 or even 22 (Monticelli et alii, 2017). The reading of the results indicates that lightweight technologies allow designers a high degree of freedom in shaping geometries and shapes, while only their optimization will ensure effective LCA sustainability results. This optimization process can be effectively achieved by a broad surface development (principle 1) and by a balanced ratio of the weight of the support structure in relation to the envelope (principle 2).

5. Conclusions and further developments

The improvement and application of this eco-efficiency analysis will be significant for optimizing the design of lightweight structures, from a technological, economic and environmental point of view, providing ideas and clear references available to designers and manufacturing companies. The three principles, developed from the interconnection between research and design and production and realization areas, require a deepening of the experts, to avoid a purely theoretical vision and analyse the validity of these three principles and their convenience, also in the practicality of installation and maintenance. Looking at the principles, in terms of eco-efficiency, these solutions are optimal but in the design phase it is necessary to consider different approaches to balance. The designer, for example, might prefer a single cushion for an aesthetic factor or for a visual matter, to allow the greatest amount of light to enter. However, the other phases of a building's life cycle have to be considered in the whole assessment. In fact, this solution could lead to risks during installation of a single cushion/panel, which should then be replaced entirely in case of damage. It is understandably more handily and safe to install a structure divided into many cushions, therefore with a global longer profile length, despite to the environmental impact. It is, therefore, appropriate to find the right balance between many factors, with respect to the context of the project.

Further steps of the research are oriented to investigate the third principle, which needs a more sophisticated tool to correlate the design of the structure, its optimization and the minimizing of the involved materials. The trend is going towards the elaboration of a parametric procedure to be easily interfaced with the changing choices during the design process, in order to immediately observe the results of the three principles, adding the possibility of a real time variations of materials and quantities for the optimization of the environmental impacts. In the construction sector one the recent trends is the integration of building information modelling with the life cycle assessment (LCA) and life cycle costing (LCC) (Santos et alii, 2019).

Acknowledgments

The authors would like to demonstrate their gratitude to the collaborators of the TAN group Mariangela Centrulli, Beatrice Pratobevera, Chiara Martinelli e Giulia Resmini, for their contribution in the selection of case studies and search of the needed information. The authors wish to acknowledge the support provided by Form TL, Maffei Engineering, Canobbio Engineering, Vector Foiltec, Taiyo Europe sharing drawings, quantities of the case studies.

References

- Chilton J., Pezeshkzadeh S. A. and Afrin S., *Embodied energy in ETFE foil construction*, in: H. Bogner-Balz, M. Mollaert, E. Pusat (ed) *[RE]THINKING Lightweight Structures*, Tensinet Symposium Proceedings 2013, pp. 457-466.
- COST ACTION TU1303 *Novel structural skins - Improving sustainability and efficiency through new structural textile materials and designs*, <http://www.novelstructuralskins.eu>, 2013 – 2017.
- Di Vivian Y. Tam, Khoa N. Le (2019), *Sustainable Construction Technologies: Life-Cycle Assessment*, Butterworth – Heinemann, Elsevier, Cambridge, USA.
- European Commission (2018), *Sustainable buildings* [cited February 2019], available from <http://s3platform.jrc.ec.europa.eu/sustainable-buildings>.
- Monticelli C., Zanelli A. (2016), Life Cycle Design and Efficiency Principles for Membrane Architecture: Towards a New Set of Eco-design Strategies. In: *Procedia Engineering*, vol. 155 (pp. 416-425).
- Monticelli C., Zanelli A. (2017), “Application and validation of eco-efficiency principles to assess the design of lightweight structures: case studies of ETFE building skins”, in: *Proceedings of the IASS Annual Symposium 2017 “Interfaces: architecture. engineering. science”*, International Association for Shell and Spatial Structures (IASS), 25-28 September, Hamburg, Germany, pp. 1-10.
- Santos R., Costa A. A., Silvestre D., Pyl L. (2019), Integration of LCA and LCC analysis within a BIM-based environment, in *Automation in Construction*, 103:127-149 DOI: 10.1016/j.autcon.2019.02.011

Proceedings of the TensiNet Symposium 2019

Softening the habitats / 3-5 June 2019, Politecnico di Milano, Milan, Italy
Alessandra Zanelli, Carol Monticelli, Marijke Mollaert, Bernd Stimpfle (Eds.)

Development and testing of a new glass fibre reinforced fluoropolymer membrane

Maxime DURKA*

*SIOEN industries, Fabriekstraat 23, 8850 Ardoonie, Belgium
Maxime.durka@sioen.com

Abstract

Coated textiles for permanent membrane structures rely on very few products, the predominant membranes are polyvinylchloride (PVC) coated and polytetrafluoroethylene (PTFE) coated fabrics. These products have been adopted by the market due to their versatility and price/performance ratio. PVC and PTFE are limited with regards to advanced properties that have been intensively developed in other construction materials in recent years.

A laminated membrane that consists of PVDF films reinforced with glass fibre mesh (called Fluoscrim™) was developed to explore additional solutions for permanent architectural membrane structures. This newly produced membrane has been tested according to membrane industry standard test methods and other internal test procedures to prove its potential as a permanent membrane for tensile architecture.

Keywords: membrane, tensile architecture, translucency, glass fibre mesh, fluoropolymers, development, testing, manufacturing.

DOI: 10.30448/ts2019.3245.27

Copyright © 2019 by Dr. M. Durka. Published by Maggioli SpA with License Creative Commons CC BY-NC-ND 4.0 with permission.

Peer-review under responsibility of the TensiNet Association

1. Introduction

The tensile architecture community have expressed enthusiasm over the decades for the dramatic architectural and engineered forms they developed since the pioneering work in the 50's.

Today there is still enthusiasm for the elegance of minimalistic forms and widespan fabric structures. These constructions are capable of softly enclosing large surface areas only by slender cables, mast supports and a membrane only a millimeter thick. Indeed, unique shapes are achievable with membranes; more importantly the ability to harness natural light creates a unique sense of well-being.

Key benefits of architectural membranes are now counterbalanced by accelerating demands for advanced building materials that combine improved environmental efficiency with flatter designs, which are not ideal for membrane structures. Furthermore, tensile architecture has been dominated by polyvinylchloride (PVC) coated fabrics, polytetrafluoroethylene (PTFE) coated fabrics and ethylene tetrafluoroethylene (ETFE) foils to develop permanent prestressed membrane structures.

In order to develop further, the membrane for tensile architecture is going through the transition of free form material to a system solution that must prove its efficiency and competitiveness in developing cutting edge performance and ecological building envelopes.

As technical textile innovators, we acknowledge that a material evolution is urgently needed. A proper evolution must be envisioned as a component of a system solution to rejuvenate the attractiveness of tensile architecture. On one hand we must deal with the limited market size and its specificities; and on the other, we can observe that the integration of advanced features in such highly customized, thin skin structures remain a challenge for the entire industry supply chain. As a result, the general lack of deep collaboration combined with limited economical impact should make one accept that we can mainly be innovators, benefiting from ideas and materials created for adjacent industries that have the budget and the means to invent new ones.

With the previous assessments taken into consideration, the goal of this work is to develop and evaluate the performance of a new kind of glass fibre reinforced fluoropolymer membrane for tensile architecture construction. This material represents a “range extender” combining a few advanced features that can be beneficial for this specialized industry.

2. Tensile architecture membranes for permanent buildings: preamble

To conduct the development of new membrane materials, we mapped first the accepted tensile architecture products. We can rapidly notice that the industry is mainly using PVC coated fabrics, PTFE coated fabrics and ETFE foils to develop permanent prestressed membrane structures.^[1,2]

Noteworthy, from the business point of view, one can notice that there is not always early and intensive collaboration within the protagonists of the project (from the owners, designers, engineers, material suppliers, installers and the service team responsible for the maintenance of the structure). Therefore, the introduction of a new material can be successfully foreseen only with intensive and trustworthy collaboration with all the project's partners not only in the preparation phase but also long after the material has been installed.

Today, a key challenge which must kept in mind is the overall environmental impact of developing a new object. To be proper stewards to the environment we need to assess, understand and reduce impact that this new item will have on the world around us. This mindset is rather new in the field, twenty years ago the environment was not the main concern for professionals. Today one can consider that by design, the object is not only faulty when it does not perform but also when its eco-efficiency is poor.

3. Material development

For this development we decided, after analyses and interviews of the tensile community, to investigate the development of a reinforced ETFE material in order to create a membrane material at the crossroads of PTFE coated membranes and ETFE foils.

Two similar products were appearing on the marketplace during the development of our first prototypes: PTFE and THV (terpolymer of Tetrafluoroethylene, Hexafluoropropylene and Vinylidene) films or foils sandwiching glass fibre meshes. There are very few groups to work on such similar product concepts.

Internally, a vast set of prototypes was executed from a broad range of building blocks and production techniques. They were characterized following an internal stage gate method:

- Material properties
- Material availability
- Prototype physical performances and aspect at lab scale
- Up-scalability & recyclability perspectives
- Validation of physical performance at production scale
- Product placement in the perspective of commercialization
- Advanced physical performance and final validation.

It is not the intention to explain in detail the different properties and iterations being made but highlighting some technical issues that were key during the development stage,

- a) Membrane ageing under artificial accelerated weathering tests
- b) Confectioning of the membrane materials using high frequency (HF) welding techniques
- c) Biaxial properties of the membrane

a) Membrane ageing under artificial accelerated weathering tests

The configuration of the equipment and this specific method for tested material is made to assess material's chemical stability through artificial weathering test.

Artificial weathering is aimed to reproduce natural weather conditions an architectural membrane will endure throughout its useful lifespan. Testing simulates the main degradation factors of temperature, UV, humidity and a combination of mentioned. Secondary degradation factors like microorganisms, pollution and corrosive gases were not the subject of these studies and we realize they can take a predominant role in some areas.

In QUV artificial weathering, the aim is to assess the coating stability against cycles of high temperature and high UVA exposure together with water condensation cycles.

The time the material is stressed and the temperature during ultraviolet (UV) and water stresses are the primary variables in natural weathering. The scope of this study is limited by defining weathering as degradation which occurs when a material is exposed to universal stresses of ultraviolet energy in sunlight, water as rain or dew, and temperature. It is recognized that there are other stresses from salt water, biological and air pollution. These weathering stresses that occur in some environments are not evaluated in this test method. Suggested limits and methods of operating the apparatus have been recently standardized and published in ASTM G-53-77: Recommended Practice for Operating Light and Water Exposure Apparatus (Fluorescent UV-Condensation Type) of Non-Metallic Materials.

The test equipment consists of a QUV accelerated weathering tester equipped with UVA-340 lamps (Figure 1) and solar eye which measure and control the emitted radiations that is received by the samples.

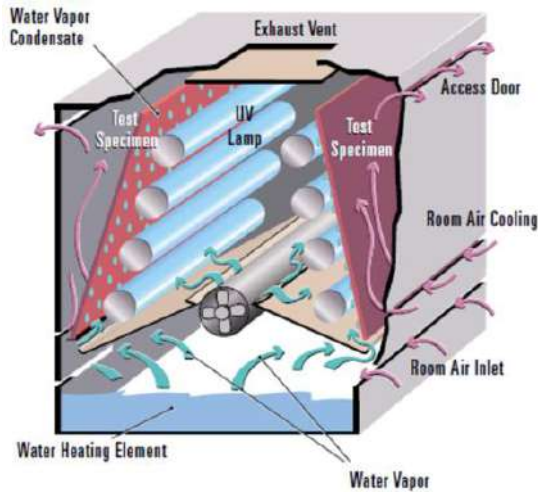


Figure 1: Scheme of a QUV accelerated weathering tester (scheme extracted from the Weathering testing guidebook from Atlas Corporation).

Test conditions are calibrated following the Q-lab Technical Bulletin LU-8160, and for correlation of laboratory to natural weathering, please refer to Q-lab Technical Bulletin LU-0824. In summary, we used UVA 340nm lamps with a normal irradiance of 0.68W/m^2 in order to mimic closely the UV irradiation of the membrane at the surface of earth (Figure 2).

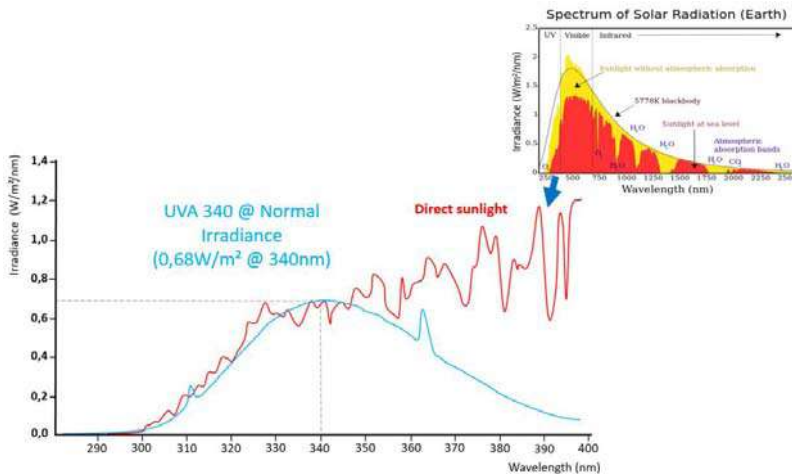


Figure 2: UVA 340 lamp irradiance and direct sunlight comparison calibration.

Different ageing stresses exist through the profile of a material as water is absorbed and desorbed (figure 3), these are mimicked in the QUV test cycle described in table 1.

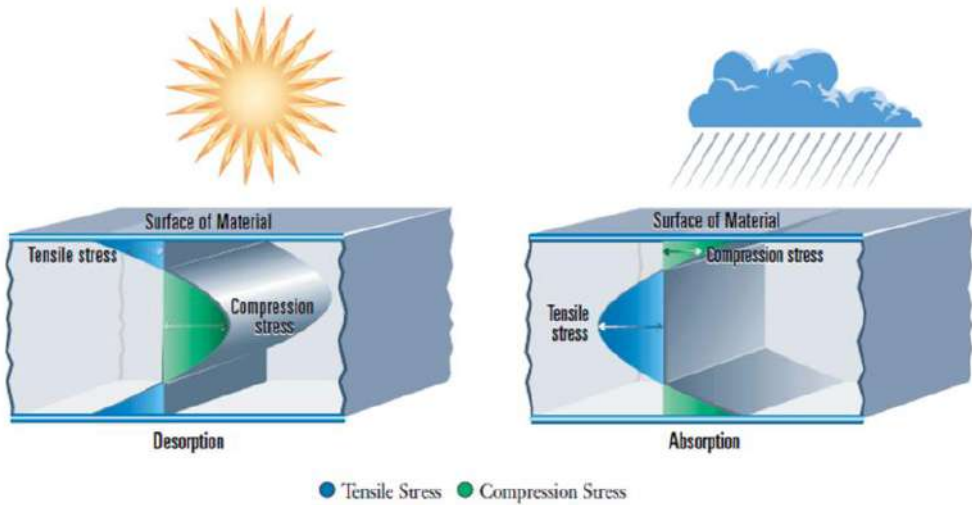


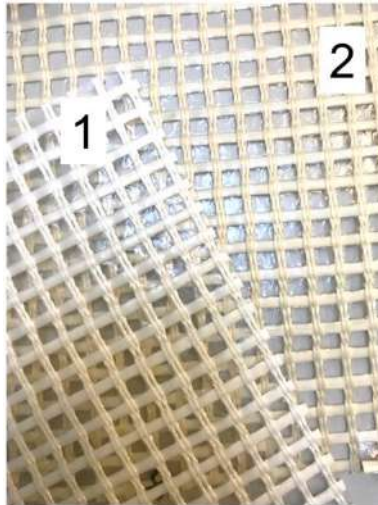
Figure 3: Representation of material stresses due to absorption and desorption of water (scheme extracted from the Weathering testing guidebook from Atlas Corporation).

Step	Function	Irradiance (W/m ²) @ 340nm	Temperature (°C)	Time (hh:mm)
1	UV irradiation	0,68	60	04:00
2	condensation	0	40	04:00
3	repeat	Go to step 1		

Table 1: Test cycles used in the QUV testing protocol

As a preliminary test, the Fluoscrim™ membrane was exposed to 4000h of the above calibrated cycles in order to provide an assessment of the UV, temperature and water absorption and desorption ageing.

Inspection of the material indicated no physical damage of the test sample with remarkable whitening of the fabric under UV exposure (Picture 1).



Picture 1: Inspection of the 4000h test piece (1) against the reference (unexposed) material (2)

Additionally a weathering test under Florida weather conditions is running. So far, after 100 weeks, the results obtained are in line with laboratory conditions picture 2.



Picture 2: Inspection of the Fluoscrim™ membrane test piece after 100 weeks in Florida weather conditions.

From these preliminary tests, we ensured that the developed Fluoscrim™ laminate has promising stability to external simulated and real UV conditions. Compared to other membrane materials being tested in this simulation, Fluoscrim™ laminate is performing as the most stable membrane available.

The tests are still running in order to investigate the impact of long stress exposures to the investigated conditions.

We also understand that the above tested conditions are not representative of all climates nor outdoor conditions but are giving the first positive indications of material stability against temperature, UV and water condensation cycles. These studies are corroborated with jungle

and temperature stability tests. These tests simulate additional intense temperature and humidity stress conditions.

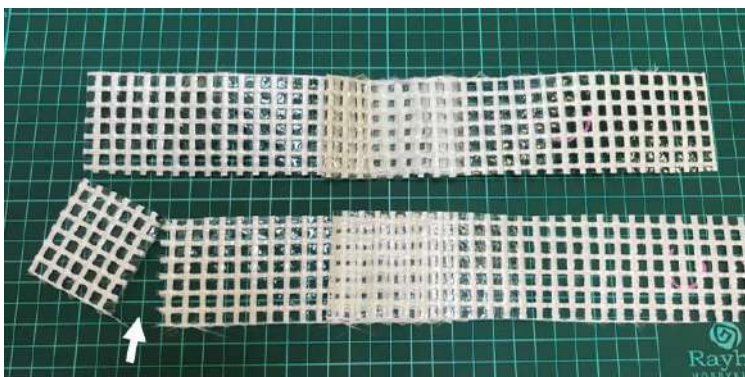
b) Confectioning of the membrane materials using high frequency (HF) welding techniques

An interesting feature that we were eager to develop with this material was the possibility to offer to the market the possibility to use HF welding techniques to fabricate structures. Contrary to PTFE or ETFE membranes that requires the fabricators to equip with additional specific equipment, the developed Fluoscrim™ membrane material is aimed to be confectioned using standard HF welding machinery used for PVC coated PES fabrics.

In the early development stage, the material selection allowed us to envision this unique feature for a glass fibre reinforced fluoropolymer laminate. The HF welding properties of the materials were not only developed to allow the welding of the material on itself but also to other types of architectural materials (mainly PVC coated PES fabrics) confectioned using the same equipment.

The optimal machine parameters for welding the Fluoscrim™ on itself need to be preliminarily tested by the operator, and so far, the numerous tests done at third party facilities were successful using HF conditions close to the ones usually used for tensile architecture PVC fabrics.

The obtained welds were tested following the EN ISO 1421:2016 (Rubber or plastics coated fabrics- determination of tensile strength and elongation at break) and EN ISO 2411:2017 procedure (Rubber or plastics-coated fabrics- determination of coating adhesion) at different temperature as proposed in the JRC's science and policy report number 100166.^[3] Noteworthy testing such glass fibres materials requires adaptation of the clamp system test equipment to avoid misleading results where the glass fibres will break at the clamp end tip (picture 3).



Picture 3: Welded Fluoscrim™ pieces tested under EN ISO 1421 protocol. The bottom sample shows a failure due to the use of an inappropriate clamp system.

The weld and adhesion performances were tested for both mesh directions and for each condition with a minimum 5 sample pieces taken from 2 different production batches. The table 2 displays the obtained test results.

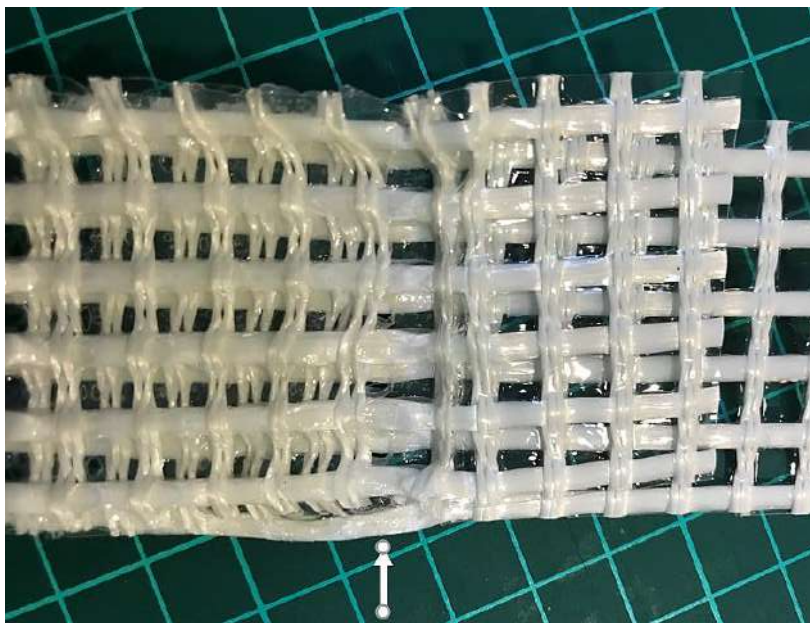
EN ISO 1421 “Seam’s tensile strength at break”

Temp.	Direction	Weld width (cm)	Min (N/5cm)	Max (N/5cm)	Average (N/5cm)	Observations
20°C	Warp	6cm	4240	5560	4670	Avg.elong. at break 4.9%
	Weft		4180	5430	4750	Avg elong. At break 5.0%
	Weft	5cm	3110	3755	3600	Creep at weld
	Weft	4cm	2516	2973	2733	Creep at weld
70°C	Warp	5cm	1860	2730	2230	Creep at weld
	Weft		2040	2670	2440	Creep at weld

EN 2411 “coating adhesion”

Temp.	Direction	Min (N/5cm)	Max (N/5cm)	Average (N/5cm)	Observations
20°C	Warp	172	248	224	
	Weft	183	274	238	

Table 2: Test results weld seams strength and coating adhesion for Fluoscrim™ on itself

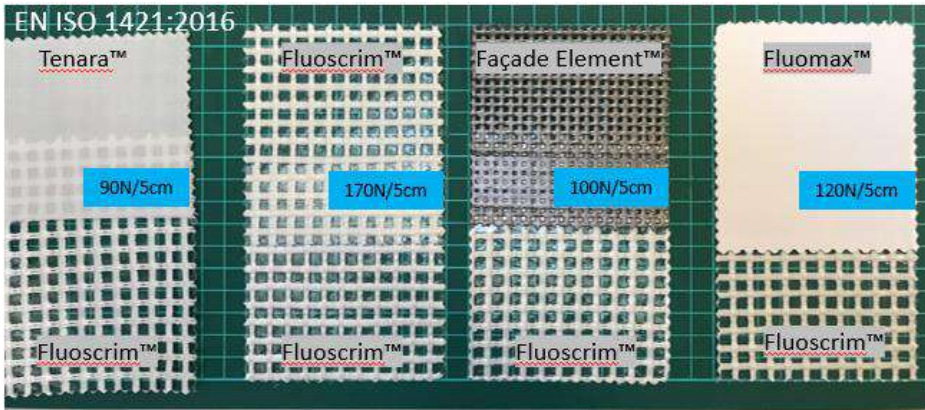


Picture 4: Illustration of the “creep at weld” for the test EN ISO 1421 at 70°C on Fluoscrim™ sample

For the EN ISO 1421 tests, the seam width of 6cm resulted in the glass fibre breakage, this leads us to think that the optimum seams width in our welding conditions is 6cm. Smaller seam widths (<6cm) or higher temperature resulted in the sliding of the mesh at the seams (like exemplified in picture 4). We believe the creep is mainly is due to the e-modulus to temperature value of the film’s resin.

For the EN ISO 2411 tests, we can observe that the complexation of the films on the glass mesh offers a reliable and consistent adhesion. The adhesion consistency is best achieved when using soft electrodes during the welding.

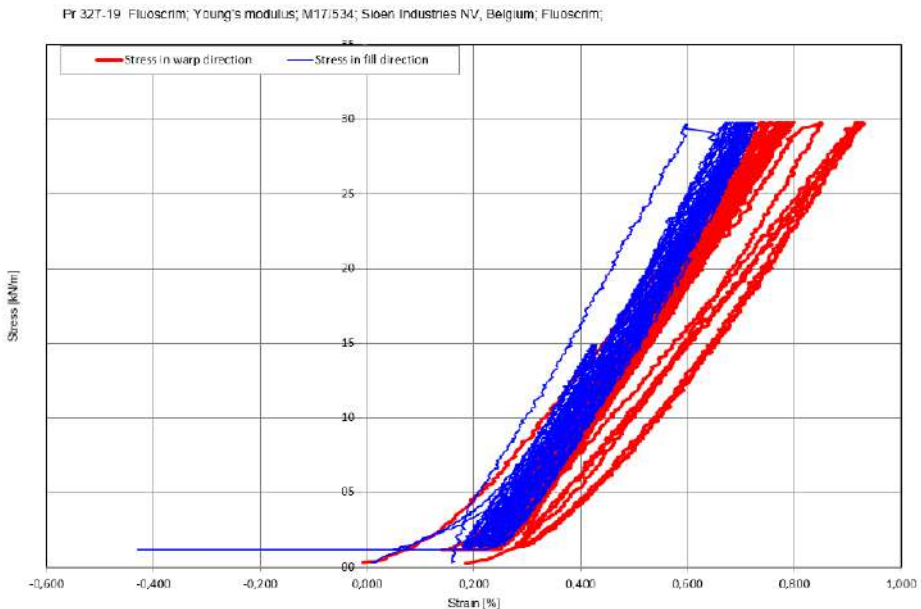
We conducted similar preliminary studies to weld the Fluoscrim™ with other membrane materials. We were successful to weld the Fluoscrim™ with PVC coated PES membranes, results showed best adhesion for PVC coated membranes with PVDF topcoats (such as Fluomax™ and Fluo²max™). Tenara™ coated membranes were also welded effectively but this time using an adhesion tape film made of FEP or PVDF. Values obtained for different materials are preliminarily indicated in picture 5.



Picture 5: 2cm width welding results with different materials under EN ISO 1421 test method

c) Biaxial behaviour of the membrane

Another important point for us during the development was to create a material that has predictable and reliable elastic behaviour in warp and weft directions. Internal weaving knowledge lead us to the design of a leno weave mesh with reliable 4500N/5cm tensile strength in warp and weft directions. The developed Fluoscrim™ was tested following the MSAJ Biaxial test procedure. As a result the membrane showed high stiffness and very close e-modulus results as showed in the graph 1.



Graph 1: Stress = f(strain) under the MSAJ biaxial procedure for the Fluoscrim™ membrane

4. Conclusion and perspectives

As a conclusion, we believe the preliminary test results give promising information related to the use of Fluoscrim™ in projects where long-term high translucency wide span structures are envisioned. This material is now available for use in tensile architecture projects. Some advanced properties are currently being optimized for a standard product offering.

One important perspective to Fluoscrim™ material is the ability to be recycled thanks to material separation. Recycling and the completion of the life cycle analysis will surely provide insight, leading us to reduce our production and logistic processes. These insights are needed to bring a more sustainable approach on material development for the tensile architecture construction industry.

5. Acknowledgements

The Author would like to thank Brian Coughlin and Matthias Kleibel for their contribution in reviewing this paper.

References

- [1] Knippers J., Cremers J., Gabler M., Lienhard J., (2011), *Construction Manual for Polymers + Membranes*, Detail ed.
- [2] Houtman R., Ignasi J. (Ed), (2016), *Fabric structures in architecture*. Woodhead Pub.
- [3] Stranghöner N. *et al.*, (2016), *Prospect for European guidance for the structural design of tensile membrane structures*, European Union.

Proceedings of the TensiNet Symposium 2019

Softening the habitats / 3-5 June 2019, Politecnico di Milano, Milan, Italy

Alessandra Zanelli, Carol Monticelli, Marijke Mollaert, Bernd Stimpfle (Eds.)

Increasing the safety of tensile structures

Heidrun BÖGNER-BALZ*, Jochen KÖHNLEIN*, Rainer BLUM^a

*DEKRA Automobil GmbH, Laboratory for Technical Textiles and Films, Breitwiesenstr. 13, D 70565 Stuttgart, Germany,

heidrun.boegner-balz@dekra.com

^a Dr.-Ing. habil. Rainer Blum, Ludwig-Finckh-Weg 17, D 71229 Leonberg, Germany

Abstract

An actual issue arising from daily work in the quality assessment of large structures is the safety of structures. Considering the most common failures of membrane roofs we can detect two main causes: either detail failures or failures of the material. To avoid failures of details in Germany e.g. a quality assurance system for every project is being executed. Testing all structural important details of a structure before and during fabrication confirming the necessary safety factors minimizes risks very effectively.

However this does not avoid all problems occurring on site as many failures are caused by harming the material itself. In this paper failures will be shown on which the origin of the problems will be demonstrated: mechanical damages, folding etc. caused during manufacturing, transport and use. The following questions will be discussed: Where do tears come from, how could they be avoided on one hand and on the other hand, in case they have happened: how can we predict the influence on the safety of the structure? Safety reducing aspects and test methods to elaborate the residual strength of materials will be presented.

Keywords: quality assessment, safety of structures, residual strength, creases, folds, tear propagation

DOI: 10.30448/ts2019.3245.03

Copyright © 2019 by Bögner-Balz Heidrun, Köhnlein Jochen, Blum Rainer. Published by Maggioli SpA with License Creative Commons CC BY-NC-ND 4.0 with permission.

Peer-review under responsibility of the TensiNet Association

1. Introduction

In tensile architecture, we usually are dealing with coated fabrics or films. If we talk about coated fabrics we can basically distinguish three failure types: defect of the yarn, defect of the coating and propagation of a defect. Defects of the yarn are usually already detected during weaving or during the cloth inspection if not happening in the later process. Defects of the coating influence the long term resistance of the fabric. Damages of the coating could be damages of the surface, destruction of the adhesion between coating and fabric either through movements perpendicular to the fabric plane or in plane through shearing.

Before starting the origins of damages the relevant terms and definitions shall be mentioned.

Folds may be seen as a doubling of material around a diameter.

Creases are ridges in a material that are caused by a fold or wrinkle being placed under pressure. These damages may occur in all materials used for tensile architecture. However the severity of the impacts varies strongly from material type to material type. While ETFE should be handled with special care to avoid scratches, creases and folds having a direct influence on the breaking strength by reducing the thickness of the film, scratches on PVC coated polyester fabrics have got a long term effect. They should only be used with special care and expert's knowledge for retractable roofs taking into account a shorter lifespan. Going into detail with all material types would lead too far for this publication. Thus here the main attention will be turned to PTFE coated glass fibre fabrics. It is a matter of common knowledge that glass fibres due to their residual stress condition are sensitive to mechanical impacts.

2. Origins of damages

Having enough experience, in most cases the origin of defects can clearly be detected. A variety of folds and creases and their formation shall be explained below.

2.1. Damages happening during material production

Damages happening from material production can either be classified as weave defects or coating defects. Furthermore the yarn direction in weft direction may deviate from rectangularity with the warp yarn direction either as a weft bow (largest deviation in the centre of the material width) or as an angle deviation over the total width. These types of defects should be detected and marked during a cloth inspection at the material supplier and later be considered during manufacturing (leaving out sections or respect the weft yarn direction for compensation if of remarkable size).

2.2. Damages happening during manufacturing

The first main origin of defects in coated fabrics results from handling during manufacturing. The material rolls will be delivered to the manufacturing company where the cutting process starts. This is usually being done by an automatic cutter, or also using (paper) templates. Then all pieces will have to be transported to the welding machines to connect them which may be done by transport wagons.

Adding one piece to the other the membrane panel is step by step getting larger and heavier. The panel or parts of it have to move along the welding machine or vice versa.

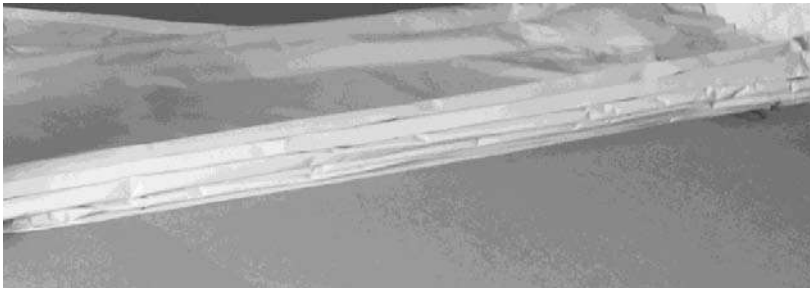


Figure 2.1: Looped material [DEKRA]

Loops may occur occasionally or where desired and necessary due to limited space for large panels (Figure 2.1).

As soon as these loops are loaded with more loops and material or due to inattention a sharp crease may happen.



Figure 2.2: Typical crease, image post processed [DEKRA]

Another type of folds occurring during manufacturing is the running fold. It happens when an unloaded crease – often perpendicular to a loop - is moving e. g. by pulling the material parallel to the loop (compare Figure 2.3a).



Figure 2.3a: Creation of a running fold [DEKRA]

The effect may be seen in the following Figure 2.3b.



Figure 2.3b: Rolling fold, image post processed [DEKRA]

A running double crease happens as soon as local double fold is torn out when moving the panel. This may happen over a great length and may harm the glass fibres severely.

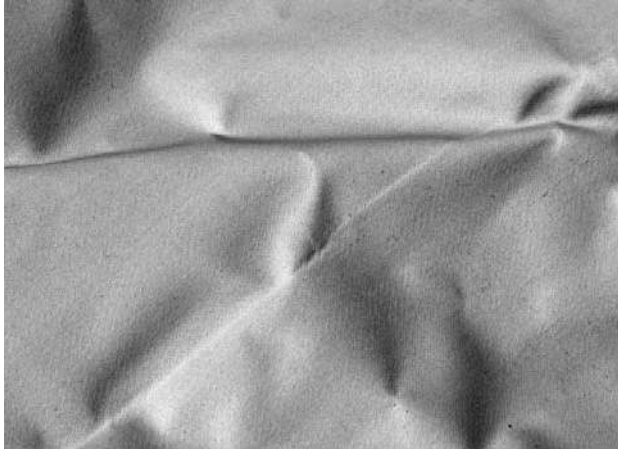


Figure 2.4: Running double crease in the center of the picture and running folds from the center to the left corner and bottom, image post processed [DEKRA]

2.3. Damages happening during packing and transportation

Due to the fact that membranes are typically wide-span doubly-curved structures the single panels are of a certain size and not easy to pack geometry. Thus the best method of packing should be planned in advance already taking into account the erection procedure and cutting pattern. The less the material will have to be moved the less damages will occur.



Figure 2.5: Typical creases resulting from packing, image post processed [DEKRA]

2.4. Damages from unpacking and installing

PTFE-glass membranes should be unpacked very carefully. The unpacking place should be clean, possibly layed out with carpets, free of objects which may harm the material. It is of advantage if the place where panels are being layed out is not accessible for untrained people.

Severe damages may already lead to panel rupture while stressing the panel due to the fact that an over stressing is necessary for the introduction of the pre stress.

Over the years initial damages are regions where deterioration may faster proceed.



Figure 2.6: Initial folding lines and scratches on an aged membrane surface [DEKRA]

2.5. Damages in use

Damages in use may happen from bird's picking, sharp parts falling onto the membrane, sliding sheets of ice, careless inspection etc.

3. Testing procedures to estimate the level of damage by folds and creases

3.1. ASTM crease fold testing

For creases a standard test method may be used: Breaking strength after crease fold according to ASTM D4851 - 07 (Reapproved 2011) [8].

3.2. Simulation of running folds

For the simulation of running folds DEKRA has designed an apparatus which creates the same folds as detected during inspections. Comparative tests between materials damaged by running folds taken from manufacturing and materials where the running fold has been applied in the running fold device have been compared and showed reliable results.



Figure 3.1: Application of running folds according to DEKRA method “Running fold” [DEKRA]

3.3. Simulation of running double crease

Running double creases are produced by folding the material twice producing a sharp edge. This sharp edge is then torn out along the first fold. The glass fibres are sharply creased and might crack, “white cracks” occur.

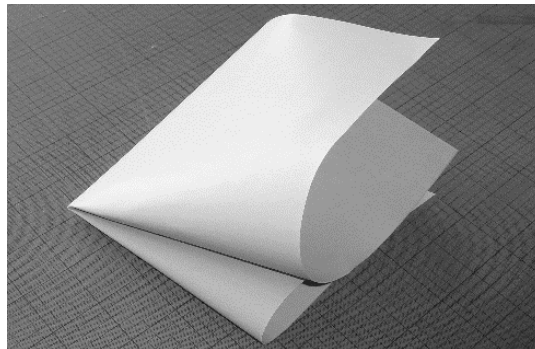


Figure 3.2a: Application of running double crease, DEKRA method “Running double crease” [DEKRA]

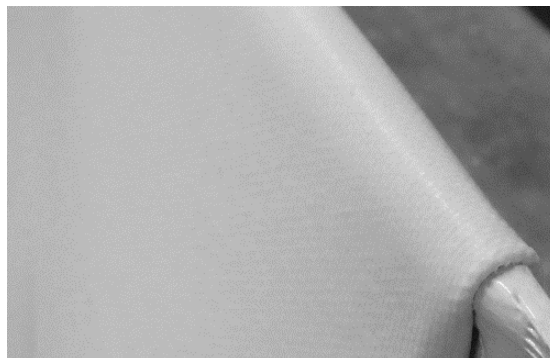


Figure 3.2b: Application of running double crease, DEKRA method “Running double crease” [DEKRA]

3.4. Biaxial tear propagation testing with simulated running double creases

3.4.1 Biaxial tear propagation testing with cuts

Uniaxial tear propagation tests do not refer to the practical stress states of large panel membrane structures. Thus it has become a state of the art procedure to execute large-panel biaxial tear propagation tests.

The execution and evaluation of biaxial tear propagation tests have been described in [6], [7], [8] and [9]. Typically tear propagation were tested with applied cuts of different length in the centre of a biaxial sample or as wide panel tear tests. An experimental set up with a 70 cm by 70 cm wide sample is shown in Figure 3.3 below.

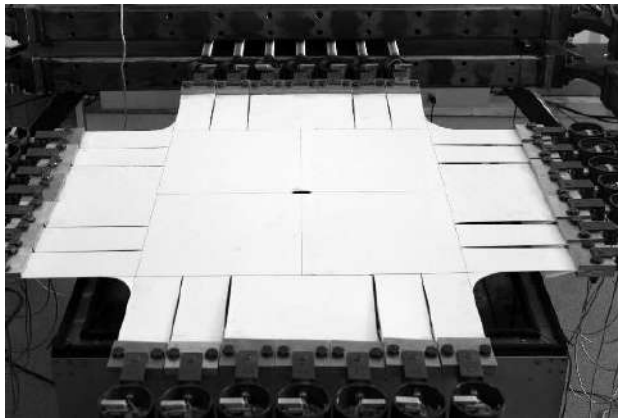


Figure 3.3: Biaxial tear propagation test at DEKRA [DEKRA]

Example results for a 15 cm wide cut parallel to fill direction are shown in Diagram 3.1

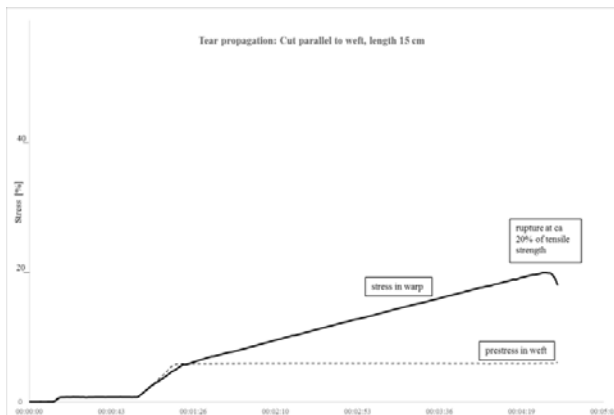


Diagram 3.1: Results of biaxial tear propagation test with a 15 cm wide cut for material A [DEKRA]

3.4.2 Biaxial tear propagation testing on samples with simulated running double crease

The procedure of biaxial tear propagation tests on folds is similar to the one described above. Here instead of a cut a damage with a defined fold will be applied in the centre of the sample. Then the membrane stress perpendicular to the damage will be increased until the failure of the sample.



Diagram 3.2b: Results of biaxial tear propagation test with a 15 cm wide running double crease for material A [DEKRA]

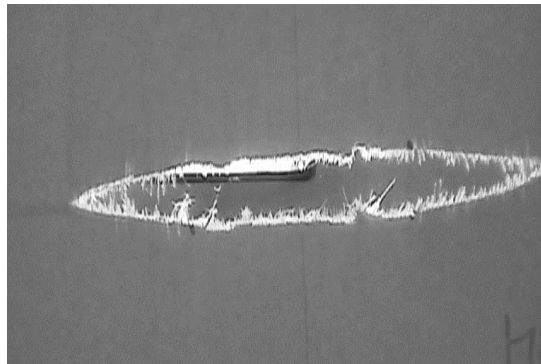


Figure 3.4: Suddenly propagating tear [DEKRA]

Comparing the test methods one can state that the tear propagation for cuts of the same length as the running creases starts at lower fabric stresses. It starts slowly with one thread cracking after the other before the total rupture happens. Contradictory to this the rupture of the sample with an applied crease happens suddenly without advance notice. There is no need to emphasize that this might be very critical for a structure in use. The difference of breaking strength is not so much influenced by the length of the damage in the tested range between 5 and 15 cm length (between 40 and 45 % of uniaxial ultimate tensile strength) as it is typically for cuts.

4. Evaluation of intensity of folds of different PTFE coated glass fibre fabrics

The breaking strength of different PTFE coated glass-fibre materials has been tested on 10 cm wide strips following the procedure of ISO 1421. To other sets of samples the three test methods described in here have been applied (ASTM Crease fold, running fold and running double crease). The 5 %-fractile of the initial breaking strength of the material has been set to 100 % and the decrease after folding has been expressed by the rel. strength compared to the initial strength. Two measured materials of two different producers are shown below.

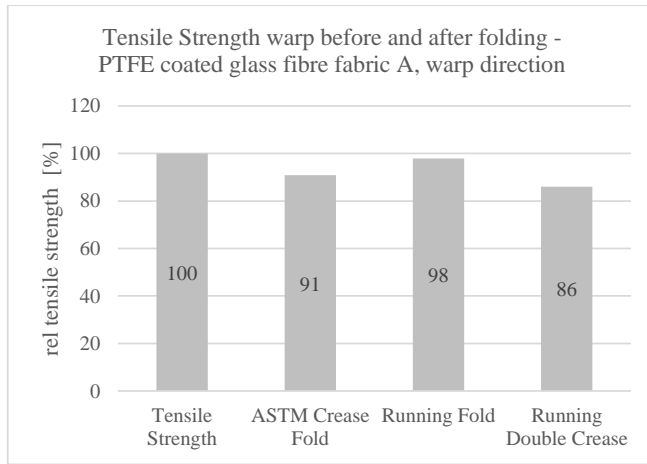


Diagram 4.1a: Comparison of relative tensile strength before folding (100 % equal to 5 % fractile according to DIBt guideline) and after folding, PTFE coated glass fibre fabric, material A in warp direction [DEKRA]

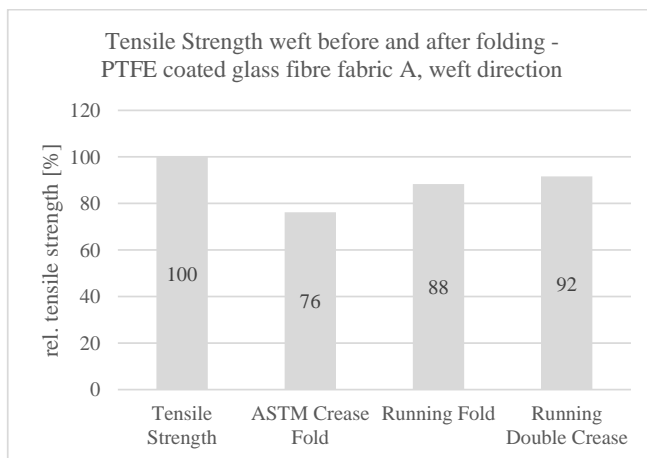


Diagram 4.1b: Comparison of relative tensile strength before folding (100 % equal to 5 % fractile according to DIBt guideline) and after folding, PTFE coated glass fibre fabric, material A in weft direction [DEKRA]

Tests executed on a material of another producer showed a different behaviour (Diagram 4.2).

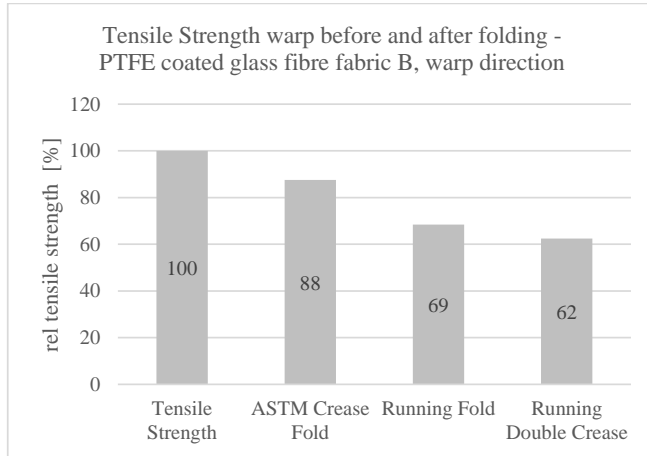


Diagram 4.2a: Comparison of relative tensile strength after folding compared to initial strength, PTFE coated glass fibre fabric, material B, warp direction [DEKRA]

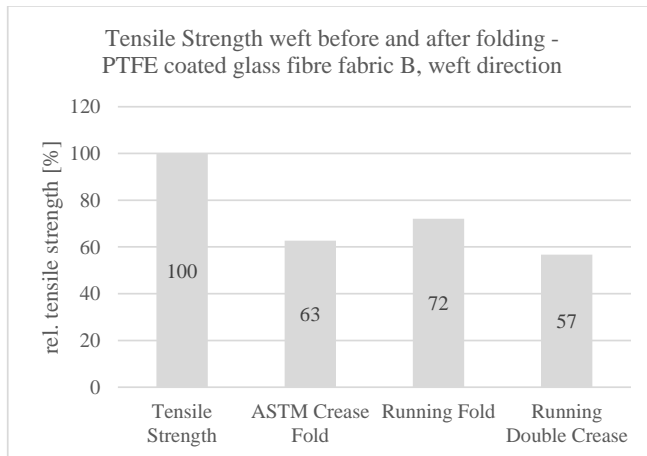


Diagram 4.2b: Comparison of relative tensile strength after folding compared to initial strength, PTFE coated glass fibre fabric, material B, weft direction [DEKRA]

The decay in strength depends on material type, direction, producer and sometimes even on a smaller measure on batches.

5. Consequences for the practice - Guidelines for the design

To prevent failures due to damages before use a detailed planning as and a well-organized and surveyed quality assurance system are essential. The life span of membrane structure is directly depending on the quality of the installed panel. In case of careful handling during

manufacturing, transport and installation and regular inspections including minor repairs and in some cases cleaning, the life span of PTFE coated glass fibre structures may exceed 35 years.

On the basis of biaxial tear or wide panel tear tests the stress concentration factor may be calculated and a critical damage length may be evaluated [7, 8]. The reduction in strength may be considered for design by applying a safety factor based on the proposed test results.

References

- [1] Blum, R., Bögner-Balz, H., Köhnlein, J.: On the mechanical behaviour of ETFE-films: Elastic range, yielding conditions, break determined by different test methods and the influence of the results on the analysis of ETFE-structures, Tensinet Symposium Newcastle 2016
- [2] Bögner-Balz, H., Blum, R., Köhnlein, J.: Structural behaviour of fabrics and coatings for architectural fabric structures, in: *Fabric Structures in Architecture*, Woodhead, 2015
- [3] Bögner-Balz, H., Blum, R., Reimann, K.: The Stress-Strain-Behaviour for Coated Orthotropic Fabrics and its Influence on the Analysis of prestressed Membranes, an Approach, IASS 2011
- [4] Blum, R., Bögner-Balz, H., Stegmaier, Th., Schneider, P., Vohrer, A., Planck: Developing and testing textiles, coatings and connections for buildings and constructions, in: *Textiles for Construction*, Woodhead, 2010
- [5] Bögner-Balz, H., Zanelli, A. (Hrsg.): *Tensinet Symposium – Ephemeral Architecture, Time and Textiles*, Mailand 2007
- [6] Barnes, M., Forster, B., Dencher, M.: *Structural Design Basis and Safety criteria*, in: *European Design Guide for Tensile Surface Structures*, Brussels 2004
- [7] Blum, R.; Bögner, H.; Némóz, G.: *Material properties and testing*, in: *European Design Guide for Tensile Surface Structures*, Brussels 2004
- [8] Blum, R.; Bögner, H.; Némóz, G.: *Testing methods and standards*, in: *European Design Guide for Tensile Surface Structures*, Brussels 2004
- [9] Bidmon, W.: *Zum Weiterreißverhalten von beschichteten Geweben*, Dissertation, University of Stuttgart 1989
- [10] ASTM D4851-07 (Reapproved 2011)

Proceedings of the TensiNet Symposium 2019

Softening the habitats / 3-5 June 2019, Politecnico di Milano, Milan, Italy

Alessandra Zanelli, Carol Monticelli, Marijke Mollaert, Bernd Stimpfle (Eds.)

Reliability-based analysis of a cable-net structure designed using partial factors

Elie DE SMEDT*, Marijke MOLLAERT, Maarten VAN CRAENENBROECK,
Robby CASPEELE^a, Lincy PYL

*Vrije Universiteit Brussel
Pleinlaan 2, Brussels 1050, Belgium
elien.de.smedt@vub.be

^a Universiteit Gent

Abstract

The design of tensioned membrane structures is not yet addressed by standards like the Eurocode. Currently, in cooperation with the TensiNet Association, Working Group 5 of CEN TC250, is working on a general standardised design approach for membrane structures, consistent with the partial factor framework used in the Eurocode (EN1990). To achieve such design approach, research towards a method to verify the reliability of a membrane structure is needed. The structural behaviour of a tensioned membrane can be represented by a tensioned cable-net. Herein a cable-net structure is firstly investigated because cables are addressed by the Eurocode (EN1993-1-11). Further research will investigate the established method for membrane structures. This paper explains and evaluates the influence of the partial factor for pretension. If the cables are dimensioned according to a partial factor 1.0, the obtained reliability indexes are lower than the considered target reliability index. If the cables are dimensioned according to a partial factor 1.35 the obtained reliability indexes are higher than the considered target reliability index.

Keywords: reliability index, cable-net, Latin Hypercube Sampling.

DOI: 10.30448/ts2019.3245.18

Copyright © 2019 by Elie De Smedt, Marijke Mollaert, Maarten Van Craenenbroeck, Robby Caspeele and Lincy Pyl. Published by Maggioli SpA with License Creative Commons CC BY-NC-ND 4.0 with permission.

Peer-review under responsibility of the TensiNet Association

1. Introduction

Since the 1950^s, the tensile surface structure industry has emerged and evolved, resulting in the wide variety of membrane structures and membrane materials available today. Although the membrane structure concept is generally approved, the design of membrane structures is not yet addressed by current standards like the Eurocode. Working Group 5 of CEN TC250 is working on a general standardised design approach for membrane structures. To obtain a design procedure that can be used by architects, engineers and contractors, such as the partial factor framework used in the Eurocode (EN1990), some partial factors need to be proposed and evaluated for membrane structures. So, research towards reliability analysis in combination with membrane structure analysis is needed to obtain such framework.

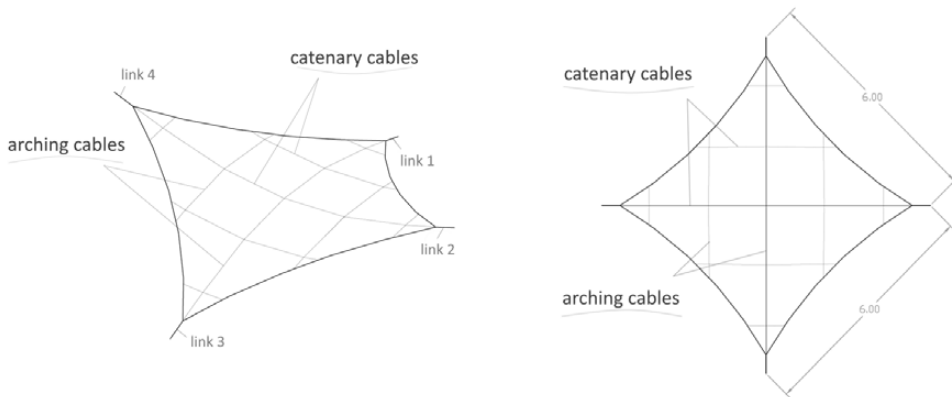
Gosling et al. (Gosling, Bridgens, & Zhang, 2013) and Thomas et al. (Thomas, Schoefs, Caprani, & Rocher, 2015) already studied the combination of reliability analysis with membrane structural analysis. Gosling et al. proposed and evaluated a method to perform a reliability analysis for membrane structures. The method consists of a sensitivity analysis and a reliability analysis based on the most important uncertain parameters. The found reliability indexes are lower than the target reliability indexes specified in the Eurocode. They concluded that the method is applicable for membrane structures if sufficient information is available about the stochastic models of the parameters. Thomas et al. investigated the reliability analysis of an inflated beam. The authors concluded that the obtained reliability indexes are in line with the target reliability indexes in the Eurocode.

The study presented in this paper also investigates a method to estimate the reliability of a membrane structure. The overall focus of the paper is on the used method. The structural behaviour of a tensioned membrane can be represented by a tensioned cable-net. Steel cables are addressed by the Eurocode (EN1993-1-11) and therefore a cable-net structure is firstly investigated and discussed in this paper. For the reliability analysis, the first order reliability method (FORM) (Sørensen, 2004) is used in combination with Latin Hypercube Sampling (LHS) (Olsson, Sandberg, & Dahlblom, 2003).

Further research will investigate the established method for membrane structures (ongoing research Round Robin exercise IV (De Smedt et al., 2018)). This paper explains and evaluates the influence of the partial factor for pretension. Therefore, the cable-net is designed with a partial factor for pretension of 1.0 and 1.35. Afterwards the reliability index β is calculated for both structures under snow load and under wind uplift load. The index is calculated for the catenary as well as for the arching cables.

2. Description of the cable-net

The studied cable-net structure is a hyperbolic paraboloid with five catenary cables, five arching cables, boundary cables and a turn-buckle in each of the four corner-points (Figure 1).



The in-plane distance from high point to low point is 6 meters.

Figure 1: Perspective view (left) and top view (right) of the cable-net.

Steel cables are used for the cable-net. The cross-section is calculated as follows (CEN, 2006):

$$A_{cc/ac} = \frac{N_{max,cc/ac}}{f_d} \quad (1)$$

$$f_d = \frac{f_u}{1.5\gamma_m} \quad (2)$$

where $A_{cc/ac}$ = area of the catenary and the arching cables; $N_{max,cc/ac}$ = maximum axial force in the catenary and the arching cables; f_d = design strength of the material; f_u = ultimate tensile strength = 1770 N/mm² (CEN, 2006); γ_m = material safety factor for steel (= 1.0).

Note that the cross-section is optimally dimensioned and considered as one circular section (so no bundle of steel wires like used for real steel cables). The structure is subjected to snow load and wind uplift load. For the dimensioning two cases are considered:

Case 1: 1 x pretension + 1.5 x snow load,

1 x pretension + 1.5 x wind uplift load.

Case 2: 1.35 x pretension + 1.5 x snow load,

1.35 x pretension + 1.5 x wind uplift load.

The partial factors are according to the Eurocode and correspond to a target reliability index of 3.8 for a 50 years reference period and a reliability class two (Table 1) (CEN, 2001).

Table 1: Target reliability indexes according to Eurocode, for a 1 year and a 50 years reference period.

Reliability class	Minimum values for β	
	1 year reference period	50 years reference period
RC3	5.2	4.3
RC2	4.7	3.8
RC1	4.2	3.3

Table 2 shows the values for the different loads. The values for snow load and wind uplift load are in line with the Eurocode.

Table 2: Values for pretension, snow load and wind uplift load.

	Value loads	Unit
Pretension	7.5	kN
Snow load	-0.6	kN/m ²
Wind uplift load	1	kN/m ²

The focus of this study is to evaluate a reliability analysis method and not to reach the safety requirements specified in the Eurocode. Therefore, the pretension of the cable-net is 7.5 kN for both directions so that a minimum tension of ± 0.75 kN remains present in both cable groups under loading.

The cross-section of both cable-groups for case 1 and 2 are given in Table 3.

Table 3: Cross-section of the catenary cables (CC) and the arching cables (AC) for case 1 and 2.

	CC	AC	Unit
Case 1	10.51	13.14	mm ²
Case 2	12.85	15.64	mm ²

As expected, the cross-section of both catenary and arching cables increases when the partial factor for pretension is increased from 1.0 to 1.35.

3. Reliability analysis

There are four methods to measure the reliability of a structure or structural element, called level I to IV methods. Level I is the partial factor approach used in the Eurocode (CEN, 2001), level II uses the mean values and the standard deviation of the uncertain parameters, level III uses the joint distribution functions and level IV incorporates the costs of failure (economic aspect) (Sørensen, 2004). The reliability analysis in this study is performed by level II methods together with first order reliability method (FORM). FORM means that the limit state function is linearized (Sørensen, 2004). In this study, the considered limit state function is ULS, considering the resistance R of the material and the effect E (CEN, 2001):

$$z = R - E \quad (3)$$

Figure 2 visualises the failure surface $z = 0$, the reliability index β and the design point P in a standard space u . The standard space is introduced by Hasofer and Lind (Hasofer & Lind, 1974). The variables R and E are transformed to respectively U_R and U_E .

$$U_R = \frac{R - \mu_R}{\sigma_R} \quad (4)$$

$$U_E = \frac{E - \mu_E}{\sigma_E} \quad (5)$$

where $\mu_{R/E}$ is the mean value of R and E and $\sigma_{R/E}$ is the standard deviation. The straight, inclined line in Figure 2 is called the failure surface. The surface represents where the limit state function z is zero. The structure is in the safe state when z is larger than zero (right of the failure surface) and in the failure state when z is smaller than zero (left of the failure surface). To measure the reliability of a structure, the reliability index can be calculated:

$$\beta = \frac{\mu_z}{\sigma_z} \quad (6)$$

where μ_z is the mean value of z and σ_z is the standard deviation.

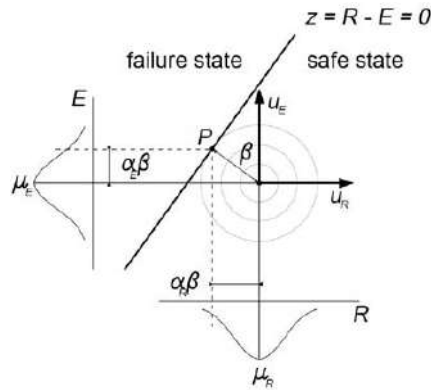


Figure 2: Visualisation limit state function z , design point P and reliability index β (CEN, 2001).

Design point P is the indication on the failure surface where failure of the structural element or structure is the most probable. The distance from this design point to the origin is the representation of the reliability index, which is the smallest distance from the origin to the failure surface (CEN, 2001).

2.1. Latin Hypercube Sampling

A reliability analysis is performed by taking into account the stochastic models of the uncertain parameters (Sørensen, 2004). This means that a range of values of the parameters based on their mean value, coefficient of variance (COV), etc., has to be evaluated. In order to obtain the reliability index, different simulation sets containing variations of the uncertain parameters are put together. The sets are established by means of Latin Hypercube Sampling (LHS) (Mckay M.D. et al. 2000). The method allows to estimate the reliability of a structure with a limited amount of simulations. In Figure 3, a schematic representation of the LHS concept on a cumulative density function (CDF) is shown. The distribution of the parameter is divided in a certain number of equal parts (grey lines) and from each part one value is randomly taken (black crosses). Like this, the whole distribution of the parameter is taken into account.

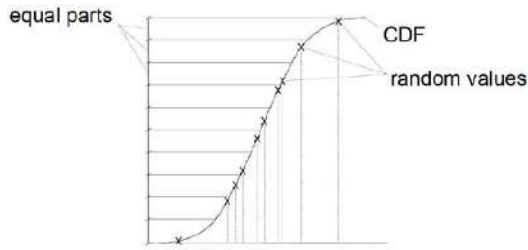


Figure 3: Schematic representation of the LHS concept with a CDF.

2.2. Parameters

The considered parameters and their stochastic models (the type of distribution, the nominal value, the mean value, the standard deviation and the COV) are given in Table 4.

Table 4: The stochastic models of the considered parameters.

	RA 1/RA 2	Distribution	Nominal values	μ	σ	COV	unit
l_{1-4}	1, 2	Normal	0,5	0,5	0,002	0.004	m
EA_{cc}^*	1, 2	Normal	1734	1734	34,68	0.020	kN
EA_{ac}^*	1, 2	Normal	2168	2168	43,36	0.020	kN
f_u	1, 2	Normal	1770	1830	30	0.016	MPa
Q_{snow}	1	Gumbel	-0,6	-0,66	-0,20	0.300	kN/m ²
Q_{wind}	2	Gumbel	1	0,7	0,25	0.350	kN/m ²

In total, eight parameters are considered: the length of each turn-buckle l_{1-4} , the axial stiffness of both cable groups $EA_{cc/ac}$ (catenary and arching cables), the ultimate strength of the steel cables and the load $Q_{snow/wind}$. The lengths of the turn-buckles are considered as an installation uncertainty. During construction, the pretension of the cable-net is set by means of the turn-buckles, that are adjusted in length on the construction site. Variation on the lengths affects the geometry and the pretension of the cable-net, which means that there is an indirect uncertainty on the geometry and the pretension. The axial stiffness of the catenary and the arching cables is the modulus of elasticity of the steel cables multiplied with the area of the cross section of each cable group:

$$Stiffness = EA_{cc/ac} \tag{7}$$

where E = modulus of elasticity = 165×10^3 MPa (Krishna P. 1978). The stochastic models of the lengths of the turn-buckles and of the stiffness of the cables are based on expert advice. According to expert advice, a variation of pretension of 0.75 kN/m is to be expected after

installation of the cable-net. The COV of the length of the turn-buckles is chosen so that the expected variation of pretension is met.

Due to the lack of available data of these stochastic models, the normal distributions are a straightforward choice for this first reliability analysis of a tensioned cable-net structure. Normal distributions can imply negative values. It proved not to have a significant influence on the outcome for this case study. The models of the yield strength, snow load and wind uplift load are taken from a publication of the Joint Committee on Structural Safety (JCSS) (Holicky & Sykora, 2010).

The length of the turn-buckles, the stiffness and load values are used in the simulations. The ultimate strength is used in the limit state function. For this study 100 simulations proved to be sufficient to perform an accurate reliability analysis.

4. Results

The reliability analysis is performed by FORM and LHS in combination with the form finding and structural analysis software Easy (Easy, 2017). After the simulations are completed, the reliability is measured with the results of each set according to:

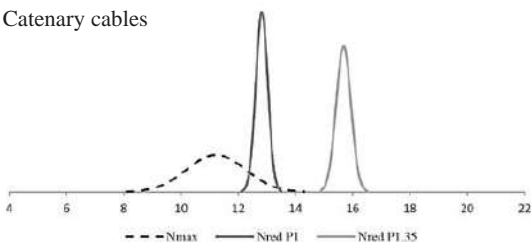
$$z = N_{red,cc/ac} - N_{max,cc/ac} \tag{8}$$

$$N_{red,cc/ac} = f_{red}A_{cc/ac} \tag{9}$$

$$f_{red} = \frac{f_u}{1.5} \tag{10}$$

where $N_{red,cc/ac}$ is the reduced tensile force of respectively the catenary and the arching cables; f_{red} is the reduced tensile strength of the steel cables. The distribution of the resistance and the effect of both cable groups are visualised in Figure 4 and Figure 5.

Reliability analysis under snow load:
Catenary cables



Reliability analysis under wind uplift load:
Arching cables

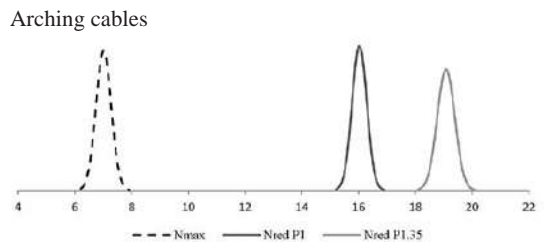
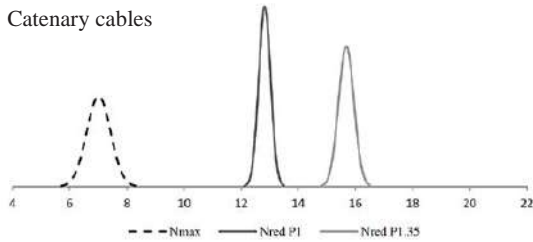


Figure 4: Distributions of the resistance and the effect for the catenary (left) and the arching cables (right) under snow load.

Reliability analysis under wind uplift load:
Catenary cables



Reliability analysis under wind uplift load:
Arching cables

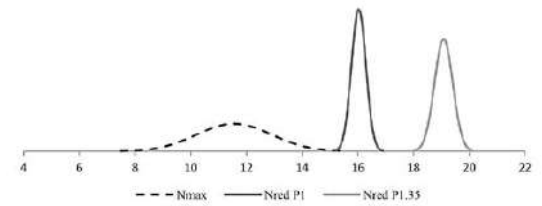


Figure 5: Distributions of the resistance and the effect for the catenary (left) and the arching cables (right) under wind uplift load.

Figure 4 shows the results of the reliability analysis under snow load and Figure 5 under wind uplift load. For the structural dominant direction (CC under snow load and AC under wind uplift load) the ‘distance’ between the distribution of the resistance and the effect is smaller than for the non-dominant direction. For the dominant cables dimensioned according to a pretension factor 1.0 there is an overlap of the distribution of the resistance and the effect, which means that the cables do not reach the specified safety requirements.

The reliability of the cable-net structure is determined with the lowest reliability index. The obtained reliability indexes obtained for the structural dominant cables under snow load (catenary cables) and wind uplift load (arching cables) are given in Table 5.

Table 5: The obtained reliability indexes for CC and AC dimensioned with a factor 1 and 1.35 for the pretension.

		Snow load	Wind uplift load
		CC	AC
Case 1	1 x pretension	1.52	3.21
Case 2	1.35 x pretension	4.01	5.61

As expected, from Figure 4 and Figure 5, the target reliability index of 3.8 is not reached for the structural dominant cables designed with a pretension factor 1, which is 1.52 under snow load and 3.21 under wind uplift load. For both case 1 and 2 the reliability index is lower for the reliability analysis under snow load than under wind uplift. This is most likely due to the fact that the simulations for the reliability analysis are performed with the mean values of the snow load and wind uplift load (respectively 0.66 kN/m² and 0.7 kN/m², Table 4) which is for the snow load higher than the nominal value (0.6 kN/m²) and for the wind load lower than the nominal value 1 kN/m²) wherefore the cable-net is dimensioned.

For case 1, the reliability index under wind uplift load for the arching cables (3.21) and for case 2, the reliability index under snow load for the catenary cables (4.01) are in line with the specified target reliability index (3.8).

From Table 5 it is noticed, that for this specific steel cable-net structure, the cables dimensioned according to a pretension factor 1.35 meet the safety requirements and are safe according to the considered limit state function (equation (8)).

5. Conclusion

This study evaluates a method to estimate the reliability of a tensioned cable-net structure. The cable-net is designed according to the partial factor method described in the Eurocode. The steel cable-net structure is dimensioned according to two partial factors for pretension 1 and 1.35. The cross-section increases from 10.51 to 12.85 mm² for the catenary cables and 13.14 to 15.64 mm² for the arching cables. The increase of the cross-section results in an increase of the reliability index. The reliability index for the structural dominant direction under snow (CC) increases from 1.52 to 4.01 and under wind uplift load (AC) from 3.21 to 5.61. As according to the Eurocode the partial factor for a permanent load should be 1.35, the reliability index obtained in case 2 is confirmed to be larger than the target reliability index 3.8. The safety requirements are met if the cable-net is designed according to a pretension factor 1.35.

The proposed reliability analysis method proves to be a valid tool to estimate the reliability of a tensioned cable-net structure. The method is very generic, because it allows inserting the parameters specific to the case study and therefore it can easily be applied to other cable-net structures. A next step is to evaluate the described method for the reliability analysis on a membrane structure and to calibrate the partial factors, which are not yet available in current standards.

References

- CEN. (2001). EN 1990: Eurocode 0: Basis of Structural Design. European Committee for Standardization.
- CEN. (2006). EN 1993-1-11: Eurocode 3: Design of steel structures - Part 1-11: Design of structures with tension components. European Committee for Standardization.
- De Smedt, E., Mollaert, M., Pyl, L., Gosling, P. D., Uhlemann, J., & Thomas, J.-C. (2018). Round Robin Exercise IV: Reliability analysis of a simple membrane structure: a hyperbolic paraboloid. Retrieved from https://www.tensinet.com/files/Announcement__calls/Round%20Robin%20exercise%20IV%20-%20call%20-%20version%202.pdf
- Easy. (2017). (Version 2017.0.6.33). technet gmbh. Retrieved from <https://www.technet-gmbh.com>
- Gosling, P. D., Bridgens, B. N., & Zhang, L. (2013). Adoption of a reliability approach for membrane structure analysis. *Structural Safety*, 40, 39–50. <https://doi.org/10.1016/j.strusafe.2012.09.002>
- Hasofer, A., & Lind, N. C. (1974). An exact and Invariant ReFirst Order Reliability Format. *Journal of Engineering Mechanics*, 100, 111–121.
- Holicky, M., & Sykora, M. (2010). Stochastic Models in Analysis of Structural Reliability. Presented at the The International Symposium on Stochastic Models in Reliability Engineering, Life Sciences and Operations Management, Beer Sheva, Israel.
- Olsson, A., Sandberg, G., & Dahlblom, O. (2003). On Latin hypercube sampling for structural reliability analysis. *Structural Safety*, 25(1), 47–68. [https://doi.org/10.1016/S0167-4730\(02\)00039-5](https://doi.org/10.1016/S0167-4730(02)00039-5)
- Sørensen, J. D. (2004). Notes in Structural Reliability Theory and Risk Analysis.
- Thomas, J.-C., Schoefs, F., Caprani, C., & Rocher, B. (2015). An Application of Reliability Analysis to Inflatable Structures, 36.

Proceedings of the TensiNet Symposium 2019

Softening the habitats / 3-5 June 2019, Politecnico di Milano, Milan, Italy
Alessandra Zanelli, Carol Monticelli, Marijke Mollaert, Bernd Stimpfle (Eds.)

Strain-rate dependent tensile strengths of PTFE-fabrics by using the Strip Method

Kübra TALAK*

* Str.ucture GmbH
Lindenspürstraße 32, 70176 Stuttgart
talak@str-ucture.com

Abstract

In this work, the strain-rate dependent tensile strength of membrane materials made of pure PTFE-fabric were analyzed. Strain-rates were determined by assessing the dynamic structural response of an umbrella membrane with 53 m span based on numerical FEM simulations. The evaluation of 5%-tensile strength fractiles from tests using various testing velocities show a notable increase of up to 1.3-fold compared to standardized testing methods. For the tensile tests clamping-methods were developed to prevent the gliding of the PTFE-testing-strips out of the clamps. They were successfully tested up to a loading limit of 8 kN and a loading rate of 500 mm/min. Overall, this is the first study showing a high potential of tested PTFE-fabrics for using the material beyond its standardized tensile strength and furthermore the demand for more detailed analyses especially in view to the definition of strain-rates for other construction types.

Keywords: PTFE-fabric, strain-rate dependent strength, dynamic analysis, strip method, clamping systems

DOI: 10.30448/ts2019.3245.05

Copyright © 2019 by Kübra Talak. Published by Maggioli SpA with License Creative Commons CC BY-NC-ND 4.0 with permission.

Peer-review under responsibility of the TensiNet Association

1. Introduction

Textile membrane structures containing PTFE-fabric provide particular mechanical properties such as high tensile strength. These uncoated PTFE-fabrics are preferred for membrane structures and particularly for special constructions like convertible roofs where high demands on the durability is required. However, their main disadvantage is their high market price compared to alternative membrane products. The price of the membrane material is closely related to the thickness of the chosen fabric which again is the result of the dimensioning of the membrane structure for the decisive load case. Membrane structures have in common that wind load is always the decisive case. Specifically, the gust wind is usually used to be applied on the structures for dimensioning. Considering the fact that gust wind is a short-time and strong wind load, the PTFE-fabric was investigated against its potential of increase of strength for a testing speed corresponding to the gust wind. An increase in strength under higher load speeds is already known for several other materials. Therefore, strain-rates were determined by dynamic structural analysis of an umbrella with 53 m span based on time-dependent c_p -values out of wind tunnel tests. The structural response provided strain-rates for decisive areas in membrane from which the loading rate was determined to 500 mm/min. This rate was used for the strip tensile tests, so that the loading rate corresponds to a short-term gust effect. For comparison reasons the tests were also performed with a loading rate of 100 mm/min according to DIN EN ISO 13934-1.

2. Properties of PTFE

Polytetrafluorethylen (PTFE) is a non-branched, linear, partially crystalline polymer made from fluorine and carbon and belongs to the polyhalogenolefines. The material is categorized as thermoplastic resin but also shows properties of a duroplastic resin. The fluoropolymer consists of carbon chains which are almost completely hermetically shielded by a helical arrangement of fluorine atoms and exhibits a very compact construction. As a result of these properties in combination with the characteristic strong connection between fluorine atoms and carbon atoms PTFE offers the highest chemical and thermic resistance among all synthetics. The material is resistant even against aqua regia. One very characteristic property of PTFE is its very low coefficient of friction which is known to be about 0.09. Here it becomes apparent, that the main challenge will be to prevent the specimens from sliding out of the clamps. Two other special characteristics of PTFE are a pronounced creep under tension and an anomaly of thermal expansion coefficient which is to be observed especially at a temperature of 19°C. The latter is attributed to a crystallization from triclinic to hexagonal (figure 1 and 2) which leads to an increase in volume of about 1% and a nonlinear relative length change. The creep behavior of pure PTFE is a non-desirable characteristic and needs to be minimized. Therefore PTFE fabrics are modified in the type of weave. Herewith the creep in material can be reduced so far that the suitability for practice is given.



Figure 1: Hexagonal crystal ($> 19^{\circ}\text{C}$)



Figure 2: Triclinical crystal ($< 19^{\circ}\text{C}$)

3. Numerical simulation of strain-rates from the membrane of U53

3.1. Reference project U53

To perform the tensile tests which shall be equivalent to a gust load the according testing speed needs to be determined. The herefore used model is the dynamic analysis of an umbrella with 53 m span (figure 3). The dynamic response of the structure provides strain-rates which can be transferred to a loading speed related to the length of the regarded specimens. This reference project provides an area of 2500 m² and an eaves height of 30 m. The umbrella was developed to protect the piazza of the Great Mosque of Mecca – United Kingdom of Saudi Arabia - from direct sun radiation and therewith to ensure a climatic comfort [Bradatsch].



Figure 3: Reference project U53

There are already measurements out of a comprehensive investigation of wind tunnel tests for the membrane of U53, which gives time-dependent c_p -values with a distribution over the membrane surface which are used for the following dynamic simulation of the umbrella-membrane. Thereby the wind load as a product of wind pressure and c_p -value needs to be applied to the FEM-model according to the distribution from the wind tunnel test model.

3.2. Simulation of the dynamic structural response

The analysis of the dynamic structural response is made with the program modul ASE 2016 from SOFISTIK AG. ASE calculates the structural response of three-dimensional finite element models. In this work the structural system consists of the membrane itself which is supported

at the points where the connections to the steel part are used to be. The membrane surface as well as the belts in the membrane are created as three-dimensional elements. The membrane is modelled as a homogeneous material with anisotropic and nonlinear material properties and the section forces are determined according to 3rd order theory (figure 4).

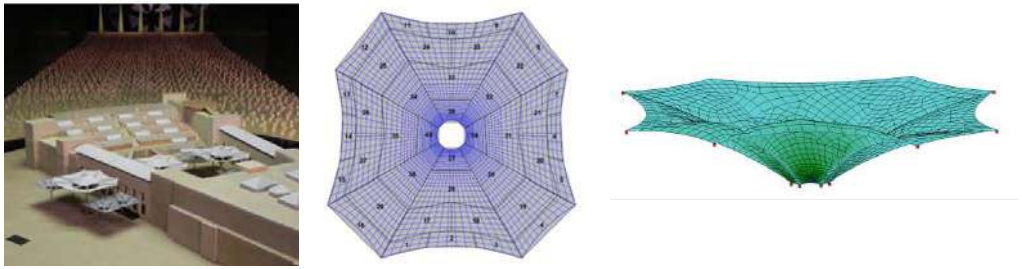


Figure 4: Base of dynamic analysis

The dynamic analysis is based on the time-dependent cp-values that are calculated with a direct time integration according to the Newmark-Wilson-Method and provides the time-dependent section forces for the structure. From the resulting data, the strain-rates can be specified with the formulas (1)-(4). To transform the strain-rate into a speed, only those values are considered which occur beyond the design resistance values of the membrane material. Given the fact that with low membrane forces the strain-rates are higher, a conservative average value of the strain-rates near to a peak is obtained.

$$d\dot{\varepsilon}_{x,total} = d\varepsilon_{x,total} / dt \quad (1)$$

$$d\varepsilon_{x,total} = d\varepsilon_x - d\varepsilon_{x(y)} \quad (2)$$

$$d\varepsilon_x = dn_x / E_x \quad (3)$$

$$d\varepsilon_{x(y)} = dn_y / E_y * v \quad (4)$$

The velocity per time step can be determined for a given length with (5). Therefore the length of the specimens is applied to 200 mm which is chosen according to DIN EN ISO 13934-1.

$$dv_{tensile\ test} = d\dot{\varepsilon}_{x,total} * l_{stripe} \quad (5)$$

The arithmetic mean in a chosen range gives the testing speed and is determined to 512 mm/min. A rounded testing speed of 500 mm/min is set for the strip tensile tests.

4. Mono-axial stiffness behaviour

4.1. Aim

With the dynamic structural analysis, a constant young's modulus is estimated. In order to justify the assumption that the loading speed has no influence on the material stiffness and therewith to ensure the quality of the dynamic structural analysis, mono-axial stiffness tests are performed. At the same time different temperatures around the temperature for crystallization, which is 19°C, are applied to observe if there is an influence on the stiffness when the crystal shape is subject to change from triclinic to hexagonal, as described in chapter 2. The stiffness tests were carried out at the University Duisburg/Essen in Laboratory for Lightweight Structures (ELLF) by testing four different pure PTFE-fabrics applying varying load speeds and temperatures.

4.2. Evaluation of the measurement results

An evaluation of the measurement results showed that the stiffness behavior of pure PTFE-fabric is rather stable against the tested load speeds and temperatures. The young's modulus varies by a factor of maximum 1.3 which is assessed to be insignificant. The tests were conducted in a mono-axial mode. Hence, the values can only be considered as an orientation to evaluate the material's behavior in general. In order to calculate the actual young's modulus, biaxial tensile tests need to be conducted. As a consequence, the factor of deviation would decrease even further. However, this conclusion shall be treated with caution due to the low number of tests been conducted and the load speeds which are distinctly lower than those of further strip tensile tests. Nonetheless they can be adopted as a preliminary assessment for the aim of this study. To specify the strain-rate and temperature dependent stiffness behavior of pure PTFE-fabric in greater detail, more extensive research with a higher number of specimens and higher load speeds needs to be done.

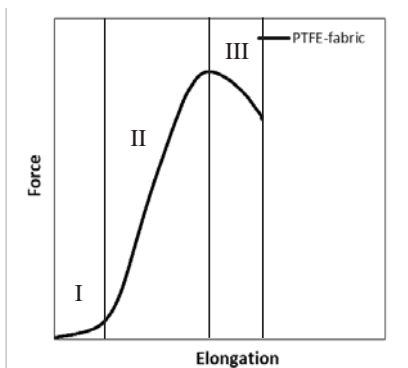
5. Mono-axial tensile tests – strip method

5.1. Aim

A preparatory study in chapter 3 provides the load speed determined for specimens equivalent to a load speed caused by a gust wind. In this chapter strain-rate dependent tensile strengths are examined for the provided testing speed of 500 mm/min and as reference with the standardized testing speed of 100 mm/min. It is expected, that higher strain-rates will cause higher tensile strengths, which further means that manufacturers' specifications, based on the standardized testing speed, might be exceeded by this new approach.

5.2. Definitions

Usually force elongation graphs are generated for tensile tests, where all relevant phases during the entire testing period are illustrated. They all have similar curve characteristics in common. Hereby essentially three phases, which are typical for force-strain curves of pure PTFE-fabrics, can be defined according to figure 5. In phase I the fibers in the fabric, which typically have a waviness are straightened from the beginning of loading until phase II, also known as *construction stretch*. In phase II the fibers are fully straightened and the actual elongation of the fibers begins. During phase II, where the force-strain curve shows an approximately linear-elastic course, the material reaches its *maximum tensile force* and corresponding *maximum tensile elongation* in the graph peak. With phase III fibers begin to tear, which leads to a decrease of force in the strip until the *breaking force* and corresponding *elongation at break* is reached.



Phase I: construction stretch

Phase II: actual elongation + tensile strength

Phase III: fiber tear + breaking force

Figure 5: Definitions for typical force-elongation curve related to PTFE-fabric

A further term is a *jaw break* in tensile tests. This is the case, when specimens break up to 5 mm close to one of the clamping edges. These tests need to be excluded from the evaluation of measurements according to DIN EN ISO 13934-1 and be repeated until the tear occurs optimally in the middle of the strip or more than 5 mm from the clamping edges away.

5.3. Test setup

5.3.1. Tensile testing machine and clamping systems

The tensile tests with the strip method were conducted in the laboratories of the Institute of Building Structures and Structural Design (ITKE) at the University of Stuttgart with the tensile testing machine Zwick/Roell Z 100. For measuring the actual elongation in the specimens with high precision, an extensometer was used. Initially, the suitability of the clamps was examined within test runs which showed that even with various clamping surfaces, either a jaw break or sliding out of clamps occurs. Regarding the test realization, PTFE-fabric has the disadvantage

that its very low coefficient of friction is a challenge to holding the specimens during the tensile test and preventing them from sliding out. On the other hand, too rough surfaces of clamping jaws, like sand paper, causes jaw breaks. Based on this knowledge new clamping systems were developed with the aim to prevent sharp edges in the clamps by using a bolt for an evenly transmission of force into the strip ends. Especially further clamping systems with more than one bolt based on the principle of a pulley were tested successfully. Their big advantage is the halved tensile force in strip ends which avoids jaw breaks exceptionally when testing stronger materials with higher tensile strengths and therewith more concentrated tensile force in the clamps. The clamping systems were tested successfully up to a maximum force of 8 kN and a maximum testing speed of 500 mm/min. Following figures 6-8 show the used clamping systems implemented in the tensile test machine. The associated sketches to the right hand side give an overview of the setup.

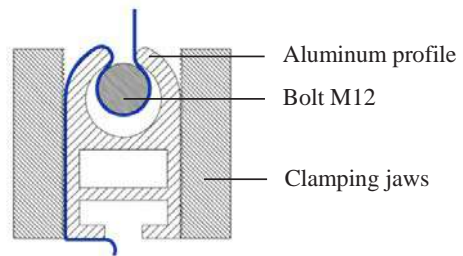
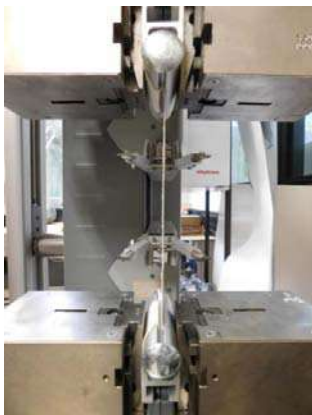


Figure 6: Clamping system 1

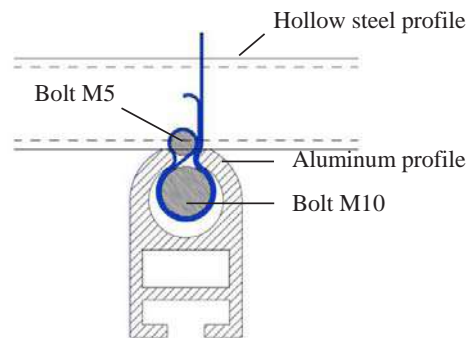


Figure 7: Clamping system 2

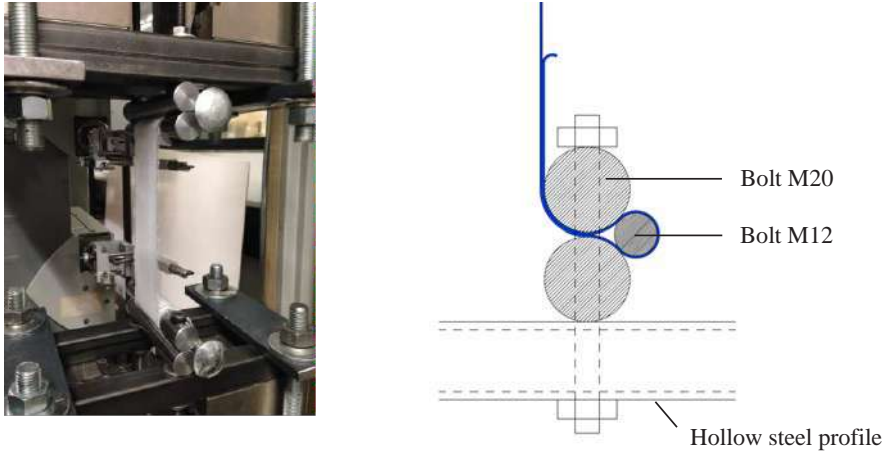


Figure 8: Clamping system 3

5.3.2. Conformity check for clamping systems

To prove the comparability among all measurements by the use of three different clamping systems a conformity check was carried out. All three clamping systems were tested once with the same material and fiber direction as well as the same testing speed. Figure 9 shows the resulting force-elongation curves which prove a high comparability with each other. Thus, hereinafter all measurements will be considered equivalent.

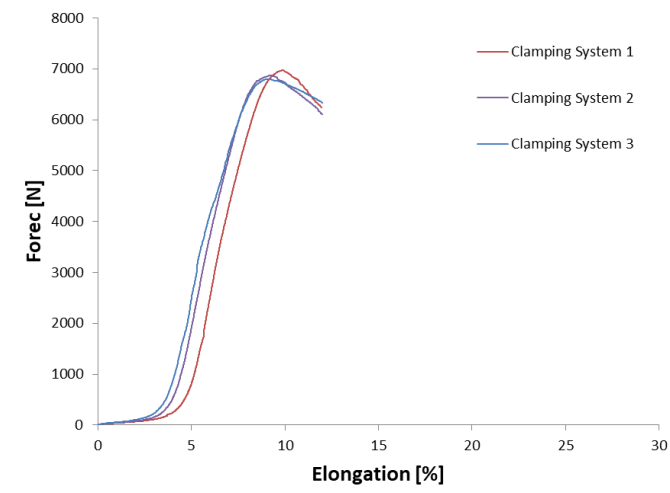


Figure 9: Conformity check for clamping systems

5.3.3. Tested Materials

Four pure PTFE-fabrics from the manufacturers C. Cramer GmbH & Co. KG (CCC) and Sefar Holding AG with differing weaves and grammage were tested as listed in table 1.

Table 1: Properties of tested materials

Tested material	Grammage [g/m ²]	Weave
SUNWEAVE CCC 216 (CCC)	310	Twill
SUNWEAVE CCC 222 (CCC)	770	Special
EL-40-T1 (Sefar)	340	Panama 2-2
EL-35-T2 (Sefar)	550	Linen 1-1

The strips were prepared according to DIN EN ISO 13934-1. For all materials and fiber directions a minimum of 5 specimens were tested for the standardized testing speed of 100 mm/min and a minimum of 3 specimens were tested for the testing speed of 500 mm/min depending on the available amount of testing material.

5.4. Test results and evaluation

For evaluation, only valid tests were considered. Figures 10-12 show one unloaded and same loaded strip for the standardized testing speed and one strip for the testing speed 500 mm/min which picture valid tests.



Figure 10: Unloaded strip



Figure 11: Loaded strip – 100 mm/min



Figure 12: Loaded strip – 500 mm/min

Following figures 13-16 are showing the force-elongation graphs for the materials SUNWEAVE CCC 216 and EL-40-T1. For comparison the curves for both testing speeds are presented together for each case.

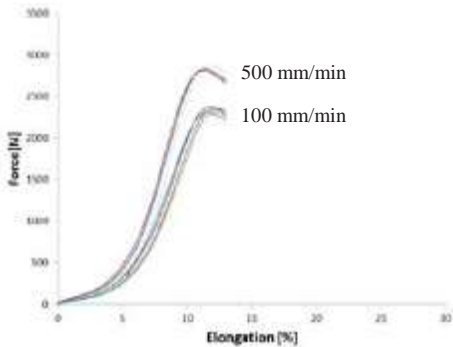


Figure 13: SUNWEAVE CCC 216 (warp)

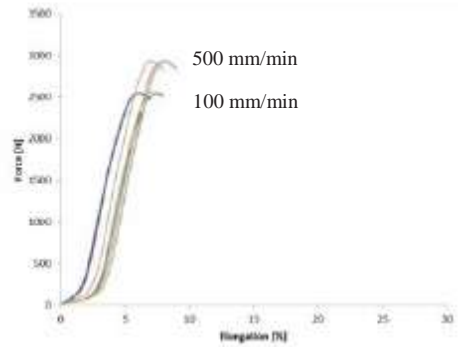


Figure 14: SUNWEAVE CCC 216 (weft)

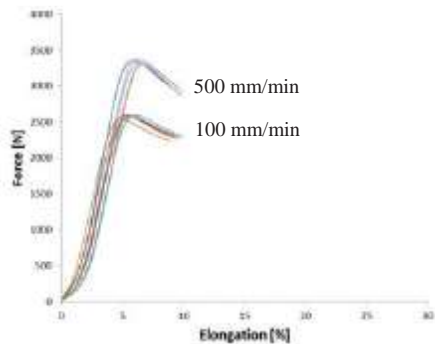


Figure 15: EL-40-T1 (warp)

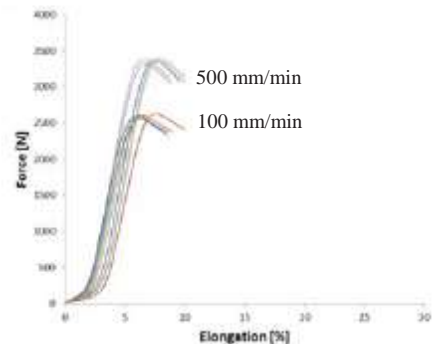


Figure 16: EL-40-T1 (weft)

A statistical evaluation of the test results according to DIN EN 1990-1 (appendix D) provides the 5%-fractiles and therewith the characteristic value for tensile strength. Comparing these, factors are created to clarify the increase in strength due to these two different load speeds. The following table summarizes the factors with the maximum increase being a factor of 1.3.

Table 2: Factor of increase for tensile strengths

SUNWEAVE CCC 216 warp	SUNWEAVE CCC 216 weft	EL-40-T1 warp	EL-40-T1 weft
1.2	1.1	1.3	1.3

It can be observed, that the material EL-40-T1 with a weave-type Panama has a higher increase than the material SUNWEAVE CCC 216 with the weave-type Twill. Other than that, both materials have a comparable grammage and have no further significant differences. This can be explained with the fact, that the PTFE-fibers in fabric are sensitive against perpendicular compression which is closely linked with the type of weave. While the fabric with a structured weave undergoes relatively early a perpendicular compression, the material EL-40-T1 with a more simple form of weave reaches a higher tensile strength because of the later occurrence of perpendicular compression. This phenomena appeared also while developing the clamp system 2 by an occurrence of press between bolt and aluminum profile. Nevertheless it can be summarized that all materials show a considerable increase in tensile strength which makes a more comprehensive investigation interesting.

6. Conclusion

In this study the strain-rate dependent tensile strength of pure PTFE-fabrics was analyzed taking into consideration, that membrane structures underlie the design relevant gust wind load. This load causes higher strain-rates than the recommended testing speeds from the ISO standard for determination of the tensile strength of fabrics. For comparison both, the standardized testing speed and a testing speed in accordance to a gust wind, were carried out. The evaluation of the test results give ground to the expectations and deliver factors for increase of the characteristic tensile strength (5%-fractile) up to 1.3 towards the results based on standardized testing speed. However this knowledge serves as a basis for a first evaluation and needs further investigations. The determination of strain-rates is based on one reference membrane structure with boundary conditions as the membrane geometry, degree of pretension, existing belt elements and others which apply only for this system. To achieve more general conclusions for the strain-rate dependent tensile strength of pure PTFE-fabric a more extensive research needs to be done. Here we especially recommend tests based on various systems to investigate the range of strain-rates for main system boundary conditions, as well as a higher number of specimens for the conducted tensile tests.

Acknowledgements

A very special thanks go to the Institute of Construction Materials (IWB), the Institute of Building Structures and Structural Design (ITKE) at the University of Stuttgart and the Institute for Metal and Lightweight Structures at the University of Duisburg/Essen who supported this work. Further thanks go to A. Arnegger GmbH for providing the test materials.

References

Bradatsch, Michalski, Wagner (2017/2018), *Großschirme für wandelbare Klimadächer*. In: *Bauingenieur*, vol. 2017/2018 (pp: 68-80).

DIN EN 1990 – 2002-12: *Basis of structural design*.

DIN EN ISO 13934-1 – 2013-08: *Textiles – Tensile properties of fabrics – Part 1: Determination of maximum force and elongation at maximum force using the strip method*.

Knippers, Cremers, Gabler, Lienhard (2011): *Construction Manual for Polymers + Membranes*. First edition. Munich.

Natalie Stranghöner, Jörg Uhlemann et al. (2016): *Prospect for European Guidance for the Structural Design of Tensile Membrane Structures. Support to the implementation, harmonization and further development of Eurocodes*. Luxembourg.

Pro-K Fluorpolymergroup – Industrieverband Halbzeuge und Konsumprodukte aus Kunststoff e.V., Technisches Merkblatt 02 – *Einführung in die Verarbeitung von PTFE-Kunststoffen*, www.pro-kunststoff.de.

Sina Ebnesajjad (2017): *Expanded PTFE Applications Handbook – Technology, Manufacturing and Applications*. USA

SOFISTIK AG – FEM.

Proceedings of the TensiNet Symposium 2019

Softening the habitats / 3-5 June 2019, Politecnico di Milano, Milan, Italy
Alessandra Zanelli, Carol Monticelli, Marijke Mollaert, Bernd Stimpfle (Eds.)

Architectural woven fabrics: Is it possible to classify stiffness values in correlation with strength values?

Jörg UHLEMANN*, Natalie STRANGHÖNER*

*University of Duisburg-Essen, Institute for Metal and Lightweight Structures, Universitätsstr. 15, 45141 Essen, Germany,
joerg.uhlemann@uni-due.de

Abstract

Down to the present day, the determination of stiffness parameters for architectural fabrics, mainly used as coated woven fabrics, is a field of intense discussion. Designers and material producers are affected by an existing uncertainty. The present contribution investigates the possibility to provide tables of stiffness parameters for specific materials in which stiffness values are given dependent on the material's tensile strength. The focus is on PVC-coated polyester fabrics as the most commonly used material for textile architecture. Materials of four different material producers and of different strength classes have been tested experimentally. Stiffness parameters have been determined based on a standardized test and evaluation method and have been statistically evaluated and compared. In order to achieve a required basis, standardized and project specific biaxial test procedures are presented and analysed in combination with established evaluation procedures.

A tabulation of stiffness parameters would be of great help for design engineers and material producers. The presented results indicate the possibility of a classified tabulation for the investigated materials.

Keywords: architectural coated woven fabrics, PES/PVC fabrics, mechanical properties, stiffness parameters, biaxial test

DOI: 10.30448/ts2019.3245.06

Copyright © 2019 by Jörg Uhlemann and Natalie Stranghöner. Published by Maggioli SpA with License Creative Commons CC BY-NC-ND 4.0 with permission.

Peer-review under responsibility of the TensiNet Association

1. Introduction

The material behaviour of coated architectural fabrics is well known to be nonlinear, viscoelastic and usually orthogonal anisotropic (orthotropic). Due to the lack of technically mature alternative models, the actual nonlinear viscoelastic material behaviour is modelled in the design practise with a linear elastic approach. The inhomogeneous composite is idealized as a homogenous continuum, assuming a plane stress state. Besides the low shear stiffness of fabrics – which is neglected in the frame of this contribution – tensile stiffnesses E (Young’s moduli) and Poisson’s ratios ν in both principal directions warp and weft are used:

$$\begin{bmatrix} \varepsilon_x \\ \varepsilon_y \end{bmatrix} = \begin{bmatrix} \frac{1}{E_x} & -\frac{\nu_{xy}}{E_y} \\ -\frac{\nu_{yx}}{E_x} & \frac{1}{E_y} \end{bmatrix} \begin{bmatrix} \sigma_x \\ \sigma_y \end{bmatrix} \quad (1)$$

where ε is the strain and σ is the membrane stress (for fabrics given in the unit force per length [kN/m]). The compliance matrix is composed of four elastic constants. For the indices of the Poisson’s ratios the following is defined: the first index indicates the direction of contraction, the second index indicates the direction of stress that causes the contraction. The x-direction refers to warp and the y-direction to weft.

The requirement for a symmetrical compliance matrix leads directly to the fact, that the terms with Poisson’s ratios are identical. Herewith, only three of the four elastic constants are independent of each other. Usually, a set of elastic constants is given by the two tensile stiffnesses E_x and E_y and is completed by one Poisson’s ratio. In case of anisotropy and assuming $E_x > E_y$, one will get $\nu_{yx} > \nu_{xy}$.

Different from isotropic materials, the Poisson’s ratios have not to fulfil the requirement of $\nu < 0.5$. According to the theory of anisotropic elasticity, the requirement $\nu_{xy} \cdot \nu_{yx} < 1$ must be fulfilled (Lempriere, 1968). As some fabrics show huge transverse contractions, this is of great advantage.

Biaxial tensile tests are conducted on plane test specimens under in-plane stress in order to determine the stiffness parameters. The magnitude of stiffness parameters depends very much on the applied stress ratios warp:weft as well as on the stress magnitude and the load protocol, i. e. number of load cycles and whether hold times are scheduled or not etc.

Because stress ratios and stress levels for prestress and maximum stress under service loads are different for every membrane structure, stiffness parameters obtained from standardized methods cannot be used – or only as a rough approximation. Modifications or adjustments of the load protocol and/or the evaluation methods are essential and must be specified individually

for each project. This leads to “design elastic constants”. However, to provide the design engineer a tool with which stiffness properties of different materials can be compared, a standardized test and evaluation procedure is desired (Schmidt, 2012). This leads to “comparative elastic constants“, see Figure 1.

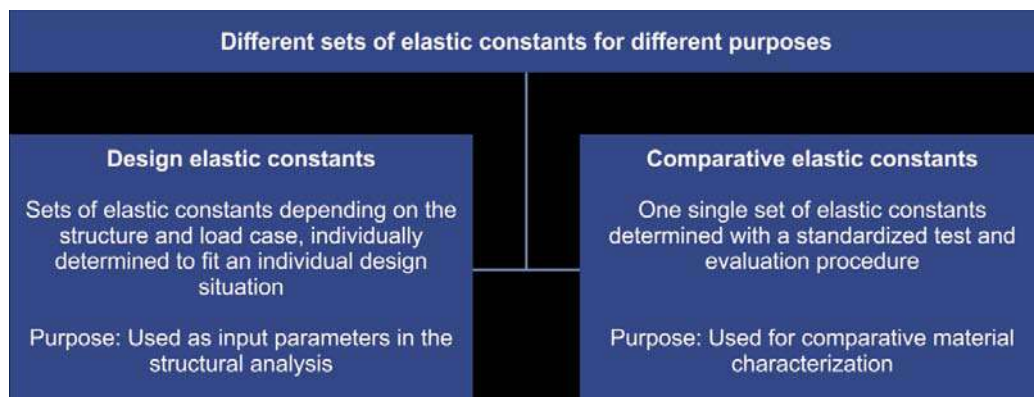


Figure 1: Different sets of elastic constants for different purposes

In a first step, the present contribution discusses possibilities for (a) a standardized determination of elastic constants (comparative elastic constants) and (b) individual determination methods, tailored for individual structures and load cases (design elastic constants). In a second step, it is investigated whether stiffness properties of PVC-coated polyester(PES)-fabrics can be classified. This investigation is conducted experimentally by means of random samples of strength types II, III and IV. A classification would enable a tabulation of stiffness parameters. Such a tabulation would be of great help for design engineers for appropriate assumptions of stiffness parameters as well as for material producers to support the material characterization. The present contribution is an updated version of Uhlemann & Stranghöner (2017).

2. Standardized comparative vs. design oriented stiffness parameters

In the past, several attempts tried to standardize biaxial test and evaluation methods for the determination of elastic constants of architectural fabrics (ASCE/SEI 55-10; Blum, Bögner, & Némóz, 2004; MSAJ/M-02-1995; Société d'Édition du Bâtiment et des Travaux Publics, 2009). Nevertheless, the Japanese guideline MSAJ/M-02-1995 was the only one providing a sufficient precise procedure for reproducible biaxial testing and for the evaluation of the recorded test data (Uhlemann, 2016). However, the results are rather “fictitious” elastic constants: they are a linear approach to nonlinear material behaviour and they are not able to model all measured stress-strain paths in acceptable approximations simultaneously. For a more detailed background on MSAJ/M-02-1995, see Uhlemann & Stranghöner (2017).

Recently, the novel European biaxial test standard EN 17117-1 for the determination of elastic constants for coated fabrics has been published. This standard emphasizes the importance of design elastic constants and offers principles to set up individual design oriented load protocols and evaluation procedures. Examples known from literature are listed as a first orientation. On the other hand, EN 17117-1 provides also a precisely defined load protocol and evaluation procedure to achieve reproducible comparative elastic constants. The basic features are oriented towards the Japanese guideline MSAJ/M-02-1995, e. g. the load profile consists of the three biaxial stress ratios warp:weft 1:1, 2:1 and 1:2 as well as of the two monoaxial stress ratios 1:0 and 0:1. But single weaknesses of the Japanese guideline (van Craenenbroeck et al., 2016; Uhlemann, 2016) are improved, e. g. a prestress level is considered in the load protocol and further load cycles are added so that for all stress ratios three load cycles are scheduled. For the determination of comparative elastic constants, a precise evaluation procedure is stated based on the least squares method minimizing the strain error. As comparative elastic constants are not used as input parameters in a structural analysis, they do not have to fulfil the mechanical restrictions described above, i. e. the Poisson's ratios are not limited. Thus, the measured stress-strain behaviour can be characterized more accurately and different materials that behave differently can be better distinguished.

As the linear elastic orthotropic constitutive model is not able to completely cover the fabric behaviour, i. e. acceptable modelling of all stress ratios simultaneously is impossible, it is required to determine structure and load case dependent sets of elastic constants individually. This is possible for instance by focusing on the evaluation of specific stress ratios of MSAJ- or EN 17117-1-tests. Stress ratios that are not expected to occur in a specific membrane structure or in a specific load case are disregarded in the evaluation. For instance, monoaxial stress ratios do not usually appear in synclastic structures, thus they can be disregarded in the evaluation. This method has already been intensely discussed in Uhlemann, Stranghöner, Schmidt & Saxe (2011).

Apparently, it is more appropriate to tailor the load protocol as well. This is actually demanded and performed in practise, see e. g. Stimpfle & Günther (2016). Refined methods for individual load protocol set ups and evaluation procedures are stated in Uhlemann (2016). However, all tailored methods require sufficient assumptions of the stress ratios over a membrane surface under a specific load. These assumptions can be made in the frame of a preliminary structural analysis. A sufficient preliminary structural analysis, in turn, requires appropriate start values for the stiffness parameters. The presentation of appropriate stiffness parameters fitting the basic shapes of membrane structures and the most relevant fabrics in a tabulated form would be of great help for design engineers for this task.

3. Investigations into tabulating stiffness parameters for architectural fabrics

This contribution presents comparisons of standardized stiffness parameters of PVC-coated PES fabrics types II, III and IV. Products with similar tensile strength properties of four different material producers are compared. The material producers are numbered arbitrarily in order to maintain anonymity. Only “traditionally coated” fabrics are considered here, i. e. fabrics which are prestressed in weft direction during the coating process are not included. All experimental tests have been performed in the Essen Laboratory for Lightweight Structures (ELLF), belonging to the Institute for Metal and Lightweight Structures of the University of Duisburg-Essen.

The tensile strength properties of all investigated materials have been measured at $T = 23\text{ }^{\circ}\text{C}$ according to DIN EN ISO 1421 and are given in Table 1 as mean values. The fabrics are classified according to the type classification presented in Stranghöner et al. (2016). Table 1 illustrates that the investigated materials have similar strength magnitudes when compared typewise.

Table 1: Tensile strength (mean values) and statistical data at $T = 23\text{ }^{\circ}\text{C}$ of the investigated coated fabrics of different material producers

Producer	Warp			Weft		
	Tensile strength $f_{m,23}$ [kN/m]	Standard deviation [kN/m]	Coeff. of variation [%]	Tensile strength $f_{m,23}$ [kN/m]	Standard deviation [kN/m]	Coeff. of variation [%]
PES-PVC Type II						
1	95.5	2.7	2.9	93.3	1.4	1.5
2	87.5	3.1	3.6	92.6	4.6	4.9
3	91.4	0.7	0.7	84.1	1.8	2.1
PES-PVC Type III						
1	127.3	1.2	0.9	113.6	1.3	1.2
2	129.4	1.4	1.1	120.2	2.8	2.3
3	118.9	2.1	1.8	104.1	1.6	1.5
4	123.7	5.6	4.5	107.8	4.4	4.1
PES-PVC Type IV						
1	167.4	1.3	0.8	162.0	0.8	0.5
2	167.9	2.9	1.7	160.6	3.4	2.1

Stiffness parameters have been achieved from biaxial tests and have been computed as fictitious elastic constants according to MSAJ/M-02-1995 using the least squares method minimizing the strain error. They are fitted to all five tested stress ratios simultaneously. Note, that in the original MSAJ-evaluation – as used here – the stress-strain paths of the unloaded directions in the monoaxial stress ratios are disregarded. The resulting sets of fictitious elastic constants are given in Table 2 for PES-PVC type II, in Table 3 for PES-PVC type III and Table 4 for PES-

PVC type IV. As an example, Figure 2 illustrates for all type III biaxial tests the small deviation of the evaluated stress-strain paths in the five stress ratios.

The deviation of tensile stiffness values (Young's moduli) is found to be very low. The impact of this deviation range on structural analysis results can be assumed to be negligible, see Bridgens & Birchall (2012), Uhlemann & Stranghöner (2013), Uhlemann, Stranghöner & Saxe (2015), van Craenenbroeck (2016). On the contrary, the deviations of the Poisson's ratios are higher. Nevertheless, the absolute values of the Poisson's ratios are still small, so that only a small impact is expected on structural analysis results (Uhlemann et al., 2015; Uhlemann & Stranghöner, 2013). From a practitioner's point of view, the stiffness properties appear to be independent of the material producer in this random sample. Comparing Tables 2, 3 and 4 with Table 1, a positive correlation of tensile stiffness and strength can be observed. Additionally, distinct differences of stiffness properties of types II, III and IV become obvious. The small deviations of stiffness properties – from batch to batch (Schmidt, 2012) as well as from producer to producer – indicate, that standardized stiffness properties of PES-PVC fabrics of types II, III and IV can be tabulated.

On the basis of the presented experimental investigations and statistical evaluations, a first proposal of sets of fictitious elastic constants according to MSAJ/M-02-1995 for PES-PVC fabrics types II, III and IV is presented in Table 5 based on mean values.

Basically, a classification is only possible for standardized and reproducible tests. It seems likely to carry out such a classification on the basis of the new European biaxial test standard EN 17117-1 instead of MSAJ/M-02-1995. Tabulated stiffness values according to the procedure of EN 17117-1 could serve as a first rough approximation of stiffness properties for preliminary design calculations in a European design context. However, it must be ensured that for an individual fabric structure all relevant stress-strain paths can be modelled in acceptable approximation by the tabulated sets of elastic constants and that the mechanical constraints are considered. In order to ensure safe and economic stiffness parameters, it is recommended to evaluate stiffness parameters from design oriented biaxial tests. Nonetheless, for fabrics that can be tabulated in general it is imaginable to tabulate design oriented stiffness parameters for different structural configurations. They could be tabulated depending on specific stress ratios and stress magnitudes. Herewith, the designer could directly specify appropriate stiffness parameters for the use as input parameters in the design of different shapes of membrane structures and different load situations.

Biaxial “compensation tests” – performed to measure pattern compensation values which in turn ensure a target prestress in the membrane structure – are not affected by the proposed classifications. The determination of compensation values is based on the irreversible constructional stretch of a fabric after unloading. It is well known that this measure strongly

deviates from producer to producer and from batch to batch. That means, project oriented biaxial compensation tests remain inevitable.

Table 2: Sets of experimentally determined fictitious elastic constants according to MSAJ/M-02-1995 for PES-PVC fabrics type II of three different material producers

PES-PVC Type II			
Producer	Tensile stiffness		Poisson's ratio ν_{yx} [-]
	E_x [kN/m]	E_y [kN/m]	
1*	738	456	0.21
	758	534	0.17
	744	462	0.21
Mean value producer 1	747	484	0.20
2**	664	530	0.05
	720	542	0.04
Mean value producer 2	692	536	0.05
3	699	508	0.13
Statistical evaluation including all producers			
Mean value***	713	514	0.12
Standard deviation***	30	27	0.08
Coefficient of variation [%]***	4.2	5.3	62.9

* Three coating batches were available from producer 1.

** Only one coating batch was available from producer 2.

*** The statistical evaluation is based on mean values per producer, if available.

Table 3. Sets of experimentally determined fictitious elastic constants according to MSAJ/M-02-1995 for PES-PVC fabrics type III of four different material producers

PES-PVC Type III			
Producer	Tensile stiffness		Poisson's ratio ν_{yx} [-]
	E_x [kN/m]	E_y [kN/m]	
1*	978	650	0.10
	990	662	0.10
	974	648	0.10
	972	646	0.10
Mean value producer 1	979	652	0.10
2**	972	646	0.00
	972	646	0.00
	984	658	0.00
Mean value producer 2	976	650	0.00
3	963	644	0.09
4	1060	708	0.03
Statistical evaluation including all producers			
Mean value***	994	663	0.06
Standard deviation***	44	30	0.05
Coefficient of variation [%]***	4.5	4.5	87.2

* Three coating batches were available from producer 1. One batch has been tested two times.

** Two coating batches were available from producer 2. One batch has been tested two times.

*** The statistical evaluation is based on mean values per producer, if available.

Table 4. Sets of experimentally determined fictitious elastic constants according to MSAJ/M-02-1995 for PES-PVC fabrics type IV of two different material producers

PES-PVC Type IV			
Producer	Tensile stiffness		Poisson's ratio ν_{yx} [-]
	E_x [kN/m]	E_y [kN/m]	
1	1274	786	0.13
2	1222	812	0.03

Table 5. Proposal of sets of fictitious elastic constants according to MSAJ/M-02-1995 for PES-PVC fabrics types II, III and IV (mean values)

PES-PVC			
Type	Tensile stiffness		Poisson's ratio ν_{yx} [-]
	E_x [kN/m]	E_y [kN/m]	
II	710	510	0.12
III	990	660	0.06
IV	1250	800	0.08

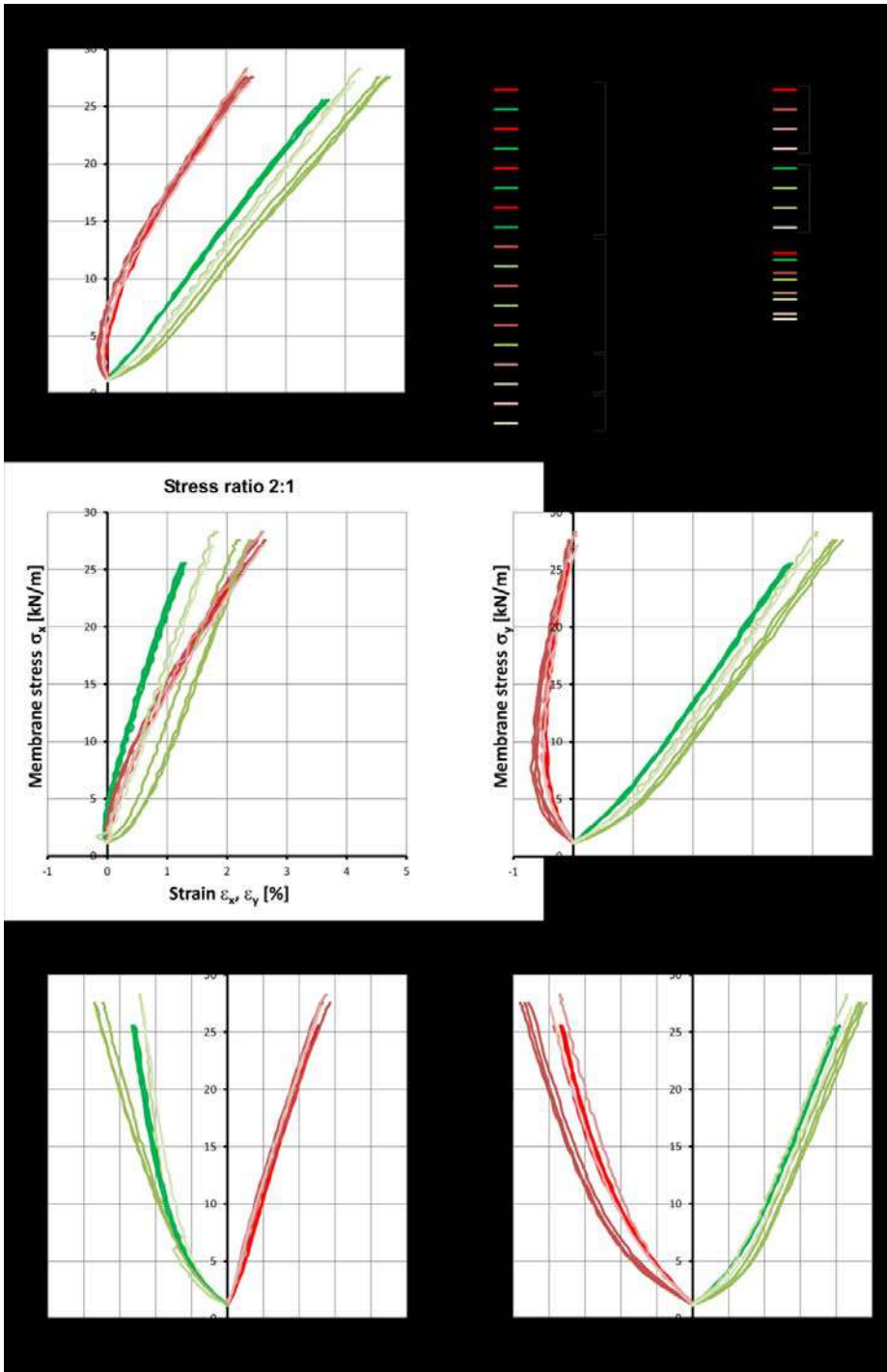


Figure 2: Evaluated stress-strain paths for all PES-PVC type III tests

4. Conclusions

In a first step, methods for a standardized as well as for a design oriented determination of stiffness parameters have been presented and discussed. In a second step, it could be shown that stiffness parameters of PVC-coated PES-fabrics can be classified correlated only to the tensile strength or strength classification, respectively. To come to this conclusion, a random sample of fabrics types II, III and IV has been tested.

A tabulation of either standardized or structure and load case dependent stiffness parameters appears to be possible for the investigated PES-PVC fabrics. This can be of great help for design engineers handling the difficult task of choosing appropriate stiffness parameters for architectural fabrics. As a first proposal, on the basis of the presented experimental investigations and statistical evaluations, sets of fictitious elastic constants according to MSAJ/M-02-1995 for PES-PVC fabrics types II, III and IV are presented as mean values. Thereby, the stress-strain paths of the five tested stress ratios of the MSAJ test procedure are implicitly fitted simultaneously by the fictitious elastic constants – as good as achievable by the MSAJ evaluation procedure.

In the framework of the research project „Charakterisierung und Modellierung des nichtlinearen Materialverhaltens von beschichteten Gewebemembranen für Membranstrukturen im Bauwesen“ (Characterization and modelling of the nonlinear material behaviour of coated fabrics for membrane structures), funded by Deutsche Forschungsgemeinschaft DFG (German Research Foundation), the determination of appropriate stiffness parameters is going to be further developed at the Institute for Metal and Lightweight Structures of the University of Duisburg-Essen. Simultaneously, the suitability of simplified assumptions for stiffness parameters as it is used since decades in the membrane structure design will be reviewed systematically with the help of membrane component tests on a novel membrane component test stand.

Acknowledgements

The authors would like to thank the following material producers for providing testing material for the presented investigations (given in alphabetical order): Heytex Bramsche GmbH, Bramsche, Germany, Mehler Technologies GmbH (now: Low & Bonar), Hückelhoven, Germany, Sattler AG, Gössendorf, Austria and Verseidag-Indutex GmbH, Krefeld, Germany. Furthermore, the authors would like to thank Deutsche Forschungsgemeinschaft DFG (German Research Foundation) for funding the research project “Charakterisierung und Modellierung des nichtlinearen Materialverhaltens von beschichteten Gewebemembranen für Membranstrukturen im Bauwesen” (Characterization and modelling of the nonlinear material behaviour of coated fabrics for membrane structures) (STR482/5-1).

References

- ASCE/SEI 55-10 (2010). Tensile Membrane Structures. American Society of Civil Engineers.
- Blum R., Bögner H. & Némoz G. (2004). Testing Methods and standards. In: Forster B. & Mollaert M. (Eds.), *European design guide for tensile surface structures* (pp. 219–241), TensiNet.
- Bridgens B. & Birchall M. (2012). Form and function: The significance of material properties in the design of tensile fabric structures. *Engineering Structures*, vol. 44, pp. 1–12.
- DIN EN ISO 1421:2017-03. Mit Kautschuk oder Kunststoff beschichtete Textilien – Bestimmung der Zugfestigkeit und der Bruchdehnung (ISO 1421:2016); Deutsche Fassung EN ISO 1421:2016.
- FprEN 17117-1:2018-05. Rubber or plastics-coated fabrics – Mechanical test methods under biaxial stress states – Part 1: Tensile stiffness properties.
- Lempriere B. M. (1968). Poisson's ratio in orthotropic materials. *AIAA Journal*, vol. 6(11), pp. 2226–2227.
- MSAJ/M-02-1995 (1995). Testing Method for Elastic Constants of Membrane Materials. Membrane Structures Association of Japan.
- Schmidt H. (2012). Steifigkeitseigenschaften textiler Membranen: Studie zur Gewährleistung durch den Hersteller – Schlussbericht August 2012: Auftraggeber: Verseidag Indutex GmbH, Krefeld. unpublished.
- Société d'Édition du Bâtiment et des Travaux Publics (Ed.) (2009). Recommandations pour la conception, la confection et la mise en oeuvre des ouvrages permanents de couverture textile: Édition 2009 (Éd. 2009). Paris: SEBTP.
- Stimpfle B. & Günther D. (2016). A Project Oriented Approach to Determine Membrane Properties. *Procedia Engineering*, vol. 155, pp. 81–88.
- Stranghöner N., Uhlemann J., Bilginoglu F., Bletzinger K.-U., Bögner-Balz H., Corne E., Gibson N., Gosling P., Houtman R., Llorens J., Malinowsky M., Marion J.-M., Mollaert M., Nieger M., Novati G., Sahnoune F., Siemens P., Stimpfle B., Tanev V., Thomas J.-Ch. (2016). Prospect for European guidance for the Structural Design of Tensile Membrane Structures: Support to the implementation, harmonization and further development of the Eurocodes. JRC Science and Policy Report, European Commission, Joint Research Centre, Editors: Mollaert M., Dimova S., Pinto A., Denton St., EUR 25400 EN, European Union.
- Uhlemann J., Stranghöner N. & Saxe, K. (2015). Tensile structures: Investigations into the determination of elastic constants of fabrics. *Journal of the International Association for Shell and Spatial Structures*, vol. 56(1), pp. 25–35.

- Uhlemann J. (2016). *Elastic Constants of Architectural Fabrics for Design Purposes*. Dissertation, Schriftenreihe Institut für Metall- und Leichtbau, Universität Duisburg-Essen, Band 3, Shaker Verlag, Aachen.
- Uhlemann J. & Stranghöner N. (2013). Einfluss fiktiver elastischer Konstanten von textilen Gewebemembranen in der Tragwerksanalyse von Membranstrukturen. *Stahlbau*, vol. 83(9), pp. 643–651.
- Uhlemann J. & Stranghöner N. (2017). Steifigkeitskennwerte von Gewebemembranen – standardisiert auf Produktebene und bauwerksspezifisch für die Konstruktion. *Stahlbau*, vol. 86(4), pp. 357–365.
- Uhlemann J., Stranghöner N., Schmidt H. & Saxe K. (2011). Effects on Elastic Constants of Technical Membranes Applying the Evaluation Methods of MSAJ/M-02-1995. In: Proceedings of the STRUCTURAL MEMBRANES 2011, Barcelona.
- van Craenenbroeck M. (2016). *Biaxial testing of fabrics – test methodologies and their impact on material parameters and the structural design process*, PhD-Thesis, Vrije Universiteit Brussel.
- van Craenenbroeck M., Puystiens S., de Laet L., van Hemelrijck D. & Mollaert M. (2016). Quantitative Study of the Impact of Biaxial Test Protocols on the Derived Material Parameters for a PVC Coated Polyester Fabric. *Procedia Engineering*, vol. 155, pp. 220–229.

Uniaxial Strip and Grab Test Methods for Tensile Testing of Architectural Fabrics

Hastia ASADI*, Jörg UHLEMANN*, Natalie STRANGHÖNER*

*University of Duisburg-Essen, Institute for Metal and Lightweight Structures, Universitätsstr. 15,
45141 Essen, Germany,
hastia.asadi@uni-due.de

Abstract

One of the most important mechanical properties of architectural fabrics is the tensile strength, which is measured by uniaxial tensile tests. Considering gripped width of the specimens, there are two principal kinds of uniaxial tensile strength tests: strip and grab tests. In the strip test, the test specimen is clamped over the whole width whereas in the grab test only the middle part of the width is clamped. Both are included in test standards for uncoated and coated fabrics. These test standards are also applied in the context of textile architecture. Until now, only few studies have focused on them. The users and constructional partners are left alone to decide which test method fits better for structural applications. Frequently it is assumed that the choice depends on the specific architectural textile to be tested, e. g. woven or knitted fabric, coated or uncoated, rather stiff or rather flexible coating etc. In one standard, the grab test is recommended as an alternative when the strip test leads to clamp fractures. In this paper, these two uniaxial tensile testing methods are compared based on experimental investigations according to EN ISO 1421. Different types of architectural fabrics have been investigated to carve out the differences regarding their tensile strength and modes of fracture observed by each test method. The objective is to assess a general applicability and to compare the shortcomings of both test methods. A recommendation for tensile testing for structural engineering applications is provided.

Keywords: architectural fabrics, mechanical properties, tensile strength, uniaxial strip test, uniaxial grab test.

DOI: 10.30448/ts2019.3245.07

Copyright © 2019 by Hastia Asadi, Jörg Uhlemann, Natalie Stranghöner. Published by Maggioli SpA with License Creative Commons CC BY-NC-ND 4.0 with permission.

Peer-review under responsibility of the TensiNet Association

1. Introduction

The strength of coated fabrics is significantly influenced by the strength of their yarns. But the yarn's strength decreases due to the weaving and coating process, and also because of the yarn deformation while crossing perpendicular yarns. Due to this deformation, tensile bearing capacity is reduced by the occurrence of an additional bending moment. This effect can cause different tensile strengths in warp and weft direction while the material of the yarn is the same. Herewith, it can be concluded, that the strength of woven and coated fabric is less than the sum of the strength of individual yarns at a specific width, see also (Blum, Bögner and Némoy, 2004). For structural fabrics, the design engineer needs to know the tensile strength of the material, i. e. the maximum membrane stress or the membrane stress at break. For fabrics, the membrane stress is given in the unit force per length (e. g. kN/m). For the design process, the experimentally achieved tensile strength is reduced by further factors to consider e. g. ageing effects and safety requirements, so that a design value for the tensile strength is acquired. The design engineer can compare this design value to the computed membrane stress in a membrane structure, ensuring that the occurring membrane stress is smaller than the design value of the tensile strength of the material used. To get the material's tensile strength, a test method is strongly required where the stress distribution over the specimen width is well known. Only this knowledge makes it possible to compute the tensile strength from the breaking (or maximum) force directly measured by the testing machine. Any tensile test performed for structural design purposes must fulfill this requirement. Moreover, the design engineer is interested in the uniaxial stress-strain behavior of a structural fabric in order to get first information on the stiffness of the material. For further characterization of the material stiffness, biaxial tensile tests are recommended.

To quantify the tensile strength of fabrics, two testing methods are available: strip and grab tests. The strip method tests a strip gripped in the jaws over the full width and provides both the breaking (or maximum) force and its corresponding elongation, see Table 1. The second technique, the grab test, measures the uniaxial force on a sample which is gripped only in the middle part of the width. Regarding the European testing standards, EN ISO 1421 and EN ISO 13934-2, it is capable to extract only the maximum force, see Table 1. Both testing methods were originally developed for uncoated clothing textiles. Today, both testing methods are included in test standards which are also used to test structural fabrics. In the presented investigation, it is analyzed in how far the strip and the grab test method according to EN ISO 1421 fulfill the aforementioned requirement for architectural fabrics with different properties. Two main attempts have been carried out to accomplish the relationship between grab and strip test empirically by Walen (1916) and Eeg-Olofsson and Bernskiöld (1956). Furthermore, Pan (2003) developed a physical relationship assuming a roughly linear mechanical behaviour. In the following, Wu and Pan (2005) verified this theoretical model.

In general, the preparation of a grab test (cut strip method) is easier than the preparation of a strip test (raveled strip). In addition, the accidental stretching of fabrics in the cloth industry usually occurs on a portion of the cloth, i. e. a local stretching while adjacent regions are unstretched. This means, that the grab method is more useful here. But on the other hand, results of strip tests are easier to interpret and in real fabric structures under different loading combination, stretching occurs on larger areas of the structure. In these areas, all yarns are contributing in carrying loads. This phenomenon is more similar to the strip method.

In this study grab and strip tests are compared using PVC-coated woven polyester (PES/PVC), uncoated woven polyester (PES) and polyurethane-coated knitted polyester (PES/PU) according to EN ISO 1421. All tests have been performed in the Essen Laboratory for Lightweight Structures (ELLF), belonging to the Institute for Metal and Lightweight Structures of the University of Duisburg-Essen, Germany.

2. Tensile tests for fabrics

For fabrics, the tensile strength is the force at which a large number of yarns break simultaneously in either warp or weft direction. The test standards, e. g. EN ISO 1421, aim to measure the maximum tensile or breaking force. But for structural membrane applications, the design engineer requires the strength given as a stress. For fabrics, stress is given in form of “membrane stress”, i. e. in force per unit length. Thus, the force measured in the tensile test must be converted to a membrane stress. To be able to do this, the stress distribution over the specimen width must be well known. In this contribution, the term tensile strength is related to the membrane stress. It is not possible to develop the same probabilistic test or analysis approach suitable for measuring the tensile strength of all type of architectural coated fabrics, because of the existence of different coatings and yarns (Lei, 2010). Lei stated that “a practical approach is to establish a specific test procedure and analysis methodology suitable for several given fabric material types, and then to modify the methodology to other types of fabric materials”.

The tensile strength of the base material or seams are measured by tensile tests. This test is specified in international and European standards as EN ISO 1421, EN ISO 13934-1, EN ISO 13934-2. Particularly for Germany, DIN 53354 and the guideline of Deutsches Institut für Bautechnik (DIBt) for acceptance tests of coated fabrics and their joints exist. In the US, ASTM D 5034 and ASTM D 5035 regulate tensile tests for fabrics. Three different types of tensile testing machines can be used: constant rate of extension (CRE), constant rate of load (CRL) and constant rate of traverse (CRT). For tests according to EN ISO 1421 and also to EN ISO 13934, a CRE machine is required. As already mentioned, EN ISO 1421 specifies two methods: the strip method which is used for the determination of the tensile strength (force) and its corresponding elongation and the grab method which is only used for the determination of the tensile strength (force). They are described to be interchangeable and for some cases it is

proposed to use the grab method instead of the strip method. On the other hand, ASTM D 5035 and EN ISO 13934-1 are specifying only strip tests, while ASTM D 5034 and EN ISO 13934-2 are limited to grab tests. In Table 1, the uniaxial test procedures for strip and grab tests according to EN ISO 1421 are summarized.

Table 1: Comparison of strip and grab test procedure according to EN ISO 1421.

Parameters	Strip Test	Grab Test
Jaw distance	200 mm \pm 1 mm or 150 mm \pm 1 mm or 100 mm \pm 1 mm	100 mm \pm 1 mm or 75 mm \pm 1 mm
Width of specimen	50 mm \pm 1 mm	100 mm
Gripping Width	50 mm \pm 1 mm	25 mm \pm 0.5 mm
Mounting state	Pretension setting or slack mounting	-
Rate of moving clamp	Constant rate of 100 mm/min \pm 10 mm/min	
Slippage	Disregard test results where specimen slips asymmetrically or by more than 2 mm. Or record them when they are useful.	
Jaw breaks	Disregard the test results where test piece breaks within 5 mm of the face of a jaw or outside the reference marks on the specimen. Or record them when they are useful.	Disregard the test results where test piece breaks within 5 mm of the face of a jaw. Or record them when they are useful.
Results	Maximum force, force at break (if it differs from maximum force), elongation at maximum force and elongation at break (if it differs from elongation at maximum force)	Maximum force

3. Strip and grab tensile strength

As already explained, in strip tests, the width of specimen is gripped completely while in grab tests, the specimen is gripped only in the middle of the width. Therefore, the grab specimen is basically divided in to two portions, the gripped part and the ungripped parts on both sides (Pan, 2003). When the clamps start to move away from each other, first only the gripped threads between them are elongated (see A and A₁ in Fig. 1). But little by little, transverse threads (a and a₁) cause some elongation in adjacent yarns (B and B₁) and gradually this trend is continuing

until rupture. For a coated fabrics, the force distributing function of the transverse yarns can additionally result from the coating, depending on the stiffness of the coating.

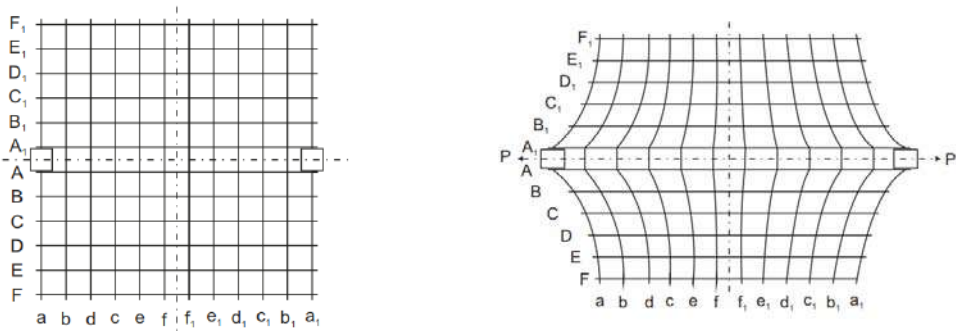


Figure 1: Grab test specimen, left: before stretching and right: while stretching (Eeg-Olofsson and Bernskiöld, 1956).

Eeg-Olofsson and Bernskiöld (1956) carried out grab and strip tests with the same specimen size (same length while widths of the strips were equal to gripping width of the grab specimens) on continuous filament rayon (viscos rayon 120/30 den in warp and weft). They changed the width of the jaws and observed that the breaking force achieved from grab tests is higher than the one achieved from strip test of the same width by a constant value which is independent of the width of the jaws. They also implied that the difference between the grab and strip test results should vary by changing the clamp distance (specimen length). While the clamp distance is decreasing, the difference of the results of both testing types is decreasing as well. It should be noticed that under practical conditions, only the testing methods according to ASTM D 5034 and ASTM D 5035 provide the same length and gripped width for grab and raveled strip specimens: the distance between the clamps is equal to 150 mm and the gripped width in both tests is equal to 25 ± 1 mm (whole width of the grab specimen is 100 ± 1 mm).

In 2003, Pan developed an analytical approach by means of the aforementioned theory of Eeg-Olofsson and Bernskiöld (1956). He offered a herringbone deformation mode, assuming roughly linear mechanical properties and neglecting the Poisson's ratio. The shear force within the elements of this model contribute to generating of tensile stresses into the ungripped parts of the test specimen width. Finally, it was concluded that overall tensile loads and stress distributions at the free region are a function of the fabric mechanical properties, the dimensions of specimen, and the grip size (Pan, 2003). Two years later, Wu and Pan carried out some tests on four woven fabrics (two types of plain cotton, one satin wool and plain polyester) and one polyethylene film. They approved the herringbone relationship (Wu and Pan, 2005). But on the other hand, Sommer (1941) investigated the strip test method on uncoated cotton fabric and found a non-uniform stress distribution over the specimen width, see Fig. 2 left. Sommer

assumed that this non-uniform stress distribution results from a non-uniform stiffness of the longitudinal yarns over the specimen width. This non-uniform stiffness, in turn, was presumed to originate from different magnitudes of enforcements of the longitudinal yarns by the orthogonal yarns over the width: the decrimping of the longitudinal yarns in the middle of specimen is more hindered than of those at the specimen edges. In fact, Sommer assumed that out of plane pressure at the weave points prevents longitudinal yarns from decrimping during uniaxial loading and that this effect is higher in the middle yarns than in the border ones. He observed the transverse contraction of orthogonal yarns is restrained in the middle of the specimen and causes more out of plane pressure while on the edges it is almost not restrained. Thus, the middle yarns behave stiffer than the edge yarns and carry more load than the latter ones. Those yarns carrying the highest load would break first and initiate the break of the fabric. Because of this, Reumann (2000) supposes that only a portion of the theoretical strength can be reached in strip tests, see Fig.2 left, while the theoretical strength is defined as the sum of the breaking forces of all yarns over a specific width. For avoiding this non-uniform stress distribution, it was offered in DIN 53857 to cut the strip specimen a little wider than the gripped width. The longitudinal yarns in the “overwidth” are then cut in the middle of the length. In this way, two extra edges of fabric can provide restrained transverse contraction while simultaneously the cut longitudinal yarns do not carry any extra loads. Sommer developed and tested extra clamps along the specimen length with which a transverse contraction along the specimen length could be avoided. Using these clamps, higher tensile forces can be reached in the strip tests.

The grab test method can be seen as another approach for achieving uniform stress distribution. For uncoated woven fabrics, Reumann (2000) assumed a uniform stress distribution in a grab test specimen because the longitudinal yarns at the edge of the gripped width are stiffened by the orthogonal yarns in the same way as those in the middle, see Fig. 2 right. The hypothesis is, that due to the uniform stress distribution, an actual strength approaching the theoretical strength can be measured. But the assumption that the load is carried only by the gripped yarns with a uniform stress distribution is obviously contradictory to what was discussed above, cf. Figs. 1 and 2. An elongation of non-gripped yarns would lead to stresses in these yarns and a non-uniform elongation cannot lead to a uniform stress distribution.

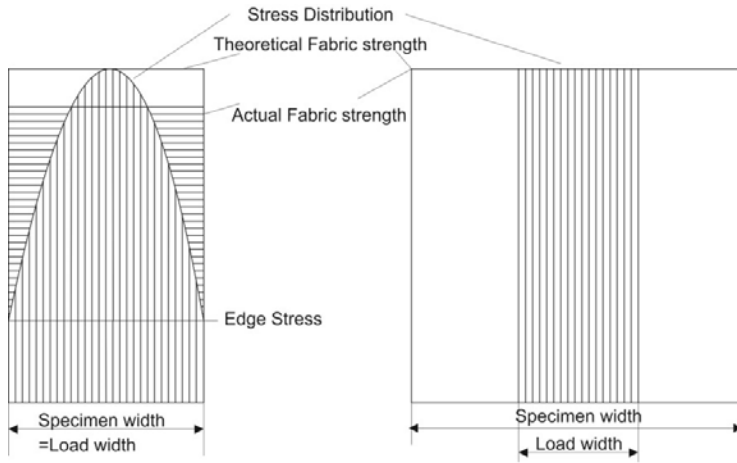


Figure 2: Assumed stress distributions over the gripped width of test specimens according to Sommer and Reumann; left: for strip test specimen (Sommer, 1941), right: for grab test specimen (Reumann, 2000).

The aforementioned investigations disregard another effect: Due to the transverse contraction of the specimens – originating from a variation of yarn enforcements during the loading process – the edge yarns are forced to elongate more than the middle yarns. This effect might lead to an over-proportional force increase in these yarns. Moreover, the transverse contraction is restrained at the jaws. This effect leads to local stress peaks at the specimen edge at the jaw.

4. Materials and Methods

4.1. Materials

The study in this paper was carried out on woven and knitted polyester fabrics. PVC-coated and uncoated woven PES fabrics were investigated. The coated fabric – a type II according to Stranghöner et al. (2016) – was made of the same fabric batch than the uncoated one, so that they are directly comparable. The third material was a knitted polyurethane-coated polyester fabric (PES/PU).

4.2. Methods

Uniaxial tests were carried out using both the strip and grab test method. For non-coated fabrics, EN ISO 13934-1 and EN ISO 13934-2 and for coated fabrics with rubber or plastic EN ISO 1421 should be used. But in fact, in all aforementioned standards, almost all test specifications, especially the sample sizes are the same while the clamp geometry shows some deviations for the grab tests. Therefore, it was decided to use EN ISO 1421 as the only standard to ensure a better comparison of the results. For the determination of the tensile strength (force) and its corresponding elongation, two sets of specimens were used, one in warp and one in weft direction. Additionally, in non-coated specimens, transverse yarns were pulled out after

clamping them. The aim was to assess the influence of transverse yarns on the mechanical properties.

5. Results and discussion

5.1. Uniaxial tensile behaviour in strip and grab tests

Force-elongation curves of all tested materials subjected to uniaxial loading are shown in Figs. 3 and 4 for strip and grab tests respectively. According to these curves, all coated and uncoated polyester fabrics show a nonlinear mechanical performance during the full uniaxial loading. Three out of four graphs of the uncoated fabrics in Fig. 4 are converging to horizontal paths and reflect slippage in the clamps. No fractures could be obtained for these materials within the grab tests.

For the PES/PVC and PES/PU samples, the maximum force and breaking force are identical while for uncoated polyester fabrics ruptures happen a little after the maximum force was reached. Figs. 5 and 6 show the different tested materials in the strip and grab tests.

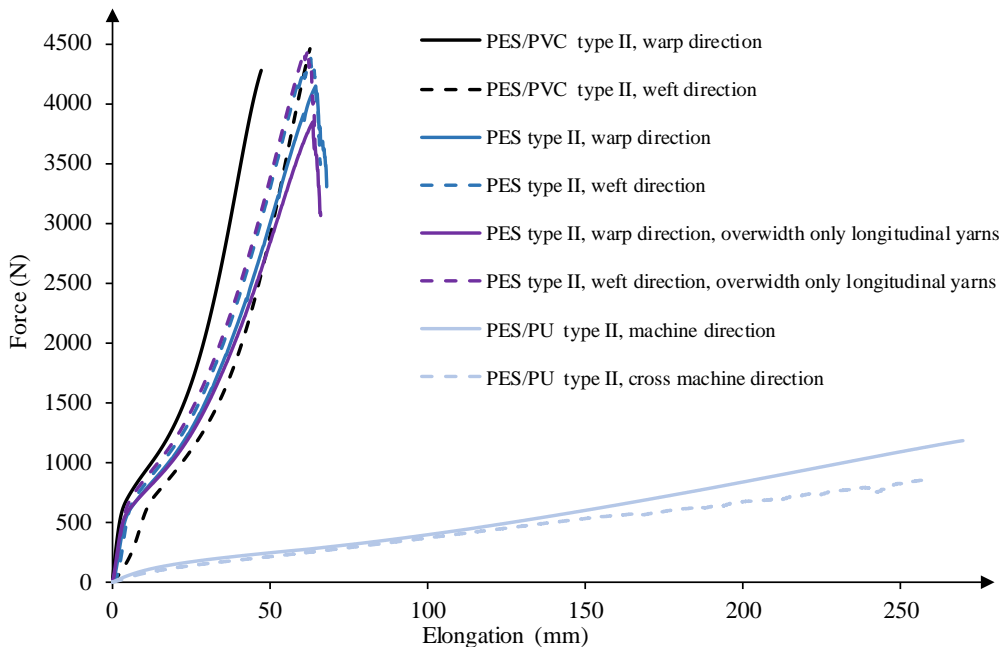


Figure 3: Force-elongation curves of investigated materials for strip tests according to EN ISO 1421

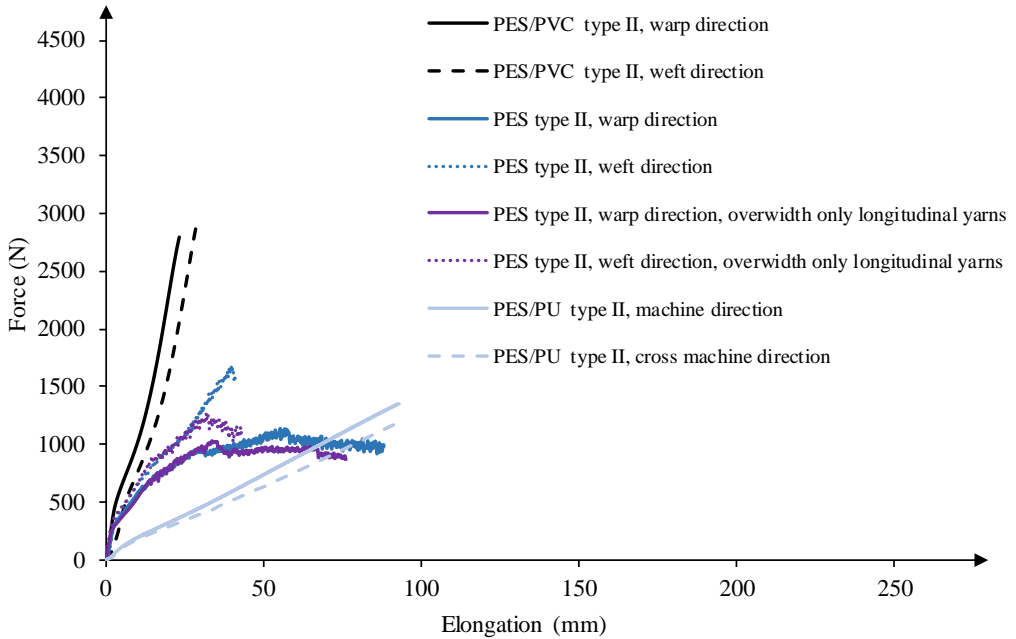


Figure 4: Force-elongation curves of investigated materials for grab tests according to EN ISO 1421

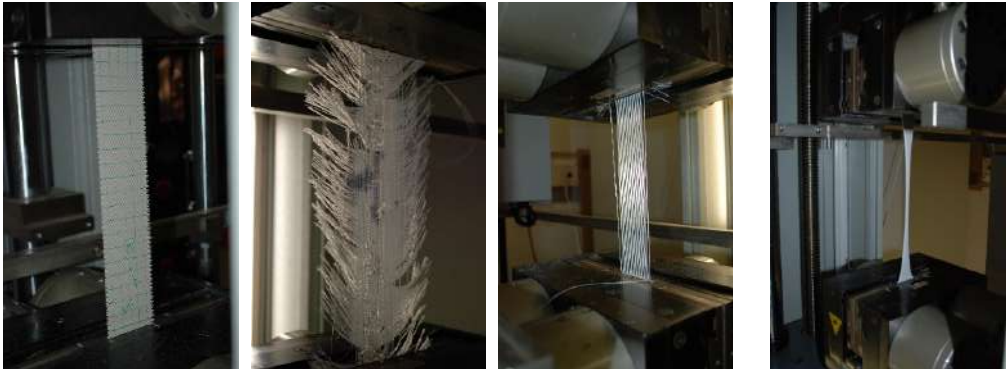


Figure 5: Strip test method according to EN ISO 1421, from left to right: PES/PVC, uncoated PES, uncoated PES with only longitudinal yarns and PES/PU



Figure 6: Grab test method according to EN ISO 1421, from left to right: PES/PVC, uncoated PES, uncoated PES with only longitudinal yarns, and PES/PU

In all grab tests where fracture occurred, clamp fractures were observed while for the strip tests also material fractures could be achieved. Material fractures are the preferred mode of fracture, because the measured breaking (or maximum) force is independent of local influences at the clamps. From this point of view, the grab tests showed a very unfavourable behaviour. Presumably the inclination of the grab test to slippage and clamp fracture is provoked by a high stress concentration at the corners of the clamps where forces carried by the ungripped parts are collected. The small clamping area of just 25 mm in a square may support slippage as well. However, the grab tests are not appropriate as a replacement of strip tests in order to avoid clamp fractures as EN ISO 1421 recommends it.

5.2. Comparison of maximum force results of strip and grab tests

According to EN ISO 1421, the only valuable parameter to obtain from a grab test is the maximum force. However, for strip tests it is mentioned that “if in spite of taking care, all breaks are within 5 mm of the face of a jaw or outside the reference marks, use method 2 (grab method)”. For that, maximum force (the only common result) of strip and grab methods should be interchangeable. To check, if this is the case, the mean value of maximum forces of both methods for different materials are compared in Table 2, as relation of $F_{\max S} / F_{\max G}$. For the uncoated fabrics, maximum forces could not be measured in the grab tests. This was because of clamp slippage – although the same clamp surface and pressure were used as in the strip tests. This illustrates, that for some materials it can be more difficult to sufficiently clamp the specimens with the grab test clamps – or even impossible.

Table 2: Comparison of results (mean values) of strip and grab tests according to EN ISO 1421

Material	Warp or machine direction			Weft or cross machine direction		
	Strip ¹⁾	Grab ²⁾	$F_{\max S}/F_{\max G}$	Strip ¹⁾	Grab ²⁾	$F_{\max S}/F_{\max G}$
	Maximum force $F_{\max S}$ (N)	Maximum force $F_{\max G}$ (N)		Maximum force $F_{\max S}$ (N)	Maximum force $F_{\max G}$ (N)	
PES/PVC II	4191	2794.5	1,50	4466.2	2943.6	1,52
PES II	3897.6	-*	-*	4466.8	-*	-*
PES II (with only longitudinal yarns)	3816.8	-*	-*	4450.6	-*	-*
PES/PU	1204.6	1355	0,89	834.4	1170.8	0,71

¹⁾ Gripped width: 50 mm

²⁾ Gripped width: 25 mm

* Fracture did not appear because of clamp slippage, thus no breaking (or maximum) force can be given.

Based on Table 2, for PES/PVC, the strip tests with a gripped width of 50 mm yield to higher maximum forces than achieved in the grab tests with a gripped width of 25 mm which is in principle an expected result. But it has to be kept in mind, that – as already mentioned – in case the width of a strip specimen is equal to the gripped width of a grab test, maximum forces of grab tests are higher than those achieved with strip tests, see Table 3. As it can be seen from Table 2, for PES/PVC type II, the maximum forces of the strip tests are about 150 % of the maximum forces of the grab tests for both warp and weft direction. Assuming a uniform stress distribution in both test methods, the strip test with double grip width should lead to somehow double maximum forces. The fact that the strip test leads only to a maximum force which is about 50 % higher than that of the grab test, indicates that more yarns than those in the gripped width of the grab test participate in carrying the load. Furthermore, a highly non-uniform elongation over the width was observed in the grab tests, see Fig. 6, comparable to Fig. 1 right. This is correlated to a highly non-uniform stress distribution over the width, which inhibits to calculate the maximum stress required for structural applications. The actual highly non-uniform elongation and stress distribution proofs that the stress assumption of Reumann, cf. Fig. 2 right, seems not to be adequate. The highly non-uniform elongation and the severe out-of-plane deformations also mean that it is not possible to measure the strain or the stress-strain

behaviour, respectively, of a material with the grab test. From this point of view, the grab test is useless for the design engineer.

For the uncoated PES fabric of the same weaving batch, the grab tests led to clamp slippage without fracture. The same happened to PES fabric strips that were clamped over just 25 mm with the grab clamps, see Table 3. Other clamping conditions or surfaces were not tested in the frame of this contribution, but the slippage illustrates that the small grab clamps are even more difficult to handle.

When removing the orthogonal yarns from the weave before applying the tensile force in the strip tests, the results are very similar to those of the unmodified woven PES fabric. This shows that transverse yarns do not play an important role in the uniaxial load carrying behaviour of woven PES fabrics. It also means that the derivation from the uniform stress distribution in the stress assumption of Sommer, cf. Fig. 2 left, can only be of insignificant magnitude.

PES/PU knitted fabrics are generally more stretchable and elastic than woven fabrics. In this way, tensile force can be distributed more to the edges in the grab test. That means, that the ungripped areas highly participate in carrying the load. Presumably this mechanism leads to the result that for the investigated knitted PES/PU the maximum forces of the grab tests with 25 mm gripped width (but total width 100 mm) were even higher than those of the strip tests with 50 mm width. It should be noticed, that in the grab tests, severe out of plane deformations were observed, see Fig. 6.

Generally, it can be summarized that the maximum forces achieved with each method show large differences and the methods are not interchangeable. For a direct comparison between grab and strip test results, a test series was carried out in a way that the length and gripped width of the specimens in both tests were the same (size of strip test specimens 25 mm × 75 mm and size of the grab test specimens 100 mm (25 mm gripped) × 75 mm). According to the results shown in Table 3, in PES/PVC fabrics, the differences between strip and grab tests are about 20 %. This means that the maximum force of the strip test is only about 80 % of the maximum force achieved in the grab test, in warp as well as in weft direction. For PES/PU, the maximum forces achieved in both testing methods yield to much higher deviations. The maximum force of the strip tests in warp direction is only about 45 % of the grab test, in weft direction this relation is a little lower about 37 %. These results show that in knitted PES/PU more ungripped parts of the fabric can carry loads than in PVC-coated woven polyester fabric. This might be because of the extreme stretchability of the knitted PES/PU which leads to high elongation even in the edge yarns.

Table 3: Comparison of results (mean values) of strip and grab tests with the same length and gripped size

Material	Warp or machine direction			Weft or cross machine direction		
	Strip ¹⁾	Grab ²⁾	$F_{\max S}/F_{\max G}$	Strip ¹⁾	Grab ²⁾	$F_{\max S}/F_{\max G}$
	Maximum force $F_{\max S}$ (N)	Maximum force $F_{\max G}$ (N)		Maximum force $F_{\max S}$ (N)	Maximum force $F_{\max G}$ (N)	
PES/PVC II	2209	2794.5	0,79	2402	2943.6	0,82
PES II	_*	_*	_*	_*	_*	_*
PES/PU	607	1355	0,45	430	1170.8	0,37

¹⁾ Gripped width: 25 mm, total width: 25 mm, grab clamping system used

²⁾ Gripped width: 25 mm, total width: 100 mm

* Fracture did not appear because of clamp slippage, thus no breaking (or maximum) force can be given.

6. Conclusions

According to the existing testing standards, both grab and strip tests can be used for measuring the tensile strength of fabrics. In some standards they are separated from each other while in EN ISO 1421, they are considered as interchangeable tests. EN ISO 1421 recommends to use grab tests when jaw breaks are inevitable in strip tests. The objective of this contribution was to present investigations into the interchangeability of grab and strip tests for testing fabrics intended to be used as structural membranes. It could be shown that for the investigated woven fabric – PES/PVC type II – the maximum forces achieved with both methods show large differences which are not proportional to the difference of the geometry. Based on the presented study it can be summarized that the results of grab and strip tests are not comparable at all.

In the grab tests, a highly non-uniform elongation distribution over the width was observed, usually combined with severe out of plane deformation. Of course, the highly non-uniform elongations go hand in hand with highly non-uniform stress distributions. During a grab test, transverse yarns of the whole length of the specimen (both between jaw distance and inside clamps), together with the coating (in case coating is applied), are transferring loads to adjacent ungripped areas. The more flexible the test material is, the bigger is this effect. This was observed with the extreme flexible PU-coated knitted polyester fabric. In all cases till now, the stress distribution and the effective width (sum of the gripped and extra ungripped width, which are participating in carrying loads) have been completely unknown in grab tests. Thus, by using the current version of EN ISO 1421 it is impossible to derivate the maximum stress from the

measured maximum force. Although the grab test might be sufficient for clothing textiles, the grab test method is unfeasible for structural design applications. Additionally, the grab test method has led to unfavourable clamping fractures in every single test of the presented test series where fracture appeared. Thus, grab tests are not interchangeable with strip tests and cannot replace them.

The design engineer is interested in the stiffness and stress-strain behaviour of a tested material. But: the strain cannot be measured within the grab test due to the severe out of plane deformations of the test specimens and also occurrence of slippage especially for uncoated fabrics.

Overall it can be summarized that for structural purposes, the strip test method according to EN ISO 1421 is the far more reliable testing method compared to the grab test method of the same standard. Nevertheless, the strip test method actually shows also little uncertainties in the stress distribution which might result from the stiffness variation over the specimen width and from transverse contraction effects. But the problems linked to these effects are much smaller than those arising from the grab tests. This conclusion holds for all materials tested: rather stiff PVC-coated and uncoated woven PES fabric and very flexible PU-coated knitted PES fabric.

References

ASTM D 5034 – 08, *Standard Test Method for Breaking Strength and Elongation of Textile Fabrics (Grab Test)*. USA: ASTM.

ASTM D 5035 – 95 (Reapproved 2003), *Standard Test Method for Breaking Strength and Elongation of Textile Fabrics (Strip Method)*. USA: ASTM.

Blum R., Bögner H., Némoz G., Material Properties and Testing, in: Forster B. and Mollaert M. (eds.) (2004), *European design guide for tensile surface structures*. TensiNet.

DIN 53354:1981–02 (withdrawn). *Prüfung von Kunstleder; Zugversuch*.

DIN 53857-1:1979-09 (withdrawn). *Prüfung von Textilien; Einfacher Streifen-Zugversuch an textilen Flächengebilden, Gewebe und Webbänder*.

Draft DIBt-Richtlinie (1983), *Richtlinien für die Zulassungsprüfung beschichteter Gewebe und deren Verbindungen*.

Eeg-Olofsson T., Bernskiöld A. (1956), Relation Between Grab Strength and Strip Strength of Fabrics. *Textile Res*, vol. 18, pp. 431– 436.

EN ISO 13934-1:2013-08. *Textile – Tensile properties of fabrics – part 1: Determination of maximum force and elongation at maximum force using the strip method*.

EN ISO 13934-2:2014-06. *Textile – Tensile properties of fabrics – part 2: Determination of maximum force using the grab method.*

EN ISO 1421:2017-03. *Rubber- or Plastics-Coated Fabrics – Determination of Tensile Strength and Elongation at Break.*

Lei Zh. (2010), *Reliability analysis of fabric structures* (Doctoral dissertation). School of Civil Engineering and Geosciences at Newcastle University, Newcastle, UK.

Pan N. (2003), Relationship Between Grab and Strip Tensile Strength for Fabrics with Roughly Linear Mechanical Behavior. *Textile Res*, vol. 73, pp. 165–171.

Reumann R.D. (2000), *Prüfverfahren in der Textil- und Bekleidungstechnik*, Springer, Berlin, Heidelberg, 2000.

Sommer H. (1941), Grundlagen der Berstfestigkeitsprüfung von Geweben I. *Melliand Textilberichte*, vol. 22, pp. 414-416.

Stranghöner N., Uhlemann J., Bilginoglu F. et al. (2016), *Prospect for European Guidance for the Structural Design of Tensile Membrane Structures*. JRC Science and Policy Report, European Commission, Joint Research Centre, Editors: M. Mollaert, S. Dimova, A. Pinto, St. Denton.

Walen E. D. (1916), Comparison of Strip and Grab Methods of Testing Textile Fabric for Tensile Strength. *ASTM Proc.*, Part 1, vol. 16, pp. 370-376.

Wu J., Pan N. (2005), Grab and Strip Tensile Strength for Woven Fabrics: An Experimental Verification. *Textile Res*, vol. 75, pp. 789–796.

Experimental assessment and interpretation of biaxial material parameter variation of a polyester-PVC fabric

Maarten VAN CRAENENBROECK*, Lars DE LAET*, Elien DE SMEDT^a,
Marijke MOLLAERT*

*Vrije Universiteit Brussel – Department of Architectural Engineering
Pleinlaan 2, 1050 Brussels, Belgium; maarten.van.craenenbroeck@vub.be

^a Vrije Universiteit Brussel – Department of Mechanics of Materials and Constructions

Abstract

Designing tensile fabric structures can be rather challenging due to the relatively complicated mechanical response of the coated textiles used in these structures. Its composition of interwoven fibres surrounded by different interacting layers of coating, and a lack of normative documents, assessing and interpreting a fabric's mechanical response unambiguously is challenging and requires a great deal of experience and expertise. Through various biaxial tests on a single Type II polyester-PVC material, and the utilisation of different test and interpretation methods, the inherent variability of the measured mechanical response and derived material constants could be assessed in function of test and interpretation methodology. By then relating these variations to the respective alteration in test or interpretation methodology, several important relations can be derived between the test methodology and derived stress-strain response/material constants. The presented paper compares various biaxial test and interpretation procedures and shows that altering any of these can have a significant impact on the results, even when the test is conducted on the same batch of material and within the same test environment. The obtained results not only illustrate the need for a unified international framework for testing of fabrics, but also the importance of interpreting test results and acknowledging the uncertainty/variability on the obtained results.

Keywords: Biaxial testing, computational simulation, polyester-PVC, fabric, tensile surface structure

DOI: 10.30448/ts2019.3245.16

Copyright © 2019 by Maarten Van Craenenbroeck, Lars De Laet, Elien De Smedt, Marijke Mollaert. Published by Maggioli SpA with License Creative Commons CC BY-NC-ND 4.0 with permission.

Peer-review under responsibility of the TensiNet Association

1. Introduction

Biaxial testing forms an integral part of the design process for tensile fabric structures. Whether it serves for the derivation of generalised material constants, assessment of tear strength or shear stiffness or establishing reduction factors for the cutting patterns, being able to accurately assess a fabric's mechanical response in a multi-axial stress state is an important aspect. (Beccarelli, 2015; Bridgens, 2004; Bridgens 2012; Uhlemann, 2016; Van Craenenbroeck, 2017)

Despite recent efforts towards a standard for designing and building tensile architecture (Stranghöner et. al., 2016), there still exist a considerable amount of variation in the way biaxial tests are conducted and the data is interpreted. Ranging from the design of the test benches and sample geometries to the mathematical process used to translate test results to a numerical material model, these inter-institutionary variations can lead to some variation, and thus uncertainties, on the test outcomes and the resulting material parameters.

Within this paper, several potential causes of uncertainties were identified and their impact on both the experimental stress-strain results as well as the derived material constants was assessed for a Type II polyester-PVC fabric (Sioen T2103) (Sioen Industries, 2018). The conducted experiments and analyses provided some insight to the effect of certain decisions and assumptions, but also allowed us to establish a base line for the expected variability for the tested material in function of commonly present differences.

2. Test and derivation methodologies

The presented research observes the three main steps in testing a fabric material and interpreting the outcome: (1) testing the material, (2) post-processing the raw data and (3) fitting a material model. For each of these three steps various variables were defined and investigated individually, assessing their impact on the stress-strain response and the material constants.

2.1. Test setup and methodology

2.1.1. Biaxial test setup

All tests described in this paper were conducted at the Vrije Universiteit Brussel. The biaxial bench used for these tests consist of four fixed actuators which stress the sample. Each actuator is equipped with a 100kN load cell which measures the applied force throughout the experiment. By constantly monitoring the force difference between two opposing actuators and adapting the actuators' position, a balanced and uniform stress state can be maintained.

The biaxial sample consists of a central area-of-interest measuring 30cm x 30cm. Each of the four arms is equipped with twelve 25mm wide slits to reduce stress reduction in the centre of the specimen. A welded loop at the end of each arm then allows the connection of the sample to the actuators.

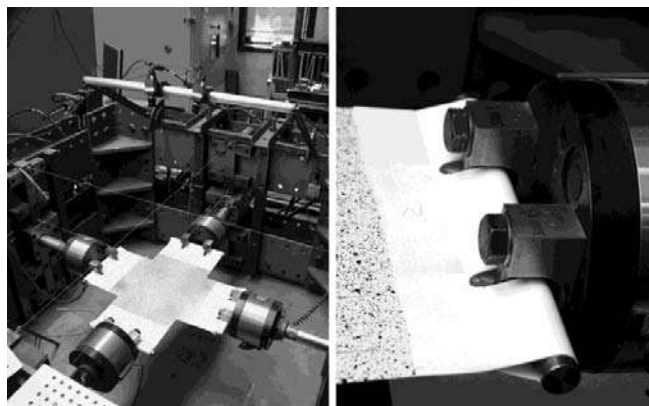


Figure 1: During the experiment, strains are measured using DIC through two cameras mounted above the sample (left). The sample is connected to each of the four actuators through a welded loop and bar system (right). (Van Craenenbroeck, 2017)

Strains in the sample were measured using a three-dimensional Digital Image Correlation (DIC) setup consisting of two AVT Stingray F-504 cameras mounted above the sample (Figure 1). Each of the tested sample was provided with a full-field speckle pattern which allows for the visualisation of the strain field throughout the entire sample in addition to the measurement within the area-of-interest.

2.1.2. Applied load profiles

The first, and one of the more significant, variations investigated during this research is the applied load profile. With no modern standard currently governing the biaxial testing of fabrics, many institutions have developed their own load profile in function of their needs and experience. Due to their woven and nonlinear nature the load history has however an important effect on the observed mechanical behaviour (Galliot and Luchsinger, 2011; Van Craenenbroeck et al., 2015). During this investigation, the results obtained from five different load profiles were compared: (1) the load profile as proposed in MSAJ-M-1995 (Membrane Structures Association of Japan, 1995); (2) the default load profile used at the VUB, (3) a variation with an asymmetric warp-dominant prestress ratio, (4) a variation with an asymmetric warp-dominant prestress and normalisation ratio and (5) an interpretation of the load profile presented by EMPA (Galliot and Luchsinger, 2009) (Figure 2).

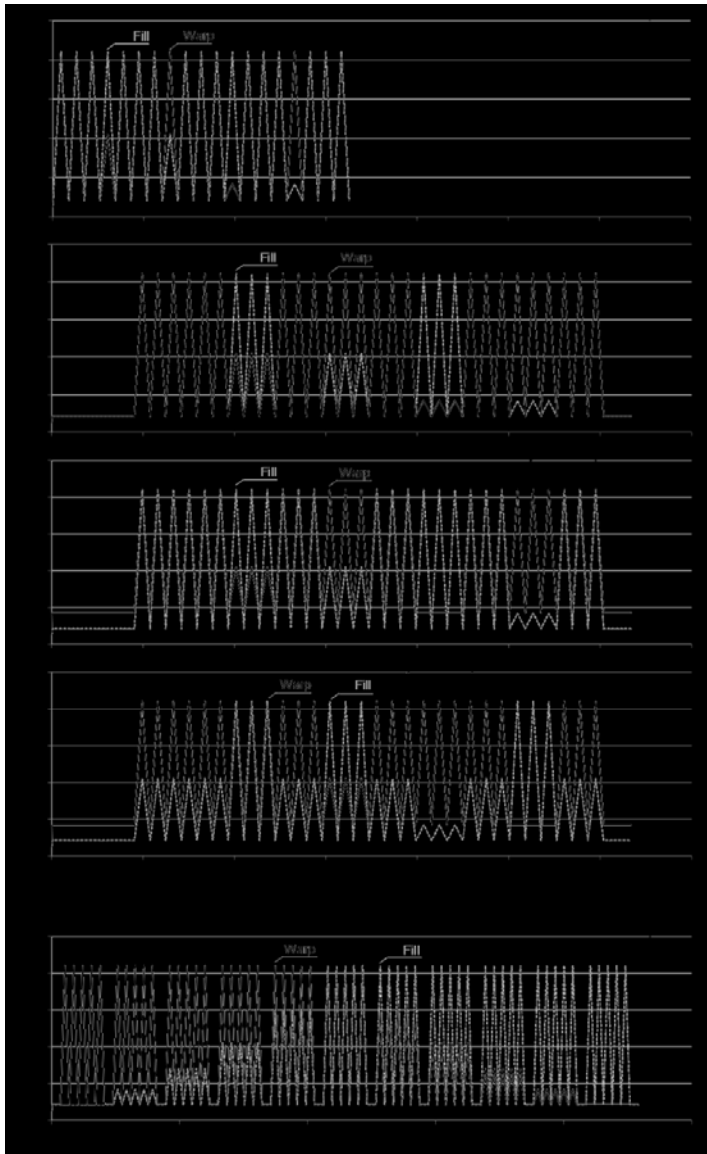


Figure 2: This investigation compares a total of five different load profiles, each targeting a specific type of variation in the test methodology. (Van Craenenbroeck, 2017)

2.2. Parameter derivation

Although different material models to numerically describe the mechanical behaviour of fabrics exist, the presented research limits itself to the linear elastic orthotropic model. Despite some limitations, such as its inability to model the non-linear behaviour or permanent deformations occurring in the fabric, it is still a commonly used material model both in academic research and

engineering practice. The recently published European Standard regarding biaxial testing on fabrics also limits itself to this linear elastic model (CEN/TC 248, 2018), further consolidating the model's relevance within the research presented in this paper.

The linear-elastic material model, under the assumption of a plane stress state given the negligible thickness of a textile, describes the stress-strain response by means of five constants: two Young's moduli, E_{warp} and E_{fill} , two Poisson's ratios, ν_{wf} and ν_{fw} , and the shear modulus G_{wf} :

$$\begin{bmatrix} \varepsilon_{warp} \\ \varepsilon_{fill} \\ \varepsilon_{wf} \end{bmatrix} = \begin{bmatrix} 1 & \frac{\nu_{wf}}{E_{fill}} & 0 \\ \frac{\nu_{wf}}{E_{warp}} & 1 & 0 \\ 0 & 0 & \frac{1}{2G_{wf}} \end{bmatrix} \begin{bmatrix} \sigma_{warp} \\ \sigma_{fill} \\ \sigma_{wf} \end{bmatrix} \quad (1)$$

As biaxial tests aim to minimise the shear stresses introduced in the sample, the shear term is typically disregarded. Although the remaining equation contains four material parameters, these are not fully independent. Due to the conservation of energy, the compliance matrix for elastic materials must be symmetrical, which means that:

$$\frac{\nu_{fw}}{E_{fill}} = \frac{\nu_{wf}}{E_{warp}} \quad (2)$$

or:

$$\frac{E_{warp}}{E_{fill}} = \frac{\nu_{wf}}{\nu_{fw}} \quad (3)$$

The above, known as the "reciprocal relation", effectively reduces the number of independent material constants to three. During this research, the impact of not enforcing this reciprocal relation during the process of deriving material constants has been investigated as well.

2.2.1. Selection of the data set

One of the very first steps when interpreting biaxial test data is selecting the data to be used during the regression analysis with the theoretical model. Aside from removing the permanent strain at the start of each load cycle as well as the stress-strain data obtained from the unloading cycles, we also consistently removed the very first load cycle of each group of a specific load ratio, provided more are present, to remove any residual effect of the previous load cycle and ratio.

The question which remains at this point is which experimental data points get selected to be used during the derivation of the material constants. Within this research, four different cases were considered:

1. All data points of all load ratios are considered.
2. Only the peak values of all load ratios are considered.
3. The peak values of subsequent and identical load ratios are averaged.
4. The peak value of all identical load ratios throughout the test are averaged.

2.2.2. Minimisation methodology

Once the data set is selected, the model's constants can be fit to the experimental data through 2 methods: either by using the experimental strain as input data for the regression analysis and minimising the difference between the theoretical and experimental stresses (= "stress minimisation") or by using the stress as input data and minimising the strains (= "strain minimisation"). Within the presented research both methods are compared.

2.2.3. Regression analysis method

Finally, two possible approaches to conduct the regression analysis were considered: minimisation of the sum of the squared differences (= "least-squares method") or minimisation of the maximum error (= "best approximation" or "minimax method"). Both approaches are part of the MSAJ M-02-1995 guide, although a preference for the least squares method is expressed in this document. (Membrane Structures Association of Japan, 1995)

To summarise, we will be discussing the impact of a total of 5 parameters in this paper: (1) the applied load ratio, (2) the initial data selection, (3) stress minimisation vs. strain minimisation, (4) the regression analysis method and (5) the effect of not enforcing the reciprocal relation.

3. Results and discussion

3.1. Stress-strain results

Before proceeding to comparing the derived material constants, the normalised stress-strain results from the various tests were considered as a first comparison of the various load profiles (Figure 3).

At a first glance, these curves already clearly show a rather large variation amongst them, with strain variations of 1% at maximum load not being uncommon. In terms of relation between the obtained data and the load profiles, we do note that the profile as presented by the MSAJ M-02-1995 results in the least stiff response for most load ratios. In addition, the outcomes of the standard VUB profile and the EMPA-based load profile tend to lie close to each other whereas

both profiles containing the asymmetric prestress ratio tend to deviate from these results, most notably in case of a fill-dominant load ratio (1/2 and 1/5 ratios).

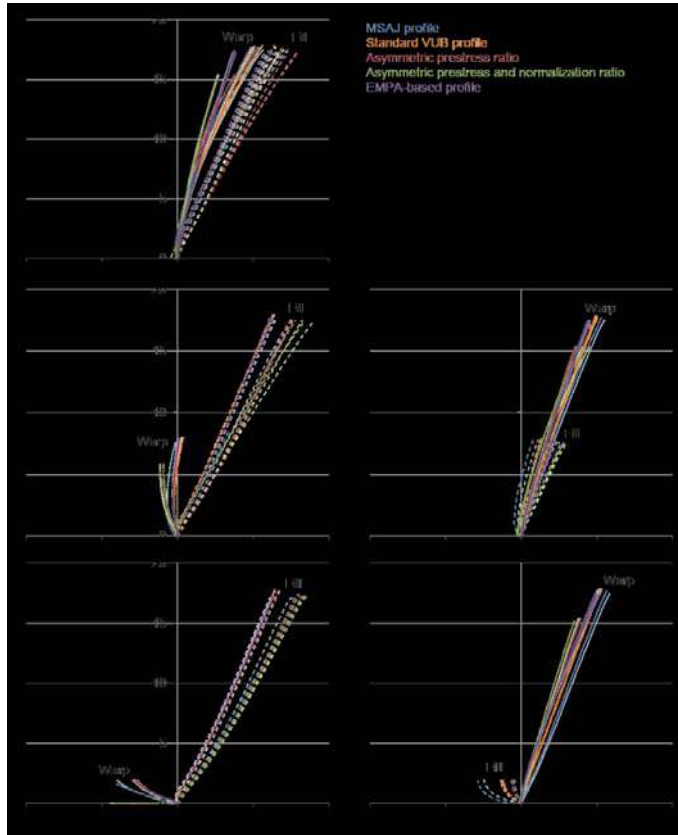


Figure 3: Comparing the direct stress-strain results already showed a fairly large variation when comparing the results obtained from the different load profiles. (Van Craenenbroeck, 2017)

3.2. Derived material constants

3.2.1. Impact of the load profiles

Summarising all material constants in two scatter plots, immediately shows the extent of the variation which exists on both the Young's moduli and the Poisson's coefficients (Figure 4). With stiffness variations of up to 300kN/m, the various alterations to the test and derivation method did have a very noticeable effect.

The most obvious factor in this is the application of different load profiles. Both scatter plots show clear groupings of material constants in function of the load profile. Following the observations made from the stress-strain curves, the MSAJ profile leads to low Young's moduli in both fibre directions while the EMPA based profile and the standard VUB profile lead to

higher Young’s moduli. Both profiles with the asymmetric prestress load ratio show a more asymmetric set of stiffness constants where the warp stiffness is higher than the values observed from the other profiles. Also note the apparent lower consistency in the results of these two test profiles in function of the other adaptations as compared to e.g. the MSAJ or standard VUB profile.

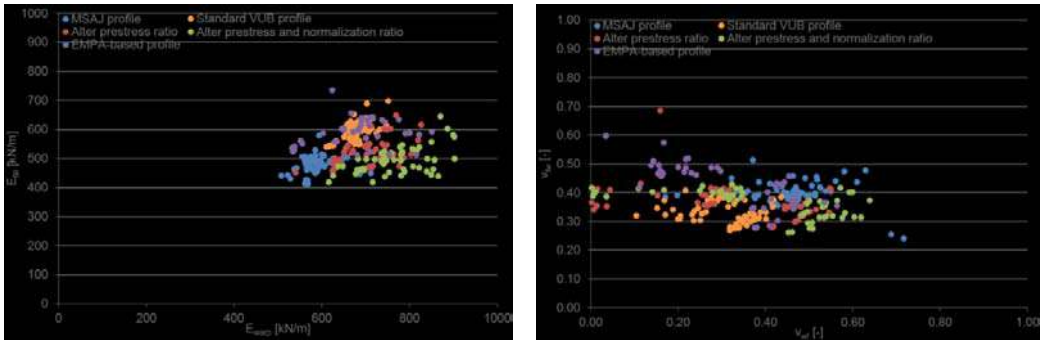


Figure 4: Separating the material constants in function of the applied load profile generates clear “clusters”. (Van Craenenbroeck, 2017)

3.2.2. Impact of the data selection

For further investigation of the distribution of the obtained material constants in function of the different applied variations, the point cloud has been reinterpreted into box plots in function of each of the target variables. This allows us to better assess the impact each variation has on the material constants not only in terms of average value, but also in terms of its variability.

When representing the data this way for the four different data selections, no clear distinction can be made between the possibilities (Figure 5). Whether the data has been linearized, averaged or whether all intermediate data points were used didn’t seem to impact the overall outcome to a significant degree, or at least not within the scope of the existing variations due to the other variables.

3.2.3. Impact of the minimisation and regression method.

Doing the same for the minimisation and regression methods, results in 4 categories: least squares with stress minimisation (“LS – Stress”), least squares with strain minimisation (“LS – Strain”), minimax method with stress minimisation (“MM – Stress”) and minimax with strain minimisation (“MM – strain”).

Observing the different boxplots (Figure 6), shows clearly that the warp stiffness E_{warp} is affected by the choice of minimisation method where strain minimisation leads to a slight increase where no such difference could be found for E_{fill} . Considering the Poisson coefficients however shows that utilising the minimax method instead of the least squares method not only increases the variability in the values for ν_{wf} , but also has a slightly stronger tendency to result in more extreme

values for this parameter. It is thus recommended to use the least squares method for the regression analysis unless specific constraints prevent this.

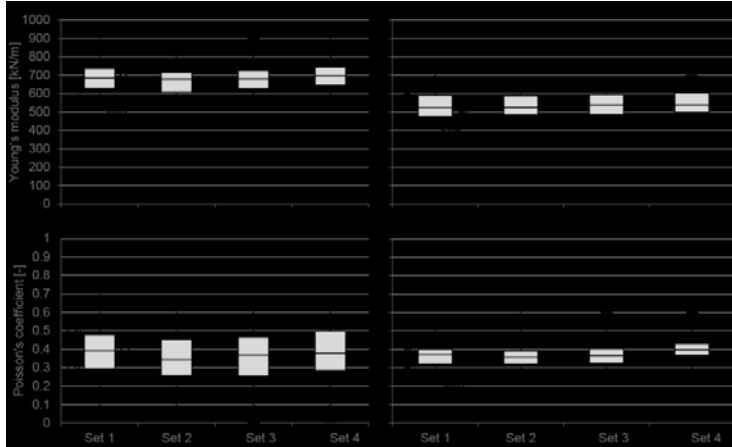


Figure 5: Comparing the constants in function of the selected data set did not reveal a clear impact. (Van Craenenbroeck, 2017)

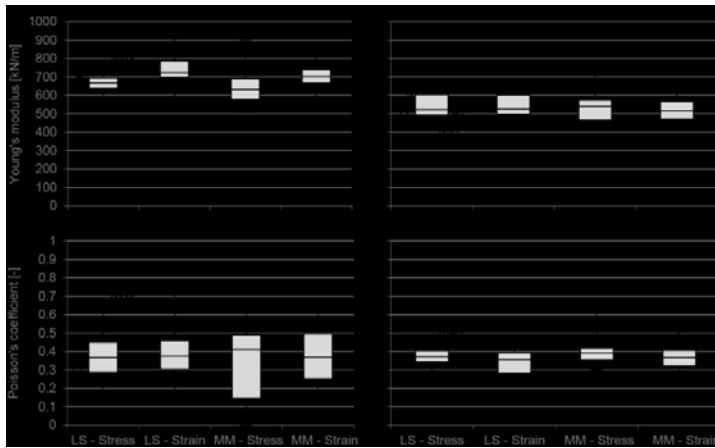


Figure 6: Whereas the choice between stress and strain minimisation affected mainly E_{warp} (top left), the difference between the least squares and minimax regression analysis methods affected mainly the variation of ν_{wf} . (Van Craenenbroeck, 2017)

3.2.4. Impact of the reciprocal constraint

As a final comparison, the impact of not enforcing the reciprocal constraint during the derivation of the material constants was investigated. Although the outcome of such analysis is physically meaningless as it violates the law of the conservation of energy, the difference between the sets on constants derived with and without application of the constraint can be a measure to how far the theoretical model deviates from the experimentally observed behaviour.

Returning to the scatter plot of the elastic constants (Figure 7), reveals that removing this constraint does not really have a notable impact on the Young’s moduli aside from a slight increase for E_{warp} and decrease for E_{fill} . For the Poisson’s coefficients the effect is more drastic, resulting in a clear shift to the left for most results. This sudden decrease in the outcome for v_{wf} , indicates that the experimentally observed fill strain is less affected by the stress in the warp direction than the linear elastic orthotropic model assumes. This discrepancy mainly comes from the non-uniform composition of the material and the geometrical displacements that take place within the weave, leading to a mechanical behaviour which seemingly violates the fundamental symmetry of the compliance matrix.

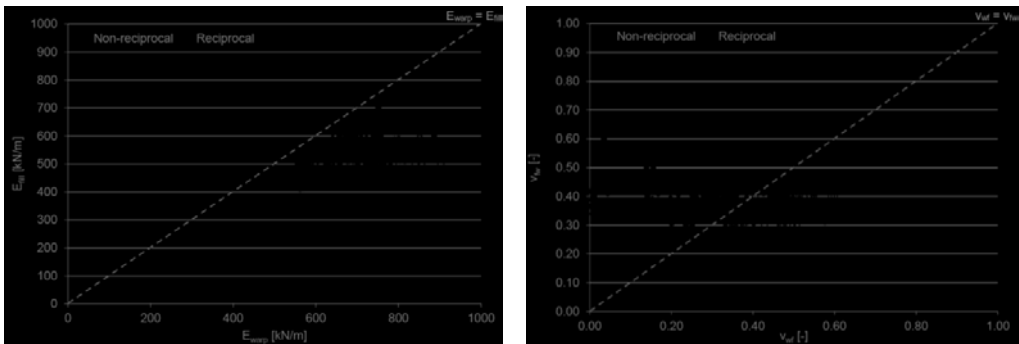


Figure 7: When not specifically enforcing the reciprocal constraint during the derivation of the linear-elastic material constants, the values found for v_{wf} decrease significantly. This suggests that the numerical model overestimates the impact warp stresses have on the fill strain. (Van Craenenbroeck, 2017)

This rather significant difference in the outcome illustrates one of the main limitations of the linear-elastic orthotropic model when it is applied to coated textiles. The model’s simplicity does provide some clear advantages in terms of deriving its constants and implementing it in numerical software, but when it comes to properly characterising the complex straining behaviour of coated textiles more refined material models will yield more accurate results.

4. Conclusions and further research

This paper gave a short overview of how different approaches and decision can influence the outcome of biaxial tests in terms of the stress-strain curves as well as the derive linear-elastic orthotropic material constants. The impact of the applied load profile, selection of the data set for further analysis, minimisation and regression methods, and the removal of the reciprocal constraint during the derivation of material constants has been investigated.

As expected, the applied load profile lies at the cause of the biggest overall differences. The load profile as presented in MSAJ M-02-1995 results in a notably low set of Young’s moduli as compared to the other load profiles used in this research. Changing the applied prestress ratio from symmetric to an asymmetric warp-dominant stress resulted in an increase of the warp stiffness while at the same time decreasing consistency in function of the other variations.

Changing the data set which was extracted from the tests did not seem to impact the resulting material constants to any significant degree, or at least not within the scope of the other parameters that were investigated.

The difference between the stress and strain minimisation methods was however apparent with the latter leading to a small increase in the resulting warp stiffness E_{warp} . The other parameters did not seem to be affected by this. And although the choice in regression analysis did not seem to impact the actual values of the resulting parameters, using the best approximation/minimax method instead of the least squares method did result in a noticeable increase in the variability of v_{wf} as well as a tendency to provide more “extreme” sets of material constants.

Finally, the impact of not forcefully imposing the reciprocal constraint during the derivation of material constants was investigated. Important to realise in this is that the derived material constants are physically meaningless but can be used as a measure to assess how much the observed behaviour deviates from the assumptions made by the linear-elastic model. Removing the constraint from the analysis did not seem to significantly affect the Young’s moduli aside from a small increase in the warp stiffness. A much more noticeable impact was the decrease of the Poisson’s coefficient v_{wf} . Considering the underlying equations, this shift suggests that the impact of the warp stress on the fill strain is much less than what the linear-elastic model suggests.

Although the presented research already allows us to draw certain parallels between specific decisions and assumptions applied during the process of biaxial testing of fabrics and deriving their material constants, the above is still relatively limited. Important causes of variations such as the influence of sample geometry and test bed design should be investigated on an international scale. Aside from merely establishing this variation, a method to cope with this material uncertainty should be developed to ensure a reliable design.

Acknowledgements

The research described in this paper has been funded by the government agency for Innovation by Science and Technology (IWT) and has been carried out at the department of Architectural Engineering at the Vrije Universiteit Brussel (<http://vub.ac.be/ARCH/ae-lab/>) with the support of COST Action TU 1303. The authors would also like to thank Sioen Industries (<https://sioen.com>) for providing the material to carry out this investigation and the department of Mechanics of Materials and Constructions (MeMC) of the Vrije Universiteit Brussel for their logistic support.

References

Beccarelli P., *Biaxial Testing for Fabrics and Foils*, SpringerBriefs in Applied Sciences and Technology, Springer International Publishing, Cham, 2015.

Bridgens B. N., Gosling P. D., A new biaxial test protocol for architectural fabrics, *Journal of the International Association for Shell and Spatial Structures* (December 2004).

Bridgens B. N., Birchall, M. (2012). Form and function: The significance of material properties in the design of tensile fabric structures. *Engineering Structures*, 44:1 – 12.

CEN/TC 248, *FprEN 17117-1 Rubber or plastic-coated fabrics – Mechanical test methods under biaxial stress states – Part 1: Tensile stiffness properties*, European standard, Brussels (2018).

Galliot C., Luchsinger R. H., A simple model describing the non-linear biaxial tensile behaviour of PVC-coated polyester fabrics for use in finite element analysis, *Composite Structures* (2009) 1-25.

Galliot C., Luchsinger R. H., Determination of the response of coated fabrics under biaxial stress: Comparison between different test procedures, in: E. Oñate, B. Kröpling, K.-U. Bletzinger (Eds.), *5th International Conference on Textile Composites and Inflatable Structures, Structural Membranes 2011*, 2011.

Membrane Structures Association of Japan, *Testing Method for Elastic Constants of Membrane Materials (MSAJ/M-02-1995)*, Tech. rep., Tokyo (1995).

Sioen Industries, T2103.pdf, <http://www.sioencoating.com/sites/default/files/T2103.pdf>, accessed: 01-10-2018.

Stranghöner N., Uhlemann J., Bilginoglu F., Bletzinger K.-U., Bögner-Balz H., Corne E., Gibson N., Gosling P. D., Houtman R., Llorens J., et. all., *Prospect for European Guidance for the Structural Design of Tensile Membrane Structures*, 2016.

Uhlemann J., *Elastic Constants of Architectural Fabrics for Design Purposes*, Ph.D. thesis, Universität Duisburg-Essen (2016).

Van Craenenbroeck M., De Laet L., Puystiens S., Van Hemelrijck D., Mollaert M., Biaxial testing of fabric materials and deriving their material properties A quantitative study, in: *Proceedings of the International Association for Shell and Spatial Structures (IASS) Symposium 2015*, Amsterdam Future Visions, International Association for Shell and Spatial Structures (IASS), Amsterdam, 2015.

Van Craenenbroeck M., *Biaxial Testing of Fabrics - Test methodologies and their impact on material parameters and the structural design process*, Ph.D. thesis, Vrije Universiteit Brussel (2017).

Proceedings of the TensiNet Symposium 2019

Softening the habitats / 3-5 June 2019, Politecnico di Milano, Milan, Italy
Alessandra Zanelli, Carol Monticelli, Marijke Mollaert, Bernd Stimpfle (Eds.)

Soft Spaces: Hybrid systems from structural membranes and conventional building technologies

Günther H. FILZ*, Gerry D'ANZA^a

* Aalto University, ENG Department of Civil Engineering, ARTS | Department of Architecture
Rakentajanaukio 4 A, 02150 Espoo, Finland
guenther.filz@aalto.fi

^a Gerry D'Anza Lightweight Architecture, Centro Direzionale Isola G8 , 80143 Naples, Italy

Abstract

Tensile structures and conventional building techniques are both highly developed, but they have never been explored as coalescent architectural and structural unity. We are proposing hybrid configurations, which will merge 3 aspects, firstly architectural design from the complex interplay of conventional and fluent forms, secondly structural design from the 3D-bracing-effect by membranes, and thirdly benefits in assembly, costs and sustainability, from the pin-joint connection related ease of assembly, alongside minimum amount of material and high degree of prefabrication. For the benefit of a global system, the role of membrane structures has been moved from intrasystem purposes to an integral structural and architectural element.

As a first step, this paper looks into the structural performance of structural membranes spanning two planar, bending resistant elements, such as floor slabs, which are held at a predefined distance by vertical pin-joint struts only.

It is shown that combining the ease of assembly of conventional members and the 3D-bracing-effect of membranes result in highly efficient architectural structures.

Keywords: structural membranes and conventional building technologies, hybrid structures, textile architecture, performance, built environment, new applications, design rules and structural analysis, sustainability.

DOI: 10.30448/ts2019.3245.25

Copyright © 2019 by Günther H. Filz, Gerry D'Anza. Published by Maggioli SpA with License Creative Commons CC BY-NC-ND 4.0 with permission.

Peer-review under responsibility of the TensiNet Association

1. Global and (Inter-) Disciplinary Context

Due to the growth of world's population the increasing demand, which is accompanied by increasingly complex and dynamic requirements, challenges the "production" of built environment and architecture. This means that architecture increasingly considers their generated objects no longer as isolated discrete objects, but rather they have to be seen as systems embedded in systems. Pioneering architecture is on the move to emergent systems, which are informed by multiobjective goals. More and more examples in architecture are developed in response to climate change, rational energy consumption, lifecycle analysis, workplace health, overall well-being and customized architected spaces. Current architectural design is also directly linked to and dependent on advances in material development, analysis tools and architectural and structural design methods. Therefore, it is essential to gain a deeper understanding of the multifaceted, complex demands and its resulting interaction respectively coaction, in order to create buildings, which have a responsive behavior to their environment, their users and within the structure itself. On the other hand, such requirements and resulting, emergent architecture are very quickly categorized as individual, unique and bespoke solutions, which have the image of representative showcases only and which are supposed to be expensive. These phenomena directly conflict with the questions of resources, which are needed and consumed by our society, and even more with our mostly profit-oriented industry. Over the decades, the building industry established conventional and standardized structures with an eye on optimized use of space, recognized construction technology, ease of construction and its well-known structural behavior. As a result, these approaches many times are over-simplified and reduced to a 2D-thinking in plan and section, resulting in 2D material and formats and vice versa. Usually a change in mindset is forced by political decisions and/or achieved by material incentives. Material incentives for example can be reward systems or gaining additional benefits, like uniqueness on the market, compensation of higher costs by shorter construction time, or a product's enhanced performance.

Textile building has been developed from an ancient technique to today's structural membranes by architects, engineers and researchers in cooperation with the industry. Due to their anticlastic curvature and applied prestress, especially minimal surface membranes show inherent structural advantages as well as architectural qualities such as fluent shapes or complex geometrical and visual effects. In a simultaneous way, such structures offer unique properties that other, more conventional, building elements often do not possess, and low self-weight, extremely high flexural strength, translucency and the capability of forming architecturally expressive shapes that enhance the urban environment with a minimum amount of material are interdependent. The complex interplay of all these features, which is achievable by interdisciplinary approach only, can result in highly advantageous projects. Still, structural membranes represent a special discipline, mainly restricted to projects with wide span or landmark buildings and isolated from other building techniques. Consequently, conventional building components and tensile

structures are both highly developed on a material and structural predictable level, but they have never been explored as coalesce architectural and structural unity. So far, mentioned spatial and structural qualities have been used for intrasystem purposes, but not for the benefit of a global system.

2. Hybrid systems from structural membranes & conventional building techniques

In the long run, we are aiming for synthesizing hybrid solutions from conventional building technologies and lightweight membrane/cable-net structures. In this sense, we will merge approaches from conventional building techniques with high degree of standardization for the analysis, design and realization, and approaches in membrane structures, in which form finding, appropriate design strategies and advanced technologies are crucial. So, the focus of our research clearly lies on “hybrids”, where elements, which are part of the hybrid constellation, inform each other and establish inseparable “spatial-structural-tectonic” emergent configurations. Our approach is firstly based on the dissertation and long-term research on “Soft Spaces” (Filz, 2011) and secondly on experimental structures like the “cut.enoid.tower”, “Cloud for fresh Snow” (Klasz & Filz, 2015) or “2Landscapes” (Filz and Naicu, 2015) amongst others.

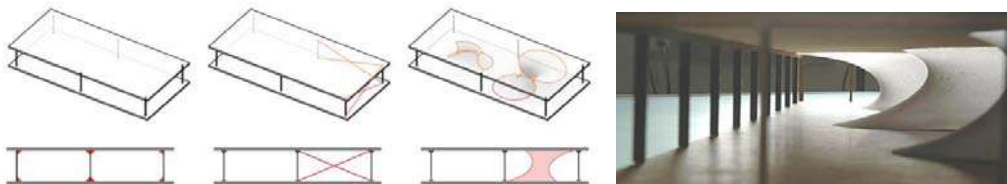


Figure 1: From bending resistant connection detail to 2D-bracing to 3D-bracing-effect by spatially curved, structural membranes, and spatial impression of a possible setup

Proposed hybrid configurations will cover architectural design aspects, structural design aspects as well as benefits in terms of assembly, costs and sustainability, but as a first step, this paper looks into the structural performance of structural membranes spanning two planar, bending resistant elements, such as floor slabs, which are held on distance by vertical pin-joint struts only. In that sense, we are combining the ease of assembly (tectonic) with the 3D-bracing-effect of spatially curved, structural membranes, which are advantageously replacing conventional 2D-bracing elements.

3. Structural membranes replacing traditional elements

For the ease of investigation into hybrid performance as described above, this research uses spatially curved, structural membranes as integral components of architecture, replacing conventional, usually planar elements. As shown in more detail in the dissertation “DAS WEICHE HAUS _ soft.spaces” by Filz, 2010, the range of exploration covers wall-like

elements, T-shaped connections, solutions for corners and the tubular shape of the catenoid. At present, experiments are restricted to minimal surfaces in soapfilm analogy. This means that the applied prestress is equal for warp and weft. Linear, maximal 2dimensionally curved, bending resistant, line supported boundaries have been defined as interface between membranes and conventional, planar floor slabs.

The results of above mentioned dissertation show surprising and partly new correlations between form and boundary proportions and so far unknown rules of the self organizing processes of Minimal Surfaces – especially in the field of the catenoid. The overview and the comparison of the results regarding their Gaussian curvature analysis allowed for a targeted selection of those setups, which show the highest percentage of curved surface. These surfaces are supposed to be the most efficient in terms of structural performance and therefore these surfaces have been selected for further investigation in a hybrid configuration. The following sections give an overview of investigated elements and Case Studies (CS).

3.1. CS 01 Minimal Surfaces between straight lines and boundaries consisting of segments of a circle

All experiments related to this series (Figure 2) show, that for this boundary condition it is not possible to find a fully anticlastic curved Minimal Surface. Those surfaces which show few flat areas concentrate on boundary conditions consisting of semicircles with a diameter that corresponds to the vertical distance of the boundaries.



Figure 2: Minimal Surfaces between straight lines and boundaries consisting of segments of a circle

3.2. Minimal Surfaces between boundaries consisting of segments of a circle

In this case the boundaries of wall like Minimal Surfaces can have the same direction or they can be arranged inversely.

3.2.1. CS 02 Minimal Surfaces between boundaries consisting of segments of a circle in the same direction

Boundaries that are curved in the same direction (Figure 3) generally effect strong anticlastic curvature of Minimal Surfaces. Boundary conditions consisting of semicircles with a diameter that equals the distance of the boundaries can be qualified as 100% spatially curved. Section lines show the smallest circle of curvature exactly on half height and harmonic development of the surfaces (Figure 4).

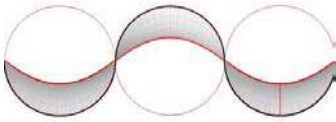


Figure 3: Boundary configurations consisting of segments of circles having the “same direction”

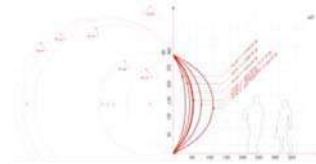


Figure 4: Vertical section of digital models and their circles of curvature at half height.

3.2.2. CS 03 Minimal Surfaces between boundaries consisting of inversely arranged segments of a circle

Curved and inversely arranged boundary conditions effect anticlastic curvature covering most of the surface, even if the boundaries have little oscillation from the longitudinal axis. The mostly curved surface can be developed with boundaries consisting of semicircles with a diameter of $2/3$ of the distance of the boundaries (Figure 5). Areas with less spatial curvature can first of all be found exactly at the maxima of boundary curvature and on half height.

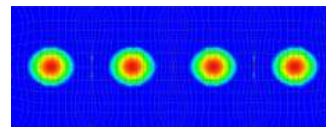
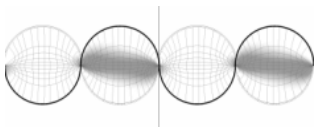


Figure 5: Minimal Surfaces between boundaries consisting of inversely arranged segments of a circle and Gaussian Curvature analysis

3.3. CS 04A, CS 04B, CS 05 Right-angled T-connections with symmetric wing length [FL]

Surfaces meeting in a T-connected boundary (Figure 6) generate a Y-intersection (Figure 7). This happens independently from the angle of the boundary connection. The 3 different parts of the Minimal Surface meet with 120° and form an arch-like intersection. This arch is less curved at its angular point and more curved the closer it is to the T-connection of the boundary. „In very special cases only, a circular intersection can be formed.” (Otto, 1988). These special cases were used to form compression only arches for real structures.

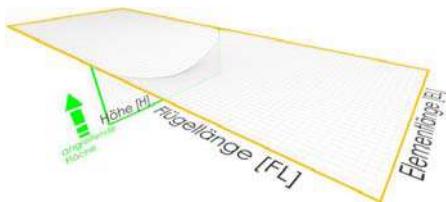


Figure 6: Geometry of right angled T-connection

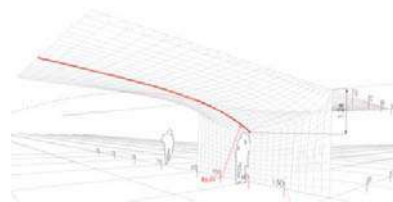


Figure 7: Minimal Surface generated from a right angled T-connection

In terms of right-angled configurations the leg length of H (Figure 6) has no influence on the form of the generated Minimal Surface as long as it is longer than the deflection of the Y-

intersection. This happens to be the same, independently from the wings being arranged symmetrically or asymmetrically.

For symmetric wing length [FL] we can determine that the magnitude of the Y-intersection is directly connected to the ratio of wing length and element length (Figure 8). For all boundary conditions with $FL \geq EL/2$ the magnitude of the Y-intersection equals 20,6% of the element length. For wing length shorter than the element length, a nonlinear behavior of the Y-intersection can be determined. So the boundary condition $FL=EL/2$ represents the borderline between linear and nonlinear development of displacement in the direction of H (Figure 9).

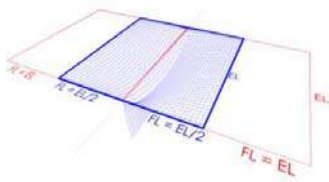


Figure 8: T-connection with square boundary geometry $FL = EL/2$

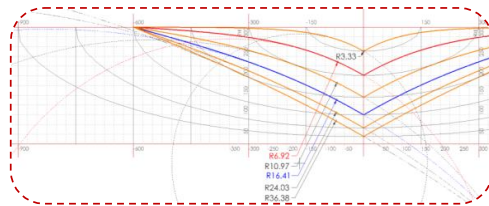


Figure 9: linear increase of displacement at increasing element length up to $EL/2=FL$, then nonlinear

A square geometry in plan causes evenly distributed curvature in the surface (Figure 8). The curved Y-intersection is similar to a basket arch (Figure 9). Starting from a square geometry in plan increased wing length results in the generation of insufficiently curved areas at the ends of the wings. Strong anticlastic curvature is limited to the areas of the T-connection of the boundary. Variations in the boundary setup, such as Asymmetric wing length [FL] and Non-right-angled T-connections do not show improved results in terms of surface curvature.

3.3. CS 06 Catenoids between circular rings

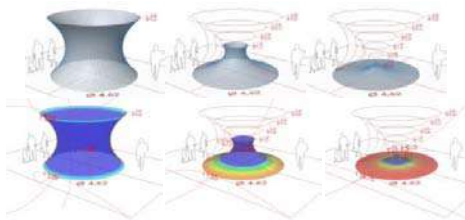


Figure 10: Change of form / change of Gaussian Curvature of a Catenoid with decreasing diameter of upper ring and therefore decreasing height

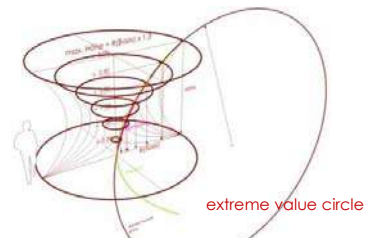


Figure 11: 3dimensional diagram for catenoids between circular rings of different diameters

The shape of the catenoid is generated by a catenary that rotates around a longitudinal axis. It is the only rotational body that can be minimal surface at the same time. As we know from SFB230 the maximum attainable height of a catenoid spanning two circular rings is approximately 1,3 times the radius of a ring. (IL, SFB 230, 1992) For conceptual designs in architecture, boundaries different from two identical circles but with different diameters, not

being arranged in one axis and/or not being symmetrically arranged are needed. So the maximum attainable heights of catenoids with different boundary geometries and arrangements were examined. New rules could be found for major boundary configurations (Filz, 2011). The resulting diagrams can be scaled at will. Starting from the extreme of 1,3 times the radius of a ring the maximum height of a catenoid is decreasing if one of the rings diameter is decreasing (Figure 10, 11). Figure 10 also illustrates that upper rings smaller than 1/5 (upper ring /lower ring) result in very little maximum attainable height and surfaces with little Gaussian Curvature at the same time. Several experiments showed that all the attainable maxima in dependence from the given diameters are located on a common circle - the extreme value circle. This circle again is in direct proportion to the circular base ring. (Figure 11).

4. Software, membrane material and general setup applied

The used software for this research has been IxCube 4-10 v 2.2.4, a system for tensile structure design, engineering and manufacturing. IxCube 4-10 uses and combines features from different disciplines like CAD (Computer Aided Design), FEA (Finite Element Analysis) and Production process (CNC and others). The user interface has most of the tools of a modern CAD software, plus a FEA section for editing FEA based objects like nodal coordinates, object orientation, meshing tools and material specifications based on engineering properties (E-modulus, Poisson, etc.). For the problem of form-finding ixCube 4-10 incorporates the following 4 techniques, namely the Force Density Method, the Update Reference Strategy, the Direct Stiffness Method, and the Natural Force Density Method, which has been used in our analysis.

For our simulation and structural analysis, Ferrari Preconstraint 702 S2 – material with a breaking load of 56/56 kN/m and a working load of 11.2/11.2 kN/m (with Sf= 5) has been applied. According to the manufacturer, Ferrari Preconstraint Flexlight Perform 702 S2 offers a very high level of translucency for unrivalled weight/mechanical and aesthetic performance for all tent types. S2 varnish and Low Wick treatment ensure lasting whiteness and resistance to the most demanding environments (dust, pollution, UV, etc.). These Type 1 fireproof fabrics are ideal for public use tents: frame, kedar, pole and clearspan. The manufacturer provides the following technical specifications on Preconstraint Flexlight Perform 702 S2 and its standards:

weight	22.1 oz/yd ²	EN ISO 2286-2
width	98.4 in / 105.1 in	
standard format length	54.6 yds / 382.7 yds	
tensile strength	280/280 daN/5 cm	EN ISO 1421
tear strength	30/28 daN	DIN 53.363
finish	Weldable S2 fluorinated varnish	

5. Structural analysis of Case Studies (CS)

As a general rule two floor slabs of 12m x12m are connected by pin joint struts of 3m of length. The prestress of 1 kN/m for warp and weft has been applied on all minimal surfaces. The horizontal loads are applied until the membrane reaches its maximum allowable stress.

CS 01

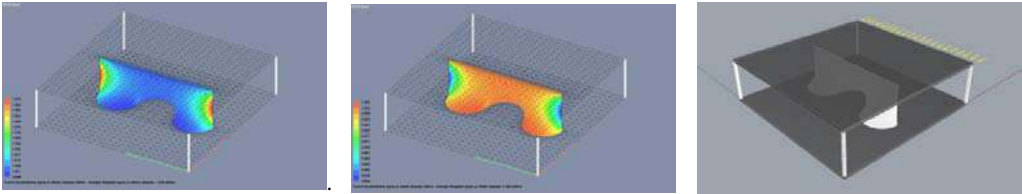


Figure 12: Form-Find-Warp sigma xx stresses 0.996-1.070(kN/m), Form-Find-Weft sigma yy stresses 0.934-1.009(kN/m), Maximum applicable Horizontal Load 10.5 (kN);

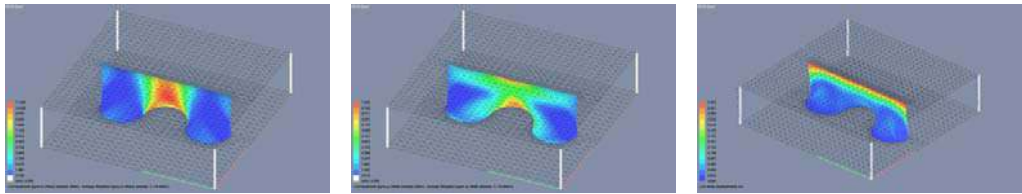


Figure 13: Warp-Maximum sigma xx = 11.058 kN/m < 11.2 kN/m, Weft-Maximum sigma yy = 7.246 kN/m < 11.2 kN/m, Maximum Node Displacements: 0.303 (m)

CS 02

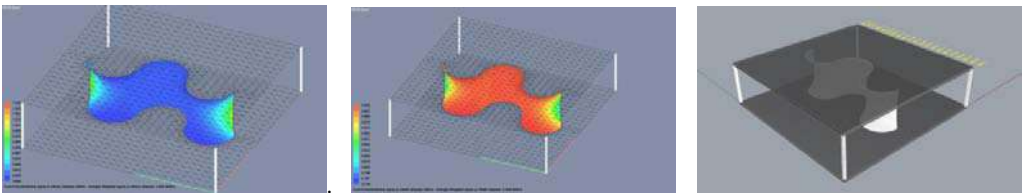


Figure 14: Form-Find-Warp sigma xx stresses 0.894-1.044(kN/m), Form-Find-Weft sigma yy stresses 0.778-0.906(kN/m), Maximum applicable Horizontal Load 19.95 (kN);

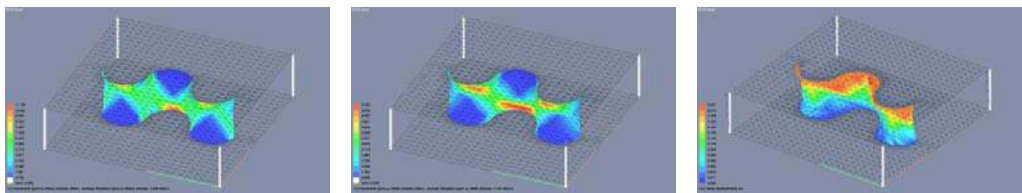


Figure 15: Warp-Maximum sigma xx = 11.136 kN/m (avg.3.438) < 11.2 kN/m, Weft-Maximum sigma yy = 9.750 kN/m < 11.2 kN/m, Maximum Node Displacements: 0.231 (m)

CS 03

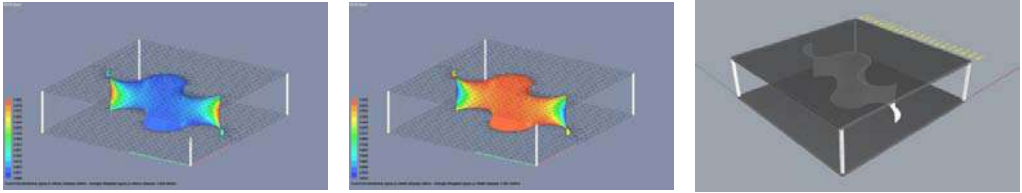


Figure 16: Form-Find-Warp sigma xx stresses 0.894-0.985 (kN/m), Form-Find-Weft sigma yy stresses 0.823-0.906(kN/m), Maximum applicable Horizontal Load 25.20 (kN);

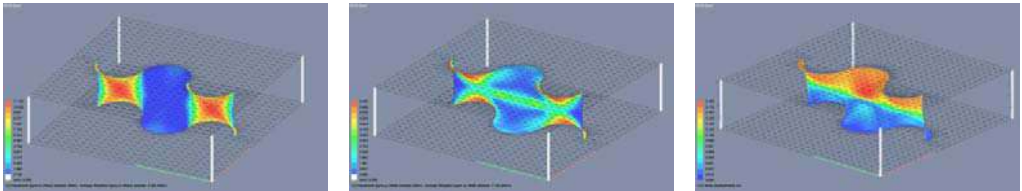


Figure 17: Warp-Maximum sigma xx = 11.120 kN/m < 11.2 KN/m , Weft-Maximum sigma yy = 6,446 kN/m < 11.2 kN/m , Maximum Node Displacements: 0.190 (m)

CS 04 A – Horizontal Load pulling

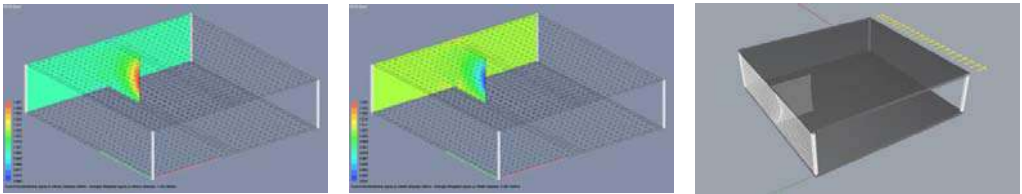


Figure 18: Form-Find-Warp sigma xx stresses 0.962-1.067 (kN/m), Form-Find-Weft sigma yy stresses 0.937-1.040(kN/m), Maximum applicable Horizontal Load 24.60 (kN);

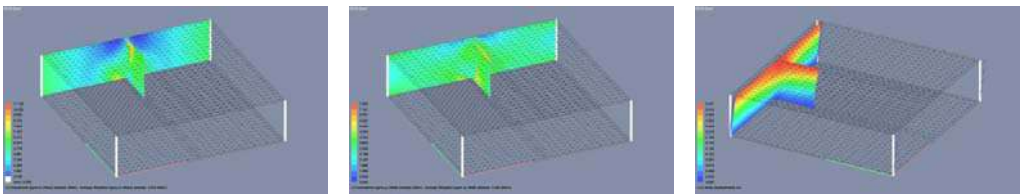


Figure 19: Warp-Maximum sigma xx = 11.148 kN/m < 11.2 kN/m , Weft-Maximum sigma yy = 7.690 kN/m < 11.2 kN/m , Maximum Node Displacements: 0.341 (m)

CS 04 B – Horizontal Load pushing

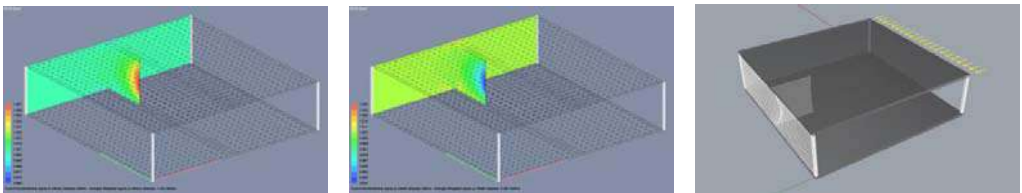


Figure 20: Form-Find-Warp sigma xx stresses 0.962-1.067 (kN/m), Form-Find-Weft sigma yy stresses 0.937-1.040(kN/m), Maximum applicable Horizontal Load 21.80 (kN);

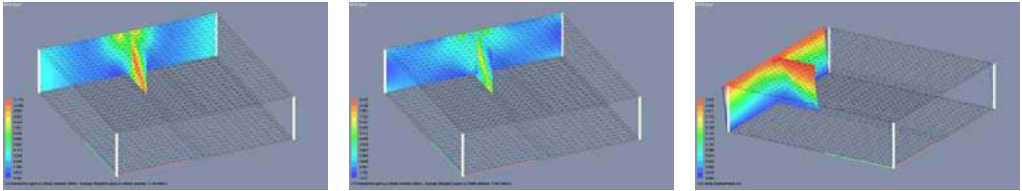


Figure 21: Warp-Maximum $\sigma_{xx} = 11.173 \text{ kN/m} < 11.2 \text{ kN/m}$, Weft-Maximum $\sigma_{yy} = 8.735 \text{ kN/m} < 11.2 \text{ kN/m}$, Maximum Node Displacements: 0.246 (m)

CS 05

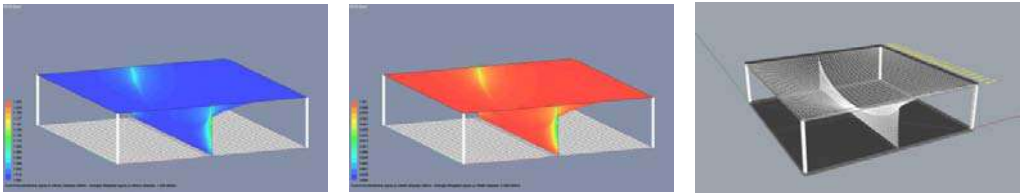


Figure 22: Form-Find-Warp σ_{xx} stresses 1.000-1.225 (kN/m), Form-Find-Weft σ_{yy} stresses 0.826-1.001(kN/m), Maximum applicable Horizontal Load 50.80 (kN);

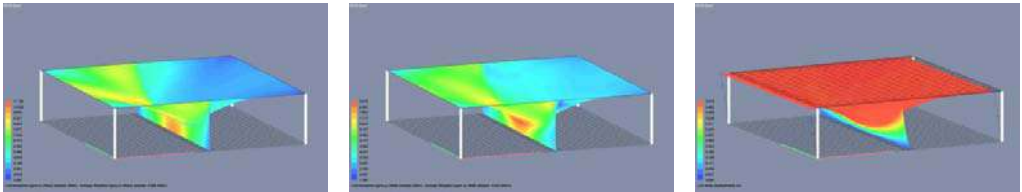


Figure 23: Warp-Maximum $\sigma_{xx} = 11.138 \text{ kN/m} < 11.2 \text{ kN/m}$, Weft-Maximum $\sigma_{yy} = 8.572 \text{ kN/m} < 11.2 \text{ kN/m}$, Maximum Node Displacements: 0.519 (m)

CS 06

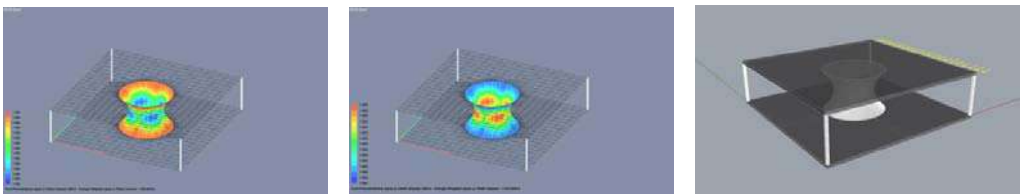


Figure 24: Form-Find-Warp σ_{xx} stresses 1.000-1.000 (kN/m), Form-Find-Weft σ_{yy} stresses 1.000-1.000(kN/m), Maximum applicable Horizontal Load 44.10 (kN);

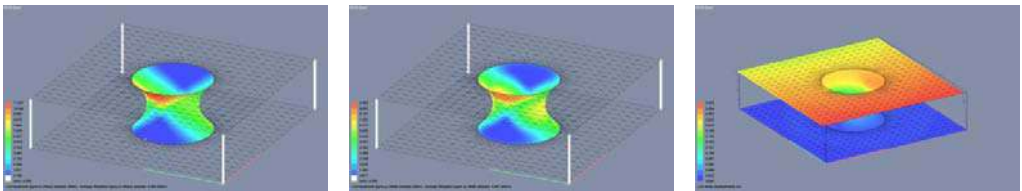


Figure 25: Warp-Maximum $\sigma_{xx} = 11.037 \text{ kN/m} < 11.2 \text{ kN/m}$, Weft-Maximum $\sigma_{yy} = 9.482 \text{ kN/m} < 11.2 \text{ kN/m}$, Maximum Node Displacements: 0.305 (m)

6. Evaluation and comparison of Case Studies (CS)

Looking at the maximum horizontal loads we can understand, which model reaches which stiffness. The comparison of models allows for an evaluation of which setup is stiffer – the higher the applicable horizontal loads the better the membrane is able to compensate these, without exceeding its allowed working load of 11.2/11.2 kN/m.

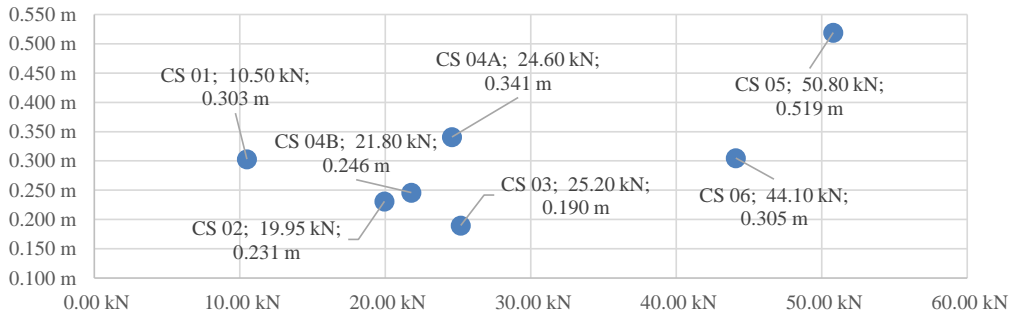


Figure 26: Warp-Maximum Displacement (m) at maximum applicable horizontal load without exceeding the membrane's allowed working load of 11.2/11.2 kN/m

First, it is verified that structural membranes can act as spatial bracing of structures. The structural analysis of Case Studies 01 to 06 (Figures 12-25) and above shown diagram (Figure 26) provide clear results, which can be already predicted from the evaluation of the minimal surfaces' Gaussian curvature. As expected CS 01 Minimal Surfaces between straight lines and boundaries consisting of segments of a circle lack of constellations, which allow for fully anticlastic surfaces. Accordingly, the applicable horizontal loads are low and the resulting displacements of the structure are high. CS 05 T-connections with symmetric wing length, used as a sort of T-intersection of roof and wall is able to resist high horizontal loads (50,80kN) at reasonable displacements (0,519m). Probably this result can be improved by replacing the straight lined boundary of the wall by an oscillating curve. Overall, CS 06 Catenoid between circular rings shows best results, when simultaneously considering the surface content of the catenoid, the maximum applicable horizontal load of 44,10kN, which equals 87% of CS 05 and the resulting displacement of 0,305m, which equals to 58% of CS 05's displacement.

7. Future questions and Case Studies

Future investigations will look into the comparison of minimal surfaces and non-uniform prestressed membranes as well as more complex load cases and load combinations, including earthquake. Last but not least more complex constellations will showcase the merger of 3 aspects, firstly architectural design from the complex interplay of conventional and fluent forms, secondly structural design from the 3D-bracing-effect by membranes, and thirdly benefits in assembly, costs and sustainability, from the pin-joint connection related ease of assembly, alongside high degree of prefabrication of elements.

References

- Filz, G. H. (2010), "DAS WEICHE HAUS soft.spaces", Dissertation, Leopold-Franzens-Universität Innsbruck, Fakultät für Architektur, Juli 2010
- Filz, G. H. (2011), „minimal is maximal _ soft.spaces“, IABSE-IASS 2011 London Symposium Report, Taller, Longer, Lighter, meeting growing demand with limited resources, London, UK, 20-23 September 2011, 204.
- Filz, G. H. (2011), „SOFT.SPACES Anticlastic Minimal Surfaces as Elements in Architecture“, TensiNews, Newsletter of the European based Network for the Design and Realisation of Tensile Structures, September 2011: 21:10-15, ISSN 1784-5688.
- Filz, G. H. (2011), „SOFT.SPACES_Analog and Digital Approaches to Membrane Architecture on the Example of Corner Solutions“, Computational Design Modeling, Proceedings of the Design Modeling Symposium Berlin 2011, Springer-Verlag Berlin Heidelberg, 2011, 105-113, ISBN 978-3-642-23434-7, e-ISBN 978-3-642-23435-4.
- Filz, G. H. (2013): cut.enoid.tower [kʌt.ənɔɪd.taʊə]. In: Bögner-Balz, Heidrun; Mollaert, Marijke; Pusat, Emre: Proceeding TensiNet Symposium 2013. [RE]THINKING Lightweight structures. Brüssel: The TensiNet Association, ISBN 9789072325068, pp. 577 - 584.
- Filz, G. H. (2013): Low-tech or High-tech? "cut.enoid.tower" - three times two facets of irregularity. In: Bletzinger, K.-U.; Kröplin, B.; Onate, E.: Structural Membranes 2013. VI. International Conference on Textile Composites and Inflatable Structures 2013. 9-11 October 2013, Munich, Germany. ISBN 978-84-941531-9-8, elektronisch.
- Filz, G. H. (2013): Minimal-Surface-T-Connections in Architecture. In: ICSA 2013: The 2nd International Conference on Structures and Architecture. Guimaraes, Portugal, 24.-26.07.2013.
- Filz, G. H., Naicu, D. I. (2015): "2 Landscapes" - interaction of 2 gridshells based on a modified Stewart-Gough-principle. In: Falk, Andreas; Vegh, Petr; Chilton, John: IASS Working Groups 12 + 18 - Joint International Colloquium Tokyo, 2015, p.elekt..
- Klasz, W., Filz, G. H.; (2015): A Cloud for Fresh Snow - Research Lab - a hybrid solution of minimal Surface prestresses by bending active boundary conditions forming a spherical tetrahedron. In: IASS Symposium 2015, Amsterdam. Future Visions. Madrid: International Association for Shell and Spatial Structures (IASS), p. elekt..
- SFB230, Heft7, Sonderforschungsbereich 230, "Natürliche Konstruktionen – Leichtbau in Architektur und Natur", Sprint Druck GmbH, Stuttgart 1992
- Otto, F. (1988), *IL 18, Seifenblasen*, Karl Krämer Verlag, Stuttgart 1988

Proceedings of the TensiNet Symposium 2019

Softening the habitats / 3-5 June 2019, Politecnico di Milano, Milan, Italy
Alessandra Zanelli, Carol Monticelli, Marijke Mollaert, Bernd Stimpfle (Eds.)

TemporActive Pavilion: first loop of design and prototyping of an ultra-lightweight temporary architecture

Carlotta MAZZOLA ^{*}, Bernd STIMPFLER ^a, Alessandra ZANELLI ^b, Roberto CANOBBIO ^c

^{*}Politecnico di Milano, via Ponzio 31, Milano, 20129, Italy, carlotta.mazzola@polimi.it

^a FormTL ingenieure für tragwerk und leichtbau gmbh, Güttinger straÙe 37, 78315, Germany

^b Politecnico di Milano, via Ponzio 31, Milano, 20129, Italy

^c Canobbio Textile Engineering Srl, Strada Sgarbazzo snc, Castelnuovo Scrivia (AL), 15053, Italy

Abstract

The paper presents the project development of an ultra-lightweight temporary structure consisting of bending active GFRP arches, a restraining system made of stainless steel cables, and a translucent membrane envelope, with particular focus on the prototyping phase leading to the first construction of the pavilion. A multi-disciplinary team has collaborated to the realization of the first full-scale prototype, built with the aim of deepening a wide range of aspects related both to the optimization of the innovative mix of structural components and to the understanding of the installation constraints, typical of temporary architecture. The paper concludes by showing the results derived from the study and the lesson learned from the first prototype and foreshadowing further studies of the interface between structure and coating, also in relation to the different cycles of use and life-span of the pavilion.

Keywords: temporary architecture, ultra-lightweight structure, bending-active, hybrid structure, membrane, translucent envelope, design, simulations, structural analysis, optimization, prototyping, performance, construction, assembly

DOI: 10.30448/ts2019.3245.40

Copyright © 2019 by Carlotta Mazzola, Bernd Stimpfle, Alessandra Zanelli, Roberto Canobbio. Published by Maggioli SpA with License Creative Commons CC BY-NC-ND 4.0 with permission.

Peer-review under responsibility of the TensiNet Association

1. Introduction

Temporary structures are increasingly present in urban areas: built for temporary events or ephemeral installations that last from a few days to a few months, they are meant to be disassembled and in some cases remounted elsewhere. When designing temporary structures, which have to be erected and dismantled regularly, costs, weight and the size of the prefabricated components have to be limited (Forster, 2004). Reducing the weight of the building materials seems a good prospect for temporary applications from an environmental point of view, in terms of limiting the resources used for the transportation, assembly and usage phase of the structure. Furthermore, designing demountable solutions optimized in weight allow the structure to occupy a limited volume when not in use.

Ultra-lightweight structures, such as hybrid bending-active structures (Slabbinck *et al.*, 2017), represent an efficient response to these needs because both the high performance and the adaptability of their components make these structures suitable for ephemeral and temporary uses (Lienhard *et al.*, 2013). The ongoing research conducted by the authors on ultra-lightweight temporary structures deals with specific requirements (e.g. transportability, easy assembly and disassembly, reuse) that are verified in an experimental application. The present paper describes the project development of an ultra-lightweight temporary structure called TemporActive, with particular focus on the prototyping phase leading to the construction of the first prototype. In particular, the first loop of design of the project investigates, on the one hand, the structural efficiency of the proposed ultra-lightweight system and on the other want to verify the effectiveness of the simplified installation process of the active bending arches. The construction of a full-scale preliminary prototype has been an integral part of the iterative design process that aimed at optimizing the erection process and of detailing the first construction of the pavilion in a public space in front of the Politecnico di Milano. Then the second loop of design will be focused on studying the envelope performance of the pavilion for providing a good level of internal comfort regardless of its thin and transparent building skin.

The challenging goal of ultra-lightweight structures is to find the right equilibrium between structural efficiency and a minor redundancy that makes the system resilient to different scenarios and modes of use of the structure over time. The weight reduction of structural components aimed at facilitating transportation and (dis)assembly, which at the same time had to strike a balance with the minimum requirements of temporary structures and with the requirements that a structure built in a public space must fulfil (e.g. above ground foundations, safety, and accessibility). The use of composite materials for the loadbearing structure aof the arches and the H-section beams of the platform allows to considerably reduce the weight of the whole structure. This affected the design of details, by combining the requirements of the bending- active structure and the interfaces between different materials.

2. Project presentation

TemporActive is an ultra-lightweight temporary pavilion that experiments the combination of a bending active structure and a translucent envelope with the aim of facilitating the transportability and accelerating the assembly and disassembly processes, even by non-specialized installers and therefore to promote multiple uses of the structure after the first use. The name TemporActive refers not only to the juxtaposition of the terms “temporary” and “active bending”, but also to a wider objective of the project of creating a temporary but, at the same time, active and dynamic space for users, able to change according to the functions and activities that are hosted inside.

The pavilion is a hybrid structural system that combines bending-active fibre-reinforced arches, a restraining system made of stainless steel cables, and covered by a form-active translucent membrane. It consists of 2.00x7.00 m modules, reaching a maximum of 3.50, made of double-wing shape restrained arches. The self-supporting module is designed to be structurally efficient and extremely lightweight, weighing only 50 kg. The modularity of the coupled arches allows the realization of different configurations (e.g. single module, tunnel, S-shape curve, flower shape, etc.) and makes the structure capable of hosting different functions. As first use, the structure in a tunnel-like shape will host in June 2019 the Entrance Pavilion of the TensiNet Symposium 2019 "Softening the Habitats" during one week of events connected to the international conference and the related exhibition IN.TENSION. After the disassembly, a second use of the structure it is planned since the structure will be rebuilt inside the PoliMi Campus as leisure time facility for students. The multiple usages and possible locations of the projects - that are often unknown during the design stage - determine design choices to meet requirements compatible with different functionalities. Given the temporariness of the structure, the technological choices and details have been designed and optimized to facilitate the (dis)assembly process and transportability. For this purpose, the detailed design phase has been made in close collaboration with manufacturers and suppliers to find the most suitable solutions to meet the project requirements.



Figure 1. Different usages of TemporActive

2. Structural behaviour

The shape of the structure is determined by a form-finding numerical model based on both static and architectural aspects. The polycentric arch geometry of the project, when compared with a semi-circumference of the same diameter, allows a considerable optimization of the indoor space. To obtain this form, instead of using pre-formed rigid elements, bending active arches are used, by bending linear elements on site and restrained them with cables. Bending active structures are structural systems which are obtained by elastically deforming an initially straight set of load-bearing elements (Lienhard and Knippers, 2014). The use of straight elements simplifies the assembly process since the actively-bent elements can be pre-assembled on the ground and erected afterwards (Liuti *et al.*, 2018). A cable restraining system is located in the inner part of the arch with a threefold function of obtaining the desired geometry, limiting and controlling the deflection of the bent elements and making the structure more resistant to external loads. The restraining system enables the total stiffness of the structure to increase despite the reduced size of the structural profile that can, therefore, be kept smaller and optimized for the bending process (Alpermann *et al.*, 2012).

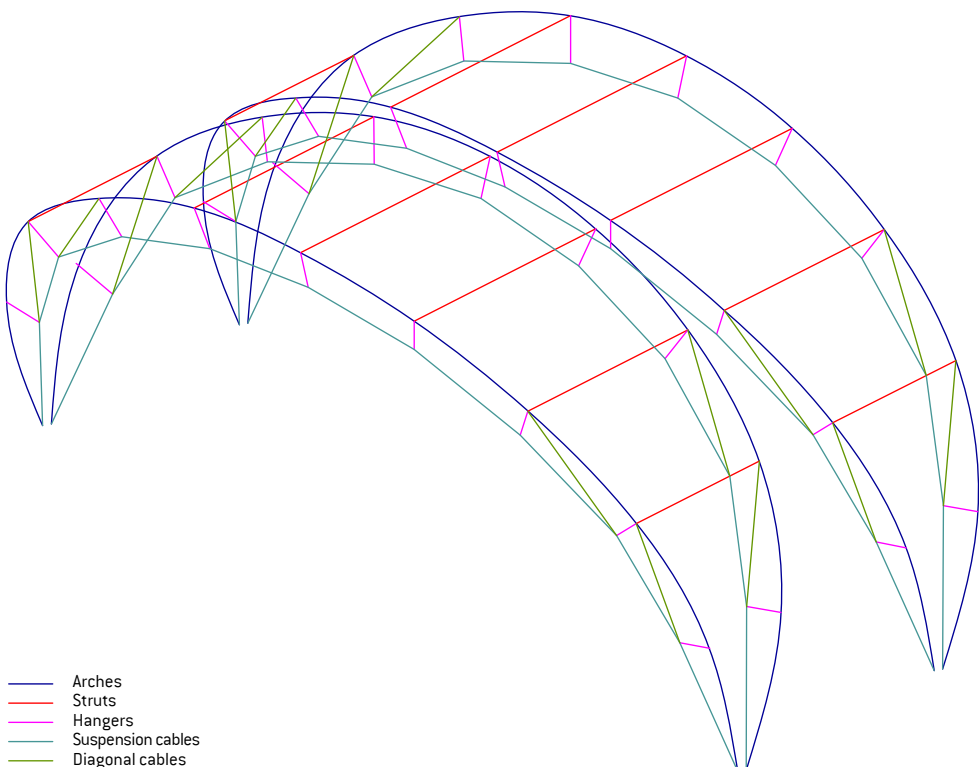


Figure 2. Structural elements

To bend the structural profiles in the polycentric arch geometry the right material needed to be found, able to be easily bent but at the same time to withstand the design loads. Glass fiber-reinforced polymers (i.e. GFRP) meets the criteria required in terms of elasticity and strength (Kotelnikova-Weiler *et al.*, 2013). Considering the safety factor of the material, it was found that the GFRP tube could be bent in the lateral part of the polycentric arch (minimum radius of curvature $R = 220$ cm) only if each tube had a cross-section diameter of less than 2 cm. Due to the limited dimension of the profile, three tubes are combined to form a triangular-shape profile. Each arch consists therefore of a bundle of tubes made up of three GFRP tubes 26x19 mm, 11.50 m long, with a span of 7 m. The combination of multiple smaller diameter tubes allows the arch to be bent according to the required geometry but, at the same time, to resist design loads without buckling.

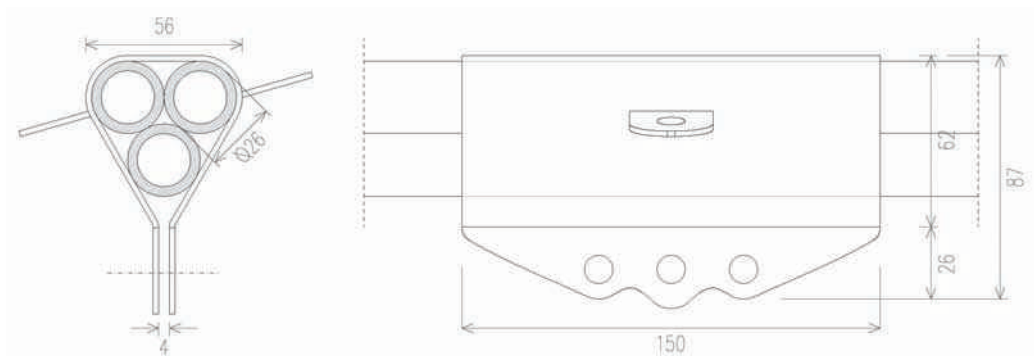


Figure 3. Structural profile composed of a bundle of three GFRP tubes 26x19 mm and its connector

The form-finding and structural behaviour of the structure have been analysed with TLLoad, developed by Mike Barnes / formTL, using the dynamic relaxation method. The structure composed of i) GFRP arches made of bundles of three $\text{Ø } 26 \times 19$ mm actively-bent tubes, ii) stainless steel cable restraining system in the inner part of the arches, iii) GFRP struts placed between the two-wings arches to stiffen and stabilize the structure, and iv) the transparent envelope made of 200 μm ETFE foil results suitable and resistant to the applied loads in accordance with EN13782 - Temporary structures (i.e. snow load $s = 0.2$ kN/m, wind load $q = 0.5$ kN/m²).

3. Full-scale preliminary prototype

The first prototype was built with the aim of i) demonstrating proof of concept for this design approach; ii) verifying the installation process, i.e. easy bending of the GFRP tubes; iii) better understanding the structural performance of the system and comparing its behavior to the form-

found geometry; and vi) to check the technological details (e. g. connections, membrane behavior, etc.).

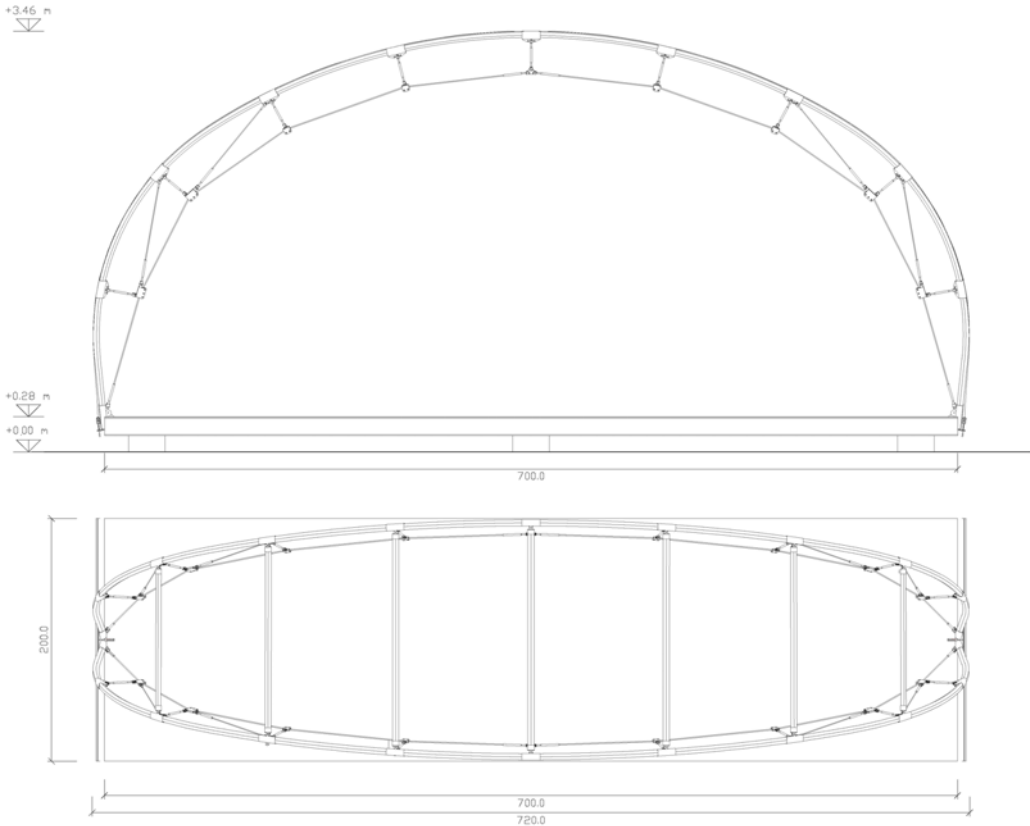


Figure 4. Dimensions of one module of TemporActive

3.1. Specifications

The full-scale preliminary prototype made of two modules of TemporActive covered a footprint area of 7 x 4 m and was 3.20 m high. Each of the four arches was built up from a bundle of three GFRP tubes connected together with 3 mm stainless steel connectors folded in a triangular shape. The restraining system consisted of: i) Ø8mm stainless steel cables parallel to the arches; ii) Ø6mm stainless steel diagonals cables in the lateral part of the polycentric arch, which do not have high tension force but that contribute to increasing the overall stiffness; and iii) turnbuckles 250 mm long to connect the cable clamp with the arch connector, by means of both ends double fork. The length of the cables and the tension required was derived by the form-found geometry. Five struts, made of coupled GFRP tubes 26x19 mm, were placed in the topper part of the arches to spread the arches out and to balance the inner forces resulting from the foil that introduced a lateral force into the end arches and wanted to press the arches together. As a

consequence to the large deformations of bending-active structures during the erection process and the consequent transition from straight to curved elements, the connection details must be carefully designed to allow movement during the erection/bending phase of the structure and then to be blocked once the structure has reached the final geometry. The arches were connected to the ground by means of two-piece stainless steel connectors. A hinge between the two parts of the connector allowed the arch to rotate during the assembly phase and was locked once the arch was in position. Folded stainless steel brackets served as intermediate connectors, allowing the sliding of the lower tubes of the bundles during the bending phase. The connectors were tightened once the arch was erected, before fixing the restraining system.



Figure 5. Base and intermediate connectors details

The envelope was realized with a clear ETFE foil, 200 μm thickness. Given the reduced size of the structural profile (52 mm total width of the arch vs 60 mm width of the standard double keder rail profile), a research was done to find a suitable connection system for the membrane in terms of size and flexibility. Initially, it was thought to use plastic single rail keder profiles since there was not too high force. However, this option has been abandoned in favor of aluminium profiles because the PVC profile deformed too much. To test two different options in the prototype, an aluminium single keder rail was installed on one side and an aluminium single keder rail coupled with an aluminum strip on the other. The second solution resulted more efficient because it prevented the keder rail buckling when the cloth was under tension. The one-piece foil was connected to the first and last arches, without any intermediate fixation, by means of an aluminum single keder rail bolted to the stainless steel connectors every about one meter. The frontal keder rails must be installed after the erection of the structure because otherwise, they behave as active bending elements as well.

3.2. Assembly process

The assembly procedure was first studied with the help of scaled models but it was mainly verified during the first full-scale prototype installation. The prototype construction required the intervention of at least three people who worked full-time for two days. In some phases, e.g. during the membrane erection, the intervention of a greater number of people was necessary. No high forces are necessary to bend the arches and to tension the restraining system, therefore no strong machinery were required for the installation.

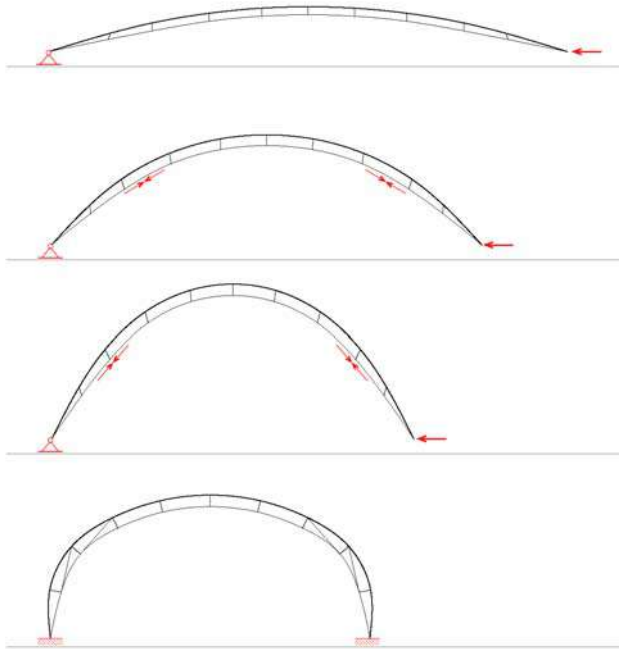


Fig. 6. Bending sequence during the erection of the arches: from the ground to the catenary shape until reaching the final geometry.

The arches were pre-assembled on the ground (i.e. by inserting both base and intermediate connectors, and connecting the restraining system and the struts) e then bent with the help of a manual wire rope hoist. Once the first phase of the arches erection was finalized, reaching the catenary/semicircle shape, the restraining system was fixed to the lower part of the arch and cables were tensioned in order to obtain the final geometry. After completing the erection procedure, it was verified that the geometry obtained corresponded with the project form-found geometry. During the prototype construction, this phase took longer than expected because the geometry has been affected by the asymmetrical assembly mode of the structure. Once the correct geometry had been obtained, the connectors were fixed in place following the marking on tubes, the clamps were tightened at the cable markings and the base connector hinges were locked in order to obtain a rigid joint.



Figure 7. Second module erection during arches bending

Afterwards, the one-piece ETFE foil - rolled and placed at the top centre part of the structure - was unrolled and then fixed to the two end arches with the help of ratchet bands and elastic ropes as tensioning devices for the foil. The ETFE foil was tensioned by pushing in two directions: first perpendicular to the arches to fix the keder rail along the arches' development, then parallel to the arches in the lateral part with the help of a threaded bar. The foil did not cooperate much with the arch-struts structure, having mainly a bracing function; however, after the ETFE installation, the structure was found stiffer and less subject to lateral deformations. ETFE foil is more rigid than textile membranes and it seems not allow to accommodate the movements and high deformations of the bending active structure. For this reason, the hypothesis of changing the envelope material for the final construction is being considered or, otherwise, lower compensation should be given to ETFE for best results. or, otherwise, lower compensation should be given to ETFE for best results. Further studies about the integration of foils in bending active structures should be performed in a new mock-up.



Figure 8. ETFE foil installation



Figure 9. Views of the finished full-scale prototype

4. Discussion and optimization

Both the assembly procedure (e.g. tensioning system and adjustments of the restraining system only on one side) and technical details (e.g. base connectors and plates) has affected the behavior of the final geometry of the first prototype. The erection procedure will therefore be optimized, pre-assembling the straight arches with the un-tensioned restraining system on the ground and then only bending the structural profiles and tensioning the inner cables. In addition, optimization of technical details can further simplify the assembly procedure (e.g. shaping the intermediate connectors to allow the rotation of the restraining system during bending, adding tensioning devices in the inner cable to reduce the length of the cable symmetrically from the two parts of the arch simultaneously) and improve the performance of the structure (e.g. increasing the number of struts to give greater rigidity to the structure).

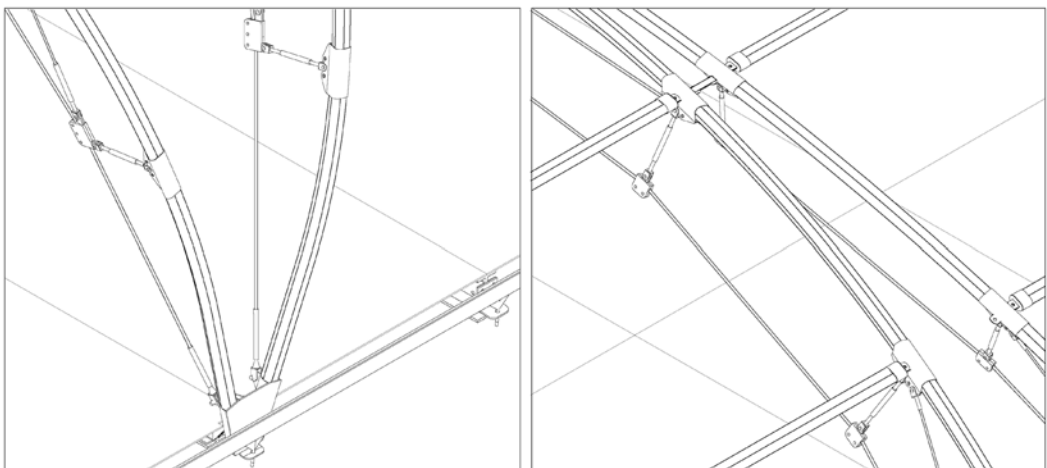


Figure 10. Details after the optimization phase

For the first construction of TemporActive in occasion of the TensiNet Symposium 2019, seven modules will be built, covering a footprint area of around 100 m² in front of the Politecnico di Milano in a public square. The location of the structure in an open public place has influenced the optimization of the tested details and the implementation of the post-prototyping project in two aspects: i) the bending active arches will be connected to a platform made entirely of GFRP H-section beams with adjustable legs and suspended ballast; ii) the installation procedure, having only two days for occupation of the square before the event begins and only one day after the event. This has resulted in scheduling the pre-assembly phase of the straight arches and modules of the platform the week before and then transporting them to the site for assembly. For the pre-assembly and assembly phase, a group of students will be involved. The methods and tools of communication of the pre-assembly and assembly phases to non-specialized people will also be considered in the study.

5. Conclusions and further steps

The construction of the prototype was a fundamental development and verification phase of the TemporActive project before the first construction; however, it is not the arrival point since the research will continue both in the construction phase of the structure and after the event when the pavilion will be reassembled elsewhere for its second use.

The possibility to build an innovative temporary structure is the opportunity to present results of the most recent scientific researches to international researchers, students and citizens, and at the same time to monitoring the structure in order to measure its performance over time. With the first design loop, we verified the behaviour of this hybrid structural system and we had developed the assembly procedure. In the coming months, the research will continue with a second design loop focused on the envelope and in particular on the study of comfort for a transparent envelope by testing and monitoring the performance of different materials and typologies. In parallel, the studies already started on the Life Cycle Assessment (LCA) will be carried out to evaluate the environmental impact of TemporActive. The reflection on the environmental impact of ultra-lightweight temporary structures aims on the one hand to use less metal and materials with a lower embodied energy and on the other to include the time variable in the design process, considering the multiple cycle of use of the structure and not just the single use.

Acknowledgements

The realization of TemporActive involved an interdisciplinary collaboration between Politecnico di Milano TAN, Textile Architecture Network (design and coordination), formTL (structural analysis and engineering) and Canobbio Textile Engineering (engineering, manufacturing and installation).

References

- Alpermann H., Lafuente Hernández E., Gengnagel C. (2012), Case-studies of arched structures using actively-bent elements, Conference Paper IASS-APCS 2012: From Spatial Structures to Space Structures, Seoul
- CEN, EN 13782: 2005, Temporary structures. Tents, Safety, European Committee for Standardization, 2005
- Forster B. and Mollaert M. (2004), *European design guide for tensile surface structures: TensiNet*
- Lienhard J. and Knippers J. (2014), Bending-active structures, PhD Dissertation, University of Stuttgart
- Lienhard, J., & Knippers, J. (2015). Bending-active textile hybrids. *Journal of the International Association for Shell and Spatial Structures*, 56(1), 37-48.
- Lienhard J., Alpermann H., Gengnagel C., and Knippers J. (2013), Active bending, a review on structures where bending is used as a self-formation process, In: *International Journal of Space Structures*, vol. 28, no. 3-4, pp. 187-196.
- Liuti A., Mazzola C., and Zanelli A. (2018), Where design meets construction: A review of bending active structures, *Proceedings of IASS Annual Symposia*, no. 15, pp. 1-8, 2018.
- Kotelnikova-Weiler, N., Douthe, C., Hernandez, E. L., Baverel, O., Gengnagel, C., & Caron, J. (2013), Materials for actively-bent structures, In: *International Journal of Space Structures*, vol. 28, no. 3-4, pp. 229-240.
- Mollaert M., Dimova S. and Denton S. (2016), "Prospect for European guidance for the structural design of tensile membrane structures", *Science and Policy Report (SaP-Report). Draft Version to be published by the Joint Research Centre (JRC) of the European Commission.*
- Slabbinck, E. L. M., Suzuki, S., Solly, J. J., Mader, A., & Knippers, J. (2017), Conceptual framework for analyzing and designing bending-active tensile hybrid structures, *Proceedings of the IASS Annual Symposium 2017 "Interfaces: Architecture.Engineering.Science" 25 - 28th September, 2017, Hamburg, Germany, Annette Bögle, Manfred Grohmann (Eds.)*

Proceedings of the TensiNet Symposium 2019

Softening the habitats / 3-5 June 2019, Politecnico di Milano, Milan, Italy

Alessandra Zanelli, Carol Monticelli, Marijke Mollaert, Bernd Stimpfle (Eds.)

Achieving complex bending-active structures from flexible planar sheets. Hybrid structure introducing the use of spacer fabrics in architectural field.

Elena KRIKLENKO*

*Politecnico di Milano Architecture, Built Environment & Construction Engineering Department

elena.kriklenko@mail.polimi.it

Abstract

This paper presents an innovative structural system based on interactive work of tensioned and bended elements equilibrating each other, made with soft materials. The structural system implies the behavior of elastic sheet material pre-stressed by active bending, thence the investigation is referred to almost unlearned structural field of complex bending-active continuous flexible sheets (CBA-CFS) structures. Blind sheets of common materials used for bending-active structures are basically hardly yield to the complex bending, nevertheless use of particularly customized material with a high grade of elasticity doesn't require introduction of holes or cuts in the surface to allow the bending process. Since all of the materials used are soft, each element of the system is unstable alone but while working together create a shell rigid enough to bear self-weight and additional distributed loads. Principal acting elements of the structure are: customized flexible sheet based on spacer fabric and system of tensioned membranes which deform the spacer sheet in a desirable configuration. Given paper develops the constructive method by research, physical and digital simulations.

Keywords: hybrid structure, bending-active planar, self-formation, mold-less, lightweight, soft structure, synclastic and anticlastic surfaces, spacer fabric, material design, complex bending.

DOI: 10.30448/ts2019.3245.48

Copyright © 2019 by Elena Kriklenko. Published by Maggioli SpA with License Creative Commons CC BY-NC-ND 4.0 with permission.

Peer-review under responsibility of the TensiNet Association

1. Introduction

The demand for complex customized double curved surfaces is increasing in contemporary architectural design and construction. The complex curved shapes are attractive not only from aesthetical point of view, but also may have an advantageous structural performance. A structure, possessing this qualities, together with lightness of construction, being easily assembled without molding (that is very requested for individualized designs), which has in the same time an advanced thermal insulation properties comparing with regular tents, is of high interest for the temporary multiple use. Moreover, for creation of smoother surfaces would be preferred to avoid tessellation since it cause difficulties with erection and connection strategies (Bruetting, 2017). Sufficiency of the structure owning all mentioned parameters may be reached by developing a continuous unique structure based on specific material behavior. Concerning the subject, this paper provides an investigation on a complex bending-active continuous flexible sheets (CBA-CFS) which will be described as a hybrid structure with an alternative behavior induced by its innovative structural and material concept.

2. Background

This chapter provide an introduction into bending-active structures and a brief overview through the categories of structural systems in order to define the main outlines of the designed system and to find a proper place for CBA-CFS into the classification space. The term “bending-active” by Knippers defines curved beam and surface structures that base their geometry on the elastic deformation of initially straight or planar elements (2011). Another definition of bending-active, is a wide range of structural systems that employ large deformations as a form giving and self-stabilizing strategy (Lienhard, 2014).

A part of classification matrix elaborated by Knippers (2011) and reprocessed by Lienhard (2014) presents different types of load bearing structures categorised according to structural action. Although the following classification discern the bending-active structures into a distinct category, this type may be understood instead as a strategy or an approach based on systemized elastic deformation, rather than a distinct structural type.

In the most general view, CBA-CFS is a hybrid structure (fig. 1, structure 19) which is defined as a result from the linkage of two parental systems of dissimilar internal load transmission into a coupled system that presume an intentional combination of load transfer mechanisms (Lienhard, 2014). Whereas, by its different attributes, it can be referred to the bending-active or even vector-active structures. CBA-CFS is a bending-active planar structure because the main acting element of it is a planar sheet of spacer fabric material (fig. 1, structure 6). In the same time CBA-CFS is partially referred to a vector-active planar structure because the inner structure of spacer fabric is similar with those of spatial frameworks (fig. 1, structure 9). If being more specific the CBA-CFS is a Hybrid system based on bending-active planar flexible sheet which has a significant thickness comparing with solid materials used for bending-active structures and has spatial-framework-like inner geometry. The sheet is actuated by system of

tensioned membranes or cords. In the figure 1, types of structures related to the CBA-CFS structural system are highlighted in red. Some referent images of the CBA-CFS added on the right, help to understand and classify the designed structure.

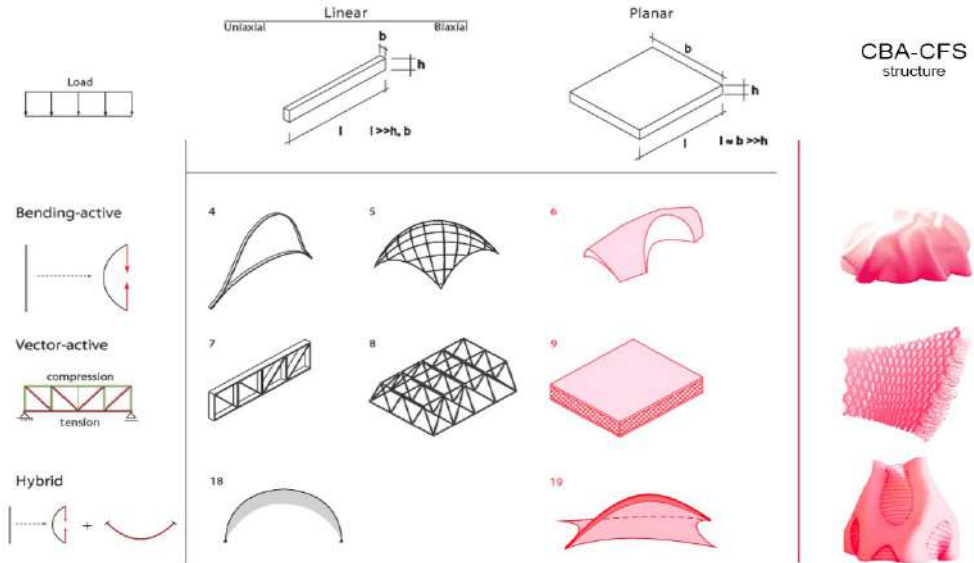


Figure 1: Integrator of CBA- CFS into the loadbearing structural matrix elaborated by Knippers (2011) reprocessed by Lienhard (2014). Highlighted in red - type referred to CBA- CFS structure.

CBA-CFS is a flexible structure, nevertheless some insight regarding stress distribution and consequently form-finding process was inspired by considerations of Mark West (2016) on buckling of the fabric soft formwork in order to obtain concrete shell. One of these considerations is that pull-buckles in fabrics are basically formed in the direction from pull-point to pull-point. In case of fabric hanged from four points, considering the direction of gravity, the material buckling along the principal compression lines, while a buckle itself is directed along the maximum tension stress-lines (figure 2, a). Once the tensioned membrane is reversed into compression shell, the buckling weaknesses of the fabric turn into a deep corrugation of buckling resistance to compression. Another very useful consideration is that push-buckles, unlike pull-buckles, has an infinity of geometric solutions, when pushing (compressing) the sheet of fabric from both directions, but one noticeable detail is that they always form branching y-like shapes (figure 2, c and d). On the figure 2, b it is seen that the buckling pattern doesn't always follow continuously from one pull-point to another but interrupts meeting the restriction of fabric behavior (West, 2016). These findings on fabric stressed in diverse directions were taken into account while searching a form for the CBA-CFS structure. This will be explained in the corresponding chapter.

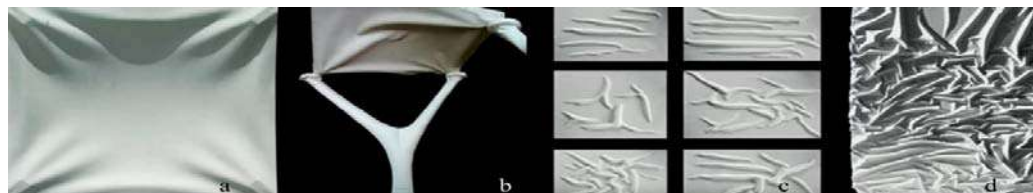


Figure 2: Experiments on fabric behavior under applied stress by Mark West (2016). a- a piece of fabric hung from four points; b- interruption in buckling pattern; c, d- branching shapes of push-buckles.

3. Innovative concept of CBA-CFS structure

In this chapter I would like to underline an innovative contribution of CBA-CFS in terms of textile architecture, structural systems and lightweight constructions.

The textile architecture is typically associated with structures based on tensioned membranes. In case of CBA-CFS the structure is also based on a kind of fabric (3d spacer), moreover, all the structural elements of the CBA-CFS are based on textile and in their disassembled state are not stable, but when achieving their proper bending geometry, gain stability. The structure made just with various textiles is extremely lightweight but the work of this elements differs from the usual membranes and belongs to bending-active type rather than to the tensioned type.

From structural point of view, particular difference of CBA-CFS as a Hybrid, from those known case studies (like Hybrid Tower, 2016 and many others) is that bending action is commonly realized by slender beams while the role of shelter in this kind of structures is usually given to a membrane. In CBA-CFS instead, the bending agent with function of shelter is an actively prestressed bended sheet, while separate membranes stabilize the whole structure. The Bending-active planar structures made with regular materials always meet an issue of compromising the thickness of the sheet to achieve required bending properties and strength. CBA-CFS solves this problem by a particular approach to the material inner geometry. CBA-CFS uses a continuous sheet of material without introducing additional holes to allow bending happen. It is dealing with a complex bidirectional bending that allows creation of double curved shapes made by a uniform piece of the material. The term “Complex bending” presumes that the planar structural element is bent to achieve multiple buckles while the radius of curvature of this buckles is considerably small relatively to the thickness of the element as well as to the size of entire structure. In terms of production and installation CBA-CFS is a fully prefabricated structure released by a kit which includes the spacer sheet with Velcro joints mapped on it and a set of tailored membranes. The kit may be packed in a vacuum bag and be minimized in its size. The volume of spacer fabric is easily restored after the depressurization. All the mentioned peculiarities of the structure and its use are mainly connected to the material aspect. Particular choice of the material derived from another industrial field gives new opportunities of its exploration. From the other hand, reflections on tectonic of curved surface makes the author seek an appropriate material with minimal restrictions. This two factors lead to emerging of a specific architectural expression.

4. The material choice

The following chapter reveal the materials appropriate for designing the CBA-CFS system. For this aim first of all it presents materials generally used for bending-active structures and structural issues related to the material choice.

4.1. Materials for bending-active structures

Appropriate materials for the bending-active structures may be found among those traditional like wood or those in the way of exploration like Fibre Reinforced Polymers (FRP). In general, the request to their properties is low density and high strength combined with low bending stiffness. The minimal bending radius is proportional to the ratio of stiffness divided by strength. For bending-active structures, the most important variables to set into relation are Young's Modulus E and permissible bending stress $\sigma_{M,Rd}$. Adequate materials offer a ratio of $\sigma_{M,Rd} / E > 2.5$ [MPa]/[GPa]. This combination of properties is more important than a singular aspect of mechanical behaviour (Lienhard, 2014). An effective way of depicting such materials for a certain design task is developed by Ashby. He introduces design guidelines in his diagrams to define 'search regions' which identify the design spaces for certain applications (Ashby, 2005).

4.2. Materials for bending-active planar structures

When dealing with planar elements instead of linear one, even more constraints are met due to the inability of bending such material bidirectionally. This problem is often solved by dividing the sheet of material on smaller pieces or stripes (tessellation) or introducing strategically placed holes in order to remove the material from the most stressed areas (La Magna, 2017). This method makes this structures similar to the linear one since the combination of stripes of the material can be seen as a grid of linear elements with a wider section rather than like a uniform surface. Two noticeable projects representing this type are Buckminster Fuller's Plydome built in 1957 and striped structure of ICD/ITKE Research Pavilion built in 2010. This kind of structures can be seen as an intermediate step from linear to planar bending-active structures (5, 6 in figure 1). From the other hand, uniform continuous sheets with properties mentioned above (like plywood, aluminium, bamboo, many types of GFRP etc) are suitable for creating simple shapes bent in one direction (conic and cylindrical surfaces) but does not allow complex bending. Another approach involving the material aspect to be mentioned is an Embedded approach (La Magna 2017) which is dealing with an inner structure of the planar element by introducing a map of auxetic properties and their gradient change throughout the sheet. This method requires a very complex, highly controllable design of inner heterogeneous structure of the material. Instead, the material for CBA-CFS structure deals with a regular structural pattern.

4.3. Materials for CBA-CFS

The material choice for the structure presented in this paper lays on reflections on above mentioned issues. Spacer fabric as well as variable polymer foams from structural point of view has necessary properties to face the need of temporary, easy-assembled monolithic bending-

active lightweight structure. Spacer fabric is commonly used by other industries rather than in architecture, but nowadays it is moving also in this field. The main application of it is cushioning for amortization or reinforcement in composites. But it is not considered as an autonomous structural material for bending-active planar structures, mostly due to its actual fabrication size. Nevertheless, if scale it up to 10-15 cm of thickness or achieve such a thickness by combining several layers, a proper result for CBA-CFS could be born (figure 3).

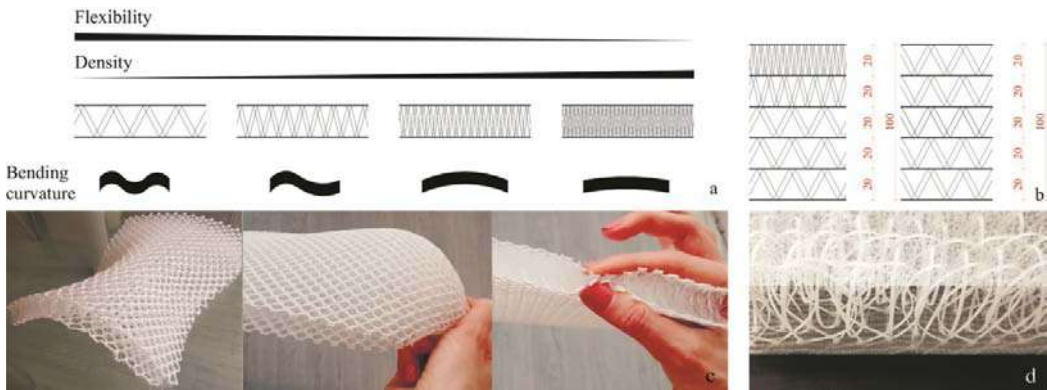


Figure 3: a- Grades of flexibility in the materials with complex inner geometry and different ratio of void space to solid material. The mechanical properties can be tailored to meet the specific bending geometry by varying the fabric structural parameters; b- Structural section of made by coupling several layers; c- spacer fabric of 2 cm able to take synclastic and anticlastic shape when bending; d- prototype of scaled up spacer.

The 3D knitted spacer fabric consists of two separate fabric layers (top and bottom surfaces) that are connected by intermediary yarns. The top and bottom fabrics can be weft or warp knitted fabrics with or without inlays (Ciobanu, 2011). The flexibility of it can be controlled by thickness of the sheet, quantity of layers, density of spacer, layer pattern, thickness and material of yarns (figure 3, a). The compression properties depend a lot on the spacer yarn type and arrangement. Bending properties are closely related to the fabric type, structure, spacer yarn type and density, while stretch and recovery properties mostly depend on fabric type and spacer yarn type (Yip, 2008). This customized set of properties partially solve the problem of bidirectional bending. And finally the high grade of flexibility allow complex geometry bending that is used as an instrument to create a shelter with a double curvature. The inner geometry of the spacer fabrics has structural similarities with a spatial frameworks but in different scale and made with an alternative material. This allows to benefit from manipulating by voluminous ultra-lightweight elements instead of slender and less resistant sheet. This difference of material distribution in spacer fabric and in solid sheet can be compared with difference between a beam and a truss action. The chosen material due to its inner structure and the grade of elasticity is not rigid enough to resist any significant load within its relaxed state, and it can be easily rolled and packed in the vacuum bag for transportation. But being bent strategically, gains stability enough to satisfy need of a temporary shelter. The main issue concerning the work with spacer fabrics to be faced is scaling it up (preferably) or joining together several layers.

5. Design methodology and development of the CBA-CFS

5.1. Functioning parts of the system

The work of the CBA-CFS Hybrid system lays on interaction between bending-active initially planar structure (so called *Bended layer*) and system of separate tensioned membranes (by which the *Tensioned layer* is composed). Geometrically the *Tensioned layer* almost repeats an initial shape conceived by the designer while the *Bended layer* always follows this shape in the near proximity. For the aim simplification of the description the terms of *General shape* (shape conceived by designer) and *Final shape* (the one build up with the *Bended layer*) are introduced. Following descriptive scheme of structural elements of the system explains the geometrical concept. *Bended layer* as the *Final shape* is drawn in blue, *Tensioned layer* as the *General shape* drawn red. In this case (figure 4) the *General shape* hasn't curvatures and presented by a rectangular plane. The whole hybrid system built up as follows: 1- The desirable *General shape* is intersected with an analytically defined (see the next chapter) *Final shape*; 2- Due to the differences in the two shapes, some parts of the *General shape* are seen above and another under the *Final shape*; 3- Outlines of this parts become the guidelines for tailoring the system of tensioned membranes on the top and the bottom of the *Final shape*. The top part, the bottom part and the *Bended layer* joined together, stabilize each other and the whole structure.

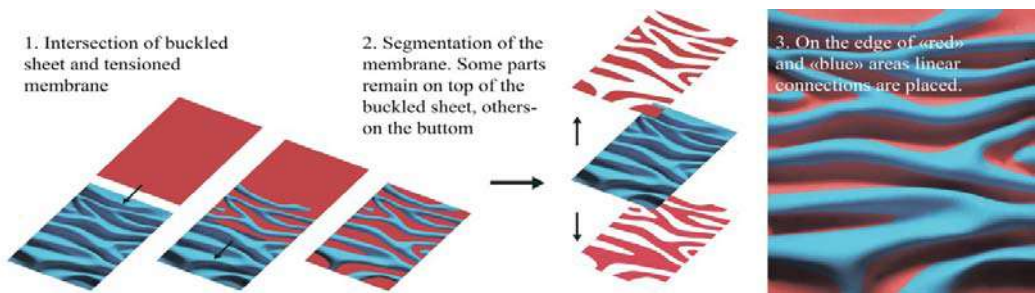


Figure 4: Geometrical concept of CBA-CFS Hybrid system and its functioning parts

5.2. Form-finding rules (Height, Intensity, Direction, Displacement)

The way the *Bended layer* is shaped coming up from the logic of stress flows, numerous physical and digital experiments and some insight gathered from the reference material (See the “Background” chapter, Mark West). Buckling of the *Bended layer* creates an additional height to the section of the structure. Distribution of the material throughout the structure is also related to the intensity of buckling. The proper direction of the buckles plays significant role in the stability of the whole structure thence is decisive in the form-finding process. Stress-lines pattern advises the direction of buckles alike with corrugation in the metal sheet which create additional rigidity. Thus, the major factors which lead the buckles form-finding process are: 1- overall height of the buckled section (amplitude); 2- intensity of buckling (frequency); 3- the direction of buckling pattern. This three factors are related to the stiffness optimization of the structure. The curvature is tightly connected to the proper tailoring, prestress and placement of

the *Tensioned layer* in relation to the center of the section (figure 5). Displacement of *Tensioned layer* in the direction of desirable curvature leads to self-formation of this curvature.

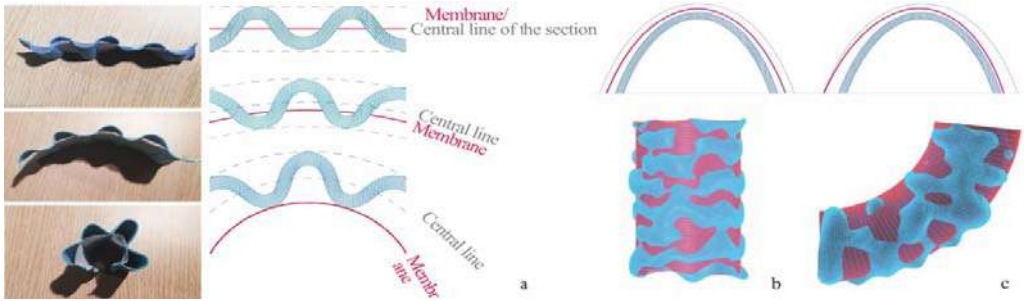


Figure 5: Displacement of *Tensioned layer* in the direction of curvature: a- self forming curvature actuated by displacement of *Tensioned layer* from the center of the section. b- photos of the section samples and drawings; b- section and plan of cylinder shape; c- section and plan of toroid shape.

5.3. Design workflow and digital analysis

In order to clarify the whole logic of the design flow the “step by step” definition is given in the following part: 1- First, the desirable *General shape* of the whole structure should be defined. This example based on the simple synclastic dome-like surface; 2- It is loaded with its self-weight (some additional loads can be added depending on the design case); 3- The produced *General shape* goes under structural analysis (figure 6) to pick information about the stress distribution and the lines of principal stresses in the loaded shell; 4- According to the information received, a decision on the optimization and preliminary definition of the *Bended layer* can be taken according to the Form-finding rules. It is seen from the diagram of stiffness



Figure 6: Digital analysis. a- Diagram of Von Mises stress; b- Diagram of principal stresses distribution; c- Stiffness optimization; d- Stress-line pattern; e- Distribution of material in the section of a regular shell; f- optimized material distribution.

optimization (figure 6 c) that the lighter areas should be more resistant (have more material distributed, have higher section). Diagram of principal stress-lines (figure 6 d) determines the direction of buckles, i.e. defines the buckling pattern; 5- Ones the requirements are set, we can start to design the *Bended Layer*. Since the pre-stressed sheet (in its bended state) closely follows the geometry of the *General shape*, can be concluded that the flat template may have a variety of shapes from rectangular to circular one in order to form a cone/cylinder wrapping the given dome (figure 7). In this case the ratio between external and internal perimeter of the *Bended Layer* is defined by ratio between stresses in upper part of the dome and its lower part.

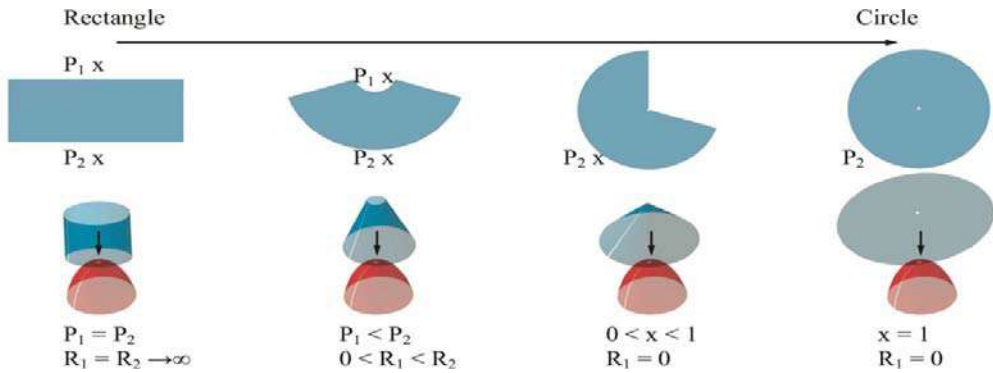


Figure 7: Defining the flat sheet material outlines. P1x- upper perimeter segment, P1x- lower perimeter segment, R1-radius of upper segment, R2-radius of lower segment.

This ratio varying the quantity of the material distributed in each part; 6- The buckles pattern can coincide to the pattern of stress-lines or move away from it without the obvious contradiction to the stress flows but according to the free will or necessity of the designer. It is noticed that for better formation of overall shape, buckles can shape an interrupted branched pattern instead of strictly following a regular continuous pattern of stress lines (figure 8). Also the choice between the circular template or conic/rectangular one can be guided by the will to introduce the seamless structure or introduce an entrance or another opening; 7- After defining the template outline and buckling pattern, the whole *Bended Layer* is ready to be simulated with the Particle Spring System (in Kangaroo 2) or by Marvelous Designer. The definition for the Kangaroo simulation is written in a way that parameters R, P, X (from figure 7), and consequently the outline of the flat material, as well as the buckling pattern can be easily changed to meet the desirable *Final shape*. 8- If the shape received is adequate and satisfactory,

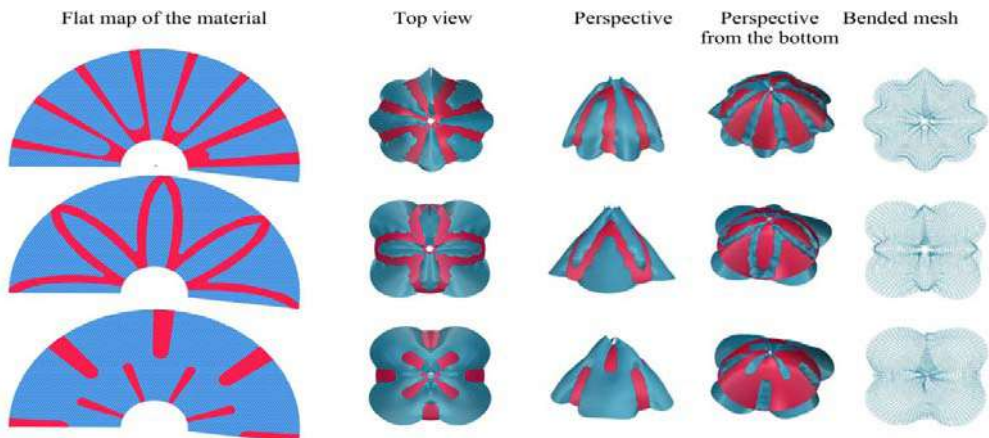


Figure 8: Different buckling pattern follows the main concentric direction of the stress-lines. line1- regular pattern; line 2,3- branched pattern;

it goes under the second round of structural analysis, after which a decision on its further optimization can be taken (figure 9). Process of designing CBA-CFS is cyclic, and can be significantly free, since the grade of pure optimization can vary accordingly (and should be proportioned) to the aesthetic expression.



Figure 9: Shapes generated with circular piece of material and deflection diagrams for each shape

9- After the *Final shape* is found, analyzed and satisfy the need by its stress distribution and aesthetic qualities, the problem of its stabilization comes out. In a way it was described in the part 5.1, the two layers intersecting each other. From this intersection we get the set of top and bottom tensioned membranes (figure 10 a). The membranes should be pre-stressed according to the direction of curvature of the *Bended Layer*, rather it is one direction or two (figure 10 c). The membranes should have considerably low elasticity in order to provide better stabilizing effect, but enough elastic to ensure a smooth tensioned surface. Due to its segmentation, the *Tensioned layer* can approximately repeat any *General shape* either it is synclastic or anticlastic, with high or low curvature. Segmentation is also needed to place the membrane in the center (or close to the center) of the section since the placement of the membrane to the very top or bottom of the section cause the decrease of stability; 10- The lines of intersection with the *General shape* should be mapped on the *Bended layer* in order to define the two-layer connection placement. Sets of the membranes are tailored by flattening the top and bottom segments and modifying it considering the stretching properties of the membrane (figure 10 b); 11- When the flat piece of the *Bended layer* is mapped by connection lines and the set of membranes get their shape, the set is ready for or the final digital simulation and production.

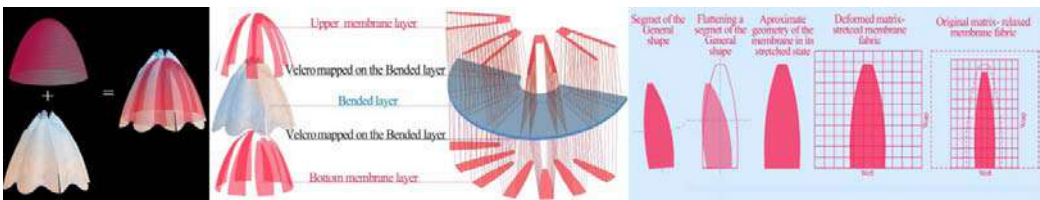


Figure 10: Tailoring the membranes

6. Fabrication of scaled prototypes

The following chapter describes the fabrication of scaled CBA-CFS models. The very first set of models was made with flexible polyurethane foam by threading it through. Material was buckling when pulling the threads, the same thread was passing through several buckles. This revealed a problem of fixing the thread since the foam sheet was sliding along it (figure 11 a). The second model was produced by joining the *Bended layer* to the prefabricated soft net of hemispherical shape to control the final shape giving to it synclastic curvature. The connections

of *Tensioned net* and *Bended sheet* were fixed and didn't slide (figure 11 b) but the *Tensioned layer* in this case was displaced on the bottom of the section, that caused the decrease of stability. Third set was made by pinning the material on the “dummy”. The challenge here was to save the dummy shape and fix it by *Tensioned layer* which had to be placed close to the center of the section. The model in the figure 11 c was fixed by threads as well, but this time each thread was fixing just one buckle setting two borders similar to shoelaces. Both external and internal sets of threads built up a shape similar to those of dummy but slightly extruded outside. Here came an idea that the *Tensioned layer* can almost repeat the *General shape* and that the denced set of threads can be replaced by membranes in order to control the tension in both directions. The small scale models formed with membranes can be tailored by sewing two layers of pretensioned fabric with the *Bended layer* in between (figure 11 d), but in bigger scale with a material of around 15 cm of thickness the problem of connection and needs an alternative solution. On the figure figure 11 e, f the two types of connections are presented. The linear connections made with the Velcro are suitable for the membranes and dot connections are adapted for the system of threads or cords. The last 1:5 model realized with two layers of spacer fabric (2 cm each), gradually assembled by pulling threads and fixed by membranes.

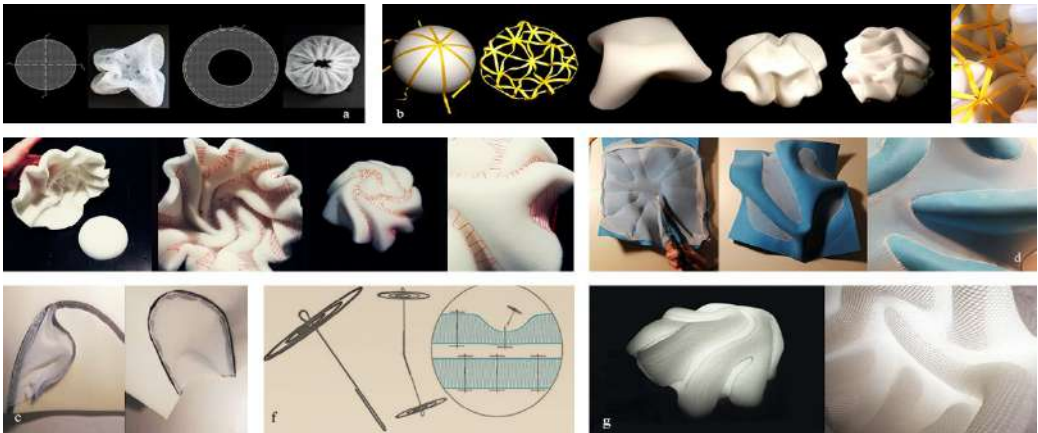


Figure 11: a- First models; b - Second model with spherical tensioned net; c- Third model pinned on a dome dummy with new system of thread placement; d- Shapes formed by the membranes; e- membrane tension layer system- velcro tape connection. The velcro are sewn by the perimeter of a membrane. f- set of connectors and cords for *Cords-tensioned layer*; g- exterior and interior view of 1:5 model made with spacer fabric with overall thickness of 4 cm.

6. Results and discussion

The concept and the method of CBA-CFS system explores opportunities for development of a wide range of shapes easy assembled, lightweight and owning a high potential for aesthetic expression due to the innovative structural approach and application of new family of materials. The work of the structure practically shown by numerous physical prototypes. The paper defines

an overall method of CBA-CFS design process, describes bases of formation logic, highlights the aspect of material application and opens a field for the further explorations.

The next steps of the development could be an investigation on coupling several layers of existing material, and further quantitative structural analysis. However, investigation on opportunities for scaling up the spacer fabric seems to the author more challenging. An innovative approach of using scaled knitted spacer structure as a self-sufficient element in architectural field states a question of emerging of a new customized products and machinery. Development of an “architectural spacer fabric” is a challenge that opens a whole new sector of architecture which deals not only with its autonomous application as a structural material but also gives alternatives in its more traditional application as reinforcement. For instance, concrete, polymer foams or even water impregnation (with further solidification) to build a rigid ice shell in extremely cold climate. Other alternatives for further research can be use of cellulose foam for the *Bending Layer* due to its reversible properties of hardening after drying. An investigation on the development of particular solution for controllable hardening of cellulose is a topic for a research in the chemistry field. Moreover, a spacer structured fabric based on cellulose yarns can be developed for CBA-CFS application. There are numerous directions of moving the ongoing research on CBA-CFS structures which open vast opportunities to benefit from the emerging of a new structural type and new sector of material application.

Acknowledgements

The research realized as a part of master thesis at the Polytechnic University of Milan TEXTILESHUB Department of Architecture, Built Environment and Construction Engineering

References

- Ashby M. F., “Materials selection in mechanical design.” MRS Bulletin, 2005
- Bruetting J., Koerner A., Sonntag D., and Knippers J., “Bending-active segmented shells,” in Proceedings of the IASS Annual Symposium 2017, HafenCity Universität, Hamburg, 2017
- Ciobanu L., “Development of 3D knitted fabrics for advanced composite materials.” In: Attaf B, editor. Advances in Composite Materials-Ecodesign and Analysis. InTech, 2011.
- Fuller, R. Buckminster. 1959. Self-strutted geodesic plydome. US Patent 2,905,113, filed April 22, 1957, and issued September 22, 1959.
- Knippers J., Cremers J., Gabler M., and Lienhard J., “Construction manual for polymers and membranes: materials, semi-finished products, form finding design.” Basel: Birkhäuser, 2011.
- La Magna R., “Bending-active plates: strategies for the induction of curvature through the means of elastic bending of plate-based structures,” Ph.D. disser., ITKE, Univ. of Stuttgart, 2017.
- West M., “Pressure Building: A New Architectural Language of Fabric-Formed Concrete”, presentation for the NYIT School of Architecture and Design on October 17, 2016 in NYC.

Proceedings of the TensiNet Symposium 2019

Softening the habitats / 3-5 June 2019, Politecnico di Milano, Milan, Italy
Alessandra Zanelli, Carol Monticelli, Marijke Mollaert, Bernd Stimpfle (Eds.)

Computational Knitting in Architecture: an Experimental Design Process for a Performative Textile System

Ingrid PAOLETTI*, Elena CLARKE^a, Andrea GIGLIO^b,

*Politecnico di Milano, ABC Department
Ingrid.paoletti@gmail.com

^aHarvard Graduate School of Design, Cambridge, MA (USA)

^bPolitecnico di Milano, ABC Department

Abstract

Today's possibility to design the performance of fabrics thanks to computational tools has broadened the application of knitting techniques to AEC. This paper will introduce a practical and computational trial to produce a knitted shading structure for a pavilion through a preliminary experimental process. The first part of this paper will focus on the practical knitting technique, in which the geometry and derived properties of a knitted stitch will be examined. A rule is defined within the knitted pattern to increase the number of stitches per course, resulting in diagonal outer edges with specific slope. Using this rule, three distinct geometric textile modules are defined where the relationship between the edges of each module provides the possibility for their combination into different patterns. The second part of this paper will introduce possible pattern simulations of the combination of textile modules. Varying degrees of enclosures can be produced through the pattern simulation and adapted to the diverse program of the pavilion and its orientation within the project site. Various structural technologies will be examined in an effort to demonstrate the possibility of integrating such a textile system through existing technologies.

Keywords: (knitting techniques, geometric textile design, geometric patterns, shading structure, textile pavilion design, computational design).

DOI: 10.30448/ts2019.3245.11

Copyright © 2019 by I. Paoletti, E. Clarke and A. Giglio. Published by Maggioli SpA with License Creative Commons CC BY-NC-ND 4.0 with permission.

Peer-review under responsibility of the TensiNet Association

1. Introduction

Knitting is a traditional and complex method of manipulating fibers in which the loops of a fiber are gradually intermeshed in order to produce a fabric. The knitted pattern of the loops, referred to as stitches, brings elasticity to the fabric. Different stitch types, bringing different knitted patterns, introduce varied properties to resulting fabrics, allowing manufacturers to tailor the shape, rigidity, and consistency of their product, thus producing customized results.

Developments in computational design have expanded the possibilities of applying knitting techniques on an architectural scale. Traditional practices of knitting have been integrated and adapted through computational tools to move beyond their traditional methods and uses, providing incredible inspiration and innumerable possibilities to contemporary designers.

This paper explores the possibility of applying traditional knitting techniques through computational tools to the design of a prototype for an architectural pavilion. Through preliminary physical testing and investigation, three unique geometric textile modules are defined and later simulated using computational tools. The possible patterns that their combination creates produces the possibility of various “degrees of enclosure” that can be customized to accommodate different program for the pavilion. Integrated within the pavilion’s structural system, the combinations of textile modules appear as one “continuous” fabric, while creating multiple “interior” spaces defined by the separation of knitted fabric “walls.”

2. Knitting geometric modules

This section of the paper introduces practical knitting techniques that have traditionally been used to produce patterns within knitted fabrics. First, common pattern-producing techniques are presented, including the possibility to join two unique fabric pieces along a diagonal seam. The possibility of “scaling up” these joining techniques is presented through a physical trial that joins 10mm hemp rope and common stainless steel hardware.

The textile pieces presented here are simulated through the “Stockinette” stitch. One of the most common knitted stitches, “Stockinette” is produced by knitting complete alternating rows of “purl” (or “under”) and “knit” (or “over”) stitches, giving the stitches a distinct “V” shape on the front of the fabric piece.

The second part of this section examines the geometry of the “Stockinette” stitch, producing a method to determine the length and weight of each completed stitch. After setting a rule to “increase” one stitch for every row of purl stitches, three unique geometric textile modules can be produced by “mirroring” the resulting base shape of a right triangle. Potential combinations of the three unique modules are explored to understand the possibilities of joining the textile pieces along their edges.

The proposed textile modules are investigated through physical trials and conceptual diagram during the design of the pavilion prototype. At a later date during a workshop held at the Politecnico di Milano, the pieces are computer simulated by a team led by Ingrid Paoletti (modeling the “Stockinette” stitch in Grasshopper and the textile modules in Kangaroo).

2.1. Pattern joining in traditional knitting

The diverse hand techniques that have evolved from traditional knitting permit a variety of patterns and designs for knitted fabrics.

2.1.1. “Picking up a stitch”

It is common practice in traditional knitting to create multicolored geometric patterns by “picking up the stitches” of a completed fabric section (see Figure 1.). This is accomplished by looping a new strand of yarn through the crossed “end stitches” of the completed piece, thereby creating a new row of loops that permit a new fabric section to be attached to the existing piece.

Often this is accomplished by using strands of contrasting colors, in order to create a pattern that is embedded within a knitted fabric and creating a “knitted seam” between the two distinct fabric pieces. A variation of the technique can also be applied to join two fabric pieces that have already been completed.

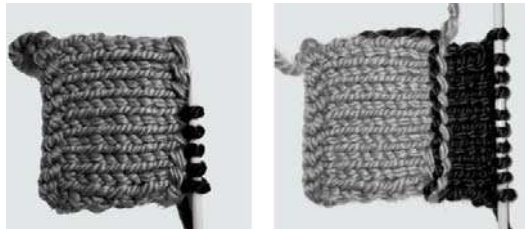


Figure 1: Hand trials of “picked up stitches” along a vertical edge, using two different colors and strands of yarn. 10mm knitting needles are used.

2.1.2. Creating a diagonal seam

A diagonal seam can be created along the edge of the knitted fabric by either “increasing” the number of stitches in a row (or by “decreasing” them). “Increasing” a stitch is accomplished by “knitting twice” on one stitch. “Decreasing” is accomplished by knitting two stitches together. Physical trials with Stockinette stitch were completed by increasing one stitch for every purled row (so alternating rows of stitches increase by one). This method produces a diagonal on a single side of the fabric piece (while the opposite side remains straight, see Figure 2.). Other methods (such as “knitting twice” or more on every row – which causes opposite sides of the fabric piece to simultaneously increase) produce diagonals of different slopes.

The method used (increase one stitch every other row) produces the possibility of a right triangle (increasing only along one edge). By “knitting twice” with the first stitch of every purled row, a crossed loop shape is produced along the diagonal seam, similar to the crossed ends of a straight seam. These loops can then be “picked up” to join the diagonal seam to a new piece of fabric in the same way that straight seams can be joined (described in 2.1.1).



Figure 2: Hand trials of “picking up stitches” along a diagonal seam, using two different colors and strands of yarn. 10mm knitting needles are used.

2.1.3. Possible attachments to existing hardware

Traditionally, these methods are used to produce flat patterns that are integrated within a single knitted fabric. This project however, investigates whether these joining methods could produce a joint between unique large-scale fabric pieces that could then be folded along their seam to produce inhabitable space.

At an architectural scale, modular textile pieces would likely be produced as completed fabric sections (easily transportable from manufacturer to the project site) and then integrated within a cable system (a common structural system for tensile fabrics and one that could be used, in this case, to create large-scale “seams”). Here, the possibility of looping the closed stitches of a completed textile piece to a piece of closed steel hardware are explored. Using hardware to attach the ends of the textile modules along a structural cable (versus attaching the ends directly to the cable) produces a structural “break” (that can help to prevent the textile from deforming during installation and also enables the piece to be more easily installed, removed, or replaced). The principle of “picking up the stitches” of a completed knit fabric (common in traditional knitting techniques) is used to loop the closed end stitch of the textile to the hardware.



Figure 3: Physical trial to test attaching a “closed stitch” to a closed hardware. Completed with 10mm three-strand synthetic hemp rope and a stainless steel swivel eye hook loop.

2.2. Determining proportions for three geometric modules

Three geometric textile modules are defined by examining the proportions of and the diagonal slope created by “increasing” with the Stockinette stitch.

2.2.1. The geometry of the stitch

The geometry of the Stockinette stitch is explored through its proportions, understanding that each stitch has an “optimal geometry” to produce optimal stretch. In terms of material, three-strand synthetic hemp rope of 10mm diameter is considered (which has its own elastic material property that must be taken into consideration). Recalling that the properties of manufactured fabrics is dependent on the type of stitch used (see Introduction: different stitches in knitting produce different fabric properties), a single “V” stitch is diagrammed. The proportions of a single stitch will be used to determine maximum and minimum areas of stretch and also to determine the diagonal slope achieved by increasing by one stitch.

This diagram allows multiple stitches to be considered through their proportions to produce a method of counting that can be used to estimate the length of 10mm rope necessary to produce a Stockinette stitch (a necessary consideration in the manufacturing of the textile pieces, and one that also allows the weight of each module to be determined).

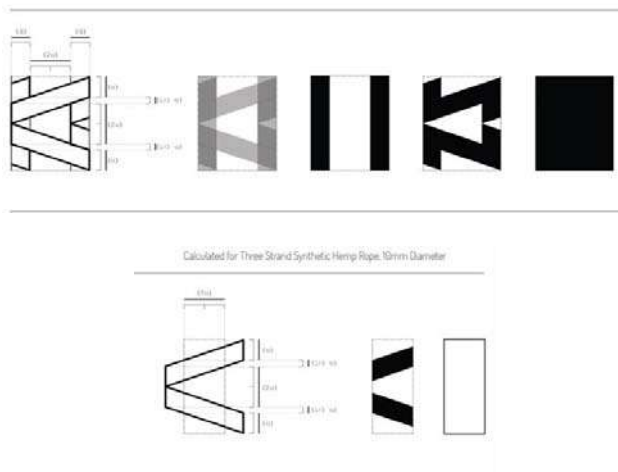


Figure 4: Diagram of the proportions of the Stockinette stitch. (Note: the length of rope needed to “loop under” and create a new stitch is not pictured in this diagram, but was taken into consideration).

	Length of Rope		Weight of Rope
■	48 cm	■	0.02182 Kg
□	45 cm	□	0.00205 kg
Table 1: Estimated length of rope for a 10mm diameter.		Table 2: Estimated weight of rope for a 10mm diameter.	

2.2.2. Defining shape based on set slope

Using the rule of increasing one stitch for every purled row (see 2.1.2), a specific slope is defined, creating a right triangle. By “mirroring” the same right triangle in two different positions, three geometric modules are produced in proportion to one another (see Figure 5.). The slopes of the geometric modules match, allowing for the possibility of their combination into various fabric “patterns.” These fabric modules are imagined to be arranged in combinations along their edges, and attached along their seams, in order to create inhabitable space in the pavilion prototype.

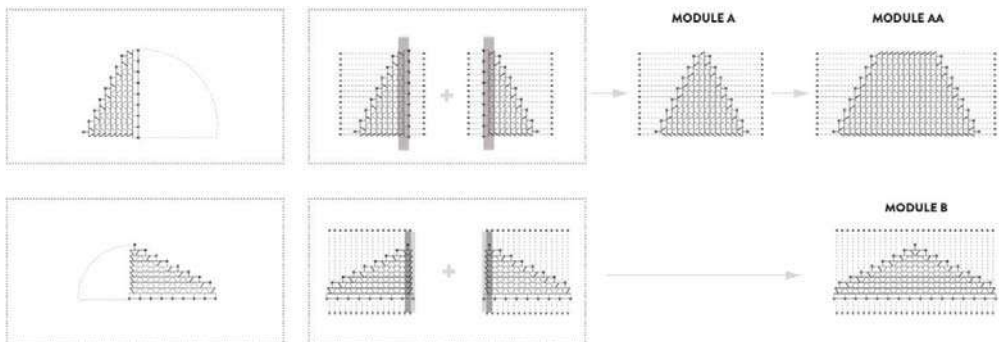


Figure 5: Three geometric textile modules are defined by “mirroring” a single right triangle. For clarity of drawing, dashed lines show the “direction” of the Stockinette stitch.

2.2.3. Exploring geometric combinations

Possible pattern combinations of the proposed textile modules are explored by understanding the relationships between the edges of their geometries (see Figure 6.).

Once the length of the straight edge of each geometric module has been set, the maximum and minimum values achieved through stretching the fabric can be determined for each textile module (this must, of course, take into consideration the elastic properties of both the Stockinette stitch and also the material properties of 10mm three strand synthetic hemp rope). This can be determined by calculating maximum and minimum areas, using the resulting calculations to determine maximum and minimum lengths of the sides. Additional pattern combinations of the fabric modules then become possible through the range of length possible from stretching each side.

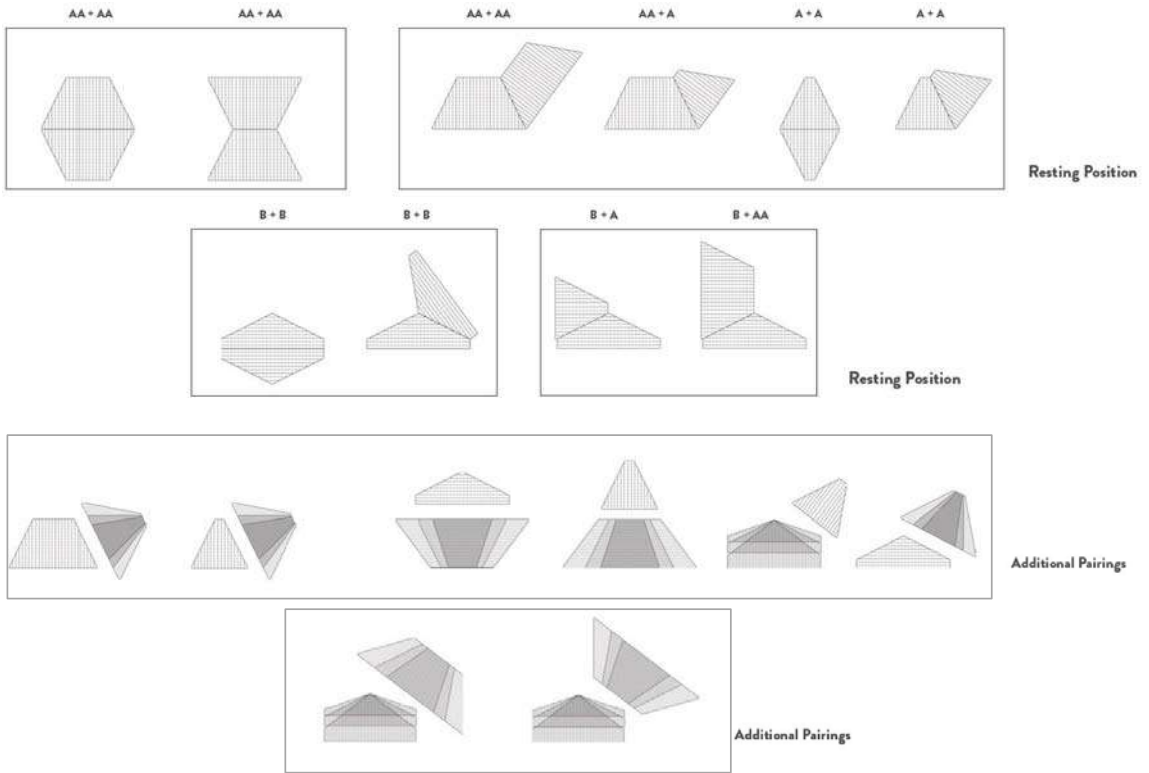


Figure 6: Possible combinations of the textile modules are simulated, based on the relationship between the edges of each module.

3. Combination of textile modules for a prototype design

This section explores the possibility of combining the three geometric modules into various pattern combinations to create space suitable for different pavilion program. The resulting open shading structure is a seemingly continuous patterned fabric that acts as to delineate space both through overhead shade and also through vertical fabric “walls.” The possibility of securing the patterned fabric between an external frame (composed of four curved triangular space trusses) and a system of curvilinear steel bars “hidden” beneath a raised wooden deck is investigated and developed through the adjustment of existing structural technologies.

The prototype proposed is for a country pavilion for the 2020 World Exposition in Dubai. The site is situated within the Dubai Expo with its main entry facing North/Northwest. The knitted composition of the textile modules produces a porous condition, allowing wind to traverse through the pavilion site and also reducing wind loads considerably. The tropical desert climate of Dubai is taken into consideration, and low-consumption cooling systems are explored.

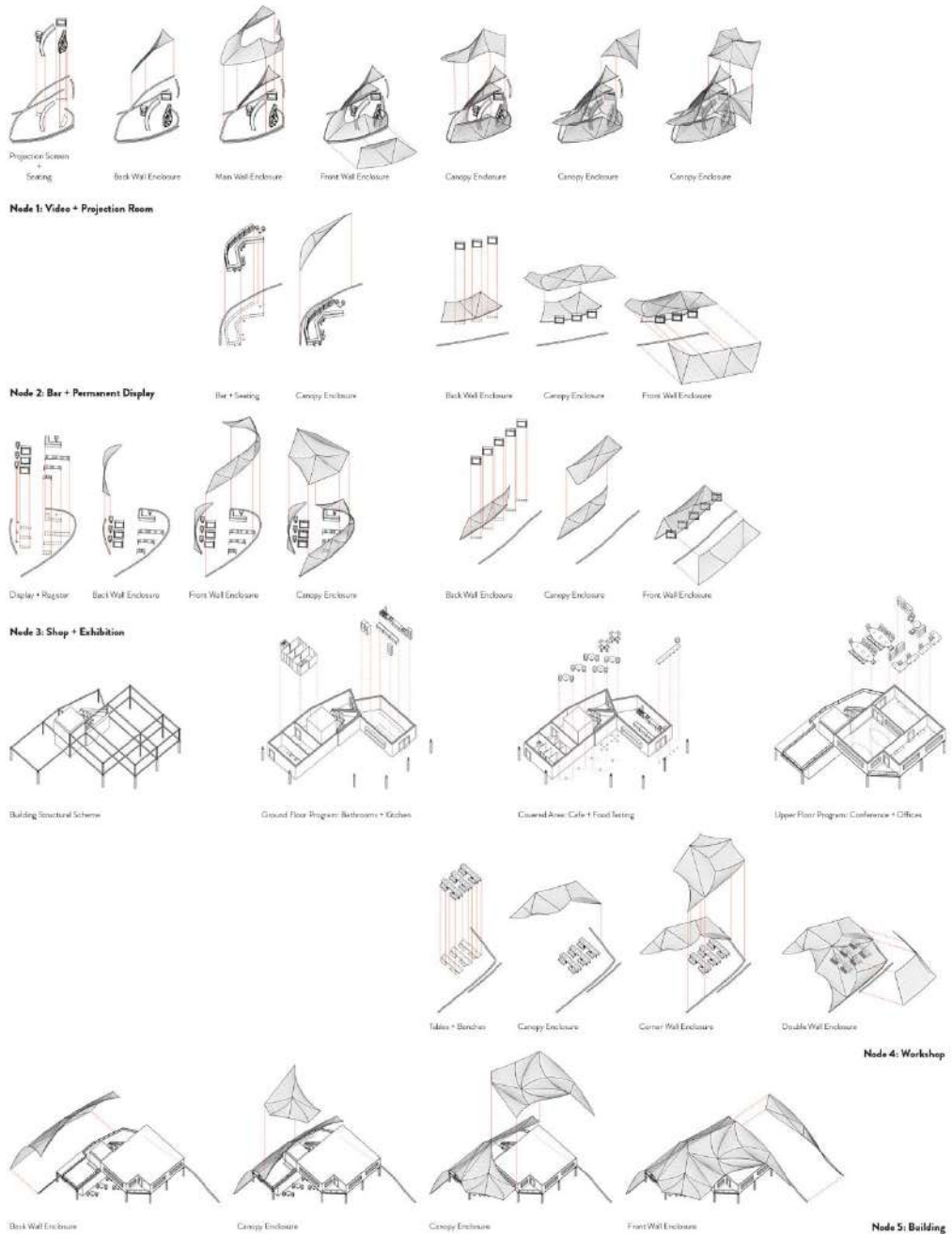


Figure 9: Exploded axonometric drawings simulating possible pattern combinations of the textile modules into geometric nodes that “wrap” various pavilion program.

3.1.2. *Wrapped enclosures and fabric “walls”*

The geometric textile modules are attached to one another through connecting structural cables. At the ground, the textile modules are secured at their ends and then along their edges by a system of curvilinear steel bars hidden beneath a raised wooden deck. This way, the textile “meets” the inhabitable ground, creating the appearance of fabric “walls.” The textile modules are held in tension above by structural cables that connect the consolidated modules to an external frame composed of four triangular curved space trusses.

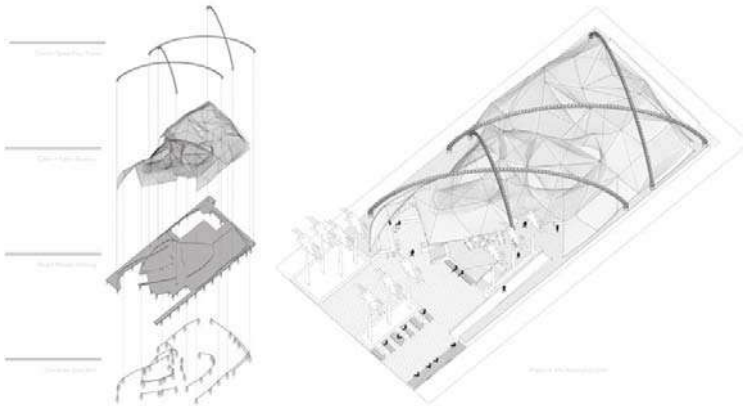


Figure 10: Axonometric drawing (right) of the project in site and exploded axonometric (left) demonstrating the curvilinear steel bar system that secures fabric modules below the raised wooden deck.

3.2. Integration of textile modules through existing structural technologies

The adjustment and modification of existing structural technologies is explored in order to demonstrate the possibility of integrating the textile modules into a larger system.

3.2.1. *Hardwares and connections*

Early physical testing explored the possibility of attaching completed fabric pieces to a stainless steel swivel eye hook loop (a common hardware used to secure ropes – see Figure 3.). In this section, the possibility is presented of modifying one end of this common hardware so that it has a flat metal plate that can be screwed into cable clips (to secure textile pieces to structural steel cables) or to a membrane plate (used to secure corners of tensile fabrics).

The knitted end stitches of the textile modules, once looped to the hardware, can be secured to adjustable cable clips (see Figure 11.). These cable clips can be secured in multiple positions to accommodate the direction of the textile stitching, and they can be easily replaced if necessary without disturbing the adjacent textile piece. At the ground, the end stitches of textile modules (once looped to hardware) can be secured at their corners to a membrane plate. Multiple

membrane plates and structural steel cables can then be consolidated and attached to foundations through a semicircular steel anchor plate (see Figure 12.). Along its edges at the ground, the end stitches of the textile modules (once looped to hardware) are secured along a curvilinear steel bar using an adjustable nylon rope (see Figure 12.). These adjustable systems are necessary in order to “tighten” the fabric system (which inevitably stretches over time).

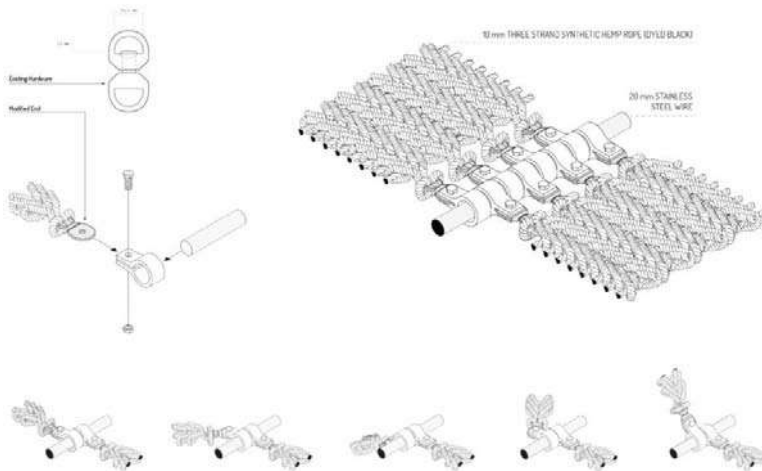


Figure 11: Diagrams depicting the adjustable connection of textile modules to structural cables.

3.2.2. Making use of a raised deck

The raising of the inhabited ground plane by a wooden deck allows for the integration of a fan system embedded in the floor. Integration of geothermal cooling can cut energy costs, to create a low-consumption cooling system that is integrated into the pavilion design. A fan system releases cooled air through perforated wooden panels embedded in the deck.

3.2.3. Integrating connections with an external frame

An external frame of four curvilinear space frame triangular trusses holds the textile modules in tension. The steel cables that secure the textile modules to one another are consolidated at the top corners of the fabric pieces, along with the corner membrane plates, and secured to a structural cable that is anchored to one of the exterior trusses.

The resulting structure holds the combined textile modules in tension between the embedded steel bars in the “ground” of the raised wooden deck and the “sky” of the external framing system.

4. Conclusion: experimental possibilities

The experimental prototype design presented here uses the geometric and material properties of knitted fabrics to inform the design and production of an architectural pavilion through the combination of knit textile modules. In particular, the process intends to explore and analyse an experimental process that allow to collect data to transform the control-by-hand work into digital modelling. Developments in computational tools in recent years have produced the possibility to incorporate traditional knitting techniques into large-scale productions, enhancing existing innovative technologies. Students at the ETH Zurich in collaboration with ZHCODE and R-Ex have worked in the past year to produce a four meter tall installation through a 3D-knitted design. As the development of computational knitting continues to progress, the experimental possibilities of applying knitting techniques at an architectural scale will expand, extending the opportunity for the integration of textiles in large-scale innovative designs and giving designers the opportunity to develop their own skills by challenging a very old technique like knitting in an innovative way.

References

Walther, M. (2018, October 29). 3D-knitted shells save on construction materials and time. Retrieved November 2, 2018, from <https://www.ethz.ch/en/news-and-events/eth-news/news/2018/10/knitted-concrete.html>

ACADIA 14: Design Agency [Proceedings of the 34th Annual Conference of the Association for Computer Aided Design in Architecture (ACADIA) ISBN 9781926724478] Los Angeles 23-25 October, 2014), pp. 267-276 http://papers.cumincad.org/cgi-bin/works/Show?acadia14_267

ACADIA // 2016: POSTHUMAN FRONTIERS: Data, Designers, and Cognitive Machines [Proceedings of the 36th Annual Conference of the Association for Computer Aided Design in Architecture (ACADIA) ISBN 978-0-692-77095-5] Ann Arbor 27-29 October, 2016, pp. 280-289 http://papers.cumincad.org/cgi-bin/works/Show?acadia16_280

Au, K. F. (2011). *Advances in knitting technology*. The textile Institute. Woodhead Publishing. ISBN 978-1-84569-372-5).

Ahlquist S., Menges A., October 2013, Frameworks for Computational Design of Textile Micro-Architectures and Material Behavior in Forming Complex Force-Active Structures. Conference: Association for Computer-Aided Design in Architecture (ACADIA) 2013 International Conference At: Cambridge, Ontario, Canada

Proceedings of the TensiNet Symposium 2019

Softening the habitats / 3-5 June 2019, Politecnico di Milano, Milan, Italy

Alessandra Zanelli, Carol Monticelli, Marijke Mollaert, Bernd Stimpfle (Eds.)

FlexHab

Edoardo MARCANDELLI*, Nicola GIULIETTI^a, Francesca PEREGO^b,
Eleonora TERUZZI^b, Eleonora VALLE^b

*Politecnico di Milano | Alta Scuola Politecnica, Piazza Leonardo da Vinci, 32, 20133 Milano, Italy,
edoardo.marcandelli@asp-poli.it

^a Composite Research s.r.l., Piazza Avis, 9, 10064 Pinerolo (TO), Italy, n.giulietti@composite-research.com

^b Politecnico di Milano | Alta Scuola Politecnica, Piazza Leonardo da Vinci, 32, 20133 Milano, Italy

Abstract

The FlexHab project of Alta Scuola Politecnica aims to study an application solution for the MadFlex (developed by Composite Research s.r.l.). It is a composite material panel, with a layered structure, basically a sandwich-like structure. Thanks to its innovative mechanical feature, the panel is flexible, even rollable, on one side, while it is absolutely crushproof on the other. The preliminary analysis of different fields of application has shown how the potential of MadFlex is addressed in the critical context of disaster management, for the construction of emergency shelters. In the Italian context, the "Recovery period" is conventionally split into "Medium-term supplementary reconstruction sub-period" and "Definitive reconstruction sub-period", in which shelter solutions are wooden houses, containers and SAE. The FlexHab project proposes a solution able to eliminate the first sub-period and to significantly reduce the overall timing of the "Recovery period". Crucial elements of the research are the interface with an innovative material with no applications and any technical tradition, and the conception of a constructive and technical system coherent both with it and with the specific requirements of the emergency shelters topic (adaptability to different weather conditions, reversibility, high performance, easy to transport, easy to storage, sustainability, affordability, flexibility and modularity). The objective of FlexHab is to conceive a shelter solution both for the private market and for a revolution of the disaster management processes, combining the requirements of comfort, flexibility, smart technical solutions and life cycle sustainability.

Keywords: emergency shelter, lightweight structure, composite material, innovation, performance, comfort, sustainability, modularity

DOI: 10.30448/ts2019.3245.37

Copyright © 2019 by E. Marcandelli, N. Giulietti, F. Perego, E. Teruzzi, E. Valle. Published by Maggioli SpA with License Creative Commons CC BY-NC-ND 4.0 with permission.

Peer-review under responsibility of the TensiNet Association

1. Introduction

The FlexHab project investigates a possible field of application for a new composite material, the MadFlex, and develops a specific construction technology regarding flexible housing solutions. The material has been developed by Composite Research srl.

Some crucial points of the research are how to approach an innovative material with no existing applications and to define a constructive and technical system consistently with the materials' properties and with the specific requirements of the emergency shelters' topic.

The preliminary analysis carried out, concerning the different possible fields of application, has shown how the potential of MadFlex is addressed to the critical context of disaster management and can be efficiently deployed in the construction of emergency shelters. In the Italian context, the "Recovery period" is conventionally split into "Medium-term supplementary reconstruction sub-period" and "Definitive reconstruction sub-period", in which shelter solutions are wooden houses, containers and SAEs (Soluzioni Abitative in Emergenza meaning "emergency housing solutions"). The FlexHab project proposes a solution able to eliminate the first sub-period and to significantly reduce the overall timing of the "Recovery period".

2. Project description

The project is concentrated on creating a technology push for a new material. The MadFlex (PCT WO2016120785 A1) is a lightweight asymmetric composite material panel, having a sandwich-like structure. It exhibits a two-order-of-magnitude difference in bending stiffness, depending on the direction of the applied bending moment, thanks to a reversible buckling phenomenon of one of its skins: it is flexible, even rollable, on the one side, while it is rigid like a traditional sandwich panel on the other one. In addition, the foam core confers to the MadFlex good insulation properties.

The design and the development of a novel flexible habitat starting from the potentialities of the new material face a multiplicity of research needs which has been integrated into a systemic approach and organized in four main steps:

1. The requirements identification: at the material / building component / habitat level. The new material is tested and its characterization orients the right matching with a set of technical requirements for adaptive structures and flexible skins;
2. The form + structure integrated design process: supported by advanced form-finding design tools and performance-based modelling tools;
3. The experimental phase, where a first demonstrator of the new adaptive skin is installed and tested to validate the behaviour of the new habitat and to optimize its final design;

4. The study of different application of the novel habitat solutions and the evaluation of social, economic and environmental impact by using multi-criteria analysis, Life Cycle Cost (LCC) and Life Cycle Assessment (LCA).

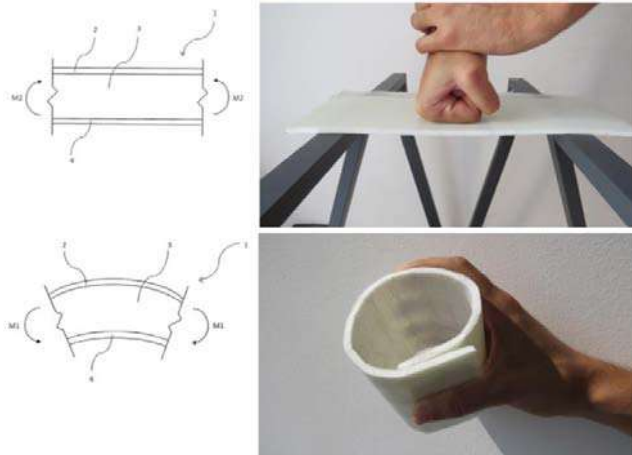


Figure 1: The two-order-of-magnitude difference in bending stiffness of the MadFlex.

The goal of the FlexHab project is then to design and develop a novel flexible habitat starting from the potentialities of the MadFlex. The main objectives are:

- Apply a multi-functional, flexible, “aeronautics-derived” composite material (MadFlex) to figure out futuristic habitat solutions;
- Improve a revolutionary approach to the building system introducing an innovative technology;
- Envision an innovative building skin, seamless and integrated with the structure, considering the industrial production requirements.;
- Satisfy user needs through an economical and social sustainable solution;
- Investigate performances and the economic feasibility of a basic adaptive habitat.

3. Problem understanding and opportunities exploring

The MadFlex is a composite material panel with a layered structure. The uniqueness of the MadFlex consists in its mechanical feature: the panel of MadFlex is flexible, even rollable, on the one side, while it is crushproof on the other. Investigating the possible scenarios where MadFlex properties could be determinant to perform a revolution inside the market, emerged

that the Emergency Shelter field was the most suitable to develop new innovative solutions. In fact, in the Emergency field the more relevant requirements are transportability (MadFlex is rollable and lightweight), constructability (MadFlex is lightweight and could be equipped in the production phase), performances (MadFlex has good thermal and mechanical performances), and customizability (MadFlex could be customized with many different finishings).

Looking for possible stakeholders involved in the Italian scenario and analyzing their needs, the main requirements have been outlined. Victims of calamitous events demand an increasing of comfort and quality of life inside the emergency shelters as well a more user-friendly solution closer to their houses. Institutions as the government and the Protezione Civile department require a decreasing of costs and time of the solution and an increasing of performances and social sustainability within the Recovery period. Finally stakeholders interested in trade, production and advertising of the FlexHab proposal are looking for the competitiveness of the project solution, that must be more sustainable, in terms of cost and social impact, of the existing ones.

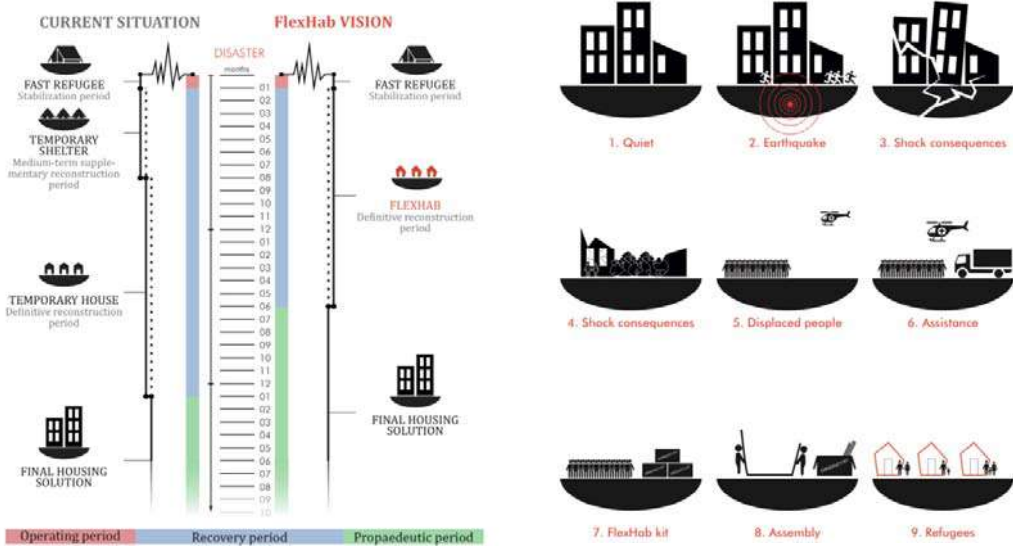


Figure 2: The emergency management process, Current situation applied in Italy and FlexHab innovative scenario.

In Italy, the Recovery period is conventionally split in different phases to which correspond different emergency housing solutions. Firstly, temporary shelters as containers and wooden houses are used to provide an immediate aid; nevertheless, they are not positively evaluated by the population because of the lack of comfort and security. Meanwhile, SAEs (meaning

“emergency housing solutions”) are built to host the disaster victims. They are well appreciated because of their tendency to look like as permanent houses, but, on the other hand, they are available too far from the catastrophic event. The FlexHab project introduces a solution able to eliminate the first sub-period, and consequently to change the nature of the Recovery period in the field of costs, time and social impact.

The MadFlex can be efficiently deployed in the construction of emergency shelters in the critical context of disaster management, thanks to many peculiarities intrinsic in the material, such as being flexible and rollable on one side, and stiff and crushproof on the other. It allows both an easy and efficient transportation/stock, and a rigid livable skin. Then one of the main assets was to design a shelter that would be easily stocked in a FlexHab kit that, as for common tents kits, is easy to transport, built and dismantled for future uses. Moreover, conversely to many composite materials, MadFlex can be moulded and accessorized in a continuous flow process, saving up to 50% of the cost spent with a warming process and meanwhile, addressing constructive needs as introduction of joints, during the production phase. Facing the emergency shelter issues, low cost and easy and fast implementation are fundamental requirements. As a consequence, modularity becomes a smart answer to fit industrial production necessities as well for the settlement and the architectural composition of the artefact. Furthermore, from an energetic point of view, it has good thermal and acoustic performances in relation to its thickness guaranteeing good thermal level of comfort for the shelter.

4. Project features

4.1. Innovativeness

The shelter’s design embraces, in single solution, the technology of the tent, easy and fast to deploy, and the “archetype” of the house, as a private and human scaled space. The goal of the design is to provide a just-in-time housing shelter being easy and fast to assemble, in order to avoid the need of temporary shelters as containers and temporary houses as SAEs. As a consequence of its being rollable and lightweight, meanwhile preserving its mechanical and physical performances, the MadFlex, in terms of transportation, is more competitive than the majority of construction materials available on the market. This was a further proof to start envisioning an innovative emergency shelter, easily folded into a FlexHab kit that, as for common tents equipment, is easy to transport, built and dismantle for future uses.

Analyzing the competitive solutions on the market and mostly looking into the Italian scenario, two emergency habitat solutions are deployed. Firstly the big emergency tents, then containers and other temporary shelters are used to provide an immediate aid, usually not positively

evaluated considering the temporality of the alienating situation. Afterwards, SAEs are built to host the disaster victims; even if they are quite well appreciated thanks to their homely look, they arrive too late from the emergency break.

The FlexHab kit ensures a just-in-time deployment, while its peculiar design, made possible by Madflex flexibility, reminds the archetype of the house, making it more likely to be appreciated by the users. The main feature of our design is the irregular pentagonal shape of the shelter. This asymmetry is conceived to allow, on each side, a different function as services, light and furniture with a high freedom for a user-based customization. Moreover, the pentagonal design, coming from the use of the modular Madflex panels, enables to set up the whole envelope through a single construction gesture. The shelter entrance is defined by a threshold, symbol of privacy and ownership. The interior space is composed by modules of 1,5 m that can be easily assembled in different combinations, adapting the shelter to the hosting group or family.

The shelter is equipped with basic services as kitchen and a soundproofed bathroom. Natural and artificial lights and interior spaces are carefully designed to fit man and its daily activities. The structure supporting the Madflex is designed on the whole length with wooden supports for extra furniture, allowing the customizability of the spaces. All those features allow FlexHab a valuable competitor in the market, able to supply both medium term and definitive reconstruction sub-period solutions.

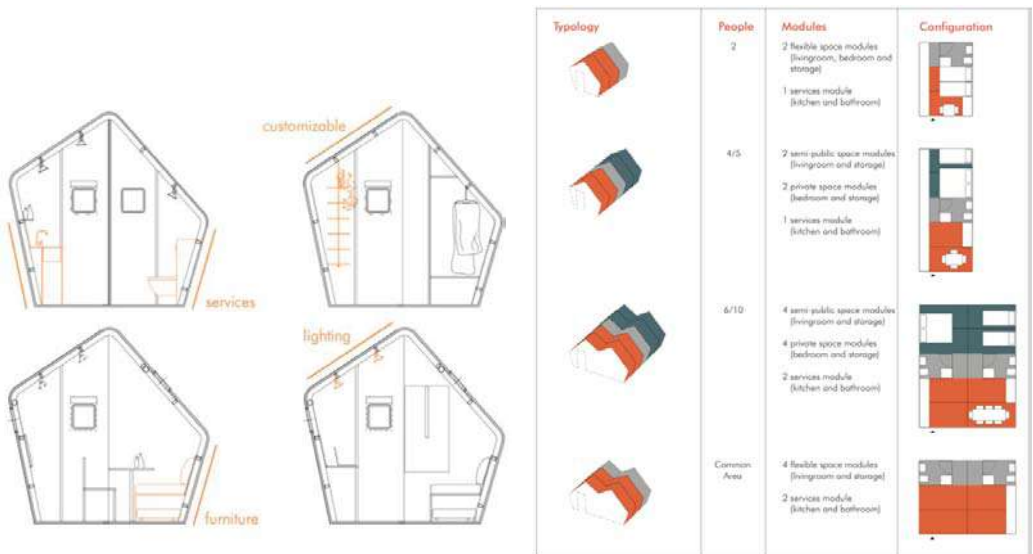


Figure 3: Different modular configurations of the shelter and transversal section definition.

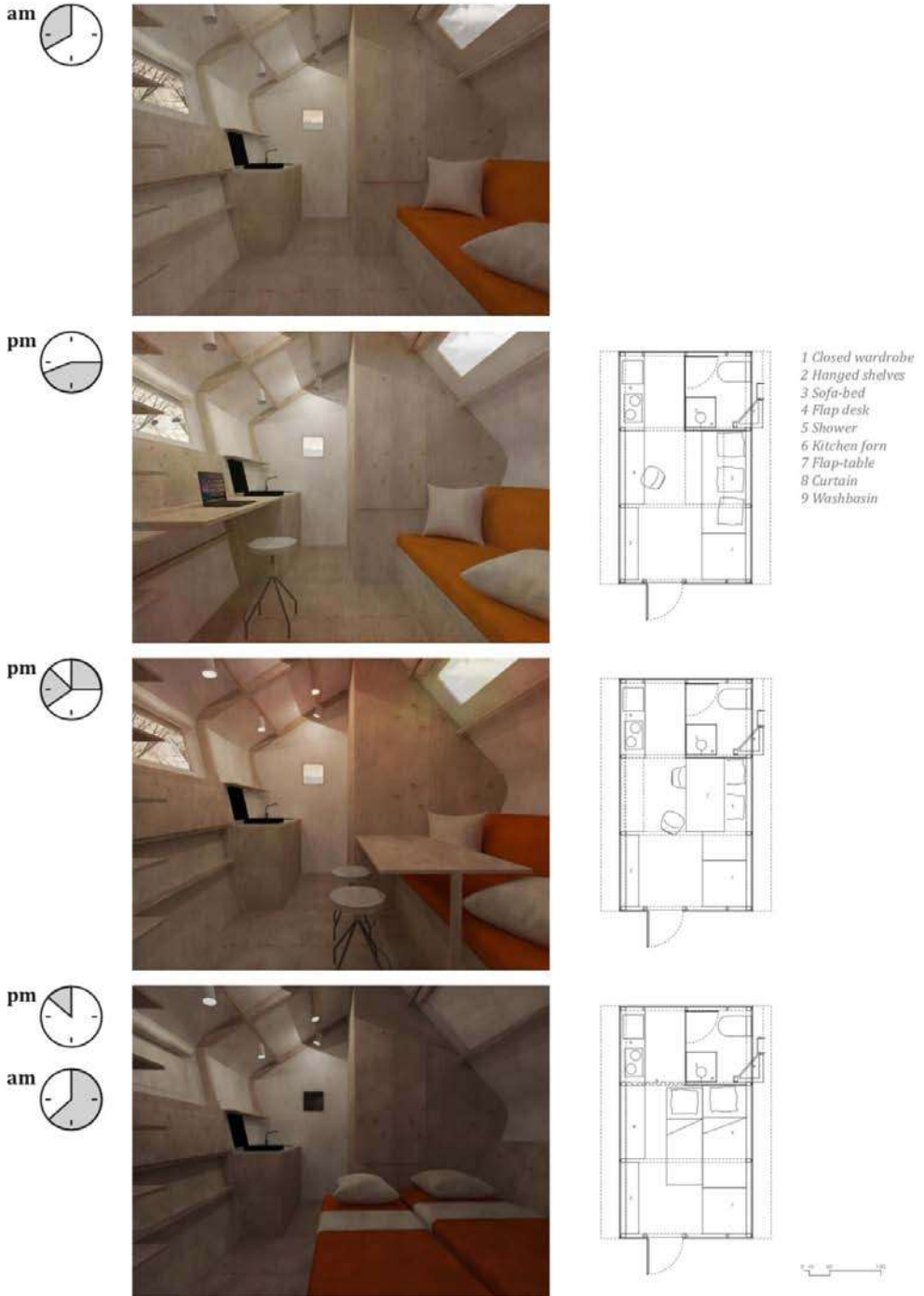


Figure 4: Rendering and plans of the shelter interiors depending on daily activities.

4.2. Technical soundness

Composite materials are usually produced with long and expensive techniques as wet/hand lay-up to shape composites on a predesigned mold. MadFlex can be produced through different industrial processes. It can be molded with a high cost warming process, or with a continuous flow process at 50 % less cost. Furthermore, during that process, it can be easily accessorized to be further implemented and joined with other materials or MadFlex panels. Facing the emergency shelter issues, low cost as easy and fast implementation are fundamental requirements. Therefore, a continuous flow process was considered as a constraint for the whole design, that allows the production of panels of 1,5 m width and unlimited length, justifying the choice to introduce modularity to fit industrial production necessities. Furthermore, the issue of fast assemble of MadFlex panels is faced through the implementation of specific joints and polycarbonate windows straightly during the industrial production process. Between possible joints' alternatives, t has been selected the most suitable for fast and simple employment, avoiding the necessity of specialized craftsmanship. To fix the MadFlex to the structure specific "socks" are implemented, made of the same strong material of MadFlex panels. These "sock joints" create a circular void to be inserted through the metal cables connecting each structural wooden frame. The MadFlex panels are afterwards joined through an high resistance and waterproof zip. As a result, no specialized craftsmanship, specific tools or heavy machineries are needed: MadFlex is the component with the easiest and fastest implementation of all the shelter and of any other envelope solution used in the market.

4.3. Feasibility

The level of feasibility of the solution has been verified from multiple points of view. The chosen Madflex configuration has been tested to verify its mechanical and thermal characteristics by Composite Research srl. Moreover, the durability to fold and unfold actions is already been tested and proved by the startup. Without any finishing touch the solution wouldn't be user friendly and probably not accepted by the disaster victims, because of its alienating aspect. To overcome this constraint and provide an adequate aesthetic touch to the shelter, an exterior and inner finishing is applied and tested. The construction feasibility is proved with an intermediate model that have been built in scale 1:15. A mock-up real scale prototype and a whole shelter model at 1:20 scale has been also built to verify the feasibility of the construction process. They have been useful tools to verify and adapt technical solutions during an integrated and heuristic design phase. Further verifications regarding transportation issues have been carry out, designing the whole arrangement of the FlexHab kit in a standard shipping container. Each container is able to host a total of 6 FlexHab modules of 1,5 m, the equivalent of two shelter for two persons each, or a whole shelter for eight/ten people, including services and furnitures. One of the main goals of the project is to ensure that the solution is economically sustainable

to guaranty competitiveness facing other solutions in the market. SAEs and solutions realized with traditional methods cost 1000 euro/m². A preliminary costs' survey on which all the construction elements as well as furnitures and services has been carried out, clarifying the sustainability of the solution. The whole shelter costs around 950 euro/m². This amount would probably decrease if the price of several objects and system would be purchased on large scale.

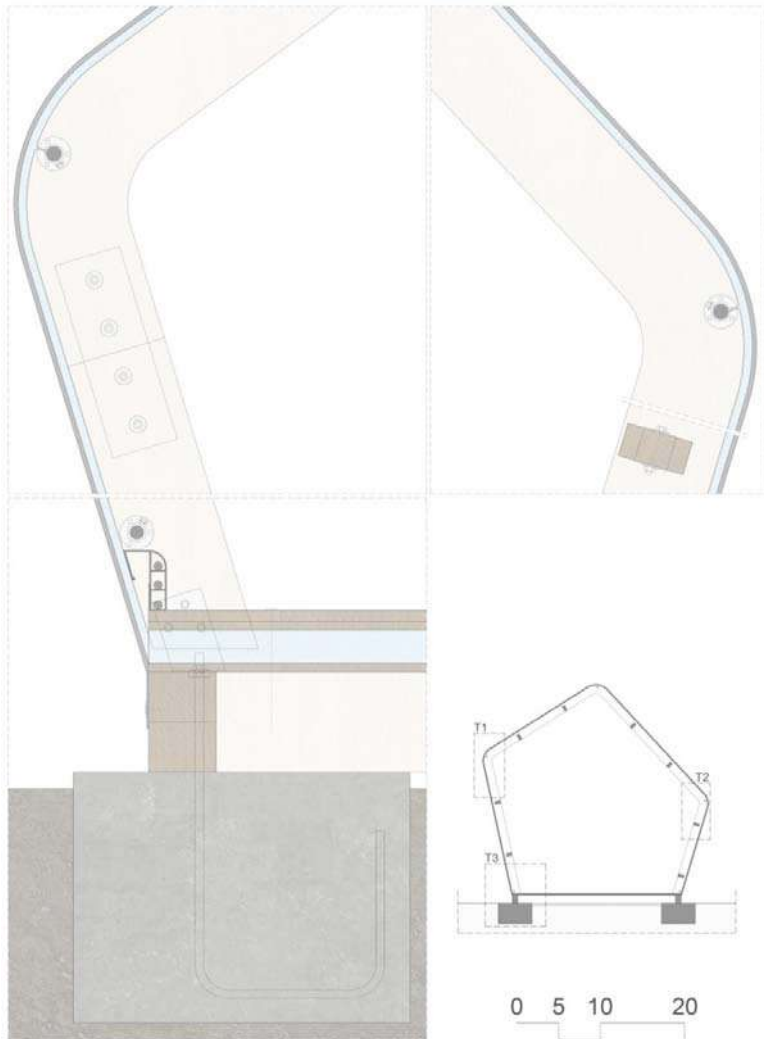


Figure 5: Technical transversal section focusing on the main interfaces.



Figure 6: 1:1 Prototype - Overview and detail of the “sock guide”.

5. Conclusion

The FlexHab project proposes an efficient solution to manage the “Recovery period”. This revolutionary impact on the disaster management is allowed by the integration of the tent technology, as an easy and fast solution to deploy, with the home archetype, as private and human scaled space, in a unique FLEXible HABitat. “Flex” stands as flexible, since the initial point for the project has been the innovative material of MadFlex and its main peculiarity. Its morphology mirrors some of the potentialities of the materials. “Flexible” is referred both to the material’s behavior and to the internal space’s conception: in fact the design of the furnitures, integrated in the structure, allows for a different arrangement of the living areas according to day-times and night-times. “Hab” refers to habitat, the space of domesticity, a new and starting living fulcrum to heal the loss of a house.

Thanks to the pentagonal modular design and innovative joints introduced in the production phase, the whole envelope can be set up through a single construction gesture. No specialized craftsmanship, avoiding the need of specific tools and heavy machineries: only a complete “kit” with assembly instructions and technical support would be provided.

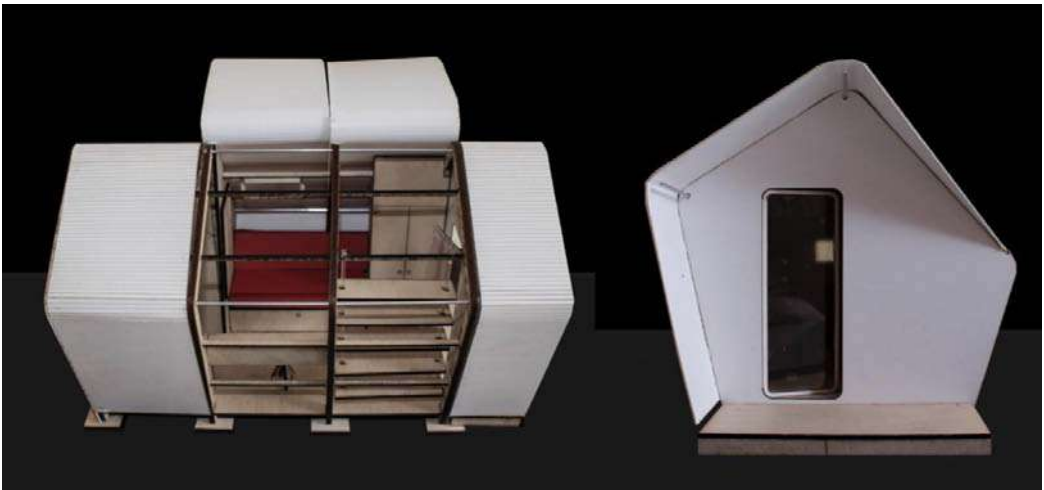


Figure 7: 1:20 Prototype - Final solution

References

Bignami D.F. (2010), *Protezione civile e riduzione del rischio disastri*, Maggioli, Sant'Arcangelo di Romagna (RM).

Composite Research srl, *Introducing the MadFlex: Building & Architecture*, Turin, Italy.

Composite Research srl, *MadFlex: Sample book*, Turin, Italy.

International Organization for Migration, (2012), *Transitional Shelter Guidelines*, Shelter Centre, maggio 2012.

MadFlex Patent (International Publication Number WO 2016/120785 A1), International Publication Date 4 august 2016.

O'Brien-Bernini F. (2011) *Composites and sustainability - when green becomes golden*, Elsevier.

Rosaspina E. (2017), *Guardare oltre l'emergenza*, Abitare, Settembre 2017 (n. 567).



SOFT SKINS

HIGHLIGHTED LECTURES

SOFT SKINS FOR THE BUILT ENVIRONMENT

TERMAL, OPTICAL AND ACOUSTIC COMFORT

Proceedings of the TensiNet Symposium 2019

Softening the habitats / 3-5 June 2019, Politecnico di Milano, Milan, Italy

Alessandra Zanelli, Carol Monticelli, Marijke Mollaert, Bernd Stimpfle (Eds.)

A tensile screen for the windows of Castello Sforzesco: integrating anemometric, optical and mechanical tests in the early-stage design of bespoke textile hybrid structures in historical contexts

Alessandra ZANELLI *, Elpiza KOLO ^a, Carol MONTICELLI ^a, Elisabetta ROSINA ^b,
Tiziana POLI ^c, Alberto SPERONI ^c, Andrea Giovanni MAININI ^c

* Textile Architecture Network (TAN), DABC, Politecnico di Milano; Via E. Bonardi 9, Milano 20133, Italy, alessandra.zanelli@polimi.it

^a Textile Architecture Network (TAN), DABC, Politecnico di Milano; Via E. Bonardi 9, Milano 20133, Italy

^b Experimental Mobile Laboratory, DABC, Politecnico di Milano; Via E. Bonardi 9, Milano 20133, Italy

^c SeedLab, DABC, Politecnico di Milano; Via Ponzio 31, Milano 20133, Italy

Abstract

This paper presents an interdisciplinary methodology of implementing bespoke, low-impact, lightweight structures as additions to historical buildings with the aim of enhancing their performance in terms of visual, lighting and hygrothermal comfort. To do this, the study focuses on the renovation of Sala delle Asse, one of the most relevant rooms of Castello Sforzesco in Milan. The design task at hand is to produce self-standing vertical screens for the large-scale windows in the room, in order to reduce the amount of sunlight that reaches the frescos, as well as to block air drafts that bring humidity inside the room. The main challenge of the project proved to be the fragility of the direct context, since the screens must be sealed in the borders, but no perforations are allowed on the vaulted edges of the windows. Thus, a textile-hybrid structure is proposed as a solution, due to its self-standing principle that would not require drilling on the vault. The experimental campaign starts by performing preliminary anemometric measures on the room and by modelling the illuminance level based on the definition of the optical properties of the glazing surfaces. These analyses, combined with parametric simulations, gave results on the preferred position and optical requirements of the curtains.

DOI: [10.30448/ts2019.3245.34](https://doi.org/10.30448/ts2019.3245.34)

Copyright © 2019 by Alessandra Zanelli, Elpiza Kolo, Carol Monticelli, Elisabetta Rosina, Tiziana Poli, Alberto Speroni, Andrea Giovanni Mainini. Published by Maggioli SpA with License Creative Commons CC BY-NC-ND 4.0 with permission.

Peer-review under responsibility of the TensiNet Association

After a selection of materials with the right visual qualities was made, these textile materials went through further optical tests to check their compatibility with the comfort requirements. Design choices were updated with these test results and were followed by mechanical studies on the stretching properties of the unconventional knitted textile materials to define the project's feasibility. This feedback loop of empirical data, in addition to a computational simulation of the structure's behavior, was applied to the construction of a real-scale mock-up to test the bending active principle. The mock-up also gives experimental results on how to change the structure in further design steps. In conclusion, this paper proposes an integrated feedback process, started from the very early-stage of design, that is not commonly applied in the architectural practice. In addition, the paper argues that the presented methodology and design process can be potentially applied in further historical contexts.

Keywords: lightweight structures, historical context, textile hybrid, interdisciplinary, experimental campaign, mechanical tests, anemometric tests, optical tests, bespoke, design methodology.

1. Introduction

One of the challenges that contemporary applications of membrane structures face today is the way they can improve the attributes of the built environment. This paper explores a specific potential application of ultra-lightweight architecture to one of the most important listed historical buildings of Milan, Italy, with the aim of projecting this singular case into the broader theme of minimizing the effect of added structures in restoration interventions, as well as giving a framework of collaboration between different fields of expertise when it comes to their design.

Recent relevant lightweight structure applications in historical contexts include the temporary canopy for the annual festival of the Olavinlinna Castle in Finland and the roof covering the biggest courtyard in the Vienna City Hall in Austria, 2000. In the case of the Olavinlinna Castle, the lightweight structure was installed and dismantled recurrently throughout its lifespan. The permanent membrane canopy for the Vienna City Hall gives an even better example of how the potential of retractability was exploited to provide a flexible solution that can be adapted seasonally (Koch, 2004). Both these notable case studies show that membrane architecture is highly compatible with historical buildings, which require a careful and non-invasive approach when it comes to contemporary interventions.

In this paper, the project's context is Castello Sforzesco, a castle initially built by the Duke of Milan, Francesco Sforza, in 1452 and later rebuilt by architect Luca Beltrami in 1893. In the light of the restoration of Leonardo da Vinci's frescos in Sala delle Asse (Fig. 3), there was a need to install window curtains on the two 6-meter-high and 3-meter-wide windows of the room. These curtains are required to perform as shading devices that stop harmful UV radiation from reaching the frescos, but also as window screens that stop air currents from going in and passing through the room. The existing window frames were installed in the '50s and thus perform badly in terms of airtightness. However, they cannot be replaced due to being designed

by the renowned Italian architectural office BBPR, which adds to their historical value. Thus, the requisite that became a priority for the project was the one of minimal impact on the surroundings and drilling as few perforations as possible on the walls. This room is located on the first floor of the Falconiera tower on the north-east corner of the castle (Fig. 1), one of the windows facing north-east and the other north-west (Fig. 2). The windows are similar in shape and dimension, but given the historical context, they are not identical. Thus, the idea of a flexible hybrid structure emerged, one that could be adjusted on site at the phase of installing it, in order to adhere to the wall inconsistencies and be fixed with the help of bending-active elements. This was also thought as a solution to the maintenance requirement of dismantling the structure and transporting it easily outside for proper textile cleaning (given that the doors of the castle are very small, the option of a rigid frame would make this process more difficult).

Hybrid structures have been widely explored in the field of lightweight architecture, since they were only recently added as a separate structural type as defined based on structural action and load transfer. The main structural types were limited to section-active, vector-active, surface-active and form-active structures (Engel et al., 1997). Bending-active and hybrid structures are later classified by Lienhard (2014), defining their former as *'curved beam and surface structures that base their geometry on the elastic deformation of initially straight or planar elements'* and introducing hybrids as the combination two other complementary structural systems. Textile hybrid structures gain their efficiency in force distribution due to reciprocal stress compensation and opposite system deflection, factors that make a hybrid structure more rigid than the components it



Figure 1: the Falconiera tower and its affected windows.

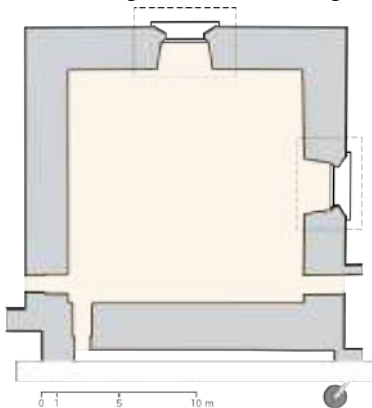


Figure 2: Floor plan of Sala delle Asse, that shows the orientation and location of the windows



Figure 3: On-site photo of the current restoration works in Sala delle Asse

started with (Lienhard, 2014). The first notable precedents in terms of textile hybrid structures came as a result of the research of Ahlquist, with the first one being the M1 Textile Hybrid exhibited in 2012, later his StretchPLAY sensorial project, and further the 2013 Toroidal Structure exhibited in the Material Equilibria installation by ICD in Copenhagen, Denmark. The latter is the first CNC-knitted fabric with a structural differentiation, aiming to optimise the stretchable fabric for maximum tensile strength and obtain the desired form (Ahlquist, 2014).

However, the most architectural examples in the category are the hybrid gridshell prototype by Kuma (Taichi, 2016) and the Hybrid Tower by the Centre for Information Technology and Architecture (CITA) at KADK. These two examples tested the ability of textile hybrids to resist extreme weather conditions. Hybrid Tower especially brought together all the knowledge about hybrid structures by implementing custom-made pockets embedded in the knitted fabric, slender elastic GFRP rods and computational analysis to produce a self-standing structure reaching a height of 9 meters (Thomsen et al., 2016).

The project in this paper tries to combine the knowledge gained from the previous expertise in textile hybrid structures to tackle problems surfacing from a multidisciplinary analysis of the site. The differentiation potential of the knit pattern is thought to contribute to the optical and anemometric requirements in terms of the screen's performance and the slender elastic GFRP rods are aimed at providing a low-impact installation rather than a structure withstanding extreme loads. While previous textile hybrid applications are ground-breaking in their structural and customisation achievements, they are usually designed as installations. The challenge posed in this paper is to provide a textile hybrid with a very specific purpose, the one of a window screen that is capable of satisfying climate controlling and comfort requirements.

2. Design requirements

The project for the window screens posed a challenge because of the many design requirements to fulfil, some of which being in conflict with each-other. These requirements were emphasized by the Castello Sforzesco officials that are in charge Sala delle Asse's cultural heritage, thus had to be respected to the largest extent. Firstly, the window screens must provide shading for the room and frescos, but it was crucial to have a visual connection to the surroundings of the castle and the Sempione Park, because the room will be used as part of the museum. A translucent fabric would need to be used in this case and this is where the idea of knitted textiles emerged, given their ability to provide a visual connection with the outside as well. This factor was significant also because the structures for the two window screens are meant to be fixed. The Castello officials reported that the current curtains, which consist of ordinary sliding drapery, are often moved by the museum employees and sometimes used to access the windows and open them. This is highly detrimental to the controlled climatic conditions inside the museum, that are supposed to be kept at a constant humidity level for a proper conservation of the artefacts. In addition, humidity and air drafts are a major problem of the room because of the poorly performing window frames that date back to 1954, but that cannot be replaced since

they were designed by BBPR and thus carry a historical value. In order to tackle the humidity and especially the air draft problem, the new curtain structures would have to be sealed in the borders and one of the requisites was to make as few perforations as possible on the walls, especially on the arched part of the vault. However, another conflicting requirement was to have the ability to remove the fabric and wash it for future maintenance. This is where textile hybrid structures started to be consolidated as a solution.

3. Multidisciplinary approach

The conducted interdisciplinary experimental campaign aimed at optimizing the window screens for visual, lighting and hygrothermal comfort, in addition to evaluating the feasibility of the project and satisfying the imposed design requisites. The full scheme of the interaction between several sectors of different expertise is shown in the diagram of Figure 4, which proposes an integrated feedback process instead of the usual linear one that is commonly applied in conventional architectural interventions. The exchange of information between the various fields starts at an early stage of the design process and continues throughout the later stages by constantly refining the design product.

The preliminary campaign started by performing anemometric measures on the current conditions of the room and by modelling the illuminance level based on the definition of the optical properties of the glazing and of the internal and external surfaces. These analyses, combined with parametric simulations of optimized solar transmittance values, gave results on the preferred position and optical requirements of the window screens. The chosen materials to be implemented in the project are required to be flame retardant to abide by the national safety regulations, thus the choice of the types of knitted fabrics was limited to the ones using the flame-retardant polyester yarn. Among these, the ones with the right visual qualities were chosen, in order to guarantee adequate levels of illuminance, avoid glare and filter direct radiation. The textile materials then went through further optical tests to check their compatibility with the comfort requirements, such as measurements of solar and visual transmittance.

Design choices were updated with these test results and were followed by mechanical studies on the stretching properties of the knitted textiles to define the project's feasibility. These data served as an input to a computational simulation of the structure's behavior, which aided the construction of a real-scale mock-up to test the bending active principle and the dimensioning of the glassfibre-reinforced elements. The mock-up is also seen as an element of the loop, which gives experimental results on how to change the structure in further design steps.

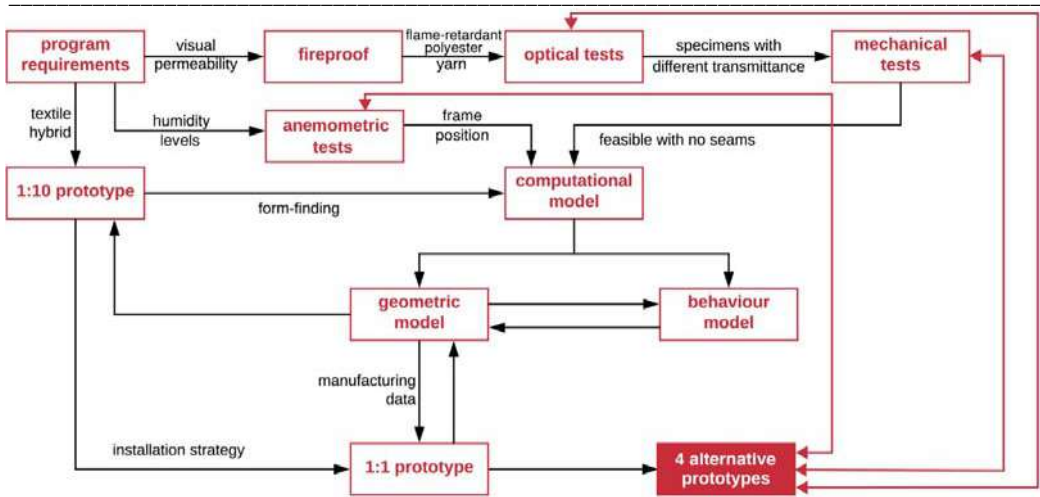


Figure 4: Flow chart of the various competences involved in the project, showing the feedback loop of their interaction; black arrows show exchange that was already applied, while red arrows show future exchange

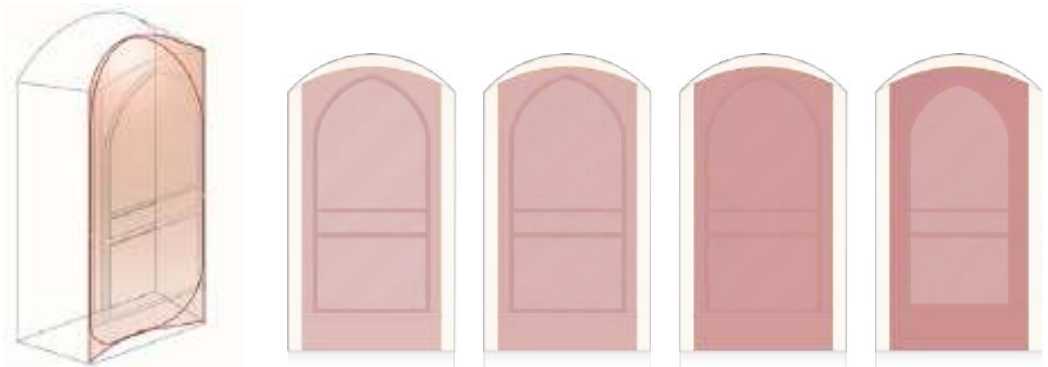


Figure 5: Shape of the bending-active self-standing structure and the 4 alternative prototypes to be tested

In refining the workflow, it was concluded that the final step of verification would be to test four alternative prototypes on site with different densities of the textile, in order to conduct final tests in each field of competence about the fulfillment of the comfort and feasibility requirements. These four options consist of low, medium and high-density fabrics that are chosen based on the transmittance range results from the optical tests and simulations, with the addition of a fourth mixed-density fabric that was thought as an experimental solution that is customized specifically for this design task. This final solution will have a denser fabric in the borders to stop air drafts and a finer knit on the inside portion, following the shape of the window, that will let more light in the room, given its northern orientation (Fig. 5).

4. Experimental testing campaign and modelling

4.1. Anemometric measurements

After an extensive restoration few years after World War II, Sala delle Asse went under few maintenance interventions. Since 2010, the conservators of Castello Sforzesco, in addition to the department of the Galleries of the Municipality, have led an articulated and well-supported program of study, analysis and research involving several Institutions for conservation research and for cultural heritage restoration, with the aim of achieving the best understanding, the most suitable project of conservation and finally, the restoration of the frescos. One of the results of these investigations attributed the main cause of damage to the microclimatic unbalance and the diffusion of soluble salts (Rosina et al., 2017). Microclimatic monitoring has been performed by probes (hourly rate of data recording), psychrometric mapping of the hall and surrounding rooms (every three months for one year and half), anemometric measures in the square areas of about 3x5 m close to the windows (different weather condition: with high speed wind, different direction of the wind, etc). The climate was monitored (T°C and RH, direction and speed of wind) with probes installed on the top of the tower that hosts Sala delle Asse. All the acquired data were processed, plotted and scaled on the plan, with the aim of overlapping the microclimatic map representing the recorded data with the geometric map of the Sala. The aim was to connect the recorded changes in balance with the location of openings in the hall.

4.2. Lighting Modelling and Optical measurements

The objective of the analysis was twofold and provided the input for the research and selection of the types of technological fabrics and their optical-radiative properties. In particular the main intent was retaining the availability of natural light and ensuring the most appropriate quality of light, and, on the other hand, controlling the direct and diffuse radiation (hourly variation) in order to prevent glare and damage of Leonardo's frescoes and the decorated vault.

The mean illuminance (lux) on the horizontal and vertical surfaces, the distribution of the illuminances (% area with illuminance <100 lux; % area with illuminance between 100lux and 2000lux; % area with illuminance >2000lux) and the occurrence of direct radiation have been considered as parameters for the analysis of the effectiveness of the shading systems.

Modelling has been performed for days with maximum and minimum incidence of radiation (summer and winter solstice). Our reference test case was the Sala delle Asse without the application of textile element in correspondence of the window. The light transmission of the glass and the reflectance of the internal surfaces was known or was considered according to scientific literature.

4.2.1. Solar Radiation mapping

The first analysis carried out has been used to map the presence and average extent of direct radiation on the surfaces inside the "Sala delle Asse" during different periods of the year and

for different time slots. The images are representative of the cumulative value of direct sunlight during day twenty-first for each month.

This analysis has shown that in this particular day the surfaces with Leonardo's frescos are never affected by direct radiation; on the contrary, they are the less illuminated surfaces.

4.2.2. Daylight Modelling

A parametric approach has been adopted for modelling the availability of natural light. The variables considered have been: a) the sky conditions (cloudy and Clear sunny); b) the visible transmittance of textile (3 macro-categories); c) the componet glass + fabric shading performance. The position of the fabric has been considered constant (inner). This parametric analysis has allowed to identify the threshold of textile optical properties (effectiveness) and it considered as a preliminary benchmark to reduce the selection of the textile samples and whose optical performance was to be measure. The textile properties considered were below reported:

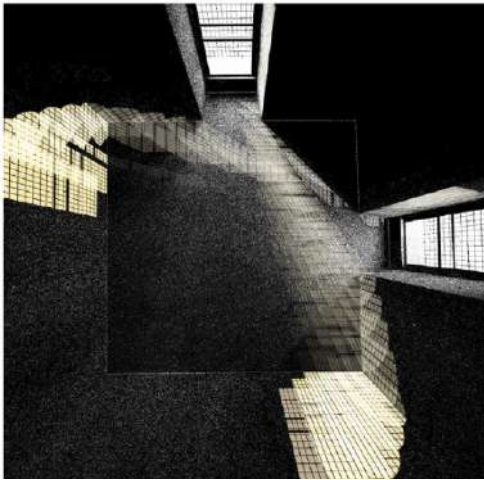


Figure 6: Top view of the Sala delle Asse and the presence of direct radiation, June 21, 4 am - 9 pm.

Type 1: τ_{vis} 4%, $\tau_{vis,tot}$ component 3,6% (glass τ_{vis} 88% + textile);

Type 2: τ_{vis} 28%, $\tau_{vis,tot}$ component 27,5% (glass τ_{vis} 88% + textile);

Type 3: τ_{vis} 50%, $\tau_{vis,tot}$ component 44,4% (glass τ_{vis} 88% + textile).

The results show that during the period of maximum exposure of the radiation and availability of natural light in the environment the optimal values of T_{vis} are below 25%-28% to prevent glare and to provide appropriate levels of illuminance (with direct radiation).

4.2.3. Material and experimental test

Five types of textile samples were tested with different patterns, V/P ratio and colour. Measurements for the determination of light and solar transmittance properties (τ_v , τ_e) were performed with a Perkin Elmer Lambda 950 dual beam UV-Vis-NIR spectrometer, equipped with a 150 mm diameter integration sphere (with PMT/PbS detectors). Measurements were made with a resolution of 5 nm, in the spectral range between 250 and 2500 nm. The average curve for each product was calculated, and therefore the values of solar reflectance, UV, visible and NIR reflectance, weighing the curve with respect to the spectral distribution of global solar irradiance on a horizontal plane with air mass equal to 1.5, according to ISO 90501. Additional measurements were made to identify for some samples: a) the influence of stretching feasibility

on the solar transmittance measurement; b) the influence of the orientation of the fabric with respect to measuring port (0° and 90°). (Table 1). Some samples were excluded because of the type and size of the texture. In these cases, the ratio between the geometry of the yarn (texture) and the characteristic size of the light source of the instrument did not allow to obtain a significant measure of the material properties. For all large textures, other measurement techniques must be used (sample 5, 6 and 7).

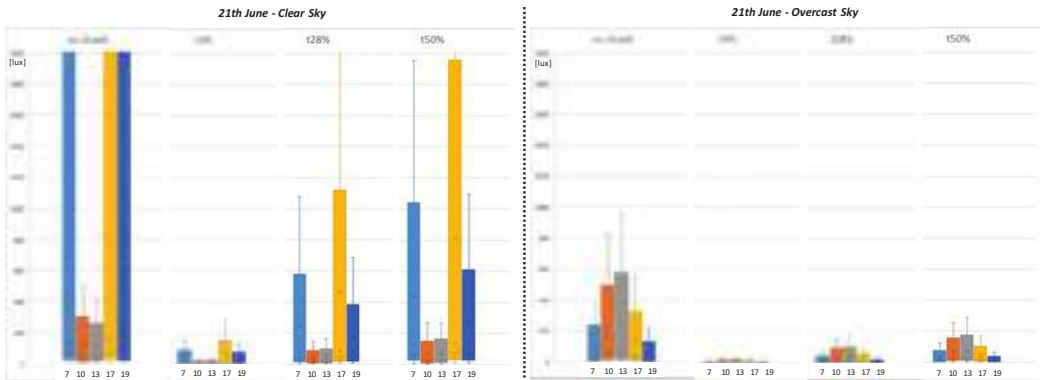
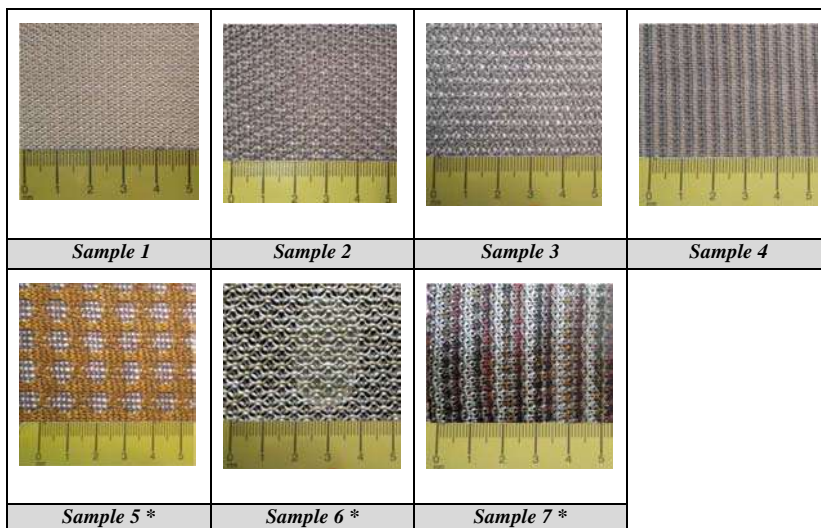


Figure 7: Simulation results for different 21th of June sky condition (clear and overcast sky) with different shading condition hypothesis: no shade, shade τ_{vis} 4%, shade τ_{vis} 28%, shade τ_{vis} 50%. With a clear sky, the peak value can reach higher value. Despite this, to have comparable results, the axis that shows Lux values has been set with a peak value of 2000lux. The optimized solutions are textile type 1 and 2.

Table 1: Textile samples (reference: SeedLab.ABC, ABC Dept, Politecnico di Milano). Samples from 1 to 4 are measured in non-tensioned condition and with controlled pre-tensioning. * Sample measured, but results are not shown because of their wide mesh and high variation in possibility to be tensioned.



In general, measurements for samples with low stretching feasibility have a repeatability and stability characteristic of the result, while for samples with a high degree of deformability, the measurement of transmittance depends on the degree and homogeneity of tensioning of the fabric itself. Below, as an example, are the measurements of the optical properties of some samples stretched and not stretched.

As regards light performance, the samples that most effectively satisfy the requirements are Sample 1 and 2, which optimize light performance while simultaneously providing control over the UV component of the radiation. In fact, a sample with the densest and most compact yarn and the thickest texture makes it easier to control the transmission of solar radiation.

Table 2: UV and VIS transmittance measurements for samples 1, 2, 3 and 4.

Sample number	τ_{VIS} [%] (ISO 9050)	τ_{UV} [%] (ISO 9050)	Comparison of stretched with non-stretched samples
Sample 1	27.6	21.7	
Sample 1 pre-tensioned	28.2	22.3	
Sample 2	14.7	13.1	
Sample 2 pre-tensioned	16	14.7	
Sample 3	41.2	40.3	
Sample 3 pre-tensioned	47.6	47.1	
Sample 4	18.9	16.4	
Sample 4 pre-tensioned	25.8	22.0	

4.3. Mechanical tests

The textiles that were selected from the optical measurements, corresponding to Sample 1, 2, 3 and 5, went through mechanical testing. A limitation of knitted fabrics is the maximum width in terms of production, that depends on the CNC-knitting along the weft direction. In large-scale projects, the maximum elastic elongation can inform the feasibility of a designed structure. The specific project calls for the installation of a 3-meter-wide textile screen, while the selected knitted textiles are produced with a weft width ranging between 1.75 and 2.4 meters (4spaces, 2018). A further objective was to avoid sewn seams for a more uniform appearance, controlling

elongation precisely. In this regard, uniaxial and biaxial stress tests were performed, focusing on the elastic deformation, in order to achieve the requirement of reversible installation and to unmount the fabric, wash it and then reassemble it on site. Even though the topic of knitted fabric testing is recent and unexplored, some important precedents were selected as a basis for the testing methodology. One of the earliest attempts in uniaxial testing of knitted fabrics was performed on interlock-knit textiles made of a reinforced composite thread (Huang et al., 1999), applying the standard ASTM D3039M-93. As far as biaxial testing is concerned, the examples of previous research highly differ from each-other. For instance, square shaped samples were tested following a non-standard method (Jinyun et al., 2010), whereas in the Hybrid Tower project (Thomsen et al., 2016), the samples were cut into cruciform shapes and standard MSAJ M-02-1995 was used. In this case the same standard was applied, but consolidating the edges with an elastic overlock stitch to protect them against unravelling of knitted material.

Based on these precedents, uniaxial stress tests were held according to EN ISO 13934 and biaxial tests were held according to the MSAJ M-02-1995, with a customized load history. Samples 1 and 2 exhibited a firm behaviour and were not prone to unravelling during the first tests, thus the elastic overlock was not used and the yarns of cut edges were left to act freely. However, in the case of Sample 3 and 5 an elastic overlock was necessary. Biaxial tests were applied a customized load history, since uniaxial tests showed that 1/4 of the ultimate tensile strength (UTS) resulted to be too high, because in this portion of the stress/strain graph knitted textiles already reach a considerable irreversible deformation. Uniaxial tests show a similar behaviour in Sample 1 and 2 (Tab. 4), whereas 3 and 5 behave more like each-other (Tab. 5). As sample 2 is produced at a 1.75m width, the tests proves its limited extension. Furthermore, the biaxial tests revealed another property of knitted textiles, which is their extensive retraction in warp when stretched considerably in the weft direction (Tab. 3).

As a conclusion, Sample 3 will be used for the highest transmittance prototype (Tvis when tensioned 47.6 %) and Sample 1 for the low one (Tvis 27.6 %). A less dense version of Sample 1 was also produced for the medium transmittance one, in addition to the customised mixed-density fabric. This proved to fall in the right range between Sample 1 and 3 (Tvis 38.9 %), while it will go through the testing loop again to assess its mechanical properties.

Table 3: Biaxial strain over time graph of Sample 1

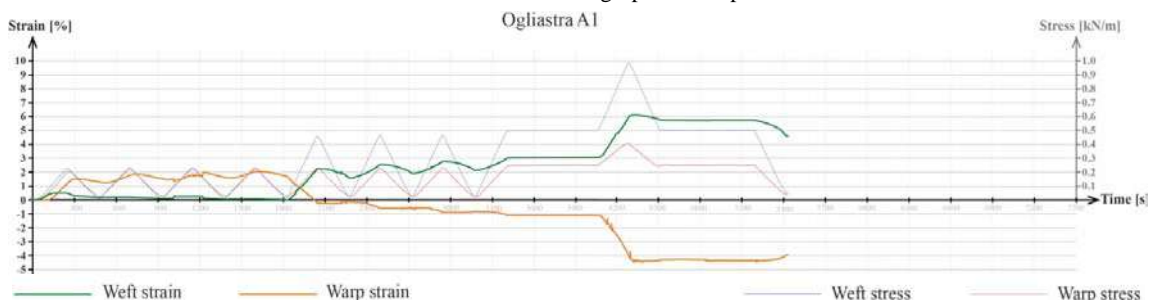


Table 4: Uniaxial strain/stress graph comparison of Sample 1 and 2

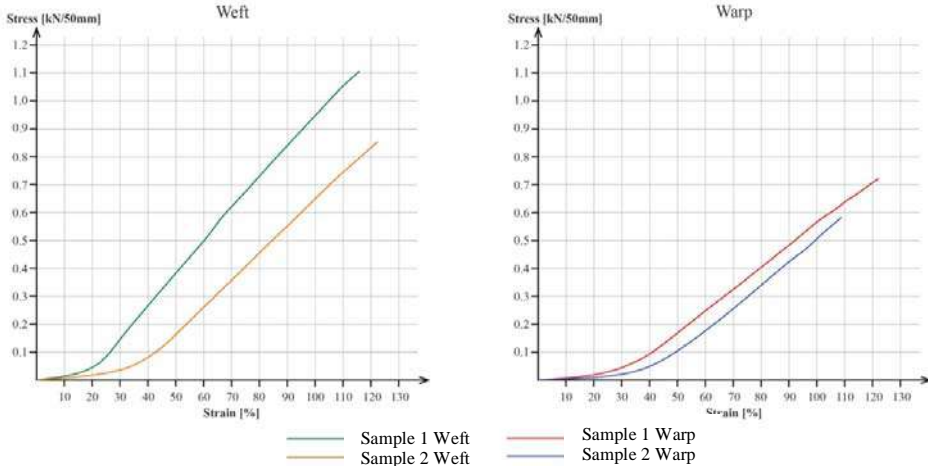
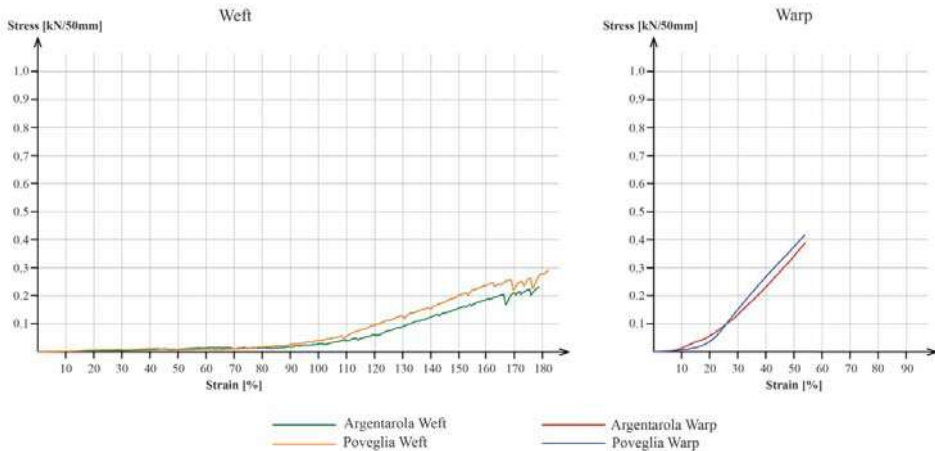


Table 5: Uniaxial strain/stress graph comparison of Sample 3 and 5



5. Real-scale prototype

The real-scale prototype consisted of a 1 to 1,5 model and it aimed at assessing the behavior of the top arch. Firstly, two vertical C-shaped profiles were anchored on the ceiling and on the ground, which were afterwards closed with an L-profile to achieve a pocket to slide the keder in. Then, the reinforcing bar was fixed in the right position by being passed through hooked elements and then secured with cable clamps at its ends. The next step was proceeding to cutting the pattern of the textile, using Sample 1. The keders were passed through the vertical edges and GFRP elements in the arched portions. Afterwards, it was proceeded to lifting the textile from the upper GFRP bar, fixing it in the corresponding hooks and connecting it to the

reinforcement bar. The textile was then inserted with the help of the keders into the vertical profiles and properly tensioned. The prototype confirmed the validity of the GFRP cross-section dimensioning coming as a result of computer simulations, which gave diameters of 8 mm for the principal bent rods and 6mm for the reinforcing ones (Kolo, 2018). The elongation extent of the textile was also confirmed in the horizontal weft direction, but from the prototype it was concluded that there is need for slightly more stretching compensation in the vertical arched portion (fig. 8) These considerations are then applied to the cutting pattern of the four options tested on site (fig. 9).



Figure 8 (left): Assembly process of the prototype in Lab.

Figure 9 (right): first full-scale prototype installed in Sala delle Asse at Castello Sforzesco.

6. Conclusion

The developed multidisciplinary workflow helped refine the project proposal in advance, in order to provide a more context-aware solution, that could target the design requirements and the different aspects of comfort at the same time, as opposed to an evaluation post-proposal. The anemometric measurements guided the design towards a mixed-density alternative, that would not be considered without the tests showing that the most humid areas were located in the borders of the windows. The optical measurements helped define the desired transmittance and the knitting requirements. Finally, the mechanical studies gave crucial information on the selection the textiles and their compensation values for the final installation process.

Acknowledgements

We express our gratitude to the Director of the restoration works, Dr. Arch. Michela Palazzo, and to the Director of the Art Archives at Castello Sforzesco, Dr. Arch. PhD. Francesca Tasso, for giving us the opportunity to tackle a project in such an important context of cultural heritage. We would also like to thank all the suppliers which supported us during the materials' choices: 4spaces, Giorgio Piovano Home Textiles, and Eos Design.

References

- 4Spaces. (2018), Products. <https://www.4spaces.ch/collections/collection-a> [13 Apr. 2018]
- Ahlquist, S. (2014). Post-forming Composite Morphologies: Materialization and design methods for inducing form through textile material behavior. In: *Proceedings of the 34th ACADIA: Design Agency*. Los Angeles, USA: p. 267-276.
- Campioli, A., Mangiarotti, A., and Zanelli, A. (2007). Learning from the past to renew ephemeral architecture in the Italian context. In: *Tensinet Symposium 2007*. Libreria Clup: p. 187-201.
- Castello Sforzesco. (2018). *Milan Castle - The History*. [online] Available at: <https://www.milanocastello.it/en/la-storia> [Accessed Sep 2018]
- Engel, H., and Rapson, R. (1997). *Structure systems*. Stuttgart, Germany: Hatje Cantz Pub.
- Huang, Z. M., Ramakrishna, S., Dinner, H. P., Tay, A. (1999), Characterization of a knitted fabric reinforced elastomer composite. *Journal of reinforced plastics and composites*, 18(2), p. 118-137.
- Jinyun, Z., Yi, L., Lam, J. and Xuyong, C. (2010). The Poisson ratio and modulus of elastic knitted fabrics. *Textile Research Journal*. 80(18): pp. 1965-1969.
- Koch, K. M. (ed.) (2004). *Membrane structures: innovative building with film and fabric*. Munich, Germany: Prestel Publishing.
- Kolo, E. (2018). New meets old: textile hybrid architecture in the historical context of Castello Sforzesco in Milan. Master thesis, Politecnico di Milano. <http://hdl.handle.net/10589/140681>
- Lienhard, J. (2014). *Bending-active structures: form-finding strategies using elastic deformation in static and kinetic systems and the structural potentials therein*. PhD thesis. ITKE, University of Stuttgart. [online]: <https://elib.uni-stuttgart.de/handle/11682/124>
- Rosina, E., Sansonetti, A. and Erba, S. (2017). Focus on soluble salts transport phenomena: The study cases of Leonardo mural paintings at Sala delle Asse (Milan). *Construction and Building Materials*, 136, p. 643-652.
- Taichi, K. (2016). Iterative design process between physical modelling and computational simulation for pre-tensioned grid shell structure. In: *Proceedings of the 21st International Conference on Computer-Aided Architectural Design Research in Asia (CAADRIA)*. Melbourne, Australia: p. 249-258.
- Thomsen, M.R., Tamke, M., Karmon, A., Underwood, J., Gengnagel, C., Stranghoner, N. and Uhlemann, J. (2016). Knit as bespoke material practice for architecture. In: *Proceedings of the 36th ACADIA: Posthuman Frontiers*. Ann Arbor (MI), USA: p. 280-289.

Proceedings of the TensiNet Symposium 2019

Softening the habitats / 3-5 June 2019, Politecnico di Milano, Milan, Italy
Alessandra Zanelli, Carol Monticelli, Marijke Mollaert, Bernd Stimpfle (Eds.)

Textil Akademie Mönchengladbach, Job Report

Bernd STIMPFLE*, Jürgen TRENKLE*

*formTL Ingenieure für Tragwerk und Leichtbau GmbH, Güttingerstraße 37, 78315 Radolfzell, Germany,
bernd.stimpfle@form-tl.de

Abstract

The textile façade for the Textil Akademie in Mönchengladbach, Germany, is developed as a pretensioned membrane and cable structure with valley and ridge cables. The cables are the forming and load carrying elements which are vertically spanned along the façade. This paper presents the development of the façade from the architectural concept to a shape that is suitable for membranes, the supporting steel structure attached to the concrete wall, the connection details, patterning process and the installation.

Keywords: PTFE, mesh membrane, cable structure, analysis

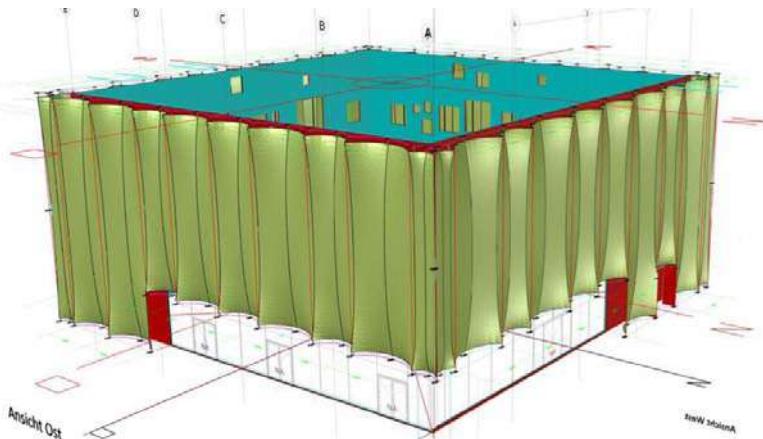


Figure 1: isometric view textile façade

DOI: 10.30448/ts2019.3245.10

Copyright © 2019 by Bernd Stimpfle, Jürgen Trenkle. Published by Maggioli SpA with License Creative Commons CC BY-NC-ND 4.0 with permission.

Peer-review under responsibility of the TensiNet Association

1. Introduction

In Mönchengladbach a new school of the textile industry has opened in autumn 2018. The school is surrounded by a textile facade, and transporting with its appearance also the contents of the teaching. The surface area of the façade membrane is approximately 2100m².

On the top and the bottom a steel structure is attached, which acts as upper and lower fixation. To shape the membrane, the attachment lines consist of arches, which are connected in the peaks. Vertical cables span between these lines and shape the membrane into its undulation.

In order to allow the view from the class rooms to the outside, an open mesh material with 42% opening was chosen. This mesh is coated with silver PTFE, and gives a shiny surface to the project.

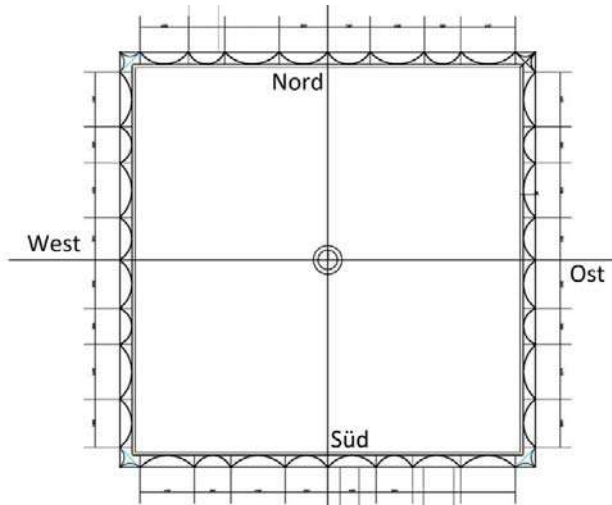


Figure 2: plan view academy building

2. Structural system

Between the undulated support system span membrane panels. The height of the facade is up to 16 m. With the chosen boundaries the membrane would have become almost flat, and would not be able to carry the applied wind load. Furthermore the textile facade should form higher folds.

Vertical cables in distances between 1.5 and 2.5 m are spanning from top to bottom. They carry the wind loads and form at the same time the membrane, Alternating, these cables are sitting as ridge cables behind the membrane and as valley cables in front of the membrane.

Even with these cables, it is difficult to shape the membrane, that is why a relative high prestress in the cables was required, as well as in the vertical direction of the membrane.

3. Analysis

The analysis of the membrane has been performed with the software TL_form and TL_Load, special software for membrane and cable systems, taking into account large deformation, as well as the orthotropic behaviour of the membrane. The stiff supporting structure was analysed with the truss software Rstab.

The façades in the North and in the West were representative for the whole façade. In the west the panel has the full height, in the North we have over one half a glass façade under the membrane, and we have one integrated door frame.

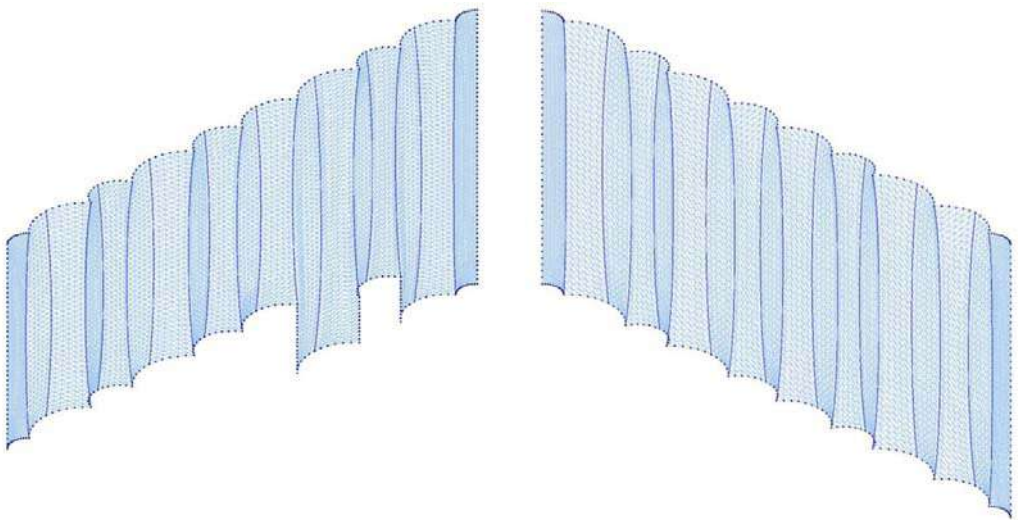


Figure 3: Numerical model membrane and cables North and West

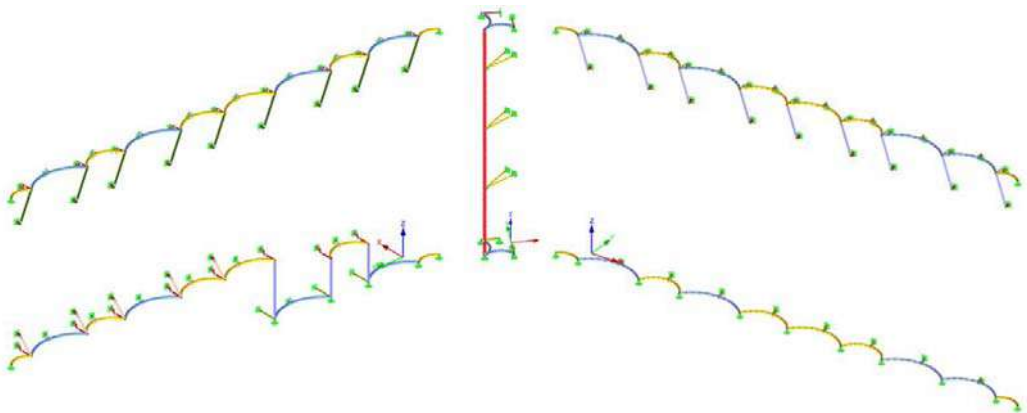


Figure 4: Numerical model supporting structure North, Corner and West

Wind has been applied according to Eurocode 1 for a cubic building. Due to the undulation also wind friction along the façade has been taken into account. The stiffness of the membrane has been determined in a biaxial test, which has also been used to determine the compensation factors. Beside this only prestress and selfweight were applied.

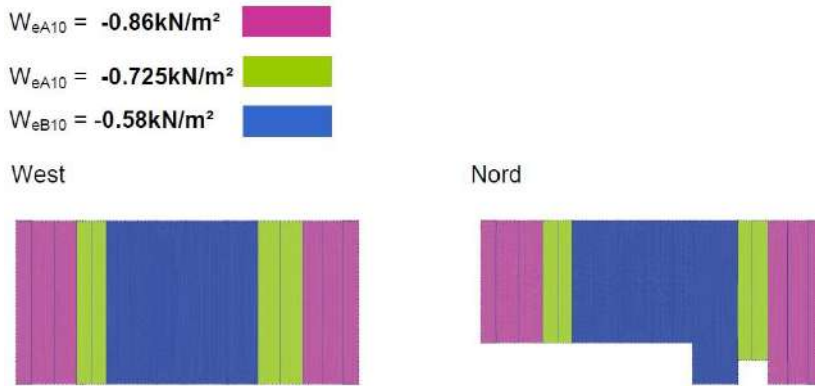


Figure 5: Distribution of the wind load for the two representative façades

The prestress in the membrane is 4 kN/m in warp and 3 kN/m in weft. Under windload the stress in warp is increased to 18 kN/m and in weft to 8 kN/m. The warp direction is vertical.

The cables are prestressed with 50 kN. Under wind load the inner cables get a maximum force of approx. 130 kN in the service limit state.

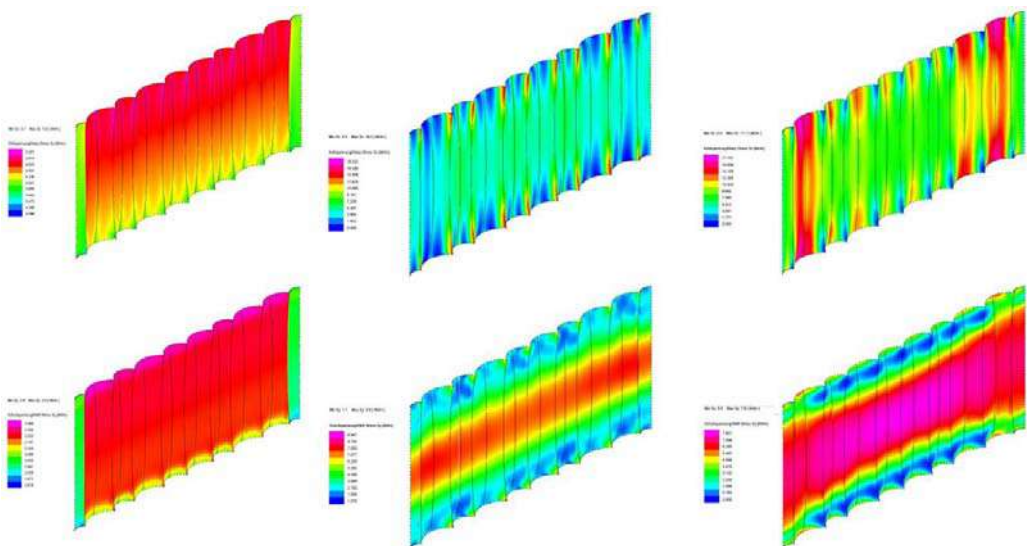


Figure 6: Membrane stress: prestress, wind pressure and windsuction West

4. Detailing

The architecture required minimised details, as well as a minimised distance to the insulated wall, that is why adjustable details have not been used along the rigid edges. The only adjustability is within the cables, which have threaded sockets at their upper end.

4.1. Upper connection detail

At the upper end the cable has a threaded fitting that allows to adjust the cables in case of tolerances. To ensure the rotation, the cable is sitting on a spherical washer.

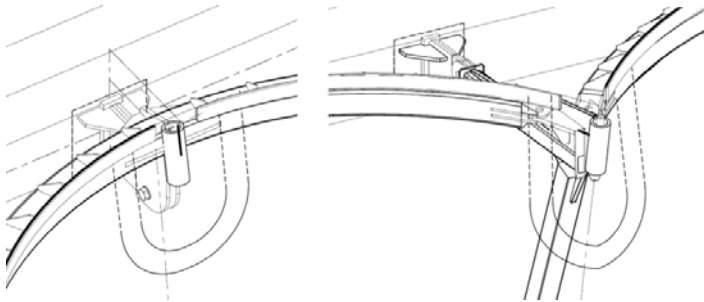


Figure 7: Upper detail wind suction and wind pressure cable

4.2. Lower connection detail

At the lower end, the cable has a fixed connection that allows for rotation perpendicular to the façade.

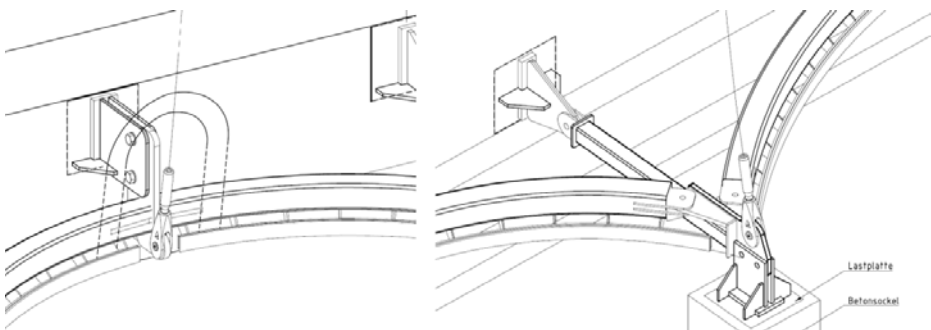


Figure 8: Lower detail wind suction and wind pressure cable

4.3. Lateral detail

The horizontal fixation of the membrane panels is made with rigid linear supports. The membrane is clamped to a U-shaped steel profile. With V-shaped struts this is fixed in-between the upper and the lower attachment line.

At the top and the bottom, this vertical beam is fixed to the circular arches of the neighbour panels.

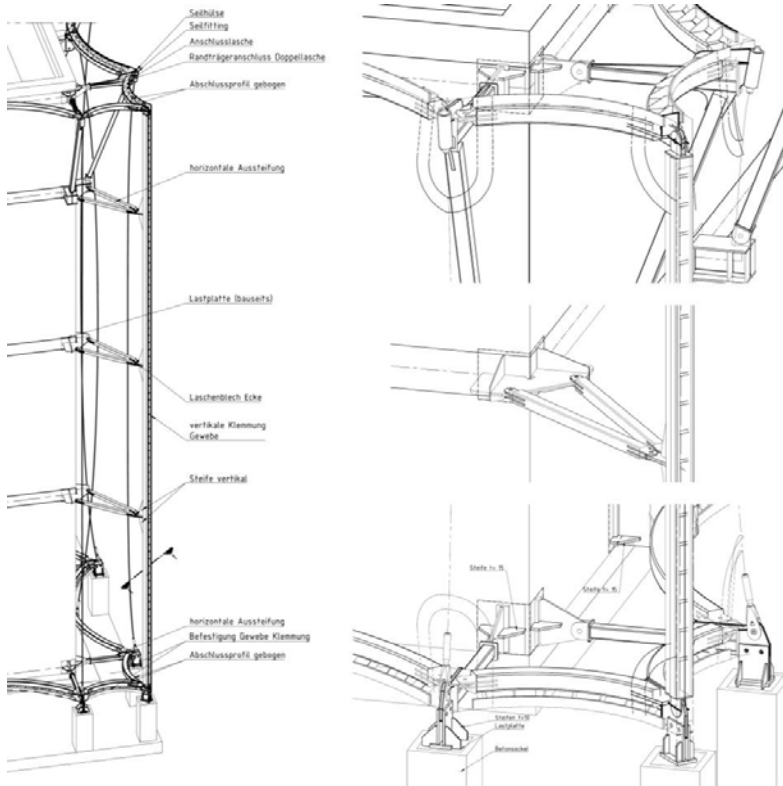


Figure 9: Corner detail from Top to Bottom

4.4. Membrane connection details

As mentioned before, the details were required to be almost invisible. Therefore along all edges we have a small clamping detail without any adjusting. The covering clamping plates were made so that also the keder disappeared behind the plate.

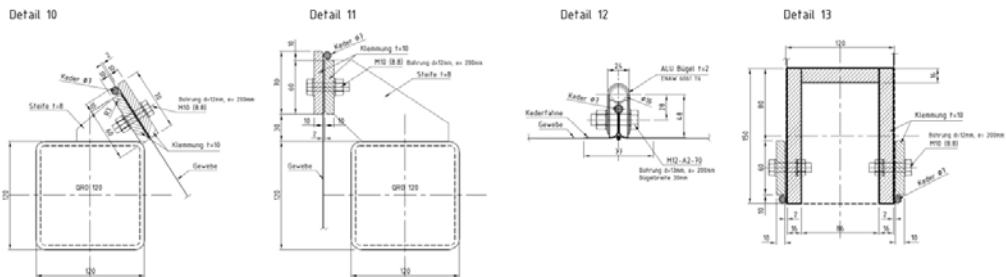


Figure 10: Clamping details of the membrane panels

5. Cutting pattern

To minimize the visual impact all bays have their welds only in the lines of the cables. The compensation has been determined in a biaxial test. Due to the specific behaviour of the glass mesh, the final compensation was very low, which caused additional effort to the installation.

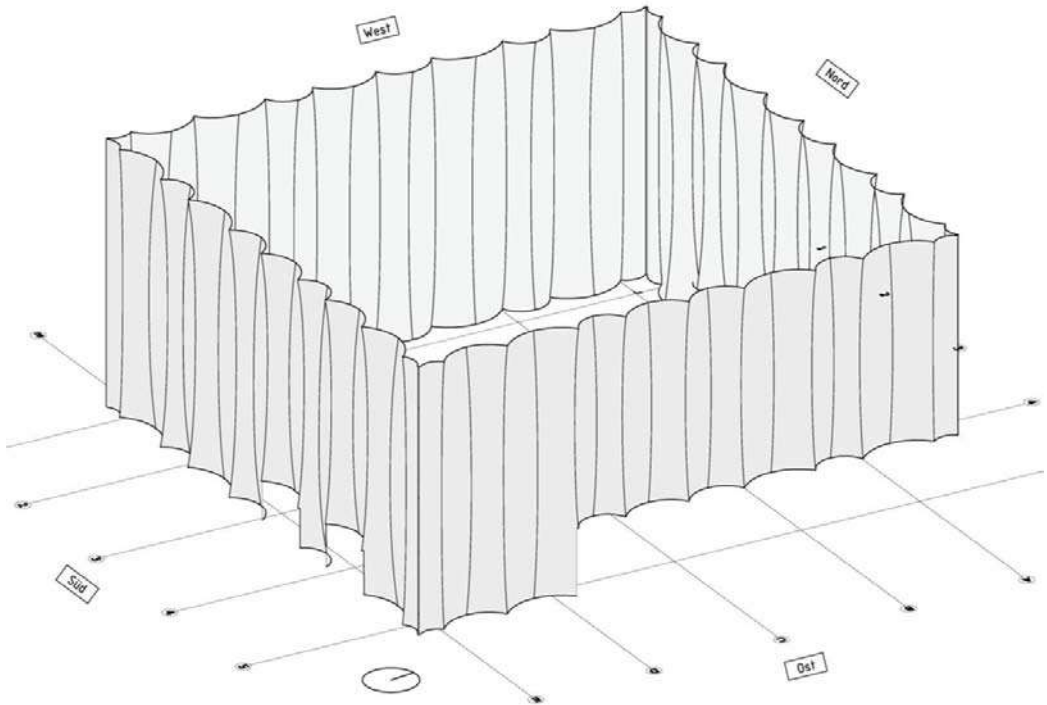


Figure 11: Final seam layout

6. Installation

The textile façade is fixed on the concrete wall of the building. Embedded steel parts had been placed in the formwork, where later the brackets had been attached with site welds. The wall was then covered with thermal insulation and plaster.

The supporting steel structure was then connected to these brackets, and geometrically surveyed for a final geometry check.

The membrane installation has been made per facade. The panels have been unfolded and laid out on the ground. With the help of mobile cranes, the panels have been lifted and attached to the upper attachment line.

The cables have been installed to the final length, and the membrane panels were stressed and clamped in the final position.



Figure 12: Support structure installed



Figure 13: Attaching of the membrane panel



Figure 14: Stressing and fixing along the lower edge



Figure 15: View from below at a door frame



Figure 16: East and North façade



Figure 17: South façade



Figure 18: East façade in the twilight



Figure 19: Transparent appearance during the night

7. Conclusion

The result of the project comes close to the design intent. The textile appearance is remarkable, and gives already an idea what might be taught in this school. From inside the façade is nearly transparent but still provides shading, while from the outside its appearance depends on the light conditions and ranges between reflecting and semi-transparent.

The use of almost invisible details made the detailing and the installation quite complex. Adjustable details would have allowed more tolerances, and a simplified installation, but they would remain visible. The installation team has worked out suitable methods to deal with these constraints. The developed installation tools can be used for future maintenance.

The textile character of the chosen mesh material appears also from far. The wish of client and architect to have a remarkable undulation over the full height of the façade leads to high tensile forces in the vertical direction. The final shape is a good balanced compromise, still appearing undulated, but with reasonable tensile forces.

Acknowledgements

Client: Textilakademie NRW gGmbH

Architect: slapa oberholz pszczulny | architekten | sop GmbH & Co. KG, Düsseldorf

Structural design of the façade structure: formTL ingenieure für tragwerk und leichtbau gmbh

Contractor: Koch Membranen GmbH, Rimsting

Picture credits: Figures 1 to 15 formTL, Figures 16 to 19 thomasmayerarchive.de

Tension-actuated textiles for architectural applications

Timothy LIDDELL*, Isabella FLORE*, Massimo FONTANA*, Nina ROMANOVA*,
Mahsa B. ZAMANI*, Nataliia ANTONENKO*, Haykaz POGHOSYAN*

* Politecnico di Milano, Alta Scuola Politecnica,
Piazza Leonardo da Vinci, 32, 20133 Milan, Italy
timothy.liddell@asp-poli.it

Abstract

This paper discusses the formal characteristics and architectural potential of tension-actuated textiles. Specifically, it shows how dynamic 3D surface geometries may be generated by printing rigid 2D patterns onto pre-stretched fabric. The resulting surfaces have aesthetic and structural properties similar to adaptive skins found in nature and, if scaled up, could bring a new degree of softness and responsivity to the built environment.

The hybridized textiles presented herein exhibit complex double-curvature. The final shapes are affected by many variables including material elasticity, bending resistance and ambient temperature. However, in all cases, the principal factor is the initial 2D print-pattern itself, where even small variations can result in drastically different surface curvatures. Through an extensive physical prototyping process, the causal link between 2D-input and 3D-output geometry was explored and several designs were developed with performative qualities such as incidental bending and snap-buckling.

The practical implications of the proposed shape-making technique are far-reaching. Along with CNC knitting, the method is among only a few fabrication techniques capable of generating complex surface curvature without the need for molds, formwork or manual labor. Since input patterns may be adjusted without incurring additional tooling costs, the

DOI: 10.30448/ts2019.3245.20

Copyright © 2019 by T. Liddell, I. Flore, M. Fontana, N. Romanova, M. B. Zamani, N. Antonenko, H. Poghosyan. Published by Maggioli SpA with License Creative Commons CC BY-NC-ND 4.0 with permission.

Peer-review under responsibility of the TensiNet Association

process is highly controlled and customizable. For these reasons, the process promises to be competitive with traditional fabrication techniques – offering new and exciting opportunities for design and manufacturing in the coming years.

Keywords: Smart Textile, 3d Printing, 4d Printing, Programmable Materials, Self-Assembly, Smart Facade, Shading, Biomimicry

1. Project introduction

The findings presented in this paper are drawn from a 14-month interdisciplinary project conducted by students enrolled at the *Alta Scuola Politecnica* in Milan, Italy. The project started from the premise that buildings account for an outsized proportion of energy consumption in the world today and do not adequately safeguard the wellbeing of occupants. These shortcomings are largely attributable to underperforming building envelopes that fail to properly regulate the flow of heat and light from the outdoors. Smart materials and control systems provide opportunities for better performing building envelopes. Indeed, many of today's state-of-the-art facades perform quite well. But, like works of art, they tend to be expensive, singular designs for premium new buildings. To have a more widespread impact, façade solutions must remain economical and applicable to a variety of existing, underperforming buildings.

With these considerations in mind, the team proposed the use of a lightweight 'second-skin' to improve the aesthetic and environmental performance of ageing glass curtain-walls. Such a system would block excess heat gain and visual glare, while optimizing natural daylight and views. Textiles are an ideal material for such applications, as they are highly customizable in terms of size, color and translucency. However, the surface geometry of soft, woven textiles can be difficult and costly to control, involving complex cut patterns and structural frameworks. Therefore, it was deemed necessary to explore new means of shape-making wherein planar surfaces acquire three-dimensionality autonomously, without extensive tooling or labor.

The proposed manufacturing process is situated at the intersection of digital fabrication and smart materials. It leverages the inherent elasticity of textile as an actuator, capable of inducing physical transformations. By depositing a pattern of rigid material onto the textile when outstretched, the textile's elasticity is selectively inhibited, causing non-uniform yet predictable surface deformation. This permits extremely complex 3D curvatures to be achieved with the application of simple 2D patterns [fig. 1].

The project builds upon the work of scholars in the emerging field of programmable materials (Yao, 2015). The prototyping process has been tested at several institutions with objectives ranging from the mathematical (Guseinov, 2017) to the aesthetic (Co-de-it, 2017). This project

is unique in placing emphasis on large-scale, real-world building applications, arguing that the use of smart textiles with an economic shape-making process could be a game-changing innovation in the world of high-performance building facades.

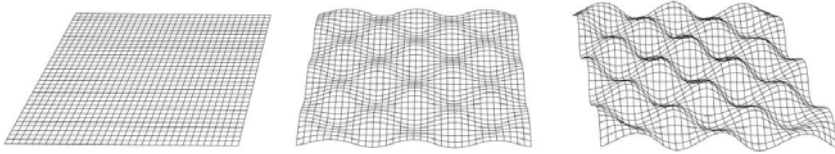


Figure 1: Prescribed deformations of plane from 2D to 3D.

2. Performative Skins

Building envelopes are increasingly seen as active systems meant to regulate environmental flows. They absorb daylight, block excess heat, shed water, filter pollutants and so forth. In short, they are expected to perform many of the same tasks as living skins found in nature, which respond to their environments in adaptive, resource efficient ways. There is much to be gained, therefore, in developing new building skin concepts with an eye toward the natural world, emulating its material intelligence wherever possible.

2.1. Living skins

The living skins of plants and animals are case studies in good design, with physical characteristics that have been proven and improved over millions of evolutionary cycles. Human builders have long borrowed from nature's catalog – either *directly* through the use of animal hides and plant fibers, or *indirectly* through the simulation of organic materials and systems. But the extent of biomimicry in architecture should not be overstated; today's buildings have more in common with the solid, inanimate confines of a cave than they do with the soft, dynamic skins of living organisms. Most buildings remain square and static.

In contrast, plant and animal skins are often characterized by (a) complex double-curvature and (b) softness and/or movement [fig. 2]. Curvature helps in achieving structural stability with minimal material input, while range-of-motion allows for better adaptability and resilience to changing environmental conditions. If buildings were not limited by manufacturing constraints and tradition, they might acquire these same shape characteristics, which are so effective and widespread in the natural world.

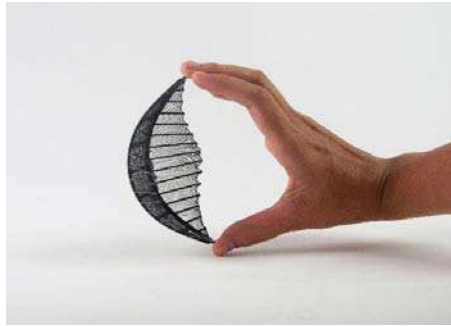


Figure 2: A prototype designed to replicate the shape and movement of the Bird of Paradise plant.

2.2. Technological skins

Textiles are perhaps the building material best suited to simulate the performance of living skins. They share many shape characteristics with plant and animal surfaces, including the capacity for softness, movement and double-curvature. This is by no means an accident as the first textiles were developed specifically as substitutes for animal hides in building and clothing applications. Textiles met and exceeded the performance requirements of earlier materials, while also being *economical*, *scalable* and *customizable*.

This biomimicry success story is considered one of the first examples of human ‘technology’ (Postrel, 2015). Time and again, textiles have been a driver of innovation – kicking off the Industrial Revolution with mechanized production and anticipating the Digital Age with binary punch cards. The future of smart buildings and dynamic building facades may very well be propelled by the next big breakthrough in the textile industry.

2.3. Programmable materials

It is popular today to talk about *smartness*, which in the age of smartphones is often associated with digital technologies and processing power. Search ‘*smart textiles*’ online and the top image results will inevitably feature digital circuitry. Yet, smartness goes far beyond the digital. Indeed, in the natural world, smartness is manifest in the physical shape and structure of organic materials; it is baked into the biology of living things.

The emerging field of *programmable materials* borrows this natural logic, embedding smartness into the composition of materials themselves (Yao, 214). A ‘programmed’ assembly is one that responds directly to external stimuli in a predictable and desirable way. Textiles, being highly customizable and kinetic, are an ideal medium for this type of material programming. So rather than resembling circuit boards, the *smart textiles* of the future are likely to be as dynamic and life-like as living skins.

3. The Shape-making Method

While it may be advantageous to emulate the high-performance surface geometries found in nature, economic and manufacturing constraints have largely precluded the idea. Today's methods of replicating organic shapes are complex and costly, typically involving custom molds. Complex forms are certainly achievable, but high tooling costs lead to shape-standardization and loss of variety. A new shape-making method, leveraging recent innovations in smart textiles and digital fabrication, could change all of this. The following sections describe the prototyping process and offer observations about the resulting forms.

3.1. Prototyping process

Prototypes were produced by printing rigid thermoplastic onto flat, pre-stretched fabric [fig. 3]. The design input is a 2D pattern, which is bonded to the fabric layer, locking the fibers in their outstretched position. When the fabric swatch is released from its frame, the printed areas remain elongated, resisting both compression and bending. Meanwhile, the unprinted areas of textile contract, causing distortion of the entire plane.

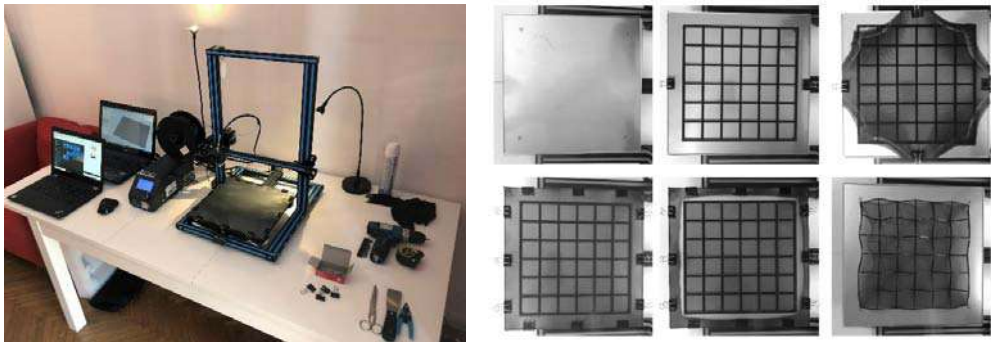


Figure 3: The Creality CR-10 3D-printer used by the team and six main steps of the fabrication process: (a) clean and pre-heat bed; (b) print lower layers; (c) stretch and clip fabric; (d) print upper layers; (e) cut away excess material; (f) remove part from printer bed and allow 3D deformation to occur.

Through the course of the study, different fabrics and plastic filaments were used. The best results were achieved with an elasticized tulle net, sandwiched between multiple layers of TPU flex-filament. Fabrics were stretched bi-laterally to about 150% of their original dimensions and deposited plastic patterns were permitted to cool before removal from the machine. The nozzle temperature and height were fine-tuned to achieve as strong a plastic bond as possible without inadvertently damaging the textile.

3.2. Shape characteristics

After having optimized the process, a *catalog of shapes* was printed using consistent materials and print-settings. By holding these variables constant, it was possible to identify how variation in the 2D print patterns impacts 3D form. The following observations were made:

- The interplay between elongation and contraction generates complex, non-developable, Gaussian curvature, but not simple one-dimensional bending.
- Patterns with more plastic toward the center (e.g. an ‘X’) result in ‘dome-shapes’ with positive Gaussian curvature; whereas patterns with more plastic toward the perimeter (e.g. an ‘O’) result in ‘saddle-shapes’ with negative Gaussian curvature [fig.04].
- Depending on the print pattern, the resulting parts will have two or more states of structural equilibrium. When an adequate force is applied, the surface ‘pops’ from one state of equilibrium to another in a process called snap-buckling.
- Two main pattern logics were used for the plastic deposition: linear elements (ribs) and rasterized gradients of dots (tiles) [fig.05]. While tiles are a more nuanced method of generating curvature, they offer no bending resistance and collapse like a limp sock. Ribs, on the other hand, serve as a built-in structural frame that helps to maintain form.
- Though a formal distinct exists, the surfaces produced in this method have much in common with *developable surfaces*. Both geometric families achieve 3D shape from 2D planer input; both achieve overall structural stability despite being locally thin.
- Folding is possible and may even be self-induced, resulting in origami-like assemblies.

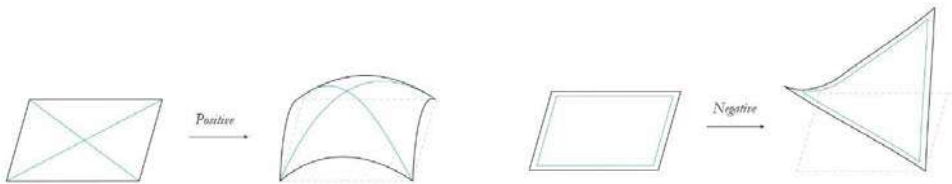


Figure 4: The shape of structure applied determines the final shape of the 3d form



Figure 5: The pattern typology of the print pattern (ribs or tiles) affects bending resistance

3.3. Software applications

Though not strictly necessary to achieve quality results, software may be used during the design process both as a predictive visualization tool and as a generator of pattern. Shape prediction is the most valuable and computationally challenging of these functions, as the software must account for many physical variables at play like material stiffness, fabric tensioning and ambient temperature. This study made use of the Kangaroo plugin for the NURBS modeling software Rhinoceros 3D. While Kangaroo and similar physics-modelers give an indication of what is possible, they remain cumbersome and error-prone for non-expert users.

Software may also be used to ‘reverse engineer’ from the desired 3D output to an unrolled 2D input pattern. Two projects cited by this paper focus entirely on this problem. The first contribution, CurveUps by scholars at IST Austria, proposes a custom algorithmic approach (Guseinov, 2017). The second contribution, Self-Forming Structures by Nervous Systems, proposes the use of a surface-unwrapping tool used in the game design industry called Boundary First Flattening (Sawhney, 2017). The idea is to ‘unwrap’ the 3D surface onto a flat plane and identify the zones of minimum and maximum distortion. The distortion map generated by the unwrapping tool is then used to create a corresponding rasterized pattern that can be printed (Fields, 2018).

4. Process Fundamentals

There were many practical considerations to understand and overcome during the prototyping process to achieve clear results. However, the scientific value of the project goes beyond the specific equipment or settings being used. This section focuses on the fundamental aspects of the shape-making process that are valid regardless of fabrication process or scale. These principles represent the conceptual groundwork on which real-world innovation may be built.

4.1. Developability

One fundamental aspect of the process is the *2D-to-3D* transformation. In contrast to *developable surfaces* like origami that assume three-dimensionality through bending and folding alone, the hybridized surfaces assume their shape through a process of planar distortion. Furthermore, the transformation is *self-actuated* by intrinsic material properties like elasticity and/or environmental stimuli like heat. There is no need for external/manual manipulation other than removing the assembled part from the machine.

4.2. Patterning

Structural patterning is the principal variable governing the shape and stability of the final form. The pattern determines the location and extent of surface distortion, which in turn determines

the location and extent of curvature. Distortion is a relative variable, meaning that what happens in any given zone is dependent on what happens in neighboring zones. If the entire surface is distorted equally, it will remain flat. Surface curvature results from distortion differentials, mathematically defined by the input pattern.

Structural patterning may also affect the assembly's overall bending resistance. A rasterized non-continuous 'dot' pattern will generate surface distortion and curvature but will not resist bending. In contrast, a linear 'ribbed' pattern may resist bending and, in doing so, will provide greater overall stability. Structural patterns with more continuity ensure more continuous curvature and fewer inflection/buckling points [fig. 6].

4.3. Hybridization

The final form is a composite of two or more input materials. These may be referred to as *surface* and *structure* respectively. In the context of this study, *surface* may be thought of as a thin, flexible membrane that acts in tension. Whereas, *structure* is a relatively solid deposited material forming a pattern that acts in compression and, at times, also bending. A third material, such as a *coating*, may be introduced to augment the performance of the final assembly [fig. 7].

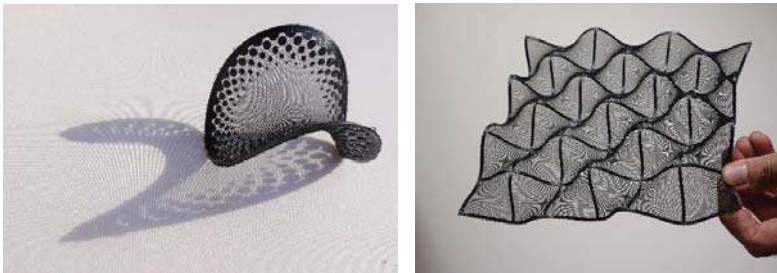


Figure 6: Patterning variation in (a) a singular, circular form and (b) a repeating, square grid.

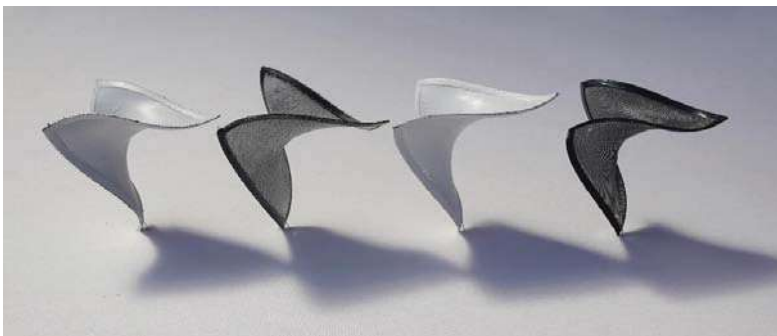


Figure 7: Four 'Hypar' structures generated by the interplay between surface and structure. Each has been treated with a different coating, affecting aesthetic and performance characteristics.

4.4. Typologies

The prototypes presented in this paper are composed of an *active* surface and a *passive* structure. But this may not always be the case. In fact, there are at least three distinct material typologies, each involving a different self-actuation process:

(1) *Pre-stretching* is the method described earlier in this paper. It involves stretching a surface and bonding it with a more rigid structure. The hybridized surface is actuated by the contraction of the surface when it is released from its frame.

(2) *Post-contraction* is a method wherein structure is bonded to an unstressed surface material, possibly a thin-film polymer that can be contracted through a chemical or mechanical process. The hybridized surface is actuated by the contraction of the surface when exposed to a reaction agent (chemical, heat, etc.).

(3) *Post-stretching* is a method differing from the previous two approaches in that the structure itself elongates after being bonded with the elastic surface. The hybridized surface is actuated by the elongation of the structure when exposed to a reaction agent (pneumatics, heat, etc.).

5. Market Viability

The proposed shape-making method could significantly impact many disciplines, from fashion to interior design and beyond. It points toward a future where softness and variation are as widespread in the built environment as in the natural world; where engineered materials are as responsive as living skins. The viability of the idea is a function of both feasibility and value: *how can programmed textiles be produced at scale? and will their end-value outweigh costs?*

5.1. Scaling up

There are several manufacturing techniques that might be used to replicate the team's prototyping process efficiently at a larger scale. These include large-format 3D-printing, laser cutting and CNC weaving/knitting – digital processes that offer pattern variation at no extra cost. The machinery need not be complicated. For example, the structural material could be deposited with a simple 2D 'plotter' onto moving sheets of stretched fabric. The hybridized surface could then be collected onto a roll, shipped to construction sites and deployed with reduced overall material, transportation and installation costs. An analogous process could occur in reverse to efficiently remove and recycle the textiles at the end of their optimal lifespan.

The success of these manufacturing and recycling processes depends largely on the selection of appropriate materials. Many textile surfaces already exist for building applications, including some that are fully reusable (technical nutrients) or fully biodegradable (biological nutrients).

It is critical, however, that the chosen *surface* material have enough elasticity to generate and retain the desired surface deformation. Furthermore, the *structural* material should be easily formable into the desired pattern and securely bondable to the selected surface through chemical and/or mechanical means. A third material, such as a spray-on coating, may be used to improve structural performance, protect from the elements and/or reduce flammability [fig. 7]. The long-term durability of these assemblies need not be a major constraint, provided they are situated within healthy economic and environmental ecosystems. The ephemerality of the engineered skin, as with living ones, may be the key to sustained performance and appropriateness in cities as urban and climactic conditions rapidly change.

In today's economy, companies specializing in smart textile materials are distinct from those specializing in additive manufacturing. The realization of high-performance 3D-printed-textiles requires the merger of competencies and equipment of these two fields. If and when this occurs, the production of tension-actuated textiles could be as affordable as screen-printing is today.

5.2. Value proposition

Hybridized textiles could be used to wrap buildings in a second-skin, improving façade appearance and performance. The textile would be tuned to site-specific needs, offering different degrees of shading, daylighting, views and urban-identity. The low-cost and versatility of such a system makes it suitable for ageing buildings, which are among the lowest performers in cities today. In this case, the fabric layer could easily be attached to existing buildings with a modular, lightweight structural system like scaffolding. Through a case study in the Porta Nuova district of Milan, designs were developed and evaluated with regard to stakeholder needs and requirements [fig. 8]. Environmental and visual simulations show that when shaped correctly, even a thin layer of textile can significantly reduce energy consumption and improve human comfort, which creates value for building occupants and owners alike.

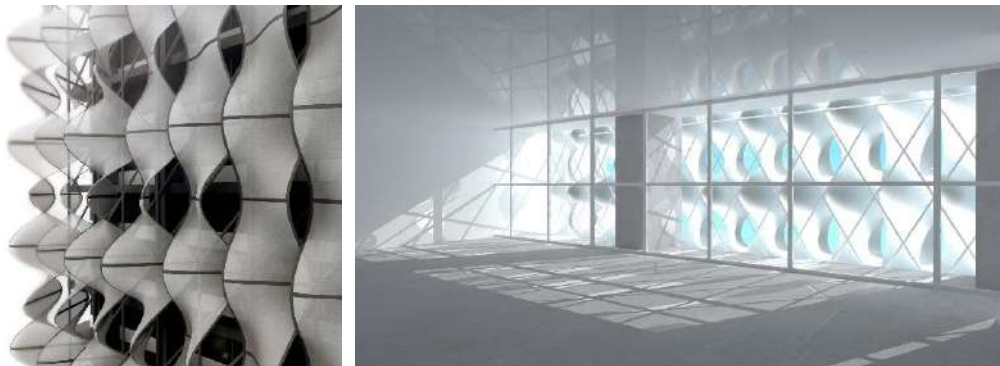


Figure 8: Rendered exterior and interior views of an office building with an undulating textile second skin.

5.3. Final remarks

One might question the logic of wrapping buildings in textile, opting instead for more traditional and durable building materials like stone and glass. But textiles are in fact one of the oldest and most technological of building materials. What they lack in longevity, they make up for in adaptability – a quality they share with the living skins of plants and animals.

If people change their clothes daily and animals change skins/coats through the course of the year, why don't building envelopes change too? For centuries, the performance of buildings has been limited by material and manufacturing constraints. The introduction of an innovative new fabrication method for textiles could overturn this paradigm and change the look and feel of cities in the years to come.

References

Callens, S. J., & Zadpoor, A. A. (2018). From flat sheets to curved geometries: Origami and kirigami approaches. *Materials Today*, 21(3), 241-265.

Co-de-it (2017) InFORMed Flexible Matter. *Workshop Summary*, 16 June. Available online: <http://www.co-de-it.com/wordpress/informed-flexible-matter.html>. [Accessed on 19 June 2018].

Fields, G. (2018). Self-Forming Structures: An exploration into 3d printing on pre-stretched fabric. *Nervous System Blog*, April 24. Accessed at <https://n-e-r-v-o-u-s.com/blog/?p=8011>

Guseinov, R., Miguel, E., & Bickel, B. (2017). CurveUps: Shaping objects from flat plates with tension-actuated curvature. *ACM Transactions on Graphics*, 36(4).

Kuusisto, T.K. (2010). *Textile in Architecture*. Tampere, Finland: Tampereen teknillinen yliopisto [Master's Thesis].

Postrel, V. (2015). Losing the thread. *Aeon Essays*, June 05. Accessed at <https://aeon.co/essays/how-textiles-repeatedly-revolutionised-human-technology>

Sawhney, R., & Crane, K. (2017). Boundary First Flattening. *ACM Transitions on Graphics*, 37(1), Article 5.

Tibbits et al. (2016). *US Patent No. 2016/0339627 A1*.

Wertheim, M. (2017). How to play mathematics. *Aeon Essays*, February 7. Accessed at <https://aeon.co/essays/theres-more-maths-in-slugs-and-corals-than-we-can-think-of>

Yao, L (2014). Matter Matters: Offloading Machine Computation to Material Computation for Shape Changing Interfaces. *UIST'14 Doctoral Symposium*, Honolulu

Proceedings of the TensiNet Symposium 2019

Softening the habitats / 3-5 June 2019, Politecnico di Milano, Milan, Italy

Alessandra Zanelli, Carol Monticelli, Marijke Mollaert, Bernd Stimpfle (Eds.)

Coating of ETFE – Solar Shading for Architectural Applications

Carl MAYWALD*

*Vector Foiltec GmbH
Steinacker 3, 28717 Bremen, Germany
Carl.maywald@vector-foiltec.com

Abstract

Due to the high transmission rate of ethylene tetrafluorethylene (ETFE) films over the whole solar spectrum cladding systems for architectural applications may result in heating up inside areas, thus increasing the energy requirements for air conditioning. In order to enhance user comfort and reduce cooling loads the foils have to be specially treated or coated. The low surface energy (23 mN/m) of ETFE foils inhibits surface adhesion thus offering maintenance advantages from self-cleaning effects which simultaneously raises considerable challenges for the design and application of stable coatings. Additionally, ETFE foils as part of the cladding system undergo significant in-service deformation, both plastic and elastic. Coatings have to cope with this specific requirements. This article will provide a brief introduction into the development of coating and printing on ETFE in particular, as well as an introduction into different techniques for solar shading of ETFE cladding systems in architectural buildings. In order to allow for quality assessment of these coatings taking into account elastic and plastic deformation of the target material, a new test procedure for coated ETFE will be introduced.

Keywords ETFE- ethylene tetrafluoroethylene, Texlon® systems in architecture, solar shading, quality assessment of coatings, transmission and reflection

DOI: 10.30448/ts2019.3245.43

Copyright © 2019 by C. Maywald. Published by Maggioli SpA with License Creative Commons CC BY-NC-ND 4.0 with permission.

Peer-review under responsibility of the TensiNet Association

1. Introduction

Extruded ethylene tetrafluoroethylene (ETFE) films were first identified as an ideal material for transparent building envelopes by Dr. Stefan Lehnert, founder of Vector Foiltec, in 1982 and were subsequently developed as the primary component of a multi-application building cladding system under the brand name “Texlon®”. The first project built by employing this technology was the Mangrove Hall of the Burger’s Zoo in Arnhem, The Netherlands, in 1982. The basis of a standard Texlon® multilayer system is an airtight cushion formed by welding together a minimum of two ETFE foil layers held within an extruded aluminum alloy perimeter frame, connected to a low pressure (250 Pa) air supply. A more detailed introduction to the technology can be found in “ETFE – Technology and Design” by Annette LeCuyer (LeCuyer A., 2008).

Early architectural projects utilizing the ETFE cladding technology were built with uncoated, clear ETFE films, which are highly transparent across the full band width of the solar spectrum (see Figure 1).

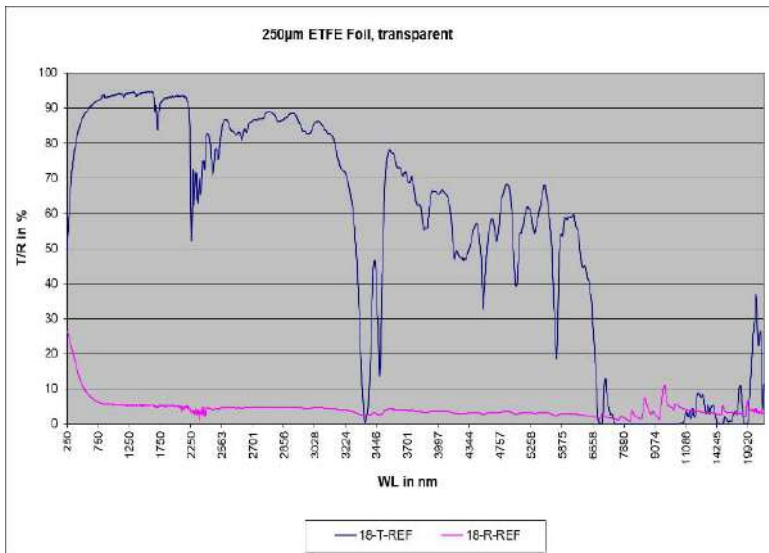


Figure 1: Transmission T and Reflection R of 250 µm ETFE foil up to 20.000 nm wavelength

The transmission of nearly 90 % of photosynthetically active radiation (PAR) is ideal for enhancing plant growth, but for human habitats the high transmission may result in heating of inside areas, thus increasing the required energy for air conditioning. Furthermore, the high surface area to perimeter ratios and the lightweight ETFE cladding panels, which are a significant advantage for sustainability and costs, increase the total solar energy transmission. Therefore careful consideration must be given to any requirement for solar control.

The first solar control for ETFE cladding systems in architecture was the application of a coating on an ETFE film for the atrium roof at the Schlumberger Research Institute in Cambridge, UK, in 1992 (Figure 2a).



Figure 2a: ETFE atrium roof Schlumberger Research Institute, Cambridge, UK, outer foil printed on inner surface, print pattern DM 4:65, light optical density ink (1992)

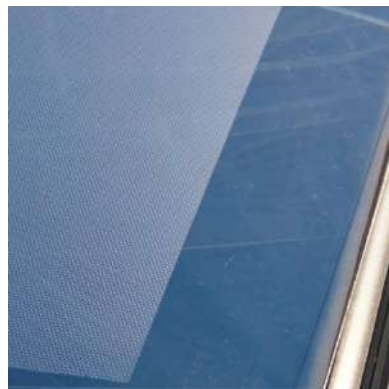


Figure 2b: Details of stable print pattern, after 23 years installation on the roof of the atrium (2015)

The application of the print pattern on ETFE film was achieved by the development of a rotogravure, roll to roll printing process by Vector Foiltec. The print pattern employed was a 4 mm dot matrix covering 65 % of the foil surface (DM 4:65) with relatively low optical density. The shading performance though effective was limited and thus supplementary blinds were still required in front of the windows on the ground floor. Despite the technical difficulties mentioned before the detailed view (see fig.2b) exhibits the good status of the coating even after 23 years of exposure (photos taken in 2015) to environmental conditions. In order to protect the ink, the printing is always applied on the inner side of the outer foil of the cushion. In addition, the self-cleaning effect of the outer face of the foil due to the low surface energy is preserved.

Indeed, even though the modification of the transmission for solar radiation is the primary driver for development of coatings on ETFE foils, they have also been utilized for purely aesthetic purposes. Finally, the development of high reflectance printing on ETFE foils was the key technological advance that expanded the application range of Texlon® towards a universal cladding product for high transparency roofs and façades. One example for the success of such a high reflective cushion system is 'The Avenues Mall', the largest shopping mall complex in Kuwait and the second largest in the Middle East. Phase III 'The Grand Avenue' encloses a main boulevard and adjoining side streets under 25.000 m² of ETFE roof (Figure 3) creating a comfortably conditioned space with the experience of an open sky, that is not only a major commercial success but has become a social hub for the whole region (Maywald C., and Riesser,



Figure 3 The Avenues Mall, Kuwait – Texlon® ETFE cladding system printed with DH 7:84 medium

F., 2016) and (Urbán et al., 2016). Since then further phases IVa and IVb have been completed creating a range of additional commercial and social spaces well-protected from the harsh external environment under a total of nearly 100,000 m² of Texlon® ETFE roofing system. Despite the high external temperatures a low overall heat transmission resistance (high U-value) for the roof system has only minor influence due to the temperature stratification effects. In this building category with its full height large volume spaces the warm air is forming a stable inversion layer immediately beneath the roof with comparable or even greater temperature than outside. The temperature gradually decreases downwards to the comfort zone at ground level. During night time the temperatures outside the building are lower. So the loss of thermal energy through the roof is beneficial to reduce daytime cooling demand. However, the necessity for control of radiative solar gain is of paramount importance. The reflective coatings used at The Avenues Mall are a third generation medium opacity ink printed in a 7 mm hexagonal matrix pattern covering 84 % of the foil area (DH 7:84) to the inner surface of the uppermost foil.

For the 3-layer system (200 µm – 80 µm – 200 µm), with outer foil printed on the inner side, the performance is given in Table 1:

	UV-light	Visible light	Solar light
Transmission (%)	16	21	21
Reflectance (%)	44	46	46
Absorption (%)	40	33	33
g-Value/SHGC	0.23		
Shading Coefficient	0.27		
U-Value (W/m ² K)	1.25		

Table 1: Optical and thermal properties of 3-layer cushion system at The Avenues Mall, Kuwait.

2. Printing and Coating on ETFE

Printing and coating on ETFE-foils is highly demanding for both the formulation of the lacquer systems and the physical coating process. This follows from the material characteristics of the foil itself and the wide range of environmental stresses that the printed foil as the primary element of a building envelope cladding system must withstand. The material properties of the ETFE foil that mostly influence the physical and chemical stability of the applied coatings during the printing process and in-service are:

1. Low surface energy ≤ 23 mN/m;
2. Elastic and plastic deformation under load up to 5%;
3. A relatively low melting point of approximately 280° C;
4. Water vapour permeability – approximately 2 g/(m²d) for a 200 μ m ETFE foil;
5. UV transparency – approximately 80 % for a 200 μ m ETFE foil.

The installed Texlon® cushion has to withstand a range of extreme environmental stresses:

1. Temperature - ETFE cladding systems have to survive external temperatures between minus 40° C up to plus 50° C.
2. Wind Loads - building envelopes are subject to high wind loads of varying gust durations and load distributions causing high and nonuniform stresses
3. Snow loads – create loading scenarios maintaining high stresses in the ETFE foils over extended periods of time.
4. High humidity, rainfall and condensation can cause vapour pressure gradients in both directions across ETFE membranes.
5. Partial water ponding – certain partial deflation scenarios can result in localised water ponding resulting in very high local loads and associated stresses.
6. Folding, bending and buckling - during the production process, transportation and installation of the ETFE cushions and single layers repeated or sustained folding and buckling can occur.

Both sets of parameters define the requirements for coating formulations, their mechanical and chemical properties, the printing process, and for the treatment systems:

1. Before coating, the surface of ETFE foils should be pre-treated by either corona or plasma discharge to increase the surface energy. The best results regarding adhesion have been identified at a surface energy value of around 56 mN/m. This can be achieved by a corona treatment of a single side of the ETFE foils during the extrusion process. Unfortunately, the surface energy will decrease with time after treatment. Thus, it is strongly recommended to renew this treatment directly before coating.
2. After the coating process the ink must be dried by controlled heating within a drying tunnel. To prevent deformations of the ETFE foil an uniform temperature distribution below 70°C should be applied.
3. The roll to roll process induces longitudinal stress in the foils. However, elongation deformation is not acceptable as multiple pieces of foil with short lengths must be welded together to form larger sheets for cushion production. The print patterns should be aligned across the seams. For this purpose, marks are printed along roll edges to ensure the correct alignment prior to welding.
4. As the primary component of a cladding system foils will be deformed elastically and to some degree plastically during service life. Coating adhesion must be sufficiently robust to withstand shear stresses at the interface between foil and pigments whereas cohesion has to perform sufficiently elastic in order to resist disruption or cracking of the matrix.
5. The coating must remain stable under 100 % humidity within a cushion under simultaneously high external temperatures. Despite pressure from water vapour permeability neither degradation nor generation of plaque due to micro-cracks and micro-channelling is acceptable.
6. The coating must have long-term UV stability
7. The coating must retain adhesion and cohesion
 - a. under dynamic stresses from wind loading across a wide material temperature range of -40° C up to +50° C,
 - b. in areas of sustained high strain and peripheral buckling induced by snow loads,
 - c. in localised zones of high strain caused by folding and buckling during welding as well as production and installation activities.
8. To facilitate many production welding scenarios it is necessary to be able to remove coatings precisely from localised areas of foil. Despite the need for extremely high levels of stability under the circumstances reported above it must also be possible to economically, effectively and safely remove coatings when required as part of the cladding production process.

2.1. Development of ink for printing on ETFE

In close cooperation with a company specializing in the research and production of varnishes and paints Vector Foiltec developed a coating system for use with ETFE foils in 1990 and undertook rigorous testing of its application in an automated gravure printing production process. Eight years after the first architectural application (Schlumberger Research Institute in Cambridge, UK, in 1992) the technology was transferred to a German printing company. Since then it has become the standard system for printing on ETFE for architectural applications. Accordingly, this technology is now used by nearly all suppliers of ETFE cladding systems. With the exception of zoological and botanical buildings where high levels of solar transmission are required, printing is employed in almost all ETFE cladding installations in order to control incoming solar radiation. Vector Foiltec have continuously worked on further optimization of printing ink formulation for exclusive use in their ETFE cladding products with a particular emphasis on enhanced system performance, environmental sustainability and occupational health and safety. In close cooperation with a high-tech printing company in Austria major advances were achieved regarding optical density and reflectivity in 2010. In contrast to the previously used fluoropolymer resin lacquers the new ink is based on an acrylic lacquer enabling the use of much less harmful solvents (bio-ethanol) for the removal of printed ink for welding purposes. The continuous improvement over time in the solar control capabilities of specialist ETFE printing inks is demonstrated in Table 2 below.

Table 2: development of print performance (the more recent acrylic based system is indicated by the prefix H and the former resin system by the prefix R

	T _{UV}	T _{vis}	T _{sol}	R _{UV}	R _{vis}	R _{sol}	ε*	g-value
	%	%	%	%	%	%		
R01249	41,9	41,7	41,4	30,8	39,9	39,7	0,56	0.46
R01249	9,7	12,6	12,8	38,2	51,5	51,1	0,47	0.25
R78185	6,6	7,2	7,1	48,4	57,7	54	0,43	0.21
H560110	2,5	2,7	2,6	53,9	56,6	55,4	0,40	0.18

For a standard 3-layer ETFE cushion system similar to that deployed in Phase III ‘The Avenues Mall’ Kuwait (200µm transparent outer foil, 80µm transparent middle foil, and 200µm transparent inner foil, outer foil printed on the inner face with DH 4:84, 4mm hexagonal matrix with 84% coverage), the g-values calculated for the 4 different print systems are indicated as well.

It should be noted that transmission and reflectance characteristics for both the visible portion T_{vis} and the solar transmission T_{sol} are closely related. Reduced solar gain resulting from a higher percentage of the surface covered by ink and/or enhanced reflectivity will result in a similar reduction in visible light transmission with these coating systems.

2.2 Texlon® “Vario” system

The Texlon® “Vario” system was developed to provide a cladding solution that could react to changing demands for solar control or visible light transmission in response to customer requirements or variations in the external environment. The system can be triggered to switch modes by automated sensor driven controls or manual push button operation.

In the standard ‘Vario’ arrangement the two outermost layers of a three layer panel are printed with a complementary offset print on their inward facing surfaces. The middle or innermost printed layer can be moved upwards to rest against the uppermost printed layer or down to meet the bottom layer by pumping air from one side of the middle foil to the other creating a pressurised chamber either below or above the middle foil. A detailed description has been given by Annette LeCuyer (LeCuyer A., 2008, p. 94).

The optical and the thermal performance of a Texlon® vario system with one of a number of different print pattern combinations (SQM 200-197:45 dark) for open and closed position is given in table 3.

Table 3: optical and thermal performance of a Texlon® vario system for open and closed position. Print pattern is SQM200-197:45

Texlon vario	open			closed		
	UV light	Visible light	Solar light	UV light	Visible light	Solar light
	UV light	Visible light	Solar light	UV light	Visible light	Solar light
	%	%	%	%	%	%
Transmission	15	26	26	5	9	10
Reflectance	14	40	38	14	53	52
Absorption	71	34	35	81	38	39
g-value / SHGC	0,37			0,14		
Shading Coefficient	0,42			0,16		
U-value [W/m²K]	2,78			2,78		

Solar light transmission is 10 % in the closed position and 26 % when open and the associated g-value or Solar Heat Gain Coefficient SHGC are 0.14 closed and 0.37 open. It should be noted that in the standard arrangement the middle foil is always in contact with the uppermost or bottom foil in the closed or open position respectively and therefore for the purpose of thermal insulation this is always a single chamber system with a corresponding U-value of around 2.78 W/m²K.

3. Test procedures for coatings on ETFE

As outlined in section 2.0 the demands on the stability of ETFE coatings for building applications are sophisticated, yet it must still be possible to efficiently remove these coatings as part of the production process. Probably the most demanding of all is the retention of

adhesion and cohesion under long and short term deformation, typically up to 3-5 %, under dynamic environmental conditions.

Classic accelerated weathering test methods like EN ISO 4892-2 (2013) and EN ISO 4892-3 (2016) within climate chambers simulating rain, alternating temperatures and UV impact had been applied and revealed no difference in performance for a range of ETFE coatings. However, in-service external exposure in mock-ups and historic installations had led to print degradation or loss of adhesion, showing the limits of the standard test methods for the determination of ageing performance of coatings on ETFE foils. Therefore, a long term corrosion test under stress load and a hysteresis test were developed.

3.1 Long term corrosion test under stress

In the long term corrosion test a 15 mm wide, coated ETFE strip with a foil thickness of 250 μm is loaded by a weight of 6.5 kg fixed at one end of the strip (cf. fig. 4) inducing a nominal stress of approximately 17 N/mm² (HUECK FOLIEN, 2010).



Figure 4: weight for creation of 17 N/mm² load on an ETFE stripe of 15 mm width

Once loaded, the specimen is inserted into a container, which will be filled with 10 mm distilled water and closed afterwards. The strip is led through a slot in the cap of the container, the container is sealed and the strip is tensioned by rolling it up a metal stick (see fig. 5, 6, and 7).



Figure 5: ETFE stripe loaded with weight up to 17 MPa



Figure 6: cap with small opening for ETFE stripe



Figure 7: containment closed with cap

The test assembly is placed into a climate chamber for 10 days at a temperature of 80° C. The tension in the strip was maintained permanently. The ongoing elongation of the strip was

corrected by further reeling over the metal stick. Afterwards the stability of the print is determined by applying the Tesa-/Tape-Test (ASTM F2252-3, 2003) (EN ISO 2409, 2013).

The strip has undergone significant elongation (356 % over the period of the test) resulting in a reduced optical density. No defects like cracks or delamination caused by this test were found for any of the H samples, neither for H 318105 nor for H 560110 print system.

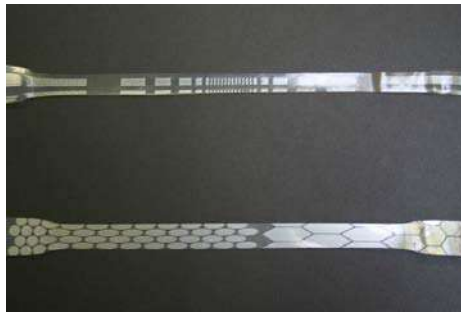


Figure 8: Two strips of ETFE after long-term corrosion test stressed with constant load of 17 N/mm^2 at 80° C and 100% humidity

Comparison with results from former ink showed significantly enhanced stability for the new H lacquer.

3.2 Hysteresis Tests

When installed in roof and façade cladding systems ETFE foils undergo frequent exposure to wind loads imposed by a wide range of wind speeds. Gusting wind speeds are typically 40 % higher than basic wind speeds. For the purpose of analysis wind gusts are generally considered to last for about 3 seconds (Eaddy and Melbourne, 2004). Texlon® ETFE cushion systems are stabilised by an inner air pressure of approximately 250 Pa inducing a permanent pre-stress load of approximately 4 N/mm^2 to the outermost foils. Single layer systems are pre-stressed to approximately 6 N/mm^2 . In order to simulate these load conditions a hysteresis test procedure using a mono-axial tensile test machine has been designed. In order to simulate extreme wind conditions the load cycling was determined to be between 9 N/mm^2 and 18 N/mm^2 . The strain-stress diagram is shown in Figure 12. The diagram also illustrates the ageing performance of the ETFE material itself. Cyclic loads will cause reduction of strain with increasing number of cycles even under 18 N/mm^2 loads. The ETFE foil becomes stiffer with mechanical ageing (Maywald C., and Mißfeld M., 2018)

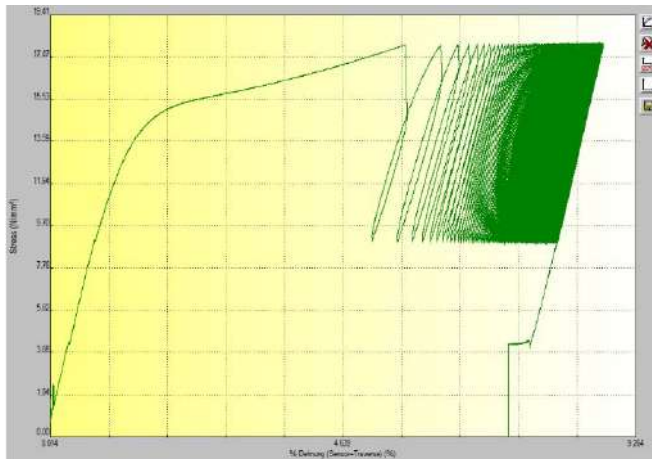


Figure 9: strain-stress diagram 250µm ETFE foil, 300 cycles; test for print stability

After the test strips with the coating under examination have been subjected to 300 load cycles, they are exposed to accelerated weathering tests according to standard norms (EN ISO 4892-2, 2013) and (EN ISO 4892-3, 2016). The load test of various coated samples from different printing companies gave evidence regarding long term stability of the coatings.

4 Summary

Over the last 28 years printing and coating technology on ETFE foils for architectural applications has improved significantly, especially reflectivity and optical density has been increased by more than a factor of 2. For that reason, the g-value of a standard 3-layer ETFE Texlon® cushion was decreased from 0.46 for the first printing generation to a value as low as 0.18 for the state-of-the-art system.

It should be mentioned that foils with embodied pigments introduced into the foil matrix prior to extrusion are also available from ETFE foil manufacturers. These embodied pigments also contribute to the selective control of transmission and reflection. The use of coloured ETFE foils in combination with additional printing expands the potential for further solar control and opens an even wider range for tuning the cladding systems according to local project related requirements. Beside printing and coloured ETFE foils there are approaches towards selective solar shading by metal film sputtering on ETFE foils. However, no solution is currently available to the construction market. This is mainly a consequence of the physical properties of ETFE foils, which are both permeable to water vapour promoting oxidation, and flexible causing micro cracks and delamination of the metallic film coatings.

In order to simulate ageing effects of coatings on ETFE foils new specific methodologies have been developed for laboratory based tests. These tests do not only provide evidence regarding

the loss of adhesion of coating on ETFE foil systems resulting from cyclic stretching of the foils under environmental conditions but are essential for the assessment of the in-service ageing characteristics of the material itself. In contrast to most of the other materials used for the building cladding systems foils and membranes are constantly deflected by environmental loads which has a major impact on ageing behaviour and therefore has to be taken into consideration. Therefore, the current test procedures and methods as specified in the standards are not sufficient for quality control of textile membranes and foil treatment systems.

References

ASTM F2252-03 (2003), Standard Practice for Evaluating Ink or Coating Adhesion to Flexible Packaging Materials Using Tape, ASTM International, West Conshohocken, PA, 2003

Eaddy M., Melbourne W.H. (2004), MEL Consultants Pty Ltd Report 30C/02, 'Addendum C to MEL Consultants Report 30/02, Wind Tunnel Measurements of Pressures on the Proposed Spencer Street Station Redevelopment, Melbourne'

EN ISO 2409:2013-06 (2013), Paints and varnishes - Cross-cut test

EN ISO 4892-2 (2013), Plastics - Methods of exposure to laboratory light sources - Part 2: Xenon-arc lamps

EN ISO 4892-3: 2016-10 (2016), Plastics - Methods of exposure to laboratory light sources – Part 3: Fluorescent UV lamps

HUECK FOLIEN (2010), Baumgartenberg, Austria

LeCuyer A. (2008), ETFE – Technology and Design, *Birkhäuser Verlag AG*, Basel, CH

Maywald C., and Mißfeld M. (2018), Zum Alterungsverhalten von ETFE-Konstruktionen, *Stahlbau 7/18*, Wiley Press, Wilhelm Ernst & Sohn Verlag für Architektur und technische Wissenschaften GmbH & Co. KG, Berlin, Germany

Maywald C., and Riesser F. (2016), Sustainability – the art of modern architecture, in: *Procedia Engineering*, Elsevier, Vol. 155, pp. 238 – 248

Stranghöner N., Uhlemann J., Llorens J. (2015), CEN/TC 250/WG 5 *Membrane Structures Scientific and Policy Report - SaP-Report*

Urbán D., et.al. (2016), Acoustic comfort in atria covered by novel structural skins, in: *Procedia Engineering*, Elsevier, Vol. 155, pp. 361 – 368

Proceedings of the TensiNet Symposium 2019

Softening the habitats / 3-5 June 2019, Politecnico di Milano, Milan, Italy

Alessandra Zanelli, Carol Monticelli, Marijke Mollaert, Bernd Stimpfle (Eds.)

Optimization of a membrane structure design for existing project of children's playground in the city of Krupina

Vojtech CHMELÍK*, Jozef KURÁŇ*, Monika RYCHTÁRIKOVÁ^a

* Department of architecture, The Faculty of Civil Engineering, STU Bratislava, Radlinského 11, 810 05 Bratislava, Slovakia

^a KU Leuven, Faculty of Architecture, Hoogstraat 51, 9000 Gent/ Paleizenstraat 65, 1030 Brussel, Belgium

Abstract

In this article, we discuss the impact of structural membrane (with a covering function) placed above already existing children's playground situated in a residential area, on the overall acoustic comfort. Without any doubt, covering of the playground, allows the usage of the place during the whole year cycle. This in principle good intention consequently increases the number of present people and number of sound reflections between ground and covering structure, and thus, in terms of acoustics, it will result in increased amount of sound sources. Frequent objection of inhabitants of residential areas at close neighborhood from playgrounds is a concern about noise and acoustic discomfort. This paper deal with an impact of a membrane structure (shading element) on the noise conditions in the given outdoor public place. Discussed possibilities aim at design optimization such as suitable material choice, shape and suspension height of the structural skin from an acoustic point of view. Consideration process is based on number of calculations and acoustic simulations performed for different cases. Result is an optimized and multi-functional design for covering membrane structure, fulfilling aesthetic, operational and acoustic requirements. Resulting optimized design will be also compared with situation in which a similar glazed covering structure would be used.

Keywords: playgrounds, sound absorption, room acoustics, acoustics, membrane structure, acoustic comfort

DOI: 10.30448/ts2019.3245.22

Copyright © 2019 by J. Kuran, V. Chmelik, M. Rychtáriková. Published by Maggioli SpA with License Creative Commons CC BY-NC-ND 4.0 with permission.

Peer-review under responsibility of the TensiNet Association

1. Introduction

Deficiency of safe, contemporary and valuable outdoor public spaces and playgrounds for children in Slovakia belongs to often discussed topics on city level, which most often leads to planning and designing of completely new facilities. In most of the cases the initiative is taken by city councils together with urban planners. Structural membranes with shading functions are, in this context not completely explored yet and might therefore open new strategies with variety of possibilities.

Revitalization of existing urban places especially in less developed regions in Slovakia and a focus on establishment of attractive and up-to-date living environment that would strengthen the identity of the given environment are essential in term of slowing down the economic and social migration. Children's playgrounds belong to important identifying elements in children's education. They establish bond and establish the relationship with the place where children grow up and gave them a chance to perform safe activities and to keep healthy physiological habits (van Mechelen, 2000, p.1610) They also serve as an alternative to the emerging dependence on digital information tools. General trend is also focused on connection of different social groups, such as seniors, children, foreigners etc. towards social integrity of the residential community. In a view of inclusive design, it is necessary also necessary to place the inclusion elements for the integration of disabled children into the game process (Shaw, 1987).

When designing children's playgrounds, the convenient accessible distance must be guaranteed, in order to keep an optimal form of social control. On the other hand, the proximity of playgrounds can cause acoustic discomfort to the surrounding dwellings on the other hand. Well-chosen acoustic solutions can reduce the noise disturbance associated with the use of playground elements and properly applied roofing above playgrounds can help in (1) Increase in perceived visual attractiveness, (2) improvement of acoustic comfort and (3) longer playing times over the whole year.

The use of children's playgrounds on average is 26.7 times during the summer and 18.9 times during the winter. Applying a suitable covering construction can increase the usage in adverse weather conditions (Gundersen, 2016, p.116).

2. Description of the case study

For this article a real study case was chosen, located in the eastern part of the small historic town of Krupina in residential part Majersky rad. From the western side of the site is a river with a regulated flow and reinforced shores. The existing terraced roads, pathways, hardened areas of smaller scale, outdated children's areas, grasslands, green areas, growing greenery of deciduous and coniferous trees of different species are placed here (Figure 1).

The project for the revitalization of the inter-block has resulted in the reconstruction of the whole urban public spaces. The main aim of the revitalization was to increase its attractiveness, aesthetics, functional and cultural-social values by creating space for relaxation, restoring public greenery, restoring the urban and park furniture, design of new park paths ways and pedestrian routes, building of the playground and outdoor fitness facilities meeting current safety standards in the meaning of the applicable legislation and standards.

Design of layout, functional use as well as material choice and design of technical aspects of new elements for playgrounds, outdoor fitness facilities and community areas is addressed with a strong emphasis on safety. All proposed assemblies needed to meet the requirements mentioned in standards (STN EN 1176, 2018; STN EN 117, 2018). Position also takes into account the suitability of orientation on the cardinal directions. The top layer of impact surfaces is formed by mats of recycled rubber of the prescribed thickness, optionally surfaces with natural materials.

The northern part of the area is focused on socio-cultural activities and active children play. The southern part predominantly hosts children's activities. The middle part focuses on active use. The proposal considers revitalization of the existing longitudinal pedestrian path in the north-south direction, alongside the Krupinica River. The sports and fitness activities will also be added to the existing playgrounds in the form of a multipurpose field set up on an area of existing green in the central part. Concerned territory is complemented by small areas with furniture for seating and communication of the visitors. Concerned territory has a linear character, functional territories are predominantly situated in the extended parts of inter-space areas. The division of the solved territory is based on the main pedestrian path, situated along the Krupinica watercourse. The color of individual areas depends on their use. Playing surfaces have an applied rubber surface on EPDM base.



Figure 1: The overall view on the solved are

As the surface under the gaming elements, a single-shell rubber granulate based on EPDM plays a role of a shock absorber. The surface is easy to move with a stroller and accessible for immobile children. In the design, the surface is graphically represented by mountain meadows. Natural materials are used for impact area beneath the rope-play assembly. The functional area is accessible by bicycles. Within the social and community area, it is proposed to build a gazebo for the needs of the community, parked seating, and petanque playground with natural materials. Design in the northern part of the treated area resolves the reclamation of the existing grassy area, the addition of the green vegetation, planting of hedges, reconstruction and completion of existing pedestrian communications.



Figure 2: Chosen middle part of solved area in detail

Pedestrian corridor in the form of an asphalt walk along the river Krupinica, as the development of longitudinal communication, is proposed in the middle part of the designed area. Near the footbridge, in the middle part of the solved territory, functional area designed for fitness and active sports as well as community use is proposed. The area is placed along the length of the pedestrian street, embedded in the existing green (Figure 2).

Inspired of previously conducted studies (Kiyama, 1998, p. 239; Sakagami, 1996, p. 237; Polomová, 2016, p. 306; Urbán, 2017, p. 93; Maywald, 2016, p. 238), in this article we will discuss the influence of covering of the playground by structural skins (ETFE) and its benefit in terms of noise situation when compared to glass.

3. Assessment of the acoustic comfort

In order to understand the acoustic situation in the playground better, 3D acoustic models were constructed, and several acoustic simulations were performed. Room acoustic prediction algorithm (Odeon software) was used, that is based on an image source method and special ray-tracing method with advanced scattering model (Christensen, 2013).

3.1. Description of the acoustic model

Predictions were performed for two kinds of roof shapes (Fig.3) and two types of playground covering materials: (1) glass and (2) ETFE foil – 2 layer cushion, i.e. in total 4 different architectural cases were compared. Values of sound absorption coefficient of both materials could be found in Table 1. From acoustic point of view, first, the simulations were done for one sound source (representing an instructor, teacher or parent present in the playground) and 7 receivers (listening kids) and second, the situation with 8 sources (kids playing) and receivers’ grid (to monitor the distribution of sound pressure level they produce together). The curved surface of cushions was taken into account through increased scattering of particular surfaces.

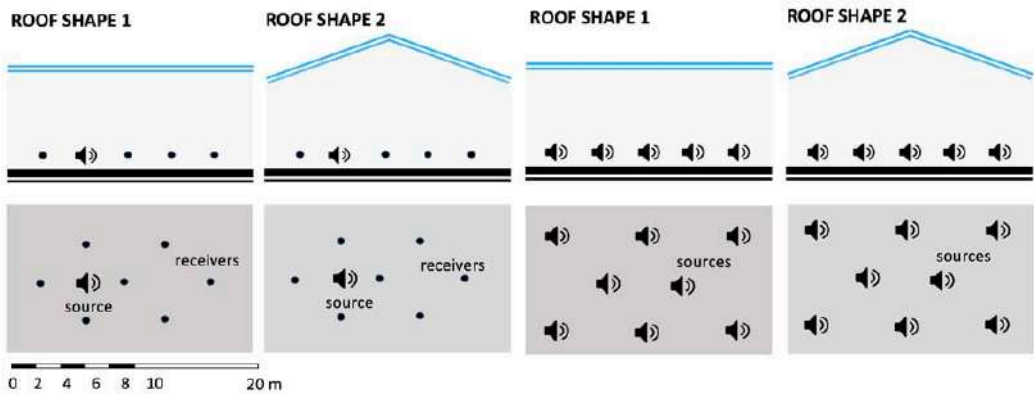


Figure 3: Spatial models of playground with two kinds of roof shape and material

3.2. Results and analysis

Sound pressure level in this paper is expressed through parameter sound strength G (dB) defined in ISO 3382 (ISO 3382, 2012). G values allow comparisons between different measured or simulated cases with different absolute sound power levels of sound source. G presumes sound power level of sound source $L_w = 31$ dB, resulting in sound pressure level of 0 dB at 10 m distance from the source in free field situation. By using G values, we can compare different cases and re-calculate very fast the noise situation cause by any sound power level. For instance, the L_w of a talking person is around 70 dB. In such a case we can simply add +40 dB to all simulated results, to get an idea about the resulting absolute sound levels in case of talking person.

Table 1: Values of sound absorption coefficient $\alpha(-)$ over frequencies for both roof materials used in simulations

	63	125	250	500	1000	2000	4000	8000
GLASS	0,1	0,1	0,07	0,05	0,03	0,02	0,02	0,02
ETFE	0,41	0,41	0,21	0,26	0,17	0,08	0,02	0,02

Figure 4 shows the results of sound pressure level decay with distance from the sound source in case of 4 alternatives mentioned above. Picture-left shows the situation at low frequencies (125 Hz), middle one for 1000 Hz and picture-right results for very high frequencies (8 kHz). All data are compared to free field situation, which expresses the fastest sound level decay with distance (if no obstacles are present in free field situation). From simulated results we can conclude, that at low frequencies, the sound pressure level at the playground will be ca 2 dB lower in cases with roof shape 1 and when ETFE is used. Interestingly in high frequencies the material of roofing doesn't matter anymore. It is because the sound absorption of high frequency sound by air is very high.

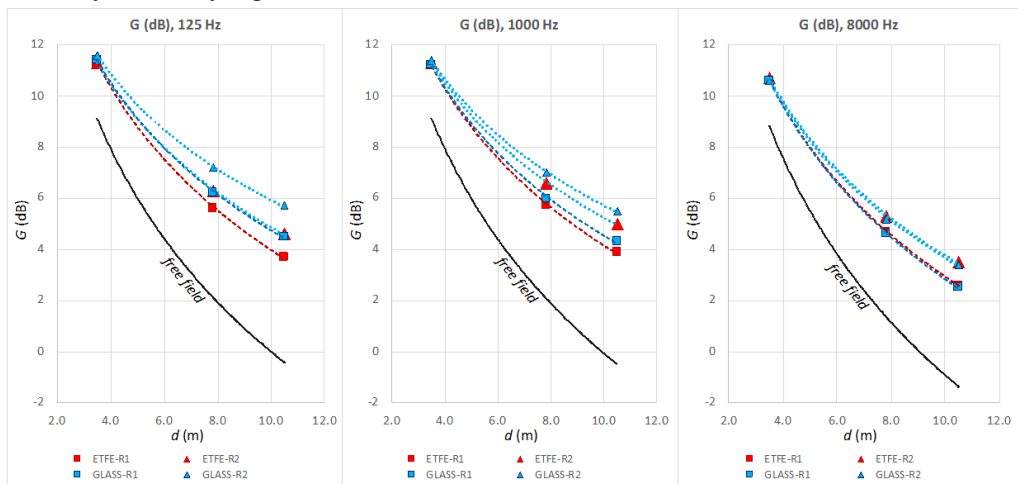


Figure 4: Spatial model of playground with two kinds of roof material

The second experiment was based on simulation of multiple sound sources under the four roof conditions. If we look at the results in so called audience place, we will see, that the differences are very small. This means that in case of the roof, placed very high above the ground, its influence will be low, and the type of material used for the roof will not influence the acoustic conditions much. Figure 5 shows the noise levels for roof shape 1 made out of ETFE (left) and glass (right) at 125 Hz. It is clear, that the roof material will influence the values of sound pressure level only little and only inside the playground and thus not significantly out of the covered part.

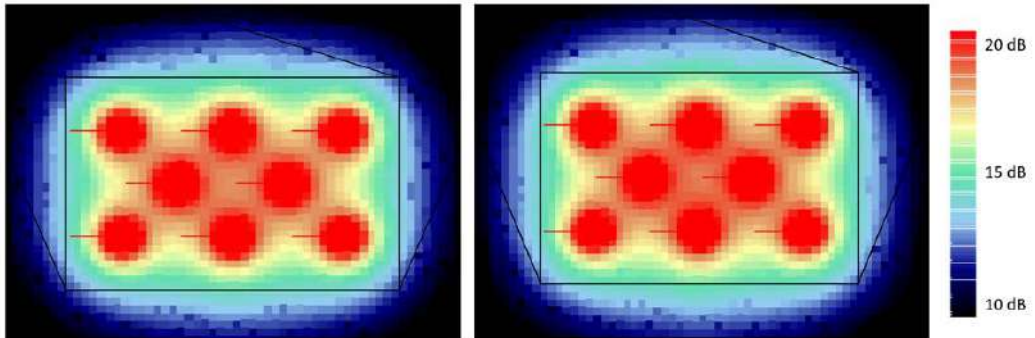


Figure 5: Sound strength G , as simulated from multiple sources equally distributed over the playground for roof shape 1, in height of 1.5 m (horizontal plane). Results at low frequencies (125 Hz) in case of ETFE (left) and glass roofing (right),

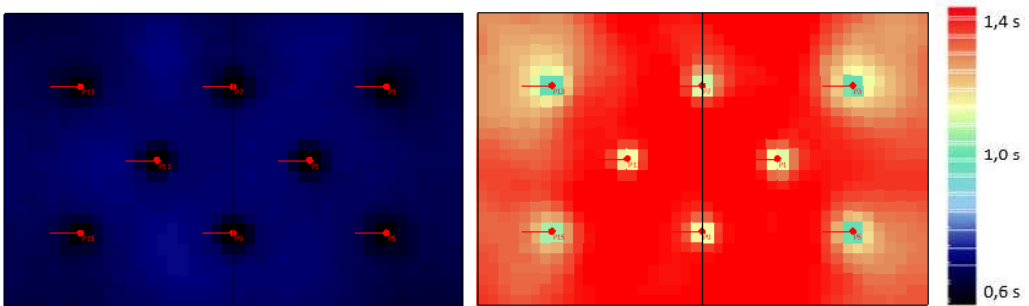


Figure 6: Reverberation time T_{30} (s) for cases with roof shape 2. Results at low frequencies (125 Hz) in case of ETFE (left) and glass roofing (right).

4. Conclusions

It can be concluded, that in architectural design and urban planning, choice of the shapes and materials should be influenced not only by aesthetic features. In prediction of a visual comfort, a lot can be resolved by proper visualisation of spaces. In terms of soundscape, acoustic prediction software is necessary and is a very useful tools important to understanding the overall comfort issues.

Based on the simulation results in the performed study we can conclude, that in semi-open spaces such as children playgrounds, the covering will influence noise situation mainly at low frequencies. However, once the shape of the roof is not flat, creating a certain “room effect” and annoying reverberation can cause acoustic discomfort, once the roof is based on hard material as glass. Here, the benefit of structural skins can be seen.

Results have thus confirmed that the overall sound pressure level in semi-open spaces will be most significantly influenced by direct sound and therefore only small differences were found between the two material cases with flat roof in terms of noise levels. However, the roof shape, if made out of hard materials, such as glass, can locally contribute to reverberation of sound and create less pleasant space.

References

- Christensen C. L. , Koutsouris, G. and Rindel, J. H. The ISO 3382 parameters. Can we measure them? Can we simulate them? *International Symposium on Room Acoustics*, Toronto, Canada. June 2013.
- Gundersen, V., Skår, M., O'Brien, L., Wold, L.C., Follo, G. (2016): Children and nearby nature: A nationwide parental survey from Norway, *Urban Forestry & Urban Greening* 17, 116-125.
- Kiyama, M., Sakagami, K., Tanigawa, M., & Morimoto, M. (1998) A basic study on acoustic properties of double-leaf membranes. In *Applied Acoustics*, 54(3), p. 239-254,
- Maywald, C., (2016) Sustainability-The Art of Modern Architecture, In: *Procedia Engineering* 155, p.238 – 248
- van Mechelen W., Twisk, J.W., Post, G.B., Snel, J., Kemper, H.C. Physical activity of young people: the Amsterdam Longitudinal Growth and Health Study. In: *Med Sci Sports Exerc.* 2000 Sep;32(9):1610-6.
- Polomová, B., Vargová A. (2016), Night Image of Tensile Facades, *Procedia Engineering* 155, 306-312
- Sakagami, K., Kiyama, M., Morimoto, M., & Takahashi, D. (1996) Sound absorption of a cavity-backed membrane: A step towards design method for membrane-type absorbers. In *Applied Acoustics*, 49(3), p. 237-247
- Shaw L.G. (1987) Designing Playgrounds for Able and Disabled Children. In: *Weinstein C.S., David T.G. (eds) Spaces for Children.* Springer, Boston, MA
- Urbán, D., Zelem, L., Maywald, C., Glorieux, C., Rychtáriková, M. (2017): Influence of transparent roofing systems on room acoustic properties of large atria, *Akustika* 29, Czech Republic, 93-98. ISSN 1801-9064.
- ISO 3382:2012 Acoustics -- Measurement of room acoustic parameters. ISO/TC 43/SC 2 Building acoustics. 2012

STN EN 1176 Playground equipment and surfacing - Part 1: General safety requirements and test methods. SUTN 2018

STN EN 1177 Impact attenuating playground surfacing - Methods of test for determination of impact attenuation. SUTN 2018

Proceedings of the TensiNet Symposium 2019

Softening the habitats / 3-5 June 2019, Politecnico di Milano, Milan, Italy

Alessandra Zanelli, Carol Monticelli, Marijke Mollaert, Bernd Stimpfle (Eds.)

Static assessment of selected transparent and translucent designs of roof over railway exposition

Eva VOJTEKOVA*, Matus TURIS^a, Michal VANEK^b, Olga IVANKOVA^a

* STU Bratislava, Faculty of Architecture, Institute of Structures in Architecture,
Nám. Slobody 19, 812 45 Bratislava, Slovakia.
vojtekova@fa.stuba.sk

^a STU Bratislava, Faculty of Civil Engineering, Dep. of Structural Mechanics

^b STU Bratislava, Faculty of Architecture, Institute of Structures in Architecture

Abstract

The area of the First steam railway station in Bratislava built in 1848, is situated on the territory of the monument restoration zone of the Slovak capitol Bratislava. This railway station functioned as the end terminal of the Hungarian Railway in 19th century. In 1871 the station was substituted by a new station building, which was built along the new passing railway track close to the original area. Nowadays the whole area of the First steam railway station became a monument registered in the Central List of the Monument Fund. Original objects built in 19th century along the rail tracks, which later served as warehouses, became in 1999 together with rail tracks a part of Museum of Transport. The rail tracks are used as an external exposition presenting locomotives, wagons and steam cranes.

Faculty of Architecture STU in Bratislava was addressed by contemporary management of the Museum of Transport to work up designs of the roof over the rail tracks protecting the exhibited showpieces. Because of the registration in the Central List of the Monument Fund, we approached to the task by working up several alternative designs (Figure 1). The roofs were designed with the use of various materials of support structures (timber, steel) and also different cover structures (glass, textile membrane and polycarbonate).

DOI: 10.30448/ts2019.3245.47

Copyright © 2019 by E. Vojtekova, M. Turis, M. Vanek, O. Ivankova. Published by Maggioli SpA with License Creative Commons CC BY-NC-ND 4.0 with permission.

Peer-review under responsibility of the TensiNet Association

Keywords: lightweight structure, transparent and translucent roof, glass, textile membrane, support structure, static analyses, railway exposition

1. Introduction

Museum of Transport in Bratislava is situated on the raised territory, bordered by Prazska Street and Square which creates traffic hub in front of the Main railway station. Three monument protected buildings, which served as warehouses, are used as museum exposition. In front of these buildings there are monument protected rail tracks serving for presentation of exhibited showpieces. The protection of the exhibited showpieces against unfavourable weather conditions was the reason for searching an appropriate shelter above the rail tracks. The architectural style of the former storages is typical for the operating factory objects from the period around the year 1900. Non-mortared brick architecture is combined with stone tectonic elements, which have aside from support also decorative function. Rougher pilasters bear the large roof. Infill walls as fulfilments between pilasters are perforated by wide doors to the particular arrays of the storages. The storage objects are covered by gable truss roof.

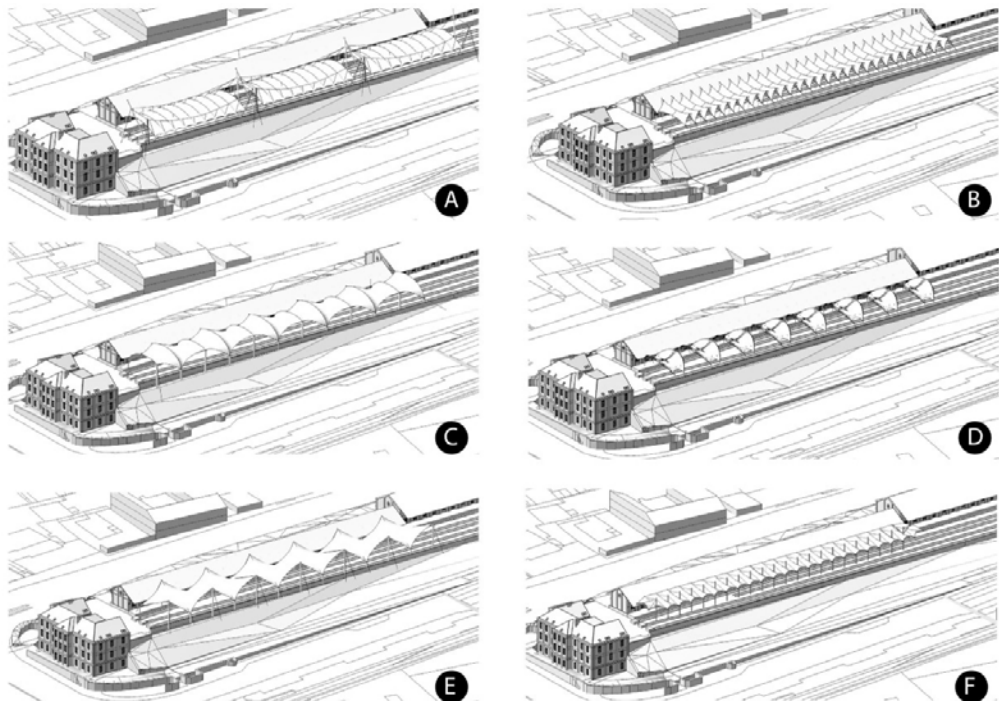


Figure 1: Alternatives of the architectural designs of the roof in textile membrane.

Beside an evaluation of the new added architectural layer to the protected monument area we considered a static analysis of the structure and its loads as important. The comparison of two architectural designs with the use of textile membrane roofs differentiated in shape and one

architectural design of the glazed roof was evoked of two possible ways of inserting new architectural object to the monument protected territory. The traditional approach is presented by design with application of traditional materials (timber) and traditional structures and shapes (gable roof) in maximal ratio. The method of contextual new added design is presented by application of new materials (PTFE membrane) and new structural elements and shapes (steel columns, arches), which have to be in harmony with monument protected surroundings.

Selected designs were modelled in computer RFEM static program and loaded by the most unfavourable combinations of the loads: dead load of bearing structures, permanent loads (cover structure), variable loads (wind, snow) according to the actual standards (Melcerova, O. 2014). The cross-sections of the separate structural elements were suggested and reviewed in both structural materials (timber, steel). The results obtained in static assessment would serve for the optimal design from the static point of view.

2. Alternatives of the architectural designs

The span of the projecting roof, the number of the rail trucks (changing from 5 to 2) and the rhythm of the industrial architecture in longitudinal direction were the main limits for the design of the new reversible roof. The shape of the projecting roof and its altitudinal position considering the height of the cornice gutter of the storage objects in cross section was important. The cornice gutter of the gable roof is by some designs in contact with the projecting roof above the rail tracks. The gable roof's shape of the origin objects didn't determine the design of the new roofs above the rail tracks. There is possible to consider the new style design of the roof as an element of new historical level. The composition of the new textile membrane roof with curvature shapes regarding the simple shape of existing gable roofs of the storage objects had to be taken in account. From the structural point of view the following types of the roofs were designed and calculated:

2.1. Timber truss frames in shape of the gable roof

Timber truss system in gable roof's shape made of timber laminated glued prisms laid on a pair of the columns (Figure 2, 3). Axial distance of the frame system's columns implied from their emplacement with regard to the position of the monument protected rail tracks and it is variable according the account of the tracks and their line. In modelled situation for the static design of the cross sections we thought over the axial distance about 4,5m. The axial distance of the trussed frames in longitudinal direction regarding the used material was designed 4,55m and corresponds with axial distance of the façade pilasters on the origin warehouses in longitudinal direction. The shape of the design comes out of origin non-existent timber shelter above the platform station from the year 1848-50. The design by shape, material and structure relates on the traditional architecture of warehouses and encourages the industrial expression

of the whole museum area. Based on static calculation the truss was designed of glued timber GL 20 with following dimensions: top and bottom chord 2*100/350mm, vertical and diagonal web members 100/200mm, load transfer from the roof will be secured via nuds to the structure. The columns are designed as 400/400mm in variant with use of glued timber profiles. To get the slender profile of the columns, we decided to use composite timber-steel profile with dimensions 250/250mm. In upper part of the frame the steel rod element $\text{Ø}57/10$ mm will be inserted for better static effect. The maximal deflection value is higher than 1/350 of the span regarding to the glazed roof. In the longitudinal direction the truss frames are stiffened by secondary aluminium steel grid created by cable trusses. The roof is created by glass laminated plates (4/PVB/6) fixed by spiders or in transom-mullion grid.

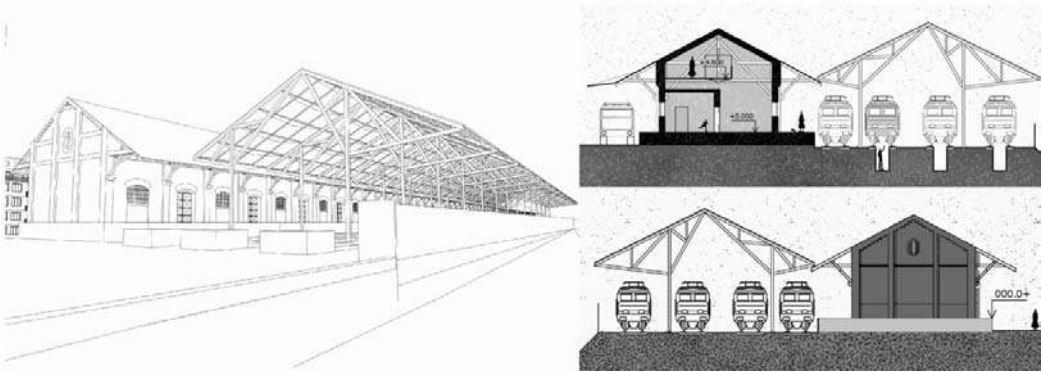


Figure 2: Glazed roof on timber truss frames - cross-section and elevation.



Figure 3: Glazed roof on timber truss frames - visualization.

2.2. Column structures with double-sided cantilevers in cross direction

Primary support structure is created by steel columns with circular cross-section in the shape of Y in the middle of the rail tracks (Figure 4, 5). Axial distance between columns in longitudinal direction corresponds with axial spans of the pilasters on historic façade. Design of this roof presents new element as a new contemporary layer to the industrial area and reacts with the shape of steel primary structure on the origin gable roof in reversed form. Wave-arched shape of the membrane presents possibilities of new contemporary material in lightweight roof structure (Sumeč, J. 2010).



Figure 4: Membrane roof on column structures with double-sided cantilevers - cross-section and elevation.



Figure 5: Membrane roof on column structures with double-sided cantilevers – visualization.

Bended steel profiles with circular cross-section create secondary support structure in longitudinal direction. The span of the structure is 16,8m and the height of the roof is 8,8m. Textile membrane PTFE with Teflon layer is used as material of the roof. Membrane is tensed by method of the edge tension and in cross direction fixed by edge clamping, and stiffened in longitudinal direction by arched steel profile (Kalesný F. 2011). Membrane precasts are connected by combined sewing-welding (Seidel M. 2008). Rain water is drained through inner columns. Based on static analysis the columns were designed with hollow circular cross-section $\text{Ø}660/14,2\text{mm}$, cantilever cross elements with hollow circular cross-section $\text{Ø}355,6/10\text{mm}$ and rods with hollow circular cross-section $\text{Ø}355,6/10\text{mm}$.

2.3. Combination of the steel frames in shape of the gable roof and arched frames

Steel frames in the shape of the gable roof and steel arched frames are alternately laid in longitudinal direction in axial distances corresponding in this case with axial double-spans (9100mm) of the pilasters on origin object. The frames with gable roof shape are used as reference on the origin roof's shape in new transformed material version. Alternately settled arched frames in doubled module distance provide dynamics to whole mass in longitudinal section. This design also presents new added design inserted contextually to the industrial area (Figure 6, 7).

Membrane is tensed by method of the edge tension and stiffened in longitudinal direction by steel cables. Membrane precasts are connected by combined sewing-welding. Primary structure is due to using doubled module distance light. The cross-section for the elements of the frames implied from the static analysis. Cross-sections of the columns and rafters of the steel frames in shape of the gable roof were designed with hollow circular dimension $\text{Ø}406,4/10\text{mm}$. The steel profiles for the arched frame are designed with hollow circular dimension $\text{Ø}273/4\text{mm}$.

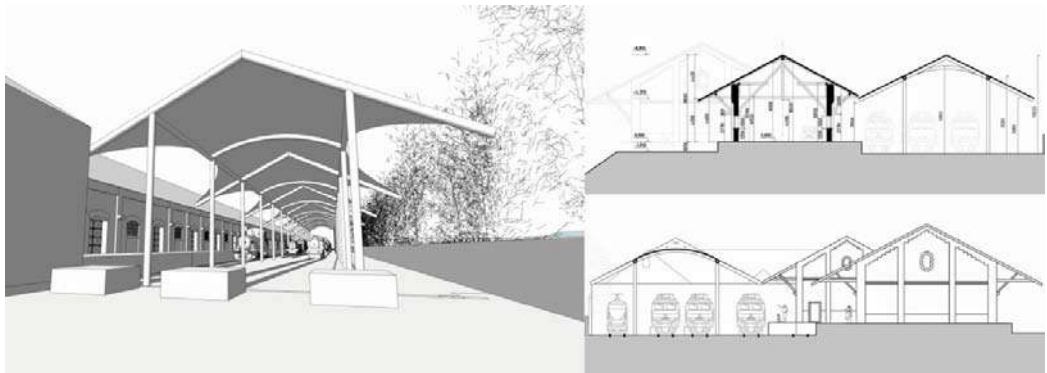


Figure 6: Membrane roof on combined gable roof frames and arched frames.



Figure 7: Membrane roof on combined gable roof frames and arched frames - visualization.

3. Results of the research

All three roof designs were modelled in static program SCIA Professional and loaded with the most unfavourable combinations loads: own weight of the support structures, permanent load from the roof, changeable load (wind, snow) according to the actual codes (EN 1990, EN 1991-1-3, EN 1991-1-4). For each model the profiles of particular support elements were calculated. In analysis due to the snow load the II. Snow territory for Slovakia was taken in account with characteristic value of the snow load $s_k = 1,05 \text{ kN m}^{-2}$ (annual maximum for 50-year period). The calculation of the wind excitation we came out from the II. Wind territory for Slovakia, where the fundamental basic wind velocity is $v = 26,0 \text{ m s}^{-1}$. Twelve loading states were calculated for generation of 72 the most unfavourable combinations of the load.

The support structure of all three models were assessed for the First limit state (the resistance of the designed profiles) and for the Second limit state (the applicability of the structural elements) comparing with limit values settled by code (EN 1993, EN 1995).

It is possible to compare models 2 and 3 from the point of expenditure and steel consumption. The weight of the steel support structure in model 2 is 103,2t and in model 3 is 33,8 t.

4. Conclusion

The designs of the new shelters above the railway trucks in monument protected area of the Museum of Transport in Bratislava were analysed from the point of the architectural approach and statics point of view. Compared models present differentiated design and use various materials for the support structure and for the roof. The choice of the material and the geometry of the roof have essential importance on the statics and the material expenditure. When finished, the research will served as decision making base for the Slovak Monument Board and Museum of Transport in Bratislava.

Acknowledgements

The article was processed as an output of the research tasks of the Grant Agency of the Slovak Ministry of Education – SK-VEGA 1/0951/16 and SK-VEGA 1/0412/18.

References

- EN 1990 Eurocode. Basis of structural design.
- EN 1991-1-3 Eurocode 1. Actions on structures. Part 1-3: General actions. Snow loads.
- EN 1991-1-4 Eurocode 1: Action on structures. Part 1-4: General actions - Wind actions.
- EN 1993 Eurocode 3: Design of steel structures.
- EN 1995 Eurocode 5: Design of timber structures.
- Kalesný F. (2011), Membrane structures: membrane envelope. In: *ALFA*. vol.16, (pp. 30-31).
- Melcerova, O. and Melcer, J. (2014), Impact of standards and regulations on design of sustainable communities. *Proc. Inter. Multidisciplinary Scientific GeoConf. Surveying Geology and Mining Ecology Manage.* SGEM, vol. 2, 549-55614th, Code 109829.
- Seidel M. (2008), Textile Hüllen, Bauen mit biegeweichen Tragelementen: Ernst&Sohn.
- Sumec, J., Jendželovský, N., Kormaníková, E. and Kotrasová, K. (2010), Architectural bionics in civil engineering - applications. In: *Media4u Magazine*, Vol.7, (pp. 122-131).

Proceedings of the TensiNet Symposium 2019

Softening the habitats / 3-5 June 2019, Politecnico di Milano, Milan, Italy

Alessandra Zanelli, Carol Monticelli, Marijke Mollaert, Bernd Stimpfle (Eds.)

Casa Corriere – RCS Media Group pavilion for Expo 2015

Paolo BECCARELLI*, Monica ARMANI^a, Roberto MAFFEI^b

*The University of Nottingham
University Park, Nottingham NG7 2RD, UK
paolo.beccarelli@nottingham.ac.uk

^a Monica Armani architects, via Falzolgher 29b, Trento, Italy

^b Maco Technology srl, Via U. La Malfa 86/88, Provaglio d'Isèo (BS), Italy

Abstract

In 2014 Rizzoli-Corriere della Sera Media Group S.p.A. decided to have a pavilion at the Milan Expo 2015 in order to promote the activity of the group in daily newspapers, magazines and books, radio broadcasting, new media and digital and satellite TV. This paper presents the design philosophy, the project development and the construction of the demountable pavilion designed by Monica Armani architects and based on a transparent volume made of XLAM columns and inflated PVC crystal cushions. The lightness of the inflated part contrasts with the weight and the mass of the vertical and horizontal wooden structure. The result is a sophisticated construction with a lightweight envelope which can be adapted to the weather conditions and solar radiation. The main structure of the pavilion, with a main ground floor and a small mezzanine, is based on an XLAM structure composed by a rigid basement, vertical rectangular columns with different orientations, a rigid central core and a flat roof with two large skylights. The series of rectangular two-layers air cushions used for the facades and the two skylights are connected to the glulam with keder rail profiles. The facade of the pavilion is the most characterizing element of the construction and is based on a two-layer system stabilized through the air pressure. This solution minimized the weight of the pavilion and provided adequate insulation of the internal spaces. The pavilion has been dismantled in November 2015 and it will be used in several temporary events planned in the next years.

Keywords: Expo 2015, Corriere della Sera, RCS, PVC-Cristal, ETFE, Pneumatic, facade, roof

DOI: 10.30448/ts2019.3245.24

Copyright © 2019 by R. Maffei, M. Armani, P. Beccarelli. Published by Maggioli SpA with License Creative Commons CC BY-NC-ND 4.0 with permission.

Peer-review under responsibility of the TensiNet Association

1. Introduction, Monica Armani Architects and Maco Technology

Monica Armani Architects is a design studio based in Trento, Italy. It is based on an interdisciplinary approach with a solid background on materials and construction. For Monica Armani Architects design means ideas, small and great inventions, endless care of every detail, synthesis between the observation of the evolution of behaviour and experiences. A very powerful tool, which can be applied to everything that man impends, a set of activities that increase the value of each work and make it at the same time sustainable and coherent. A design object is not just what you see, but all that it represents. The design approach of the studio reflects feelings and thoughts, the story of the team of architects involved and the deep connection with the territory in which the studio was established and operated: the northern alpine region of Italy, where tradition and innovation have found a sophisticated balance and design is the common thread.

The recent projects range between architecture, industrial design and teaching. The design studio focuses its attention on finding the harmony between form and timeless design, in a continuous process of research and innovation. The aim is to create a unique language that allows Monica Armani Architects to collaborate with different partners, all with a common denominator: great passion and ability to do things.

The design activity of the studio is based on a constant cross-over between research and innovation, this approach put Monica Armani Architects in a leading position in the current Italian and international panorama in the field of contemporary architecture and industrial design.

Casa Corriere for the Milan Expo 2015 (figure 1) is the first collaboration between Monica Armani Architects, the first step of a long-term collaboration which led to cutting edge projects such as the pneumatic structures developed for the Trento Economics Festival in 2016 and 2017. Founded in 2012, Maco Technology srl approached the market of membrane structures with a strong academic background of the co-founders with PhDs on pneumatic structures and the mechanical performances of architectural coated fabrics and foils. The focus of the company gradually moved towards the advanced design of complex lightweight structures and artistic installation. The holistic approach includes digital parametric tools for the 3D modelling of the components, FEM simulations, environmental analysis and optimisation of the storage and transportation volumes (Beccarelli et al., 2015). The file-to-factory approach allows the rapid and accurate manufacturing making possible challenging projects within a tight timeframe. Recent projects include collaborations with the main international architectural firms such as Diller Scofidio +Renfro (New York), MAD architect (Shanghai) and Foster + Partners (London).



Figure 1: View of the EXPO 2015 site in Milan

2. The design approach for Casa Corriere, the RCS pavilion for Expo 2015

In 2014 Rizzoli-Corriere della Sera Media Group S.p.A. decided to have a pavilion at the Milan Expo 2015 in order to promote the activity of the group in daily newspapers, magazines and books, radio broadcasting, new media and digital and satellite. Monica Armani Architects developed an innovative project based on a prefabricated timber construction able to be easily assembled and disassembled, in line with the principles of **TIMELY ARCHITECTURE** developed by Monica Armani Architects for the temporary structures.

The design approach is based on CAD-CAM technologies, which allowed to meet the demanding requests from the client delivering at the same time a customized pavilion structurally safe and easy to assemble. The connections allowed the disassembly of the pavilion at the end of the EXPO 2015 and the efficacious transportation and storage until the next use. Reduced installation costs, reusability, high standards and quality of the details are the main features of Casa Corriere, the pavilion designed and manufactured for RCS Media Group for Expo 2015 (Figures 2 and 3). The built project includes sophisticated connections and technical solutions with the integration of advanced manufacturing technologies and systems for environmental control.

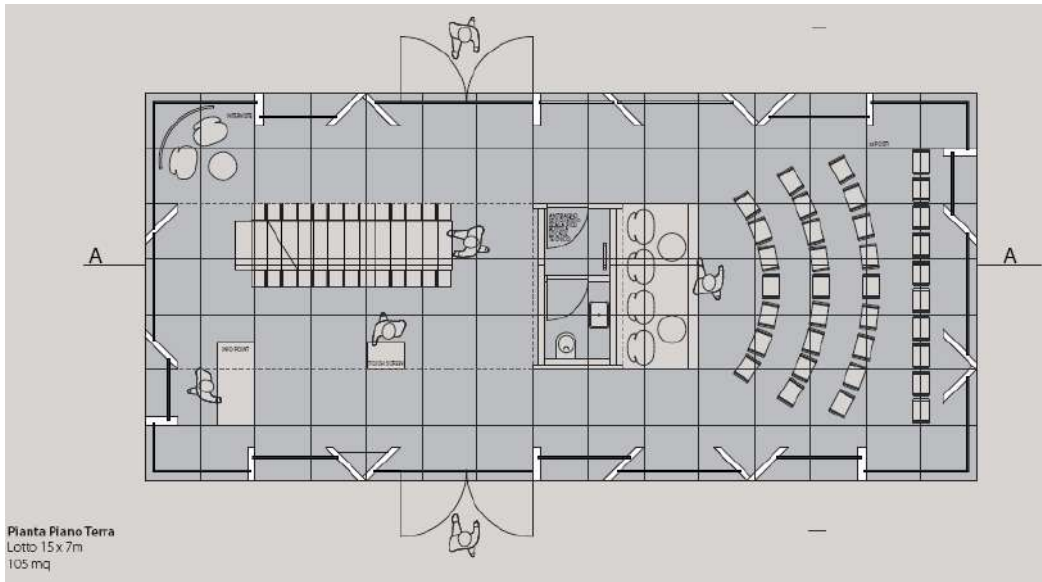


Figure 2: Plan view of the pavilion.

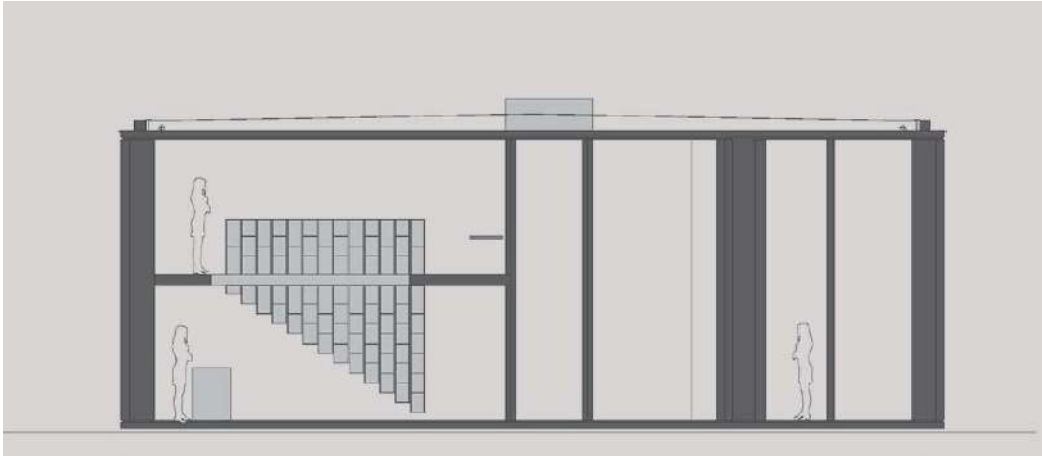


Figure 3: Section of the pavilion.

3. Timber structures

The main load-bearing structure of the RCS pavilion is based on a timber structure made of structural panels made of cross-laminated timber-XLAM arranged overall a regular grid of 140cm x 110cm to support the pavilion with a total dimension of 8m x 14m and an external high of 6m (figure 6).

The façade is strongly characterised by large timber columns 5120mm high with a cross-section of 100mm x 950mm. The 24 columns are arranged around the external perimeter of the pavilion inclined at 90 and 45 degrees providing at the same time support for the roof and a filter between the indoor and the external spaces of the pavilion. The columns are connected with bespoke connectors to the solid timber slab used for the ground floor and the timber beams used to support the roof and the inflated skylights.

The lateral stability is increased by the central core of the pavilion which is also made of cross-laminated timber. The central core is used to host the small toilet and the cabinet for the services of the building, including the pumps for the ETFE roof.



Figure 4: Assembly of the timber structure on site.

4. Inflated envelope

The original project included multilayer glass panels placed in between the timber columns arranged around the perimeter of the pavilion. Due to the short life span of the temporary pavilion, during the development of the project, it became obvious that a traditional glazed façade was not the right solutions for the RCS pavilion. Monica Armani Architects decided to investigate alternative solutions characterised by a similar thermal performance with a fraction of the embodied energy of a glass panel. An inflated membrane façade became the ideal solution able to provide the required structural and thermal performance with a limited

amount of embodied energy. The concept uses air under pressure to achieve the required load-bearing capacity. In addition, the pressurised air chamber considerably increases the insulating performance of a typical single layer membrane facade, which can progressively be improved with multiple layers. Compared with double- or triple-glazed façades, the thermal performance is considerably compromised by the dimensions of the air chambers, which allow a not-insignificant movement of the enclosed air with consequent energy losses due to convection. However, considered the short life span of the pavilion, the overall benefit of this solution was still positive compared with traditional glazed alternatives (Beccarelli, 2015).



Figure 5: Assembly of the PVC envelope on site.

Inflated envelope, based on two layers of clear PVC foils, has been designed to maintain a relatively small thickness of the envelope in order to avoid the waste of floor area. The shape of the cushions is a rectangle with a width variable between 1268mm and 2060mm and a maximum high of 5200mm. On the basis of the results of the structural simulation, due to the reduced mechanical performance of the clear PVC foil, the designer decided to integrate strips of coated fabric, 1300mm far from each other, to retain the external layers of the cushions and reduce the level of stress/elongation in the foil. The membrane envelope includes two large skylights 6318mm x 6488mm and 5720mm x 6488mm. They are based on a three layers cushion with the intermediate layer and the external layer printed with a positive/negative strip pattern. The manufacturing of the fabric panels was executed in safe and clean spaces by highly specialised workers and specific equipment such as computerised cutting tables and

high-frequency welding machines. The manufactured membrane has been easily packed, stored and shipped due to the reduced weight and volumes of the fabric once folded. Once on site, the assembly process was relatively fast and efficient due to the accuracy of manufacture, the aluminium boundary profiles and the reduced weights and volumes to be handled, which required less (and smaller) lifting equipment (figure 5). The result was an overall cost-effective product able to offer an alternative to the main traditional solutions and materials currently in use for transparent façades (Beccarelli and Chilton, 2013).



Figure 6: The external roll blinds (left) and the detail of the connection with the timber frame (right).

Picture by A. Liverani

5. Environmental performance and building services

If compared with a standard double-glazed window, the solution adopted was able to provide similar thermal performance with a total weight of 2kg per square meter compared with the 30 kg per square meter required by traditional double-glazed panels. In order to reduce the heat gains during the day and the warm season, the façade is protected by vertical blinds with an open mesh fabric Serge Ferrari SOLTIS86 ALU/WHITE 2051.

The two large skylights (figure 7) are based on a triple layer solution in order to provide an integrated control of the solar radiation based on a positive/negative pattern printed on the external and intermediate layer which can be overlapped by changing the air pressure in the inner chambers. The air in the cushions is continuously blown through two fans which keep the facade and the roofs at different pressure. Roof cushions are equipped with motor valves which deviate the flow of air in the two different chambers. Through this system, the light transmittance can be adjusted according to needs. At night the translucency of the pavilion is emphasized by LED lights which attract the interest of the visitors and transform the construction in an ideal venue for events.



Figure 7: Detail of the two large skylights with the printed pattern designed to control the daylight.

The pavilion is equipped with a Heating, Ventilation, and Air Conditioning – HVAC system which can operate in summer and in winter. The main unit is placed in the space of the central core of the pavilion. The ventilation conducts and the ventilation nozzles are integrated in the timber structure of the pavilion in order to minimize the aesthetic impact.

6. Conclusions

This paper described the design philosophy, the project development and the construction of the demountable pavilion designed by Monica Armani and Luca Dallabetta of Monica Armani architects and based on a transparent volume made of cross laminated timber columns and inflated PVC crystal cushions. The result is a sophisticated construction with a lightweight envelope which can be adapted to the weather conditions and the solar radiation. The pavilion has been dismantled in November 2015 at the end of the Expo and, thanks to the reduced weight and demountable concept, will be used to promote Rizzoli-Corriere della Sera Media Group S.p.A. in several temporary events planned in the next years.



Figure 8: Casa Corriere – RCS Media Group pavilion for Expo 2015

Acknowledgements

The authors would like to thank GIPLANET spa (general contractor), Monica Armani Architects (art direction, design, supervision of the manufacturing), F&M ingegneria (structural design, Health and Safety, coordination with EXPO 2015).

References

Beccarelli P., Maffei R., Galliot C. And Luchsinger R.H., (2015). A new generation of temporary pavilions based on Tensairity® girders, *Steel Construction*, 8(4), pp. 259-264

Beccarelli P. (2015). Biaxial Testing for Fabrics and Foils: Optimizing Devices and Procedures, Springer.

Beccarelli P. & Chilton J. (2013). Advantages of lightweight tensioned coated fabrics and foils façades for the building sector In: *Structural Membranes 2013 VI International Conference on Textile Composites and Inflatable Structures*, 9-11 October 2013, Munich, Germany.

Proceedings of the TensiNet Symposium 2019

Softening the habitats / 3-5 June 2019, Politecnico di Milano, Milan, Italy

Alessandra Zanelli, Carol Monticelli, Marijke Mollaert, Bernd Stimpfle (Eds.)

Textile architecture: "dressing the Aurelian walls"

Federica OTTONE*, Alessandra ZANELLI^a, Dajla RIERA^b

* School of Architecture and Design "Eduardo Vittoria", University of Camerino 63100 Ascoli Piceno (Italy),
mariafederica.ottone@unicam.it

^aPolitecnico di Milano, Architecture, Built Environment and Construction Engineering Dept., Milan (Italy),

^bUniversity of Camerino, School of Architecture and Design, Ascoli Piceno (Italy),

Abstract

Rome has been exponentially increasing its lands use till 2030, with a rate of 3sm/minute. In the near future developers and authorities will have to face not only the restorations of existing building stocks, but also the environmental and social sustainable regeneration of wider open-air zones and still empty urban spaces (Ottone, Cocci Grifoni, 2018; Gehle, 2017). The study focuses on a representative cultural heritage built system in Rome - the Aurelian walls - which is listed as outstanding part of a new green infrastructure by the city regulatory plan. This ancient wall-ring surrounding the historical centre of Rome has seen as a potential area where to apply novel strategies of urban regeneration, due to the presence of several neglected urban zones and uncomfortable public spaces. Taking inspiration from Christo and Jean-Claude's artistic avant-gardes interventions, the authors are envisioning the temporary application of lightweight composite meshes as a sun-shading protective path, able to interact with the thermal mass of the ancient walls, in order to increase the level of thermal comfort of the open-air urban spaces. The final goal is, on one hand, to simulate the performances of the developed textile shells' building system and to assessment its potential of heatwaves mitigation, and, on the other hand, to investigate the replicability rules of temporary textile-based architecture as a mean for re-activating - in a sustainable and reversible manner - the urban live and the care of ancient and delicate, cultural heritage contexts.

Keywords: outdoor comfort, fiber design, parametric design, composite meshes, urban heatwaves mitigation.

DOI: 10.30448/ts2019.3245.19

Copyright © 2019 by Federica Ottone, Alessandra Zanelli, Dajla Riera. Published by Maggioli SpA with License Creative Commons CC BY-NC-ND 4.0 with permission.

Peer-review under responsibility of the TensiNet Association

1. Introduction

Starting from the visionary experiences of technological and constructive avant-gardes and taking inspiration from Christo and Jean-Claude's specific artistic intervention, that covered 259 meters of urban walls with polypropylene and rope for 40 days, this essay investigates how to improve climatic conditions through the use of technological textile shells matched to the thermal mass of the walls. The study aims to verify - through a performative design process and comparative analysis of simulated constructive alternatives - the hypothesis that, thanks to the application of light and breathable materials connected to a massive long-line construction system as the Aurelian Walls in Rome, a comfortable open-air zone can be created, offering a new quality to the urban areas adjacent to ancient wall ring.

The material taken into consideration, a key factor and the power supply of new locations, is based on an innovative technology, composed of multi-axial natural fibers, with high solar reflectance and high thermal emissivity (Cocci Grifoni, Tascini, Cesario, 2017).

The thermal characteristics of textile depend on the fiber type and the density of the "weaving" technique, for instance the specific pattern created by the overlapping of several fibers before the finishing lamination process. Through a parametric design, it is possible to modify not only the aesthetic yield of the material but, after a survey of the stress agent on the surface, it is possible to make the texture itself structural, optimizing the use of the installation systems.

This fiber-designing methodology can shape a novel kind of soft, sinuous, light, non-invasive and reversible architecture. Through the Aurelian Walls' case study we are willing to validate this design methodology, which allows:

- the definition of innovative technological systems that use external thermal comfort as one of the main requirements to consider in the design phase.
- the integration of the parametric climatic simulations already carried out (Ottone-Cocci Grifoni, 2017) with further data deriving from the material and its structure.

The optimization of the life span of textiles materials in relation to the desired structural form and functional needs; the replicability of the technological solution to be applied in historical urban contexts.

The dissemination of these reproducible, temporary and transformable systems could contribute to the environmental regeneration of parts of untapped urban fabric, using the thermal mass already present and expanding its effectiveness as a climate mitigation mean.

2. The Aurelian walls: an urban resource

The Aurelian Walls were built in only 5 years in 270-275 a.C. by the Emperor Aureliano and elevated by Onorio start of 4th Century a.C. were developed for about 19 km. The Walls have been restructured and reinforced along the centuries, depending on the functional and military requirements, and saved almost the total integrity until the modern age.

The modifications realized on the original structure in course of the ages, such as the modernization of the original doors and the introduction of new passages, have been necessary for the development of the road networks. Only 13 km are currently left of the ancient walls: it is an open-air monument, at the same time an urban infrastructure symbol of the identity of Rome.

Though the Aurelian Walls are a unique patrimony of their kind, being an inestimable source of historical/cultural- and social value, continuous changes happened over the years, the rapid changes of the city, as well as several social and historical changes, made this monument loose identity and value. A program strategy for the realization of a linear park along its perimeter has been introduced the last **General town development plan**, with the aim of "recovering all the open spaces that can be redeveloped or restructured to enhance this exceptional building". (Municipality of Rome, PRG, 2008).

In particular, the case-study project of "**Dressing the Aurelian walls**" focuses on just a part of the Aurelian' Walls, exactly between Porta San Giovanni and Porta Maggiore, which identify the limit of the historical centre of Rome. This is a problematic area because of the concentration of car traffic and the lack of green areas able to regenerate air quality. Currently, a small linear garden runs along the stretch of walls without giving a significant contribution to this area's microclimate.

3. The problem of heatwaves mitigation in Rome

In just one year, the City of Rome has transformed 54 hectares of soil, the highest value in front of the Italian big cities - Turin 22 hectares, Bologna 17 hectares. In numbers, land use passed from 31.064 to 31.594 hectares (24,58 %) between the 2012 and the 2016. If this current trend continue, we can foresee up until 2030 an increase of 2.895 hectares , 161 hectares per year, it means 3 square meters per minute, so + 9,32% (source ISPRA).

One of the easily predictable effect of this soil loss is, for sure, the rise in temperature.

According to the report “Future heat-waves, drought and floods in 571 European cities”, drawn up by a team of the Newcastle University and the Willis Research Network (Guerreiro, Dawson, Kilsby, Lewis, Ford, 2018), which has analyzed the climate changes in European cities, noting an aggravation of the heatwaves in all of these 571 examined cities (Rome is in the high eight of this ranking).

The United Nations’ International Panel on Climate Change (IPCC) recognized the key role of the cities to deal with climate change, and it highlights «Micro-climates at urban/city scales and their associated risks for natural and human systems, within cities and in interaction with surrounding areas. For example, current projections do not integrate adaptation to projected warming by considering cooling that could be achieved through a combination of revised building codes, zoning and land use to build more reflective roofs and urban surfaces that reduce urban heat island effects (Hoegh-Guldberg, Jacob, Taylor, 2018).

Starting from these considerations, we can state that, in the near future, professionals, construction companies and city administrators will have to identify new possibilities of under-exploited urban spaces transformation, without further soil consumption, with the goal to turn them into new urban resources, improving climate, social and economical conditions.

We therefore imagine an architecture for the open space, which can modify the framework of the city, enhancing environmental quality and connecting with the city from a physical-perceptive point of view.

Furthermore, ephemeral installations can be seen as a valid alternative to create contemporary architecture within the city of Rome, due to the very restrictive limitation of the authority dedicated to the protection of historical and architectural heritage.

4. The need and the opportunity of temporary and soft architecture in cultural heritage contexts

“To design sustainable buildings means to get in touch directly with the weather and the core concept of place. This process seems a step towards the complexity of the nature rather than the man-made mechanicals. We need buildings with a high degree of empathy, a creative empathy” (Mario Cucinella, 2016).

Through the design of a big, ephemeral, light and soft architecture, we imagine a different use of an almost forgotten portion of the city, even if it is placed in the central urban fabric and near to the public transport infrastructures.

The design simulation process here presented has to be seen as a programmatic research exercise, which is motivated by the need to carry out a verification of the effects that the project can achieve on the microclimate, acting on a grand scale (almost hyperbolic), in order to stress the result and make it more meaningful.

The project idea starts from the utopian thoughts, looking on the one hand at Buckminster Fuller's utopias (Emili, 2003), like the geodesic climatic dome above the center of Manhattan in 1960, but on the other hand at the radical architecture of the 60s and 70s (Archigram, Superstudio, Cedric Price), that aimed at the creation of a functional urban superstructure for the city. These theories however were at the time impossible to carry out in the practice, due to technological lacks. «But we're at time when Bucky said that there would be ample resources to support all life at a higher standard of living than anyone has ever known. All we need to do is shift our focus and resources from weaponry to "livingry" as Bucky championed for most of his life» (Sieden, 2013).

Approaching Rome's specific case, the limitations for the protection of ancient monuments have generated, since the 1980s, a reflection on temporary and ephemeral architecture as an opportunity to intervene in historic cities with events capable of re-activating neglected sites that would suddenly come alive. The artwork "The Wall - Wrapped Roman Wall" (1974) by Christo and Jean-Claude, who wrapped part of the Aurelian wall with 259 meters of polypropylene fabric and ropes for 40 days, is the main example of the creative possibilities of this area. Other crucial references are the experimentations conducted by Renato Nicolini, Petroselli and Costantino Dardi's art exhibition "Transavanguardia, Mura Aureliane".

The goal is therefore to transform these conceptual and visionary experiences into a methodology of intervention within historical contexts, using the same communicative and symbolic force to obtain an environmental result that would transform some areas of the city, making them less exposed to the effects of climate change.

Through this study, we want to put forward the use of a light material, an innovative fabric, reusable and able to not only to regenerate an urban context left unused, in totally abandoned, but also to generate a system able to improve the urban comfort from several points of view, architectural, climatic / environmental and perceptual.

In addition to the survey methodology based on the CFD simulation system (Computational Fluid Dynamics), we thought it would be appropriate to stress dimensional data using the concept of paradox, to bring the project in an ideal scenario with extreme dimensions to obtain convincing and significative responses.

5. The concept of “dressing walls”: a weather-adaptive sun-shading path for the city of Rome

This project’s conceptual idea was developed during the teaching experience of the Environmental Design Laboratory at the University of Camerino, School of Architecture and Design. A long-line of wooden portals climb over the existing walls, without interfering with the ancient structures. The preliminary study of the shadows and the measurement of the thermal mass of the walls determined the distribution of the ribs according to a rhythm able to maintain a stable shade, with the aim of contributing to the summer cooling of the intervention area. The study was then extended with the definition of the material, a completely reversible structure.

The final aims of this conceptual design proposal of a novel wood and fabric-based promenade to the ancient walls of Rome, is the simulation of the comfort benefits, and the decrease of the urban heat island effect, by the integration of massive and light materials.

Eventually two technological options for the new shading portals are here simulated and comparatively investigated. In the first scenario, the portals are designed as opaque and rigid frames, while the latter scenario redefines the portal as an ultra-lightweight screen made of I-MESH, an innovative fabric composed of interwoven mineral fibers in a multiaxial mesh, supported by a wooden structure designed according to the Segal construction method (Fabris, 2002) and based on a modular wooden grid similar to the balloon frame. (*figure 1*).

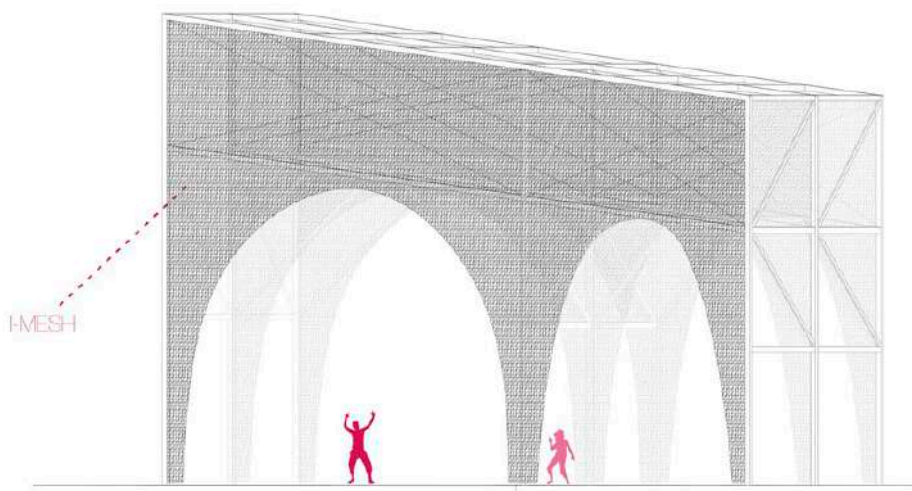


Figure 1: I-MESH with installation system_Axonometric

In both cases, the join between the structure and the ground is done through the support on plinths foundation, hidden inside a platform that divide the structure from the flooring that will host the installation. The installation is supposed to be modular and fully removable, without affecting the existing supporting surfaces.

5.1 The mesh fabric

I-MESH is an innovative fabric composed of mineral fibres coated with a polymer resin. The fibres may be fibreglass, carbon, basalt, technora, or zylon. The unique nature of the material makes I-MESH an exceptionally good outdoor performer. The energy studies conducted on I-MESH concern the effect of the material when it is used as a outdoor shading device.

The shape of I-MESH can be customized and parameterized; the characteristics of I-MESH obviously depend on the different fibres used. In this case, the fibreglass fibre was chosen for the research. (*figure 2*)

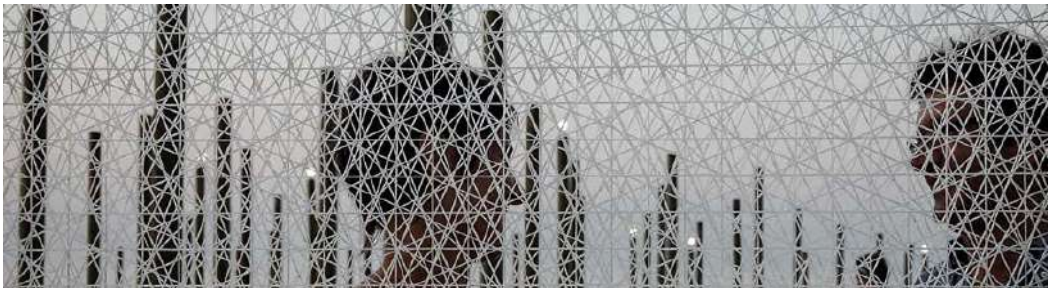


Figure 2: I-MESH fiberglass weaving with 60% opening. The extreme characterization of the material

The main physical characteristics of the fibreglass I-MESH are the following (Cocci Grifoni, Ottone, Cesario, Marchesani, 2017):

- thickness 2.5 mm;
- reflectance 0.60;
- emissivity 0.9;
- thermal conductivity 0.18 W/m*K at 20°C;
- heat capacity at constant pressure 1200 J/Kg*K at 20°C;

- specific heats $1200/1175 = 1.02$.

The pattern of the material is engineered to give the fabric an adequate stiffness, in according to a parametric design methodology, developed by the company in collaboration with the Politecnico di Milano.

The rovings that composes the material is placed freely in 2D space to create a soft mesh where both structure and decorative motives are blended. The positioning and composition of the rovings are custom. The fiber layout can be designed to absorb and distribute the loads generated by the weight of the material and wind load, in relation to the specific constraints dictated by the construction technology adopted.

5.2 The urban-scale simulation: objectives

To monitor the interaction of human-environmental phenomena, preliminary multi-level analysis were made. Each of them produced multiple information, deriving from the different sources, measured with the help of the current urban monitoring devices (mobility, climate, etc.) and, in some cases, with empirical measurements carried out on the site. To conduct the comfort estimation, a CFD (envimet) tool has been used. Such tool is able to work on an urban scale returning a map where is possible to read the values of PMV (Predicted Mean Vote), defined by the classic chromatic scale, that indicates wealth as much as they tend to zero.

First of all, the calculation was made on a larger scale considering the geometries of the actual state (*figure 3*). A subsequent enlargement of the same area, allows a better evaluation of the effects that the design project produces on the urban system of the Aurelian Walls.

The simulation has been carried on in two-steps:

- analysis of the project “Urban Portal” (figures 4.a and 4.b), that uses opaque and rigid material. The material utilized, although shading, did not offer acceptable results from the PMV’s point of view, as it was designed as impermeable full screens.
- analysis of the project, that has the same spatial composition and morphology of “*Urban Portal*”, by replacing the opaque and rigid material with I-MESH.

This investigation was simulated on August 19th. This day is considered as representative day in comparison to temperature data in the summer period (Ottone, Cocci Grifoni, 2017). The pictures show the comfort scenery at 12 o’clock, obtained by cutting the geometries at eye level,

with an air temperature of 30° and a humidity of 45%. The mean radiant temperature and the wind speeds data are obtained thanks to the software.

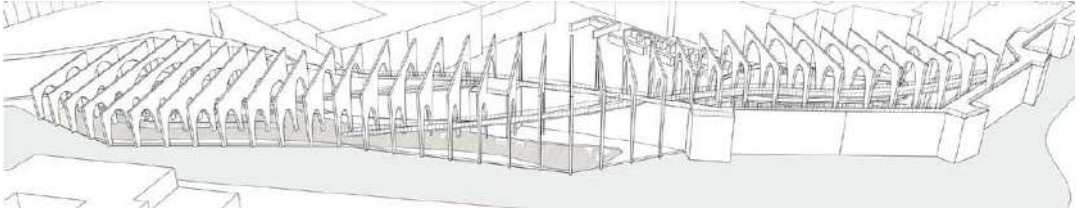


Figure 4.a: “Urban Portal” (S. Castellani e C. Vagnozzi Environmental Design Laboratory at the University of Camerino, School of Architecture and Design,, Prof. Federica Ottone)

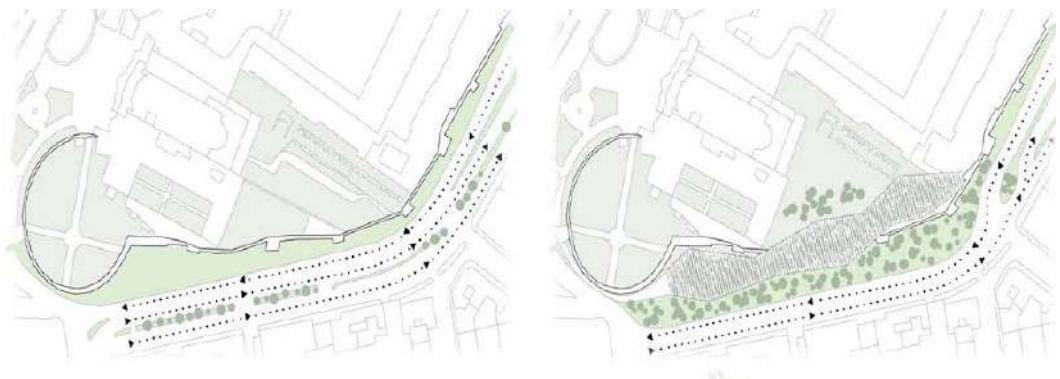


Figure 4b: plan before and after the integration of the new “urban portal” lightweight system

5.3 Results

Considering the existent scenario before the project (fig. 5) and then comparing the two alternative materials applied to the project proposal (fig. 6 and fig.7), it can be argued that the non-conventional use of vertical textile screen, instead a normal horizontally oriented shading system, may create a valid shading and filtering system, better allowing the circulation of air flows, avoiding overheated zones and creating a qualitative effect of textile promenade beside the ancient massive walls.

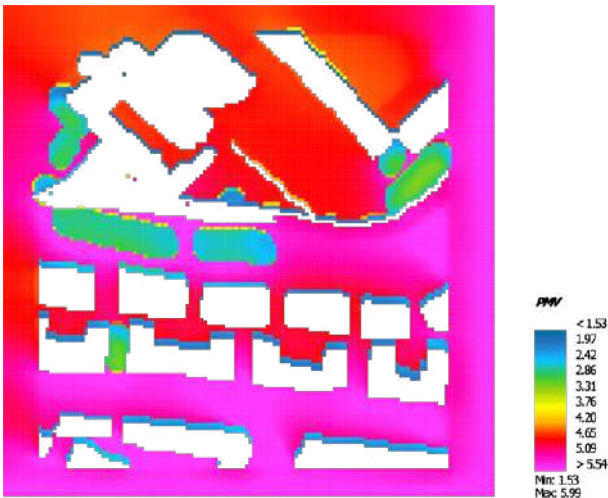


Figure 5: PMV before the project

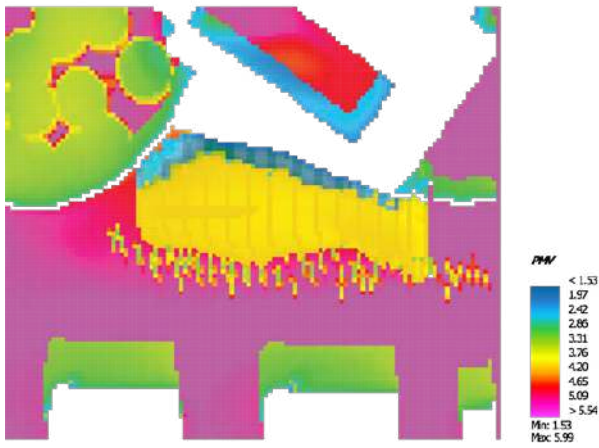


Figure 6: PMV with portals made of opaque material

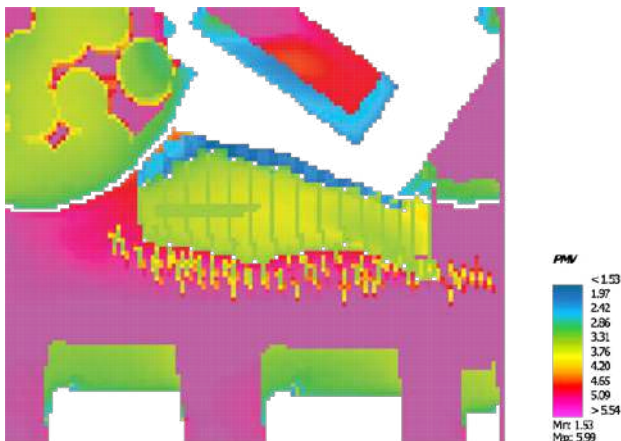


Figure 7: PMV with portals made of I-MESH composite fabrics

In particular, the characteristic of I-MESH may mean that even in a situation like the one designed, with big light portal, the installation system can become stable without the need for additional substructures, thanks to the composite nature of the material. Furthermore, it is well-known that the application of meshes in outdoor structures may improve the thermo-hygrometric comfort of a covered area. The innovative application of the I-MESH product in a large-span vertical panel opens a new way of designing shading systems, allowing the perceptive comfort of the fully open-air environment, compared to other traditional solutions. This is also possible due to the high strength performances of the I-MESH composite fabric.

Moreover, the developed portals long-line integrated to the urban existing building are thought as a easily transformable, transportable ultra-lightweight structure; the mesh material has the qualities of transparency and lightness which allow to minimize the visual impact of the new structure, integrating it with the historical presence.

4. Conclusion

This experimentation wants to be an occasion to investigate on innovative practices of intervention on important historical urban contexts, preserving their memory, and applying on them reversible, lightweight artifacts able to generate places dedicated to the development of a new urban sociality.

At the same time, we are convinced that this opportunity gives the chance to restore, through temporary installations, a fruitful relationship between history and contemporaneity, giving continuity of life and meaning to the presences and triggering new scenarios of urban regeneration, through the reconfiguration of open spaces, increasingly protagonists of historic cities.

References

ISPRA (2017), "Consumo di suolo, dinamiche territoriali e servizi ecosistemici - Edizione 2017. Rapporti 266/2017.

Guerreiro S.B., Dawson R.J., Kilsby C. , Lewis E. , Ford A. , (eds.) (2018) "Future heat-waves, droughts and floods in 571 European cities", *Environmental Research Letters*.

Cucinella M. , (eds.) (2016) "Creative Empathy", Skira Editore.

Emili, A.R. (2003), "Richard Buckminster Fuller e le neoavanguardie", Roma, Editore Kappa.

Sieden, S. (2013) Buckminster Fuller: “A Verb Who Supported All Life on Spaceship Earth” (https://www.huffpost.com/entry/buckminster-fuller-a-verb_b_2764737)

Comune di Roma, PRG, Ambito di programmazione strategica Mura – Obiettivi - (http://www.urbanistica.comune.roma.it/images/uo_urban/prg_adottato/i6_02.pdf).

Baal-Teshuva J., (eds.) (2016) Christo & Jeanne-Claude. Köln, Taschen.

Fava F., (eds.) (2017) “Estate romana. Tempi e pratiche della città effimera”, Quodlibet.

Oke, T. R. (1982). "The energetic basis of the urban heat island". Quarterly Journal of the Royal Meteorological Society. 108 (455): 1–24.

Gehl, J., (eds.) (2017) “Città per le persone”, Maggioli Editore.

Scuderi, M., (eds.) (2014). Philippe Rahm architectes. Atmosfere costruite, Postmedia Books.

Cocci Grifoni R., Tascini S., Cesario E., Marchesani G. E., “Cool façade optimization: a new parametric methodology for the urban heat island phenomenon (UHI)”, 2017 IEEE International Conference on Environment and Electrical Engineering and 2017 IEEE Industrial and Commercial Power Systems Europe (EEEIC / I&CPS Europe).

Ottone M.F., Cocci Grifoni R., (eds.) (2017) “Tecnologie Urbane. Costruito e non costruito per la configurazione degli spazi aperti”, List.

Monticelli C., Zanelli A. (2016), "Life Cycle Design and Efficiency Principles for Membrane Architecture: Towards a New Set of Eco-design Strategies", *Procedia Engineering*, Vol. 155, DOI: 10.1016/j.proeng.2016.08.045, pp.416-425.

Barozzi M.; Liehnard J.; Zanelli A.; Monticelli C. (2016), “The Sustainability of Adaptive Envelopes: Developments of Kinetic Architecture”, *Procedia Engineering*, Vol. 155, DOI:10.1016/j.proeng.2016.08.029, p. 275-284.

Butera, F.; Aste, N.; Adhikari, R.S.; Del Pero, C.; Leonforte, F; Zanelli, A. (2017), “Wet Curtain Wall: A Novel Passive Radiant System for Hot and Dry Climates”, *Energy Procedia*, Vol. 105, May, DOI: 10.1016/j.egypro.2017.03.424, p. 953-960.

Proceedings of the TensiNet Symposium 2019

Softening the habitats / 3-5 June 2019, Politecnico di Milano, Milan, Italy
Alessandra Zanelli, Carol Monticelli, Marijke Mollaert, Bernd Stimpfle (Eds.)

Application of Atrium Tensile Structure in Historic Building. Case study: Daylight Modeling of Atrium within Historic Building.

Beata POLOMOVÁ*, Peter HANULIAK^a, Andrea VARGOVÁ^a

* Institute of History and Theory of Architecture and Monument Restoration, Slovak University of Technology in Bratislava, Faculty of Architecture, nám.Slobody 19, 812 45 Bratislava, Slovakia
beata.polomova@stuba.sk

^a Slovak University of Technology in Bratislava, Department of Building Structures. nám.Slobody 19, 812 45 Bratislava, Slovakia

Abstract

The specific area of application of tensile roof structure is their use in the historical environment. They do not have the character of historical constructions considered as elements of long life spans such as masonry, wood, steel (especially in the 20th century). In general, the tensile structures represent desirable structural elements in contemporary architecture. They are suitable in the historical environment due to low bulk density (lightweight skins), and reversibility to monument structures. On the other hand, their optical properties of translucency and transparency is the reason for studying the effects in daylight exposure as well as the effects of night image. In this paper, the daylighting simulation for the selected atrium tensile roof structure is added and its effect on daylighting distribution of the historic building's rooms is evaluated. These are daylighting outputs that can help or to lead to choose a preferred type of tensile roof structure already during preliminary design phase.

Keywords: daylight modeling, atrium, tensile roof structure, refurbishment of historic buildings

DOI: 10.30448/ts2019.3245.26

Copyright © 2019 by b. Polomová, P. Hanuliak, A. Vargová. Published by Maggioli SpA with License Creative Commons CC BY-NC-ND 4.0 with permission.

Peer-review under responsibility of the TensiNet Association

1. Introduction

Many historical buildings have a new function in adapting their atriums. They transform the exterior space into the interior. New social functions for a short stay are integrated here. In this context, it is necessary to consider in advance the real impact of the new atmosphere of the future interior and the demands on technical solutions (roof drainage system, air flow, acoustics, lighting, etc.). In our contribution, we focus on the material selection effect in terms of optical properties on daylighting in the renewed atrium of a historic building, since the daylight is still considered as the healthiest form of lighting. [6] The impulse for our experimental exploration was the previous design project of atrium roof using a glazed structure (Fig. 1a-b - current state of 3D model, 1c - conventional design of glass roof in atrium). However, in variants of calculation on illuminance a glazed structure was replaced by tensile roof construction. It is a framework findings demonstrated by calculation that would be important in the initial design phase of the atrium. The following question arises: What are the impacts of tensile roof structures on the daylighting in atrium space of building, as a second variant, compared to the glazed roofing? For this reason, a model simplification was chosen for daylight modeling.

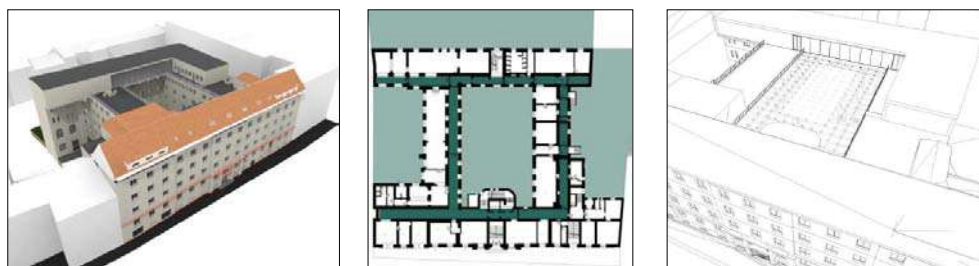


Fig. 1a-b (current state of 3D model), 1c (conventional design of glass roof in atrium)

Method for the theoretical experiment: To calculate the daylight distribution of the ground floor area and in adjacent rooms and the amount of light and its uniformity on the façade, we neglect the load bearing and supporting construction, so theoretically we consider a flat element in which two parameters are changed: the specific transparency and the particular surface area in the given shape when making a combination of two materials. By combinations of these parameters, we obtained 10 variants. Subsequently we could choose the most optimal design for different purposes.

2. Selected example of atrium at Faculty of Education Comenius University in Bratislava, Office building in Šoltéssova street.

The studied building was built in 1923 as a Young Women's Christian Association (YWCA). It had been rebuilt several times, and finally adapted to school. It still preserves its architectural cultural and historical values, especially in the street tract. It is a larger 4-storey building, has 4

wings. There are three atria located between 4 wings of building's floor plan. The new renovation of faculty will convert attic into new spaces of building and utilization of space in faculty environments (offices) will become more efficient throughout the building. We are interested in the central atrium, where a new small campus, connected to the social spaces and the school buffet will be. It is a simple shaped atrium with volume of 6960 m^3 ($25.8 \times 16.85 \times 16.0\text{m}$ of height). Only the space of staircase enters the area of the atrium. The classrooms are situated behind the fourth facade, which presents the southern facade. There are the large classroom windows in the southern façade in accordance with daylight requirements for school classes. Above this atrium space a new tensile roof structure is considered. Here, it is important to take into account daylighting (falling light on(to) the ground, into the interior – classroom and the third on the façade of the atrium). In relation to the requirements for daylight, the height of the atrium and the function of the surrounding interiors were not considered. The need of shading devices will be solved locally, depending on the requirements of individual rooms.

3. Transparency and tensile structure materials

Light transmission in membranes as an important aspect ranges from zero to 95% transparency. The control and use of daylight in the inside environment is improving, and that not only reduces the cost of artificial lighting but also improves the interior quality of the space. [2]. In the case of films or foils, the translucency as a property is the result of the very essence of this material. Consequently, these materials represent higher transparent values reaching up to 95%. [3]

Transparency of roofing material: Within fabric solutions, PVC polyester and PTFE glass fibres present blackout capabilities, the first material starts with a value around 0 and reaches up to 25% translucency, and the next material with values ranging from 4 to 22%. Silicone glass fibres presents transparency values of 10 to 20% (Pudenz, 2004). Consequently, the entrance of diffused daylight, and the regulation of the amount of daylight entering the building is allowed. [4]

For the calculation, we applied the available real transparency coefficients for the textile and foil products used for such constructions. There were two groups of variants. First one consists of homogenous material with transparency ranging from 95% to 30%. The second group consist of a combination of two materials that have different transparency 30%, 50% and 95% where the whole roofing is divided into central part with one type of material and perimeter part of a different type. The area ratio between those two parts was set to 50:50. The material composition of tensile roof structure is irrelevant for our preliminary model study. Although in real life we can count with a more diffuse behaviour of this material.

4. Results of calculation

The WDSL software (Building design package by Astra 92) was used for daylighting calculations. We used standardized uniform CIE overcast sky (the changes of luminance from horizon to zenith in ratio 1:3) that resulted into daylight factor (DF[%]) distribution outputs: minimal, maximal and average values in combination with its uniformity across the evaluated areas of the atrium’s inner surfaces. This is helpful since most climates across Europe have substantial periods of overcast skies and DF is therefore a useful metric to inform design decisions. However, for the climates with a greater portion of sunny days, a more sophisticated dynamic, year-round simulation would give us more precise outputs. We are planning to do so in a next step as an advance in our initial research.

4.1 Calculation focusing on illuminance of atrium ground floor area.

In this case, it is the amount of daylight that would fall on the working plane sufficient and allow various functions including visual tasks (reading – writing). Such conditions in accordance with STN requirements can be found across the whole area, even using the worst material combination variant in this case (central (c) 95% /perimeter (p) 30%).

From the point of view of the combination of materials, the most appropriate solution is one that prefers a higher transparency on the perimeter of the tensile fabric structure thanks to the effect of interreflections of adjacent walls of the atrium. This solution (50/95 and 30/95) is also satisfactory if shading devices are placed in the centre of the tensile fabric structure to reduce thermal gains and increase the luminous comfort resulting from glare suppression.

Calculation 4.1	min.DF	max.DF	average DF	uniformity
	[%]	[%]	[%]	[-]
variant 1 - no foil				
variant 2 - homogenous foil 95%	8.5	42.5	34	0.2
variant 3 - homogenous foil -80%	7.2	35.8	28.7	0.2
variant 4 - homogenous foil -70%	6.4	32.1	25.7	0.2
variant 5 - homogenous foil -50%	4.6	22.9	18.3	0.2
variant 6 - homogenous foil -30%	2.7	13.7	11	0.2
variant 7 - combination center 95%, perimeter 50%	4.7	30.3	23.1	0.15
variant 8 - combination center 95%, perimeter 30%	3	24.9	18.2	0.12
variant 9 - combination center 50%, perimeter 95%	8.3	34.5	28.8	0.24
variant 10 - combination center 30%, perimeter 95%	8.2	31	26.5	0.26

Tab.1: Calculation of illumination on the atrium ground floor area, comparative plane height of 0.85 m

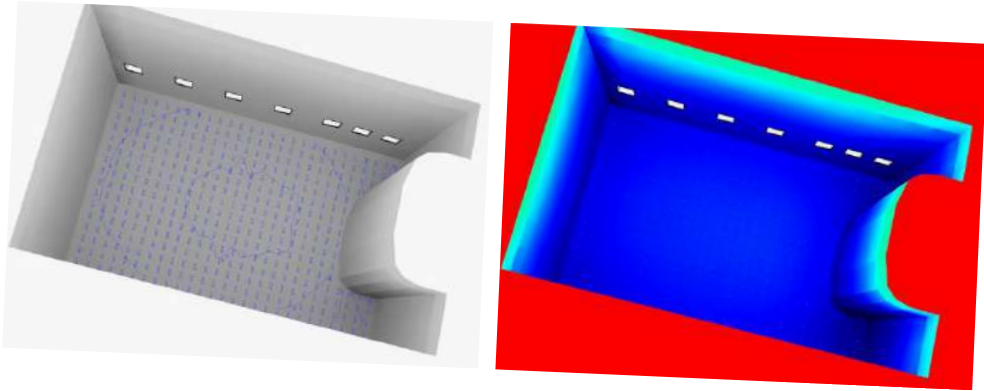


Figure 2: Typical light distribution on the atrium ground floor area at 50/95 combination, illumination (left) - false color (right).

4.2 Calculation focusing on illuminance of classroom interior.

The subject of the calculation was light distribution on the working plane in the room as a result of material selection of the tensile atrium structure. In terms of classroom design in the building space, we are limited by dimensions of the room and size of the window. This room, even without any roofing structure, does not provide enough daylighting to meet the standard for newly built classrooms, which is typical scenario by historic buildings. Therefore, we used the evaluation based on requirements for a combined lighting – daylighting and artificial lighting, with lower requirements for daylight levels. The results of the calculations show that using the composite materials combination, the best values of daylighting can be obtained with the variant 50/95 (floor ratio with sufficient daylighting is 45.85%). Therefore, designs which prefer higher transparency on the perimeter of the tensile fabric structure, are preferred for interior daylighting in this type of building geometry.

floor	Calculation 4.2	min.DF	max.DF	average DF	uniformity	area DL	floor ratio	area IL	floor ratio
		[%]	[%]	[%]	[-]	[m2]	[%]	[m2]	[%]
5th.	variant 1 - no foil	0.2	8.1	1.1	0.025	3.63	16.43278	12.81	57.99004
	variant 2 - homogenous foil 95%	0.2	7.7	1	0.025	3.47	15.71	12.35	55.90765
	variant 3 - homogenous foil -80%	0.2	6.5	0.9	0.025	2.95	13.35	9.46	42.82481
	variant 4 - homogenous foil -70%	0.1	5.7	0.8	0.025	2.55	11.54	8.48	38.38841
	variant 5 - homogenous foil -50%	0.1	4.1	0.5	0.025	1.7	7.70	5.37	24.30964
	variant 6 - homogenous foil -30%	0.1	2.4	0.3	0.025	0.8	3.62	3.31	14.98416
	variant 7 - combination center 95%, perimeter 50%	0.1	4.7	0.7	0.025	2.12	9.60	6.73	30.46627
	variant 8 - combination center 95%, perimeter 30%	0.1	3.4	0.5	0.025	1.44	6.52	5.12	23.17791
	variant 9 - combination center 50%, perimeter 95%	0.2	7.1	0.9	0.024	3.11	14.08	10.13	45.85785
	variant 10 - combination center 30%, perimeter 95%	0.2	6.8	0.9	0.024	2.95	13.35	9.06	41.01403

Tab. 2: Calculation of illuminance in the classroom on working plane at height of 0.85 m

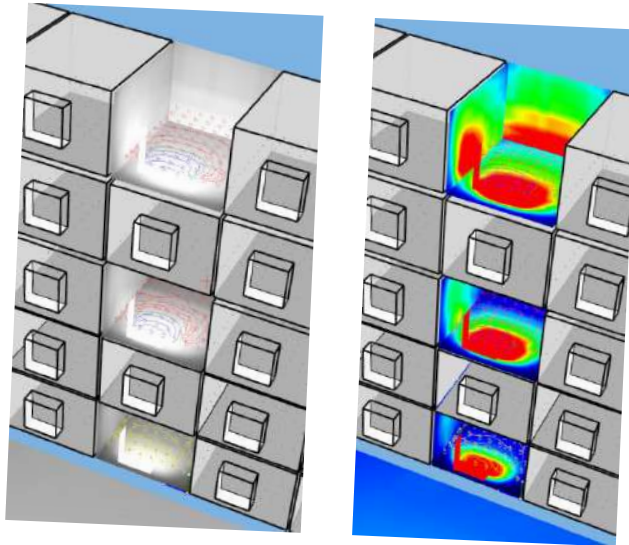


Fig.3: Daylight distribution in the room – illumination (left) , false color (right)

4.3 Calculation focusing on translucency of the facade of atrium.

Concerning uniformity of the facade illuminance by natural daylight and its aesthetic appearance, it is preferable when the uniformity, a dispersion of values of the illumination on the facade surface, reaches the highest values. In the visual image of the facade area, it means a quality of the uniformity and an exclusion of contrasting places. In our case of the atrium, different variants of the transparency of film/ foil materials V1 to V10 have been applied.

The results show that the greatest influence on uniformity (although the differences between variants seems to be small) of the facade illuminance has a combination of different film or foil materials (see Table 3). The most preferred variant (0.25) for wall luminance is a combination of materials (c95/p50), it means, the middle part offers a higher light flux towards remote parts of the facade.

Výpočet 4.3	min.DF	max.DF	avg.DF	uniformity
	[%]	[%]	[%]	[-]
variant 1 - no foil	9.9	45.3	27.9	0.22
variant 2 - homogenous foil 95%	9.4	43.1	26.6	0.22
variant 3 - homogenous foil -80%	7.9	22.4	36.3	0.22
variant 4 - homogenous foil -70%	6.9	31.8	19.6	0.22
variant 5 - homogenous foil -50%	4.9	22.7	14	0.22
variant 6 - homogenous foil -30%	3	13.6	8.4	0.22
variant 7 - combination center 95%, perimeter 50%	6.2	25.1	16.9	0.25
variant 8 - combination center 95%, perimeter 30%	4.8	19.9	12.6	0.24
variant 9 - combination center 50%, perimeter 95%	8.2	42.6	23.8	0.19
variant 10 - combination center 30%, perimeter 95%	7.6	42.4	22.5	0.18

Table 3: Calculation of illuminance and uniformity of the façade in atrium.

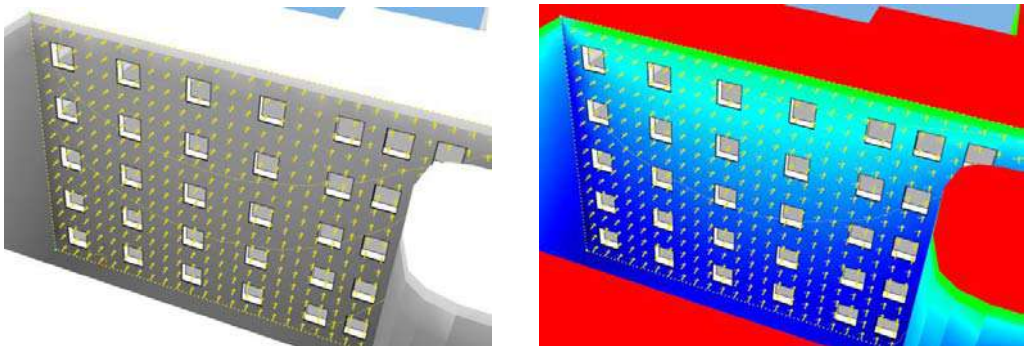


Figure 4: Light distribution on the façade in the atrium - distribution of control points. Display of illumination (left) a false color display (right)

5. Conclusion

In terms of lighting function over work surfaces, taking into account the performance of the visual tasks, the best possible options concerning material combinations are as follows: In the centre of atrium area, the material with a lower transparency is used and the most transparent on perimeter of the area.

The primary objective is to illuminate the atrium area, the secondary objective is the impact on the illuminance of the interiors (corridors, space to work or study space). In this case study, the influence of the percentage of transparency on atrium façade is only tertiary. Aesthetic inequality is not essential here.

This reduced verification procedure serves as an example that assists the author in deciding on the preference of the amount of incident light. There is a need to achieve a greater amount of incident light either on the floor area of atrium and in the space to work, eventually in the study space, behind the atrium facade (on a horizontal plane) or on the atrium facade in front of common areas (on a vertical plane with windows of different cardinal points).

We showed, that not only the parameter of transparency of a single material, but also a combination of two different materials in the roofing area of atrium can bring us different results. Therefore, a preliminary design verification is necessary. This is an example of the interdisciplinary cooperation which is needed to design the architectural project in renovation of the building. In the presented verification method, the tensile roof structure was converted into a plane and two parameters (area size and transparency in %) were considered. The simplification is both, sufficient and relevant to the expected results in architectural designing.

4. Acknowledgements

We thank for the provided graphic material about the building from the source: Šimončíčová, L. Tokovicsová, A. (2016), Design of the Faculty of Pedagogy in Bratislava, Seminar of design studio II, 2016-17, FA STU in Bratislava. This contribution was supported by VEGA no. 1/0286/15 and H2020-MSCA-RISE-2015 No. 690970 “papabuild”.

5. References

- [1] Kalesný, F., Vojteková, E. (2017), Reversible roof structures on architectural objects in specific conditions. In: *Architecture in Perspective 2017*, Vysoká škola báňská, Technická univerzita Ostrava, pp. 256-263. ISBN 978-80-248-4058-1.
- [2] Huntington, C.G., (2013). *Tensile Fabric Structures: Design, Analysis, and Construction*. American Society of Civil Engineers, Reston, Virginia.
- [3] Kaltenbach, F., (2004). *Translucent Materials: Glass, Synthetics, Metal* (Detail Practice): Glass, Plastics, Metals. Birkhäuser GmbH, Birkhäuser.
- [4] Chilton, J., Lau, B., (2015). “Lighting and the visual environment in architectural fabric structures” in Llorens, J.I., (ed) *Fabric Structures in Architecture*. Woodhead Publishing, Boston, MA, p.203-219
- [5] Polomová, B., Vargová, A., (2013). *Covering of Historic Building Atriums Due Adaptation to New Function*. In: 2nd Conference on Acoustics, Light and Thermal Physics in Architecture and Building Structures. Book of proceedings. Leuven, Belgium
- [6] Hraška, J. 2015, Chronobiological aspects of green buildings daylighting, Renewable Energy, Volume 73, January 2015, Pages 109-114

[7] STN 730580-1 amendment.2, Daylighting of buildings, part 1: Basic Requirements, Slovak Technical Standard, ICS 91.160, October 2000

[8] STN 730580-2, Daylighting of buildings, part 2: Daylighting of residential buildings, Slovak Technical Standard, ICS 91.160, October 2000

Proceedings of the TensiNet Symposium 2019

Softening the habitats / 3-5 June 2019, Politecnico di Milano, Milan, Italy
Alessandra Zanelli, Carol Monticelli, Marijke Mollaert, Bernd Stimpfle (Eds.)

Exploring fog harvesting nature-based solution tensile membrane structures towards sustainable development in the Italian urban context

Gabriela FERNANDEZ*, Gloria MORICHI^a, Lucas B. CALIXTO^b

* Department of Architecture & Urban Studies, Politecnico di Milano
Via Bonardi 3, 20133 Milan, Italy
gabriela.fernandez@polimi.it

^a Department of Architecture, Built Environment and Construction Engineering, Politecnico di Milano

^b Department of Architecture and Design, Politecnico di Torino

Abstract

Current practices are depleting the planet's finite resources, changing its climate and damaging its natural ecosystems. Due to population growth trends and fresh water resource depletion, it is estimated that by 2050 global water demand will face a 55% increment, mainly related to higher demands from manufacturing, thermal electricity generation, and domestic use (United Nations, 2015). In order to preserve global water supplies and relieve the stress on conventional, over-exploited fresh water sources, fog water harvesting tensile membrane structures stand as a promising yet relatively unexplored solution (Fernandez, 2018). The study focus on maximizing the ecology of system boundary processes and offer fog harvesting lightweight architecture design opportunities and tailor the circularity of a city based on geography and climate characteristic conditions (Morichi, 2018). The threefold study: (i) applied a step-by-step replicable material flow analysis data collection pyramid model method, (ii) proposed a fog harvesting smart system tensile membrane design approach, and (iii) policy guidelines in the Mediterranean region of Emilia Romagna, in the cities of Parma and Piacenza (Italy).

Keywords: fog-harvesting, sustainable development, lightweight material, data collection, Italy, Po Valley, water, data collection, material flow, smart technology, urban metabolism

DOI: 10.30448/ts2019.3245.36

Copyright © 2019 by G. Fernandez, G. Morichi and L. B. Calixto. Published by Maggioli SpA with License Creative Commons CC BY-NC-ND 4.0 with permission.

Peer-review under responsibility of the TensiNet Association

1. Introduction

The planet Earth's surface is composed of 70% water, but almost all of that liquid is seawater and undrinkable. As our population grows and temperatures rise, the global water crisis makes cities vulnerable and unsustainable. According to the Joint Monitoring Programme for Water Supply and Sanitation (2015), half of the world will be living in areas where water is not easily available by 2025, while other reports show that global water shortages pose a threat to national security. There is a high alertness on the availability of water resources, uncertainty related to climate changes, which is exacerbating the risks associated with variable precipitation patterns, droughts, and extreme weather events. Many countries already began to experience direct/indirect negative effects on the hydrological cycle (Distefano and Kelly, 2017 and Stein et al., 2016). Among numerous factors influencing water demand, one of the greater stresses applied to water resources is related to population growth and urbanization.

According to the Water Exploitation Index (in which values above 20% and 40% exploitation indicates stress and severe stress, respectively), many Mediterranean countries are yearly using up 20% of their long-term resource supplies (EEA, 2016). Due to pressing and evident environmental challenges, there is a need to characterize, monitor, forecast and transform the current linear paradigm of urban economies. With high levels of urban resources and water consumption, cities are vulnerable due to their dependency on a global hinterland. As cities continue to grow both in territorial and economic aspects, their vulnerabilities also increase while their resilience decreases. The Urban Metabolism approach can help to address these major environmental challenges by better understanding these complex interconnections between an urban area, its economy, its resource requirements and pollution impact (Wolman, 1965). This evaluation is an important aspect to identify the nexus between environmental degradation, socio-economic behaviors of citizens and urban form. Through nature-based technological solutions, monitoring and evaluation of resource flow, cities can shift from a centralized government to a more sustainable decentralized resilient society.

This study proposes an innovative methodology to integrate the unexplored fog harvesting technology – that allow water collection from fog masses – within urban environment, to understand and tailor the circularity of a city based on geography and climatic characteristic conditions. The outcomes provide fog harvesting design guidelines and policy recommendations at the building level using real case scenarios in the urban built environment, with reference to the Italian context of Emilia Romagna (Northern Italy).

2. Fog harvesting state-of-the-art technology and design

Fog is often present in temperate regions, where in Italy it is characterized by its nocturnal formation, configuring the radiation fog type. Fog is made up of water droplets, 1 μm and up to 40 μm in diameter, suspended in the air (Schemenauer and Cereceda, 1994). Fog is also known for being able to provide both clean water (Schemenauer, Cereceda and Osses, 2015) and an environment for aggregation of air pollutants and microbiological life (Fuzzi, Mandrioli and Perfetto, 1997), all depending on pollution levels and on the ecosystems of given area. According to Domen et al., 2014, fog can form and dissipate in the arc of a few hours, and sometimes can persist over many days or weeks. In the majority of cases, the shape and arrangement of fog collectors make use of similar harvesting design processes. As shown in Figure 1, the process functions through a simple surface impaction process, where fog droplets are carried by the wind and are intercepted while the air passes through the mesh. Minute fog droplets coalesce and form larger water droplets on the mesh fabric – the most diffused for fog collection purpose is the *raschel mesh* – and trickle down into an attached gutter. In this way, water can be collected, stored and later used.

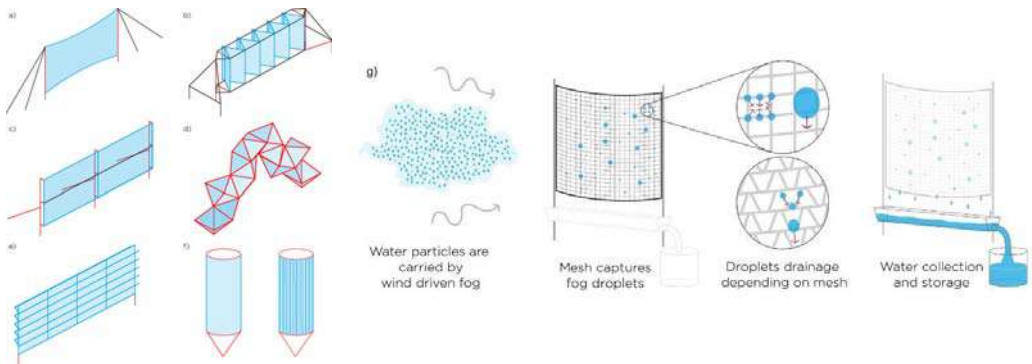


Figure 1: Fog collector schemes: a) Semi-rigid large fog collector, b) Multi-modular funnel large fog collector. c) Rigid two-dimensional collector, d) Macro-diamond collector, e) Rigid composed fog collector, f) Cylindrical mesh and wires fog collectors; g) fog droplet collection process (Morichi, 2017).

The water collection rate depends on many factors, related to fog characteristics or influenced by the mesh properties. Some fog-related parameters are the frequency of fog events (days/month or days/year); the duration of single fog events (hours/day, or hours/fog event); the moisture content of the fog (more precisely Liquid Water Content, LWC); wind speed, which is crucial for collection (Schemenauer, Cereceda and Osses, 2015). In the Chugungo (Chile) Large Fog Collectors yielded an average of 3L/m² per day of mesh area (Schemenauer, Cereceda and Osses, 2015) while in Oman, magnitudes of 30L/m²/day were achieved. Among fog-catchers, related parameters are (Fernandez et al., 2018; Rajaram et al., 2016) the size of the filaments and pores in the nets; the size of the holes between those filaments; the coating applied to the filaments.

Past scholars have designed collectors with flat, rectangular plastic nets and supported with cable posts or wooden structures arranged perpendicularly to the direction of the prevailing wind and others have scientifically design mathematical equations to measure fog collector efficiency (Ritter et al., 2008; Imteaz et al., 2011). Scientists have discovered that the most productive geographic conditions to implement fog water harvesting are found in mountains, valleys and coastal regions where the wind moves clouds over the surface of the ground (Gandhidasan et al., 2018; Regalado and Ritter, 2016). Figure 2 illustrates fog harvesting studies implemented in numerous countries around the world.

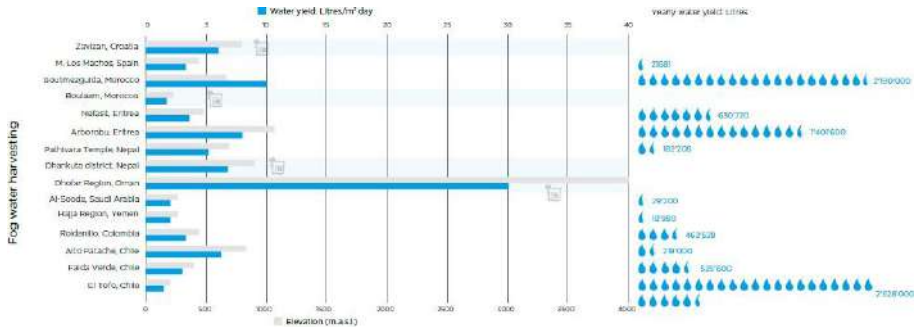


Figure 2: Worldwide fog harvesting applications. (Morichi, 2018)

3. Method

The study is composed of an extensive literature review on water, particularly emphasis on fog harvesting as an unexplored science in research that can be used as a secondary solution in cities to preserve, conserve and monitor water consumption (urban metabolism assessments) in unrepresentative areas with little to no access to water. The research is developed in three phases: 1) Material flow analysis data collection method pyramid model and assessing material, energy and pollution 2) Clustering and multi-parameters optimization techniques (guidelines). 3) Nature-based fog harvesting membrane design solution. Identifying the appropriate business model to a circular economy can create a more feasible, transparent and adaptive approach to the metabolic profile of cities while designing healthier public policy strategies. Figure 3, illustrates an urban metabolism approach using the Material Flow Analysis Metabolic Scan Pyramid Process which composes of the study method process in five steps (Fernandez, 2018):

- 1) Definition of study area, intervention area, available data, aim, and scope;
- 2) Metabolic characterization of the study area: scale and system boundaries;
- 3) Identification and characterization of the metabolic impact;
- 4) Evaluation of the proposal of and alternative scenarios;
- 5) Potentiating the metabolic efficiency using mitigation and adaptation policy actions.

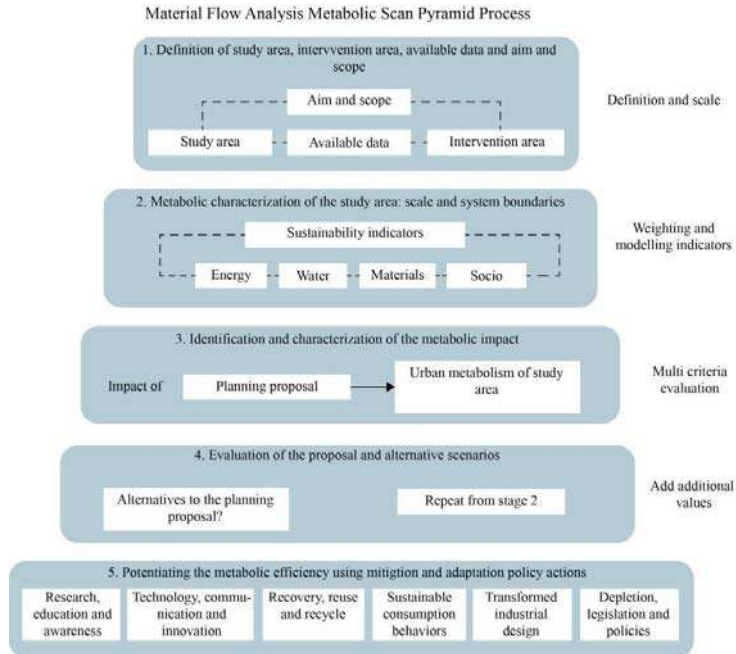


Figure 3: Material Flow Analysis Metabolic Scan Pyramid Process Diagram for Pavia and Piacenza (Fernandez, 2018).

4. Fog harvesting in Italy’s Po Valley region

The Po River Valley region is located north of Italy and hold the highest quantity of radiation fog, which stretches from Ravenna to Torino, Italy. Italy’s Po river valley is frequently cited as one of the foggier regions on the planet (Mariani, 2009; Fuzzi et al., 1996), despite its generally low wind speeds. Vicinity of strong economic centers, high population density but a still (yet strong) fog presence altogether may not represent an ideal scenario of intervention - at least according to traditional fog harvesting techniques. According to Calixto (2018), alternative fog harvesting may be a solution for the Po valley region. Exploring a combination of artificial wind generation (to compensate for the region’s weak winds) and the usage of high-efficiency Periodic-roughness Conical Copper Wires Calixto proposed a novel design fog harvester approach (Dynamic Fog Collectors) that enhances water collection by several magnitudes. An important difference between the state-of-the art in rural-based fog harvesting and this urban-integrated fog harvesting proposal is ownership. Traditionally, villagers themselves owned fog collectors and provided maintenance, of which they extracted their water for daily use. Ownership is to be granted to local regulatory water bodies, public in nature that will be in charge of the maintenance and quality of the installations. The urban furniture nature of the fog harvesters mean that their overall appearance must have an aesthetic appeal, so to not cause visual disturbances for citizens.

5. Fog-harvesting strategies for the provinces of Parma and Piacenza, Italy

Emilia Romagna is a foggy region located in the north of Italy, between the Po Valley River and the Apennine Mountains, of which the Province of Bologna serves as its capital. The Emilian provinces of Parma and Piacenza have experienced a number of droughts, and problematic wastewater management systems due to heat waves that have intensified the evapotranspiration phenomenon. Major efforts have been invested to obtain a state of emergency declaration (June 2017), which has allowed an 8.65 million euros budget to be made available for helping to meet water supply requirements in the provinces of Parma and Piacenza.

According to Agenzia regionale per la Prevenzione, Ambiente e Energia (ARPAE), and Emilia Romagna representatives, there is a situation of emergency regarding water in northern Italy following a Mediterranean trend of rising temperatures and decreasing rainfall. Figure 4 demonstrates the Southern Europe percent of normal precipitation and extreme maximum temperature in alarming digits. A number of structural measures have been situated in order to counteract or at least attenuate the consequences of the drought and climate change.

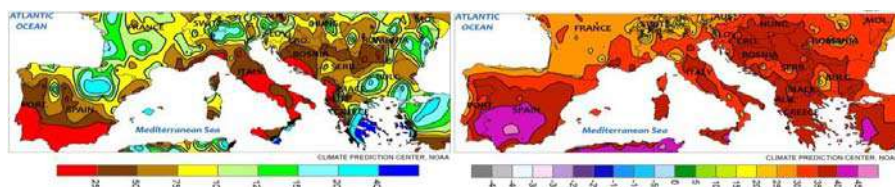


Figure 4: Southern Europe percent of normal precipitation and Southern Europe Extreme Maximum Temperature (°C) July 9-15, 2017 (NOAA, 2017)

In Emilia Romagna, water consumption has significantly decreased after the economic crisis of 2008, however, in 2015 water consumption slightly increased. In 2010, a Bolognese family of 3 people per household consume on average 130m³ per year which total 200.02 euros/per year and 0.55 euro per day, respectively (Gruppo HERA, 2014). Thus, water remain a cheap commodity to Emilia Romagna citizens. The municipality of Bologna is among the most active regions in developing awareness on the water consumption levels through the EU Blue AP initiative. As a result, there is room for improving the behaviors and educating consumers on the use of water consumption dangers and environmental health impacts.

In the last century, the Mediterranean basin has experienced up to 20% reduction in precipitation (Trigo et al., 2004; Arnell, 2004). This has put tremendous pressure on social policies, population, economies, and water supplies in these areas, as water trends are expected to worsen with increasing demand for water and reduction in rainfall in the region. Thus, reducing the water consumption from the existing water infrastructure network by using other water sources (water from air) may help reducing energy consumption, logistics and carbon footprint from the tertiary, agriculture, urban transport, residential and industry sector while improving the quality of life within the Emilia Romagna. On average, the transport of bottled

100 liters of water produces approximately 10kg of CO₂, respectively (Gruppo HERA, 2014). The expected impacts of climate change on water resources across regions include further reductions in quantity, quality and availability, with increasing frequency and intensity of droughts, especially in the summertime. For example, an increasing frequency and severity of river flow droughts could occur, with annual river flow decline and possible summer water flows reduction by up to 80% (ISTAT, 2017). Through the process of fog harvesting in the study we design a smart and feasible method that can be integrated within the built environment.

6. Urban micro-climate adaptation and funnel membrane design

According to the Koppen Climate Classification subtype both cities within the region fall under the humid subtropical climate conditions with no dry season and constantly moist with heavy continental influences due to geographical environmental conditions. Giving the Po Valley's fog dynamics and assuming they're nearly even throughout the region (Giulianelli et al, 2014), the onset of fog formation occurs at early evening and may dissipate during next morning. Water collection and usage is exemplified through Figure 5, which hypothesize a scheme of intervals of nocturnal fog water harvesting and daily water usage.

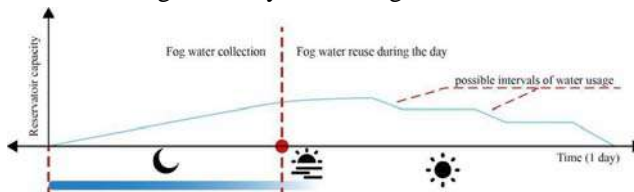


Figure 5: Hypothetical model of water collection and use.

The implementation of fog water harvesting technologies in urban environments demonstrates enormous opportunities to improve a city's metabolism towards sustainability. This technology can be especially useful in environments where cities are isolated with poor infrastructure. In addition, water consumption from natural resources such as lakes and rivers would be lowered leading towards an environmental cautious society with positive effect on water stress and improve people's attitude towards sustainable water management practices.

There are numerous variables on how to make a fog- harvesting project succeed. Wind speed, a crucially important feature, is low in the region. However, performative materials and particular micro-climatic effects originated by urban morphology and density can contribute to the increase the efficiency of the state-of-the-art technology. It has been proved that street geometry and orientation influence the amount of solar radiation received by street surfaces, the potential for cooling of the whole urban system and airflows in urban canyons, defined as the space formed by two typically parallel rows of buildings separated by a street (Ali-Toudert and H. Mayer, 2006). Moreover, higher wind speeds are found as one moves up from the surface. This leads to two possible solutions: installation on rooftops and within city streets of sufficient width to allow for the wind tunnel phenomenon to occur (see figure 6).

Considering also that only a small fraction of the water contained in the fog is actually harvested by caption meshes, the proposed fog collectors design is composed by: one funnel-like structure that canalize all possible wind flows to pass through the collector and two collection meshes placed in a row, as to increase water collection. Each of these meshes are in fact double meshes, creating a 3D-like structure that not only traps fog droplets more efficiently, but helps the water from “bouncing” away due to the wind. The model is illustrated in Figure 7.

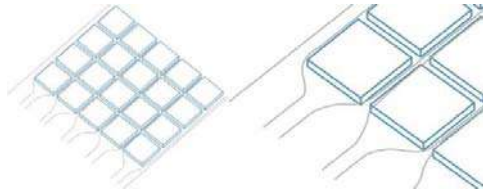


Figure 6: Fog harvesting wind tunnel direction and infrastructure hotspot installation within the city.

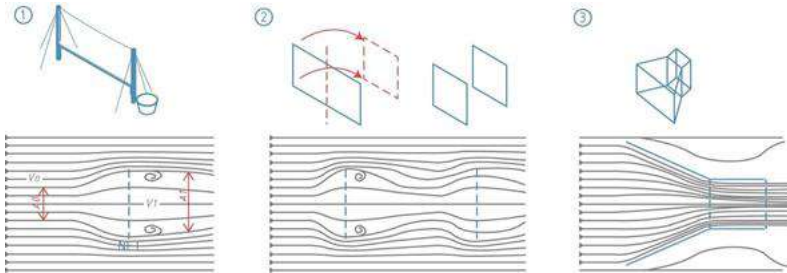


Figure 7: Fog harvesting system design model process: 1) traditional fog harvester, where significant wind flow gets deviated by the flat mesh; 2) proposed two-layer mesh where collection is enhanced by increased wind flow; 3) funnel-like structure that canalizes wind and allows for much more water collection.

There are a large number of potential services that fog harvesting can provide to the city, related to many sectors, from residential to tertiary, from industrial to agriculture. Not only multiple possible end-users but also a great variety of potential places of installation around cities from public places to private building, from new structure to old existing ones, activating a sustainable urban renovation process. The ‘fog harvesting smart system network’ measure outdoor temperature, humidity, air pressure, wind conditions, including speed and direction. It adjust to climatic conditions variables and geography using GPS, UV radiation and send data to users and operators on water to access environmental data on a smart device.



Figure 8. Proposed fog harvesting smart system network support for urban/building use. Components: 1) Funnel 2) Harvesting mesh 3) Rigid structure 4) Collection point 5) Distribution pipe and rigid axis that allows the rotation of the device 6) Support/base, where electronic and network systems are located.

Focusing on the mesh to adopt in the funnel-harvester, the most common and diffused fog harvesting systems use *Raschel mesh* but a new approach could include architecture materials used for tensile façades, shading systems and canopies. Some laboratory experiments to compare possible water droplets condensation and harvesting properties of textile meshes already present in the market have been conducted by Morichi (2018) using a climatic chamber, with 90% Relative Humidity, 40°C and 0,5 m/s wind speed (simple condensation conditions). Among the samples studied, a honeycombed textured monofilament mesh – almost a 3D material – proved to be the most efficient, with yields of 0,15 L/m² per hour. Considering that a combination of a correct upwind fog-catcher placement and the funnel shape can consistently increase water collection, we can expect yields of around 1-1,5 L/m² per hour, or rather 6 L/m² day. Moreover, a 3D mesh structure should be sufficiently rigid to withstand medium-weak winds without significant maintenance need and drainage loss.

Figure 9, demonstrates a proposed fog harvesting wastewater system support at the building level. The system model is composed of a circular movement of water that shifts in and out of the building. While incorporating a number of modes within the building as additional recycling movement features and services. The fog harvesting condensate greywater is inserted into the system model waste water system as a complimentary unexplored source of greywater to lubricate and support the existing water cycle system.

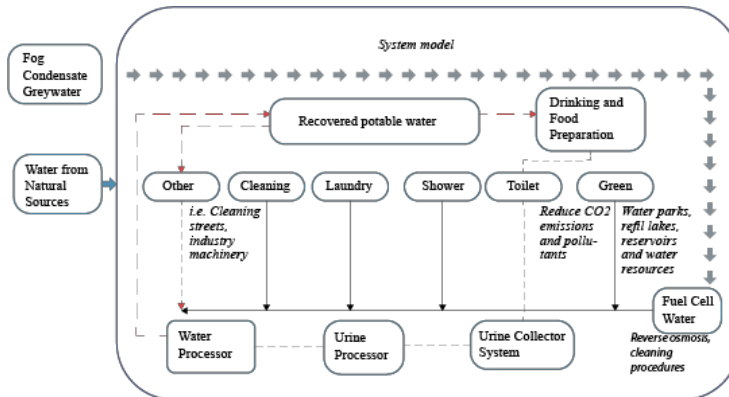


Figure 9. Proposed water fog harvesting wastewater system support for building use (Fernandez, 2018).

4. Results and discussion

Fog harvesting is far from exhausting its possibilities. Global and local wind patterns, topography, altitude, orientation of the topographic features, distance from the coastline, humidity levels and fog occurrence are some of the factors that needs to be considered before activating a fog-harvesting project. Even though fog collection projects are currently found mostly in isolated or rural areas, this research proposes an innovative fog harvesting system to have an additional water source in fog-prone urban areas. If implemented and diffused, this nature-based network system can influence the way cities are shaped and their water resource

are managed. The study recommended six policy actions (for the city of Parma and Piacenza, in Emilia Romagna region) to rethink the urban metabolism in cities. 1) Awareness, education, and research; 2) new infrastructure and system thinking: data; 3) recovery, reuse and recycling; 4) sustainable consumption and behavior, 5) transformed industrial design, and 6) depletion legislation and policies. Cities with fog have to be explored. The captured water can be utilized for various sectors such as agriculture irrigation, tertiary, industries, construction, local government, military, and domestic use. This technology can be especially useful in environments where cities are isolated with poor infrastructure. In addition, water consumption from natural resources such as lakes and rivers would be lowered leading towards an environmental cautious society with positive effect on water stress and improve people's attitude towards sustainable water management practices.

Acknowledgements

The research is a continuation of the Water for Life (WaLi) project that was developed by a team from Alta Scuola Politecnica (Politecnico di Milano and Politecnico di Torino). In addition, to the Horizon 20/20 research project Air 2 Water for Life (Air 2 Wali): Integrating natural and artificial textile mesh processes for enhancing fog-harvesting technologies applied to the urban built environment.

References

- Arnell, N.W. (2004). Climate change and global water resources: SRES emissions and socio-economic scenarios. *Global Environmental Change*, 14 (1), 31-52.
- Agenzia regionale per la Prevenzione, Ambiente e Energia (ARPA) Emilia Romagna (2018)
- Batisha, A. F. (2015). Feasibility and sustainability of fog harvesting. *Sustainability of Water Quality and Ecology* 6, 1-10.
- Calixto L. (2018). Water for Life: An experiment on fog water harvesting for the Po valley in Northern Italy. Master's thesis. Politecnico di Torino, DAD, Turin, Italy.
- Distefano T., Kelly S. (2017). Are we in deep water? Water scarcity and its limits to economic growth. *Ecological Economics* Vol.142, pp. 130-147
- Domen J. K., Stringfellow W. T., Camarillo M. K. and Gulati S. (2014), Fog water as an alternative and sustainable water resource. *Atmospheric Research*, 16, 235–24.
- European Environmental Agency (2016) The use of freshwater resources, Indicator Assessment, Diagram and maps. Kongens Nytorv, Copenhagen K Denmark, 8.

- Fernandez G. (2018), Exploring the dynamics of urban metabolism: from theory to practice. Ph.D. dissertation thesis. Politecnico di Milano, DASTU, Milan, Italy.
- Fernandez D. M., Torregrosa A., Weiss-Penzias P. S., Zhang B. J., Soresen D., Cohen R. E., Mckinley G., Kleingartner J., Oliphant A., Bowman M. (2018), Fog Water Collection Effectiveness: Mesh Intercomparisons. *Aerosol and Air Quality Research*, 18: 270–283
- Fuzzi S., Mandrioli P. and Perfetto A. (1997). Fog droplets - An atmospheric source of secondary biological aerosol particles. *Atmospheric Environment* 31(2), 187-190.
- Giulianelli L., Gilardoni S., Tarozzi L., Rinaldi M., Decesari S., Carbone C., Facchini M.C. (2014) Fog occurrence and chemical composition in the Po valley over the last twenty years. *Atmospheric Environment* 98, 394-401
- Gruppo HERA (2014). Vulnerable population numbers, over 65 and under 4 years old, retrieved from BlueAp: Emilia Romagna and Bologna Local Urban Environment Adaptation Plan for a Resilient City.
- Imteaz, M.A. Al-Hassan, G., Shanableh, A. and Naser, J. (2011). Development of a mathematical model for the quantification of fog-collection. *Resources, Conservation and Recycling*, 57, 10–14.
- ISTAT. 2017. Emilia Romagna region and Pianura Padana.
- Joint Monitoring Programme for Water Supply and Sanitation (2015). Update and MDG Assessment: Progress on Sanitation and Drinking Water. Geneva, UNICEF and World Health Organization 2015
- Klemm O., Schemenauer R.S., Lummerich A., Cereceda P., Marzol V., Corell D., Heerden J., Reinhard D., Gherezghiher T., Olivier J., Osés P., Sarsour J., Frost E., Estrela M.J., Valiente J.A. and Fessehayé G.M. (2012). Fog as a fresh water resource: overview and perspectives. *Ambio* 41, 221-234
- Mariani, L. (2009) Fog in the Po valley: Some meteo-climatic aspects. *Italian Journal of Agrometeorology* 3, 35-44.
- Morichi, G., Calixto L., Lorenzon F., Li, R. Miladinovic, S., (2017). WaLi: Water For Life Exploring Urban Landscapes for Water Harvesting with new technologies. Alta Scuola Politecnica Report, Milano Torino.
- Morichi, G. (2018), Water skin. Fog and dew harvesting integration in urban environments. Master Thesis. Politecnico di Milano, DABC, Milan, Italy.

- Rajaram, M. (2015). Enhancement of fog-collection efficiency of a raschel mesh using surface coatings and geometric changes. Master of Science in Mechanical Engineering. The University of Texas at Arlinton.
- Regalado, C.M. and Ritter, A. (2016). The design of an optimal fog water collector: A theoretical analysis. *Atmospheric Resource* 178–179: 45–54
- Rivera, J.D. (2011) Aerodynamic collection efficiency of fog water collectors. *Atmospheric Resource* 102, 335–342
- Ritter, C., Regalado, M. and Aschan, G. (2008). Fog Water Collection in a Subtropical Elfin Laurel Forest of the Garajonay National Park (Canary Islands): A Combined Approach Using Artificial Fog Catchers and a Physically Based Impaction Model. *Journal of hydrometeorology*, 9, 920-935.
- Schemenauer R.S., Cereceda P. and Osses P. (2015). Fog water collection manual. FogQuest: Sustainable Water Solutions.
- Schemenauer, R. S. and Joe P. I. (1989) The collection efficiency of a massive fog collector. *Atmospheric Research* 24 (1-4): 53-69.
- Schemenauer, R.S., Osses P., and Leibbrand (2004). Fog collection evaluation and operational projects in the Hajja Governorate, Yemen. *Proceedings of the 3rd International Conference on Fog, Fog Collection and Dew*, Cape Town, South Africa, 38.
- Schemenauer R.S. and Cereceda P. (1994). Fog collection's role in water planning for developing countries. *Natural Resources Forum*, 18, 91-100, United Nations, New York.
- Stein U., Özerol G., Tröltzsch J., Landgrebe R., Szendrenyi A. and Vidaurre R. (2016), European Drought and Water Scarcity Policies (2016) In: Bressers, H.; Bressers, N.; Larrue, C. (2016), Governance for drought resilience Land and Water Drought Management in Europe.
- Trigo, R. M., Trigo, I. F., DaCamara, C. C., & Osborn, T. J. (2004). Climate impact of the European winter blocking episodes from the NCEP/NCAR reanalyses. *Clim. Dyn.*, 23, 17–28.
- United Nations. (2015). United Nations Sustainable Development Goals 2030. Paris Agreement. Paris, France.
- Wolman A. (1965). Metabolism of Cities. *Scientific American*, 213(3), 179-190.

Proceedings of the TensiNet Symposium 2019

Softening the habitats / 3-5 June 2019, Politecnico di Milano, Milan, Italy
Alessandra Zanelli, Carol Monticelli, Marijke Mollaert, Bernd Stimpfle (Eds.)

A lightweight textile device for urban microclimate control and thermal comfort improvement: concept project and design parameters.

Anna CANTINI *, Adriana ANGELOTTI ^a, Alessandra ZANELLI ^b

*Department of Architecture, Built Environment and Construction Engineering, Politecnico di Milano
Piazza Leonardo Da Vinci 32, 20133 Milano, Italy
anna.cantini@polimi.it

^a Department of Energy, Politecnico di Milano

^b Department of Architecture, Built Environment and Construction Engineering, Politecnico di Milano

Abstract

The proposed contribution presents the design process of a lightweight device for the mitigation of the microclimate in summer conditions in the public spaces of residential urban areas. In particular, the project is part of a wider and ongoing process of regeneration in the west urban periphery of Milan, Italy: throughout its implementation, several public areas with considerable social fragility and environmental outdoor discomfort are emerging. These areas are being studied for monitoring of the microclimatic and comfort conditions, in order to evaluate the installation potential of a lightweight device for mitigating thermal discomfort. Due to the specific context, the innovative aspect of the technological design and construction process of a lightweight structure is to respond to the twofold requirement of seasonal use of the device, namely its transportability and deployability, and of its applicability in public areas in terms of security, usability and comfort performances of the materials.

Keywords: shading systems, lightweight materials, thermal outdoor discomfort, microclimatic mitigation, deployability, portability.

DOI: 10.30448/ts2019.3245.38

Copyright © 2019 by A. Cantini, A. Angelotti, A. Zanelli. Published by Maggioli SpA with License Creative Commons CC BY-NC-ND 4.0 with permission.

Peer-review under responsibility of the TensiNet Association

1. Introduction

The proposed contribution operates in the framework of environmental and technological mitigation strategies in the urban outdoor spaces which are characterized by a significant thermal discomfort.

Since the 80s, environmental research has studied the impact of the urban heat island by analyzing how urban morphology (Stewart et al., 2012), urban materials and microclimate conditions (Chatzidimitriou & Yannas, 2015; Chatzidimitriou & Yannas, 2016; Nikolopoulou & Lykoudis, 2006) influence the thermal comfort of users; on the other hand, environmental architecture (among others: Minati, 2004) analyses the link between built environment and users' behaviors. Environmental comfort is indeed essential to determine the use of spaces and thus it should be given as a design parameter in urban planning. The design approach to urban outdoor spaces can be addressed through performance analysis, which is used typically for the technological design; its extension to the design of urban spaces is recent and not yet consolidated (Dessi, 2007).

There is also room for further investigations in the matter of lightweight structures for mitigating outdoor discomfort in urban spaces. According to the state of the art, lightweight structures, combined with efficient materials under tension, are more frequently applied for covering wide span enclosures (Majowiecki, 1996). Nevertheless, in urban outdoor spaces, lightweight technologies and textiles are used mostly for their shading properties, while there is a lack of investigation on ephemerality and time-based technology as a design principle for microclimate mitigation in urban context. In this sense, there is a poor exploration of thermal micro-mitigation relying on the advantages of lightweight structures: namely minimal mass and thus transportability; adaptability in terms of modularity; retractability; structural efficiency; flexibility.

For the purpose of this project, lightweight temporariness is explored in terms of seasonal usability and transportability. In this contribution, a special emphasis is put on high-tech materials and their performances in relation to environmental comfort and, consequently, on the structural behaviors of tensioned fabric in combination of slender substructures.

1.1. The design context

The project is developed under the broader analytical work of the funded research entitled: *“West Road Project, a device for activating networks and public spaces through the diffused neglected areas”* that operates in the west urban periphery of the City of Milan, Italy. The main goal of this research-by-design programme is to provide the Municipality with an agile urban masterplan that highlights the crossovers between local resources, in terms of social and economic behavior, and governance resources, in terms of the definition of interests and design guidelines, in public and collective spaces of urban areas. Research shows, on one hand, that marginal areas are characterized by spatial deterioration, scarce mobility and high concentration

of fragile populations. On the other hand, that experimental experiences around the common goods worldwide have been spreading out by local initiatives (Orsenigo, 2018).

2. Thermal mitigation strategies for summer outdoor comfort

In environmental studies (Chatzidimitriou et al. 2015; 2016; Gaitani et al., 2011; Nikolopoulou et al., 2006), several mitigation techniques have been analyzed to counterbalance the impacts of outdoor thermal discomfort. Along with cool materials and greenery, the use of solar control as well as the dissipation of the excess heat in low/high temperature heat sinks like the ground, the water and the ambient air, are also included. A summary of referenced main passive strategies and key technologies to reduce and/or mitigate the outdoor microclimate is shown in Table 1. Green roofs are not included because not significant in terms of pedestrian comfort (Chatzidimitriou et al., 2016).

Environmental strategies	Thermal processes	Design parameters
Greening	Evapotranspiration Regulation of the air movement Solar radiation absorption	Soil humidity Tree cover Grass cover
Solar shading	Solar irradiance reduction Surface temperatures decrease	Shading canopies
Water cooling (spraying/water lines)	Evaporation Solar radiation absorption	Water cover Water injection rate Water collection ¹
Cool pavement	Solar reflection increase at the ground level Surface temperature decrease Temperature peaks mitigation	Pavements albedo Pavements emissivity Pavements thermal capacity
Green façades	Evapotranspiration Solar radiation interception Thermal insulation increase	Vegetation (low-medium size) Grass cover
Night-time heat dissipation	Evapotranspiration Radiative heat exchange increase	Tree cover Grass cover Roads Aspect Ratio (H/W ratio) Sky view factor (SVF)

Table 1: Main passive strategies and key technologies to reduce and/or mitigate outdoor air temperature. Elaboration by the authors.

Among them, the options that have been explored for the purposes of the project are: i) greening; ii) solar shading and iii) water cooling. In fact, the device aims to be deployed in different outdoor spaces that the masterplan would select as potential liveable spaces with an existing

¹ No significant applications in urban areas of fog and dew harvesting (Morichi, 2017).

outdoor thermal discomfort. In the Mediterranean climate, liveable open public spaces offer environmental comfort conditions, especially the thermal one, that change according to seasonal and daily variations and to the activities taking place there. For this study, the Thermal Budget (TB) indicator used in the COMFA model (Brown and Gillespie, 1986) and in the extended COMFA+ model (Angelotti, Dessì & Scudo, 2007) has been adopted to measure outdoor comfort conditions. In the COMFA model the human being thermal balance is calculated by taking into account the various sensible and latent heat exchanges between the person and the surrounding environment.

The energy balance equation is:

$$TB = M + K_{abs} + L_{abs} - (Conv + Evap + TR_{emitted}) \quad (1)$$

where:

- M is the net metabolic rate;
- K_{abs} is the solar radiation absorbed;
- L_{abs} is the thermal radiation absorbed;
- Conv is the heat lost by convection;
- Evap is the heat lost by evaporation;
- $TR_{emitted}$ is the emitted thermal radiation.

Therefore, a positive value of TB implies a thermal gain for the person; vice versa, a negative value indicates a net thermal dispersion. A net value around zero of TB indicates thermal neutrality and consequently thermal comfort. A comfort sensation is then assigned to the value of the Thermal Budget (TB) as shown in Table 2.

Thermal Budget TB (W/m ²)	Thermal sensations
< - 150	Very cold
- 150 ÷ - 50	Cold
- 50 ÷ 50	Comfort
50 ÷ 150	Hot
> 150	Very hot

Table 2: Comfort sensations and corresponding Thermal Budget ranges.

The original COMFA model was mainly intended for rural open spaces. In urban contexts, buildings are likely to interfere with the TB as they intercept, absorb and reflect solar radiation, they obstruct the sky view and they emit thermal radiation. The COMFA+ takes into account all these contributions to the thermal budget, allowing thus to evaluate comfort conditions also in open urban spaces.

3. Experimental Results

3.1. Microclimatic measurements

The TB data collection has been conducted on the 24th, September 2018 in the city of Milan and it was performed from 12 am to 5 pm in two urban sites: Cascina Case Nuove (CA) and via Zamagna (ZA). The two urban sites (Fig. 1) were selected due to their relevance stemming from the activities and insights achieved so far from the ongoing WRP project (see subsect. 1.1.) which has conducted a qualitative study preliminary to the measurements that suggested a thermal discomfort in the two areas.

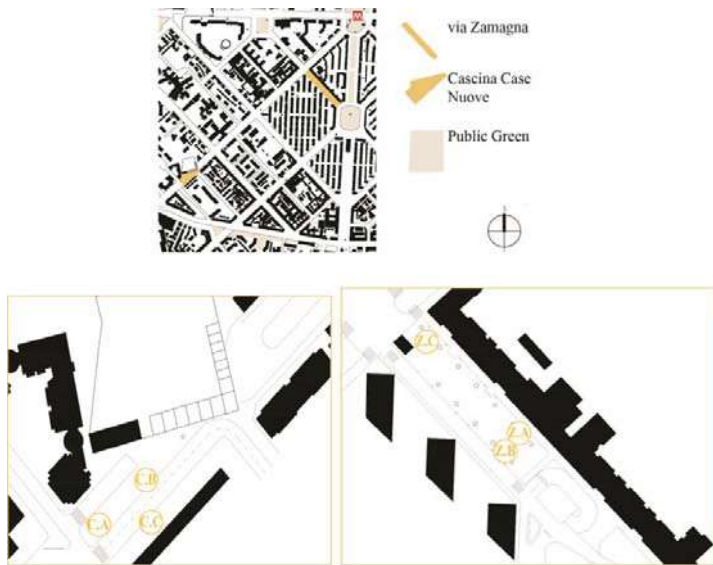


Figure 1: The monitored urban sites in Milan, Italy (latitude N45°): on the left, Cascina Case Nuove (CA) and, on the right, via Zamagna (ZA).

The first site is Cascina Case Nuove (CA), namely it is a residual space in front of a semi-abandoned ancient farmhouse, now embodied in the urban perimeter. The urban environment is characterized by high-density residential buildings and the proximity of a high traffic density road; surfaces are made essentially by asphalt and vertical materials with a medium level of albedo. There are no urban canopies and trees, while an unofficial car parking occupies the grass area next to the minor road (Fig. 2). The second site is via Zamagna (ZA), a narrow rectangular square with a high H/W aspect ratio, a poor presence of vegetation, a large variety of surface materials, such as concrete tiles and asphalt, and vertical materials with medium levels of albedo (Fig. 2). Most of the square is accessible only to pedestrians.

Measurements were carried out through a mobile data logger equipped with a thermo-hygrometer, an anemometer, a globe-thermometer and a radiometer (Fig. 2). Measured quantities are then air temperature, relative humidity, wind speed, mean radiant temperature and global horizontal solar irradiance. Microclimatic variables were mapped in three different points for each site, one of them being always in shadow and providing thus a reference condition (Fig. 2). In each point, measurements were taken for about 20 minutes.



Figure 2: Above: the measurement equipment in Cascina Case Nuove.
Below: the measurement equipment in via Zamagna.

3.2. Experimental results

The experimental results are summarized in Table 3. For each quantity, the average of the collected data in the last 5 minutes, out of the 20 minutes long measurement period, is reported. Thermal Budgets calculated through COMFA+ are shown in Table 4, where the cases of a standing person (metabolic rate 90 W/m^2) and a walking person (at 4 km/h , corresponding to a metabolic rate of 190 W/m^2) are considered. The corresponding thermal sensations, according to the scale in Table 2, are also shown.

Site	Measurement Point	Start Time	End Time	Wind speed [m/s]	Air temp. [°C]	Rel. hum. [%]	Glob. hor. solar irradi. [W/m ²]	Globe temp. [°C]
CA	C.A1	11:58	12:21	2,59	27,1	15	694	33
	C.B1	12:30	12:52	1,17	28,2	15	743	36
	C.C1	12:53	13:13	0,96	27,7	15	37	28
ZA	Z.A1	13:33	13:53	1,50	28,6	15	750	38
	Z.B1	13:53	14:13	1,08	27,7	16	51	28
	Z.C1	14:14	14:35	1,62	28,6	15	728	37
CA	C.A2	15:24	15:46	1,62	28,8	16	557	36
	C.B2	15:48	16:09	1,53	28,9	16	466	35
	C.C2	16:10	16:28	0,95	28,1	16	61	29
ZA	Z.A2	16:43	16:59	1,48	28,0	16	82	29
	Z.C2	17:01	17:21	1,04	27,9	36	331	35

Table 3: Environmental measurements on site. The input points for the measurements are named: C.A, C.B. and C.C for Cascina Case Nuove; Z.A., Z.B. and Z.C. for via Zamagna.

	M [W/m ²]	C.A 1	C.B 1	C.C 1	Z.A 1	Z.B 1	Z.C 1	C.A 2	C.B 2	C.C 2	Z.A 2	Z.C 2
TB [W/m ²]	90	159	181	-21	226	-6	217	177	160	-4	-2	139
	180	195	220	19	265	34	256	216	199	36	36	179
Therm. sensat.		Very hot	Very hot	Com fort	Very hot	Com fort	Very hot	Very hot	Very hot	Com fort	Com fort	Hot/ Very hot

Table 4: Thermal Budget (TB) calculated with a typical summer clothing thermal resistance: Rco = 0,042 m2K/W, for metabolic rate equal to 90 W/m2 and 180 W/m2.

It can be noticed that the thermal sensation in every point at a given time is generally the same for both metabolism levels considered. Experimental results show a significant outdoor thermal discomfort both in Cascina Case Nuove and in via Zamagna. Moreover, in both the sites thermal neutrality – and thus thermal comfort - is easily reached by providing solar shading (points: C.C, Z.B).

4. An integrated design concept for a lightweight textile device

4.1. Urban design typologies to mitigate outdoor microclimate

Environmental comfort has significant effects on the use of spaces and consequently it should be used as a design parameter in urban planning. Dealing with environmental comfort can be pursued through performance analysis which is used typically for technological design and that involves users' needs and environmental requirements in the definition of technological parameters. In literature, bioclimatic strategies for urban outdoor mitigation fall into two main architectural typologies: vertical elements (walling systems) and horizontal ones. The horizontal architectural components of the urban system that affect outdoor microclimate mitigation are roof structures (covering systems) and ground height differences. Covering systems normally reduce surface temperature on the ground by shading solar radiation. The best option in terms of roofing is a material with a high solar reflection, meaning a reduction of solar radiation that is transmitted and, at the same time, a low absorption of radiation and thus, a relatively low roof temperature. For thermal performances, opaque roofs with a high coefficient of solar absorption can be improved through the use of light materials, e.g. textiles and polymers, either by water irrigation of the outer side of the layer or by using double layers. Green roofs are typically a good solution if suitably designed to prevent the effects of the high coefficient of solar absorption of the vegetation. Membranes and textiles are particularly fitting the dual requirement, namely low solar absorption coefficients and low solar radiation transmission (see Table 5).

Materials	Solar absorption coefficient [%]	Solar transmissivity coefficient [%]	Solar radiation reflection [%]
Vegetation and grass	80-100	0-20	0
Textile: light color	10-20	25	55-65
Rigid polymer	10-15	13	72-77
Textile: opaque material	20-70	0	30-80
Membrane	19-11	4-17	72-77

Table 5: Solar radiation coefficients according to the different shading systems (Dessì, 2007).

While the use of membranes and textile materials in solar shading is widely common, the potential of lightweight structures is less exploited. Given the condition of the context of the site, indeed, several typical advantages of lightweight technologies could be beneficial, such as modularity, retractability, flexibility and transportability.

4.2. An integrated design concept of a lightweight textile device

Due to the specific context, the innovative aspect of the lightweight device is to explore seasonal operability and transportability in order to deploy it in different outdoor spaces that the masterplan would highlight. In the following diagram (Tab. 6) a preliminary analysis of the structural system of the device is investigated. Four main spatial configurations are introduced, according to the different structural behaviors of the components of the structure, and they are: i) open configuration: the device can be hanged to existing elements, i.e. surrounding buildings; ii) closed; iii) fix: the device is a self-standing lightweight structure, i.e. umbrellas, and vi) retractable configuration (a structural typology within the broader classification of mobile and rapidly assembled structures) if the device could be deployable thanks to the design of the structure and with a seasonal use. The greening and the water cooling are environmental strategies that can be explored either by using open and fixed covering systems, i.e. closed envelopes, or open and fix walling systems. As already mentioned, the green roofs are efficient but they need design strategies in order to induce the exchange of air in the area below. Shading canopy is the only design parameter to mitigate environmental discomfort that is supported by retractable structural covering systems.

Design Parameters (see tab. 1)	Technical requirem. (see tab. 5)	Building components	Structural systems
Soil humidity	Solar absorption Breathability	Green Roof	Open
		Green Façades	Closed
		Mesh support layer	Fix
Tree covering	Solar absorption Breathability	Green Roof	Open
		Mesh support layer	Fix
Grass covering	Solar absorption Breathability	Green Roof	Open
		Green Façades	Closed
			Fix
Solar Shading	Solar reflection	Single membrane	Open
	Solar absorption	Selective Roof	Closed
	Breathability	Green Roof	Fix
		Green Façades	Retractable
Water covering	Solar reflection	-	-
	Solar absorption		
Water collection	Solar absorption	Single membrane	Open
		Green Roof	Closed
		Green Façades	Fix
		Mesh support layer	
Cool pavement	Solar reflection	Modular pavement	Open
	Solar absorption		Fix

Table 6: Comparison of design parameters and preliminary structural systems.

In common construction practice, the main lightweight roofing to mitigate urban outdoor thermal discomfort are: i) single layer, ii) double layers, iii) multiple layers, iv) green roof and v) selective roof. The latter is particularly relevant because it combines the “dark tent” effect with high efficiency materials. The dark tent is the opposite of the greenhouse principle: the outer layer is highly reflective to the solar radiation while the inner one is permeable to infrared radiation supporting thus the heat exchange between the covered area and the area above. The best possibility to achieve good values of all the three environmental strategies coincides with the integrated design of a lightweight device in which the peculiar characteristics of high-tech materials can join the intrinsic properties of temperature decreasing of greening and water cooling design parameters.

5. Conclusion and further developments

In conclusion, the device has to perform as a temporary and transportable architecture, which can be implemented over time according to the context constraints in high density residential areas, and which assures a high efficiency cooling and solar shading performance through the use of textiles and greening. The methodology to define the technological criteria and the requirements of the thermal behavior of the device involved different levels of knowledge: 1) a field data analysis to measure real thermal outdoor discomfort in summer conditions and a field data report of the under-usage of specific spaces because of the thermal discomfort. 2) A state of the art in the matter of environmental strategies for mitigating which led to the definition of thermal performances of the device. 3) A state of the art concerning urban design parameters and architectural strategies that positively impact microclimate, which resulted in a set of best options in terms of technological performances of materials and a preliminary definition of structural sub-systems in the overall form by means of their general movement.

The presented study is to be seen as a conceptual method investigation, in which more detailed functions are to be integrated. Further and more detailed investigations are to be made upon the architectural proposal and the form finding-process of the membrane. Prototyping and model installation is going to be finalized within May, 2019.

Acknowledgements

The research moves within the activities of the broader research: “West Road Projects, a device for activating networks and public spaces through the diffused neglected areas”, a two-year funded project (2017-2019) by the Polisocial Award 2017, a programme of social responsibility of the Politecnico di Milano.

References

- Angelotti A., Dessì V., Scudo G. (2017). The evaluation of thermal comfort conditions in simplified urban spaces: the COMFA+ model. In: *2nd PALENC Conference and 28th AIVC Conference on Building Low Energy Cooling and Advanced Ventilation Technologies in the 21st Century*, September 2007, Crete island, Greece.
- Brown R. D., Gillespie T. J. (1986). Estimating Outdoor Thermal Comfort Using a Cylindrical Radiation Thermometer and an Energy Budget Model, *International Journal of Biometeorology*, vol. 30, n. 1, pp. 43-52.
- Chatzidimitriou A., Yannas S. (2015). Microclimate development in open urban spaces: The influence of form and materials, *Energy and Buildings*, vol. 108, pp. 156-174.
- Chatzidimitriou A., Yannas S. (2016). Microclimate design for open spaces: Ranking urban design effects on pedestrian thermal comfort in summer, *Sustainable Cities and Society*, vol. 26, pp. 27-47.
- Dessì, V. (2007). *Progettare il comfort urbano. Soluzioni per un'integrazione tra società e territorio*, Napoli, Italia: Esselibri – Simone.
- Gaitani N., Spanou A., Saliari M., Synnefa A., Vassilakopoulou K., Papadopoulou K., Pavlou K., Santamouris M., Papaioannou M., Lagoudaki A. (2011). Improving microclimate in urban areas: a case study in the centre of Athens, *Building Services Engineering Research Technology*, vol. 32, n.1, pp. 53-71.
- Majowiecki, M. (1996). Conception design in the reliability of long-span lightweight structure systems: observations concerning retractable roofs. In: F., Escrig and C.A. Brebbia (Ed.). *Mobile and Rapidly Assembled Structures* (pp. 351-370). Southampton, England: Computational Mechanics Publications.
- Minati G. (2004). *Teoria Generale dei Sistemi, Sistemica, Emergenza: un'introduzione. Progettare e Processi Emergenti: Frattura o Connubio per l'Architettura*, Milano, Italia: Polimetrica.
- Morichi G. (2017). *Water skin. Fog and dew harvesting integration in urban environments*. Retrieved from <https://www.politesi.polimi.it/handle/10589/140683>
- Nikolopoulou M., Lykoudis S., (2006). Thermal comfort in outdoor urban spaces: analysis across different European countries, *Building and Environment*, vol. 41, pp. 1455–1470.
- Orsenigo G. (2018). The effect of an uncertain project. In: *EURAU18: Retroactive Research*, Alicante, Spain. Conference paper.
- Stewart I. D., Oke T. R. (2012). Local climate zones for urban temperature studies, *Bulletin of the American Meteorology Society*, n. 93, pp. 1879-1900.

Proceedings of the TensiNet Symposium 2019

Softening the habitats / 3-5 June 2019, Politecnico di Milano, Milan, Italy
Alessandra Zanelli, Carol Monticelli, Marijke Mollaert, Bernd Stimpfle (Eds.)

Building Integrated Photovoltaic (BIPV) applications with ETFE-Films

Karsten MORITZ*

*Taiyo Europe GmbH, Mühlweg 2, 82054 Sauerlach, Germany, info@taiyo-europe.com

Abstract

This paper describes the design and installation of building integrated photovoltaic (BIPV) in combination with transparent structural membranes made of ETFE-films. The contribution refers to three project examples, designed and built between 2010 and 2018.

The first example is about a transparent roof with a total area of about 9,600 sqm, made of ETFE-film cushions, which spans a parking lot of the waste management services in Munich. The flexible translucent PV modules occupy an area of about three thousand sqm. The PV modules are located in the air inflated interior volume of the ETFE-film cushions. This project was finished in the year 2011. The second example shows transparent façade modules made of mechanically pre-tensioned single-layer ETFE-films with organic photovoltaic cells (OPV) and light emitting diodes (LED), applied on the weather-protected backside. An international and interdisciplinary group of researchers has received funding from the European Union's Seventh Framework Program (FP7/2007-2013) [1], to develop the façade modules from 2013 to 2017 in the frame of the project ETFE-MFM (Multifunctional Façade Module). The third and newest example shows transparent façade modules with organic photovoltaic (OPV), glued onto the printed backside of the ETFE film. Aluminum-frames of different sizes carry the pre-tensioned films. The preinstalled modules were mounted and the OPV was connected to the power inverter on site. The modules form the transparent curtain wall of a one-story brick building on the premises of the company MERCK KgaA in Darmstadt. The project was finished at the beginning of the year 2018. It can be assumed, therefore, as the world's first energy-efficient, digitally printed single-layer ETFE curtain wall façade equipped with OPV-elements.

Keywords: building integrated photovoltaic, structural membrane, transparent roof, single-layer ETFE-film, ETFE-film / foil cushion, organic photovoltaic, OPV, light emitting diode, LED, multifunctional façade module.

DOI: 10.30448/ts2019.3245.29

Copyright © 2019 by Karsten Moritz. Published by Maggioli SpA with License Creative Commons CC BY-NC-ND 4.0 with permission.

Peer-review under responsibility of the TensiNet Association

1. Introduction

The following three examples show the fast development in the field of photovoltaic and the great potential that lies in the combination of PV-cells, especially organic photovoltaic cells (OPV), with the ETFE-films.

2. Three project-examples of BIPV with ETFE-films

2.1. Project AWM carport, Munich/Germany

In the year 2011 the City of Munich (Germany) got a new membrane roof for their parking lot of the lorries for the waste management services. The reconstruction of the roof was necessary, because the former textile membrane roof collapsed in parts under snow and ice loads a few years before. The client decided for a new 9,600 sqm sized roof, made of a steel structure, covered with 220 air inflated ETFE-film cushions with 2,640 integrated PV-modules. The design from the architects Ackermann & Partners in Munich, presented here, won the competition for this new and innovative membrane roof.



Figure 1:AWM carport-roof, top view

The translucent PV modules with a total surface of about 3,000 sqm, were fixed in a removable way onto the middle layer of the 3-layers cushions by using mechanical fasteners. The PV-modules of amorphous solar cells are enclosed, therefore, by transparent ETFE-films, and kept safe from external exposures, like rain, snow, ice and dust. The outer cushion layer made of a 0.25 mm thin transparent ETFE-film reduced, of course, the solar radiation, needed for the

generation of electric energy by the PV-modules, but the reduction in solar transmission amounts only about 10%. The performance of the photovoltaic plant decreased since installation, although the modules are weather protected and the upper ETFE-film shows no clouding or significant contamination, as expected. Furthermore, the temperature inside the enclosed air space is moderate, because of the continuous air exchange.

This indicates that a few modules are defective and, therefore, affect the overall energy output. Unfortunately, the PV-producer and the used product are not available anymore.

The lower layer of the 3-layers ETFE-cushions was printed with a dot-pattern, to serve shading and to reduce the thermal impact in summer on the huge open parking lot, the workers and the lorries.

The decision for taking ETFE-film cushions for the cladding of the roof, instead of other materials, like over-head glass panes, was basing on the following advantages:

- low weight of the transparent roof cover
- low weight of the supporting steel structure
- foundation on the existing concrete-foundations of the old roof
- possibility to protect the PV-modules from external exposures
- low expense of work for maintenance and cleaning of the huge-sized smooth ETFE-film surface, because of self-cleaning by rain water
- long durability of the ETFE-film (> 25 years) because of being a fluoropolymer material
- good behavior in case of a fire (ETFE-film are classified as B-s₁,d₀ according to EN 13501-1 / EN 13823 / EN ISO 11925-2, that means self-distinguishing, no burning droplets, low fire propagation, low flammability, melting (self-opening) above a flame / hot gases)
- good recyclability of the clear ETFE-film because being a thermoplastic material (printed ETFE-films cannot be recycled, and must be utilized, therefore, thermally)
- simple replacement of single roof components and easy waste separation of the different materials at the end of the components life time
- clear and nice design vocabulary by the synclastic surfaces of the air inflated cushions
- natural lighting of the garage area and, therefore, minimization of the energy for artificial lighting, because of the high and natural light transmission of the ETFE-film
- low construction costs

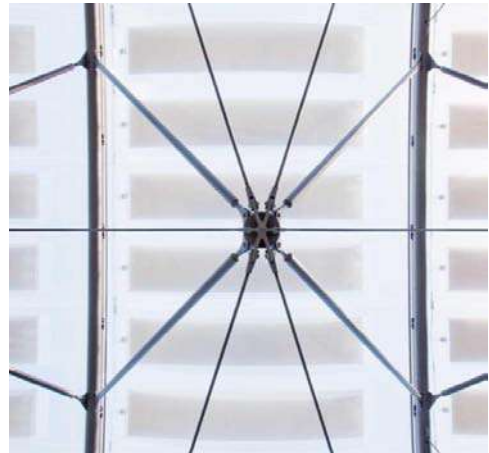


Figure 2:AWM carport-roof, view from below

For the fixation of the photovoltaic modules onto the middle layer of the ETFE-film cushion mechanical fasteners with slotted holes in the outer edge of the PV-modules were used, to resist deformations from temperature without restraint forces. The upper layer was clamped separately from the other two layers in order to exchange a defect PV module without any problems. This allows an easy access and a quick replacement of a defect module.

This innovative project is a milestone in the development of multilayer ETFE-film structures with integrated photovoltaic. The combination of both components allows the owner to get many benefits, as weather protection, light transmission, the gain of electric energy, and finally, a nice architectural appearance of his innovative building.

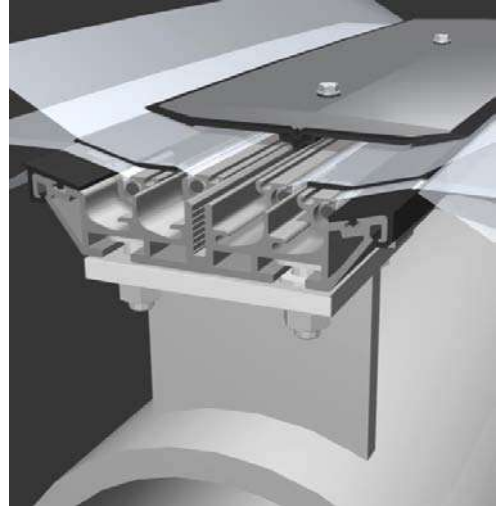


Figure 3: Isometric view of the 4-Keder-clamping system, especially developed for separated upper and lower cushion layers

Table 1: Project Data, AWM carport for the waste management services in Munich, Germany, three layers ETFE-film cushion system with integrated PV-modules, 2011

Project data	
Client	City of Munich
Architects	Ackermann & Partners, Munich
Structural Engineers	Christoph Ackermann, Munich
Membrane Engineering	Konstruk, Rosenheim; Taiyo Europe
Executing Company (GC)	Taiyo Europe, Sauerlach
Supplier (steel structure)	steel concept, Chemnitz
Surface (ETFE-film cushions)	9,600 sqm
Number (ETFE-film cushions)	220
Surface (PV-modules)	3,000 sqm
Number (PV-modules)	2,640
Rated power per module (STC)	57 W

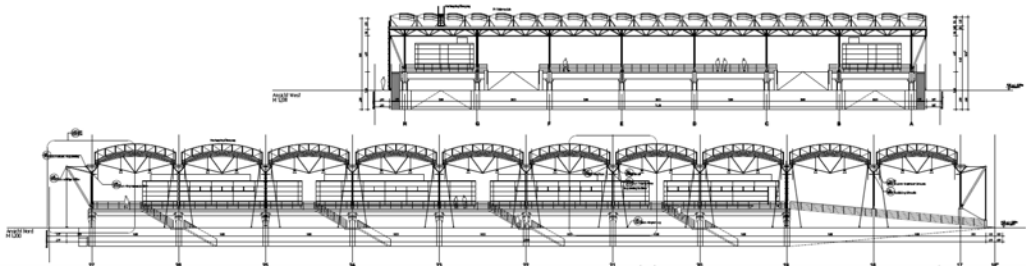


Figure 4: Sections of the building

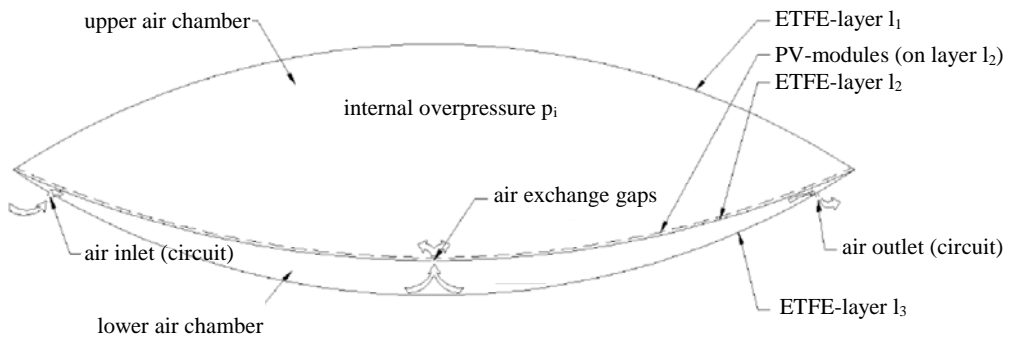


Figure 5: Principle design of the 3-layers ETFE-film cushions

2.2. Project ETFE-MFM, Pamplona/Spain

This chapter summarizes the developments, done in the context of the ETFE-MFM project. It was a research project funded and supported by the European Union Seventh Framework Programme (FP7 / 2007-2013, Grant Agreement no. 322459). The development was done by different project partners, specialized in the technologies, needed for the development of smart façade modules [1].

The project focused on the design, manufacturing and testing of a smart solution for current façade multifunctional requirements in the building sector, like load bearing, lighting, displaying and energy harvesting. The developed system is based on two ETFE-films (front and back film), embedding photovoltaic elements, in this case equipped with organic photovoltaic cells (OPV), but also equipped with light-emitting diodes (LED).

The purpose of this project was to provide a standardized semitransparent façade module acting as flexible LED display, with an electric consumption, supplied by solar energy. In this way, LED strips, organic photovoltaic cells and flexible electronics were laminated between the two ETFE-films by using Ethyl Vinyl Acetate (EVA) as interlayer-material.

The lamination process was optimized in order to provide good optical and mechanical performances without affecting the functionality of the different components.

The resulting multilayer film is held by a 1.5 m x 1.5 m sized aluminum frame, developed especially for such applications. The frame should clamp the multilayer film safely without welded keder-pocket, to prevent the embedded OPV, LED and protruding electric cables from damages at the processes of production and assembly.

Four prototypes of this module were installed vertically as a curtain wall of an existing building in Spain, to enable the one-year-lasting monitoring under real conditions. The four modules showed an average electric output of about 43 Wh per day and module and up to 90 Wh in maximum. This energy complies with the energy, needed for a video transmission that is lasting up to 150 minutes, if the consumption of the light emitting diodes is 35 W.

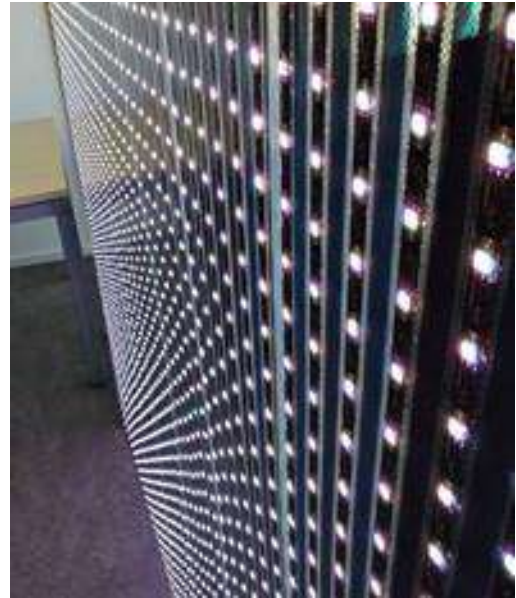


Figure 6: Prototype of the ETFE-MFM module, here with LED switched on (uniform white light) [1]

This second example shows another milestone in building with the combination of ETFE-film and photovoltaic, in this case additionally equipped with LED. The applied combination constitutes a trendsetting approach to manufacture many of identical modules, to function as a big energy-efficient façade-display as curtain wall in front of a building.

Table 2: Project Data, Research Project Multifunctional Façade Module (MFM), 2 layers ETFE with embedded OPV and LED

Project data	
Funded (2013 – 2017) by	European Commission
International Research Project Partners	Acciona, Cener, Greenovate, Itma, Opvius, Taiyo Europe
ETFE-membranes / extrusion profile	Taiyo Europe, Sauerlach
OPV	Opvius, Kitzingen
Surface (ETFE)	2.25 sqm (per 1.5m x 1.5m module)
Surface (OPV)	~ 1.75 sqm

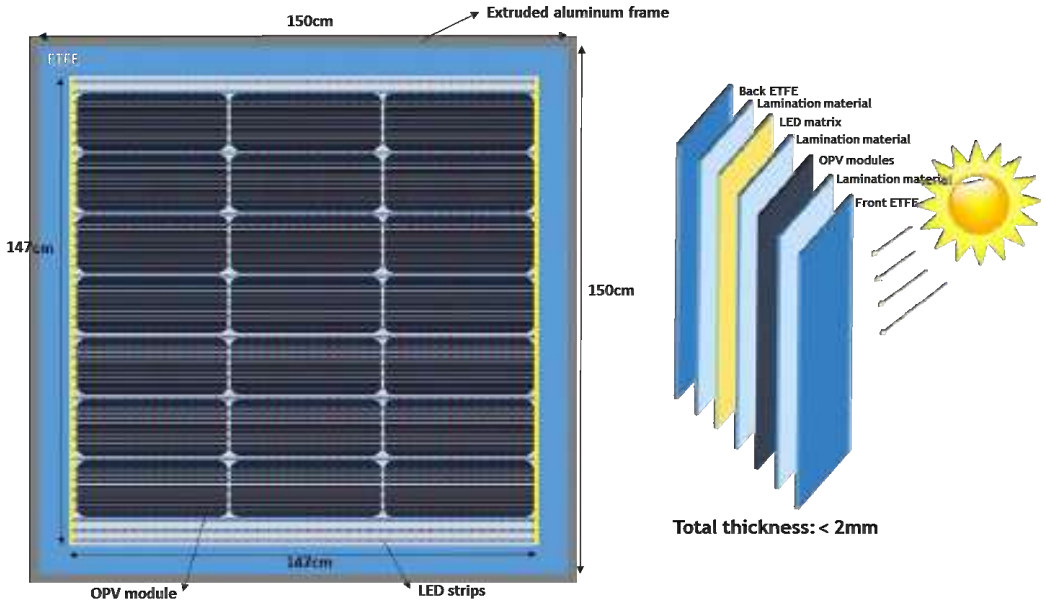


Figure 7: Layer structure of the multifunctional façade-module (ETFE-MFM) [1]

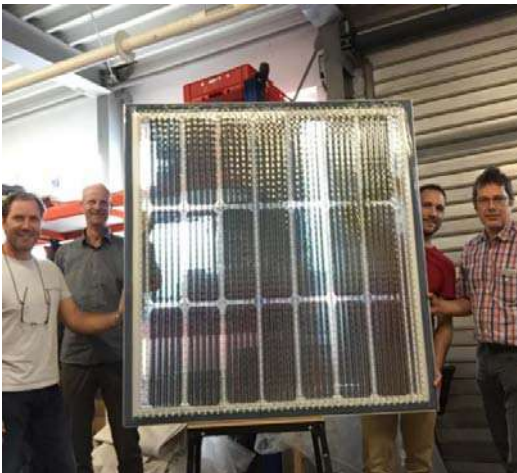


Figure 8: Pre-assembly of the first prototype, Taiyo Europe's workshop in Sauerlach, Germany



Figure 9: Installation of 4 modules of the prototype on ITMA premises in Pamplona, Spain [1]

2.3. Project MERCK Transformer Station, Darmstadt/Germany

The third example also shows a modular design for curtain wall façades, which also consists of the combination of ETFE- film and organic photovoltaic (OPV). Here, three different organic shapes of OPV elements were applied on the mechanically pre-tensioned ETFE film for the first time. The 64 membrane modules with aluminum frames form a curtain wall on the four sides of the existing transformer building on the premises of MERCK in Darmstadt in front of a wall made of fired bricks. The selected colors of the digital printing of the ETFE film follow the corporate identity of the company. Since the relatively small area of the OPV provides only a low power yield. The small façade is, therefore, a pilot project, that should demonstrate the possibilities of this technology. The direction in which this technology goes is clear: the individual design of modular, aesthetically appealing multifunctional curtain wall façades. Topics include lightness, transparency, aesthetics, careful use of resources and solar energy generation. The project uniquely combines aesthetics and multi-functionality. The result is a great architectural work of art with a high innovative demand.



Figure 10: Assembly of the 64 frames in Taiyo Europe's workshop (standard size 4.2 x 1.3 m, as shown here; special size 4.2 x 0.5 m)

Table 3: Project Data, transparent ETFE/OPV-façade, MERCK transformer building (B7/B8) in Darmstadt, Germany

Project data	
Client	MERCK KGaA, Darmstadt
Architect	Henn Architects, Berlin
Structural Engineer (curtain wall)	Leicht, Munich
ETFE-membrane/extrusion profile	Taiyo Europe, Sauerlach
OPV	Opvius, Kitzingen
Steelwork	Steelconcept, Chemnitz
Surface ETFE	300 sqm
Number of modular frames	64
Number of PV-modules	1,578 (3 types of organic shapes)

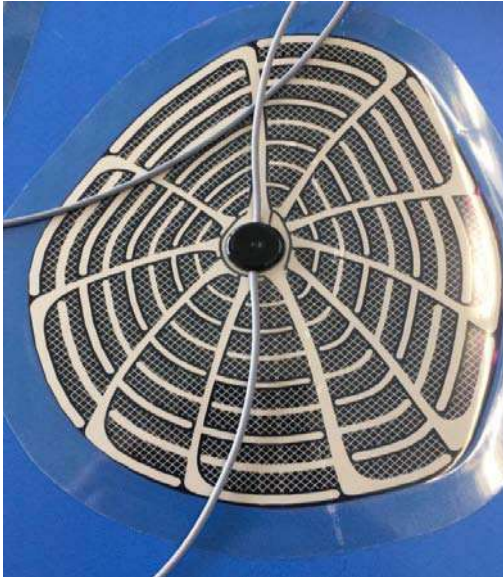


Figure 11:OPV-modules glued on the backside



Figure 12:Connecting the OPV-modules

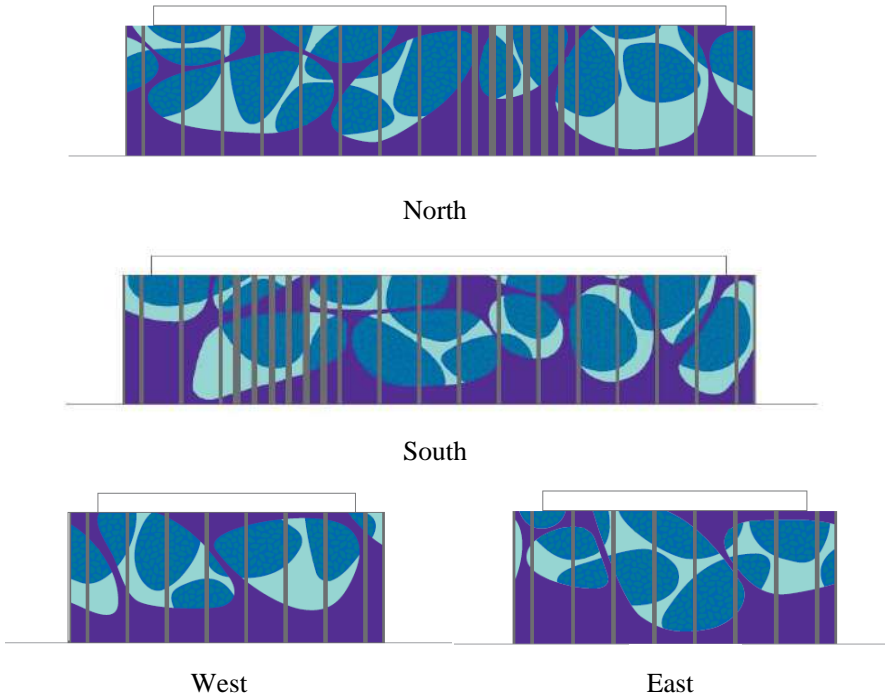


Figure 13: Side views of the building



Figure 14: Installation of the pre-fabricated façade-modules on site



Figure 15: Finished façade (MERCK premises, Darmstadt, Germany)



Figures 16:MERCK Transformer Station, Darmstadt, Germany: appearance of the original brick-façade



Figure 17:MERCK Transformer Station, Darmstadt, Germany: appearance of the new curtain wall

3. Conclusion

The projects presented above show the possibilities of building integration of photovoltaic (BIPV) in combination with transparent ETFE film, but they also show the beginning of a construction method that will only mature to a trend-setting technology after overcoming the teething troubles. However, the combination of PV and ETFE enables, like no other, the realization of modular, individual, multifunctional and aesthetically pleasing façades and roofs. The examples also show that requirements for aesthetics, transparency, lightness, load transfer, weather and fire protection, as well as the careful use of our natural resources and the solar energy production are achievable. Since the examples refer to curtain walls and open spaces, building physical requirements due to thermal insulation were not to consider, here.

Currently the membrane construction sector is changing rapidly to the extent that modular construction with multi-layered structure and multifunctional use is now part of it. Due to their low weight per unit area and their multi-functionality, modular construction also undoubtedly belongs to the field of lightweight structures. Such multifunctional modules are becoming increasingly important for architects and building owners, and, therefore, for the construction industry as well, as they allow very different applications and functional possibilities. However, they also lead to a major challenge for membrane construction companies, architects and structural engineers. This means that suitable production methods with appropriate quality assurance for modular multilayer structures must be present or developed, and the topics of building physics, fire and structural behavior, but also production and assembly technologies of modular multilayer membrane structures are to consider in design and engineering, including all interactions.

Which membrane construction company is capable of producing a large number of uniform or even different modules economically and in terms of a needed high quality? Which structural engineer is also a specialist in building physics or photovoltaic and knows the elements stress-strain behavior or its structural limits? Which architect can claim that he masters all relevant topics in such a way that he can present a harmonious execution planning of such modular constructions without involvement of experts in the early phase of the planning process already? The knowledge of all the elementary properties and requirements, but also their interactions, will increasingly determine the success of such modular membrane projects as well as the future of the planners and specialist companies involved in this new technology.

4. Referencing literature

- [1] A. Menéndez, A. Martínez, A.Santos, B. Ruiz, K. Moritz, I. Klein, J. Díaz, A.R. Lagunas, T. Sauermann, D. Gomez, “A multifunctional ETFE module for sustainable façade lighting: Design, manufacturing and monitoring”, *Energy and Buildings, Elsevier*, vol. 161 (2018) 10-21

Extreme Soft Skins: Multilayered ETFE for Challenging Environments

Nebojsa JAKICA*, Alessandra ZANELLI^a

* University of Southern Denmark
Campusvej 55, 5230 Odense, Denmark
nja@iti.sdu.dk

^a Politecnico di Milano, TextilesHUB
33 Ponzio street, Milan 20133, Italy
alessandra.zanelli@polimi.it

Abstract

ETFE has been rapidly expanding its presence in the building industry, finding its application on all parts of the envelope, especially skylights due to the superior light translucence (Monticelli, 2015). Recent technological developments of multi-layered ETFE systems coupled with advanced coatings have altered their performance and boosted their potential for applications across all latitudes. The paper presents the optical and thermal characterization of multi-layered ETFE foils performed at the TextilesHUB - the Interdepartmental Research Laboratory at Politecnico di Milano. Studies include ETFE with advanced silk-screen printed coatings and coating patterns for various real case projects in challenging environments, covering both cold and hot extremes. Special focus is placed on hygro-thermal analyses to inform the design of the frame to eliminate potential condensation caused by the high-temperature difference between both sides and very low thickness at the edge of the ETFE cushions, where all layers converge into framing gasket. Moreover, the paper presents an optimization process for improving performance of ETFE layer compositions to mitigate high environmental stresses, provide optimal indoor comfort and reduce energy demand. Finally, we present achieved performance levels of different ETFE systems implemented in three projects in Sankt Petersburg, Milan and Manama and discuss possibilities for future improvements.

DOI: 10.30448/ts2019.3245.51

Copyright © 2019 by Nebojsa Jakica, Alessandra Zanelli. Published by Maggioli SpA with License Creative Commons CC BY-NC-ND 4.0 with permission.

Peer-review under responsibility of the TensiNet Association

Keywords: ETFE lightweight structures, sustainability, optical and thermal performance, multilayered ETFE

1. Introduction

The early presence of ETFE in the building industry was characterized by its temporality and lightness. Majority of ETFE structures were auxiliary and temporal buildings, mostly for limited and not extended occupant use. Moreover, the unrivaled light-weightiness of the construction, only one hundred of the equivalent construction in glass, has enabled creation of large span structures. As a consequence, the cost of such constructions was also much lower than those made of glass. However, in this phase of ETFE development, its minimal thickness and lack of spectrally-selective coatings in the two-layered system limited its optical and thermal properties and range of suitable climates (Chilton, 2013). Recent technological developments of multi-layered ETFE systems coupled with advanced coatings have altered their performance and boost their potential for applications across all latitudes. Since then, ETFE has been rapidly expanding its presence in building industry, finding its application on all parts of the envelope, especially skylights due to the superior light translucence of 90-95% (Monticelli, 2015).

The paper presents the optical and thermal characterization of multi-layered ETFE foils with advanced silk-screen printed coatings and coating patterns for three real case projects in challenging environments, covering both cold and hot extremes. Performance levels of different ETFE systems implemented on projects in Sankt Petersburg, Milan and Manama are shown. Moreover, the paper presents an optimization process for improving performance of ETFE layer compositions to mitigate high environmental stresses, provide optimal indoor comfort and reduce energy demand. Special focus is placed on hygro-thermal analyses to inform the design of the frame to eliminate potential condensation caused by the high-temperature difference between both sides and very low thickness at the edge of the ETFE cushions, where all layers converge into framing gasket. The paper proposes and discusses potential solutions. In addition, the paper explains challenges of structural framing and gaskets detail design of multilayered ETFE to accommodate all layers and widen edge of the cushion thickness to improve u-value in these areas.

2. Methodology

The paper presents a methodology for addressing arbitrary complex thermal and optical requirements and consequently achieving high performance of the ETFE systems. Three case studies were chosen to demonstrate the range of climates and suitable ETFE structures. All three structures are atrium roof coverings in large projects located in Manama Bahrein; St. Petersburg, Russia; and Milan, Italy representing hot desert, warm-summer Mediterranean and Savanna climates respectively according to the Köppen classification (Köppen, 1884) Figure 1. Despite a large variation in environmental loads, with a range of average high summer

temperatures from 39°C to 23°C and winter from 20°C to -4°C, annual global horizontal solar irradiation from 2100KWh/m² to 900KWh/m², each project follows a general methodology that balances optimal and thermal properties.

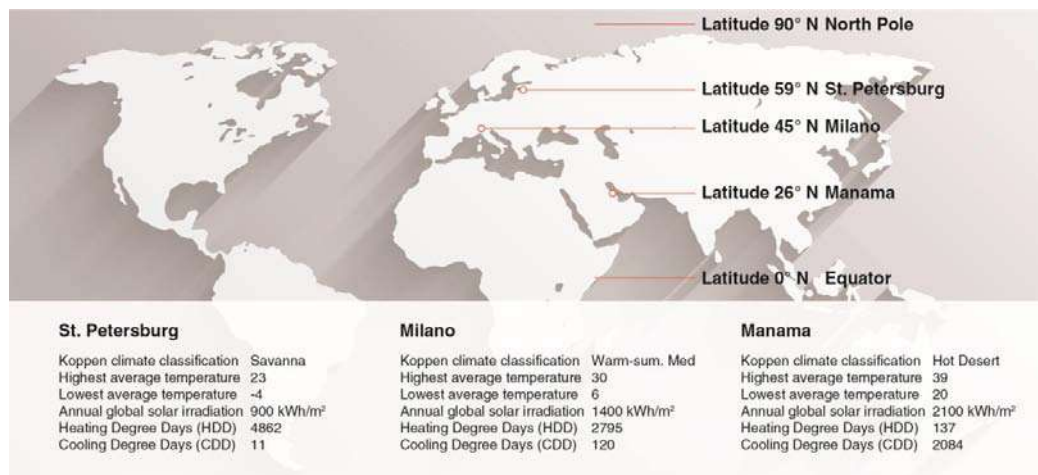


Figure 1: Climate data of cities of case studies

The methodology starts with a project brief that specifies required thermal transmittance or u-value and Solar Heat Gain Coefficient (SHGC) or g-value for a Total Fenestration Product (TFP)(NFRC, 2013). TFP is composed of Frame, Edge of Glazing (EOG) and Center of Glazing (COG) parts, where the latter is of much higher significance due to the size of ETFE cushions that may be much larger than those in the glass counterpart. TFP performance is calculated according to the standards ISO 9050, ISO 15099, EN 410 and EN 673 using validated Optics6 and Window 7.4 for COG and EOG values, while the frame has been calculated in Therm 7.4. The software is provided by the Lawrence Berkeley National Laboratory (LBNL). ETFE cushion curved surface geometry structure has been simplified to parallel flat surfaces in modeled layer configuration using a value of 100mm as an average distance of the air gap between ETFE layers that do not influence u-value. EOG area used an air gap of 20mm and has perimeter offset of 5cm. A typical frame profile and thermal analysis are shown in Figure 2. The figure also shows a schematic diagram of TFP components and the following formula used to determine TFP u-value. Environmental conditions were set to NFRC 100-2010 unless specified otherwise like in the Case Study 3 – Extreme Cold Climate: Lakhta Center, St. Petersburg, Russia. The emissivity of all ETFE surfaces was set to 0.84, with exception of coated surfaces with an emissivity of 0.57. Thermal conductivity of ETFE was set to 0.24W/mK. Since most of the currently available ETFE foils have similarly mentioned emissivity, u-value of multilayered ETFE systems will be dependent only on a number of layers, assuming exterior-facing foil is always coated. The selection process for reaching required u-value is therefore straightforward. Two-layered ETFE will have u-value of 2.6W/m²K, three-

layered 1.8W/m²K and four-layered 1.3W/m²K. Further improvements of thermal performance are possible either by adding more layers or changing spectral-selectivity of coatings. However, five-layered cushions and IR-cut coatings with the emissivity of 0.4 and below are still in experimental phases and not yet commercialized.

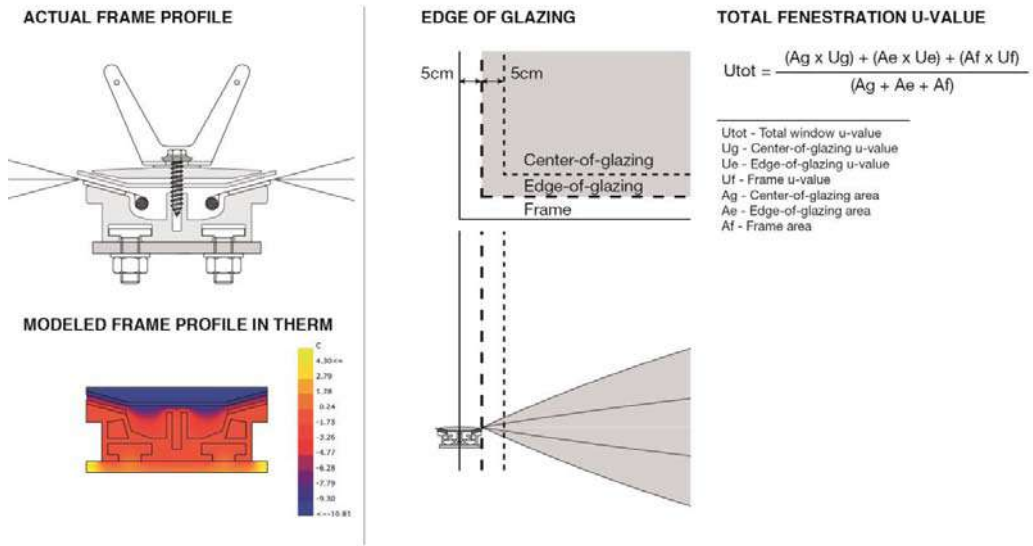


Figure 2: Total fenestration u-value calculation of multilayered ETFE

When the number of layers is defined, the process continues with an optical characterization of materials to determine g-value. This part is not straightforward as there are many parameters influencing optical behavior to various extends. Three main optical performance parameters are: foil thickness, coating type and percentage of the coated area, while pattern type is a visual parameter that affects aesthetics and may be determined by other stakeholders. In most of the cases, pattern type, percentage of the coated area and coating type are all predetermined by the ETFE foil producers to cover all range of g-values from 0 to 1. Each of the parameters has its code and each ETFE foil name is composed from parameters codes. In that way, selection filters may be applied to acquire a selection of foils with desired parameters and possible alternatives of other parameters. For standard ETFE foils, producers provide optical and thermal specifications, while custom products may be produced on demand. Additionally, producers may present spectral curves or provide optical data showing Transmittance (T), Reflectance on the front (R_f) and back side (R_b) in Ultraviolet (UV), Visible (VIS), Near-Infra-red (NIR) and Far-Infra-Red (FIR) parts of the spectrum. Optical data of ETFE foils represent a necessary step in determining multilayered ETFE system performance. Due to the very low variability in the optical performance of uncoated foils, inner-facing and middle foils are characterized with a standard spectral curve of ETFE. For uncoated foils, it is possible to adjust the spectral data to

account for different thicknesses. For exterior-facing foils, there are two types of inputs that determine further procedures. Since for ETFE foils with a very small pattern, where individual geometries are 3-4mm and less, it is not possible to perform optical characterization only through coated parts, optical data of such foils are representative for the whole surface. Alternatively, in case of larger size patterns, optical data represents only the coated part. In this case, the final optical performance of the ETFE system is determined by calculating two systems, one with coated exterior foil and one for uncoated, that are later linearly interpolated based on a percentage of the coated surface. In order to calculate the performance of multilayered systems, process use spectral data, obtained through laboratory spectral characterization of samples using UV/VIS/NIR spectrometers, from producers or measured at the ThermALab at the Energy department of Politecnico di Milano. Measurements are performed at the normal incidence and contain hemispherical T, Rf and RB at 5nm wavelength increment for the wavelength range of 380nm-2500nm. Before importing into LBNL Optics, data was processed to comply with the required data structure. Spectral data of all samples were then stored in user-defined libraries under International Glazing Data Base (IGDB) that could be accessed by LBNL Window. Detail ETFE system optical and thermal characterization of COG and EOG was performed using standard procedures. Where coating and pattern types allowed different combinations, options were computed in Excel and then for the same performance levels, final selection has been chosen according to the visual criteria.

The last component in TFP, frame, is calculated separately as it does not interfere with other components. Since ETFE cushion has a variable thickness, that decreases towards frame where it gets to zero, thermal properties in EOG areas are the most critical points of the construction Figure 3 (left). Moreover, since the thermal impact of the frame in TFP is a quite small, more important aspect in frame simulation is hygro-thermal, or water vapor transfer and condensation risk. This risk is higher in humid climates with higher dew point temperature. These climates require special improvements to the fixing detail - Figure 3 (middle and right). This can be done either by an increasing distance between the layers (proposal 1) or increasing the size of the EPDM profile to extend contact length with ETFE (proposal 2). In both cases, there is no zero path length with a high-temperature difference between exterior and interior that creates condensation on interior surfaces stimulating fungal growth.

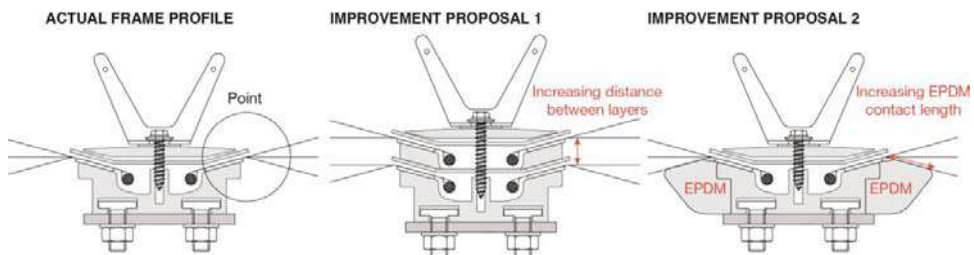


Figure 3: Improving weak spots in multilayered ETFE joints for extreme climates

3. Case Study 1 – Extreme Hot Climate: Shopping Mall, Manama, Bahrain



Figure 4: Corridor of the shopping mall in Manama (©Taiyo Europe MakMax)

The first of the case studies represent a project - Figure 4 located in extreme cooling dominated climate with the average dry bulb temperature from 6°C to 30°C and annual global solar irradiation of 2100kWh/m². Such a high environmental load required high thermal and optical protection. U-value of 1.31W/m²K was chosen to be adequate, that corresponds to the four-layered ETFE system - Figure 5. Similarly, the project required low g-value and since ETFE was placed on the roof of the shopping mall corridor, there were no constraints regarding optical clarity. The pattern with one of the highest coverages was Hexagon, with the 89% covered with silk-screen printed silver coating. This pattern allowed further adjustment of the coating type for fine-tuning g-value, one with high spectral selectivity and one with the standard.

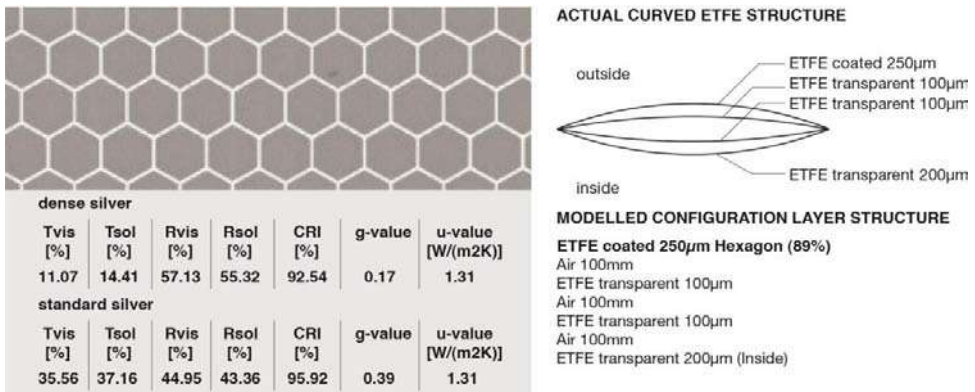


Figure 5: Multilayered ETFE properties of the shopping mall in Manama (extract of the report done by authors for Tai Europe MakMax)

4. Case Study 2 – Moderate Climate: CityLife, Milano, Italy



Figure 6: Atrium of the shopping mall in CityLife complex (©Taiyo Europe MakMax)

The second case study - Figure 6 is located in moderate heating dominated climate with the highest average summer dry bulb temperature of 39°C and annual global solar irradiation of 1400kWh/m². Moderate environmental loads required average thermal and optical protection and therefore three-layered ETFE system with U-value of 1.82W/m²K was used - Figure 7. Again, there were no constraints regarding optical clarity, yet g-value requirements were still high. In the coverage range from 70% to 80%, Negative dots in combination with dense coating provided optimal g-value of 0.34 and T_{vis} of 30%. The ETFE system was additionally successfully tested with raytracing simulations against a temporary increase of concentrated solar radiation caused by highly reflected glazing of the curved Zaha Hadid tower.

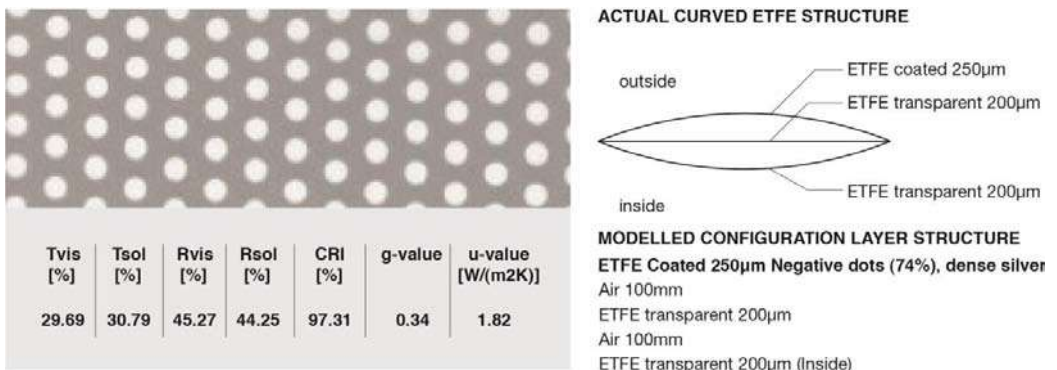


Figure 7: Multilayered ETFE properties of the shopping mall in CityLife complex (extract of the report done by authors for Taiyo Europe MakMax)

5. Case Study 3 – Extreme Cold Climate: Lakhta Center, St. Petersburg, Russia



Figure 8: Atrium of the multifunctional building in Lakhta Center complex (©Лакhta Центр)

Contrary to the previous two case studies, this project - Figure 8 is located in extreme heating dominated climate with the average dry bulb temperature from -4°C to 23°C and annual global horizontal solar irradiation of just 900kWh/m^2 . Again, high environmental loads demanded U-value of $1.31\text{W/m}^2\text{K}$ and four-layered ETFE system like in the case of Manama. Since this project is located in Russia, standards required modifications of boundary conditions to account for extremely low temperatures. All parameters followed standards ISO 15099 and NFRC 100-2010 (Wind speed: 5.5 m/s ; Indoor air temperature: 21°C ; Outdoor air temperature: -18°C ; Irradiation on surface: 0 W/m^2) except for outdoor winter temperature that was set to -26°C according to the client's requirements. Client in coordination with contractor performed experimental validation studies on a real scale prototype using the dual climatic chamber to verify simulation results. Values obtained by testing showed a minor discrepancy in comparison to the simulation ones. The project did not specify high requirements for g-value as solar radiation in this climate is considered beneficial. Unfortunately, the client did not allow the publishing of material and therefore there is no figure demonstrating the results of the study.

6. Conclusion and future works

Despite the advances in the building simulation tools, there are still challenges ahead in optical, thermal and computational fluid dynamics simulations, particularly when handling complex free-form geometries, thin materials and coatings. There are many levels of uncertainties that influence simulation accuracy. This can be caused by the simplification of geometry, materials and boundary conditions, reduction of dimensionality and parameter sets, thus neglecting angular dependency of system properties and multi-physics behaviour of the system. Therefore, future work will be focused on exploring more robust simulation approaches able to handle arbitrary complex cases with controllable deviations. In particular, the area of research will include 3-dimensional multi-physics simulation of complex geometries and materials including optical, thermal and CFD simulations. Furthermore, research will explore the dynamic and adaptive behaviour of the ETFE systems and its potential to mitigate seasonal environmental loads. A particular area of interest will be to study the angular-dependent influence of ETFE cushion curvature, material properties, air pressure states, turbulent air-flows inside ETFE cushions and middle layer movement on the optical and thermal behaviour of multi-layered ETFE systems.

On the other hand, future research will also cover simple and efficient simulation models with reasonable accuracy. In this way, research will explore the whole range of simulation tools and aim to assess accuracy for various Levels of Details (LODs) and consequently creating more effective ETFE workflows and processes. Knowing accuracy-LOD correlation for each design phase will allow greater confidence in exploring design options in early phases and gradual accuracy increase as approaching detailed design phases.

Acknowledgments

Authors would like to thank Taiyo Europe MakMax for their long-term collaboration and support providing project-based and research funding as well as field expertise and testing samples. Also, acknowledgements go also to the two labs of Politecnico di Milano: TextilesHUB - the Interdepartmental Research Laboratory (ABC department) where research took place and the ThermALab (Energy department) where ETFE samples were spectrally measured.

References

- Chilton, J. (2013). Lightweight envelopes: ethylene tetra-fluoro-ethylene foil in architecture. *Proceedings of the Institution of Civil Engineers - Construction Materials*, 166(6), 343–357. <https://doi.org/10.1680/coma.12.00049>
- Köppen, W. (1884). Die Wärmezonen der Erde, nach der Dauer der heissen, gemässigten und kalten Zeit und nach der Wirkung der Wärme auf die organische Welt betrachtet. *Meteorologische Zeitschrift*, 1(21), 5–226.
- Monticelli, C. (2015). Membrane claddings in architecture. *Fabric Structures in Architecture*, 449–480. <https://doi.org/10.1016/B978-1-78242-233-4.00014-0>
- NFRC. (2013). *ANSI/NFRC 100-2014 [E0A0] Procedure for Determining Fenestration Product U-factors*. Retrieved from https://c.yimcdn.com/sites/nfrccommunity.site-ym.com/resource/resmgr/2014_Technical_Docs/ANSI_NFRC_100-2014_E0A0.pdf

Proceedings of the TensiNet Symposium 2019

Softening the habitats / 3-5 June 2019, Politecnico di Milano, Milan, Italy
Alessandra Zanelli, Carol Monticelli, Marijke Mollaert, Bernd Stimpfle (Eds.)

Thermal performance of pneumatic cushions: an experimental evaluation

Andrea ALONGI*^a, Adriana ANGELOTTI*^a, Alessandro RIZZO^b, Alessandra ZANELLI^{ac}

*Politecnico di Milano, Energy Department,
v. Lambruschini 4A, Milano 20156, Italy,
adriana.angelotti@polimi.it

^aTextiles Hub, Politecnico di Milano, v. Ponzio 33, Milano 20133, Italy

^bCanobbio textile engineering srl, Strada Sgarbazzolo, Castelnuovo Scivria (AL) 15053, Italy

^cPolitecnico di Milano, ABC Department, v. Bonardi 3, Milano 21033, Italy

Abstract

In the recent past coated textiles and membrane structures have been increasingly implemented in architecture as either temporary or permanent external building envelopes. Double or multiple layer pneumatic cushions are frequently adopted. Therefore, one of their tasks is to guarantee suitable thermal conditions for the enclosed environment and/or limit HVAC energy consumption. The key thermal-physical parameter is then the cushion thermal resistance, which is usually assessed through simple calculations based on the assumption that cavities are approximated as rectangular enclosures. However, the impact of the actual shape of the cushions on the heat transfer has not been clarified yet. In this work, the thermal resistance of two cushions is experimentally assessed using a double chamber thermal setup. More precisely, two (double and triple layer) small vertical samples (1.1 m x 1.1 m) are exposed to a 25 °C steady-state temperature difference, to replicate Milan winter design conditions. Their exterior surfaces are divided in thermally homogeneous sub-surfaces of various sizes and temperatures are locally sampled on every sub-surface of both skins, along with the heat flux density on one side. Data are collected every 5 seconds for a time span of 12 h, in order to verify the steady-state assumption, and the average values for both temperatures and heat flux in every subsection are calculated. These data are then area-weighted and used to calculate the overall thermal resistance for each sample investigated, which are then compared with various correlations from literature.

Keywords: pneumatic cushion, thermal resistance, energy performance, measurement, heat flow, air gap, natural convection, multi-layered membrane skin.

DOI: 10.30448/ts2019.3245.02

Copyright © 2019 by A. Alongi, A. Angelotti, A. Rizzo, A. Zanelli. Published by Maggioli SpA with License Creative Commons CC BY-NC-ND 4.0 with permission.

Peer-review under responsibility of the TensiNet Association

1. Introduction

In the field of membranes structures, made of coated textiles or Fluor-polymeric foils, the pneumatic cushions are widely used with a variety of multilayered solutions, composed of 2 up to 5 layers, where the resulting air gaps are inflated to an extra-pressure of 200-300 Pa up to 600-900 Pa. Cushions can be also shaped with a quite high freedom by architects, while the manufacture optimization suggests adopting rectangular shapes, with a span of 3 meters and an almost infinite development in the other direction (Gomez-Gonzalez et al., 2011; Le Cuyet, 2008).

The thermal transmittance of the cushion (i.e. the U -value), together with the solar gain factor (i.e. g -value), is the fundamental thermal-physical property for evaluating the energy behavior of the textile envelope (Afrin et al. 2015), as in the dynamic simulations of the pressostatic sports halls analyzed in (Suo et al. 2015). The cushion thermal transmittance depends on the heat flow direction (horizontal, upwards or downwards) and on the number of layers, which determines the number of air gaps. According to (Knippers et al., 2010), both CEN EN ISO 6946 and CEN EN 673 can be used to estimate the center-of-the cushion thermal transmittance in a roughly similar way, although no calculation method is able to catch the non-steady state heat transfer mechanism connected to natural convection inside the air cavities. Following the standards calculations, for the horizontal heat flow direction, passing from a double layer cushion to a triple layer allows to reduce the wintertime U -value from about $3 \text{ W}/(\text{m}^2\text{K})$ to about $2 \text{ W}/(\text{m}^2\text{K})$.

The center-of-the cushion U -value, representing the portion where the layers are almost plane and parallel, does not take into account the impact of the curved shape of the cushion. Mainini et al. (Mainini et al., 2011) measure the thermal conductance of a double layer panel (dimensions: 1050 x 1140 mm) realized with two ETFE membranes, finding that $C = 5.158 \text{ W}/(\text{m}^2\text{K})$ and $U = 2.748 \text{ W}/(\text{m}^2\text{K})$. However, the two layers are parallel to each other and tensioned on an aluminum frame with no thermal break, therefore the effects of the typical curvature of the cushion are not considered. In turn in (Antretter et al., 2008) 2D CFD simulations on a large size double layer ETFE cushion with realistic curvature are performed, with the aim to study the flow patterns inside the cavity. For inclined cushions, one big roll is found with secondary flows in the upper and lower edges. For the horizontal cushion with heat flow upwards, several eddies are found, determining a good mixing in the cavity, a part from the edges.

Therefore further efforts are necessary to understand the heat transfer across cushions, including natural convection in the curved cavities, and then evaluate U -values more accurately than with present parallel planes assumptions.

2. Materials and Methods

This paper deals with a series of experimental tests performed on two pneumatic cushion samples of small size, namely a double layer and a triple layer with vertical orientation, in a laboratory apparatus. Collected data are processed to derive the thermal resistance and the thermal transmittance of each sample. The measured energy performances of the two cushions are then compared with each other. In the end experimental outcomes are compared to values obtained using literature correlations for free convection in vertical cavities.

2.1. The experimental setup

The experimental phase of this work consists of the evaluation of the cushion thermal resistance using a laboratory rig called Dual Air Vented Thermal Box (DAVTB), developed at the Building Physics Laboratory of the Energy Department of Politecnico di Milano. This setup is designed to test building envelope technologies under user-defined thermal boundary conditions (both in steady and unsteady state) and, if needed, to force an airflow through permeable components such as Breathing Walls. For the purpose of this study, the air flow loop is not used. A detailed description of the apparatus can be found in (Alongi et al. 2017).

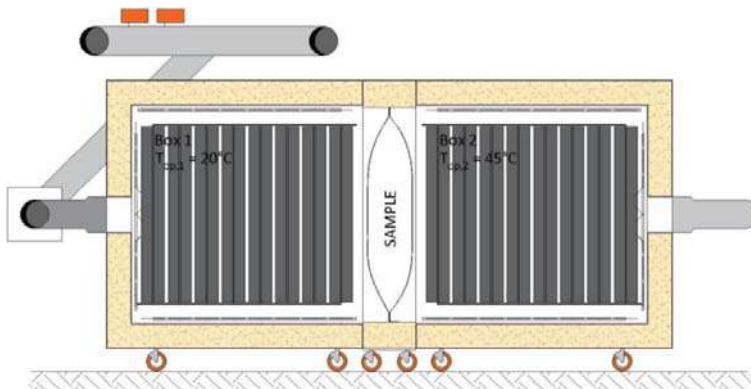


Figure 1: vertical section of the DAVTB apparatus. The radiant panels are visible both in Box 1 (left) and in Box 2 (right). The operative conditions adopted in this work are also reported, along with the cross section of one of the two samples experimentally investigated.

The DAVTB facility (Figure 1) consists of two insulated chambers (1.5 m x 1.5 m x 1.29 m each) divided by the sample and connected by the air recirculation system, used to generate an airflow through the sample, if needed. The operative temperature is set separately in each chamber, by means of a dedicated hydronic system providing both heating and cooling through radiant panels inside the boxes. The range of operative conditions achievable is between 15°C and 50°C. The sample is accommodated in a 1.5 m x 1.5 m metal frame interposed between the chambers and provided with thermal insulation, in order to minimize any edge effect. The

apparatus is supplied with two different frames: one is used to test regular 1 m x 1 m building walls with a maximum thickness of 30 cm, while the other one is dedicated exclusively to test 1.1 m x 1.1 m pneumatic cushions samples as in the present study. The measurement and control system in the DAVTB apparatus is based on an Agilent 34980A multifunctional switch unit, remotely controlled through a LabVIEW algorithm. As far as temperature measurements are concerned, they are sampled in various points of the hydraulic plant and in various locations inside each chamber, using T-type calibrated thermocouples (TC). A globe thermometer is installed in the geometrical center of each chamber to measure the operative temperature.

The thermal resistance of the cushion is measured through the heat flow and surface temperatures method, as in (GOST 26602.1-99). Therefore, 32 thermocouples and 16 heat flux meters (HFM) are installed to map temperature and heat flux density distribution on the sample surfaces. The HFMs are 5 gSKIN®-XM 26 9C (sensing dimensions 4.4 mm x 4.4 mm) and 11 gSKIN®-XI 26 9C (sensing dimensions 18.0 mm x 18.0 mm), with a ± 3 % calibration accuracy according to the manufacturer GreenTeg.

In order to experimentally assess the thermal resistance of the two cushion samples, a constant operative temperature difference across the sample has been set, reproducing equal the design winter condition in Milan i.e. $\Delta T = 25$ °C. Considering the operative temperature range achievable in the apparatus such temperature difference has been established by setting 20 °C in Box 1 and 45 °C in Box 2. Environmental data (i.e. operative temperature in each chamber) and surface data (temperature and heat flux density) have been collected every 5 s for a time period of at least 12 h, in order to obtain a stable set of data that could confirm the steady-state hypothesis.

2.2. The samples

As already mentioned, the main core of this work is based on the experimental evaluation of the thermal resistance of two pneumatic cushions samples, like the one shown in Figure 2 (cross section visible in Figure 1). Double and triple layer configurations have been investigated, i.e. SAMPLE01 and SAMPLE02 respectively, both based on PVC coated polyester fabrics with grammage of 700 g/m² and 900 g/m², to replicate the inner and the outer surfaces of a real cushion. Thermal emissivity of both layers has been found equal to 0.85 through FTIR spectrophotometry measurements. Both cushions are kept inflated at an internal extra-pressure of 300 Pa using an intermittent air compressor.

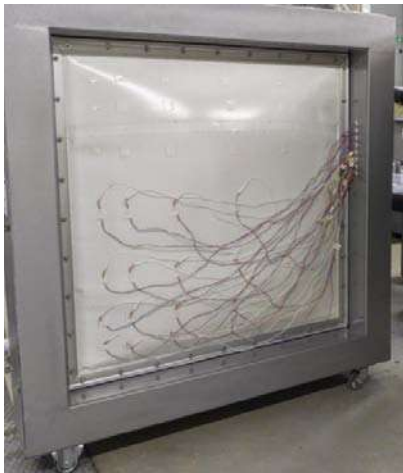


Figure 2: picture of the inflated SAMPLE01 (surface facing Box 2). Thermocouples and heat flux meters location is also visible.

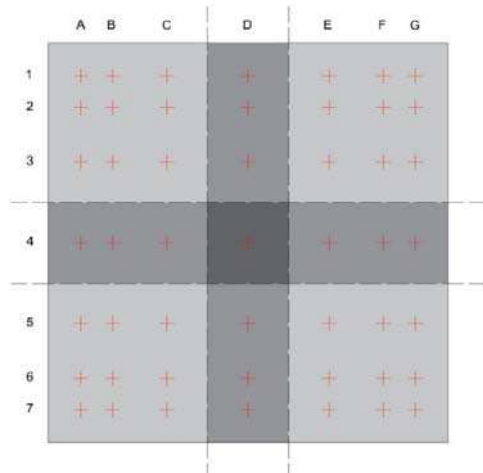


Figure 3: location on a general sample surface of the probing points, used as a reference for the mapping procedure of temperature and heat flux density. Overlapping areas are also visible.

For both cushions analyzed, the section is double-ogive shaped with a flatter region in the central section and steep tapering toward the edges. Due to this feature, temperature and heat flux density are expected to vary significantly throughout the surfaces. For this reason, the surfaces of the samples have been divided into 49 portions, with decreasing dimensions going from the center toward the edges (Figure 3). Surface temperatures and heat flows have been measured in the centers of each portion, indicated by the red crosses in Figure 3. Since the measured thermal emissivity of the heat flow meters is equal to 0.65, they are not matched in emissivity with the cushion materials. Therefore, HFMs have been covered with dedicated patches of the same textile material used to produce the cushions, to guarantee that they are subjected to the same radiative conditions of the investigated sample.

As it is possible to infer from Figure 3, the available amount of probes is not enough to cover the overall area in a single test. Therefore, the testing procedure applied to each cushion has been divided into four phases, in which temperatures and heat flux densities are measured on corresponding 4 rows-by-4 rows portions of the surfaces, as exemplified in Figure 2:

- phase 1 - from A1 to D4 on the Box 1 side and from D1 to G4 on the Box 2 side;
- phase 2 - from D1 to G4 on the Box 1 side and from A1 to D4 on the Box 2 side;
- phase 3 - from D4 to G7 on the Box 1 side and from A4 to D7 on the Box 2 side;
- phase 4 - from A4 to D7 on the Box 1 side and from D4 to G7 on the Box 2 side.

In this way, both the surfaces are covered completely, with data collected twice on column D and row 4 on both sides and four times on the D4 point. This redundancy allows to verify that

the same surface conditions have been achieved in different phases of the test, and thus all the collected data are coherent and can be treated as if they were gathered in a single test.

2.3. The data processing procedure

The most relevant data collected during every test are:

- the operative temperature $T_{op,1}$ for Box 1 and $T_{op,2}$ for Box 2;
- the surface temperature $T_{i,j,k}$ on each mapping point of both the sample surfaces, where, according to Figure 3, i represents the column (from A to G), j represents the row (from 1 to 7) and k represents the side of the sample (1 for the surface facing Box 1, 2 for the one facing Box 2);
- the heat flux density $\varphi_{i,j}$ on each mapping point of the surface facing Box 2.

Once steady state condition has been reached in a phase of the test, for every quantity mentioned above the time average is calculated. Those quantities that have been measured in more than one phase of the test have then been further averaged over the phases.

Subsequently the area weighted averages of surface temperatures and heat fluxes have been calculated using the following equations:

$$\bar{T}_{s,k} = \frac{\sum_{i=A}^G \sum_{j=1}^7 A_{i,j} T_{i,j,k}}{\sum_{i=A}^G \sum_{j=1}^7 A_{i,j}} \quad (\text{average surface temperature toward Box } k) \quad (1)$$

$$\bar{\varphi} = \frac{\sum_{i=A}^G \sum_{j=1}^7 A_{i,j} \cdot \varphi_{i,j}}{\sum_{i=A}^G \sum_{j=1}^7 A_{i,j}} \quad (\text{average heat flux density toward Box 2}) \quad (2)$$

where $A_{i,j}$ is the area surrounding the i,j mapping location on the sample surface. This comes from the hypothesis of thermal homogeneity over a given i,j area, and allows to mitigate any edge effect or singularity. The overall experimental thermal resistance of the cushion is then calculated as follows:

$$R_{\text{exp}} = \frac{\bar{T}_{s,2} - \bar{T}_{s,1}}{\bar{\varphi}} \quad (3)$$

The experimental thermal transmittance, that includes the effects of the surface heat transfer coefficient in the apparatus, is evaluated from the average values of operative temperatures and the average heat flux density calculated through (2), i.e.:

$$U_{\text{exp}} = \frac{\bar{\varphi}}{T_{op,2} - T_{op,1}} \quad (4)$$

At the same time, using the conventional values for the surface heat transfer coefficients (h_{ext} and h_{int} equal to 25 W/(m²K) and 7.7 W/(m²K) respectively), the standard thermal transmittance is calculated as:

$$U_{\text{std}} = \frac{1}{\frac{1}{h_{ext}} + R_{\text{exp}} + \frac{1}{h_{int}}} \quad (5)$$

The experimental thermal resistances R_{exp} for the two cushions derived through Eq. (3) are then compared to the thermal resistances in vertical cavities (i.e. parallel surfaces) calculated using natural convection correlations from literature, which are generally used to assess the overall performance of cushions. Neglecting the conductive resistance of the very thin fabric layers, the calculated thermal resistances of the cushions are:

$$R_{\text{calc,SAMPLE01}} = \frac{1}{h_{rd,cav} + h_{cv,cav}} \quad (6)$$

$$R_{\text{calc,SAMPLE02}} = \frac{1}{h_{rd,cav1} + h_{cv,cav1}} + \frac{1}{h_{rd,cav2} + h_{cv,cav2}} \quad (7)$$

where $h_{rd,cav}$ and $h_{cv,cav}$ are the radiative and convective heat transfer coefficients in the rectangular cavities, respectively. The first is calculated as:

$$h_{rd,cav} = \frac{4 \cdot \sigma \cdot T_m^4}{\frac{1}{\varepsilon_1} + \frac{1}{\varepsilon_2} - 1} \quad (8)$$

where σ is the Stefan-Boltzmann constant, T_m is the average between the two surface temperatures, ε_1 and ε_2 are the thermal emissivities of the two surfaces. As far as the convective heat transfer is concerned, it is calculated as a function of the Nusselt number (Nu) as:

$$h_{cv,cav} = Nu \cdot \frac{\lambda_{air}}{s_{cav}} \quad (9)$$

where λ_{air} is the air thermal conductivity evaluated at T_m and s_{cav} is the cavity thickness. Nu is then calculated alternatively using two correlations, therefore ending with two different values for the cavity thermal resistance. The first one is reported in (CEN EN 673, 2011) and is used as technical standard to deal with vertical cavities:

$$Nu = 0.035 \cdot (Gr \cdot Pr)^{0.38} \quad (10)$$

where Gr and Pr are the Grashof and Prandtl numbers respectively, calculated as:

$$Gr = \frac{g \cdot \beta \cdot \Delta T \cdot s_{cav}^3}{\nu_{air}^2} \quad (11)$$

$$Pr = \frac{\nu_{air} \cdot \rho_{air} \cdot c_{p,air}}{\lambda_{air}} \quad (12)$$

with g is the gravity acceleration (9.81 m/s^2), β is the thermal expansion coefficient of air defined, ΔT is the difference between surface temperatures, ν_{air} , ρ_{air} and $c_{p,air}$ are the air cinematic viscosity, density and specific heat at constant pressure respectively, all evaluated at T_m . The second is the Ostrach correlation reported in (Incropera et al., 2007):

$$Nu = 0.22 \cdot \left(\frac{Pr}{0.2 + Pr} \cdot Gr \cdot Pr \right)^{0.28} \left(\frac{h}{s} \right)^{-\frac{1}{4}} \quad (2)$$

where h is the height of the cavity. The validity ranges for this correlation are $Pr < 10^5$, $h/s = 2 \div 10$ and $Gr \cdot Pr = 10^3 \div 10^{10}$.

3. Results and Discussion

For both tests, the standard deviation of the boundary conditions lies in the range $0.03 \text{ }^\circ\text{C} \div 0.09 \text{ }^\circ\text{C}$, namely within the accuracy of the globe thermometers ($\sim 0.15 \text{ }^\circ\text{C}$). Therefore steady state conditions have been established with good accuracy across the samples. As an example of the outcomes of the tests, Figure 4 shows the surface temperature maps for SAMPLE01 obtained from the time-averaging process of the measurements.

First of all, a thermal stratification is clearly visible, with temperature rising from the bottom to the top of the sample surfaces. For SAMPLE01 on the central strip D the temperature increases by $3.2 \text{ }^\circ\text{C}$ on the surface towards Box 1 and by $2.9 \text{ }^\circ\text{C}$ on the surface toward Box 2. Similar results are obtained for SAMPLE02, for which the temperature increase from bottom to top on the central strip D is $3.0 \text{ }^\circ\text{C}$ on the Box 1 side and $3.8 \text{ }^\circ\text{C}$ on the Box 2 side. These trends are only partially caused by the thermal layering in both chambers (along the cushion height the air temperature increases by $0.9 \text{ }^\circ\text{C}$ in Box 1 and by $1.3 \text{ }^\circ\text{C}$ on Box 2), while the main cause are the convective phenomena inside the sample itself. It can also be noticed that the temperature variations are mainly located toward the edges, probably due to the shape of the sample section, as it is represented in Figure 1.

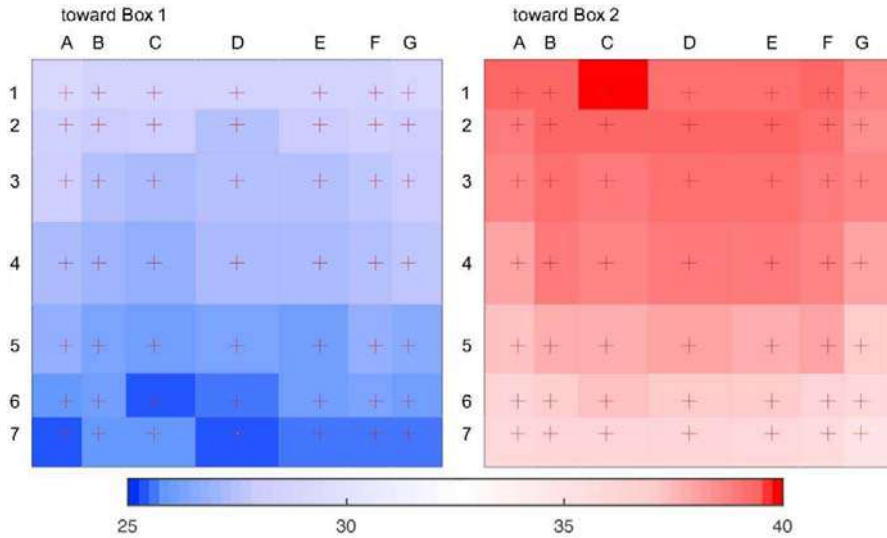


Figure 4: average surface temperature for both the surfaces (toward Box 1 and Box 2) obtained after the experimental investigation of SAMPLE01 (double layer cushion).

Table 1: average boundary conditions and weighted averages of surfaces temperatures and heat flow densities resulting from the tests performed on SAMPLE01 and SAMPLE02. Experimental thermal resistance, experimental transmittance and standard transmittance derived from tests

<i>sample</i>	$T_{op,1}$ °C	$T_{op,2}$ °C	ΔT_{op} °C	$\bar{T}_{s,1}$ °C	$\bar{T}_{s,2}$ °C	$\Delta \bar{T}_s$ °C	$\bar{\varphi}$ W/m ²	R_{exp} m ² K/W	U_{exp} W/(m ² K)	U_{std} W/(m ² K)
01	20.0	45.0	25.0	27.0	38.1	11.1	61	0.183	2.43	2.83
02	20.0	45.0	25.0	25.2	39.8	14.6	42	0.351	1.67	1.92

Table 1 shows for each cushion sample the average boundary conditions, the average surface temperatures and the average heat flow density. Under the same boundary conditions, the heat transfer through the triple layer cushion is 31% less than through the double layer one. The thermal resistance R_{exp} reported in Table 1 is equal to (0.183 ± 0.009) m²K/W and (0.351 ± 0.015) m²K/W for the double and the triple layer sample respectively, with expected combined errors equal to 4.8 % and 4.4 %. These results show that, even though the overall thickness of the sample is only increased slightly going from two to three layers, therefore switching from one larger to two thinner cavities, the overall thermal resistance of the cushion almost doubles (+ 91%). This might be explained by the reduction of the average thickness of the cavity that partially inhibits the convective motions, therefore reducing the heat transfer, as demonstrated also by the reduction of the average heat flux density and the rise of the average surface temperature difference. In terms of thermal transmittances (Table 1), the triple layer cushion U -value is about 30 % lower than the double layer U -value. The laboratory thermal transmittance U_{exp} is generally lower than the standard one U_{std} , indicating that convective-radiative heat

transfer coefficients in the boxes are lower than the standard ones. Indeed the purpose of the experimental measurements is mainly to compare the performances of the two cushions, rather than deriving U -values according to standard conditions.

By adopting air thermo-physical properties according to the thermal conditions observed during the experimental measurements and summarized in Table 1, the rectangular cavity convective-radiative thermal resistances R_{calc} have been calculated, treating the cavity thickness as a parameter. The results are reported in Figure 5 (red lines based on Ostrach correlation, blue lines based on the technical standard) and compared to the experimental results (black lines). Analysis has been performed within the range of validity and results are only taken into account when the convection is active (i.e. $Nu > 1$). For the triple layer sample, the cavity thickness indicated in Figure 5 refers to each of the two cavities.

By adopting air thermo-physical properties according to the thermal conditions observed during the experimental measurements and summarized in Table 1, the rectangular cavity convective-radiative thermal resistances R_{calc} have been calculated, treating the cavity thickness as a parameter. The results are reported in Figure 5 (red lines based on Ostrach correlation, blue lines based on the technical standard) and compared to the experimental results (black lines). Analysis has been performed within the range of validity and results are only taken into account when the convection is active (i.e. $Nu > 1$). For the triple layer sample, the cavity thickness indicated in Figure 5 refers to each of the two cavities.

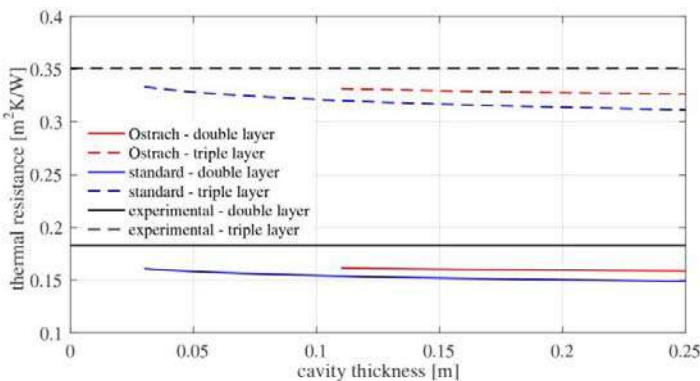


Figure 5: comparison between the experimental thermal resistances, obtained for both Box 1 and Box 2, and the results achieved using correlations from literature for vertical rectangular cavities.

As Figure 5 shows, calculated thermal resistances underestimate the measured values in both double and triple layer samples, with a slightly lower discrepancy for the thermal resistances calculated on the base of Eq. (13). If the average thickness of the double layer cushion is set to 19 cm, the calculated thermal resistance is 13-18 % less than the measured one, depending on the natural convection correlation adopted. If the average thickness of each cavity in the triple

layer sample is set to 11 cm, the calculated thermal resistance is 6-9 % less than the measured one. The discrepancy between measured and calculated values is larger than the measurement accuracy. Moreover, it can be noticed that it is not possible to find any equivalent thickness that allows to represent the heat transfer across a cushion with a vertical cavity with parallel surfaces. A possible explanation might be that the peculiar shape of the sample sections, with the tapering edges, significantly diverges from the simplified models geometry. This shape could also lead to the formation of stagnation regions inside the cushions, that might affect and reduce the overall convective phenomena, in agreement with the studies by (Antretter et al., 2008). Therefore, the next step in this work will be the assessment of this hypothesis through CFD simulations.

4. Conclusions

The main objective of this work was to compare the heat transfer performance of double layer and triple layer pneumatic cushions, by taking the effective curved geometry of the cushions into account. To this purpose, an experimental study on two small vertical samples was performed using the DAVTB apparatus, with some adaptations with respect to the original configuration in (Alongi et al. 2017). Temperature and heat flux density distributions have been mapped on both surfaces of each sample over the steady-state part of 12 h tests, and have then been used to calculate the area weighted average of the corresponding quantity. The results of this process have finally been used to calculate the overall experimental thermal resistance of the two samples, obtaining $0.183 \text{ m}^2\text{K/W}$ and $0.351 \text{ m}^2\text{K/W}$ for the double and the triple layer cushion respectively, with an estimated accuracy below 5 % in both cases. This shows that going from a single large cavity to two smaller ones almost doubles the overall thermal resistance of the cushion. No calculation of thermal resistance of a vertical rectangular cavity is able to effectively portray the actual behavior of the samples: both correlations analyzed tend to underestimate the experimental thermal resistances. This might be due to the unique shape of the sample cross-section, that could generate stagnation regions where the convective motions are inhibited, thus the overall insulating performance is better than what predicted by the simplified models behind the correlations.

In the future, this work will be developed on two sides: first of all, new samples will be experimentally investigated, possibly introducing textile materials provided with low emissivity coating; secondly, the convection inside the cushions will be further investigated by means of CFD simulations, in order to better understand the air motion with respect to what happens inside comparable rectangular cavities.

Acknowledgements

The authors warmly thank Prof. Alfonso Niro and Dr. Damiano Fustinoni for the FTIR spectral characterisation of the PVC coated polyester samples and of the Heat Flow Meters.

References

- Afrin, S., Chilton J., Benson L. (2015) "Evaluation and Comparison of Thermal Environment of Atria Enclosed with ETFE Foil Cushion Envelope" in: *Energy Procedia*, vol. 78, p. 477-482.
- Alongi A., Angelotti A., Mazzarella L. (2017), Experimental investigation of the steady state behaviour of Breathing Walls by means of a novel laboratory apparatus. In: *Building and Environment*, vol. 123, p. 415-426.
- Antretter F, Haupt W, Holm A. Thermal Transfer through Membrane Cushions Analyzed by Computational Fluid Dynamics. 8th Nordic Symposium on Building Physics in the Nordic Countries 2008. Copenhagen, Lyngby, p. 347-354.
- CEN EN ISO 6946 (2017), Building components and building elements. Thermal resistance and thermal transmittance. Calculation methods, CEN.
- CEN EN 673 (2011), Glass in buildings. Determination of the thermal transmittance (U value). Calculation method, CEN.
- Gomez-Gonzalez A., Neila J., Monjo J. (2011), Pneumatic skins in architecture. Sustainable trends in low positive pressure inflatable systems. In: *Procedia Engineering*, vol. 21, p. 125-132.
- Incropera F., Dewitt D., Bergman T., Lavine A. (2007), *Fundamentals of Heat Transfer*, 6th ed, John Wiley and Sons, USA.
- Interstate Standard of Russian Federation GOST 26602.1-99 (1999), Windows and doors. Methods of determination of resistance to thermal transmission.
- Le Cuyet, A. (2008) *ETFE: Technology and Design*, Birkhauser.
- Knippers J., Cremers J., Gabler M., Lienhard J. (2010), *Construction Manual for Polymers + Membranes*, Birkhauser, Basel, Switzerland.
- Mainini A.G., Poli T., Paolini R., Zinzi M., Vercesi L. (2012), Transparent multilayer ETFE panels for building envelope: thermal transmittance evaluation and assessment of optical and solar performance decay due to soiling. In: *Energy Procedia*, vol. 48, p. 1302-1310.
- Suo H., Angelotti A., Zanelli A. (2015), Thermal-physical behaviour and energy performance of air-supported membranes for sports halls: a comparison among traditional and advanced building envelopes. In: *Energy and Buildings*, vol. 109, p. 35-46.

Proceedings of the TensiNet Symposium 2019

Softening the habitats / 3-5 June 2019, Politecnico di Milano, Milan, Italy
Alessandra Zanelli, Carol Monticelli, Marijke Mollaert, Bernd Stimpfle (Eds.)

Assessment of building Physical Aspects of a New Angular Selective 3D – Prototype Foil (ETFE)

Jan CREMERS*, Hannes MARX*

*Stuttgart University of Applied Science, Schellingstr. 24, Stuttgart 70174, Germany,
jan.cremers@hft-stuttgart.de

Abstract

Buildings, which boast a high transparency into the façade or roof area without an appropriate sun protection, have a common problem of overheating due to solar heat gains (SHGC) in the summer. Especially lightweight-buildings with typical transparent materials, such as polymer-film of transparent ethylene-tetra-fluoro-ethylene (ETFE) have a very high solar transmission [T_{sol}] greater than 93% (200 μm).

The combination with a membrane cushion improves the thermal transmission coefficient (U-value) according to the number of layers (air gaps). A three-layer ETFE foil construction has an U-value of about 2.1 [$\text{W}/\text{m}^2\text{K}$] (Knippers, 2011, p.216)].

For the unshaded case passive solar gains (SHGC) enter the building via the transparent ETFE foil cushion resulting in considerable high cooling energy loads and the risk of thermal- and visual discomfort (glare effects) in the summer case. In this paper we assess a new selective 3D-Prototype foil (sun protection) concerning the building physical aspect of the angle-dependent transmittance [τ], reflectance [ρ] and solar heat gain coefficients (SHGC) for the building envelope. Further aspects of this new development have been published before, cp. (Cremers and Marx, 2017a, 2017b, 2017c).

Keywords: ETFE, Solar energy, membrane cushion, prototype

DOI: 10.30448/ts2019.3245.01

Copyright © 2019 by J. Cremers, H. Marx. Published by Maggioli SpA with License Creative Commons CC BY-NC-ND 4.0 with permission.

Peer-review under responsibility of the TensiNet Association

1. Introduction

In this study, special modifications of plastic foils are investigated and developed in order to achieve a targeted regulation of the visual and solar radiation for the building envelope. A single layer of transparent ETFE foil (Nowoflon ET 6235 Z) has a solar heat gain coefficient (SHGC) of about 93 % (Product Data Sheet, Nowoflon) and the combination of a three layer foil construction with 2 air gaps of each 0.50 m has a SHGC of about 75 % (Nowoflon brochure, pp. 7). A well-established form to appropriately modify the visual and radiation properties is printing, tinting, coloring or applying coatings on foils. Compared to the current state-of-the-art shading technology, the main disadvantage of shading solutions for foils is the constant transmittance [T_{sol}] and reflection coefficient [ρ_{sol}] regardless of the incidence angle of the sun.

Therefore, the new 3D foil is based on the shed roof principle (saw-tooth roof) for sun protection.

The advantage of this approach is to block off the energy intensive direct sun light and to let in diffuse sunlight for the daylight quality into the building. This reduces the cooling energy loads and improves the thermal- and visual comfort inside the building. The idea reflects on a realized ETFE building example, the shopping mall "Dolce Vita Tejo" close to Lisbon (Amadora), which possesses a shed roof principle of membrane cushion. The dimension of each membrane cushion is approximately 10 m x 10 m (Knippers, 2011, p. 256).

In this context we manufactured the selective prototype foil with a hemisphere geometry (diameter of 0.02 m) on a millimeter scale similar to a bubble wrap foil. As the first step in the manufacturing process, the foil is printed with a flat printing pattern adjusted to the sun position (Stuttgart, Germany) and the spatially transformed geometry (hemisphere), sub sequentially foil is spatially transformed.

This allows for the same geometry (hemisphere) to be simply adjusted by varying the printing pattern for each project regarding the location.

2. Pneumatic multilayer foil construction

2.1. Construction (ETFE foil cushion including the new 3D - Foil)

Basically, pneumatically stabilized multilayer foil constructions are clamped typically with an aluminum frame system at the edge, which is held by a corresponding load-bearing substructure (one layer ETFE foil $\approx 350 \text{ g/m}^2 @ 200 \text{ }\mu\text{m}$). The pneumatically stabilized foil cushions can consist from two to five layers of foil. Conventional foil width for ETFE (Nowofol ET 6235 Z) is 1550 mm, whereby the foil length is optional. In order to guarantee greater wingspan, welding

or gluing of the material (3D foil) is necessary for the future use. Conceivable joining techniques could be done by welds or UV-stable bonded joints. Characteristic foil thickness varies according to static and design requirements between 80 μm to 300 μm

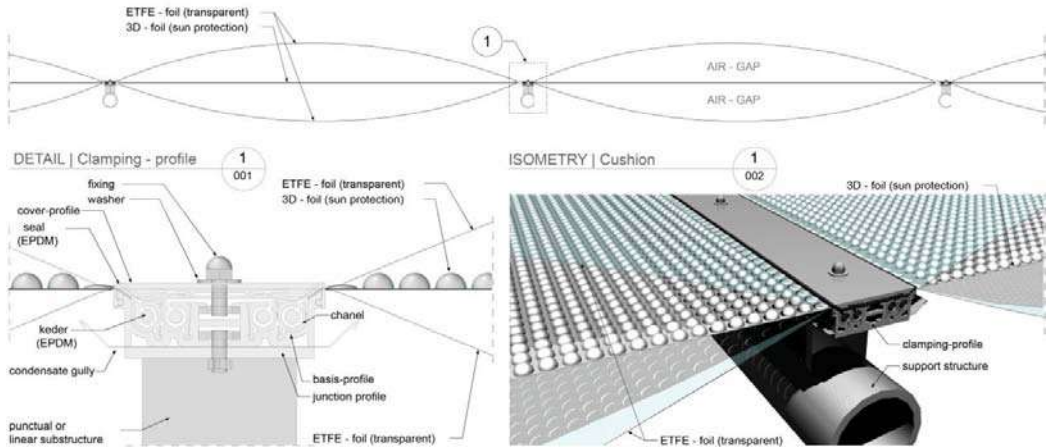


Figure 1: Pneumatic three layer foil construction: (ETFE transparent 200 μm + 3D foil 250 μm + ETFE transparent 200 μm)

The main application setup of the new 3D foil would be between two foil layers (external and internal), this means that the minimum requirement is a three-layer foil construction with an U-Value of about 2.1 [W/m²K]. The shape of the cushion geometry for pneumatic multilayer foils is stabilized by a low-pressure air system at an overpressure level of approx. 200 Pa to max. 800 Pa, depending on the cushion size. Consequently, the benefit is: no external environmental influences of weathering, soiling, chemical influences (ambient air quality), contamination and cleaning processes. Furthermore, the exposition to UV radiation on the 3D foil can be additionally reduced by the external foil layer. Stress due to pressure- and suction effects e.g. by snow, water or wind loads can be targeted by cutting a small hole into the 3D foil to enable pressure equalization. This means that practically no mechanical stress is transmitted to the middle foil layer (3D foil). The power is transferred to the following inner foil layer.

This "protected installation" improves the durability of the 3D foil. Further benefits are no complex cutting patterns of the 3D foil, which means a significant cost reduction and manufacturing process within the planning. The new selective 3D – Prototype foil

3. The new selective 3D – Prototype foil

3.1. Material and coating

ETFE has a non-polar surface so therefore is a special procedure necessary in which increases the surface energy, this allows coating on ETFE foils (Moritz, 2007). However, the complex

coating process and the random-like 3D-shape quality (no precise form) of ETFE foils (Nowoflon ET 6235 J @ 100 μm and 200 μm) after spatially transforming by thermoforming cf. Figure 2, left, have led to the choice of another suitable material for the first stage of the prototype foil. The 3D - prototype foil is made of Polycarbonate material (PC) with a thickness of 1000 μm that allows to achieve the effect.

A suitable ETFE material thickness for the 3D foil in the construction sector would be 250 μm to 300 μm for the practical usage. It is because a material thickness less than 200 μm indicates due a durable deformation regarding in manufacturing, packaging, transport and installation by one-off external power. Tests have shown this by manufactured ETFE foils in thickness of 100 μm and 200 μm . A material thickness higher than 300 μm is not suitable for economic use (referred to investment) and the technical limitations of the roll-to-roll process is max. 500 μm .

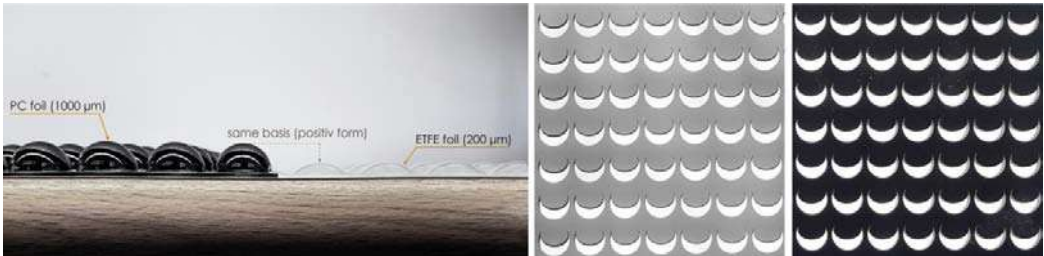


Figure 2: Prototype: spatially transforming of PC foil (1000 μm) and ETEF foil (200 μm); coating layers (silver and black).

A modified coating structure for the lighting- and radiance properties is determined by a repro- and screen printing process. The first layer is a black coating for minimum solar transmission (the view from inside). Afterwards, the second layer is a silver coating for maximum solar reflection coefficient (the view from outside).

3.2. Geometry and printing pattern

The geometry of the spatially transformed foil is a hemisphere and the additionally printing pattern considers the position of the sun by the zenith- and azimuth angles for Stuttgart, Germany. The hemisphere diameter is 20 mm (a) and the distance between each hemisphere is 3.21 mm (b), see Figure 3. The total printing proportion of the flat print (before spatial transformation) amounts to 76 % and the total printing proportion of the 3D foil changes due to spatial transformation to 63 %.

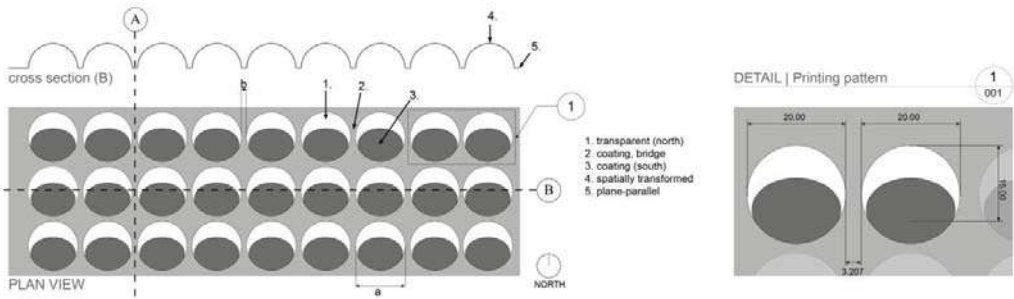


Figure 3: Plan view and Detail of the 3D Prototype

The coating on (2.) and (3.) have the same lighting- and radiance characteristics to minimise the solar transmission. Meanwhile, position (1.) should allow as much diffuse sunlight as possible to enter and does not require any additional coating (maximum visual transmission), see Figure 3.

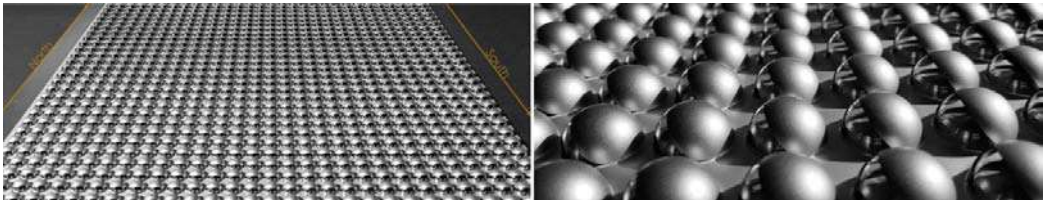


Figure 4: Finalized PC foil prototypes (dimension: 700 mm x 700 mm)

3. Building Physical Aspects

The important building physical aspects for a building envelop in summer is solar protection and in winter thermal insulation of the internal thermal condition (e.g. by thermal transfer, thermal radiation, thermal convection), sound insulation, sound absorption, control of humidity as well as the optical properties (e.g. SHGC, T , ρ , α). This is essentially for concept, planning, practical construction and utilization of a well-functioning building envelope.

Foil cushions have a highly dynamic thermal transmittance coefficient (U-value) which is significantly influenced by the thermal convection inside the cushion and radiation - and therefore by the membrane cushion geometry.

The multi-layer construction can reduce the thermal heat transfer but this leads to a change of the optical properties. Consequently, an assessment is made of the optical properties of the new angular selective sun protection (3D foil).

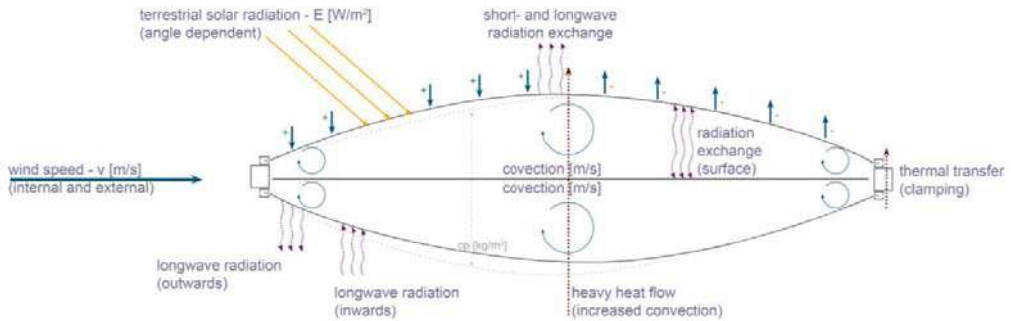


Figure 5: Building physical aspect of a multi layer foil cushion

4. Results and discussion

4.1. Optical Properties: Angular measurement data (spectral transmissions- and reflection coefficient)

For the manufactured selective prototype foil from paragraph 3, measurements of the angle-dependent variation of transmission- and reflection coefficient, in an interval of 15° to the surface normal were conducted. The vertical radiation source is at an angle of 90° . Meanwhile at an angle of 150° , the radiation source is directed towards the transparent open north side of the hemisphere. At an angle of 30° , the radiation falls on the fully printed south side.

Within the measurement, the simulation of the sun's solar path over the azimuth and zenith angles is not taken into account. There are two different variations in Figure 6, the black characteristic curve is a conventional flat printed ETFE foil with 65 % of silver printing "ETFE silver printing" and the new 3D foil with 63 % of silver printing: "hemisphere, printed".

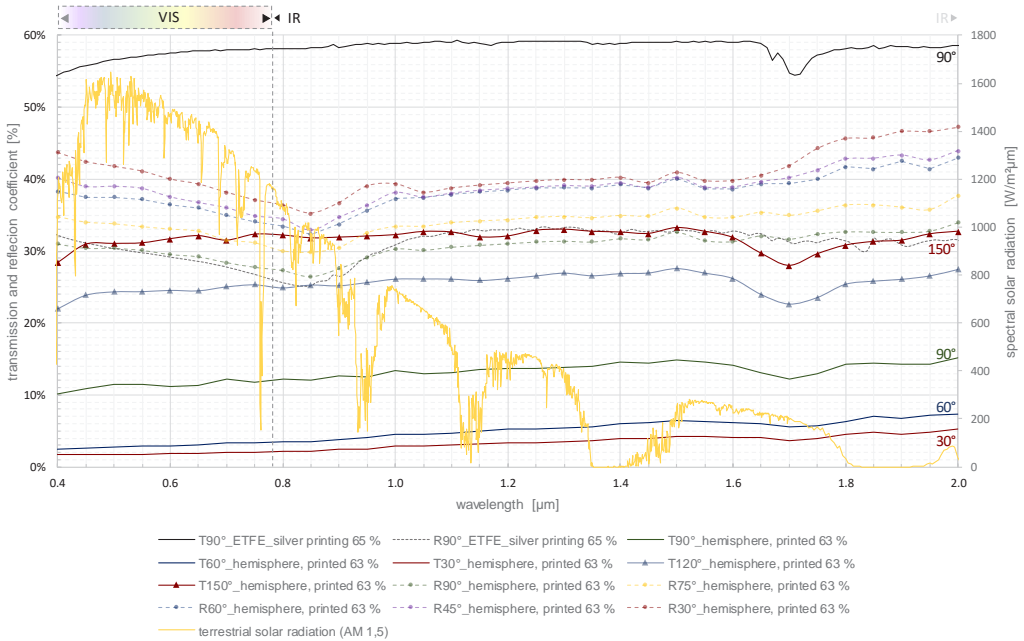


Figure 6: Spectral data (reflection- and transmission coefficient)

Figure 6 displays reflection and transmission coefficients for different angles in the wavelength range $[\lambda]$ from 400 nm to 2000 nm. The spectrum of terrestrial solar radiation (AM 1,5) $[W/m^2\mu m]$ is plotted on the secondary axis. This is the primarily reason for the solar energy inside the building and for overheating.

A decrease of the transmission with the angles between 90° to 30° is recognizable, meanwhile an increase of the transmission within the angles of 120° and 150° compared to the variant "ETFE silver printing" can be seen. As a result, the solar and visual transmittance within the 3D foil varies heavily depending on the angle of radiation. The absolute difference is around 30 % ($T_{vis}-T_{sol}$: 30-31 % at 150° and $T_{vis} - T_{sol}$: 2 % at 30°). Furthermore, the measurement indicates for the incident angle of 60° , the result of the spatial transformation can achieve an improvement by reducing the solar transmission by 87 % and the visual transmission by 82% compared to the variant without the spatially transformed (flat printing) on the basis of measurements.

Compared with the reflection coefficient of "ETFE silver printing 65 %", the 3D foil shows good agreement for the radiation incidence of 90° . The incidence of 30° shows an increase of the solar reflectance by a factor of 1.6 from 2D to 3D foil. The missing optical parameters (angles) were interpolated between the measured radiance properties done according to formula (1).

$$Y_n = Y_1 + \frac{Y_2 - Y_1}{x_2 - x_1} * (x_n - x_1) \tag{1}$$

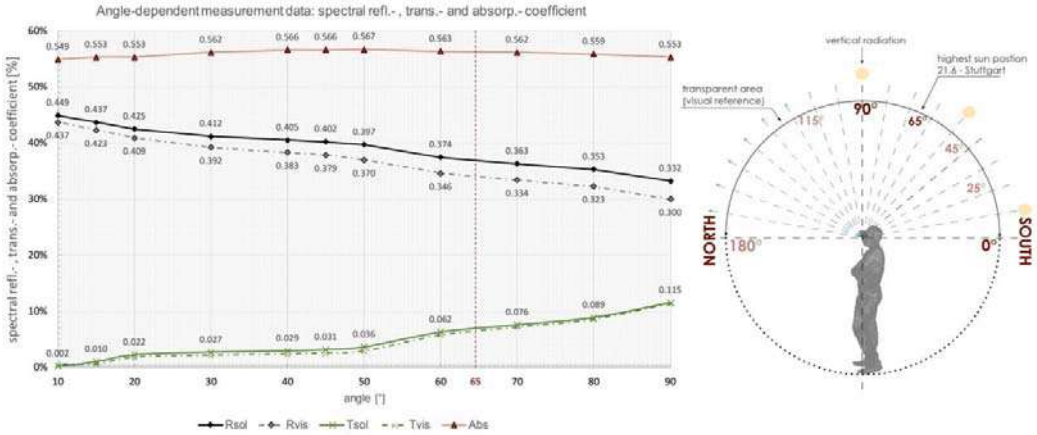


Figure 7: Angle-dependent reflection-, transmission- and absorption coefficient of new 3D foil material (Data interpolated from measurements by ZAE-Bayern e.V.)

4.1. Solar Heat Gain Coefficient (SHGC)

The "SHGC" of the new angle selective 3D foil was measured at an outside sun test facility at ZAE-Bayern in the climate region of Würzburg "WU" (49.786°, 9.967°) (Germany). The sun position is very close to Stuttgart "STR" (48.776°, 9.183°) (Germany). The highest sun position in Würzburg is on June 21st with an angle of 64° (STR 65°), the lowest sun level is on December 21st with an angle of 17° (STR 18°) and the equinox is on March 21st with a maximum of 41° (STR 42°).

There are two different measurements of the angle to the sun (90° and 55°) for two variants of foils (2D and 3D). One version is the 3D foil as described in chapter 3 with the spatial transformation. The other version is the 2D foil, before the spatial transformation but with the identical printing pattern as the 3D foil.

Table 1: Solar heat gain coefficient (outside sun stand) in Würzburg, Germany. Measurement data by ZAE – Bayern.

Description	Angle to the sun	Solar Heat Gain Coefficient (SHGC)	Deviation
3D foil, hemisphere, printed 63 %	90°	0,26	+- 0,05
3D foil, hemisphere, printed 63 %	55°	0,16	+- 0,05
2D foil, plane, printed 76 %	90°	0,29	+- 0,05

2D foil, Plane, printed 76 %

55°

0,28

+/- 0,05

The results of the "SHGC" measurement of change by spatially transforming at the angle of sun with 55° amount a reduction of 75 % (3D foil: 0,16 and 2D foil: 0,28).

5. Conclusion & outlook

This paper makes an assessment of building physical aspects, in detail of the optical properties (SHGC, T, ρ, α) of a new 3D – foil Prototype, by evaluation of measurements. The basis is the manufactured angular selective 3D – Prototype Foil for the location Stuttgart (Germany). One important special modification of the plastic foil was necessary. The foil is not only printed with a pattern, but also additionally spatially transformed through a hemisphere geometry. The modifications were made under the premise of sufficient daylight quality. Light is entering only by diffuse daylight through the transparent area of the hemisphere, in the style of the shed roof effect.

The significant aim of reducing the solar transmission (sun protection) of about the factor 2 compared to the flat printing (not additionally spatially transformed) is achieved for the relevant angles between 0° and 65° for Stuttgart.

The maximum solar transmission (T_{sol}) is 11 % at an angle of 90° to the sun. Meanwhile, at an angle of 60° to the sun transmission (T_{sol}) amounts to only 6 %. The solar reflection amounts to 37 % at an angle of 60° to the sun with a constant absorption coefficient of about 56 %. The "SHGC" amounts to 16 % at an angle of 55° to the sun.

The visual transmission (T_{vis}) amounts to 24 % at 120° and 31 % at 150°.

Table 2 lists a summary and comparison of all relevant optical properties. The angle dependent low level of "SHGC" by the 3D foil compared to the other solutions is very noticeable.

Table 2: Summary and comparison of the optical properties (ETFE, PC, Glass). Source: ¹: (Knippers 2011 p. 115), ²: (Nowoflon brochure), ³: (Schnittich 2006 p. 126), ⁴: (Glastroesch).

	ETFE FOIL			PC FOIL			GLASS		
	SINGLE - LAYER ¹ (transparent)	THREE - LAYER ¹ (transparent)	THREE - LAYER ¹ (IR-cut)	2D - SINGLE - LAYER (90°)	3D - SINGLE - LAYER (90°)	3D - SINGLE - LAYER (55°)	SINGLE ²	DOUBLE ²	DOUBLE ² (solar glass)
Thickness Composition [µm]	F-200 µm	F-200 µm F-200 µm F-200 µm	F-200 µm F(IR)-200 µm F-200 µm	F-1000 µm	F-1000 µm	F-1000 µm	G-4 mm	G-6 mm A-16 mm G-4 mm	G-6 mm A-16 mm G-4 mm
Visible light transmittance [%]	92 %	71 %	44 %	22 %	12 %	3 %	89 %	41 %	19 %
solar transmittance [%]	93 %	74 %	38 %	20 %	11 %	4 %	83 %	20 %	12 %
visible light reflection [%]	7 %	24 %	11 %	45 %	29 %	34 %	8 %	18 %	29 %
solar reflection [%]	6 %	22 %	11 %	45 %	31 %	38 %	8 %	32 %	25 %
Solar heat gain coefficient [%]	93 %	75 %	41 %	29 %	26 %	16 %	85 %	22 %	17 %
thermal transmittance coefficient [W/m ² K]	6.9	2.1	2.1	6.5	6.5	6.5	5.6	1.0	1.1
printing proportion [%]	0 %	0 %	lined	76 %	63 %	63 %	0 %	0 %	lined

The next step will be to manufacture prototypes with ETFE foil with a thickness of 250 µm to 300 µm. Furthermore, it is possible to improve the coating with regard to a better reflection coefficient and this should lead to an even lower absorption coefficient.

Acknowledgements

The project "FMESG" is funded by the German

Federal Ministry for Economic Affairs and Energy

(BMW, project code 03ET1309F).

Supported by:



on the basis of a decision
by the German Bundestag

References

Cremers J., Marx H. (2017a), 3D-ETFE: Development and evaluation of a new printed and spatially transformed foil improving shading, light quality, thermal comfort and energy demand for membrane cushion structures, CISBAT 2017, In *Energy Procedia* 122 115-120.

Cremers J., Marx H. (2017b), Improved daylight comfort by a new 3D-Foil that allows to trade off solar gains and light Individually, STRUCTURAL MEMBRANES 2017.

Cremers J., Marx H (2017c), A new printed and spatial transformed ETFE foil provides shading and improves natural light and thermal comfort for membrane structures, PLEA 2017, Volume III, 3620 – 3627.

Glastroesch, Product Data Sheet - Sun protection glasses (Silverstar), 2014.

Knippers J., Cremers J., Gabler M., Lienhard J. (2011). *Construction manual for polymers + membranes: Materials and semi-finished products, form finding and construction*. Munich, Germany, Edition DETAIL.

Moritz K. (2007) *ETFE-Folie als Tragelement*, Dissertation, Munich, Germany, Technical University Munich

Nowoflon, Product Data Sheet, Physical Properties Nowoflon ET 6235 Z (2015).

Nowoflon, brochure, Nowoflon ET 6235 Z-IR, ETFE Heat Absorbing Film (2015).

Schnittich, Staib, Balkow, Schuler, Sobek (2006), *Glasbau Atlas* Munich, Germany, Edition DETAIL.

Proceedings of the TensiNet Symposium 2019

Softening the habitats / 3-5 June 2019, Politecnico di Milano, Milan, Italy

Alessandra Zanelli, Carol Monticelli, Marijke Mollaert, Bernd Stimpfle (Eds.)

Impact of Technical Textile Envelopes on the Perception of Indoor Comfort in Minor Sports Facilities

Aldina SILVESTRI*, Teresa VILLANI*

*Dip. of Planning, Design, and Technology of Architecture, Sapienza University of Rome
Via Flaminia 70, 00196, Rome, Italy
aldina.silvestri@uniroma1.it

Abstract

The main focus of this research is the Light Envelope, a specific and not widely known type of building envelope produced with technical textiles. In particular we focus on a highly widespread type of construction, textile sports facilities. To define the scope of the present paper, the field of investigation was restricted to minor sports facilities. The focus is on the study of the impact this technology has on the users' perception of environmental indoor comfort. A direct experimentation permitted the concrete definition of the problem at the base of the research: the conditions of absolute discomfort experienced during sporting practice in these indoor spaces. –We subsequently drew an evaluation and comparison of the different products (or technical solutions) for the envelope, in order to outline the effects of each product on indoor comfort perception. This final step aimed to highlight and compare the various technical solutions currently available. This analysis is a valuable tool for end users (technician / designer) when making the appropriate choices for a correct design of the cover itself. Finally, an innovative package for the cover was proposed which, due to its characteristics, could represent a quality prototype whose utilization can be widely spread for the construction of this type of buildings.

Keywords: Sport facilities, comfort perception, comfort indoor, textile envelope, technical textiles.

DOI: 10.30448/ts2019.3245.31

Copyright © 2019 by Aldina Silvestri, Teresa Villani. Published by Maggioli SpA with License Creative Commons CC BY-NC-ND 4.0 with permission.

Peer-review under responsibility of the TensiNet Association

1. Introduction

The spread of indoor sports practiced in Italy (ISTAT, 2005) has determined the need for sports facilities on a local scale, which we could define as "minor". The smaller sports facilities can have different configurations and different construction technologies, from the traditional "heavier" to the light ones; they can be covered, uncovered or semi-open (with removable cover). The characteristic that distinguishes them from large systems is the service of neighbourhood: a limited number of users are needed; they have a low turnout; they are small in size; they do not host large events; they remain part of a "local" reality, which often also identifies the social context. These sports facilities are today the most widespread type in Italy. Precisely because of their value as an "centre of attraction" they are often overused, even if in unsuitable conditions, often reaching levels of degradation or inadequacy (technical, functional, equipment etc.), although they are also used by many professional athletes. In fact, just only in the last decade the number of professional athletes throughout the national territory increased from 3,415,905 to 4,500,327 (Uva, 2014). Therefore, the operation that should be encouraged is to promote sports activities through welcoming infrastructures and services, capable of hosting as many users as possible, and at the same time promoting the practice of sport carried out in conditions of absolute physical, physiological and mental well-being.¹ Despite a substantial European research activity that focuses on the formal architectural of minor sports facilities (or facilities for young people), in relation to their use in Italy today, many researches follow a different methodology: given the lack of construction land, the possibility of a "rebirth" of minor structures for sport is often sought through the - necessary - recovery of disused spaces, or reconversion of buildings, or through the construction of temporary and light structures. This contribution deals with minor sports facilities through the study of a very widespread light construction model. This is due to many reasons: ease of installation and maintenance (and therefore low costs), the practicality of inclusion in any urban area (with consequent control on the 'impact' on the environment), the ease of transformation (which corresponds to a reuse of the constituent elements): minor sports facilities with a textile casing. These systems are identified as light, economic, flexible and minimally invasive structures, created for the practice of all types of sports (from aquatic sports to extreme sports, such as those on ice). They are characterized by a textile cover, with a thin and non-massive shell composed mostly of polymeric products. The envelope can be made up of products that are catalogued in the T.U.T., which we can define as textile materials that meet high technical-quality requirements and that have ability to adapt to a technical function. Currently the T.U.T. represents a particularly dynamic production segment, in continuous growth, both in basic and applied research and at different levels of operations (Zanelli, 2009). The main characteristic of the use of these products is that of being extremely low cost compared to a traditional massive casing. This means this type of solution is chosen at the technical and economic feasibility stage without considering the repercussions that an envelope of this type can have in the indoor space at the level of environmental

comfort, but simply through prioritizing the economic aspect.² Unfortunately this is due to many designers' lack of knowledge of this sector of the technical textile industry and of the real functionality of sports buildings. The problem is further amplified by the low quality of the technical information which is not conveyed in a correct and synthetic way.

1.1 The aims of the study on "minor" sports facilities

To further define the set of sports facilities examined from the dimensional point of view, and in order to give a clear definition of what is meant by a "minor" sport facilities, we analyzed the minimum playing surfaces of different sports sharing the same flooring. With this operation it was possible to identify a "model" of reference (Figure 1) that contained more space for possible activities, compatible with each other both in terms of size and type of flooring. It was compared the size of the playgrounds with the same flooring joined to the respective bands on the sideline, mandatory for all sports, and see which was the largest, considering the pre-disposition of the polyvalence.

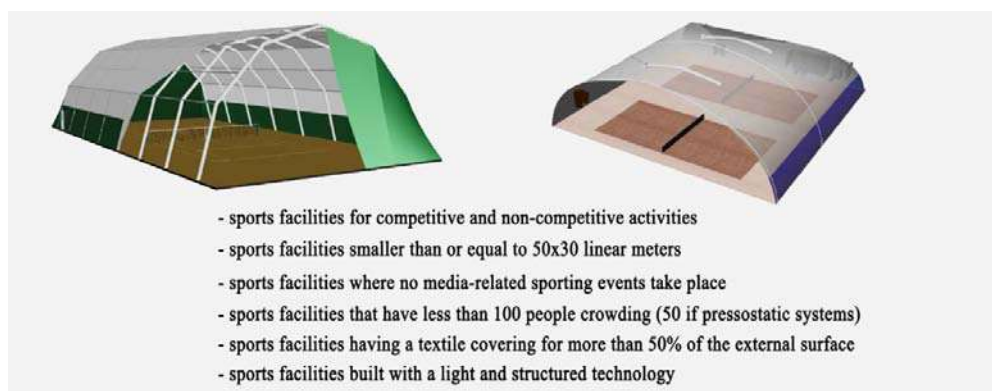


Figure 1: Characteristics of minor sports facilities with a textile casing object of the research

The model of sports facilities that this research has examined has been preliminarily deduced from a comparison proposed by the industry standards.³ The consequent characteristics were then validated through a more specific study related to the types of sports facilities, also focusing on the options that are offered by main companies offer in reference to the prefabrication of sports facilities. From the first studies of the morphological and technological type, all the technological properties of the light sports facilities have been highlighted, closely linked to the cover system: in fact the indoor performances of these sports spaces and comfort conditions depend almost totally on the textile covering that encloses, even if very often during the design phase, the right attention is not paid to the stratification of the envelope. Every athlete, who practices both amateur and agonistic activities, spends many hours in these spaces, in critical environmental conditions. Inadequate visibility, glare, noise, too high or too low temperature, poor air quality: these are just some of the discomfort factors

that each of them faces every day. To assess the indoor condition of comfort or discomfort (general objective of the research), the prevailing factors that characterize these conditions during the sports practice have been identified. Through the study of the legislation, the field of investigation has been restricted to four factors / requirements: thermo-hygrometric, visual, acoustic and air quality comfort. In order to validate the topic, a review of the few international researches that dealt with comfort during sporting activities was conducted. The first results showed prevalent insights in the field of design (sports equipment, sportswear clothing) and energy saving. This is why one of the specific objectives was to propose a monitoring and evaluation system for the various parameters that characterize the configuration of the components of the envelope (and therefore of textile materials), through the use of specific indicators that identify the effects that every requirement has on the overall perception of indoor comfort, in order to support the designer, defining a framework for evaluation and comparison which can be useful for making "thought out" choices. If the main cause of indoor discomfort is due to the lack of attention to the design of the envelope, a first result of this research was a classification of the main types of casing most frequently used, defining, for every aspect related to the building process phases, the strengths and weaknesses, and their impact on the various aspects of comfort. This aims to underline how the aspect of comfort must be considered from the planning phase, and not only at the end of the construction of the sports facility: by evaluating the incidence of comfort in every single phase of the process, it will be possible to know how much during the life span of the sport facility itself the problem of comfort will be solved.

2. Methodology

The research involved a first phase consisting of a cognitive survey on a sample of five sports facilities in the city and the province of Rome (Figure 2). Although not being representative of the totality of minor sports facilities with a textile casing, this sample can provide reliable information on the perception that athletes have of the space in which they train and on its critical issues. These sports facilities have different features, as regards age, morphology, and functions, but they all share a similar weekly attendance in terms of number of athletes (about 107). The analysis on the 5 structures was performed thanks to the collaboration of the sports management companies and the athletes themselves (over 200 athletes), who were asked to respond to a questionnaire aimed at assessing the level of comfort or discomfort perceived during sports activities. At the same time, by analyzing the building technologies used, the dimensions, the furnishings, the crowding, and the technical systems, we identified the critical situation to be improved. This phase has returned a critical reading of the most common situations on the Italian territory.

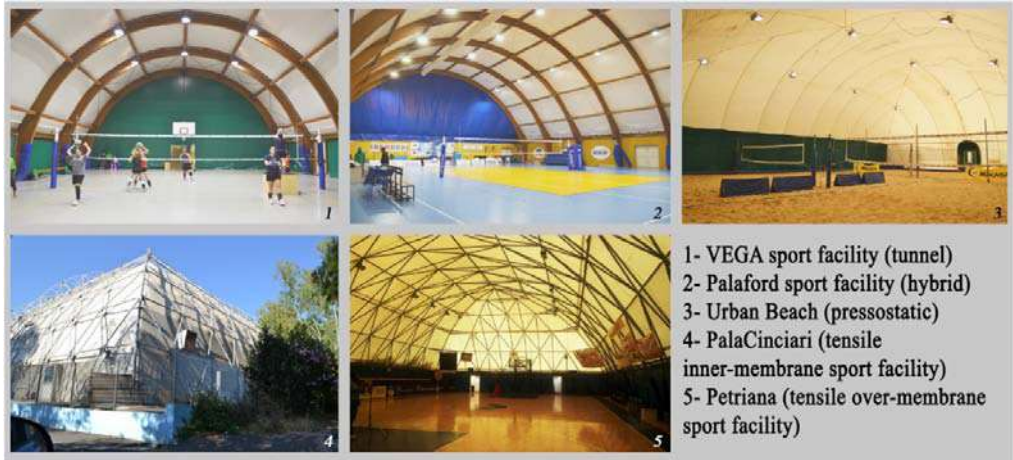


Figure 2: Sports facilities chosen for experimentation

The athletes were given the questionnaire for the assessment of perceived comfort. The questionnaire is structured into different questions with their pre-set answers, divided into groups related to different reference parameters concerning the microclimate control. This structure was very similar to the subdivision proposed by the CONI 1379/2008 technical standards, which show the limit values of microclimatic parameters for each space intended for sporting activities. This comparison (figure 3, 4) allowed to take the OfficAir questionnaire as a reference, distribute it to the users involved and evaluate it through the scales of values provided by the CONI technical standards. To obtain reliable results, calculations were necessary in order to have all the values on the same scale and to make them comparable to each other.

1 The OfficAir Study 74	
Parameter	Questionnaire Item
Temperature	Too cold (-3)- Too hot (+3) Varies too much during the day (-3)-Not enough variation (+3) Uncomfortable (1)-Comfortable (7)
Air Movement	Draughty (-3)-Still (+3)
Air Quality	Humid (-3)-Dry (+3) Stuffy (1)-Fresh (7) Smelly (1)-Odorless (7) Unsatisfactory (1)-Satisfactory (7)
Light	Natural Light: Unsatisfactory (1)-Satisfactory (7) Artificial Light: Unsatisfactory (1)-Satisfactory (7) Reflection or glare: Glare (1)-No glare (7) Light Overall: Unsatisfactory (1)-Satisfactory (7)
Noise	Noise from outside the building: Unsatisfactory (1)-Satisfactory (7) Noise from building systems (e.g., heating, plumbing, ventilation, air conditioning): Unsatisfactory (1)-Satisfactory (7) Noise from within the building other than from building systems (e.g., phone calls, colleagues chatting, photocopiers, etc.): Unsatisfactory (1)-Satisfactory (7) Noise overall: Unsatisfactory (1)-Satisfactory (7)

Figure 3: The questionnaire items of the Officair Study

2 Norme Tecniche CONI 1379/08

Tipologia	Temp. aria °C	Umidità relativa %	Illum. medio lux	Ricambi aria volumi amb./ora	Velocità massima aria m/sec ⁽¹⁾	Livello massimo rumore ambiente dBA ⁽²⁾	Locali
Sale al chiuso	16-20	50	⁽³⁾	⁽⁴⁾	0,15	40	sala di attività
	20-22	50	200	⁽⁴⁾	0,15	40	sale preatletismo
	18-22 ⁽⁷⁾	50	150	5	0,15	40	spogliatoi
	22 ⁽⁸⁾	70	80	8	0,15	50	docce
	22	60	80	5-8	0,15	40	servizi igienici
	20	50	200	2,5	0,15	40	primo soccorso
	20	50	200	1,5	0,15	40	uffici
	20	50	200	1	0,20	40	atrio
	16	50	100	0,5-1	0,25	50	magazzini
20	50	150	0,5	0,20	40	locali vari	

Figure 4: CONI technical standards (Regulation 1379/2008)

The surveys, lasting between 2 and 18 weeks, were supported by special tools⁴ and external consultancy by field experts. Thus, we arrived at a clear structuring of the reference framework and defined a system for collecting and classifying data. This surveying activity was divided into three phases:

- Phase 1: architectural and constructive analysis for a first identification of the morpho-typological parameters (framing of the urban context, descriptive synthesis and representative images). To obtain a more complete descriptive picture, the values of the reference microclimatic parameters were detected in a single moment, using specific instruments. In particular, we detected (i) the internal temperature; (ii) the relative humidity; (iii) the speed of the air; (iv) the lighting; (v) the noise level; (vi) the amount of PM2.5 particulate and the VOCs. Detecting these data in a single moment and in a single environmental position(at the centre of the facility), provides a homogeneous information framework for the indoor microclimate of the case studies.

- Phase 2: distribution of the questionnaires, preceded by a brief description of the motivation, purpose and methodology of the interview and concluded by final notes in which each interviewee was able to add observations or personal considerations. The athletes involved were required to have attended the gym for at least a year, and for at least 4 hours per week (amateur), up to a maximum of 25 hours per week (professionals). For each sports facility, 70 questionnaires were distributed, out of which only 51 were considered for each structure for evaluation purposes, as the final response rate was not 100%.

- Phase 3: data analysis. Each section was analyzed through the Likert Scale. This scale assigns a value (ascending or descending) to each response level.⁵ Once the values had been compared, some graphs were created referring to each sports facility. Radar graphs for each

macro-group were drawn to represent the variation of the responses obtained from each sports facility (Figure 5). An analysis was then carried out to evaluate the environmental comfort parameters of the individual gyms, in order to find out which was the least critical sports facility. The questions on temperature, air movement and internal humidity had a different rating scale, therefore, in order to compare the results with each other, we proceeded with the normalization of all the values until we had comparable numerical results. The final synthesis provided an estimate of the criticality level of each sports facility with respect to the parameters considered to assess the operating conditions of each of them, mainly through user satisfaction surveys.

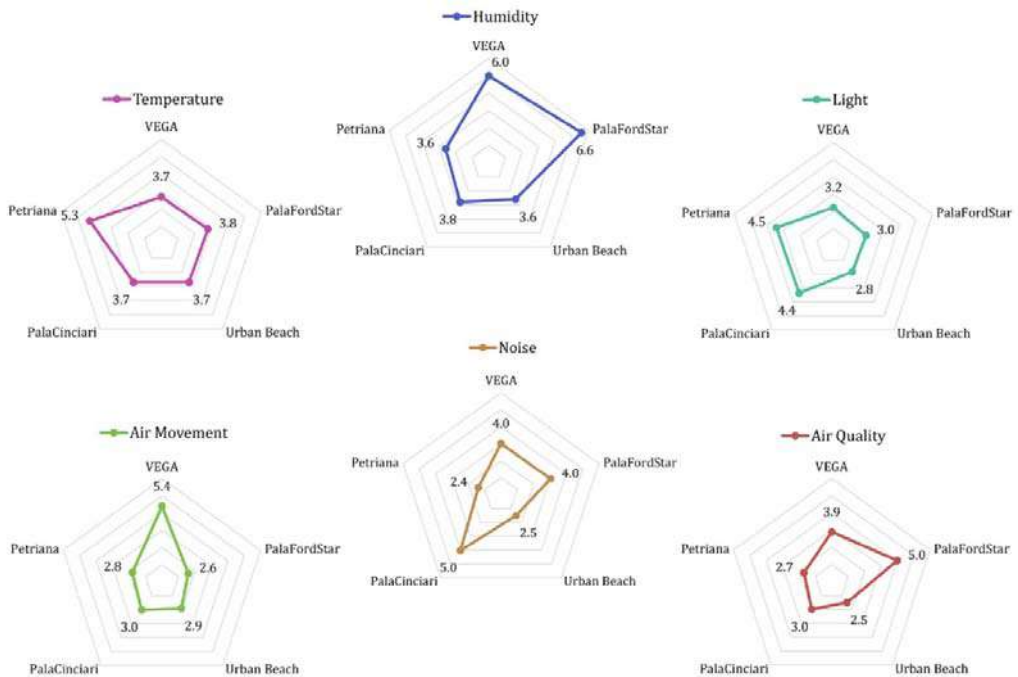


Figure 5: Comparison of the five minor sports facilities at the single parameter level investigated through the questionnaires.

The comparison shows that the five sports facilities are positioned around an average value, which therefore indicates a condition that is not completely satisfactory for the practice of the activity (Figure 6). Although there are no sports facilities with a score below +3/7 ("not bad"), it is also true that none reach the +5/7 value ("quite good"). This deficiency means an absolutely unsuitable global situation, in terms of environmental comfort, to allow sports practice. It follows that such buildings, so designed, do not meet the satisfaction of users.

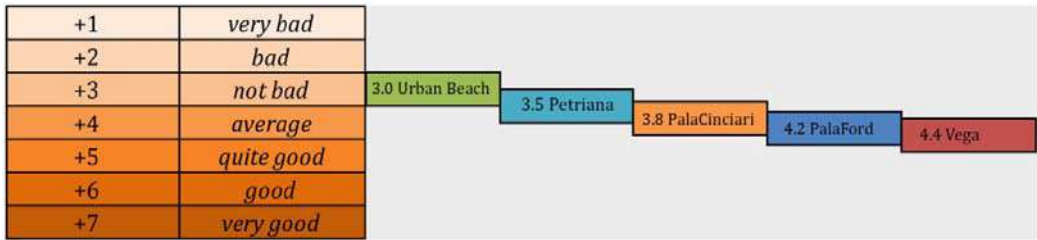


Figure 6: Evaluation scale used and comparison between the individual sports facilities.

2.1. The answer for textile cover design

Is it possible, after the previous considerations, to talk about "comfort design" in a sports facility with a textile casing? It has been established that the problem of discomfort exists and is real: how is it possible to intervene to prevent this problem, both during the planning of modifications and during the management phase of a sports facility? Considering the problem of the very low durability of these casings compared to traditional casings (estimated at around 15 years), support tools are needed for the various operators that are involved throughout the building process. In order to control "advantages" and "limits" of a textile membrane plant, one can identify items to assess the overall level of the state of conservation and operation of existing sports facilities. These items can be given a value to develop an overall synthesis of the conditions of each sports facility. By matching these items with each type of construction being studied, one can obtain different case studies that fully depict the functional image of the sports facility itself. In fact, by structuring a scoreboard, it is possible to identify lines of actions to solve various basic problems, such as (i) the low level of knowledge on these construction typologies; (ii) the poor quality of technical information related to products for the textile envelope; (iii) the lack of consideration of comfort within these structures. Through these three issues, and proceeding with the definition of an evaluation framework for the most adopted casing technical solutions for the deployment of a textile cover, it is possible to establish valid "designed" intervention strategies, performing in relation to control of indoor discomfort.

3. Results

The proposed scoreboard takes several items into consideration. For each single material for the envelope, or "package" for the envelope, a single Excel spreadsheet has been created, along with a summary sheet containing all the information concerning the adopted technical / technological composition. The first informative level is graphic (constructive details, images), to which tables are added containing the specifications of each considered item. The first table frames the product for the envelope within the building process phases; the second frames the product compared to the impact on indoor comfort that each phase can generate.

Each described feature is identifiable through a definition and description of the material / product being examined. Furthermore, a qualitative indicator is assigned to each item, to allow its evaluation and to obtain a global score qualitatively identifying the examined product. The overall sum of the scores for each product varies with the number of items actually considered, based on the score of each item and based on its influence on the indoor comfort. Finally, the single score value, ranging from 1 to 3 (Low = 1, Medium = 2, High = 3), must be entered in the score column. We chose to define an increase factor (Q_x) to be assigned only to items impacting on the relevant comfort, both positively ($Q_x = +2$), and negatively ($Q_x = -2$). In the next column, the final score will be reported, obtained from the sum between the score value and the value of Q_x . The final score can then be positive or negative, and will range between +5 and -1. A total of 10 traditional products are considered. Each product is described by qualitative indicators and by the items related to the product itself during the process phase, or when applied as enclosure elements for the construction of light sports facilities. It is therefore possible to have a clear score for each product, allowing the designer to evaluate its effectiveness and to compare it with complementary products. By comparing the analyzed products and their scores, we can order them qualitatively. Out of the examined items, the most competitive product in terms of quality / cost ratio (and of comfort, in particular) is found to be the expanded PTFE membrane. On the other hand, the less performing product from the qualitative and performance point of view related to comfort, is the glass fiber / silicone membrane: this product does not achieve optimal performance in terms of comfort, and also does not meet some important requirements (such as cleanability / durability).

With reference to innovative materials, the transparent insulation materials (TIM) were analysed. They have the same insulating capacity as the glass fibers, and a solar transmission coefficient comparable to a double glazing unit. The special optical and thermal properties allow considerable energy saving on the one hand, thanks to the passive exploitation of solar energy, and an effective improvement of the thermal and visual comfort conditions of the internal environment on the other, thanks to the low transmittance value and high transmission value of diffused light. Up to now, TIMs have never been used for roofing or textile façades. For this reason, by closely collaborating with the TIM producer Okalux, the main problem of a TIM panel with two or more layers of textile type has been identified, namely the low tensile strength of the panel itself. In fact, a TIM panel generally has a fragile behaviour; however, the use of the Oki panel product, homogeneous nature and reduced thickness, was experimented fusing the "heads" of the internal structure with a thin sheet of polyethylene or glass fiber fabric. Thus, we proposed a technical solution that entails the use of polyester fabric and PVC coating + pvdf lacquering - to be integrated with a TIM panel instead of the classic double glazing unit. This solution is composed by a casing of variable but very small (about 2 to 5 cm) thickness (according to the TIM material being used), and it could be used to cover large sports spaces, keeping its "light" nature. Moreover, this solution would combine a high degree of translucency with a good thermal resistance. Even the visual comfort would be guaranteed, thanks to the translucency of the material, which if combined with a translucent

material (such as the one proposed in Figure 7) would ensure natural light supply thus limiting the need for lighting devices, favouring high energy saving, a better insulation, and therefore thermal insulation. Certainly this solution needs to be tested, but it could draw an innovative line increasingly oriented to raising awareness about indoor comfort conditions that users who practice sports in these facilities need.

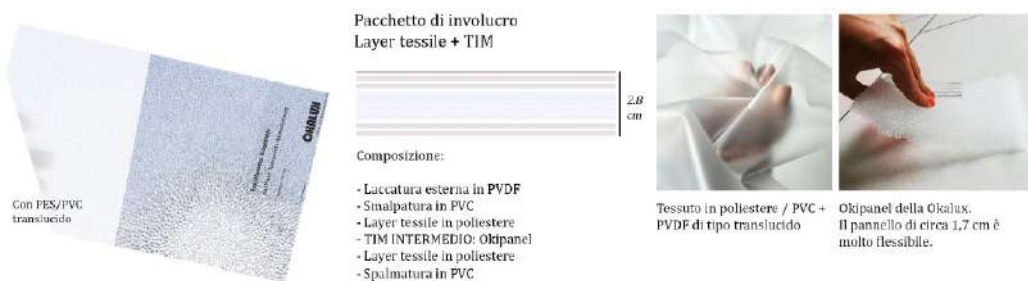


Figure 7: A possible light envelope package solution, with two textile layers + TIM

4. Final considerations

This research aims to sensitize the designers, managers, technicians, lenders of sports facilities on the importance of indoor comfort during training hours. The results of the different phases can represent useful tools for all the figures that revolve around the building process of these buildings, to support decision-making. All the processed information can be organized in digital platforms, so to be available as a basis for future studies. This data generated a "decomposable" information framework, that can be implemented according to the evolution of sports federations rules. In addition, indoor comfort has been approached in an interdisciplinary way, with different disciplines each contributing to the final result with important, specific "knowledge". Finally, without the support of figures belonging to different scientific fields, this research would have been "sectorial": it is important to underline the necessity of a continuous interaction between experts from different scientific fields, to activate an exchange of skills that leads to the definition of a quality result.

References

- [1] Campioli, A. Zanelli, A.(2009) *Architettura tessile - progettare e costruire membrane e scocche*,ed. il Sole 24 Ore, Milano
- [2] ISTAT, (2005) *Lo sport che cambia*, Report pp. (116-120) ed. CSR
- [2] Uva, M.(2014) *Lo sport in Italia. Numeri e contesto*. In: *Conference CONI- ISTAT*

- [3] Sakellaris I.A. et. al, (2016) Perceived Indoor Environment and Occupants' Comfort in European "Modern" Office Buildings: The OFFICAIR Study. In: *International Journal of Environmental Research and Public Health*, vol. 13 (pp. 444-448)
- [4] Masera G. et. al., (2017) Development of a Super-insulating, Aerogel-based Textile Wallpaper for the Indoor Energy Retrofit of Existing Residential Buildings. In: *Procedia Engineering*, vol. 180 (pp. 1139-1149)
- [5] Mondal, S. (2015) Phase change materials for smart textiles – An overview. In: *Applied Thermal Engineering*, vol. 28 (pp. 75-77)
- [6] Buratti, C., Moretti, E., (2011) Transparent insulating materials for buildings energy saving: experimental results and performance evaluation. In: *Third International Conference on Applied Energy* (pp. 1421-1432)
- [7] Capasso, A. (1993) *Le tensostrutture a membrana per l'architettura*, Maggioli Editore, Rimini
- [8] Grosso, M. (2017) *Il raffrescamento passivo degli edifici in zone a clima temperato*, Maggioli editore, Rimini,
- [9] Knipper, J., Cremers, J., Gabler, M., and Lienhard, J., (2011) Construction Manual for Polymers + Membranes, Edition Detail Birkhauser Architecture
- [10] Norme CONI per l'impiantistica sportiva, Deliberazione del Consiglio Nazionale del CONI n. 1379 del 25 giugno 2008
- [11] Zhang, L. (2006) Transparent Thermal Insulating Multi-Layer Membrane Structure for Building Envelope, In: *International Conference On Adaptable Building Structures*, vol. 8 (pp. 182-185)
- [12] Monticelli, C. Zanelli, A. (2016) Life Cycle Design and Efficiency Principles for Membrane Architecture: Towards a New Set of Eco-design Strategies. In: *Procedia Engineering*, vol. 155 (pp. 416-425)
- [13] Yeha, H., Stoneb, J., Churchillb, S., Brymerc, E., and Davidsa K. (2016) Designing physical activity environments to enhance physical and psychological effects. In: *11th conference of the International Sports Engineering Association, ISEA*

¹ In this case, well-being is understood as physical and / or mental well-being that the body feels when practicing sport.

² These choices concerned large stadiums or sports halls made with sophisticated light construction techniques (such as ETFE bearings). But also a large amount of smaller PVC structures, "sovereign" material of the sector, or other low-cost synthetic material.

³ CONI Rules for Sports Facilities, approved by resolution of the National Council of CONI n. 1379 of 25 June 2008.

⁴ The instruments used were: (1) a detector for measuring indoor air quality, and more precisely the level of VOCs (Volatile Organic Compounds) and PM2.5 particulate. The same instrument detected the temperature and the relative relative humidity; (2) an anemometer with a propeller probe to measure air velocity; (3) a lux meter with photometric probe to measure the level of internal illumination; (4) a sound level meter to record the internal sound level.

⁵ Given the presence of different scales between the various questions, it was necessary to normalize the reference values to make them comparable in a single scale.

Proceedings of the TensiNet Symposium 2019

Softening the habitats / 3-5 June 2019, Politecnico di Milano, Milan, Italy
Alessandra Zanelli, Carol Monticelli, Marijke Mollaert, Bernd Stimpfle (Eds.)

Audiovisual comfort in shopping streets covered by structural skins

Monika RYCHTÁRIKOVÁ^{*a}, Richard ŠIMEK^a, Paulína ŠUJANOVÁ^b, Jarmila HÚSENICOVÁ^a, Vojtech CHMELÍK^a

^{*} KU Leuven, Faculty of Architecture, Hoogstraat 51, 9000 Gent/ Paleizenstraat 65, 1030 Brussel, Belgium
monika.rychtarikova@kuleuven.be

^a Department of Architecture, Faculty of Civil Engineering, STU Bratislava, Radlinského 11, 810 05, Bratislava, Slovakia

^b Dep. of Building Construction, Faculty of Civil Engineering, STU Bratislava, Radlinského 11, 810 05, Bratislava, Slovakia

Abstract

This article focuses on the prediction of acoustic conditions in wide shopping streets covered by transparent roof materials. This is done by analysing the impact of common glass and ETFE cushion systems on noise levels and sound reverberation. Research is done by simulation software, using a parametric study to deduce how architectural features influence the acoustic quantities. Three basic street models are tested: (1) a street without any roof, (2) a street with roof made out of ETFE foil and (3) a glazed roof. Firstly, the impact of roof (ceiling) elevation on sound pressure level distribution and reverberation time is analysed. Secondly, the impact of the shopping street (gallery) width on selected parameters is discussed. Analysis is done in detail, per octave band, in order to show the behaviour at low and high frequencies in the rooms separately. Lastly, recommendations are given for the optimization of acoustic comfort.

Keywords: acoustic comfort, daylight, structural skins, smart city, shopping streets, urban planning, protection of building monuments

DOI: 10.30448/ts2019.3245.30

Copyright © 2019 by M. Rychtáriková, R. Šimek, P. Šujanová, J. Húsenicová, V. Chmelík. Published by Maggioli SpA with License Creative Commons CC BY-NC-ND 4.0 with permission.

Peer-review under responsibility of the TensiNet Association

1. Introduction

Evolution of market places and shopping streets has a long history influenced by economic and societal evolution. The shopping streets in the 18th century had become important for the economy of cities, yet only little attention was given to the links between shopping and shops with the changing social, economic and physical structure of towns (Stobart, 1998). In the middle of the 19th century traditional open-air markets were very popular in the central squares of cities. These were later challenged by new urban concepts of the city centre, such as construction of market halls with fish markets etc (Toftgaard, 2016). One of the most influential factors in the urban planning of public spaces has always been urban traffic. The dominance of cars in the 20th century had a large impact on the urban development (Pooley, 2005).

In all probability the oldest of large shopping streets in Europe date from the 19th century. Most of them consist of a number of stores, nowadays accessible by public transportation. Examples of such historical places with a long standing tradition are the Avenue Montaigne in Paris, Bond Street in London and Bahnhofstrasse in Zurich. In the same historical period, many shopping galleries covered by a glazed roofing were built across Europe as well (complex of Galeries Royales Saint-Hubert in Brussel, Passage du Caire in Paris, Passage in Saint Petersburg and the Galerie Vittorio Emanuele II in Milano). These shopping galleries are covered along the entire length by glazed arcades, that contribute to changes in daylight quality and soundscape perception (when compared to uncovered streets or atria). Glass belongs to acoustically reflective materials, and its presence in rooms therefore contributes to an increase of noise and sound reverberation.

Nevertheless, glass is the most common roofing material when it is required that a construction is transparent (Polomová, 2013). Alternatively, tensile structures can be used that may bring many advantages for contemporary architecture in terms of indoor comfort. However, the impact of these structures hasn't been explored yet in detail (Vojteková, 2007). So far, the most appreciated features, such as light weight, thin layers, flexibility and innovative design options have been recognized not only in contemporary architecture, but also in restoration projects (Vojteková, 2018). More related to the matter of sustainability of light and ultralight structures, such as ETFE, can be found in Maywald (Maywald, 2016).

Preliminary case studies of large atria covered by an ETFE foil structure have shown a positive impact on acoustic conditions in- and outdoors (Rizzo, 2016; Urbán, 2017; Szabó, 2018). Concerning the room acoustics, it is known, that the influence of sound absorptive properties of building interior surfaces on noise is the most prominent in small rooms, where the density of sound reflections is high. In this paper, we focus on the analysis of acoustic conditions in relatively wide shopping streets, where the impact of glass and ETFE foil systems has not yet been investigated in detail. The parametric study reveals the influence of a roofing material in

combination with a varying height and width of the shopping street with the same length of 100 m on the resulting acoustic conditions.

2. Description of the architectural case study

For the sake of understanding the influence of different architectural features and functions on acoustic situation in the shopping streets, a parametric study was performed for four virtual streets with different width and height of buildings. Cross sections of the street models for the four simulation cases are shown in the Fig. 1.

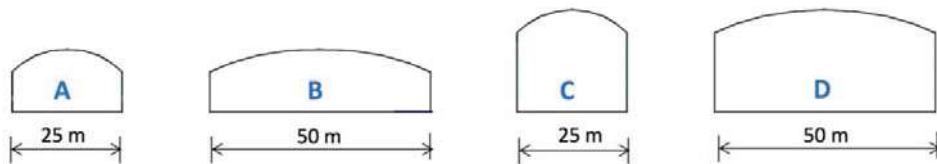


Figure 1: Four simulated shapes of shopping streets with the length of 100 m.

Variants A and C have the same street width of 25 m, and variants B and D are 50 m wide. In the first two variants (A and B) the streets are formed by buildings with the heights of 10 m, representing 3 storey buildings. In the variant C and D the surrounding houses are twice as high, i.e. 6 storey buildings. Each variant was simulated under 3 different conditions of roofing system: (1) open and thus without a roof, (2) an ETFE system, and (3) a glass roof.

All other surfaces in the simulation models (besides the roof) were the same in all variants. In the simulation model plaster was used as the finishing material of the building façade, the windows were simulated as ordinary double glass windows, and the road surfaces were simulated as an acoustically hard material, such as asphalt or concrete. An overview of the simulated models is shown in the Figure 2.

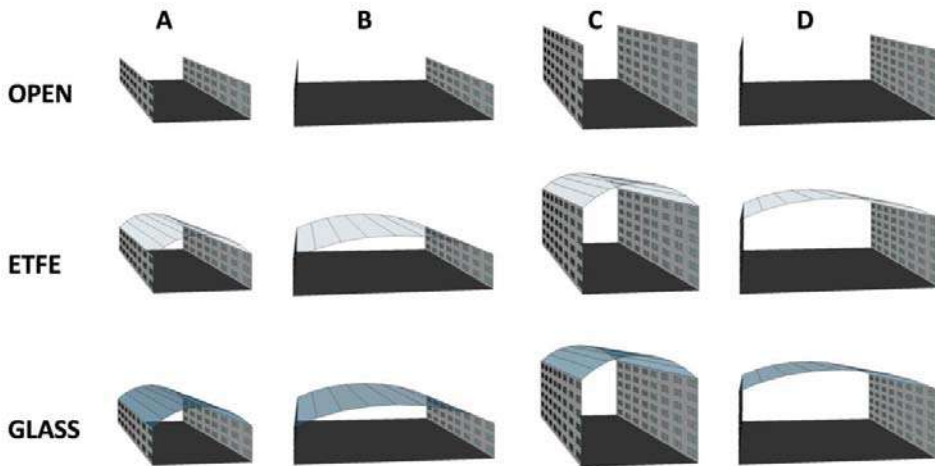


Figure 2: Overview of the twelve simulation models

3. Simulations

The simulations of the 3D models were performed in acoustic prediction software, ODEON v.14. This software uses an image-source simulation method combined with a modified ray tracing algorithm with an advanced sound scattering model (Christensen, 2013).

Each street variant was evaluated for three kinds of linear noise source position and composition (Figure 3). These sources represent typical pathways of pedestrians, tram lines or other noise sources. For this article, the detailed point receiver calculations were performed for pink noise and thus in a general way, in order to understand the sound distributions in different rooms. The simulated values were compared to the so-called free field situation (also simulated), i.e. a situation in which all the surfaces absorb 100% of sound energy. This has given us the opportunity to work with the relative sound pressure level values, instead of the absolute levels that would be valid only for one type of the noise source. In this way we didn't calculate the the absolute noise level in the street, but instead, only the contribution of buildings and roofing materials to the overall noise situation (as compared to the situation without buildings, i.e. free field). In doing so, the result of the paper is more general and more useful for comparisons with other research works.

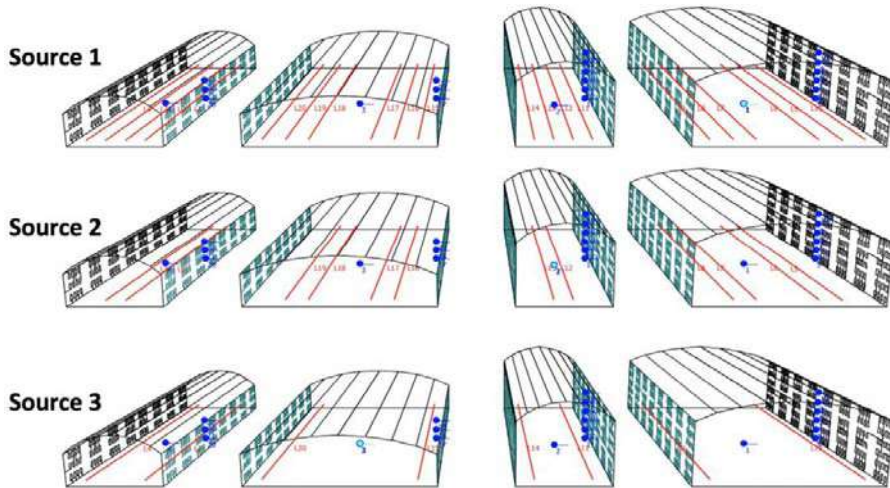


Figure 3: Each of the 12 variants were evaluated for 3 kinds of noise source compositions.

The receiver positions were chosen as follows. A point receiver was placed in the middle of each room, followed by placing several receivers at a 2 m distance from the building facades (in front of the windows), which are indicated in a blue colour in the Fig. 3. The second part of the analysis was performed in the so-called audience plane (ca 1,4 m above the ground), in order to get an overview of the sound distribution in each of the situations.

In the description of the acoustic situation of public spaces, typically only noise assessment is done. Concerning shopping galleries, there is no standardized acoustic parameter for the assessment of acoustic comfort. The equivalent noise level is surely not the only relevant parameter. Late sound reflections should be also taken into account in the assessment. They will not increase the equivalent sound levels significantly, but they are responsible for the continuous background sound in large spaces that contributes to the overall people's judgement of acoustic pleasantness or annoyance in situ. For this reason, we show also the reverberation time that might affect the perception of sound.

4. Results and analysis

4.1. Sound pressure level

For the sake of simplicity, in the graphs summarizing the results (Fig.4), we will present only the total sound pressure level L_p (dB) as an integration over all frequencies. Nevertheless, we will reflect on the frequency dependent results in the text. The Fig. 4 shows an overview of the results of the sound pressure level L_p (dB) for all the simulated cases expressed (in each case) as a difference between each of the simulated case and the free field situation. In other words,

these values show the impact of the architectural design on the increase of noise levels compared to the situation with no buildings.

In general, the noise level in the considered shopping street is lower in the cases without a roof compared to the models with a roof, which is rather logical. These simulations are useful in particular for understanding the impact of the surrounding building facades on the resulting acoustic situation. In our cases, the overall sound pressure level increase is between 2-7 dB, depending on the situation. The strongest impact of the building facades on the increase of noise is noticeable the most at the receivers' positions near the building walls.

Looking at the data from a global point of view, we can conclude, that the smallest impact of the surrounding buildings and roof on the noise level is observed in the largest shopping street (D). This is expected, since the sound reflections arriving from far distances (due to the large volume of the room) carry less sound energy, and thus result in an overall lower total sound pressure level. If we consider the receiving position in the middle of the street, the noisiest situation is the case B when glass is chosen as the roof material. When analysing the results of the receivers at the distance of 2 m from the building facades, the noisiest situation occurs in the case A, i.e. the smallest room. This can be explained by the highest density of sound reflections in such a space.

When comparing glass and ETFE systems in general, the roof made out of the ETFE scores in average better in all cases, by ca 2 dB. However, if we look in the frequency dependent analysis (Fig.5), we will see that the differences between the glassing and foil structure will become much larger, up to 4 dB at low frequencies, since these thin foils reflect less than 50% of the sound back into the space, whereas in the case of the glass this is around 80-90% (depending on the type of the glass).

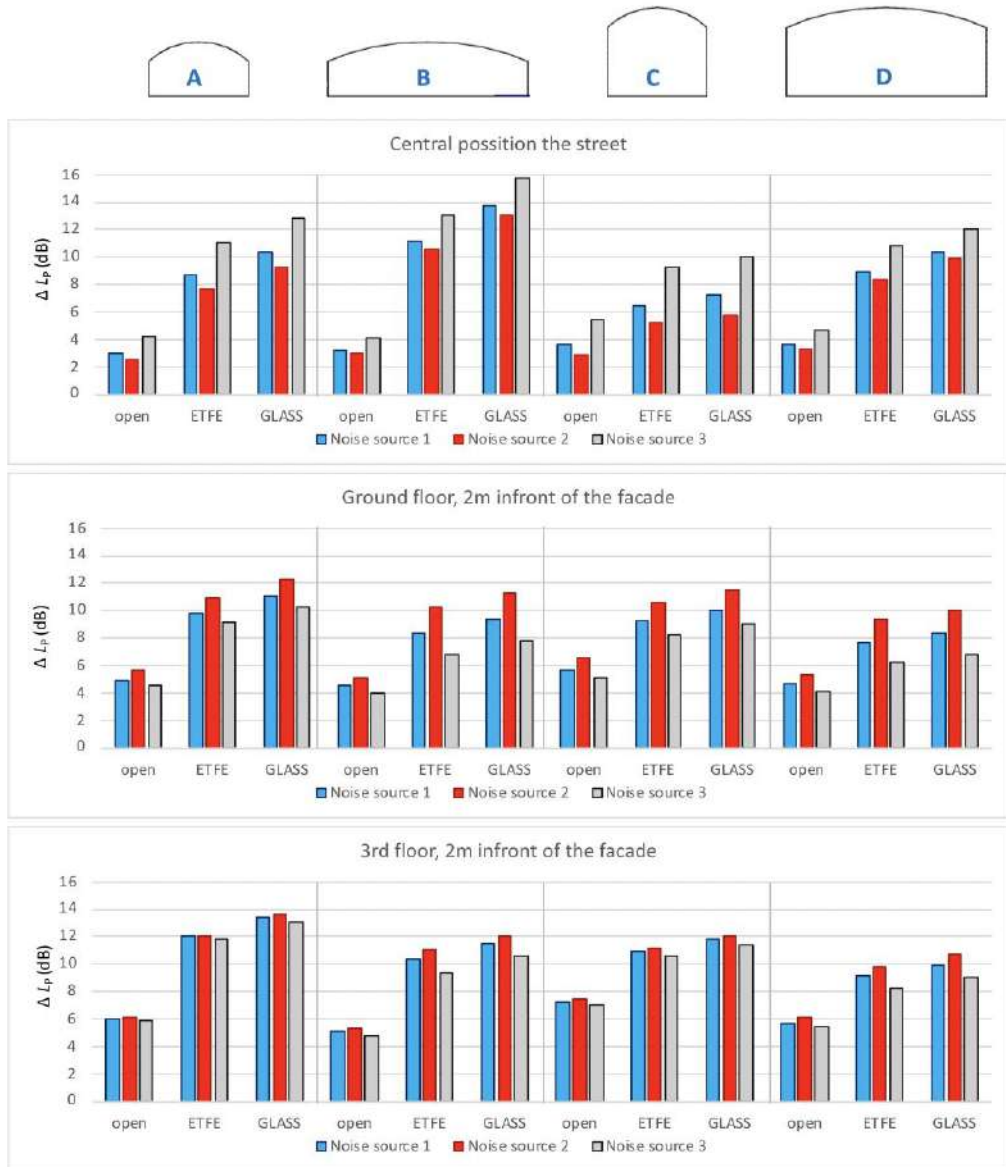


Figure 4: Differences in total the sound pressure level ΔL_p (dB) for each of the simulated case and the free field situation; the receiver position placed: in the middle of each room (upper picture); at a 2 m distance the façade in the height of 2 m (middle picture); and at a 2 m distance in front of the façade at the 3rd floor (bottom picture)

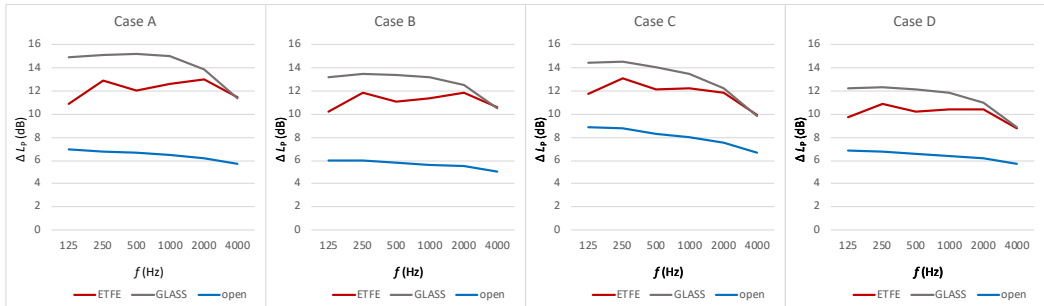


Figure 5: Differences in the total sound pressure level ΔL_p (dB) in the octave bands. Example of the situation with the sound source 2 and the receiver placed at a 2 m distance in front of the façade at the 3rd floor.

4.2. Reverberation time

As mentioned above, the overall noise is not the only performance indicator of acoustic comfort. The sound reverberation creates a special environment which influences the perception of the room quality. The reverberation time analysis (Fig.6) shows that the potential of continuous background noise due to reverberation is higher in shopping streets covered by glass. The Reverberation in spaces with bigger volumes is longer (Fig.6) and thus the roof (ceiling material) is a potential factor in acoustic comfort also in large spaces. In the case of the glass structure the reverberation time is more than twice as long.

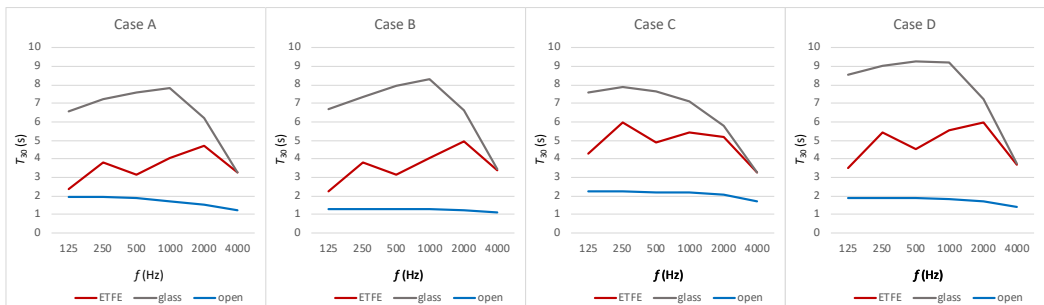


Figure 6: Average reverberation time T_{30} (s) in the four simulated cases.

5. Discussion and conclusion

While historical shopping galleries covered by glass were characterized by their narrow dimensions and high ceilings, contemporary architecture brings also other types of covered shopping street corridors. The parametric study presented in this article has shown the impact of building facades and materials used as a roof construction for relatively wide streets with a low and high ceiling. The article has shown, that in cases where the ceiling is low, the selection of the material will have a strong impact on the overall noise level. Furthermore, the positive

impact of a structural skin, in our case the ETFE roof structure, has been proven to be a better solution, not only in terms of noise, but mainly in terms of the reverberation time.

The real correlation between the reverberation time (and /or other room acoustic quantities) in relation to the unpleasant continuous background noise, background noise caused by impact noise during a heavy rain or hails storms, in shopping galleries and large covered atria still needs to be investigated in detail and a reliable parameter needs to be defined.

Acknowledgements

This paper has been made within the scope of the H2020-MSCA-RISE-2015 “PaPaBuild, project (grant agreement No. 690970). This paper was supported by national project VEGA 1/0050/18 and Slovak Research and Development Agency under the contract APVV-16-0126.

References

Christensen C. L., Koutsouris G., and Rindel J. H. (2013), The ISO 3382 parameters. Can we measure them? Can we simulate them? In: *International Symposium on Room Acoustics*, Toronto, Canada.

Maywald, C., and Riesser, F. (2016), Sustainability - The Art of Modern Architecture, In: *Procedia Engineering* vol. 155, pp.238 – 248

Polomová, B., Vargová, A. (2013), Covering of historic building atriums due to adaptation to new function, In: *ATF 2013 conference*, ATF 2013, Leuven.

Pooley, Colin G., and Turnbull, Jean (2005), Coping with congestion: responses to urban traffic problems in British cities c.1920–1960. In: *Journal of Historical Geography*, vol.31 (1), pp.78.

Rizzo, Fabio, and Paolo Zazzini. (2016): Improving the acoustical properties of an elliptical plan space with a cable net membrane roof. In: *Acoustics Australia*, vol.44.3, pp.449-456.

Stobart, J. (1998), Shopping streets as social space: Leisure, consumerism and improvement in an eighteenth-century county town. In: *Urban History*, vol.25 (1), pp.3-21.

Szabó, D., Šujanová, P., Glorieux, C., Rychtáriková, M. (2018), Impact of Building Facade Properties on Noise Levels in Street Canyons, In: *Proceedings of Euronoise 2018*, 27 – 31th May 2018, Euronoise 2018, Heraklion, Crete, Greece.

Toftgaard, J. (2016), Marketplaces and central spaces: markets and the rise of competing spatial ideals in Danish city centres, c. 1850–1900. In: *Urban History*, vol.43 (3), pp.372.

Urbán, D., Zelem, L., Maywald, C., Glorieux, C., Rychtáriková, M. (2017), Influence of transparent roofing systems on room acoustic properties of large atria, In: *Akustika 29*, Czech Republic, pp.93-98. ISSN 1801-9064.

Vojteková, E. (2007), Atria with glass roof – new phenomenon in buildings (2007), In: *proceedings of the 4th International conference in Banská Štiavnica*. Publisher FA STU Bratislava, ISBN 978-80-227-2777-8.

Vojteková, E., Gregorová, J., Ivánková O. (2018), Interdisciplinary approach in designing of the roofing Romanesque palace ruin at Spiš castle in Slovakia, In: *proceedings of ATF conference 2018*, ATF 2018, Leuven.

Proceedings of the TensiNet Symposium 2019

Softening the habitats / 3-5 June 2019, Politecnico di Milano, Milan, Italy
Alessandra Zanelli, Carol Monticelli, Marijke Mollaert, Bernd Stimpfle (Eds.)

Energy performance of film membranes in the retrofitting of Architectural Heritage: an Italian case study

Mariangela DE VITA*, Raffaella D'ANTONIO^a, Paolo BECCARELLI^b,
Pierluigi DE BERARDINIS^a

* Construction Technologies Institute of the Italian National Research Council (CNR)

Via Giosuè Carducci 32, 67100 L'Aquila, Italy

mariangela.devita@itc.cnr.it

^a Civil, Construction-Architectural and Environmental Engineering Department, University of L'Aquila, Italy

^b Department of Architecture & Built Environment, University of Nottingham, United Kingdom

Abstract

During the last decades, the development of architectural textiles led to significant innovations in the building industry. Designers, producers and researchers have invested in the technical development of textile envelopes with the aim of improving the structural performances of existing building in a cost-effective and sustainable way without sacrificing the aesthetical aspects of the historic buildings. The optimization of technical textiles properties focused particularly on the production process, on the lifespan and the end of life scenarios. Despite the technological progress, the performance of the membranes in terms of internal comfort and energy consumption still represents a critical issue constantly investigated by the academics in this field. In parallel, recent research on the use of membrane structures in historical buildings provided important references and data on the advantages of textiles application in the protection and promotion of the architectural heritage thanks to their intrinsic lightness and reversibility. For this reason, it is fundamental to evaluate the effects that the integration of film membranes has in these valuable structures in terms of energetic behaviour.

DOI: 10.30448/ts2019.3245.23

Copyright © 2019 by M. De Vita, R. D'Antonio, P. Beccarelli, P. De Berardinis. Published by Maggioli SpA with License Creative Commons CC BY-NC-ND 4.0 with permission.

Peer-review under responsibility of the TensiNet Association

The aim of the paper is to analyse the potentiality of membrane usage in the energetic retrofitting interventions. The Authors will present and analyse the hypothesis of a temporary roof installation in the courtyard of a historical building located in the town of L'Aquila (Italy) and severely damaged by the 2009 earthquake. The paper includes the results of a dynamic simulation of the entire building, carried out with the software "Design Builder", which allowed the assessment of the project from the environmental point of view on the basis of the energy consumption.

Keywords: performance, energetic retrofitting, CO₂ reduction, internal comfort, temporary roof, valuable courtyard, dynamic simulation

1. Introduction

Historic buildings have a crucial role in the exploitation of the cultural and economic potential of existing cities. Due to the numerous threats, such as an increasing level of pollution, gentrification and natural disasters, the government department responsible for monuments are constantly under pressure to ensure an adequate level of protection without interfering with the regular use of the building.

The use of lightweight membrane structures for the protection of historical sites has been successfully experimented in several key projects. The foldable roof for the Rathaus's courtyard in Vienna (Tillner, 2003) and the ETFE roof for the Palacio de Igartza, a small fortress-palace built in the 13th century in Beasain, Guipúzcoa, North of Spain (Tejera J., Monjo-Carrió J., 2010) are only two of the successful projects based on lightweight membrane structures added to historic buildings to improve the weather protection (Rosina et al. 2011) without damaging the existing buildings or compromising their structural performance.

In addition, recent projects investigated the potential of temporary membrane structures for the development and exploitation of the potential of historic buildings in the improvement of areas of the cities still underutilised. Artistic installations for the Milan Design Week, such as "Invisible Borders" (Beccarelli et al., 2016) by MAD architects and "Off the Cuff" (Beccarelli et al., 2017) by DR+R, can attract thousands of visitors in few days offering free access to public buildings and unique experience. The constructive discussion with the government department responsible for monuments shows that membrane structure can be successfully used to improve the current state of historic building

However, the increase in the number of textile interventions on cultural heritage requires detailed analyses on the impact of the membranes on the energy behaviour of valuable masonry buildings (Llorens and Zanelli, 2016; De Vita et al., 2018). This paper shows the

potential of a temporary textile cover in the internal courtyard of a historic building in the city of L'Aquila, and its positive impact on the energy performance of the building.

2. Case study: *E. De Amicis* school

2.1. The history of the building and its morphology

The construction of the building was commissioned by *S. Giovanni da Capistrano* to host the “S. Salvatore” major hospital, next to the Basilica of S. Bernardino, and it was completed in 1457. In 1779 the building hosted a Medical School as well, until the second half of the 17th century, when it was occupied by a military dispensary. In the first years of the 18th century the building became a school, until the earthquake that occurred in L’Aquila on April 2009. It is now damaged and abandoned, waiting to be restored to its original state.

The building has a rectangular shape with an inner courtyard and consists of 3 levels covered by pitched roofs (Figure 1). The ground floor has a difference in level from the south to the north side of nearly three meters, resolved by a set of stairs on the north side; for this reason, the courtyard is flat, and it is surrounded by a colonnade which sustains a hallway on the first and second floor. On the second floor, the hallway and the southern part of the building have a lower roof which is surrounded by walls that share the same roof as the perimetral walls of the East, North and West side (Figure 2).

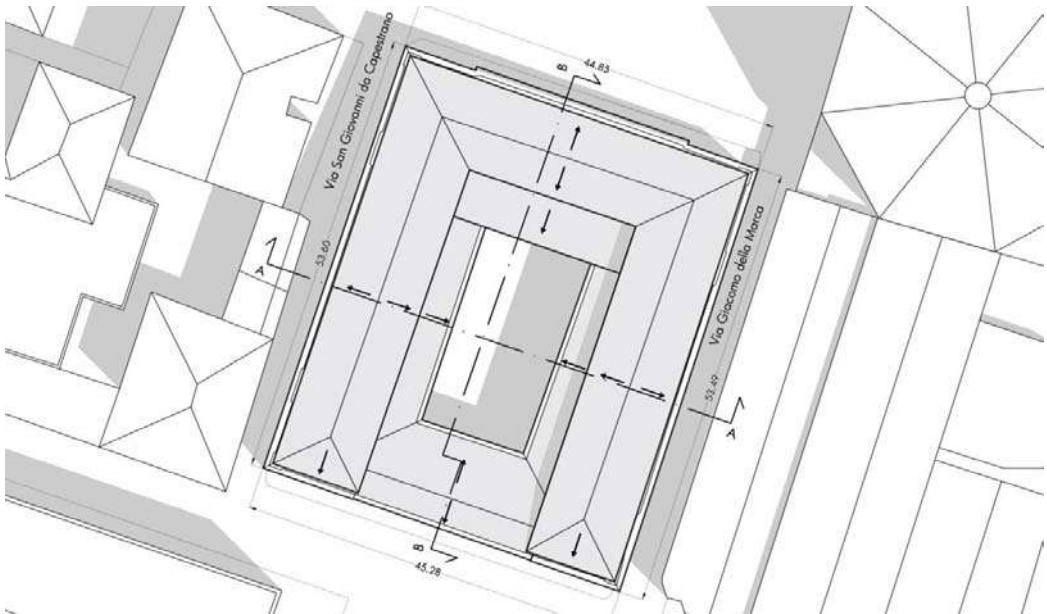


Figure 1: Roof plan of the building and context.

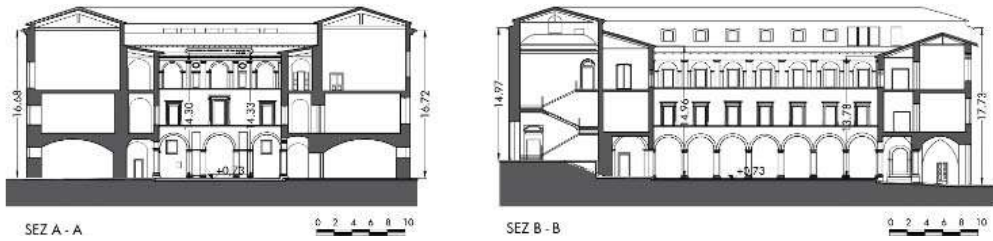


Figure 2: Transversal (left) and longitudinal section (right) of the building.

2.2. The restoration plans

The restoration plans of the historic building foresee the reconstruction of it as it was before the earthquake with the integration of all the necessary structural and energetic improvements. This research project proposes, along with the restoration plans, the covering of the inner courtyard. Such covering would be able to guarantee the use of the courtyard space even in case of adverse climatic conditions, giving the school the possibility of exploiting the courtyard during the educational activities.

The municipal administration is still developing a long-term plan for the building, one of the most important ones of the city, but it suggested that an alternative use of the building could be the transformation from a school to a social aggregation point for the city, offering a wide range of services for the population. In this case, the courtyard would represent a buffer space and a connection between the two squares adjacent to the building: the square of the municipal Theatre and the square of *S. Bernardino Church*.

For what concerns the covering of the courtyard itself, this research project proposes an adaptive textile roof, whose transparency could be altered through the use of printed patterns, if needed. The advantages of using textiles, especially if compared to a traditional transparent roof made of glass, are: a good reversibility, a low impact on the existing building in terms of both structural weight and installation repercussion, and effectiveness in preserving the architectural features of a building (Figure 3). In fact, parts of the courtyard roof can be demounted if the users require it, without compromising the architectural values and historical integrity of the intervention area.

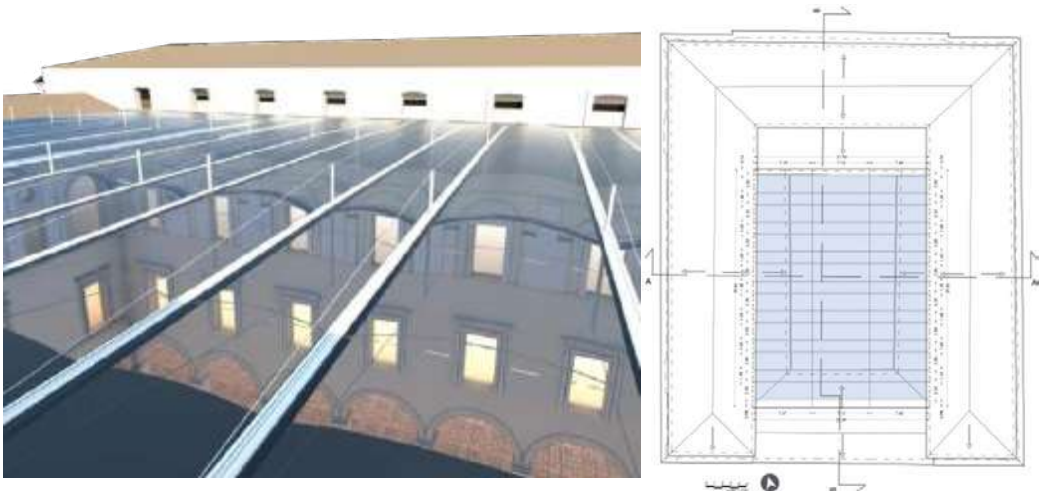


Figure 3: Rendered image of the ETFE roof seen from the top (left), installation of the ETFE roof (right).

3. The design of the courtyard textile roof: an adaptive retrofit solution

The textile roof structure is based on fixed steel beams designed to minimize the material usage. The frame is based on four edge beams and 16 double UPN160. In order to reduce the cross section despite the ambitious long span, steel bars are placed at 1/3 and 2/3 of the UPN beams and put into compression by tensioned cables. The UPN160 beams inside the frame form a series of rectangles, of 2 different widths, which are covered with ETFE cushions with an aluminium frame.

The greater challenge of this project is the measure of the energetic improvement generated by the textile installation. The energy saving has been predicted through dynamic simulations by using Design Builder software.

3.1. The dynamic model

An energetic simulation is a mathematical model of the thermo-physical building behaviour. The geometry of the structure is the basis of the initial input data. A model for energetic simulations is simplified in comparison to the architectural model to which it refers. Usually an object consisting of curved elements is discretized with a certain number of surfaces, but in this work, considered the relatively small curvature of the cushions (transversely), the textile roof is modelled as a plane surface. External loads, on the other hand, depend exclusively on the weather data used in the simulation. One of the main objectives of energy simulation software is to compare different scenarios to analyse energy consumption. In this paper specifically the energy strategy is the introduction of the courtyard roof.

In order to analyze and compare the effect that the membrane roof has on the energy behaviour of the building, two identical models have been designed: one without the coverage of the courtyard and the other with the textile integration (Figure 4). In the development of the model, the location data of L'Aquila have been set in the *Location* template using the weather data of Campobasso, available in the library of the software and with climatic conditions similar to the city of L'Aquila.

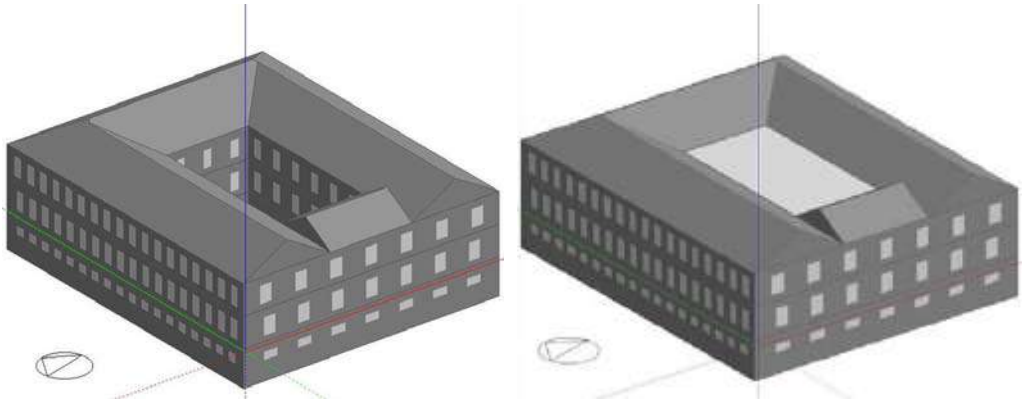


Figure 4: Design Builder model of the building without the ETFE courtyard covering (left) and with the ETFE courtyard covering (right).

The two models have the same geometry and orientation but were handled differently: the first one has one *zone* (building) with its correspondent activity while the second one has two *zones* (building and atrium) and one activity for each zone. For what concerns the building the *Activity* was set to "Generic Office Area" in both models; instead, for the *atrium*, the *Activity* Template was set to "None". Even if the building will host social events, they would only be occasional and take place when there are no office or school activities; so, the average occupancy density of the courtyard was set to 0.05 people/m². during the Office Circulation Schedule, with a "Standing/walking" Activity.

In regard to the *Construction* template, the pitched roof was chosen from the software gallery, while the exterior walls, which consist of a masonry wall plastered on both sides, were created using data from literature (De Vita et al., 2018). Three different wall thicknesses were constructed in the model, representing the average masonry thickness for each level (Table 1). The presence of the courtyard made the creation of a *void*, which is not considered by the software as part of the building, necessary in the first model. In the second model, instead, the courtyard was made in the rectangular building through partition walls and a glazed roof.

Table 1: Masonry wall characteristics used in the model

Construction elements	Thickness [mm]	Density [kg/m ³]	U-Value [W/m ² K]
Perimeter wall - level 1	1600	2100	0.647
Perimeter wall - level 2	1400	2100	0.796
Perimeter wall - level 3	800	2100	1.390

The Wall-to-Window ratios were calculated for the *Openings* and assigned to each different wall, and the window template was chosen according to the Italian Standards. In the second model, the roof of the atria had to be transparent, so it was necessary to create an opening extended through the whole roof surface and the layout of the glazing was set to “100% roof glazing” (De Vita 2018). For the membrane to be assimilated to a glass surface, the textile coverage was modelled starting from the “Project roof glazing”: within the tab of the physical and optical properties of the glass, the characteristic values of the designed membrane (ETFE of 200 µm) have been inserted from literature (Cremer et al., 2017) (Table 2). The cushion was modelled designing two transparent ETFE layers separated by an air gap of 10 cm. Since with the use of Design Builder software it is not possible to reproduce the curved geometry of the cushions, the model of the textile roof was realized through a simple plane. The surface through which the courtyard exchanges heat with the exterior was similar to the real one (≈ 350 m²), as well as the number of partitions and the characteristics of the aluminium frame.

Table 2: Textile roof characteristics used in the model

Construction elements	Thickness	Conductivity	Solar transmittance	U-Value [W/m ² K]
ETFE - clear	200 µm	0.24	0.930	-
ETFE - clear cushion	200 µm + 10 cm air gap + 200 µm	-	0.883	5.977

The *Lighting* template was automatically generated by the software according to the previously set *Activity* template. For the *HVAC* template, instead, an Air to Water Heat Pump (ASHP) heating system, was set up; the system provides the building with the DHW as well and it is powered by the natural gas network. As well as the designed covering, the model of the covering allows natural ventilation, to avoid problems of moisture and condensation.

A comparison of the results from the dynamic simulation enabled the functioning of the cushions roof. The textile model used to carry out the dynamic simulations was developed by the authors using literature results (Chilton, 2004; De Vita et al., 2018).

The period chosen for the simulation coincides with the whole solar year: from January 1th to December 31th.

3.2. Simulation results

The following outputs from the dynamic simulations were analyzed and summarized in figure 4, 5 and 6:

- CO₂ emissions calculated from total fuels with operating HVAC system;
- Electricity consumption with operating HVAC system;
- Natural Gas consumption with operating HVAC system;

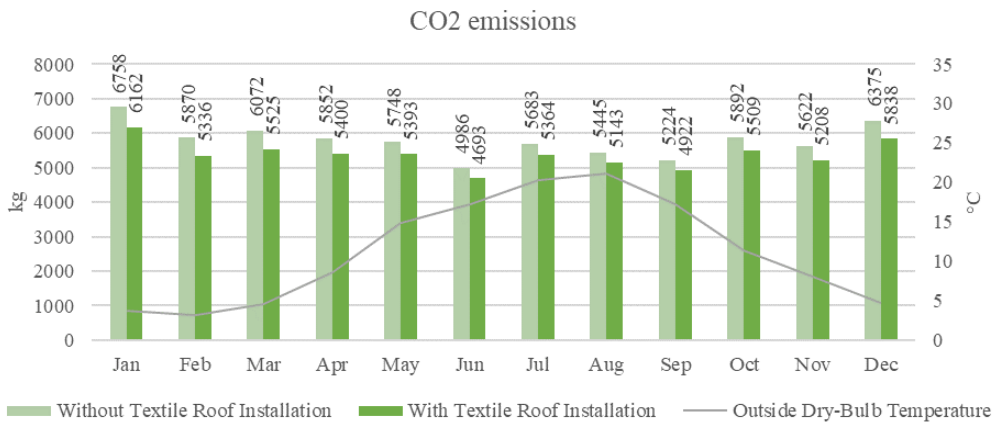


Figure 4: Chart showing the CO2 emission levels in the building during 12 months without the textile roof installation and with it.

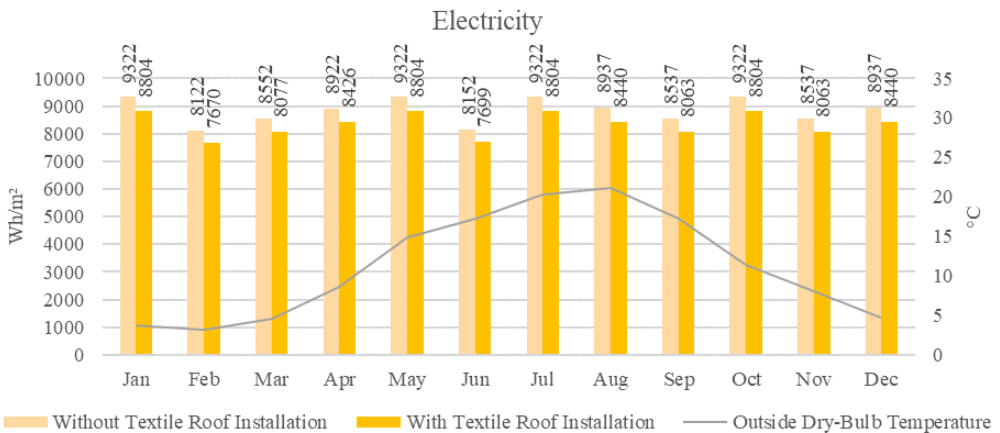


Figure 5: Chart showing the Electricity consumption levels in the building during 12 months without the textile roof installation and with it.

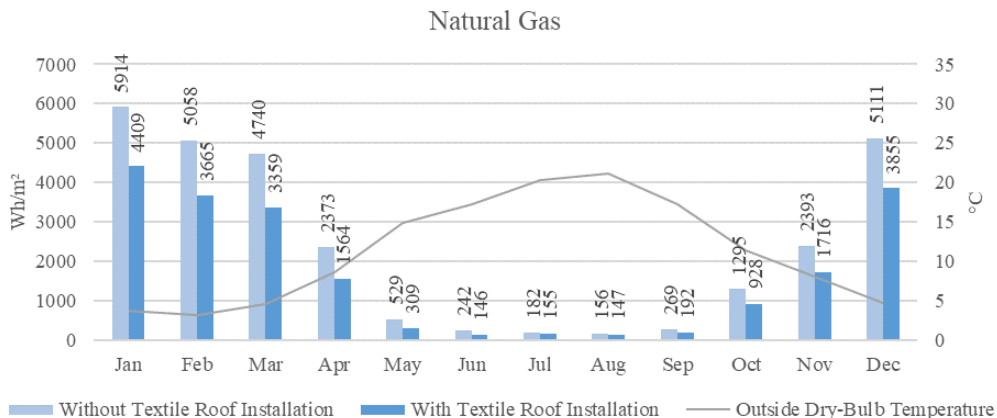


Figure 6: Chart showing the Natural Gas consumption levels in the building during 12 months without the textile roof installation and with it.

Figure 4 shows the reduction of the CO₂ through the installation of the textile roof ranges from 10% (colder months) to 6% (warmer months). The use of ETFE roof solution can even reduce the Electricity fuel of about 6% (Figure 5). The most relevant results from the dynamic simulations show that, although the percentage reduction of Natural Gas consumption level is placed between 25% (colder months) and 42% (warmer months), in winter the textile roof allows to achieve the highest energy saving, considering both the CO₂ emissions and the total fuels.

5. Conclusion

The relevance of this work consists in the possibility of managing the performance of historical buildings through the integration of membranes. The challenge that this study presented was to predict the energetic behaviour of masonry structures combined with textiles using dynamic simulation software, thus allowing the definition of the optimal technological configuration. The results of this study are extremely relevant considering that the choice of textile materials is often based on aesthetic and reversibility aspects whilst energy saving is not yet fully envisaged.

References

- De Vita M., Beccarelli P., Laurini E., De Berardinis P. (2018), Performance Analyses of Temporary Membrane Structures: Energy Saving and CO₂ Reduction through Dynamic Simulations of Textile Envelopes, *Sustainability*, 10(7), DOI: 10.3390/su10072548.
- De Vita M., Bartolomucci C., De Berardinis P. (2018), *L'adozione dei tessuti tecnici come soluzione di retrofit energetico del patrimonio culturale*, ReUSO 2018, VI International Congress, Messina, Italy, 11-13 Ottobre 2018, pp. 1513-1524.

Llorens J., Zanelli A. (2016), *Structural membranes for refurbishment of the architectural heritage*, Procedia Engineering, Vol.155, pp. 18-27.

Chilton J. (2004), Internal environment, in *The European Design Guide for Tensile Surface Structures: Tensinet*, Eds. B. Forster, M. Mollaert, Vrije Univ.: Brussel, pp. 97-146.

De Vita M., Mannella A., Sabino A., Marchetti A. (2018), *Seismic Retrofit Measures for Masonry Walls of Historical Buildings, from an Energy Saving Perspective*, Sustainability, 10(4), DOI: 10.3390/su10040984.

Tillner S. (2003). *Mobile Hofüberdachung in Wien*, Deutsche Bauzeitschrift, Wien, 4/2003, S. pp. 48-53.

Tejera J., Monjo-Carrió J. (2010), *Heritage preservation strategies through textiles*, In: *Tensile Architecture: Connecting Past and Future*, Proceedings of the TensiNet Symposium, 16-18 September 2010, Sofia, Bulgaria, pp. 1-11.

Rosina, E., Zanelli, A., Beccarelli, P., Gargano, M. and Romoli, E. (2011), *New procedures and materials for improving protection of archaeological areas Materials Evaluation*. 69(8), pp. 979-989.

Beccarelli P., Maffei R. and Binda R. (2016), ETFE envelopes for the building sector In: Proceedings of the 11th Conference on Advanced Building Skins, pp. 720-729.

Beccarelli P. and Maffei R. (2017), *Engineering and fabrication of the “Off the Cuff” pavilion*, Fuorisalone 2017, Milan, in: Structural Membranes 2017 VIII International Conference on Textile Composites and Inflatable Structures 9-11 October 2017, Munich, Germany.



AUTHORS A-Z

A	Alongi, Andrea.....	580
	Andriasyan, Mesrop.....	51
	Angelieri, Andrea.....	184
	Angelotti, Adriana.....	547, 580
	Antonenko, Nataliia.....	465
	Armani, Monica.....	505
	Asadi, Hastia.....	351
Atawula, Nuerxiati.....	220	
B	Bandeira Calixto, Lucas.....	535
	Beccarelli, Paolo.....	505, 624
	Benzi, Francesco.....	231
	Bernert, Katja.....	268
	Blum, Rainer.....	46, 304
	Bögner-Balz, Heidrun.....	304
C	Canobbio, Roberto.....	231, 390
	Cantini, Anna.....	547
	Caspeepe, Robby.....	316
	Chesnokov, Andrei.....	58, 71, 111
	Chiu, Simon K.....	46
	Chmelik, Vojtech.....	488, 614
	Clarke, Elena.....	414
	Colliers, Jimmy.....	83
	Cremers, Jan-Frederik.....	592
D	D`Anza, Gerry.....	378
	D'Antonio, Raffaella.....	624
	De Berardinis, Pierluigi.....	624
	De Laet, Lars.....	83, 366
	De Smedt, Elien.....	316, 366
	De Vita, Mariangela.....	624
	Degroote, Joris.....	83
	Di Fusco, Beniamino.....	184
	Di Muro, Emanuela.....	34
	Dolmatov, Ivan.....	58, 111
	Dragoljevic, Milan.....	208
	Dürr, Horst.....	46
	Durka, Maxime.....	292
	F	Fernandez, Gabriela.....
Filz, Günther.....		378
Flore, Isabella.....		465
Fontana, Massimo.....		465
G	Giglio, Andrea.....	414
	Gimferrer, Xavier.....	135
	Giulietti, Nicoletta.....	426
H	Habraken, Arjan.....	123
	Hanuliak, Peter.....	526

Hecht, Katharina.....241
Holl, Jürgen.....144
Houtman, Rogier.....123
Húsenicová, Jarmila.....614

I Imagawa, Norihide.....260
Ivankova, Olga.....497

J Jakica, Nebojsa.....570

K Köhnlein, Jochen.....304
Kolo, Elpiza.....439
Kriklenko, Elena.....402
Kuran, Jozef.....488

L La Magna, Riccardo.....95
Le Van, Anh.....160
Ledesma, Daniel.....196
Liddell, Timothy.....465
Lienhard, Julian.....25
Llorens, Josep.....196
Lombardini, Daniela.....34
Lussou, Philippe.....26

M Maffei, Roberto.....505
Mainini, Andrea Giovanni.....439
Marcandelli, Edoardo.....426
Marx, Hannes.....592
Maywald, Carl.....476
Mazzola, Carlotta.....220, 390
Mikhailov, Vitalii.....58, 71, 111
Mollaert, Marijke.....11, 83, 316, 366
Monteiro, Filipa.....95
Monticelli, Carol.....11, 208, 220, 280, 439
Morichi, Gloria.....535
Moritz, Karsten.....558

O Ottone, Maria Federica.....514

P Paech, Christoph.....17
Paoletti, Ingrid.....414
Pedersen Zari, Maibritt.....241
Perego, Francesca.....426
Poghosyan, Haykaz.....465
Poli, Tiziana.....439
Polomová, Beata.....526
Pyl, Lincy.....316

R Ramsgaard Thomsen, Mette.....95
Riera, Dajla.....514
Rizzo, Alessandro.....231, 580

Roithmayr, Robert.....46
Romanova, Nina.....465
Rosina, Elisabetta.....439
Rychtáriková, Monika.....488, 614

S Sastre, Ramon.....135
Schäffer, Michael.....172
Silvestri, Aldina.....602
Šimek, Richard.....614
Sinke Baranovskaya, Yuliya.....95
Speroni, Alberto.....439
Stefanucci, Alessandro.....34
Stimpfle, Bernd.....11, 172, 390, 453
Stranghöner, Natalie.....339, 351
Ströbel, Dieter.....144
Šujanová, Paulína.....614

T Talak, Kübra.....327
Tamke, Martin.....95
Teruzzi, Eleonora.....426
Teuffel, Patrick.....123
Thomas, Jean-Christophe.....160
Trenkle, Jürgen.....453
Turis, Matus.....497

U Uhlemann, Jörg.....339, 351

V Valle, Eleonora.....426
Van Craenenbroeck, Maarten.....316, 366
Van Wijk, Jasper.....123
Vanek, Michal.....497
Vargová, Andrea.....526
Villani, Teresa.....602
Viscuso, Salvatore.....208
Vojtekova, Eva.....497
Vorstermans, Rens.....123

Z Zamani, Mahsa B.....465
Zanelli, Alessandra.....11, 208, 280, 390, 439, 570

